

# PHYSICAL AGING OF MISCIBLE POLYMER BLENDS

Christopher G. Robertson

Dissertation submitted to the Faculty of the  
Virginia Polytechnic Institute and State University  
in partial fulfillment of the requirements for the degree of

Doctor of Philosophy  
In  
Department of Chemical Engineering

Garth L. Wilkes, Chairman  
William L. Conger  
Richey M. Davis  
Hervé Marand  
Thomas C. Ward

October 29, 1999  
Blacksburg, Virginia

Keywords: physical aging, volume, enthalpy, relaxation, creep,  
miscible polymer blends, cooperativity, fragility

Copyright 1999, Christopher G. Robertson

# PHYSICAL AGING OF MISCIBLE POLYMER BLENDS

Christopher G. Robertson

(ABSTRACT)

Physical aging measurements were performed on various polymeric glasses with the overriding goal of developing a better molecular picture of the nonequilibrium glassy state. To this end, aging-induced changes in mechanical properties and in the thermodynamic state (volume and enthalpy) were assessed for two different miscible polymer blends as a function of both composition and aging temperature. This investigation considered the physical aging behavior of blends containing atactic polystyrene (a-PS) and poly(2,6-dimethyl-1,4-phenylene oxide) (PPO) as well as mixtures of poly(methyl methacrylate) (PMMA) and poly(styrene-co-acrylonitrile) (SAN). Substantial attractive chemical interactions are characteristic of a-PS/PPO blends but are absent in PMMA/SAN blends. The distinct nature of interactions for these two blends resulted in differences in the compositional dependence of secondary relaxation intensity, segmental cooperativity which dictates glass formation kinetics, and density (prior to aging). The variation of volume relaxation rate with aging temperature and composition was interpreted based upon these characteristics for the two systems. In addition, a general relationship was uncovered which linked structural relaxation rates for amorphous polymers to their respective segmental relaxation characteristics (glass transition cooperativity or fragility), which in turn are well understood from a molecular standpoint. This work, therefore, established a basis for comprehending glassy state volume and enthalpy relaxation rates based upon molecular characteristics. Developing an understanding of the connection between the evolving thermodynamic state and mechanical property changes fared less well. The fact that the thermodynamic and mechanical properties can have very different relaxation time responses governing their changes in the nonequilibrium glassy state was clearly evident in an extensive study of the physical aging characteristics of an amorphous polyimide material. For some materials, interpretation of mechanical aging behavior was obscured by thermorheological complexity arising due to overlap of a secondary relaxation with the main chain softening dispersion.

## Acknowledgments

Special thanks are expressed to my family and wife for their support and encouragement.

I greatly appreciate the contributions of my committee members whose time, personal attention, and excellent courses have helped to make me a careful, thoughtful, and curious scientist. In particular, I thank my research advisor Prof. Garth Wilkes for instilling in me a passion for polymer science and for knowing exactly when to actively advise and when to allow much needed freedom.

Research discussions with David Shelby, Mark Muggli, and Sean Christian provided an excellent avenue for idea growth and development, and I express thanks to each accordingly.

I am grateful for being able to associate with past and present members of my research group. Their scientific and social interactions filled my graduate experience with learning and fun, and I am proud to call many of them close friends.

I have had the pleasure of personally interacting with numerous excellent scientists during the course of this research investigation and these interactions have greatly enhanced this present work. I specifically extend gratitude to Austen Angell, Greg McKenna, Sinee Simon, Jim O'Reilly, Shiro Matsuoka, Marty Tant, Anita Hill, Mike Roland, and Kia Ngai.

Finally, I wish to acknowledge funding support for this research by the Phillips Petroleum and Eastman Chemical Companies.

# Table of Contents

Introduction.....	1
Chapter 1: Review -- The glass transition and the nonequilibrium glassy state.....	5
1.1 Glass transition: kinetic vs. thermodynamic .....	5
1.2 Relaxation characteristics of glass-forming materials .....	13
1.2.1 Non-Arrhenius relaxation time behavior.....	13
1.2.2 Non-equilibrium nature of the glass (physical aging).....	21
1.2.3 Non-linear relaxations in the glassy state.....	35
1.2.4 Non-exponential relaxations .....	38
1.3 References .....	44
Chapter 2: Review -- Selected features of miscible polymer blends .....	48
2.1 Thermodynamics of polymer-polymer miscibility .....	48
2.2 Compositional dependence of properties .....	56
2.2.1 Glass transition temperature .....	56
2.2.2 Barrier and mechanical properties .....	67
2.3 References .....	70
Chapter 3: Review -- Previous studies concerned with the physical aging of miscible polymer blends .....	73
3.1 Enthalpy relaxation investigations.....	73
3.2 Effect of physical aging on mechanical properties.....	87
3.3 References .....	95
Chapter 4: Physical aging behavior of miscible blends containing atactic polystyrene and poly(2,6-dimethyl-1,4-phenylene oxide) .....	96
4.1 Introduction .....	97
4.2 Experimental details.....	99
4.3 Results and discussion .....	103

4.3.1	Volume relaxation.....	104
4.3.2	Enthalpy relaxation/recovery.....	108
4.3.3	Aging-induced changes in creep compliance behavior.....	111
4.4	Conclusions.....	113
4.5	References.....	135
Chapter 5:	Glass formation kinetics for miscible blends of atactic polystyrene and poly(2,6-dimethyl-1,4-phenylene oxide).....	137
5.1	Introduction.....	138
5.2	Experimental details.....	139
5.3	Results and discussion.....	141
5.3.1	Glass formation kinetics from DSC and DMA.....	142
5.3.2	Correlation between aging rates and glass transition cooperativity.....	149
5.3.3	Origin of negative excess volumes in the glassy state: kinetic vs. thermodynamic considerations.....	150
5.4	Conclusions.....	154
5.5	References.....	169
Chapter 6:	Physical Aging Behavior for Miscible Blends of Poly(methyl methacrylate) and Poly(styrene-co-acrylonitrile).....	172
6.1	Introduction.....	172
6.2	Experimental details.....	175
6.3	Results and discussion.....	178
6.3.1	Physical aging results.....	178
6.3.2	Interpretation of aging results and comparison with a-PS/PPO system....	182
6.4	Conclusions.....	186
6.5	References.....	198
Chapter 7:	Correlation between physical aging rates and glass transition cooperativity (fragility): Part 1. Experimental results.....	200
7.1	Introduction.....	200

7.2	Experimental details.....	202
7.3	Results and discussion .....	205
7.3.1	Determination of glass formation characteristics.....	205
7.3.2	Correlation between structural relaxation rates and glass transition cooperativity .....	213
7.4	Conclusions .....	221
7.5	References .....	240
Chapter 8: Correlation between physical aging rates and glass transition cooperativity (fragility): Part 2. Adam-Gibbs predictions .....		
8.1	Introduction .....	243
8.2	Results and discussion .....	245
8.2.1	Model description.....	245
8.2.2	Comparison of predictions with experimental data .....	254
8.3	Conclusions .....	256
8.4	References .....	270
Chapter 9: Physical aging of an amorphous polyimide: enthalpy relaxation and mechanical property changes .....		
9.1	Introduction .....	271
9.2	Experimental details.....	272
9.3	Results and discussion .....	275
9.3.1	Enthalpy relaxation rates .....	279
9.3.2	Changes in stress-strain response.....	281
9.3.3	Mechanical aging effects observed by creep and DMA.....	282
9.3.4	Discussion of mechanical-structural aging rate interrelationships .....	286
9.4	Conclusions .....	290
9.5	References .....	309

Chapter 10: Long-term volume relaxation of bisphenol-A polycarbonate and atactic polystyrene .....	311
10.1 Introduction .....	312
10.2 Experimental details.....	312
10.3 Results and discussion.....	313
10.4 Conclusions .....	315
10.5 References .....	319
 Chapter 11: Refractive index: a probe for monitoring volume relaxation during physical aging of glassy polymers .....	320
11.1 Introduction .....	321
11.2 Experimental details.....	322
11.3 Results and discussion.....	325
11.3.1 Effect of physical aging on refractive index.....	325
11.3.2 Determination of volume relaxation rate from refractive index data.....	326
11.3.3 Comparison of volume relaxation rates determined by refractometry and dilatometry.....	328
11.4 Conclusions .....	329
11.5 References .....	333
 Summary and recommendations for future work .....	335
 Vita .....	337

## List of Tables

Table 1-I: Comparison of Aging Effects Measured by Different Methods.....	30
Table 3-I: $\Delta H_{\infty}$ for PVME, a-PS, and 50/50wt. Blend Aged at $T_a = T_{g,f} - 10^{\circ}\text{C}$ .....	78
Table 3-II: Cowie-Ferguson Parameters Corresponding to the Illustrative Fits Indicated in Figure 3-2.....	79
Table 3-III: Enthalpy Relaxation Parameters for the SAN/SrMMA System Aged at $T_a =$ $T_g - 20^{\circ}\text{C}$ .....	86
Table 4-I: Glass Transition Temperature Results .....	115
Table 4-II: Observed Differences Between Liquid and Glassy Heat Capacities.....	115
Table 5-I. Relaxation Parameters.....	154
Table 6-I: Results from thermal contraction experiments .....	187
Table 7-I: Parameters describing glass transition and aging responses .....	222
Table 7-II: Relaxation parameters.....	222
Table 7-III: Predicted values of $E''/(E_{\infty} - E_0)$ for low $\beta$ values (using $\tau = 10$ sec).....	238
Table 7-IV: Predicted values of $E''/(E_{\infty} - E_0)$ for high $\beta$ values (using $\tau = 10$ sec)....	239
Table 9-I. Stretched exponential fitting parameters for creep .....	292
Table 9-II. Fitting parameters for linear stretched exponential decay.....	292
Table 11-I: Summary of parameters used to calculate $\beta$ from refractive index data.....	330

## List of Figures

Figure 1-1: Illustration of the kinetic behavior of $T_g$ using the generalized temperature dependence of specific volume. ....	7
Figure 1-2: Idealized thermodynamic behavior for the glass transition. Generalized figure adapted from reference 5. ....	9
Figure 1-3. Illustration of the Kauzmann paradox (entropy crisis). Schematic adapted from reference 7. ....	10
Figure 1-4: Non-Arrhenius relaxation time behavior. Curves generated using the WLF equation with the parameters $T_g = 376\text{K}$ , $\tau_g = 100 \text{ s}$ , $C_1=17$ , and values for $C_2$ equal to $50\text{K}$ for curve A and equal to $100\text{K}$ for curve B. ....	15
Figure 1-5: General illustration of occupied and total volume for an amorphous material. The difference between the two functions is the free volume.....	17
Figure 1-6: Matsuoka's depiction of cooperative relaxation domains with $z = 6$ (from reference 29).....	21
Figure 1-7: Changes in the thermodynamic state due to the physical aging process.....	23
Figure 1-8: Volume relaxation of polystyrene (replotted from reference 38).....	23
Figure 1-9: Determination of enthalpy relaxation using differential scanning calorimetry. When the heat flow is given in units of $\text{W/g}$ , then the heating rate must be used to convert the $\Delta H$ given above to the correct units of $\text{J/g}$ .....	25
Figure 1-10: Tensile stress-strain behavior (room temperature, $10\%/min$ strain rate) for amorphous poly(ethylene terephthalate) annealed in the glassy state for 90 minutes at $51^\circ\text{C}$ (curve A) and freshly quenched from above $T_g$ (curve B) (replotted from 41).....	26
Figure 1-11: Struik's generalized creep compliance testing schedule utilized for isothermal aging studies.....	28
Figure 1-12: Influence of physical aging on the time-dependent creep compliance response of rigid poly(vinyl chloride) (replotted from reference 32).....	28
Figure 1-13. Aging temperature dependence of volume relaxation rates for various glassy polymers (replotted from reference 36).....	31

Figure 1-14. Creep shift rate as a function of aging temperature for various glassy polymers (replotted from reference 32). .....	31
Figure 1-15. Relaxation map for an amorphous glass-forming material for cooling through the glass transition region followed by glassy state annealing at $T_a$ (based upon reference 7). .....	33
Figure 1-16: Portion of a hypothetical potential energy surface for a glassy material (based upon reference 77). An expanded view of the potential energy surface reveals the possible influence of secondary relaxation response which serves to coarsen the surface and enable a lower energy state to be obtained (1→ 2) for the main chain relaxation by a series of smaller energy jumps. ....	34
Figure 1-17. Long-term volume relaxation response of bisphenol-A polycarbonate at 23°C following 80°C/min quench from above $T_g$ (replotted from reference 78). ....	35
Figure 1-18: Diagram illustrating the up-jump and down-jump experiments initiated from equilibrium states. See text for details.....	37
Figure 1-19: Asymmetry of approach for poly(vinyl acetate) indicated by contraction and expansion behavior (replotted from reference 84). By comparison with Figure 1-18, $T_1=30^\circ\text{C}$ , $T_2=35^\circ\text{C}$ , and $T_3=40^\circ\text{C}$ .....	38
Figure 1-20: Illustration of the memory effect for poly(vinyl acetate) (replotted from reference 84). Curve A represents relaxation during annealing in the glassy state at 30°C following a rapid quench from 40°C (the equilibrium liquid state above $T_g$ ). Curve B represents volume response at 30°C for a sample which was first quenched from 40°C and then annealed at 15°C for 140 hours prior to being rapidly heated to 30°C. Time $t_1$ is when the temperature of 30°C is reached.....	42
Figure 1-21: Relaxation time distributions according to the KWW stretched exponential function. Relaxation times are normalized by most probable relaxation time, $\tau$ . ....	43
Figure 2-1: General phase diagram (constant pressure) for binary polymer blend system with LCST behavior.....	51
Figure 2-2: General schematic of modulus variation with temperature (constant testing rate) for miscible and immiscible amorphous polymer blends as a function of blend composition in the glass-to-rubber transition region(s) (adapted from ref. 3).....	58

Figure 2-3: Some commonly observed dependencies of $T_g$ on composition for miscible polymer blends. Additivity for $T_g$ is illustrated (b) as well as positive (a) and negative (c) deviations thereof. ....	58
Figure 2-4: Thermodynamic cycle which cannot be performed experimentally (step 4 is impossible) for an amorphous miscible blend system. Figure adapted from reference 33. ....	62
Figure 2-5: Experimental and predicted $T_g$ values for the a-PS/PPO blend system. Gordon-Taylor and Couchman-Karasz predictions as well as experimental data replotted from reference 31. Prediction using Fox equation calculated based upon the indicated $T_g$ values of the pure components.....	64
Figure 2-6: Room temperature specific volume and tensile modulus for a-PS/PPO blend system. Data replotted from references 38 and 39. ....	68
Figure 2-7: Compressive yield stress and maximum crack propagation energy ( $R_{max}$ ) at room temperature for a-PS/PPO blend system. Double-cantilever beam specimens used for crack propagation tests. Data replotted from reference 40.....	68
Figure 2-8: Specific volume at 23°C (upper plot) and n-hexane vapor sorption properties at 40°C (lower plot) for a-PS/PPO blends. Prior to testing, samples were annealed for 2 hours at $T_g+20^\circ\text{C}$ after solution casting. Sorption data obtained using a ratio of partial pressure to equilibrium vapor pressure (activity) of 0.98. Data replotted from reference 41.....	69
Figure 2-9: Specific volume at 23°C and water vapor diffusion coefficient at 30°C and 50°C for blends of poly(methyl methacrylate) and poly(styrene-co-acrylonitrile)(30 wt.% acrylonitrile). Data replotted from reference 42.....	69
Figure 3-1: Schematic of typical enthalpy recovery behavior (solid lines) following isothermal annealing in the glassy state for binary polymer blends with components possessing similar glass transition temperatures. Dashed lines represent generalized heating scans for freshly quenched blends.....	78
Figure 3-2: Example fits using the Cowie-Ferguson model for illustrative enthalpy recovery “data” which has not yet reached equilibrium. The data sets are identical with the exception of the values at $t_a = 300$ hours.....	79

Figure 3-3: Tool-Narayanaswamy-Moynihan parameters fit to normalized DSC heating scans for freshly quenched a-PMMA/SAN samples (100°C/min cooling, 10°C/min heating). Parameters replotted from reference 18. ....	81
Figure 3-4: Sample of enthalpy relaxation data used to determine $\tau$ and $\beta_H$ in Figure 3-5 (data replotted from reference 20). ....	83
Figure 3-5: (a) Relaxation time, $\tau$ , from the Cowie-Ferguson model fit to enthalpy relaxation data for a-PS/PPO blends (replotted from reference 20). (b) Enthalpy relaxation rates determined (by this author) from the same $\Delta H$ data. ....	83
Figure 3-6: Enthalpy relaxation rates for a-PS/PPO blends determined (by this author) from data presented in reference 14 (see text for possible explanation of unusually high $\beta_H$ values). ....	85
Figure 3-7. Stress relaxation aging rate as a function of composition and aging temperature for a-PMMA/SAN blend system. Aging rates determined (by this author) from KWW relaxation times given in reference 28 for aging times of 2, 4, and 8 hours. ....	90
Figure 3-8. Stress relaxation aging rate as a function of composition and aging temperature for a-PS/PPO blend system. Aging rates determined (by this author) from KWW relaxation times given in reference 28 for aging times of 2, 4, and 8 hours. ....	90
Figure 3-9: (a) Average KWW relaxation time at $t_a = 240$ min. and (b) aging shift factor, $\mu$ , determined from stress relaxation data for a-PS/PPO system. The aging temperature is scaled with respect to $T_g$ . Data are replotted from references 31 and 32. ....	93
Figure 3-10: (a) Average KWW relaxation time at $t_a = 240$ min. and (b) aging shift factor, $\mu$ , determined from stress relaxation data for a-PS/PPO system. The aging temperature is scaled with respect to $T_{g,o}$ . Data are replotted from references 31 and 32. ....	94
Figure 4-1: Representative volume relaxation data at undercoolings of 30°C and 60°C. An aging time of 0.25 hr was used as the reference for determining volume differences ( $\Delta V$ values). The negative slope of each data set represents the volume	

relaxation rate, $b_v$ , and data points between 0.6 hr and 80 hr were used in the rate determination.....	116
Figure 4-2: Volume relaxation rate as a function of composition for the indicated undercoolings. ....	117
Figure 4-3: Volume relaxation rates replotted as a function of undercooling. Midpoint and onset DSC glass transition temperatures are employed as references. ....	118
Figure 4-4: Dependence of specific volume on blend composition for freshly quenched glassy samples. ....	119
Figure 4-5: Dynamic mechanical response for freshly quenched samples using a heating rate of 2°C/min and a frequency of 1 Hz. ....	120
Figure 4-6: Dynamic mechanical response using a heating rate of 2°C/min and a frequency of 1 Hz for PPO samples with the indicated pre-treatments.....	121
Figure 4-7: Loss modulus at the indicated temperatures (a); and a comparison of property (P) ratios for loss modulus and volume relaxation rate. See text for additional details. ....	122
Figure 4-8: Representative DSC enthalpy recovery traces during heating at 10°C/min following annealing at $T_g-30^\circ\text{C}$ . The dotted lines represent the second heats after freshly quenching the samples into the glassy state at 200°C/min.....	123
Figure 4-9: Representative DSC enthalpy recovery traces during heating at 10°C/min following annealing at $T_g-60^\circ\text{C}$ . The dotted lines represent the second heats after freshly quenching the samples into the glassy state at 200°C/min. Note that the scale is different than that used in Figure 4-8. ....	124
Figure 4-10: Recovered enthalpy ( $\Delta H$ ) as a function of aging time for undercoolings of 30°C and 60°C. Each data point represents the average $\Delta H$ from three DSC enthalpy recovery experiments, and approximately 200 DSC runs were performed in order to generate this plot.....	125
Figure 4-11: Rate of change of enthalpic fictive temperature during aging. Rates were determined: (a) from the $\Delta H$ data; and (b) from the first heating scans using the software provided with the DSC instrument. See text for additional details. ....	126
Figure 4-12: Illustration of enthalpic fictive temperature assessment for a-PS/PPO50 blend aged at $T_g-60^\circ\text{C}$ .....	127

Figure 4-13: Rate of change of volumetric fictive temperature during aging. See text for additional details.....	128
Figure 4-14: Creep compliance responses for a-PS (a), a-PS/PPO50 (b), and PPO (c) aged at $T_g-30^\circ\text{C}$ . Upper plots depict the data as a function of aging time, and the lower plots are the master curves generated at a reference aging time of 6 hr as well as the stretched exponential fits to the master curve data. For clarity, only every fifth data point is included in the master curves.....	131
Figure 4-15: Mechanical aging rates determined from horizontal and vertical shift factors used during formation of creep compliance master curves.....	132
Figure 4-16: Variation of the stretched exponential function parameters $\tau$ and $\beta$ with composition for creep compliance response at $T_g-30^\circ\text{C}$ and $T_g-60^\circ\text{C}$ . ....	133
Figure 4-17: Sensitivity of mechanical creep changes to structural volume changes for the blend system at undercoolings of $30^\circ\text{C}$ and $60^\circ\text{C}$ . ....	134
Figure 5-1. DSC glass transition responses during heating at $10^\circ\text{C}/\text{min}$ following a quench from above $T_g$ at the indicated cooling rates.....	155
Figure 5-2. Relationship between the cooling rate and the fictive temperature assessed from the DSC heating scans at $10^\circ\text{C}/\text{min}$ . The fictive temperature associated with the cooling rate of $1^\circ\text{C}/\text{min}$ , $T_{f,1}$ , is used as a normalization constant for each material. The magnitude of a typical error bar associated with the normalized fictive temperature data is given in the plot.....	156
Figure 5-3. Dependence of loss modulus on frequency and temperature for PPO in the glass formation ( $\alpha$ -relaxation) region. The plot on the right is the master curve which was generated by time-temperature superposition, and the solid line represents the KWW function which was fit to the master curve data. Vertical shifting of the loss modulus data was accomplished using the temperature ratio of $T_{\text{ref}}/T$ (where temperatures are in units of K). ....	157
Figure 5-4. Dependence of loss modulus on frequency and temperature for the a-PS/PPO75 blend in the glass formation ( $\alpha$ -relaxation) region. The plot on the right is the master curve which was generated by time-temperature superposition, and the solid line represents the KWW function which was fit to the master curve data.	

Vertical shifting of the loss modulus data was accomplished using the temperature ratio $T_{ref} / T$ (where temperatures are in units of K). .....	157
Figure 5-5. NonArrhenius behavior of segmental relaxation times in the glass formation temperature range. The shift factor data and associated WLF fits (lines) were converted from the reference temperatures used during time-temperature superposition of loss modulus data to the DSC glass transition temperatures. Only selected data and fits are shown in order to maintain clarity. ....	158
Figure 5-6. Influence of blend composition on fragility determined from DSC and DMA data.....	159
Figure 5-7. Cooperative domain size at $T_g$ for the a-PS/PPO polyblends determined from DMA relaxation time scaling behavior. The dashed line represents pure component additivity. ....	159
Figure 5-8. Normalized DSC heat flow data (symbols) for a-PS/PPO blends obtained during heating at 10K/min following a quench from above $T_g$ at 10K/min. The solid lines are the AG/TNM fits to the data. See text for additional details.....	160
Figure 5-9. Role of PPO content on $\beta$ parameter assessed from DSC and DMA data..	161
Figure 5-10. Compositional dependence of the ratio of DSC glass transition breadth to the breadth assessed from DMA data. The DSC breadth was determined from heating scans at 10°C/min and the DMA transition breadth assessed from the peak width at half height of the $\tan\delta$ peaks obtained at 1 Hz and during heating at 2°C/min. <sup>39</sup> .....	161
Figure 5-11. Comparison of the trend between fragility and $\beta$ observed for the a-PS/PPO system via DMA with literature trend for polymers reported by Böhmer et al. ....	162
Figure 5-12. Variation of glass transition cooperativity, $z_g$ , (upper plot) and aging rates at $T_a=T_g-30^\circ\text{C}$ (lower plot) with blend composition. ....	163
Figure 5-13. Apparent correlation between structural relaxation rates at $T_a=T_g-30^\circ\text{C}$ and glass transition cooperativity for the a-PS/PPO blend system. ....	164
Figure 5-14. Compositional dependence of specific volume for the a-PS/PPO blend system plotted based upon results of Zoller and Hoehn. <sup>12</sup> The dashed lines connect the data points for the pure polymers and thus represent additive behavior.....	165

Figure 5-15. Thermal contraction responses for the a-PS/PPO blends during cooling at 1°C/min. The numbers represent the PPO content in wt.% .....	166
Figure 5-16. Jump in thermal expansion coefficient at $T_g$ as a function of blend composition. Data are from this study and from the investigation performed by Zoller and Hoehn. <sup>12</sup> .....	167
Figure 5-17. Compositional variation of DSC glass transition temperature, $T_g$ , and Vogel temperature, $T_0$ . Also plotted are predictions for both $T_g$ and $T_0$ .....	168
Figure 6-1. (a) DSC glass transition temperature results and (b) room temperature specific volume data. ....	188
Figure 6-2. Typical volume relaxation results for aging performed at $T_g-30^\circ\text{C}$ . An aging time of 0.25 hr was used as the reference for determining volume differences ( $\Delta V$ values). The negative slope of each data set represents the volume relaxation rate, $b_v$ , and data points between 0.6 hr and 80 hr (approx.) were used in the rate determination.....	189
Figure 6-3. Variation of volume relaxation rate with both composition and aging temperature.....	189
Figure 6-4. (a) Creep compliance behavior for PMMA following aging at $T_g-30^\circ\text{C}$ for the indicated aging times; (b) Attempt to generate a master curve via horizontal and vertical shifting in order to superimpose the entire data set for each aging time; (c) Attempt to superimpose the long time portion of the creep data. The reference response used during the superposition attempts was that obtained at an aging time of 6 hours. ....	191
Figure 6-5. Loss modulus data obtained at a heating rate of 2°C/min using a testing frequency of 1 Hz. ....	192
Figure 6-6. DSC heating traces obtained during heating at 10°C/min following cooling at 1°C/min (dashed lines), 10°C/min (solid lines), and 100°C/min (dotted lines). The numbers represent the SAN content in wt.% .....	193
Figure 6-7. Relationship between the cooling rate ( $q_c$ ) and the fictive temperature assessed from the DSC heating scans at 10°C/min. The fictive temperature associated with the cooling rate of 1°C/min, $T_{f,1}$ , is used as a normalization constant	

for each material. The magnitude of a typical error bar associated with the normalized fictive temperature data is given in the plot.....	194
Figure 6-8. Influence of blend composition on the fragility determined from the DSC data.....	195
Figure 6-9. Thermal contraction responses assessed during cooling at 1°C/min. ....	196
Figure 6-10. Ratio of property value at $T_g-15^\circ\text{C}$ to value at $T_g-45^\circ\text{C}$ for the properties of volume relaxation rate and loss modulus (1 Hz, heating at 2°C/min, freshly quenched sample). ....	197
Figure 7-1: Generalized segmental relaxation time behavior in glass-forming temperature region. The curves are generated using the Williams-Landel-Ferry expression with $T_g=400\text{K}$ , $C_1=16$ , and $C_2=50\text{K}$ for curve A and $C_2=100\text{K}$ for curve B.....	223
Figure 7-2: Dynamic mechanical loss data as a function of frequency and temperature for the amorphous polyimide. See Figure 7-3 for the symbol legend.....	224
Figure 7-3: Loss modulus master curve obtained by superposition of data in Figure 7-2. The solid line is the stretched exponential function fit to the data ( $\beta=0.45$ ) .....	225
Figure 7-4: Shift factor plot illustrating glass transition cooperativity for the amorphous polyimide investigated. The shift factors were converted from the reference temperature of 250°C used during superposition of the loss modulus data to a reference temperature of 239°C which is the calorimetric $T_g$ . The solid line represents the WLF fit. ....	226
Figure 7-5: DSC glass transition response during heating at 10°C/min for the amorphous polyimide material following cooling from $T_g+50^\circ\text{C}$ at indicated cooling rates....	227
Figure 7-6: Arrhenius plot of the cooling rate dependence of calorimetric fictive temperature for the polyimide material.....	228
Figure 7-7. Two-dimensional depiction of cooperative relaxation domains with $z = 7$ . Schematic adapted from representation given by Matsuoka and Quan. <sup>18,19</sup> .....	229
Figure 7-8: Schematic which illustrates activation energy associated with intramolecular relaxation of molecular segments: (a) independent relaxation of one segment; (b) cooperative relaxation of $z$ segments. The intramolecular relaxation depicted involves rotation of backbone bonds from second-lowest to lowest energy state ( $\phi$ is the angle of rotation).....	229

Figure 7-9. WLF behavior (curve A from Figure 7-1) and the associated temperature dependence of the most probable cooperative domain size.....	230
Figure 7-10: Departure into the non-equilibrium glassy state from the equilibrium nonArrhenius segmental relaxation response in the glass formation region. The segmental relaxation response indicated is from curve A in Figure 7-1. ....	231
Figure 7-11: Predicted loss modulus using KWW function numerically transformed to frequency domain. A fixed relaxation time ( $\tau = 10$ sec) was used in the predictions and the stretching exponent was varied as indicated.....	232
Figure 7-12: Illustration of fictive temperature changes during isothermal annealing in the glassy state.....	233
Figure 7-13: Apparent correlation between structural relaxation rates at $T_g - 30^\circ\text{C}$ and glass transition cooperative domain size.....	234
Figure 7-14. Apparent correlation between $\beta$ and most probable cooperative domain size at the glass transition temperature for amorphous polymers. The solid triangles are from this paper (Table 7-II) and the open circles are converted data from Böhmer et al. <sup>3</sup> Literature fragility data were converted to $z_g$ data using $C_1 = 16$ . ....	235
Figure 7-15. Fragility and $z_g$ plotted versus glass transition temperature for amorphous polymers. The solid triangles are from this paper (Table 7-II) and open circles are from Böhmer et al. <sup>4</sup> Literature fragility data were converted to $z_g$ data using assumption $C_1 = 16$ .....	236
Figure 7-16. Volume relaxation rates for various glassy polymers. Figure adapted from reference 27. Each solid circle marks volume relaxation aging rate at $T_g - 30\text{K}$ .....	237
Figure 8-1. Illustration of the temperature and structure contributions to the most probable cooperative domain size. The calculations use a $T_g$ (during cooling as shown) equal to 400 K and a value of 350 K for $T_2$ . For illustrative purposes, it is assumed that limited structural relaxation occurs during cooling from A to B such that the fictive temperature remains constant in the glassy state until annealing is commenced at 370 K. ....	258
Figure 8-2: AG/TNM predictions for thermal history involving cooling from $T_g + 50\text{K}$ at 1K/min, annealing for 2 minutes at $T_g - 50\text{K}$ , and heating to $T_g + 50\text{K}$ at 10K/min. The model parameters employed were assessed from DMA data for the polyimide	

material. The curves indicate the influence of including an iterative procedure for  $T_f$  evaluation during the numerical prediction using temperature step of 1.0 K.... 259

Figure 8-3: AG/TNM predictions for thermal history involving cooling from  $T_g+50K$  at 10K/min, annealing for 2 minutes at  $T_g-50K$ , and heating to  $T_g+50K$  at 10K/min. The model parameters employed were assessed from DMA data for the polyimide material. The curves represent the different temperature steps employed in the numerical technique..... 260

Figure 8-4: AG/TNM predictions for thermal history involving cooling from  $T_g+50K$  at 200K/min, annealing for 1 hour at  $T_g-30K$ , and heating to  $T_g+50K$  at 10K/min. The model parameters employed were assessed from DMA data for the polyimide material. The curves represent the different temperature steps employed in the numerical technique..... 261

Figure 8-5: AG/TNM predictions for thermal history involving cooling from  $T_g+50K$  at 1K/min, annealing for 2 minutes at  $T_g-50K$ , and heating to  $T_g+50K$  at 10K/min. The model parameters employed were assessed from DMA data for the polyimide material. The curves represent the different temperature steps employed in the numerical technique..... 262

Figure 8-6: AG/TNM predictions for thermal history involving cooling from  $T_g+50K$  at 200K/min, annealing for 100 hours at  $T_g-30K$ , and heating to  $T_g+50K$  at 10K/min. The model parameters employed were assessed from DMA data for the polyimide material. The curves represent the different temperature steps employed in the numerical technique..... 263

Figure 8-7: DSC heating scan at 10°C/min for a poly(2,6-dimethyl-1,4-phenylene oxide) (PPO) film sample (thickness approx. 0.2 mm) sandwiched between two indium samples. Indium (1.6 mg) was melted in the DSC pan, the PPO sample (8.3 mg) was then placed in the pan, and additional indium (1.0 mg) was melted on top. A lid was finally placed on top and the pan was crimped. A quench from above the  $T_g$  of PPO into the glassy state at 200°C/min was then performed prior to the heating scan at 10°C/min shown in the figure..... 264

Figure 8-8: AG/TNM predictions during annealing at the indicated aging temperatures following a quench from  $T_g+50K$  (289°C) at 200K/min. The model parameters

employed were assessed from DMA data for the polyimide material. The negative rate of change of the predicted $T_f$ with respect to $\log(t_a)$ was evaluated for aging times between 1 and 100 hours for each annealing temperature and converted to a $b_H$ value by division by $\Delta C_p$ .....	265
Figure 8-9: Comparison of AG/TNM predictions and experimental enthalpy relaxation rate data for the polyimide material ( $T_g = 239^\circ\text{C}$ ). The $\beta$ parameter was varied as indicated in the plot ( $\beta = 0.45$ for DMA data).....	266
Figure 8-10: Volume relaxation rates for atactic polystyrene. Plotted are the experimental data trend from Greiner and Schwarzl (— + —) and this work (■). Also indicated are AG/TNM predictions using the given values of the $\beta$ parameter ( $\beta = 0.4$ for DMA data).....	267
Figure 8-11: Comparison of AG/TNM predictions (lines) and normalized experimental DSC heating traces (symbols) at $10^\circ\text{C}/\text{min}$ for the polyimide material following cooling from $T_g+50^\circ\text{C}$ at: (a) $100^\circ\text{C}/\text{min}$ ; and (b) $10^\circ\text{C}/\text{min}$ . A short hold of 2 minutes at $T_g-50^\circ\text{C}$ was performed after the quench and prior to the heating scan. Refer to Chapter 7 for experimental details.....	268
Figure 8-12: Apparent correlation between structural relaxation rates at $T_g-30^\circ\text{C}$ and glass transition cooperativity (data from part 1). For the predictions, $\tau_g = 100$ sec, $T_g = 400$ K, $C_{1,g} = 16$ , and $C_{2,g}$ was varied between 31.6 and 89.4 K to give $z_g$ which varied from 160 to 20.....	269
Figure 9-1. Predominant chemical repeat unit for the polyimide used in this investigation. The incorporation of a proprietary comonomer serves to disrupt chain symmetry and prevent crystallizability of the polymer. ....	292
Figure 9-2. DSC scans ( $10^\circ\text{C}/\text{min}$ heating) illustrating enthalpy recovery behavior following aging at the indicated temperatures. Each dotted line represents the second scan immediately following a quench into the glassy state.....	293
Figure 9-3. Dependence of recovered enthalpy ( $\Delta H$ ) on aging time for aging performed at the indicated temperatures. The lines are linear fits to the data for the given axes (linear y, logarithmic x) and the slope of each line is $b_H$ . Each data point represents the average $\Delta H$ value from three samples.....	294

Figure 9-4. Enthalpy relaxation rate ( $b_H$ ) as a function of aging temperature. The dotted line indicates the location of the kinetic  $T_g$  determined via DSC for a freshly quenched sample using a  $10^\circ\text{C}/\text{min}$  heating rate..... 295

Figure 9-5. Effect of physical aging at  $T_a = 204^\circ\text{C}$  on the engineering stress-strain (tensile) behavior measured at room temperature using a rate of  $2.54 \text{ mm}/\text{min}$  (sample gauge length =  $7 \text{ mm}$ ). Each indicated curve is representative of the average response for the 10 samples tested at each condition. .... 296

Figure 9-6. Effect of physical aging at  $204^\circ\text{C}$  on modulus ( $E$ ), yield stress ( $\sigma_y$ ), and strain at yield ( $\epsilon_y$ ) determined from tensile testing at room temperature using a testing rate of  $2.54 \text{ mm}/\text{min}$ . The data plotted at  $t_a = 10\text{-}2 \text{ hr}$  are for the unaged material..... 297

Figure 9-7. Effect of physical aging at  $204^\circ\text{C}$  on toughness, stress at break ( $\sigma_b$ ), and strain at break ( $\epsilon_b$ ) determined from tensile testing at room temperature using a testing rate of  $2.54 \text{ mm}/\text{min}$ . The data plotted at  $t_a = 10\text{-}2 \text{ hr}$  are for the unaged material..... 298

Figure 9-8. (a) Tensile creep compliance response after aging at  $204^\circ\text{C}$  for the indicated aging times. (b) Master curve at a reference aging time of  $6 \text{ hr}$  generated by horizontal and vertical shifting. For clarity, only every fifth data point indicated for each aging time data set in the master curve. The solid line is the best fit of the stretched exponential function to the master curve. .... 299

Figure 9-9. Comparison of creep compliance master curves (reference:  $t_a = 6 \text{ hr}$ ) for the aging temperatures indicated. The curves represent the stretched exponential functions which were fit to the master curves..... 300

Figure 9-10. Mechanical aging rate ( $\mu$ ) as a function of aging temperature determined from the rate of horizontal shifting used in the generation of master curves for creep compliance data. Also shown are enthalpy relaxation rate ( $b_H$ ) data. The dotted line indicates the location of the kinetic  $T_g$  determined via DSC for a freshly quenched sample using a  $10^\circ\text{C}/\text{min}$  heating rate. .... 301

Figure 9-11. Rate of vertical shifting necessary for adequate superposition of creep compliance data to form master curves. Also indicated is the derivative of  $\log(\text{modulus})$  with respect to  $\log(t_a)$  for the stress-strain tensile modulus. The dotted

line indicates the location of the kinetic $T_g$ determined via DSC for a freshly quenched sample using a $10^\circ\text{C}/\text{min}$ heating rate.....	302
Figure 9-12. Dynamic mechanical spectrum for a freshly quenched sample measured in tension at a frequency of 1 Hz and using a heating rate of $2^\circ\text{C}/\text{min}$ . .....	303
Figure 9-13. Changes in dynamic storage ( $E'$ ) and loss ( $E''$ ) moduli during physical aging at $204^\circ\text{C}$ . Testing was performed using 13 frequencies ranging from 0.01 Hz to 20 Hz although only the data for 0.01, 0.1, and 1 Hz are shown. ....	304
Figure 9-14. (a) Storage modulus response after aging at $204^\circ\text{C}$ for the indicated aging times. (b) Master curve at a reference aging time of 6 hr generated by horizontal and vertical shifting.....	305
Figure 9-15. (a) Loss modulus response after aging at $204^\circ\text{C}$ for the indicated aging times. (b) Attempt to generate master curve at a reference aging time of 6 hr by horizontal and vertical shifting.....	306
Figure 9-16. Decay function for enthalpy relaxation at indicated aging temperatures. Experimental data presented as well as nonlinear predictions using relaxation time function determined from creep compliance data. The predictions employ the $\beta$ values fit to the creep data (solid lines) as well as $\beta = 0.3$ (dotted lines) and $\beta = 0.6$ (dashed lines).....	307
Figure 9-17. Enthalpy relaxation decay functions for aging at 184, 204, 214, and $224^\circ\text{C}$ . Each solid line represents the linear stretched exponential fit. See text for additional details. ....	308
Figure 10-1. Volume relaxation data for bisphenol-A polycarbonate during aging at $21^\circ\text{C}$ . ....	316
Figure 10-2: Volume relaxation data for bisphenol-A polycarbonate during aging at $21^\circ\text{C}$ (triangles) and the converted data after subtraction of a slow linear volume relaxation process (squares). See text for an explanation of the subtraction. ....	317
Figure 10-3. Volume relaxation data for atactic polystyrene during aging at $21^\circ\text{C}$ . ....	318
Figure 11-1: Refractive index at $20^\circ\text{C}$ as a function of aging time for a-PS films aged at $74^\circ\text{C}$ (a) and data replotted in the form of the Lorentz-Lorenz relationship (b). Straight lines represent linear fits to the data. ....	331

Figure 11-2: Refractive index as a function of temperature for unaged a-PS films. The solid line represents the linear fit used to determine  $(\partial n / \partial T)_{P, t_a}$  ..... 332

Figure 11-3: Volume relaxation plot for a-PS during aging at 74°C obtained using dilatometry. Volume changes referenced to  $t_a = 0.25$  hr. The slope of the linear fit is equal to  $-\beta$ . ..... 333

# Introduction

---

Physical aging is the process which manifests itself as property changes for a material in the glassy state which occur due to slow localized relaxation toward thermodynamic equilibrium, also known as structural relaxation. The effects of physical aging can be removed by heating the material into the equilibrium liquid state and then re-quenching the material into the glassy state. Permanent chemical changes do not take place during the thermo-reversible physical aging process, and it is, therefore, very distinct from chemical aging. This nonequilibrium nature of the glassy state can result in time-dependent mechanical, barrier, and opto-electronic properties for amorphous polymers.<sup>1-5</sup> After quenching an amorphous polymer into the glassy state by, for example, the final forming step of a typical melt processing operation, the common observations associated with physical aging are a densification and a concomitant embrittlement of the material which tend to occur with respect to  $\log(\text{aging time})$ . Compared to other classes of amorphous materials, glassy organic polymers are typically used at temperatures much closer to the glass transition temperature region where physical aging effects can be quite significant. Physical aging can also affect the performance of semicrystalline polymers in addition to influencing the properties of wholly amorphous polymers. High crystal contents are not common for polymers which can crystallize, and the remaining amorphous portion of these materials is subject to physical aging when the end-use temperature is below the  $T_g$  region. These issues combine to make the physical aging of polymer materials an important process to understand and predict. Certainly the accurate prediction of application lifetimes for a glassy polymer relies, to some extent, on an understanding of the physical aging behavior for that material.

The impact of physical aging on the industrial sector has helped to fuel the research in the arena of nonequilibrium glassy behavior, and numerous physical aging studies have appeared in the scientific literature.<sup>4,5</sup> Despite all of the investigative efforts which have focused upon the problem of physical aging, a comprehensive molecular understanding of physical aging has yet to be generated. One way of probing the influence of intermolecular characteristics on nonequilibrium glassy behavior is to investigate miscible blends where interactions occur between the blend components. The study of physical aging behavior for miscible polymer blends is also pertinent because of the ever increasing use of polymer blends as a means of economically achieving desired combinations of different properties, properties which may be subject to changes due to structural relaxation in the glassy state.

The main theme of the research performed is the physical aging of miscible polymer blends. To state it succinctly, the primary goal of this study was to develop an understanding of the influences of aging temperature and composition on physical aging rates for two miscible blend systems which are quite different from each other based upon the nature of molecular interactions between the blend species. Miscible blends of atactic polystyrene (a-PS) with poly(2,6-dimethyl-1,4-phenylene oxide) (PPO) were considered. Also, this research examined miscible mixtures of poly(styrene-co-acrylonitrile) (SAN) and atactic poly(methyl methacrylate) (PMMA). Specific attractive interactions are present between the blend components in a-PS/PPO blends<sup>6,7</sup> while PMMA/SAN blends achieve miscibility via a repulsion effect,<sup>8,9</sup> as will be described later in this dissertation. A secondary objective of this research was to consider the aging behavior of numerous amorphous polymeric materials to see if a molecular-based interpretation of the kinetic glass formation process could provide any generally applicable insight into the structural relaxation process which subsequently occurs after the glassy state is formed.

The basic format of this dissertation is an assemblage of self-contained manuscripts which deal with topics related to satisfaction of the research objectives which were previously stated. Before the research results are disclosed and discussed in these manuscripts, however, critical background information is first offered. A general

review of the nonequilibrium glassy state is provided (Chapter 1), and concepts of importance when considering miscible polymer blends are also presented (Chapter 2). The final literature review, Chapter 3, represents a comprehensive review of previous studies which investigated the physical aging of miscible polymer blends. The research performed on the aging behavior and glass formation kinetics of the a-PS/PPO blends is detailed in Chapters 4 and 5. Aging data assessed for the PMMA/SAN blend system are then contrasted with the results obtained for the a-PS/PPO system in Chapter 6. An intriguing connection was noted between the structural relaxation and glass formation processes for many glassy polymers. This correlation has serious implications on the potential for predicting physical aging behavior, and it is, therefore, given much attention in Chapters 7 and 8 from both experimental and modeling standpoints. Although not specifically relevant to the two main research objectives, additional physical aging studies were performed and the results are also included in this dissertation. An extensive investigation of nonequilibrium glassy behavior for a high temperature amorphous polyimide material is discussed in Chapter 9. A long-term volume relaxation study with critical implications was performed on both bisphenol-A polycarbonate and a-PS during aging near room temperature (Chapter 10). Chapter 11 reveals that refractive index was effectively utilized as a novel probe for quantifying the rate of volume relaxation for a-PS which occurred during the physical aging process. Finally, a brief section which summarizes this entire research contribution and offers some suggestions for future research is used to conclude this dissertation.

## References

- <sup>1</sup> L. C. E. Struik, *Physical Aging in Amorphous Polymers and Other Materials*, Elsevier, New York, 1978.
- <sup>2</sup> J. M. O'Reilly, *CRC Critical Rev. in Solid State and Matl. Sci.* **13**, 259 (1987).
- <sup>3</sup> M. R. Tant and G. L. Wilkes, *Polym. Eng. Sci.* **21**, 874 (1981).
- <sup>4</sup> J. M. Hutchinson, *Prog. Polym. Sci.* **20**, 703 (1995).

- <sup>5</sup> G. B. McKenna, in *Comprehensive Polymer Science, Vol. 2, Polymer Properties* (eds. C. Booth and C. Price), Pergamon, Oxford, UK, 1989, pp 311-362 (Chapter 10).
- <sup>6</sup> H. Feng, Z. Feng, H. Ruan, and L. Shen, *Macromolecules* **25**, 5981 (1992).
- <sup>7</sup> S. H. Goh, S. Y. Lee, X. Zhou, and K. L. Tan, *Macromolecules* **32**, 942 (1999).
- <sup>8</sup> M. Suess, J. Kressler, and H. W. Kammer, *Polymer*, **28**, 957 (1987).
- <sup>9</sup> N. Nishimoto, H. Keskkula, and D. R. Paul, *Polymer*, **30**, 1279 (1989).

# Chapter 1

## Review -- The Glass Transition and the Nonequilibrium Glassy State

---

---

This portion of the review is focused on establishing a general understanding of the nature of the glass transition and the glassy state. In particular, the question of whether the glass transition temperature is thermodynamic or kinetic will be addressed. Relaxation characteristics of glass-forming materials will also be described including mention of models which are utilized in an attempt to capture these relaxation features. The illustrative examples to be utilized will largely involve data for glassy polymers, although the forthcoming discussion applies more generally to all classes of glass-forming materials.

### 1.1 Glass Transition: Kinetic vs. Thermodynamic

During cooling at constant pressure, the glass transition temperature ( $T_g$ ) region marks the change in behavior from liquid-like to glassy for all materials which can be cooled without inducing crystallization. For high molecular weight amorphous polymers, the region just above the glass transition region is more appropriately described as rubbery due to the presence of entanglements which serve as physical crosslinks. For such amorphous polymers, modulus values are of the magnitude  $10^9$  Pa in the glassy state where molecular motion is highly localized, or segmental, and in the rubbery region, where long-range backbone motion between entanglements is possible, the modulus is typically on the order of  $10^6$  Pa. Because of such a difference in behavior observed for the glassy and rubbery states, the glass transition temperature<sup>‡</sup> is an extremely important application property. Even though the importance of the glass transition temperature region is widely recognized, the fundamental understanding of its origin is still lacking. It is not known

---

<sup>‡</sup> The glass transition temperature region does not display a sharp transition but often has a breadth of 10 to 30°C. Additionally, the glass transition temperature is rate-dependent as will be discussed later. Therefore, the singular term “glass transition temperature” is used solely out of convenience.

whether the glass transition is a purely kinetic phenomenon or whether it is a kinetic reflection of a true thermodynamic transition, an issue which will be more fully explored in the following discussion.

The glass transition temperature can be experimentally observed using various techniques such as differential scanning calorimetry, dilatometry, and dynamic mechanical analysis, and in all cases, there is a rate effect involved. Upon cooling a liquid through the glass transition region, the average relaxation time and viscosity increase such that equilibrium is not maintained when the glassy state is formed. Because the cooling rate defines the amount of time per unit temperature decrease which is afforded the molecules to move in an attempt to maintain the equilibrium thermodynamic state, slower cooling rates result in lower observed glass transition temperatures as is schematically illustrated in Figure 1-1 using the thermodynamic property of volume. For reasonable apparent activation energy values in the glass transition region which range from 400 to 1200 kJ/mol,<sup>1</sup> the resulting increases in  $T_g$  range from 7 to 2°C, respectively, for a ten-fold increase in cooling rate. A discussion of the experimentally determined glass transition as a thermodynamic transition is therefore inappropriate because equilibrium can never be maintained during glass formation due to the kinetics involved. However, as will be detailed later in the discussion of the characteristics of glass-forming materials, there is an apparent kinetic temperature asymptote which can be considered to represent the glass transition temperature in the limit of infinite time allowed the molecules to reach equilibrium during cooling. This extrapolated kinetic temperature limit may indicate the presence of a true thermodynamic transition which would be observed if an infinitely slow cooling rate could be utilized. The dashed line in Figure 1-1 is intended to represent such a possible underlying thermodynamic transition.<sup>2,3</sup>

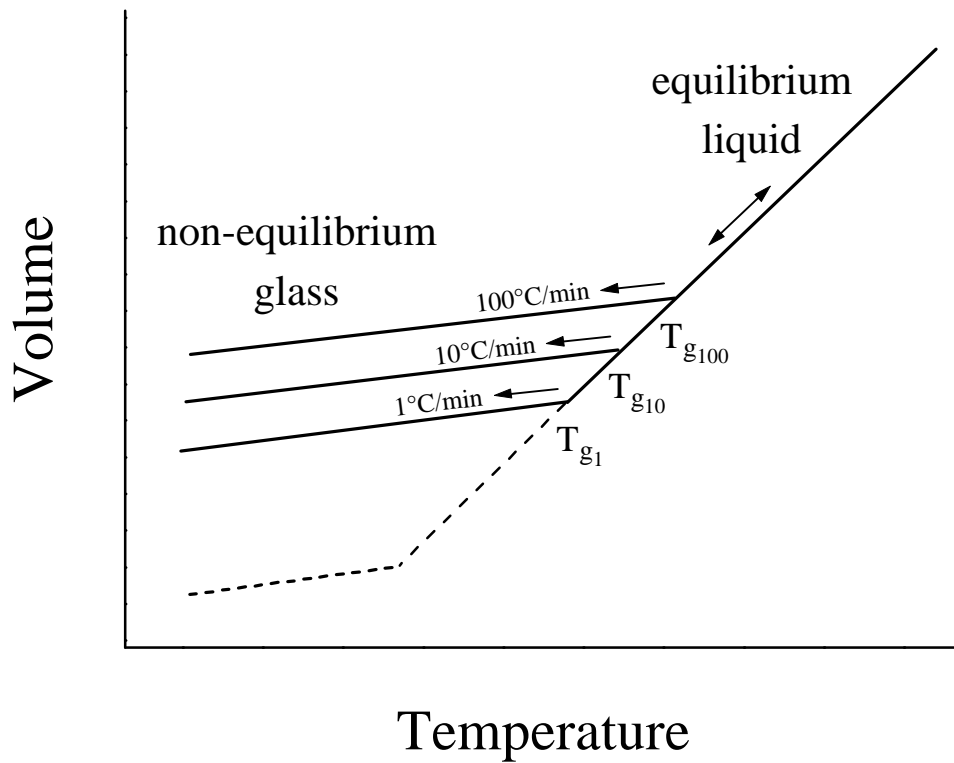


Figure 1-1: Illustration of the kinetic behavior of  $T_g$  using the generalized temperature dependence of specific volume.

If the kinetics of the glass transition temperature are disregarded,  $T_g$  has features which could classify it as a second order thermodynamic transition according to the scheme established by Ehrenfest.<sup>4</sup> A second order thermodynamic transition is defined where discontinuities occur in second derivatives of the Gibbs free energy with respect to thermodynamic variables such as pressure and temperature. Free energy expressions which are useful in the definition of a thermodynamic transition include:

$$(a) G = H - TS \quad (b) G/T = H/T - S \quad (c) G = U + PV - TS \quad \text{Eqn. 1-1}$$

where (c) is a consequence of the relationship  $H = U + PV$ . The relevant second partial derivatives of these thermodynamic relations are:<sup>3</sup>

$$\left(\frac{\partial^2 G}{\partial T^2}\right)_P = -\frac{\partial S}{\partial T} = -\frac{C_p}{T} \quad [from (a)] \quad \text{Eqn. 1-2}$$

$$\left(\frac{\partial}{\partial T}\left(\frac{\partial(G/T)}{\partial(1/T)}\right)\right)_P = \frac{\partial H}{\partial T} = C_p \quad [from (b)] \quad \text{Eqn. 1-3}$$

$$\left(\frac{\partial^2 G}{\partial P^2}\right)_T = \frac{\partial V}{\partial P} = -\kappa V \quad [from (c)] \quad \text{Eqn. 1-4}$$

$$\left(\frac{\partial}{\partial T}\left(\frac{\partial G}{\partial P}\right)_T\right)_P = \frac{\partial V}{\partial T} = \alpha V \quad [from (c)] \quad \text{Eqn. 1-5}$$

Discontinuities in the heat capacity at constant pressure ( $C_p$ ), the isobaric thermal expansion coefficient ( $\alpha$ ), and the isothermal compressibility ( $\kappa$ ) are accordingly expected for a second order transition. Jumps in these measurable quantities are observed in the glass transition temperature region probed at a constant rate,<sup>§</sup> and illustrating this is an idealized presentation of glass transition behavior in Figure 1-2.<sup>5</sup> Although the breaks in the  $C_p$ ,  $\alpha$ , and  $\kappa$  functions are consistent with the view that the glass transition temperature is a thermodynamic transition, closer inspection of the Gibbs free energy behavior upon cooling suggests otherwise. A material will undergo a thermodynamic transition in order to minimize its free energy, but the upper plot in Figure 1-2 indicates that the glassy state formed upon cooling is at a higher Gibbs free energy than the corresponding liquid state. Again, the kinetic nature of the glass transition is manifested and prevents consideration of  $T_g$  in terms of thermodynamics alone.

---

<sup>§</sup> The use of cooling rate is desirable because the initial state is the equilibrium liquid. More complex behavior in the glass transition region can be observed upon heating from the non-equilibrium glassy state.

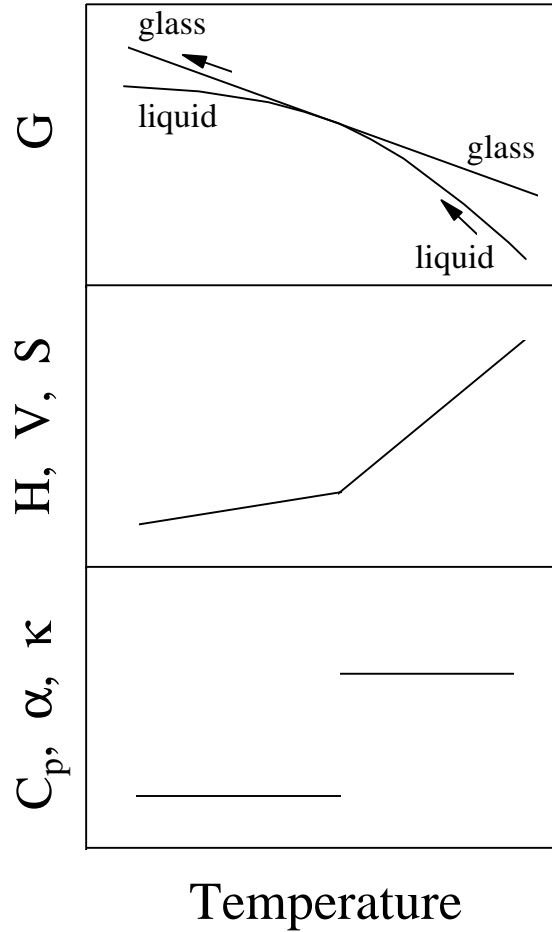


Figure 1-2: Idealized thermodynamic behavior for the glass transition. Generalized figure adapted from reference 5.

It is clear that kinetic behavior is an intrinsic part of the glass transition response, and the use of a completely thermodynamic approach to explain the experimentally observed glass transition is not adequate. A wholly kinetic interpretation of the glass transition is also inadequate, and problems exist in considering the glass as a nonequilibrium liquid. If the observed glassy state upon cooling from the equilibrium liquid is merely a frustrated liquid, then extrapolating the equilibrium liquid behavior above the glass transition region into the glassy state ought to provide an indication of the nature of the equilibrium liquid state which the system is kinetically prevented from attaining during the quench. Kauzmann<sup>6</sup> did undertake such an extrapolation exercise for various glass-forming liquids (non-polymeric), and the results have established critical insight into

the glass transition and the glassy state. In comparing the extrapolated entropy of the liquid with that of the crystalline state, Kauzmann identified an entropy crisis or catastrophe which has become known as the Kauzmann paradox. The essence of the Kauzmann paradox is depicted<sup>7</sup> in Figure 1-3 where the extrapolated entropy of the liquid into the nonequilibrium glassy state (dashed line) results in entropy values which are lower for the amorphous liquid than for the crystalline state at a given temperature, an absurd result, and a value of zero entropy is reached at a temperature well above absolute zero, a violation of the third law of thermodynamics. Developing an understanding of the glass transition invariably involves resolution of this entropy crisis.

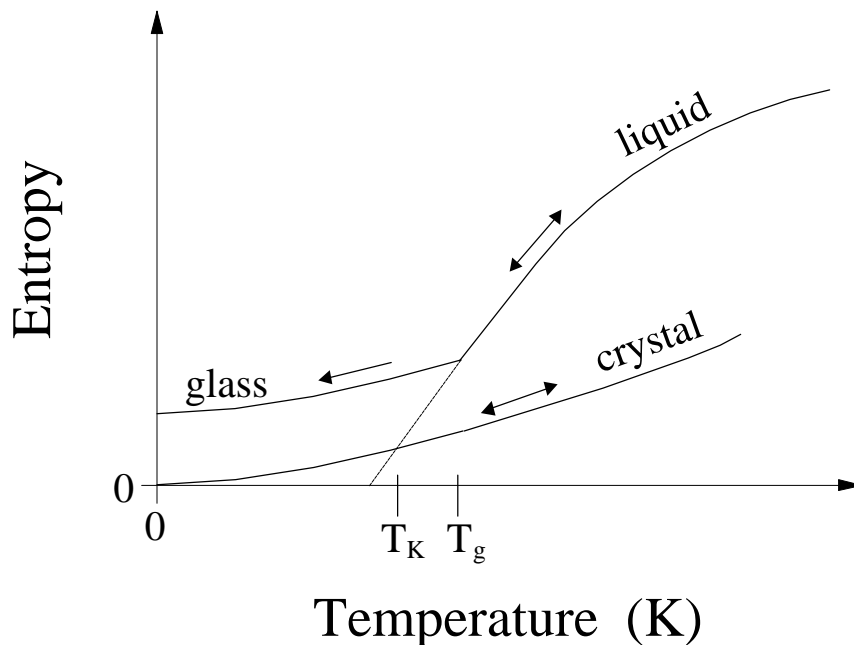


Figure 1-3. Illustration of the Kauzmann paradox (entropy crisis). Schematic adapted from reference 7.

A possible thermodynamic resolution of the Kauzmann paradox is that there exists a true underlying glass transition temperature, the lower limit of which is the Kauzmann temperature ( $T_K$ ). Gibbs and DiMarzio<sup>8</sup> have established a theoretical basis for the existence of a true thermodynamic glass transition, at least for polymeric systems which cannot crystallize. The Gibbs-DiMarzio theory makes use of a statistical mechanics lattice approach comparable to that employed in the development of the Flory-Huggins theory

for polymer solutions. Linear, monodisperse polymer chains occupy continuous paths of lattice sites due to connectivity, and the number of required sites per chain ( $x$ ) is related to the degree of polymerization or molecular weight. The possible energetics allowed the system do not include crystallization such that the approach applies to atactic,<sup>‡</sup> or otherwise non-crystallizable, linear polymers. The polymer backbone bonds are permitted two possible rotational energy states: a low energy state of  $\epsilon_1$  and a higher “flexed” state represented by  $\epsilon_2$ . Holes or empty lattice sites are also allowed and the energy associated with a hole is related to the intermolecular, or long-range intramolecular, energy ( $\alpha$ ) of the secondary bonds which must be broken between polymer segments in order for the hole to be introduced onto the lattice. The partition function for a canonical ensemble of lattice subsystems allows assessment of thermodynamic functions including the configurational contribution to entropy, and a second-order thermodynamic transition temperature,  $T_2$ , is defined in the theoretical treatment such that for all  $T \leq T_2$  the number of unique ways of configuring the system is equal to one, and the number of holes ( $n_0$ ) is constant. Above  $T_2$ , the number of lattice holes is an increasing function of temperature. For temperatures equal to or less than  $T_2$ , the configurational entropy is zero and entropy changes can only arise from altered molecular vibrations about equilibrium positions due to effects such as temperature changes. In the Gibbs-DiMarzio theory, the vanishing configurational entropy at  $T_2$  is a combined effect of the diminishing number of holes, or free volume sites, and the decline in the relative number of higher energy molecular conformations during cooling. At temperatures higher than  $T_2$  there are numerous ways the system can pack and the configurational entropy is positive. If the degeneracy of free volume sites and high energy states continued with decreasing temperature below  $T_2$ , the geometry and energy constraints would not allow the amorphous arrangement of the chains on the lattice. Therefore, the state at temperature  $T_2$  is considered to represent “the ‘ground state’ of amorphous packing”.<sup>8</sup>

The theoretical approach of Gibbs and DiMarzio allows the prediction of a purely

---

<sup>‡</sup> Atactic poly(vinyl alcohol) is an exception in that it can crystallize.

thermodynamic glass transition temperature,  $T_2$ , independent of kinetic considerations, which is a function of such molecular features as intermolecular interactions, flex energy ( $\epsilon_2 - \epsilon_1$ ) (i.e. bond rotation energetics), and molecular weight. The experimentally determined effects of molecular weight, degree of crosslinking, and other features on the kinetic glass transition of polymeric materials have been successfully represented using the Gibbs-DiMarzio theory,<sup>3,9,10</sup> suggesting that the kinetic glass transition temperature is a reflection of the theoretical true thermodynamic temperature  $T_2$ . However, the theory is lacking in that it only applies to amorphous polymeric materials while the glassy state and glass transition are generally applicable to all materials for which crystallization can be prevented, an issue recently raised by Matsuoka.<sup>11</sup>

The above discussion has indicated the unclear nature of the glass transition. No general consensus currently exists among scientists as to whether: (a) there is a true thermodynamic glass transition and there exists a fourth state of matter, an ideal glassy state; or (b) the observed glassy state simply represents a system which is kinetically impeded from attaining the desired liquid or crystalline state. The possibility given by (a) resolves Kauzmann's paradox from a thermodynamic standpoint by the existence of a true liquid-glass transition temperature which the observed kinetic glass transition temperature reflects. For case (b), the entropy crisis is averted by completely kinetic means, but a kinetic solution to a thermodynamic problem does not seem proper. A possible thermodynamic resolution of Kauzmann's paradox can be developed without the presence of an ideal glassy state and associated transition temperature by considering the equilibrium state below  $T_K$  to be the crystal instead of the liquid. This is a plausible resolution for simple liquids according to this author, but intuitively this resolution seems to be a practical impossibility for atactic polymers which cannot crystallize. One must consider, however, whether a single polymer segment "thinks" it can crystallize despite practical limitations due to connectivity and stereoregularity issues. If this is reasonable, then the theoretical equilibrium state below  $T_K$  can be the crystalline state even for atactic polymers which cannot crystallize.

## 1.2 Relaxation Characteristics of Glass-Forming Materials and Useful Descriptive Models

Although a fundamental understanding of the glass transition and the glassy state is currently lacking, comprehension of the phenomenological features of glasses is much more developed. There exist relaxation characteristics which appear to be generally applicable to most glass-forming materials, and these observed features must be accounted for in any empirical or theoretical treatment of the glassy state. Glass-formers may be considered to have four defining characteristics which are: (1) nonArrhenius scaling of relaxation times and viscosity in the glass-forming region; (2) nonequilibrium nature of the glass, also known as structural relaxation or physical aging; (3) nonlinear relaxation time response in the glassy state; and (4) nonexponential relaxations due to the presence of relaxation time distributions.<sup>12,13</sup> It is evident from the terms used to describe the behavior of glassy materials (nonArrhenius, nonequilibrium, nonlinear, and nonexponential) that the nature of a glass is more easily described in terms of what it is not rather than what it is. These four defining characteristics will be further explained in order to give a good phenomenological description of glassy materials. Throughout the discussion of these defining features will be descriptions of models which are used in an attempt to represent glassy behavior. The Adam-Gibbs cooperativity approach will be specifically highlighted because it will be employed in the proposed research.

### *1.2.1 NonArrhenius Relaxation Time Behavior*

As a material forms a glass from the liquid state, the increase of relaxation times does not follow Arrhenius behavior. Probing the alpha relaxation (glass transition) region of amorphous materials by means of dielectric spectroscopy, dynamic mechanical analysis, or stress relaxation measurements indicates instead that the activation energy increases as temperature is decreased in this region. Time-temperature superposition allows shift factors ( $a_T$  values) to be generated which indicate how the average relaxation time at one temperature compares to that at a reference state temperature, typically the inflection glass transition temperature ( $T_g$ ) measured by calorimetry.<sup>1</sup> The empirically developed Williams-Landel-Ferry equation is useful in representing the experimentally determined

relaxation time scaling behavior in the glass formation region:<sup>14</sup>

$$\log(a_T) = \log\left(\frac{\tau}{\tau_g}\right) = \frac{-C_1(T - T_g)}{C_2 + T - T_g} \quad \text{Eqn. 1-6}$$

The values for the parameters  $C_1$  and  $C_2$  depend on the choice of the reference temperature, but for the purposes of this review, the reference temperature will always be the calorimetric glass transition temperature. The nonArrhenius nature of glass formation is shown in Figure 1-4 where the WLF function is plotted using the parameters given in the caption. Although the normal applicability range of the WLF equation is from approximately 10K below to 100K above the calorimetric  $T_g$ ,<sup>3</sup> the functionality is extended in Figure 1-4 for illustrative purposes because it is the limiting behavior that provides interesting insight. The relaxation times appear to display Arrhenius behavior in the limit of high temperatures as is evident from the constant slope behavior in Figure 1-4 as  $1/T$  approaches zero. As the glass transition temperature range is approached upon cooling, the activation energy of relaxation time response increases, and the relaxation times appear to diverge due to the kinetic asymptote of  $(T_0)^{-1}$ . From the WLF expression, this kinetic temperature limit is given by  $T_0 = T_g - C_2$ . The origin of the difference between the two WLF curves in Figure 1-4 is due to variation of the  $C_2$  parameter, which has distinct values of 50K for curve A and 100K for curve B.

Angell has developed the concept of “fragility” to compare the nonArrhenius glass formation characteristics of liquids.<sup>15-17</sup> One way to contrast the difference between curves A and B in Figure 1-4 is the slope in the glass transition region, and one mathematical definition of fragility, represented by the symbol  $m$ , is given by:

$$m = \left. \frac{d \log \tau}{d(T_g / T)} \right|_{T=T_g} \quad \text{Eqn. 1-7}$$

The  $m$  parameter is essentially a normalization of the apparent activation energy ( $\Delta E_{a,g}$ ) in the glass transition region ( $m = \Delta E_{a,g} / (2.303RT_g)$ ). Recently, Angell has utilized a different quantitative representation of fragility,  $F$ :<sup>18</sup>

$$F = \frac{T_0}{T_g} = 1 - \frac{C_2}{T_g} \quad \text{Eqn. 1-8}$$

where it is assumed that the Williams-Landel-Ferry  $C_1$  parameter is a constant. Although the WLF equation is sometimes considered to have universal constants, it is clear that unique fragility characteristics require differences in the  $C_2$  parameter. The kinetic temperature asymptote,  $T_0$ , represents where the equilibrium relaxation times appear to diverge toward infinity. How close this asymptote is to the glass transition temperature dictates the severity of the nonArrhenius behavior during glass formation. If the kinetic limit represents a true thermodynamic glass transition ( $T_K$  or  $T_2$ ), then fragility given by the second definition may be considered a measure of how close the kinetic glass transition approaches the true thermodynamic glass transition temperature. Glasses with a low and high degree of fragility are classified, respectively, as strong and fragile glasses. In principle, the value of fragility can vary depending on what rate is used to define the reference  $T_g$ . As mentioned earlier, typical  $T_g$  increases are on the order of 2 to 7°C for a ten-fold cooling rate increase. The associated influence on the fragility parameter,  $F$ , is small because typical values of  $C_2$  (on the order of 50°C) are large relative to such variations in the kinetic  $T_g$  value used for reference purposes.

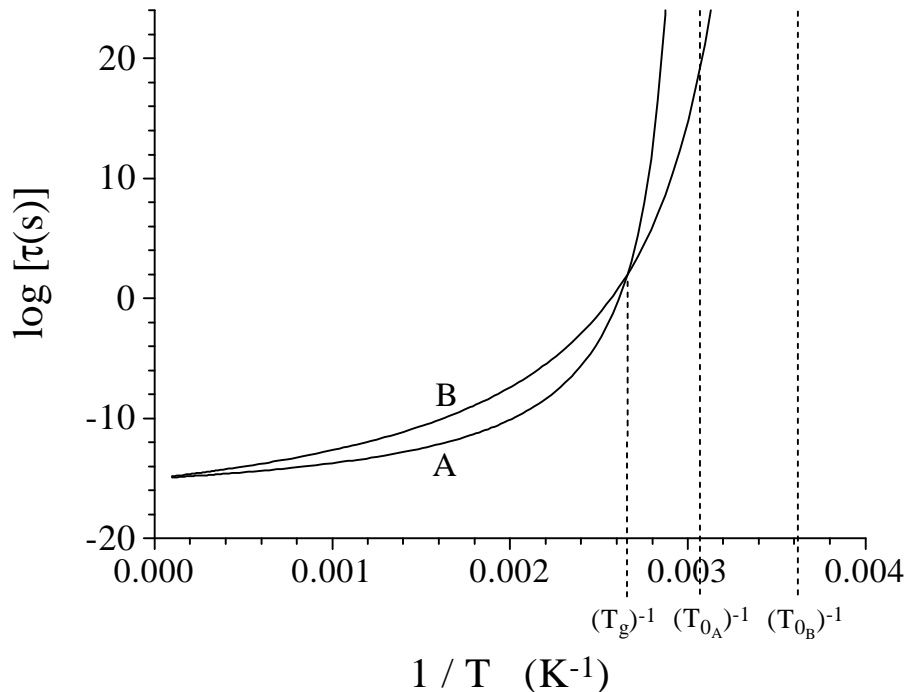


Figure 1-4: Non-Arrhenius relaxation time behavior. Curves generated using the WLF equation with the parameters  $T_g = 376K$ ,  $\tau_g = 100$  s,  $C_1=17$ , and values for  $C_2$  equal to 50K for curve A and equal to 100K for curve B.

The empirically derived WLF equation, which has exhibited success in capturing the nonArrhenius relaxation time and viscosity behavior in the glass-forming region, can be related to more fundamental free volume arguments. The basis for free volume considerations is illustrated in Figure 1-5 where the occupied and total specific volumes are schematically illustrated for an amorphous material in the liquid and glassy regions. The occupied volume represents the physical volume occupied by the molecules plus the extra volume required for vibrational motions, and it is the temperature dependence of these vibrational motions which results in the occupied volume showing an increasing function with temperature even though the actual volume of the molecules remains invariant. The free volume can be considered to be the difference between the total observed volume and the occupied volume, and the amount of free volume is expected to influence the ease of diffusive molecular motions which in turn affects relaxation times and viscosity. As the glass transition region is approached during cooling, the free volume decreases and relaxation times increase. The connection between molecular mobility and free volume was explicitly made by Doolittle,<sup>19,20</sup> and this link is represented by the following equation for viscosity ( $\eta$ ):

$$\eta = A \exp\left(\frac{b}{f}\right) \quad \text{Eqn. 1-9}$$

where  $f$  is the fractional free volume ( $f = \text{free volume}/\text{total volume}$ ) and the parameters  $A$  and  $b$  are constants. With certain assumptions, the Doolittle equation can be derived from the Cohen-Turnbull free volume theory.<sup>3,21,22</sup> Basic free volume approaches assume that the free volume fraction ( $f$ ) at a temperature above  $T_g$  can be related to the free volume fraction at  $T_g$  ( $f_g$ ) by:

$$f = f_g + \alpha_f (T - T_g) \quad \text{Eqn. 1-10}$$

The parameter  $\alpha_f$  is the free volume expansion coefficient, sometimes approximated as the jump in thermal expansion coefficient at the glass transition temperature ( $\Delta\alpha = \alpha_{\text{liquid}} - \alpha_{\text{glass}}$ ). Those who view the glass transition temperature to be an iso-free volume state typically fix a value for  $f_g$  which is approximately 0.025, and this approach to understanding the glass transition temperature assumes that the fractional free volume at

$T_g$  is largely invariable regardless of the glass-forming material being considered. The use of Eqn. 1-9 and Eqn. 1-10 in combination with the shift factor defined in terms of viscosity,  $\log a_T = \log (\eta / \eta_g)$ , can result in the derivation of the WLF equation with the following expressions for the WLF parameters:

$$C_1 = \frac{b}{2.303f_g} \quad \text{and} \quad C_2 = \frac{f_g}{\alpha_f} \quad \text{Eqn. 1-11}$$

This indicates that the use of free volume arguments results in an expression similar in form to the WLF equation. Therefore, there is a fundamental basis from a free volume standpoint for the success of the empirically derived WLF equation in describing the nonArrhenius behavior of glass formers.<sup>1,3</sup>

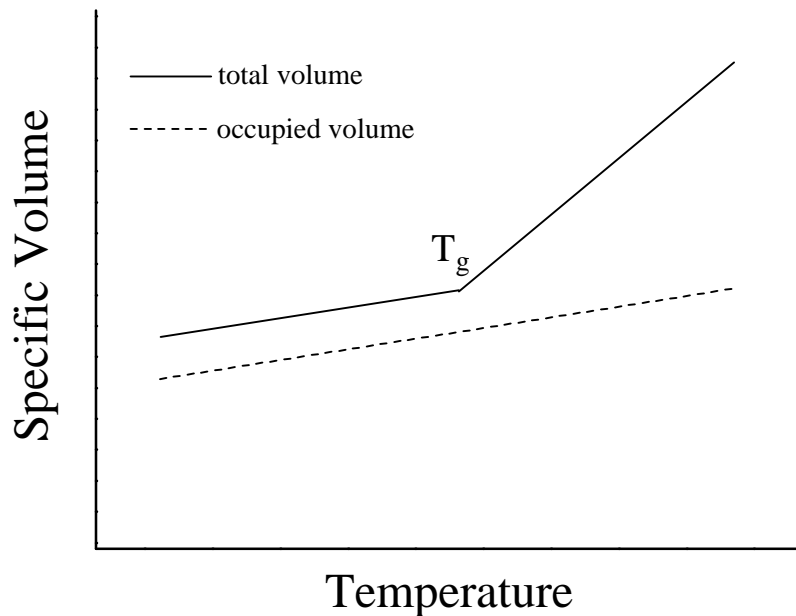


Figure 1-5: General illustration of occupied and total volume for an amorphous material. The difference between the two functions is the free volume.

A configurational entropy approach can also result in the WLF equation as will now be illustrated by an examination of the Adam-Gibbs cooperativity approach. Adam and Gibbs<sup>23</sup> combined the thermodynamics embodied by the Gibbs-DiMarzio equation with kinetic aspects of glass-forming behavior. Because configurational entropy ( $S_c$ )

diminishes toward zero at  $T_2$  and equilibrium relaxation times appear to diverge toward infinite values during cooling, Adam and Gibbs postulated that  $\log(\tau)$  was proportional to  $1/S_c$ . Hodge has provided excellent reviews<sup>13,24</sup> which present the development of the Adam-Gibbs relaxation time expression, and the reader is therefore directed to these references for additional details not provided here. The assumption that the difference between the liquid and glass heat capacities is inversely proportional to temperature allows an expression for the configurational entropy to be developed which leads to the following form for the Adam-Gibbs equation:

$$\tau = A \exp\left(\frac{\Delta\mu}{RT[1-(T_2/T)]}\right) \quad \text{Eqn. 1-12}$$

In this equation, “A” represents a constant prefactor and  $T_2$  is the Gibbs-DiMarzio transition temperature. The parameter  $\Delta\mu$  is used here instead of the B parameter employed by Hodge because the above expression should yield a primitive activation energy ( $\Delta\mu$ ) at high temperatures as will be described. As temperature approaches  $T_2$  during cooling, the equilibrium relaxation time given by the above expression diverges toward infinity, which is consistent with experimental inferences. The equilibrium Adam-Gibbs equation given above is equivalent in form to the empirical Vogel-Fulcher-Tammann-Hesse equation.<sup>25-27</sup>

An integral part of the Adam-Gibbs approach is the idea of cooperativity, wherein the actual configurational entropy at a given temperature is lower than expected for independent relaxation of the primitive segments comprising the glass-forming liquid. In the limit of high temperatures, the extrapolated activation energy is given by  $\Delta\mu$  which may be thought to represent the energy barrier for independent relaxation of the segments, an energy barrier which typically has values consistent with activation energies for intramolecular bond rotation.<sup>13,29</sup> As temperature is decreased toward the glass transition region, the observed activation energy is greater than  $\Delta\mu$  and increases during cooling as depicted in Figure 1-4. Based upon the Adam-Gibbs cooperativity approach, the observed activation energy is greater than the primitive activation energy by a factor  $z$ , the number of cooperative segments which must relax simultaneously for relaxation to occur. This means that  $\Delta E = z \Delta\mu$ , and after comparing Eqn. 1-12 with a generalized Arrhenius

expression ( $\tau \propto \exp(\Delta E/RT)$ ), it may be tempting to assign an expression for  $z$  which is equal to  $[1 - (T_2/T)]^{-1}$ . However, when one defines the activation energy ( $\Delta E$ ) in the proper manner by the derivative of  $\ln(\tau)$  with respect to  $1/T$  then it is apparent that:

$$\frac{d \ln \tau}{d(1/T)} = \frac{\Delta E}{R} = \frac{\Delta \mu}{R[1 - (T_2/T)]^2} \quad \text{Eqn. 1-13}$$

$$\Delta E = z \Delta \mu \quad \Rightarrow \quad z = [1 - (T_2/T)]^{-2} \quad \text{Eqn. 1-14}$$

Therefore, the equilibrium value of  $z$  should be given by the above expression according to this author and should not be set equal to  $[1 - (T_2/T)]^{-1}$ .

The equilibrium Adam-Gibbs expression can be shown to be equivalent to the Williams-Landel-Ferry equation, suggesting a connection between the free volume and configurational entropy approaches above the  $T_g$  region. The equivalencies between the parameters from Eqn. 1-12 and Eqn. 1-6 are as follows:

$$T_2 = T_g - C_2 \quad \text{Eqn. 1-15}$$

$$\Delta \mu = 2.303 R C_1 C_2 \quad \text{Eqn. 1-16}$$

$$\ln(A) = \ln(\tau_g) - 2.303 C_1 \quad \text{Eqn. 1-17}$$

From the Williams-Landel-Ferry expression, the activation energy in the high temperature limit (limit  $T \rightarrow \infty$ ) is  $\Delta \mu = 2.303 R C_1 C_2$  and the apparent activation energy at  $T_g$  is given by  $\Delta E_{a,g} = 2.303 R C_1 (T_g)^2 / C_2$ . Therefore, the most probable cooperative domain size at  $T_g$  ( $z_g$ ) can be given by  $z_g = \Delta E_{a,g} / \Delta \mu = (T_g/C_2)^2$  based upon the cooperativity concept, and this  $z_g$  parameter is a useful descriptor of glass-forming behavior according to this author.

Matsuoka and Quan<sup>28-30</sup> have developed a relaxation expression for segmental cooperativity similar in form to the general Adam-Gibbs expression. Their equation was developed by compressing the temperature scale for the configurational contribution to entropy to account for it going to zero at a temperature  $T_0$  as opposed to a temperature of absolute zero. The theory relies on the existence of this kinetic temperature limit ( $T_0$ ), and it is assumed that segmental cooperativity compresses the temperature scale without otherwise changing the shape of the temperature dependence. Of great utility in the presentation of cooperativity given by Matsuoka and Quan is their molecular depiction of

the process which greatly aids in understanding the Adam-Gibbs approach. Figure 1-6 represents their illustration of primitive relaxing segments or “conformers” which must relax together in a domain due to packing limitations and other intermolecular features. An approach was also established by these authors for determining the number of relaxing “beads” or conformers per polymer repeat unit with the end result being an excellent correlation between the glass transition temperature and the segmental molecular weight per bond for numerous polymers.

DiMarzio and Yang<sup>31</sup> attempted to rigorously derive the Adam-Gibbs approach using statistical mechanics and thus justify its success from basic principles. Instead, their derivation resulted in the prediction that viscosity displays an Arrhenius dependence on temperature in the equilibrium glassy state where  $S_c = 0$ . The implication of this recent theoretical work is that equilibrium values of viscosity and relaxation time do not diverge to infinity at  $T_2$ . This raises questions concerning the validity of the Adam-Gibbs and Williams-Landel-Ferry equations, equations which have exhibited much success in describing the experimentally observed nonArrhenius nature of glass formation. This controversy highlights the fact that a fundamental and comprehensive picture of the glass transition and glassy state has yet to be developed.

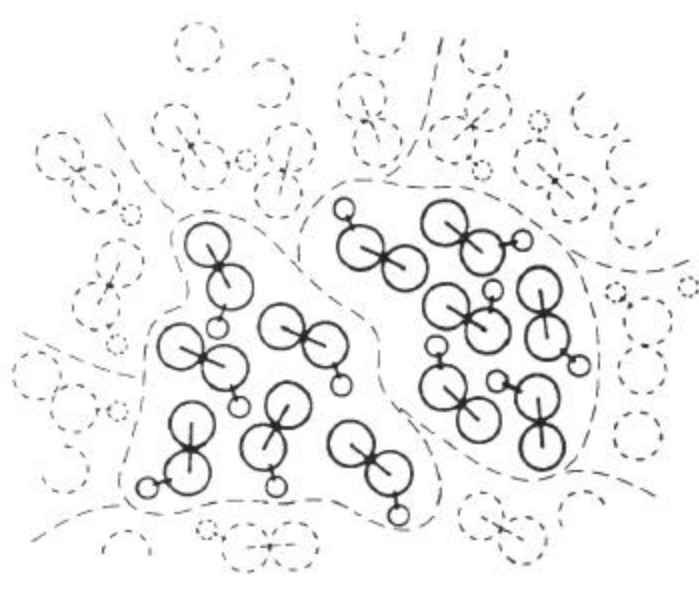


Figure 1-6: Matsuoka’s depiction of cooperative relaxation domains with  $z = 6$  (from reference 29).

### *1.2.2 NonEquilibrium Nature of the Glass (Physical Aging)*

The glass is inherently a nonequilibrium thermodynamic state, a direct consequence of the rapidly increasing relaxation times during cooling from the equilibrium liquid state. During cooling, thermal contraction occurs as the free volume surrounding the molecules decreases and the relative mobility of the molecular segments becomes increasingly inhibited, in a manner which could be considered a molecular log jam, as a nonequilibrium glassy state is formed. The formation of the nonequilibrium glass occurs when the relaxation times become large relative to the time-frame allowed for molecular rearrangements, a time-frame dictated by the quench rate. Departure from equilibrium constitutes a driving force for relaxation in the glassy state and, consequently, localized molecular motion in the glassy state allows decreases in the volume, enthalpy, and entropy to occur. The temporal changes in the thermodynamic variables of the glass are often termed structural relaxation and, considered together, result in a decrease in the free energy of the system. Considered independently, however, not all of the changes lower the free energy within the glassy state; a reduction in entropy during structural relaxation contributes to an increase in free energy although the total free energy decreases, not unlike the crystallization process. The changes that occur in the thermodynamic state, in turn, result in changes in numerous characteristics including mechanical, optical, and barrier properties. The time-dependent nature of the thermodynamic variables in the glassy state (structural relaxation) as well as interrelated changes in bulk application properties are collectively referred to as physical aging. Because physical aging is a consequence of the nonequilibrium glassy state, it is thermoreversible unlike chemical or thermo-oxidative aging, and its effects can be removed by heating into the equilibrium liquid state and then re-quenching into the glassy state.<sup>32-35</sup>

A glass-forming material departs from equilibrium at the kinetic glass transition temperature ( $T_g$ ) region during cooling, and, upon annealing at an aging temperature ( $T_a$ ), densification toward equilibrium occurs with time. This densification is indicated in Figure 1-7, and in a manner comparable to this volume relaxation, the enthalpy and entropy of the material decrease toward equilibrium. The time-dependent nature of the thermodynamic state for a glassy material can be assessed by directly measuring volume

changes via dilatometry.<sup>36,37</sup> When far from the equilibrium state, relaxation of volume in the glassy state is often found to display a linear dependence on  $\log(\text{time})$ , a consequence of the nonlinear behavior to be discussed later. This dependence is illustrated in Figure 1-8 for the volume relaxation of atactic polystyrene at various temperatures in the glassy state.<sup>38</sup> With the exception of very short times and when the volume closely approaches the equilibrium volume ( $V_\infty$ ) at long times, isothermal volume relaxation at constant pressure can be described by the following rate expression:<sup>32,36</sup>

$$\beta_V = -\frac{1}{V} \frac{dV}{d \log t_a} \quad \text{Eqn. 1-18}$$

Changes in volume during isothermal aging in the glassy state can be followed using dilatometric techniques, and the rate of relaxation can be assessed using the above expression.

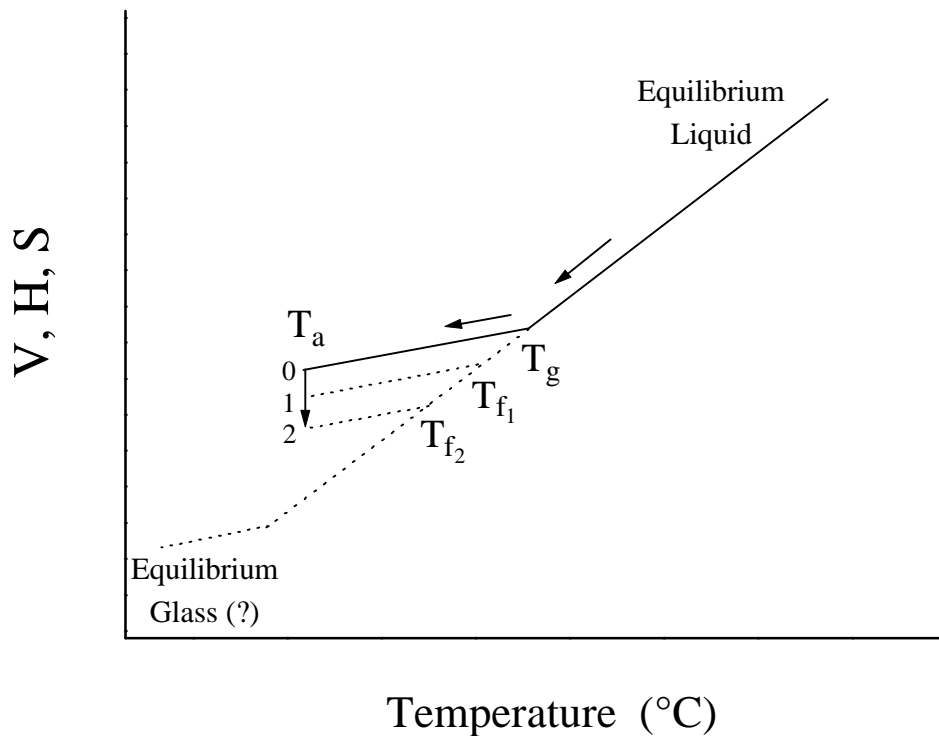


Figure 1-7: Changes in the thermodynamic state due to the physical aging process.

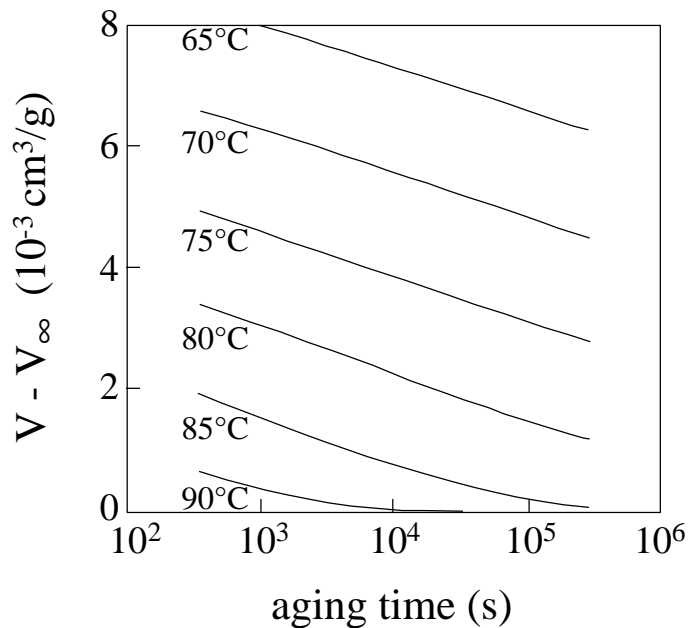


Figure 1-8: Volume relaxation of polystyrene (replotted from reference 38)

Enthalpy also decreases upon annealing in the glassy state following a quench from above  $T_g$ , but these changes cannot be directly measured but rather must be inferred from differential scanning calorimetry (DSC) techniques. After aging within the glassy state, a DSC heating scan reveals an endothermic peak in the glass transition region, and this represents the recovery of the enthalpy which was lost during aging.<sup>39,40</sup> After performing the heating scan which exhibits this enthalpy recovery, the material is quenched from above  $T_g$  in the DSC and immediately reheated to give an unaged reference scan. A generalized comparison of aged and unaged DSC scans is made in Figure 1-9. Because heat capacity represents the temperature derivative of enthalpy, the difference, or thermal hysteresis, observed between the aged and freshly quenched DSC scans is related to the amount of enthalpy decrease, or relaxation, which took place during the aging process. The determination of the recovered enthalpy from the thermal hysteresis observed between the two DSC scans is also illustrated in Figure 1-9. When aging is performed relatively close to  $T_g$ , the aged sample is usually quenched to a lower temperature prior to heating in the DSC so that the thermal inertia associated with initiating the temperature ramp does not occur near, or within, the region where the heat flow responses exhibit differences for

the aged and freshly quenched thermal histories. As the amount of aging time is increased, the recovered enthalpy increases and the location of the endothermic peak moves to higher temperatures until equilibrium is reached. When far away from equilibrium, the enthalpy relaxation/recovery often displays a linear dependence on  $\log(\text{aging time})$  like volume relaxation, and an enthalpy relaxation rate can be defined:<sup>35</sup>

$$\beta_H = \frac{d(\Delta H)}{d \log t_a} \quad \text{Eqn. 1-19}$$

The changing thermodynamic state in the glass can accordingly be assessed for both variables of enthalpy and volume.

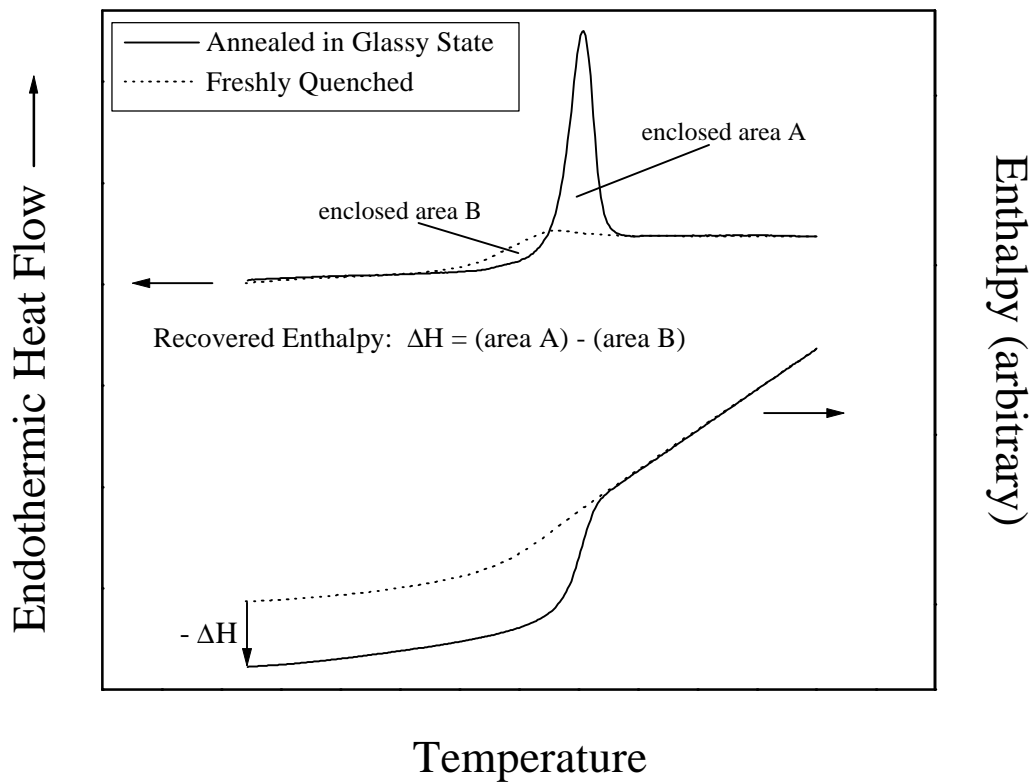


Figure 1-9: Determination of enthalpy relaxation using differential scanning calorimetry. When the heat flow is given in units of W/g, then the heating rate must be used to convert the  $\Delta H$  given above to the correct units of J/g.

Mechanical properties are observed to undergo time-dependent changes in the glassy state as a result of the changing thermodynamic state. The densification and reduction in configurational entropy which occur during physical aging cause a reduction in the molecular mobility which in turn results in changes in the mechanical response of a glassy material. These mechanical property changes can often be substantial as demonstrated by Petrie and coworkers<sup>41</sup> for an amorphous poly(ethylene terephthalate) (PET) material. The tensile stress-strain characteristics at room temperature are contrasted in Figure 1-10 for a PET sample aged in the glassy state and for a sample which was freshly quenched. The physical aging process resulted in a slight increase in modulus, and the tensile strength for the aged sample was significantly heightened in comparison to the yield stress for the freshly quenched sample. Physical aging also resulted in a substantial amount of embrittlement for PET, as is evident from the elongation to break and toughness (area under stress-strain curve) which were much lower for the aged sample relative to the freshly quenched sample.

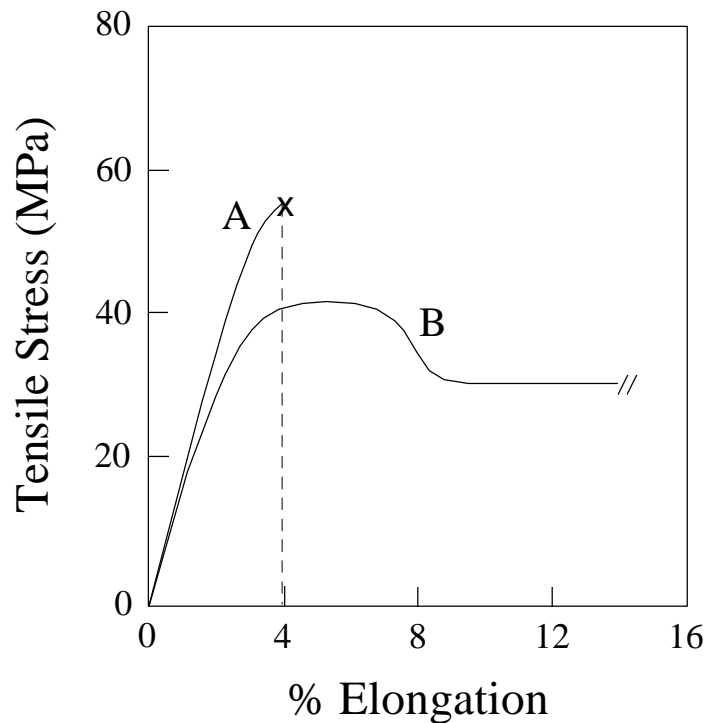


Figure 1-10: Tensile stress-strain behavior (room temperature, 10%/min strain rate) for amorphous poly(ethylene terephthalate) annealed in the glassy state for 90 minutes at 51°C (curve A) and freshly quenched from above  $T_g$  (curve B) (replotted from 41).

The rate of change in the mechanical response of a glassy material due to the physical aging process can be followed through the use of creep compliance measurements using a methodology established by Struik.<sup>32</sup> The approach utilizes creep (step-stress) testing which is performed within the small strain limit, and because the stresses used are low, the amount of total strain is also kept small (< 0.1%). This enables a sample to be intermittently tested for its mechanical response during isothermal physical aging without the testing procedure significantly affecting the state of the sample after the stress is removed and the sample is allowed to recover. This testing procedure is illustrated in Figure 1-11 where the stress input and typical strain output responses are given. Creep compliance is defined as the time-dependent strain output divided by the applied step in stress ( $D(t) = \epsilon(t) / \Delta\sigma$ ). If a small amount of unrecoverable flow occurs then subsequent strain values are determined relative to this new reference length as illustrated from the extrapolated dashed lines in Figure 1-11. The total time during which the stress is applied is one-tenth of the total cumulative aging time, such that any aging which occurs during the creep test can be neglected. The time-dependent creep compliance can accordingly be determined as a function of aging time, and typical data given by Struik<sup>32</sup> for poly(vinyl chloride) are indicated in Figure 1-12. Assuming that relaxation time distributions shift to longer times during physical aging but do not change shape (thermorheological simplicity), the compliance curves in Figure 1-12 can be horizontally shifted to form a master curve. The rate of logarithmic change of the horizontal shift factor ( $a_t$ ) with respect to  $\log(\text{aging time})$  can be used to define an aging rate,  $\mu$ :<sup>32</sup>

$$\mu = \frac{d \log a_t}{d \log t_a} \quad \text{Eqn. 1-20}$$

The shift factor represents a comparison between a relaxation time at one aging time with the relaxation time at the reference aging time:  $a_t = \tau/\tau_{\text{ref}}$ . The formation of such a master curve also requires a small amount of vertical shifting for decent superposition, but the amount of this shifting is quite small in comparison to the degree of horizontal shifting.<sup>32,42,43</sup> This superposition principle can also be applied to changes in stress relaxation and dynamic mechanical data due to isothermal physical aging.

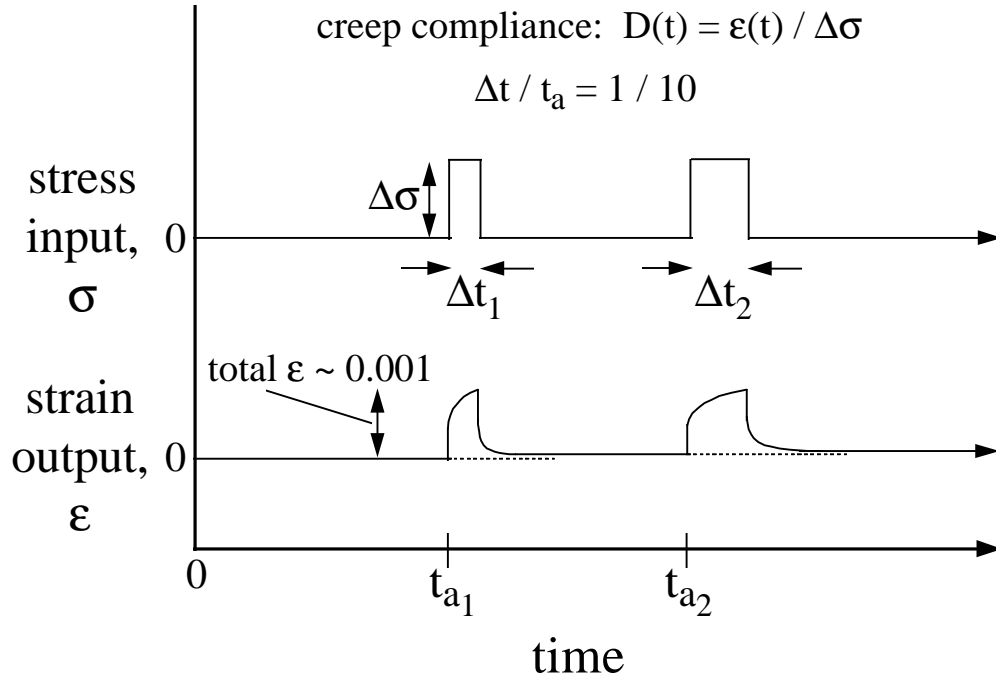


Figure 1-11: Struik's generalized creep compliance testing schedule utilized for isothermal aging studies.

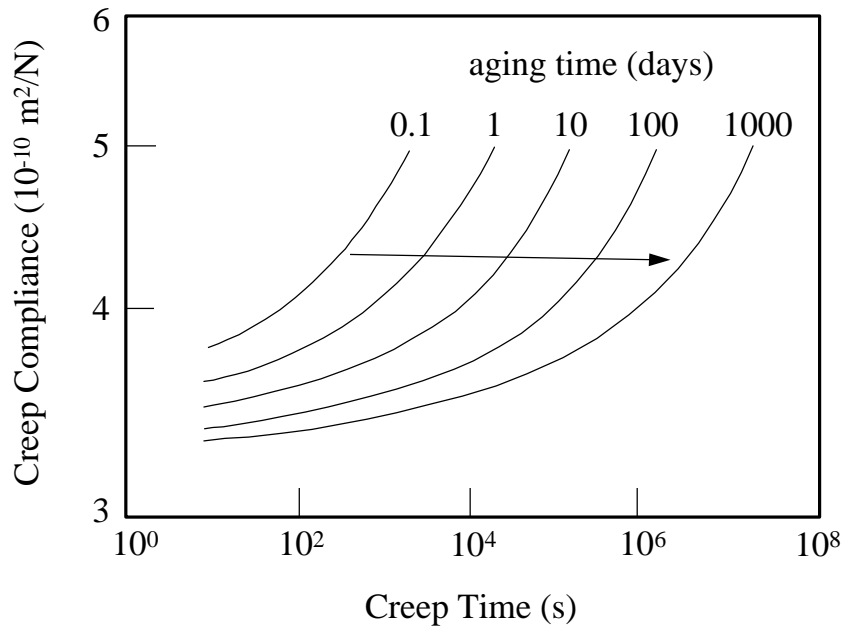


Figure 1-12: Influence of physical aging on the time-dependent creep compliance response of rigid poly(vinyl chloride) (replotted from reference 32)

To comprehensively review the literature pertaining to physical aging would be a difficult task and would not really be appropriate for the purposes of this research proposal. However, it is worthwhile to briefly discuss some controversial aspects of research on the nonequilibrium glassy state. One area of confusion in the literature is the connection between physical aging rates measured by following changes in different properties and whether all properties reach equilibrium at the same time. Simon and coworkers<sup>44</sup> have recently provided a concise review concerning research pertinent to these unresolved issues (Table 1-I), and their own work on poly(ether imide) (PEI) indicated that volume, enthalpy, and creep compliance response reach equilibrium at the same time, although the rates of approach differ. However, the different conclusions reached by the researchers whose work is summarized in Table 1-I clearly indicate the need for further research before any generalizations can be made. Close connections between changes in the thermodynamic variables of volume and enthalpy during glassy state relaxations might be expected,<sup>45</sup> but the way in which the microstructural changes transfer to changes in macroscopic mechanical properties is necessarily complex and may be material specific. Volume relaxation rates<sup>36</sup> for various glassy polymers can be compared with corresponding mechanical aging rates determined from creep compliance measurements<sup>32</sup> by examining the data given in Figure 1-13 and Figure 1-14. These data indicate that the sensitivity (S) of mechanical properties to the changing state of packing ( $S=2.303(\mu / \beta_v)$ )<sup>32</sup> not only varies for different materials but also varies with aging temperature for a given glassy polymer. Although the relationship can be complex, it seems intuitive that the densification associated with structural relaxation affects mobility and, therefore, influences mechanical response, but what is the opposite influence of stress/strain fields on the glassy structure? Connections between mechanical input and structure (e.g. volume) in the glassy state are implied from the de-aging or rejuvenation phenomenon wherein stress and deformation are thought to increase free volume, thereby removing previous volume relaxation.<sup>32,46-48</sup> However, simultaneous mechanical and volume measurements in the nonequilibrium state have been made by McKenna and coworkers which indicate a decoupling between mechanical and structural responses.<sup>49-51</sup>

Table 1-I: Comparison of Aging Effects Measured by Different Methods\*

Material	Experiments	Findings
DGEBA/PPO Epoxy	volume recovery and stress relax. changes (up- and down-jumps)	time to reach equilibrium shorter in up-jump and longer in down-jump for volume relative to mechanical property <sup>52, 53</sup>
DGEBA/DDS Epoxy	volume recovery (up- and down-jumps) and creep (equilibrium)	shift factors are the same for data reduction <sup>54</sup>
PS	volume and enthalpy recovery (up- and down-jumps)	approach rates to equilibrium for volume and enthalpy are related by a constant <sup>45</sup>
PS	volume and enthalpy recovery (double temperature jumps)	enthalpy reaches maximum faster than volume <sup>55</sup>
PS	Enthalpy recovery and room temp. creep changes (down-jumps)	enthalpy reaches equilibrium faster than mechanical property <sup>56</sup>
PS	volume and enthalpy recovery (following cooling under pressure)	volume reaches specified percent recovery faster than enthalpy <sup>57</sup>
PMMA	volume and enthalpy recovery (following cooling under pressure)	volume reaches specified percent recovery slower than enthalpy <sup>57</sup>
PMMA	volume recovery, enthalpy recovery, and dynamic mechanical property changes (down-jumps)	different decay functions with enthalpy showing fastest relaxation, followed by volume, and then mechanical property <sup>58</sup>
PMMA	enthalpy recovery and stress relaxation changes (down-jumps)	model parameters for enthalpy relaxation comparable to experimental stress relaxation times <sup>59</sup>
PVAc	volume and enthalpy recovery (down-jumps) as well as dynamic mechanical and dielectric analyses (equilibrium)	different equilibrium relaxation times from data modeling: smallest for enthalpy and largest for mechanical property <sup>60</sup>
PVAc	volume and enthalpy recovery (down-jumps)	effective retardation time smaller for volume compared enthalpy <sup>61</sup>
PEI	volume recovery, enthalpy recovery, and creep changes (down-jumps)	time to reach equilibrium same for all three although initial approach faster for V compared to H and creep <sup>44,62</sup>

\* Table adapted from Simon et al.<sup>44</sup> Consult this reference for further details

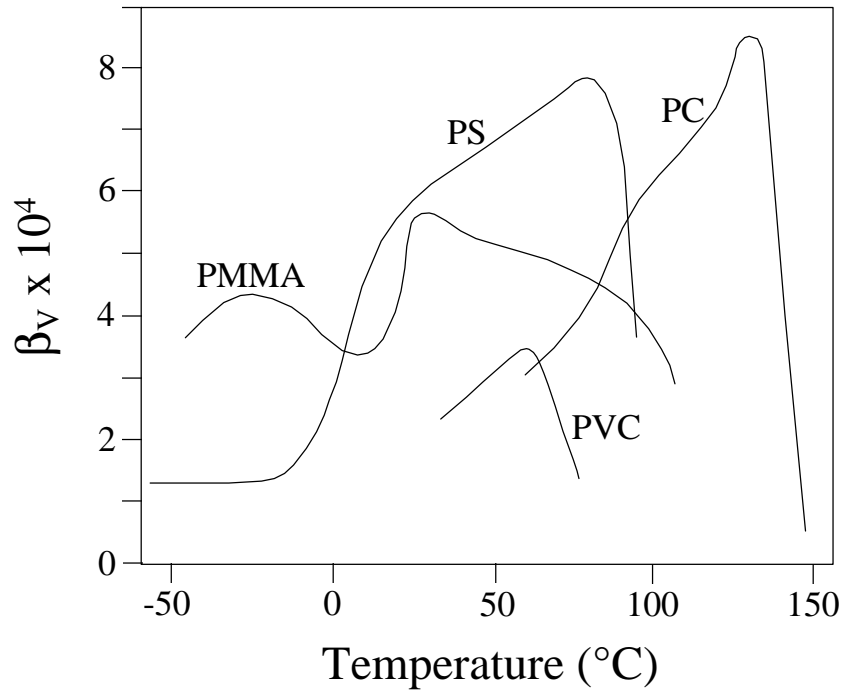


Figure 1-13. Aging temperature dependence of volume relaxation rates for various glassy polymers (replotted from reference 36)

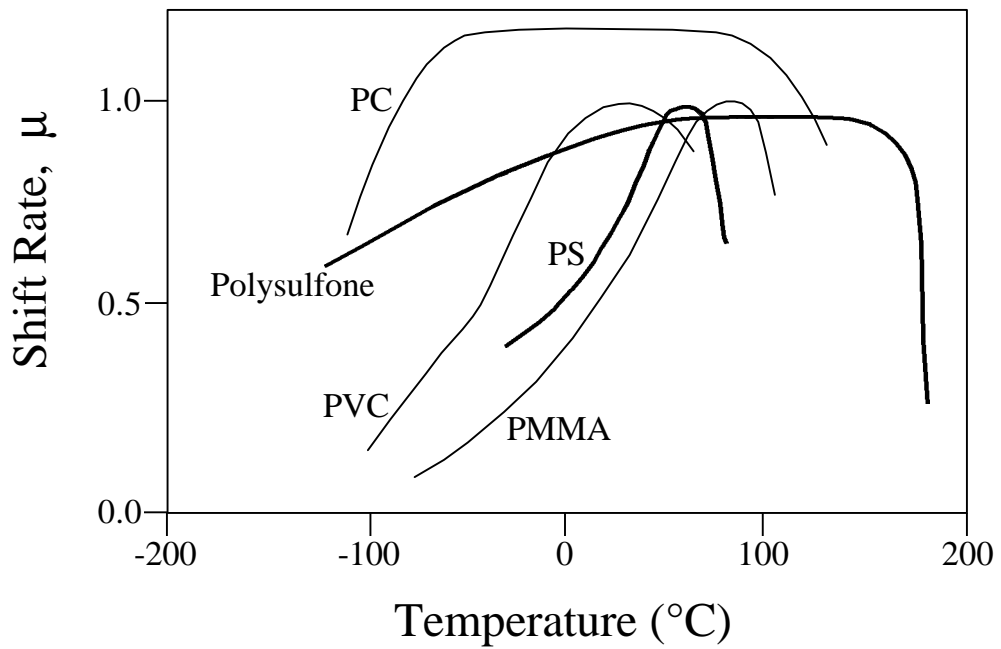


Figure 1-14. Creep shift rate as a function of aging temperature for various glassy polymers (replotted from reference 32).

Another area which has yet to be conclusively resolved in the literature is the temperature range over which physical aging occurs and the related influence of secondary relaxations on the physical aging process and vice versa.<sup>32,42,63-75</sup> Struik originally noted that the temperature dependence of volume relaxation rates appeared to mimic the shape of the dynamic mechanical  $\tan(\delta)$  response with temperature, including local increases in aging rates with respect to temperature in the vicinity of secondary relaxations.<sup>67</sup> It is well known that poly(methyl methacrylate) (PMMA) has an uncharacteristically strong secondary relaxation whose intensity observed from dynamic mechanical loss is actually greater than that associated with the main chain relaxation ( $\alpha$ -relaxation).<sup>76</sup> This broad transition, which is centered in the vicinity of 0°C when probed at 1 Hz by means of dynamic mechanical methods, may be partially responsible for the unusual temperature dependence of volume relaxation rate for PMMA relative to the behavior of other glassy polymers (Figure 1-13). In contrast to volume relaxation rates, Struik observed that creep compliance shift rates were largely independent of aging temperature ( $\mu \approx \text{constant} \approx 1.0$ ) except for close to the glass transition temperature where the rates decreased toward zero and for temperatures below the temperature range associated with the secondary relaxation where the rates were essentially zero.<sup>32</sup> This led to the generalization that physical aging of mechanical properties is limited to the temperature window between  $T_g$  and the secondary relaxation temperature. It is clear that the study of physical aging cannot ignore the role of secondary relaxations. The fact that the relaxation times associated with physical aging in the nonequilibrium glassy state are much greater than those attributed to secondary relaxations implies that the physical aging process has access to these localized secondary relaxations as is illustrated in Figure 1-15. The molecular motion afforded by the secondary relaxations may be an integral part of the structural relaxation process as is implied in Figure 1-16 by the possible coarsening of the potential energy surface.<sup>77</sup> The connection between secondary relaxations and the physical aging process is much more complex than this simple depiction, however, as is exemplified by the observation that the strength of secondary relaxations can diminish during structural

relaxation,<sup>63,65,70,71</sup> a finding which is not without controversy.<sup>32,64,72,75</sup> One of the controversial aspects is whether the aging-induced intensity reduction observed for the secondary relaxation ( $\beta$ -relaxation) is real or really reflects an influence of physical aging on the tail of the primary relaxation ( $\alpha$ -relaxation) which is partly underlying the secondary relaxation response.

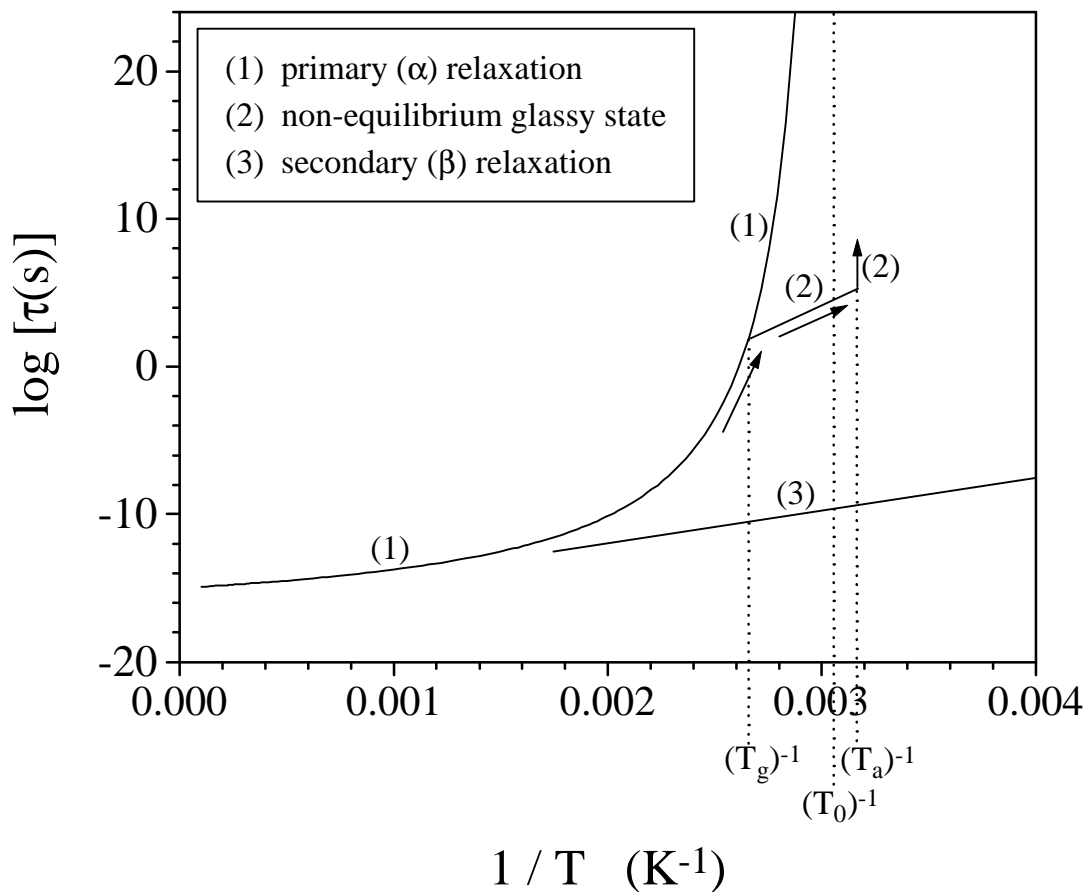


Figure 1-15. Relaxation map for an amorphous glass-forming material for cooling through the glass transition region followed by glassy state annealing at  $T_a$  (based upon reference 7).

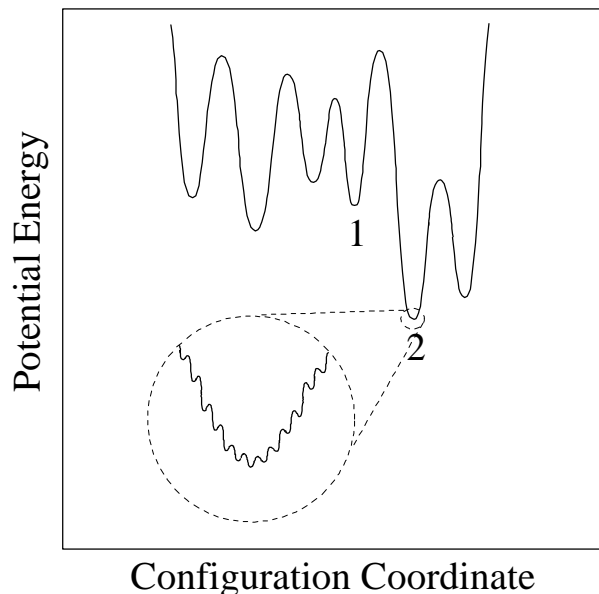


Figure 1-16: Portion of a hypothetical potential energy surface for a glassy material (based upon reference 77). An expanded view of the potential energy surface reveals the possible influence of secondary relaxation response which serves to coarsen the surface and enable a lower energy state to be obtained (1→2) for the main chain relaxation by a series of smaller energy jumps.

Recently, the prevalent view of physical aging as a self-limiting process has come under scrutiny. The behavior of isothermal physical aging in the glassy state following a quench from above  $T_g$  is often termed self-limiting because properties tend to change with  $\log(\text{aging time})$  as opposed to a dependence on linear time. As physical aging progresses, the system densifies causing mobility to decrease and further impeding additional aging from occurring, and this is the essence of the self-limiting nature of physical aging. Wimberger-Friedl and de Bruin<sup>78</sup> have recently investigated the volume relaxation of bisphenol-A polycarbonate at room temperature (23°C), and, although densification initially displayed the typical self-limiting response, the rate of relaxation increased dramatically after approximately  $10^7$  seconds ( $\sim 100$  days) as can be observed from Figure 1-17. Further confirmation of this observation for other polymer glasses is warranted given the implications on the current understanding of the nonlinear nature of glassy state relaxations, an understanding which will now be detailed.

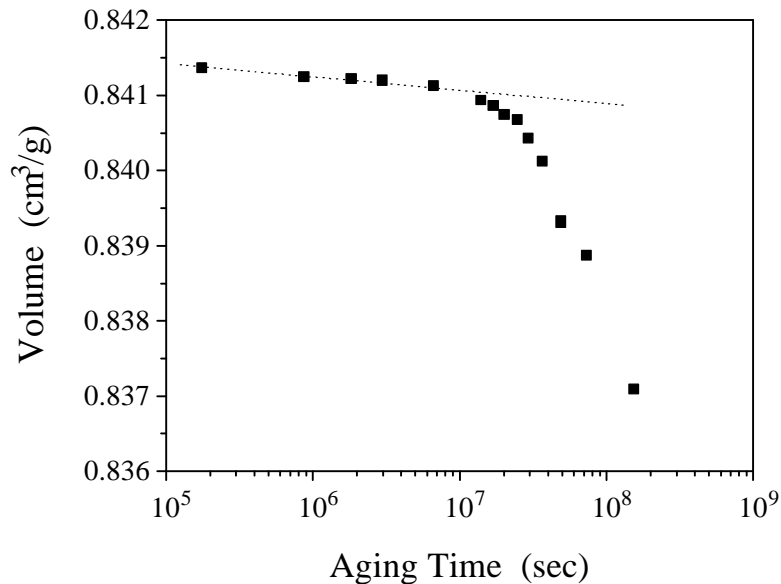


Figure 1-17. Long-term volume relaxation response of bisphenol-A polycarbonate at 23°C following 80°C/min quench from above  $T_g$  (replotted from reference 78).

### 1.2.3 NonLinear Relaxations in the Glassy State

The nonequilibrium nature of the glassy state leads to relaxation behavior which is nonlinear in character. Relaxation in glasses is termed nonlinear because relaxation times in the nonequilibrium glassy state depend not only on the temperature but also on the time-dependent thermodynamic (structural) state. It is useful to have a parameter which quantifies the structural state for a glass, and a commonly utilized order parameter is the fictive temperature,  $T_f$ , introduced by Tool.<sup>79,80</sup> The fictive temperature is defined to represent the temperature at which the system would be in equilibrium if instantaneously heated, a concept which is more easily grasped by reinspection of Figure 1-7 (figure was presented earlier). If a glass is formed by quenching from the equilibrium state to a temperature  $T_a$  then the initial state (state 0) can be represented by a fictive temperature which is equal to the glass transition temperature ( $T_{f_0}$ ). As physical aging progresses at  $T_a$ , then the fictive temperature decreases as illustrated in Figure 1-7 for states 1 and 2.

Although the actual temperature remains constant, the fictive temperature changes in the glassy state, leading to nonlinearity. This nonlinearity can be captured using the Adam-Gibbs configurational entropy approach,<sup>13,29,81</sup> and the following expression is one nonlinear form of the Adam-Gibbs equation:

$$\tau = A \exp\left(\frac{\Delta\mu}{RT[1 - (T_2/T_f)]}\right) \quad \text{Eqn. 1-21}$$

According to the above, the relaxation time increases as the fictive temperature decreases during isothermal aging. Another nonlinear relaxation time expression is the empirical relationship commonly used in the Tool-Narayanaswamy-Moynihan (TNM)<sup>24,79,80,82,83</sup> formalism to be described later. The TNM relaxation time is a function of a prefactor (A), an activation energy ( $\Delta h$ ) and a parameter (x) which partitions the response of the material between actual temperature and structural temperature:

$$\tau = A \exp\left(\frac{x\Delta h}{RT} + \frac{(1-x)\Delta h}{RT_f}\right) \quad \text{Eqn. 1-22}$$

In the equilibrium state above  $T_g$ , the fictive temperature is equivalent to the actual temperature and the TNM relaxation time function becomes an Arrhenius expression, in contradiction to the experimentally observed nonArrhenius response above  $T_g$ . When the nonlinear Adam-Gibbs equation becomes linear in the equilibrium state ( $T_f = T$ ) it appropriately yields a nonArrhenius relationship.

Nonlinearity is observed in the well known asymmetry-of-approach experiments performed by Kovacs.<sup>84</sup> These measurements involve following the densification toward equilibrium in the glassy state at a temperature  $T_2$ <sup>¶</sup> after a positive temperature jump from the equilibrium state at a temperature  $T_1$  (expansion experiment) and after a negative temperature jump from the equilibrium state at a temperature  $T_3$  (contraction experiment). The absolute value of the positive and negative temperature steps are typically the same for comparative purposes. The essence of the experimental approach employed is indicated in Figure 1-18. Before initiation of the contraction experiment, the sample is

---

<sup>¶</sup> This parameter  $T_2$  should not be confused with the Gibbs-DiMarzio temperature. The subscript “2” is used here in an arbitrary manner.

quenched from point H to A and then isothermally aged to equilibrium (state B). The temperature jump from  $T_3$  to  $T_2$  initially induces a densification (B to C) consistent with the glassy state thermal expansion coefficient, and then the contraction experiment follows the time-dependent nature of volume reduction from state C to equilibrium at state D. In a similar manner, the progression of volume from G to D is monitored in the expansion experiment. The asymmetry of approach assessed for poly(vinyl acetate) by Kovacs<sup>84</sup> is shown in Figure 1-19, and the influence of nonlinearity is clearly manifested in the differing responses for contraction and expansion experiments. During the expansion experiment, the volume increases and the relaxation times decrease leading to an autocatalytic approach to the equilibrium state  $V_\infty$  while the contraction leads to autoretarded behavior by an opposite nonlinear effect. A related phenomenon is the  $\tau_{\text{eff}}$  (“tau effective”) paradox described in detail in a review by McKenna<sup>3</sup> which involves the discrepancy between relaxation times during contraction/expansion experiments for different prior thermal histories during the final approach toward equilibrium (in the limit as  $\delta = (V - V_\infty)/V_\infty$  approaches zero) when the prior history might be expected to be unimportant.

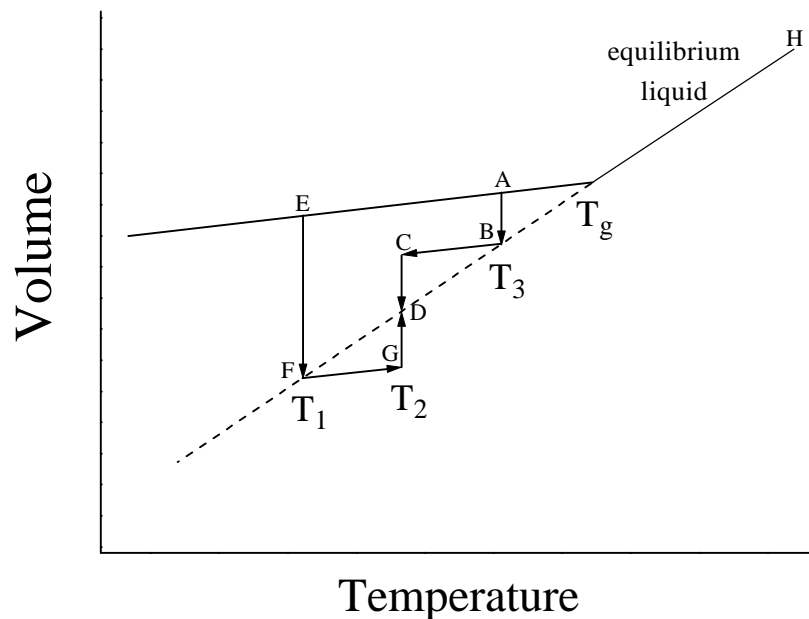


Figure 1-18: Diagram illustrating the up-jump and down-jump experiments initiated from equilibrium states. See text for details.

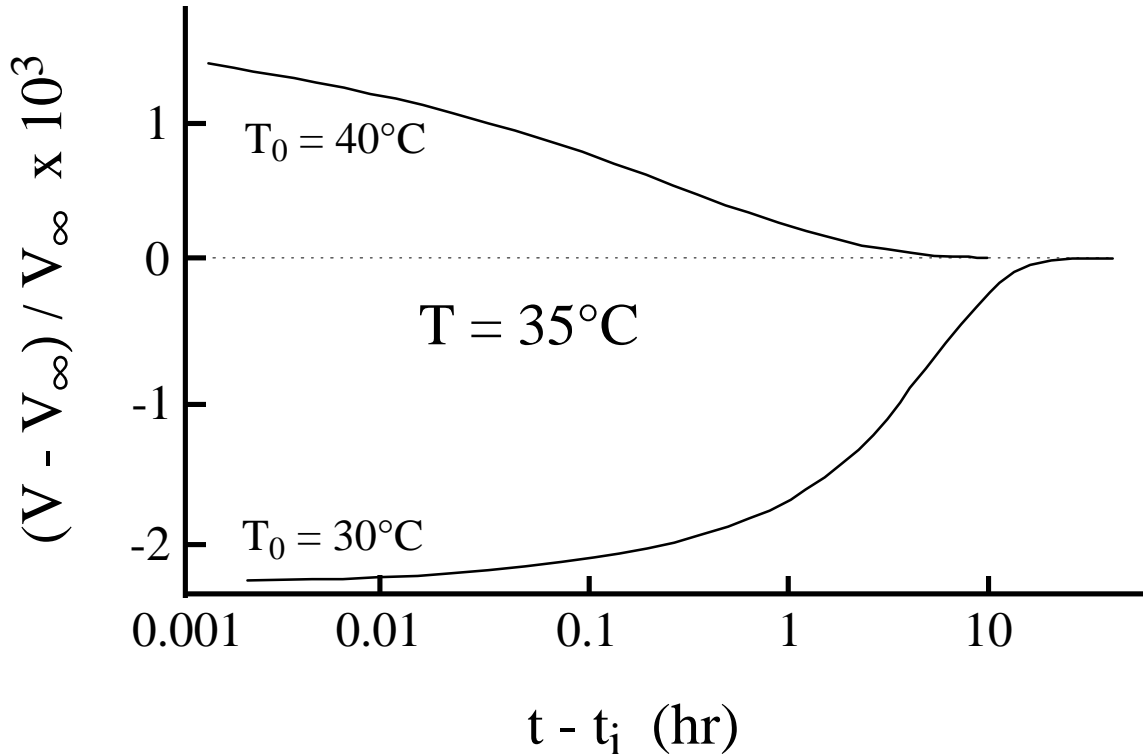


Figure 1-19: Asymmetry of approach for poly(vinyl acetate) indicated by contraction and expansion behavior (replotted from reference 84). By comparison with Figure 1-18,  $T_1=30^\circ\text{C}$ ,  $T_2=35^\circ\text{C}$ , and  $T_3=40^\circ\text{C}$ .

#### 1.2.4 NonExponential Relaxations

Up to this point, the discussion has considered the relaxation behavior of glass formers in a manner which only highlighted a single characteristic relaxation time for a material, a relaxation time which is influenced by temperature and the thermal history applied to the material. In reality, there exists a distribution of relaxation times for a glass-forming material, and the previous discussion of nonArrhenius and nonlinear characteristics only examined the relaxation behavior from changes in the average or, more appropriately, the most probable relaxation time. An exponential, or Debye,

relaxation event is only influenced by a single characteristic time constant so that relaxation behavior governed by an expanse of relaxation times is classified as nonexponential or nonDebye.<sup>13,81</sup> The presence of a relaxation time distribution for glass formers requires that the picture of segmental cooperativity not be restricted to a single domain size but rather incorporate the notion of a distribution of  $z$  values. The discussion will now address how the presence of a relaxation time distribution can affect the relaxation behavior of glass formers.

One of the most striking examples of the influence of a distribution of relaxation times is the memory effect observed in the glassy state response of materials. The term “memory” is used because the relaxation time distribution can lead to path dependent relaxation behavior in the glassy state. This behavior is distinct from the nonequilibrium and associated nonlinear complexities previously described.<sup>3,32,84-87</sup> Kovacs observed the memory effect using dilatometry, and the essence of this phenomenon, also referred to as “breathing” in the literature, is illustrated in Figure 1-20 for poly(vinyl acetate) (PVAc).<sup>84</sup> After a temperature jump from the equilibrium liquid state (40°C) to 15°C followed by 140 hours of annealing, the PVAc sample (sample B) was rapidly heated to 30°C where the log(time)-dependent volume response was then followed relative to the equilibrium volume ( $V_\infty$ ) at that temperature as is indicated by curve B of Figure 1-20. The volume response after such a thermal history is initially observed to advance through the equilibrium state where  $(V-V_\infty)/V_\infty$  is equal to zero, a feature known as the crossover effect. Following this, the volume of the sample passes through a maximum and finally approaches equilibrium in a similar manner to a PVAc sample (sample A) which underwent a temperature jump directly from 40°C to 30°C (curve A of Figure 1-20). Although sample B was annealed at the lower temperature of 15°C for a significant amount of time, upon jumping to the final temperature (where time was reset to zero), the time to reach equilibrium was not any different than sample A which was rapidly quenched directly to 30°C from the equilibrium liquid state.

The memory effect is a direct manifestation of a relaxation time distribution where the annealing time at the lower temperature is between the shortest and longest relaxation times.<sup>32</sup> It is a worthwhile endeavor to provide a simplified explanation for the connection

between the observed complex breathing response and a relaxation time distribution. To illustrate the influence of relaxation time multiplicity it is easier to assume the presence of only two distinct relaxation times, one of which is much longer than the other, apportioned evenly within the sample. The average relaxation time is between these two relaxation times and the average structural state or specific volume is intermediate to the structural states for the two distinct relaxing components of the material. Upon being quenched into the glass (to 15°C for the PVAc example) from the equilibrium liquid, the structural state corresponding to the short relaxation time relaxes much faster, resulting in densification, while very little relaxation occurs for the structural component with the long relaxation time. The act of annealing in the glassy state itself shifts the relaxation times to larger values as was mentioned in the description of nonlinearity, but to observe the memory effect, the longest relaxation times must always be greater than the final annealing time. Upon heating to a higher temperature in the glass (30°C), the volume for the fast relaxing portion of the material is below the equilibrium volume at the new temperature while the volume state attributed to the long relaxation time is above equilibrium. The volume for the structural state below equilibrium expands at a much greater rate than the contraction of the slowly relaxing state towards  $V_{\infty}$ , and, in accordance with these different directions and rates of approach to equilibrium, the average volume increases and passes through  $V_{\infty}$ . After longer times, the expansion of the fast relaxing structural state becomes complete while the slow contraction corresponding to the long relaxation time character of the material continues, and this explains the peak and subsequent volume relaxation towards the equilibrium state  $V_{\infty}$ . In reality, there exists a relaxation time distribution for a material rather than just two relaxation times, but the above explanation allows insight into the origin of the memory effect to be acquired nonetheless.<sup>88</sup>

A mathematical representation of a distribution of relaxation times is useful in modeling the complex relaxation behavior of glasses. The following expression is the most widely employed form for the decay function,  $\phi(t)$ , which describes relaxation of a dimensionless variable from a value of 1.0 at  $t = 0$  toward a value of zero at long times:<sup>13,81</sup>

$$\phi(t) = \exp \left[ - \left( \int_0^t \frac{dt'}{\tau(t')} \right)^\beta \right] \quad \text{Eqn. 1-23}$$

The linear form of this equation results when the relaxation time does not change with time:

$$\phi(t) = \exp \left[ - \left( \frac{t}{\tau} \right)^\beta \right] \quad \text{Eqn. 1-24}$$

where  $\tau$  is the most probable relaxation time and the parameter  $\beta$  is related to the breadth of the relaxation time distribution. The above equation is often attributed to Kohlrausch, Williams, and Watts<sup>89-91</sup> although this equation should be more generally called the stretched exponential function instead of the KWW equation because it cannot be simply attributed to any individuals.<sup>13</sup> When the value of  $\beta$  is equal to 1.0 then relaxation is exponential with only a single relaxation time, and as  $\beta$  decreases the relaxation time distribution broadens. The relaxation time distribution corresponding to the stretched exponential function can be approximated using Alfrey's method:<sup>92</sup>

$$p(\tau_i) \approx \beta (\tau_i / \tau)^\beta \exp \left[ - (\tau_i / \tau)^\beta \right] \quad \text{Eqn. 1-25}$$

This approximation describes the probability of a relaxation time,  $p(\tau_i)$ , and the probability distributions for various values of  $\beta$  are illustrated in Figure 1-21 as functions of the ratio of  $\tau_i$  to the most probable relaxation time,  $\tau$ . The KWW function provides a means for incorporating the concept of a relaxation time distribution when attempting to describe the relaxation behavior of glass forming materials.

There are a lot of experimental data for many different classes of glass formers which indicate a connection between nonexponentiality and nonArrhenius behavior. Specifically, it has been observed that the relaxation time distribution is broader (lower  $\beta$ ) in the glass transition region for materials which are more fragile,<sup>93,94</sup> and the coupling model of Ngai et al.<sup>95-100</sup> can capture this interrelationship. A distribution of relaxation times can either be thought of as representing the presence of a distribution of distinct intrinsic relaxation times or can be viewed as reflecting changes in a single relaxation time due to cooperativity. This latter view is consistent with the observed interrelationship

between nonexponentiality and nonArrhenius behavior. The implication of the connection is that thermorheological simplicity is not strictly valid because the distribution broadens as the relaxation times shift to longer times. From a pragmatic approach, however, thermorheological simplicity is a fair assumption in many cases and it immensely simplifies the mathematical approach to modeling glassy state relaxations as will be evident in the discussion to follow.

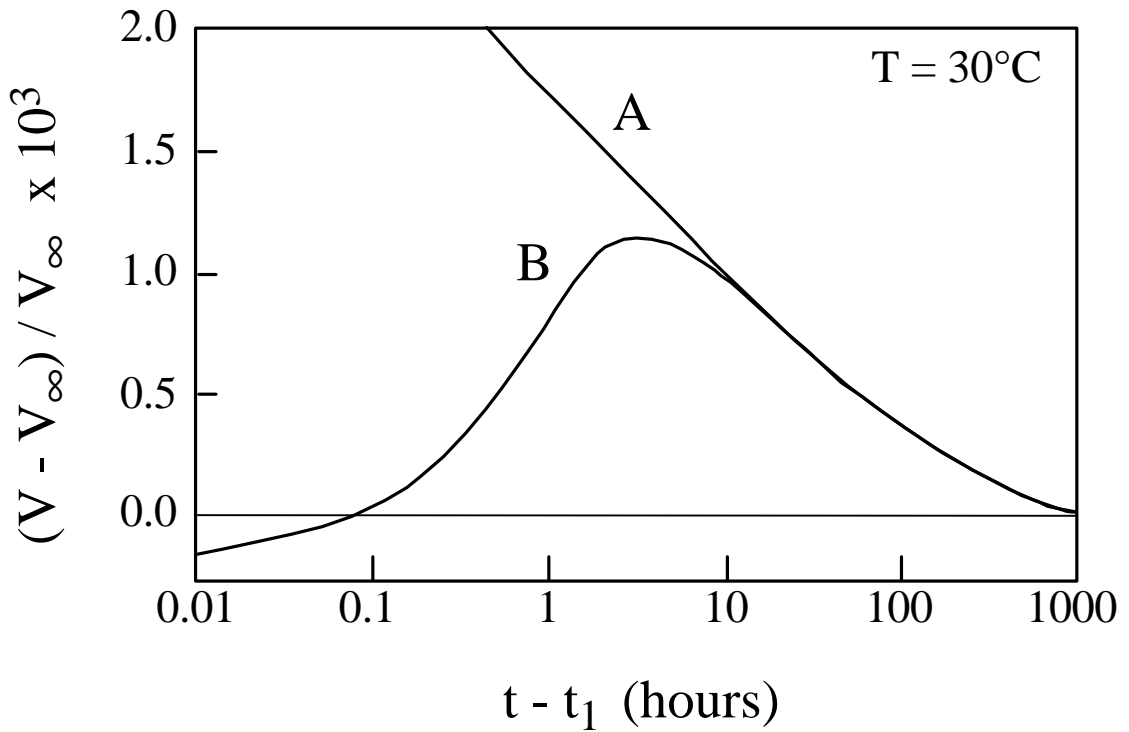


Figure 1-20: Illustration of the memory effect for poly(vinyl acetate) (replotted from reference 84). Curve A represents relaxation during annealing in the glassy state at 30°C following a rapid quench from 40°C (the equilibrium liquid state above  $T_g$ ). Curve B represents volume response at 30°C for a sample which was first quenched from 40°C and then annealed at 15°C for 140 hours prior to being rapidly heated to 30°C. Time  $t_1$  is when the temperature of 30°C is reached.

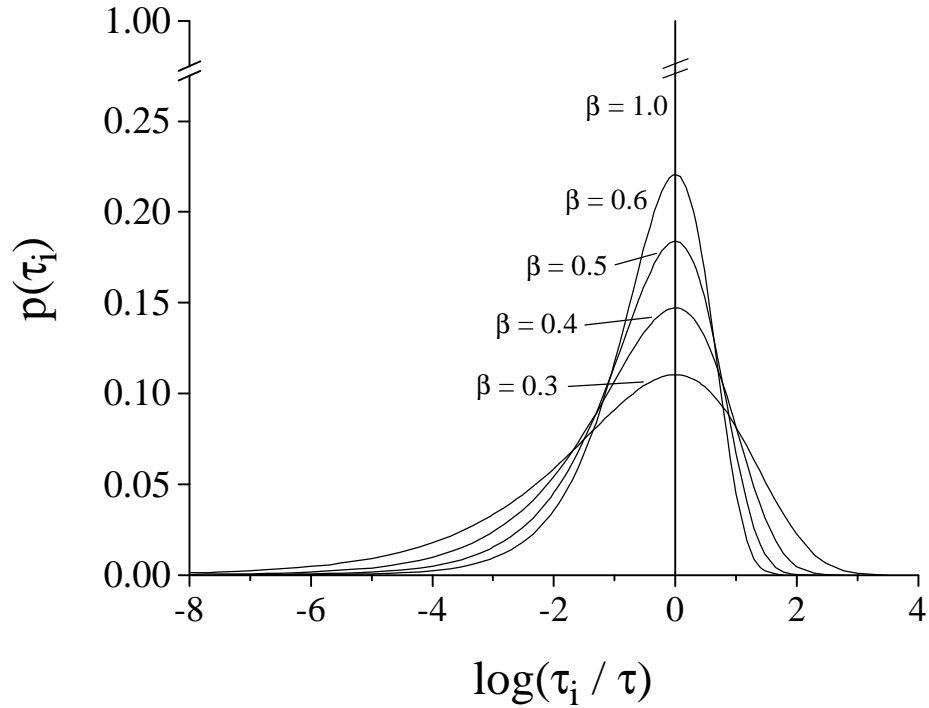


Figure 1-21: Relaxation time distributions according to the KWW stretched exponential function. Relaxation times are normalized by the most probable relaxation time,  $\tau$ .

One commonly used approach to modeling the relaxation response of a material in the glassy state is the Tool-Narayanaswamy-Moynihan (TNM) formalism<sup>24,79,82,83,101-104</sup> which allows the changing structural temperature in the nonequilibrium glassy state to be modeled by collectively superimposing the responses from the previously applied thermal history:

$$T_f(T) = T_{init} + \int_{T_{init}}^T \left\{ 1 - \exp \left[ - \left( \int_{t(T'')}^{t(T)} \frac{dt'}{\tau(T, T_f)} \right)^\beta \right] \right\} dT'' \quad \text{Eqn. 1-26}$$

The simulated thermal history is initiated at a temperature  $T_{init}$  which is in the equilibrium liquid state where  $T_f = T$ , and the above equation relies upon the assumption of thermorheological simplicity. Considering the mathematical complexity which would result

instead if  $\beta$  and  $\tau$  were both allowed to be functions of temperature and the changing structural state, one can easily see how the assumption of thermorheological simplicity ( $\beta$ =constant) greatly simplifies the modeling of complex thermal histories. The Ngai coupling model considers a characteristic relaxation time to be coupled to its environment by a functionality involving the coupling parameter,  $n$ , which is related to the stretching exponent ( $n = 1 - \beta$ ),<sup>99,100</sup> and the use of this approach adds an additional complexity because of this intimate connection between the  $\tau$  and  $\beta$  parameters. A comparable approach to the TNM methodology is the formalism developed by Kovacs, Aklonis, Hutchinson, and Ramos (KAHR) which is discussed elsewhere.<sup>3,105,106</sup> The majority of the modeling efforts using the TNM approach employ the empirical relaxation time function given by Eqn. 1-22 which does not capture the nonArrhenius behavior above  $T_g$ . When the relaxation time function utilized in Eqn. 1-26 is the nonlinear Adam-Gibbs equation (Eqn. 1-21), then the nonArrhenius, nonequilibrium, nonlinear, and nonexponential phenomenological characteristics of glass-forming materials can all be represented. This approach will be used in the execution of the proposed research investigation which will be described later.

### 1.3 References

- <sup>1</sup> K. L. Ngai and D. J. Plazek, in *Physical Properties of Polymers Handbook* (ed. J. E. Mark), AIP Press, Woodbury, NY, 1996, pp. 341-362 (Chapter 25).
- <sup>2</sup> D. J. Plazek and K. L. Ngai, in *Physical Properties of Polymers Handbook* (ed. J. E. Mark), AIP Press, Woodbury, NY, 1996, pp. 139-159 (Chapter 12).
- <sup>3</sup> G. B. McKenna, in *Comprehensive Polymer Science, Vol. 2, Polymer Properties* (ed. C. Booth and C. Price), Pergamon, Oxford, UK, 1989, pp 311-362 (Chapter 10).
- <sup>4</sup> P. Ehrenfest, *Proc. K. Ned. Akad. Wet.*, **36**, 153 (1933).
- <sup>5</sup> G. Rehage and W. Borchard, in *The Physics of Glassy Polymers* (ed. R. N. Haward), Wiley, New York, 1973, p. 54.
- <sup>6</sup> W. Kauzmann, *Chemical Review*, **43**, 219 (1948).
- <sup>7</sup> E.-J. Donth, *Relaxation and Thermodynamics in Polymers: Glass Transition*, Akademie Verlag, Berlin, 1992.
- <sup>8</sup> J. H. Gibbs and E. A. DiMarzio, *J. Chem. Phys.*, **28(3)**, 373 (1958).
- <sup>9</sup> E. A. DiMarzio, *J. Res. Natl. Bur. Stand.*, **68A**, 611 (1964).
- <sup>10</sup> G. Pezzin, F. Zilio-Grandi, and P. Sammartin, *Eur. Polym. J.*, **6**, 1053 (1970).

- 11 S. Matsuoka, *J. Res. Natl. Inst. Stand. Technol.*, **102(2)**, 213 (1997).  
12 C. A. Angell, *Proc. Natl. Acad. Sci USA*, **92**, 6675 (1995)  
13 I. M. Hodge, *J. Non-Cryst. Solids*, **169**, 211 (1994).  
14 M. L. Williams, R. F. Landel, and J. D. Ferry, *J. Am. Ceram. Soc.*, **77**, 3701 (1955).  
15 C. A. Angell, *Science*, **267**, 1924 (1995).  
16 C. A. Angell, L. Monnerie, and L. M. Torell, in *Structure, Relaxation, and Physical Aging of Glassy Polymers* (eds. R. J. Roe and J. M. O'Reilly), *Mat. Res. Symp. Proc.*, **215**, 3 (1991).  
17 C. A. Angell, *J. Non-Cryst. Solids*, **131-133**, 13 (1991).  
18 C. A. Angell, *J. Res. Natl. Inst. Stand. Technol.*, **102(2)**, 171 (1997).  
19 A. K. Doolittle, *J. Appl. Phys.*, **22**, 1031 (1951).  
20 A. K. Doolittle, *J. Appl. Phys.*, **22(12)**, 1471 (1951).  
21 M. H. Cohen and D. Turnbull, *J. Chem. Phys.*, **31(5)**, 1164 (1959).  
22 D. Turnbull and M. H. Cohen, *J. Chem. Phys.*, **34**, 120 (1961).  
23 G. Adam and J. H. Gibbs, *J. Chem. Phys.*, **43(1)**, 139 (1965).  
24 I. M. Hodge, *J. Res. Natl. Inst. Stand. Technol.*, **102(2)**, 195 (1997).  
25 H. Vogel, *Phys. Z.*, **22**, 645 (1921).  
26 G. S. Fulcher, *J. Am. Ceram. Soc.*, **8**, 339 (1925).  
27 G. Tammann and W. Hesse, *Z. Anorg. Allg. Chem.*, **156**, 245 (1926).  
28 S. Matsuoka and X. Quan, *Macromolecules* **24**, 2770 (1991).  
29 S. Matsuoka, *Relaxation Phenomena in Polymers*, Hanser Publishers, Munich, 1992.  
30 S. Matsuoka, *J. Non-Cryst. Solids*, **131-133**, 293 (1991).  
31 E. A. DiMarzio and A. J. M. Wang, *J. Res. Natl. Inst. Stand. Technol.*, **102(2)**, 135 (1997).  
32 L. C. E. Struik, *Physical Aging in Amorphous Polymers and Other Materials*, Elsevier, New York, 1978.  
33 J. M. O'Reilly, *CRC Critical Rev. in Solid State and Matl. Sci.*, **13(3)**, 259 (1987).  
34 M. R. Tant and G. L. Wilkes, *Polym. Eng. Sci.*, **21(14)**, 874 (1981).  
35 J. M. Hutchinson, *Prog. Polym. Sci.*, **20**, 703 (1995).  
36 R. Greiner and F. R. Schwarzl, *Rheol. Acta*, **23(4)**, 378 (1984).  
37 R. S. Marvin and J. E. McKinney, in *Physical Acoustics*, Vol. II B (ed. W. P. Mason), Academic, New York, 1965.  
38 L. C. E. Struik, *Internal Stress, Dimensional Instabilities and Molecular Orientations in Plastics*, John Wiley and Sons, New York, 1990.  
39 S. E. B Petrie, *J. Polym. Sci.: Part A-2*, **10**, 1255 (1972).  
40 J. M. Hutchinson, *Prog. Colloid Polym. Sci.*, **87**, 69 (1992).  
41 S. E. B Petrie, in *Physical Structure of the Amorphous State* (ed. G. Allen and S. E. B. Petrie), Marcel Dekker, New York, 1977.  
42 B. E. Read, P. E. Tomlins, and G. D. Dean, *Polymer*, **31**, 1204 (1990).  
43 R. D. Bradshaw and L. C. Brinson, *Polym. Eng. Sci.*, **37(1)**, 31 (1997).  
44 S.L. Simon, D.J. Plazek, J.W. Sobieski, and E.T. MacGreggor, *J. Polym. Sci.: Part B: Polym. Phys.* **35**, 929 (1997).  
45 E. F. Oleinik, *Polym. J.* **19**, 105 (1987).

- <sup>46</sup> S. Matsuoka, H. E. Bair, S. S. Bearder, H. E. Kern, and J. T. Ryan, *Polym. Eng. Sci.*, **18**, 1073 (1978).
- <sup>47</sup> S. Matsuoka and H. E. Bair, *J. Appl. Phys.*, **48**, 4058 (1977).
- <sup>48</sup> L. C. E. Struik, *Polymer*, **38**, 4053 (1997).
- <sup>49</sup> G. B. McKenna, *J. Non-Cryst. Solids*, **172-174**, 756 (1994).
- <sup>50</sup> G. B. McKenna, *J. Res. Natl. Inst. Stand. Technol.*, **99(2)**, 169 (1994).
- <sup>51</sup> W. K. Waldron, Jr., G. B. McKenna, and M. M. Santore, *J. Rheol.*, **39(2)**, 471 (1995).
- <sup>52</sup> G. B. McKenna, Y. Leterrier, and C. R. Schultheisz, *Polym. Eng. Sci.* **35(5)**, 403 (1995).
- <sup>53</sup> G. B. McKenna, C. R. Schultheisz, and Y. Leterrier, in *Deformation, Yield and Fracture of Polymers*, Proc. 9th Int'l. Conf., Cambridge, UK, 1994, pp. 31/1-31/4.
- <sup>54</sup> C. A. Bero and D. J. Plazek, *J. Polym. Sci.: Part B: Polym. Phys.* **29**, 39 (1991).
- <sup>55</sup> K. Adachi and T. Kotaka, *Polym. J.* **14**, 959 (1982).
- <sup>56</sup> R. J. Roe and G.M. Millman, *Polym. Eng. Sci.* **23(6)**, 318 (1983).
- <sup>57</sup> A. Weitz and B. Wunderlich, *J. Polym. Sci.: Polym. Phys.* **12**, 2473 (1974).
- <sup>58</sup> J. Perez, J.Y. Cavaille, R. D. Calleja, J.L.G. Ribelles, M.M. Pradas, and A. R. Greus, *Makromol. Chem.* **192**, 2141 (1991).
- <sup>59</sup> J. Mijovic and T. Ho, *Polymer*, **34**, 3865 (1993).
- <sup>60</sup> H. Sassabe and C.T. Moynihan, *J. Polym. Sci.: Part B: Polym. Phys.* **16**, 1447 (1978).
- <sup>61</sup> J.M.G. Cowie, S. Elliott, R. Ferguson, and R. Simha, *Polym. Commun.* **28**, 298 (1987).
- <sup>62</sup> I. Echeverria, P.-C. Su, S. L. Simon, and D.J. Plazek, *J. Polym. Sci.: Part B: Polym. Phys.* **33**, 2457 (1995).
- <sup>63</sup> G. P. Johari and M. Goldstein, *J. Chem. Phys.* **53**, 2372 (1970).
- <sup>64</sup> J. Haddad and M. Goldstein, *J. Non-Cryst. Solids*, **30**, 1 (1978).
- <sup>65</sup> G. P. Johari, *J. Chem. Phys.*, **77(9)**, 4619 (1982).
- <sup>66</sup> G. B. McKenna and A. J. Kovacs, *Polym. Eng. Sci.*, **24**, 1138 (1984).
- <sup>67</sup> L. C. E. Struik, *Polymer*, **28**, 1869 (1987).
- <sup>68</sup> B. E. Read and G. D. Dean, *Polymer*, **25**, 1679 (1984).
- <sup>69</sup> A. A. Goodwin and J. N. Hay, *Polymer Commun.*, **31**, 338 (1990).
- <sup>70</sup> A. B. Brennan and F. Feller, III, *J. Rheol.*, **39(2)**, 453 (1995).
- <sup>71</sup> R. A. Venditti and J. K. Gillham, *J. Appl. Polym. Sci.*, **45**, 1501 (1992).
- <sup>72</sup> R. Diaz-Calleja, A. Ribes-Greus, and J. L. Gomez-Ribelles, *Polymer*, **30**, 1433 (1989).
- <sup>73</sup> H. H.-D. Lee and F. J. McGarry, *Polymer*, **34(20)**, 4267 (1993).
- <sup>74</sup> E. Muzeau, G. Vigier, and R. Vassoille, *J. Non-Cryst. Solids*, **172-174**, 575 (1994).
- <sup>75</sup> E. Muzeau, G. Vigier, R. Vassoille, and J. Perez, *Polymer*, **36(3)**, 611 (1995).
- <sup>76</sup> N. G. McCrum, B. E. Read, and G. Williams, *Anelastic and Dielectric Effects in Polymeric Solids*, Dover Publications, New York, 1967, pp. 238-255.
- <sup>77</sup> F. H. Stillinger, *Science*, **267**, 1935 (1995).
- <sup>78</sup> R. Wimberger-Friedl and J. G. de Bruin, *Macromolecules*, **29(14)**, 4994 (1996).
- <sup>79</sup> A. Q. Tool, *J. Am. Ceram. Soc.*, **29**, 240 (1946).
- <sup>80</sup> A. Q. Tool, *J. Res. Natl. Bur. Stand.*, **37**, 73 (1946).

- 81 G. W. Scherer, *Relaxation in Glass and Composites*, Wiley, New York, 1986.
- 82 O. S. Narayanaswamy, *J. Am. Ceram. Soc.*, **54(10)**, 491 (1971).
- 83 C. T. Moynihan, A. J. Easteal, M. A. DeBolt, and J. Tucker, **59**, 12 (1976).
- 84 A. J. Kovacs, *Fortschr. Hochpolym.-Forsch.*, **3**, 394 (1964).
- 85 H. N. Ritland, *J. Am. Ceram. Soc.*, **39**, 403 (1956).
- 86 S. M. Rekhson, *J. Non-Cryst. Solids*, **84**, 68 (1986).
- 87 S. Spinner and A. Napolitano, *J. Res. Natl. Bur. Stand.*, **70A(2)**, 147 (1966).
- 88 S. Brawer, *Relaxation in Viscous Liquids and Glasses*, American Ceramic Society, Columbus, OH, 1985.
- 89 R. Kohlrausch, *Pogg. Ann. Phys.*, **91**, 198 (1854).
- 90 R. Kohlrausch, *Pogg. Ann. Phys.*, **119**, 352 (1863).
- 91 G. Williams and D. C. Watts, *Trans. Faraday Soc.*, **66**, 80 (1970).
- 92 J.D. Ferry, *Viscoelastic Properties of Polymers*, third edition, Wiley, NY, 1980.
- 93 R. Bohmer and C. A. Angell, *Materials Science Forum*, **119-121**, 485 (1993).
- 94 R. Bohmer, K. L. Ngai, C. A. Angell, and D. J. Plazek, *J. Chem. Phys.*, **99(5)**, 4201 (1993).
- 95 K. L. Ngai, *Comments Solid State Physics*, **9(4)**, 127 (1979).
- 96 K. L. Ngai, *Comments Solid State Physics*, **9(5)**, 141 (1980).
- 97 K. L. Ngai, *Phys. Rev. B*, **22(4)**, 2066 (1980).
- 98 K. L. Ngai, R. W. Rendell, A. K. Rajagopal, and S. Teitler, *Ann. NY Acad. Sci.*, **484**, 150 (1986).
- 99 K. L. Ngai and R. W. Rendell, *J. Non-Cryst. Solids*, **131-133**, 942 (1991).
- 100 R. W. Rendell, K. L. Ngai, and D. J. Plazek, *J. Non-Cryst. Solids*, **131-133**, 442 (1991).
- 101 J. Mijovic, L. Nicolais, A. D'Amore, and J. M. Kenny, *Polym. Eng. Sci.*, **34(5)**, 381 (1994).
- 102 C. T. Moynihan, S. N. Crichton, and S. M. Opalka, *J. Non-Cryst. Solids*, **131-133**, 420 (1991).
- 103 I. M. Hodge, *Macromolecules*, **20(11)**, 2897 (1987).
- 104 I. M. Hodge, *Macromolecules*, **15(3)**, 762 (1982).
- 105 J. J. Aklonis, *Polym. Eng. Sci.*, **21(14)**, 896 (1981).
- 106 A. J. Kovacs, J. J. Aklonis, J. M. Hutchinson, and A. R. Ramos, *J. Polym. Sci.: Polym. Phys. Ed.*, **17**, 1097 (1979).

# Chapter 2

## Review -- Selected Features of Miscible Polymer Blends

---

---

It is useful to review some features of miscible polymer blends which, in combination with the previous review of the glassy state, will serve as a knowledge resource to be drawn upon later during the assessment of literature dealing with the physical aging of miscible blends and during discussion of the research results. The thermodynamics of miscibility will be addressed, focusing on the attributes which are unique to mixtures of high molecular weight polymers. Following this will be an overview of the compositional nature of properties in binary miscible polyblends, focusing on the property of glass transition temperature.

### 2.1 Thermodynamics of Polymer-Polymer Miscibility

The phase behavior of all classes of mixtures including polymer-polymer blends is specified by the temperature and compositional dependence of the change in the Gibbs free energy upon mixing,  $\Delta G_m$ . The formation of a homogeneous blend can only occur if this combination of the two materials results in a net decrease in free energy:

$$\Delta G_m < 0 \quad \text{Eqn. 2-1}$$

This is a necessary prerequisite for miscibility, but from a phase stability standpoint the following criteria must also hold:

$$\left( \frac{\partial^2 \Delta G_m}{\partial \phi_2^2} \right)_{T,P} > 0 \quad \text{Eqn. 2-2}$$

where  $\phi_2$  is the volume fraction of component 2 in a binary blend. Because the second derivative indicates concavity, this criteria is met when the  $\Delta G_m$  versus  $\phi_2$  curve is concave upward.<sup>1,2</sup>

The effect of temperature, pressure, and composition on the above miscibility criteria dictate the phase diagram, and a typical phase diagram for a two component polymer blend system is shown schematically in Figure 2-1. This phase diagram is presented as a function of the mole fraction of species 2 ( $x_2$ ) as opposed to volume fraction because this will allow simpler illustration of how the binodal curve is determined. The phase diagrams are very similar when plotted versus  $x_2$  and  $\phi_2$ , and they are identical for the case where the number and volume of the molecular units comprising linear chains of the two polymer species are the same. Polymer-polymer blends are unique in that it is common for a miscible blend formed at one temperature to phase separate upon heating to a higher temperature (see Figure 2-1), a phenomenon known as lower critical solution temperature (LCST) behavior,<sup>3</sup> although a variety of phase behaviors are observed in polymer blend systems.<sup>4</sup> The observation of LCST response for a polyblend is contradictory to the commonly held heuristic that increasing temperature improves the solubility of one material in another. The spinodal curve is representative of where the second partial of  $\Delta G_m$  with respect to  $\phi_2$  is zero. The binodal curve represents the compositions of the stable equilibrium phases comprising an immiscible blend, and is defined by equating the chemical potential of species  $i$  ( $\Delta\mu_i$ ) in the two immiscible phases.<sup>5</sup> The chemical potential,  $\Delta\mu_i$ , is given by the first partial of  $\Delta G_m$  with respect to the number of molecules of component  $i$  ( $N_i$ ):

$$\Delta\mu_i = \left( \frac{\partial \Delta G_m}{\partial N_i} \right)_{T,P,N_{k \neq i}} \quad \text{Eqn. 2-3}$$

For a binary system with two immiscible phases, designated A and B, the binodal compositions must satisfy the following equalities:

$$(\Delta\mu_1)_A = (\Delta\mu_1)_B \quad \text{and} \quad (\Delta\mu_2)_A = (\Delta\mu_2)_B \quad \text{Eqn. 2-4}$$

When the  $\Delta G_m$  function at a given temperature and pressure is plotted versus mole fraction, a single straight line which can be drawn tangent to two points on the curve graphically defines the solution to the phase equilibrium criteria given in Eqn. 2-4.<sup>2,6</sup> The critical temperature ( $T_C$ ) at constant pressure is graphically defined by the intersection of

the binodal and spinodal curves and, mathematically, is where the third partial of  $\Delta G_m$  with respect to  $\phi_2$  is equal to zero.<sup>2,5</sup>

The thermodynamic phase diagram indicates whether two materials will form a homogenous miscible blend or a phase separated mixture at the temperature and pressure of interest. The region between the binodal and spinodal curves is a metastable miscible region which is not affected by small fluctuations in concentration and temperature. However, significant fluctuations can lead to nucleation and growth of an immiscible blend system comprised of two distinct miscible blend phases, one rich in component 1 and one rich in component 2. These two phases have compositions which correspond to the two compositions defined by the binodal curve at that temperature.<sup>5</sup> Using *Figure 2-1* to illustrate this point, a miscible blend may be initially formed at temperature  $T_2$  with a composition ( $\bullet$ ) between the nearest binodal ( $\times$ ) and spinodal (+) values of  $\phi_2$ , but large concentration fluctuations can lead to formation of nuclei with composition corresponding to the nearest stable binodal point,  $x_{2,B}$ . The end result is an immiscible blend made up of two miscible blend phases with compositions given by the two binodal points at that temperature,  $x_{2,A}$  and  $x_{2,B}$ , and with relative amounts necessary to maintain a mass balance. If the temperature of an initially miscible blend is changed at constant pressure such that the system now resides in the unstable, immiscible region of the phase diagram encompassed by the spinodal curve, then spinodal decomposition will lead to phase separation into two phases possessing the binodal compositions. However, spinodal decomposition is a spontaneous process while phase separation by nucleation and growth involves an activation barrier which must be overcome to generate the stable nuclei which can then grow to form the immiscible blend system.<sup>5,7</sup> With the characteristic phase behavior of polymer-polymer blends illustrated, the specific thermodynamic characteristics leading to miscibility will now be addressed.

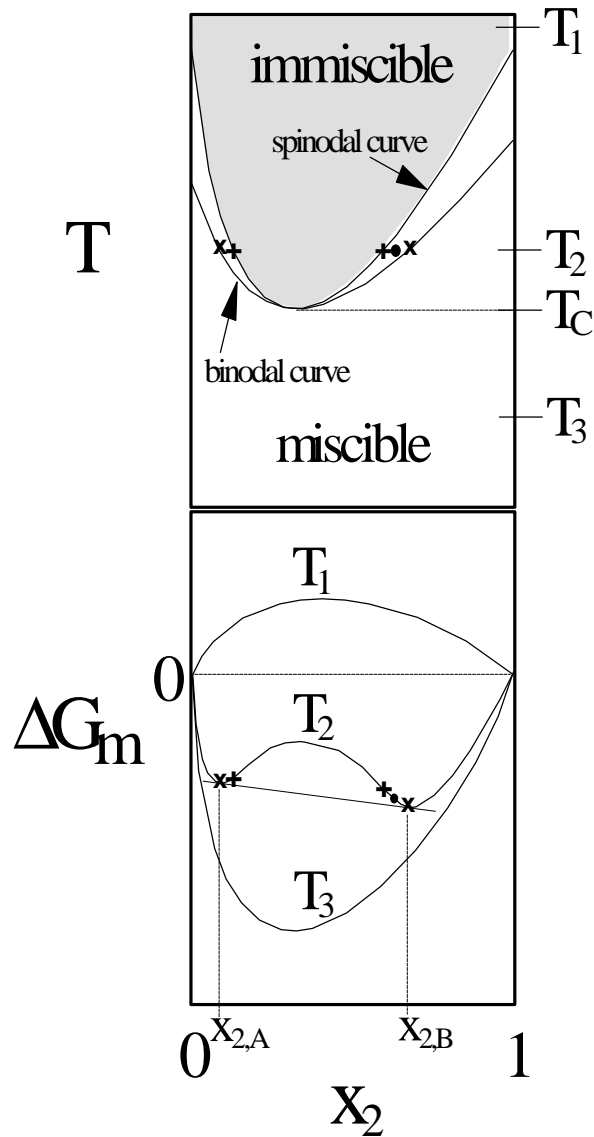


Figure 2-1: General phase diagram (constant pressure) for binary polymer blend system with LCST behavior.

The high molecular weights associated with polymeric materials influences the thermodynamic nature of miscible blend formation relative to mixtures of small molecules, and the notion of "likes dissolve likes" is not necessarily valid for polymer blends. A detailed explanation of this statement first requires brief mention of the general thermodynamic contributions to the free energy change due to mixing. Regardless of the type of mixture considered, the change in Gibbs free energy upon mixing is composed of enthalpic and entropic components:

$$\Delta G_m = \Delta H_m - T \Delta S_m \quad \text{Eqn. 2-5}$$

The  $\Delta S_m$  can be further divided into combinatorial (C) and excess (E) components:<sup>1</sup>

$$\Delta S_m = \Delta S_m^C + \Delta S_m^E \quad \text{Eqn. 2-6}$$

The discussion to follow will initially neglect the excess entropy of mixing and will focus on the combinatorial entropy component and the heat of mixing. However, the implications of the excess entropy on the thermodynamics of polymer-polymer miscibility will be mentioned later.

The Flory-Huggins lattice theory for polymer solutions<sup>8,9</sup> provides a good starting point for developing an understanding of the thermodynamics of polymer blends. Based upon this theory which was derived assuming linear, monodisperse polymer chains, the combinatorial change in entropy upon mixing two polymers, normalized per mole of lattice sites, is as follows<sup>3,7</sup>:

$$\Delta S_m^C = -R \left[ \frac{\phi_1}{n_1} \ln \phi_1 + \frac{\phi_2}{n_2} \ln \phi_2 \right] \quad (\text{per mol lattice site basis}) \quad \text{Eqn. 2-7}$$

In the above expression,  $n_1$  and  $n_2$  are the number of lattice sites occupied by polymer species 1 and 2. Therefore, these parameters are proportional to molecular weight and can be thought of as degrees of polymerization, provided that the repeat units of the two polymers have similar molar volumes. The expression for the heat of mixing according to the Flory-Huggins theory is:

$$\Delta H_m = RT\chi\phi_1\phi_2 \quad (\text{per mol lattice site basis}) \quad \text{Eqn. 2-8}$$

The symbol  $\chi$ , known as the Flory-Huggins interaction parameter or "chi" parameter, can be thought to represent the enthalpic interactions between the different segments of the two polymers, as a first approximation. Assuming that no specific interactions are present between the two species and only dispersive or van der Waals type interactions are involved, then the interaction parameter can be related to the solubility parameter ( $\delta$ ) difference for the two materials:

$$\chi = \frac{v(\delta_1 - \delta_2)^2}{RT} \quad \text{Eqn. 2-9}$$

where  $v$  is an average segmental molar volume for the components.<sup>10</sup> This definition of  $\chi$  only allows positive or zero values of  $\Delta H_m$  according to Eqn. 2-8 which does not help attain the negative  $\Delta G_m$  required for miscibility. For low molecular weight materials, the combinatorial entropy of mixing is a significant positive quantity which is favorable for attaining a negative  $\Delta G_m$ . For mixtures of small molecules, therefore, keeping  $\Delta H_m$  as small a positive quantity as possible by minimizing the difference in solubility parameters (through mixing chemically similar materials or "likes") typically results in miscibility. For a binary polymer system, however, it is clear that the  $\Delta S_m$  term approaches zero in the limit of high molecular weight polymers. This requires a negative value of  $\Delta H_m$  (exothermic mixing) to achieve the negative change in free energy of mixing required for miscibility between two polymers, a seemingly impossible result given the above expression for  $\chi$  (Eqn. 2-9). However, further examination of the interaction parameter will indicate that it can be a negative quantity.

The discovery of numerous miscible polymer blend systems suggests that the interaction parameter can be less than zero, contrary to the above expression for  $\chi$  (Eqn. 2-9). In addition, negative values for the interaction parameter of polymer-polymer mixtures have been experimentally determined using techniques such as small angle neutron scattering and inverse gas chromatography, and research has indicated that exothermic heats of mixing occur for polymer blends.<sup>11-13</sup> The definition of  $\chi$  based upon solubility parameters was developed assuming that no specific interactions are present between the two materials. Complementary chemical structures leading to specific interactions such as hydrogen bonds or aromatic donor / acceptor complexes can lead to negative values of  $\chi$  and  $\Delta H_m$ .<sup>1</sup> In blends where at least one component is a random copolymer, miscibility does not need to be a result of specific interactions but rather a negative  $\chi$  can be derived from a repulsion effect.<sup>14-20</sup> As an example, the interaction parameter can be expressed as follows for a blend of a homopolymer (A) made up of type 1 segments and a random copolymer (B) composed of molecular units 2 and 3:<sup>14,15</sup>

$$\chi_{A,B} = b \chi_{1,2} + (1-b) \chi_{1,3} - b(1-b) \chi_{2,3} \quad \text{Eqn. 2-10}$$

The variable  $b$  denotes the mole fraction of the type 2 repeat unit in the copolymer, and

the  $\chi$  subscripts indicate which two molecular units are associated with each binary interaction parameter. A negative interaction parameter between the homopolymer and the copolymer ( $\chi_{A,B}$ ) can be obtained for a range of copolymer compositions even if the interaction parameters between all of the different segments are all greater than zero. This can occur if more repulsion exists between the chemically linked copolymer units 2 and 3 than is present between either of these units and the homopolymer unit 1:

$$0 < \chi_{1,2} < \chi_{2,3} \quad \text{and} \quad 0 < \chi_{1,3} < \chi_{2,3} \quad \text{Eqn. 2-11}$$

with the magnitudes of the inequalities dictated by the copolymer composition, b. Poly(methyl methacrylate) is not miscible with either polystyrene or polyacrylonitrile but yet it can form miscible blends with poly(styrene-*co*-acrylonitrile) for statistical copolymers with approximately 9 to 30 wt.% acrylonitrile due to the copolymer repulsion effect.<sup>18,20</sup> ‡ The requirement of an exothermic (negative) value of  $\Delta H_m$  for miscibility in high molecular weight polymers due to a negligible combinatorial entropy of mixing is not necessarily applicable in cases where significant self-associations exist in the pure components to be blended. If specific interactions (i.e. hydrogen bonds) are present in a neat polymer, then blending with another polymeric species can result in a miscible mixture despite an endothermic (positive) value  $\Delta H_m$ . A positive heat of mixing will occur if breaking the intermolecular self-interactions present in the two pure species requires more heat than is given off by the formation of any interactions between the different polymers upon blending. Breaking the self-associations in the pure components can also enact a larger increase in configurational entropy upon mixing relative to that predicted by Eqn. 2-7, and this overcomes the positive heat of mixing thus leading to miscibility.<sup>21</sup>

The interaction parameter does not just simply reflect segmental attractions/repulsions which are purely enthalpic in nature as previously implied. It is now recognized that this parameter also reflects the excess entropy of mixing which is thought to be attributable in part to changes in volume with mixing, not accounted for in the

---

‡ Although aliphatic polyesters with a single repeat unit are not considered “copolymers”, it has been observed that the ratio of aliphatic backbone carbons to ester groups can affect the miscibility of polyesters with other polymers due to the repulsion effect.<sup>16,17</sup>

combinatorial entropy function. The right hand side of Eqn. 2-8 should therefore be associated with a change in Gibbs free energy<sup>2,10</sup> instead of solely a change in enthalpy and should be redefined as follows:

$$\Delta H_m - T \Delta S_m^E = R T \chi \phi_1 \phi_2 \quad (\text{per mol lattice site basis}) \quad \text{Eqn. 2-12}$$

For miscible polymer-polymer blends, especially those with specific interactions between the components, it is common for volume contraction to occur with mixing (negative  $\Delta V_m$ ), and this is expected to cause the excess change in entropy to be negative.<sup>1</sup> This is unfavorable for miscibility and must be overcome by the negative  $\Delta H_m$ . The realization of LCST behavior for polymer-polymer blends requires  $\chi$  to become less negative as temperature is increased by either  $\Delta H_m$  becoming less negative or by  $T \Delta S_m^E$  becoming more negative. According to Sanchez,<sup>22</sup> LCST behavior in polymer blends is associated with equation of state effects and can be attributed to a heightened degree of volumetric contraction upon mixing as temperature is increased, leading to an increase in the negative value of  $\Delta S_m^E$ . Another possible explanation is that increasing temperature reduces the number of specific interactions due to increased thermal "kicking" of the polymer segments which would decrease the number of specific interactions and the magnitude of the exothermic heat of mixing.<sup>23</sup> It is clear that  $\chi$  is a complex "black box" parameter which accounts for both entropic and enthalpic effects. Accordingly,  $\chi$  is often observed to be a function of temperature, blend composition, and species molecular weight in addition to depending on the nature of the repulsive/attractive interactions between the molecular segments comprising the polymers to be blended.<sup>4,7</sup>

The previous discussions have dealt only with the equilibrium thermodynamics of polymer blends in the amorphous state. Some complexities which affect the phase behavior of polymer blends are worth noting. Mechanical melt blending of amorphous polymers in the viscous liquid region above the highest component glass transition may limit the degree of attainable intimate contact between the pure polymers, thus preventing formation of the miscible state dictated by thermodynamics. It is also likely that stress and strain fields perturb the actual thermodynamics of a polymer blend. Polymers are sometimes blended by dissolution into a common solvent followed by casting, and,

although the ternary polymer-polymer-solvent system may be a homogenous mixture, thermodynamics may not be favorable for miscibility between the two polymers in the absence of the solvent. This may result in a non-equilibrium blend where the two components are in close contact with each other and appear to be miscible in the glassy state, but this is simply a consequence of their inability to obtain the desired phase-separated state due to mobility constraints. Crystallization of one or all of the polymers comprising a miscible polyblend is another complicating feature.

## **2.2 Compositional Dependence of Properties**

Polymer blends are developed for the purpose of attaining unique combinations of characteristics. Miscible polymer blends can display some properties which are intermediate to the characteristics of the pure constituents, but they can also exhibit responses not expected based upon the behavior of the neat polymers. Because the glass transition temperature is an important application property which is also interconnected with relaxations in the glassy state, the compositional behavior of this parameter in miscible polyblends will be discussed. This discussion will include an in-depth examination of predictive expressions for blend  $T_g$  values. These expressions are often used without an understanding of the basic principles and simplifying assumptions employed in their development. Typical experimentally observed dependencies of mechanical and barrier properties on blend content will also be considered. An examination of the properties of miscible blends is useful because the factors leading to unique compositional property dependencies may also contribute to the role of blend composition on physical aging rates.

### ***2.2.1 Glass Transition Temperature***

One of the most widely employed criteria used to establish miscibility for a mixture of two polymers is the presence of a single glass transition temperature for the blend. As illustrated in Figure 2-2, miscible amorphous polyblends exhibit a single glass-to-rubber transition temperature which is generally located between the glass transitions of the pure constituents. The presence of only one  $T_g$  for miscible blend systems is unlike immiscible

binary polymer blends which have two glass transitions located near the temperatures corresponding to the component  $T_g$  values.<sup>3</sup> The effect of blend composition on the glass transition is specific to the nature of each blend system. Some commonly observed  $T_g$  dependencies on blend composition for miscible polyblends are indicated in Figure 2-3, although more complex functions have also been observed including S-shaped curves.<sup>24</sup>

The observation of a single  $T_g$  in a miscible blend using a macroscopic technique such as differential scanning calorimetry (DSC) or dynamic mechanical analysis (DMA) does not infer that the homogeneous behavior extends to the molecular level or, in other words, that the segments of the two species are intimately mixed.<sup>25</sup> A “miscible” blend can possess small heterogeneous regions, but unless these regions contribute significantly to the mass of the sample, a single glass transition will still be realized using DSC and DMA techniques. The presence of microheterogeneities in polymer blends composed of polymers which have different  $T_g$  values often increases the breadth of the glass transition temperature region relative to the breadth values for the neat polymers which are typically less than 10°C. Microheterogeneities are regions in the blend where the local concentration differs from the bulk blend composition and these concentration fluctuations are thought to be responsible for the broadening of the blend relaxation response.<sup>26-28</sup> In some polymer blend systems the  $T_g$  broadening is noticeable, but small, and in other systems the blends exhibit glass transition breadths which are far greater than those of the pure constituents. A noteworthy contrast exists between a 50/50wt. miscible blend of atactic polystyrene (a-PS) with poly(2,6-dimethyl-1,4-phenylene oxide) (PPO) which exhibits a DSC  $T_g$  breadth which is approximately 20°C and a 50/50wt. blend of a-PS with poly(vinyl methyl ether) (PVME) which has a breadth of 50°C.<sup>29</sup> Despite this large  $T_g$  breadth difference for these two blends, the a-PS/PPO and a-PS/PVME blend systems are similar in other respects. For example, the differences in the pure component glass transition temperatures for the two blend systems are very similar ( $T_g(\text{PVME}) \cong -30^\circ\text{C}$ ,  $T_g(\text{a-PS}) \cong 100^\circ\text{C}$ ,  $T_g(\text{PPO}) \cong 210^\circ\text{C}$ ) and the  $T_g$  breadth values of the pure homopolymers are all on the order of 10°C. However, concentration fluctuations are likely greater in the a-PS/PVME blend system compared to blends of a-PS with PPO, causing the difference between the blend  $T_g$  breadth characteristics of these two blend

systems. Microheterogeneities have been observed in both of these blend systems<sup>26-28</sup> although their severity and associated influence on the glass transition breadth have not been directly contrasted for these two polyblend systems which are both generally classified as miscible.

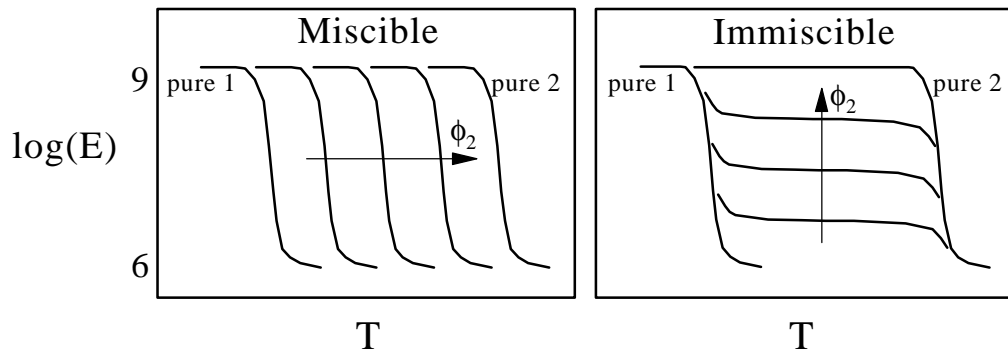


Figure 2-2: General schematic of modulus variation with temperature (constant testing rate) for miscible and immiscible amorphous polymer blends as a function of blend composition in the glass-to-rubber transition region(s) (adapted from ref. 3).

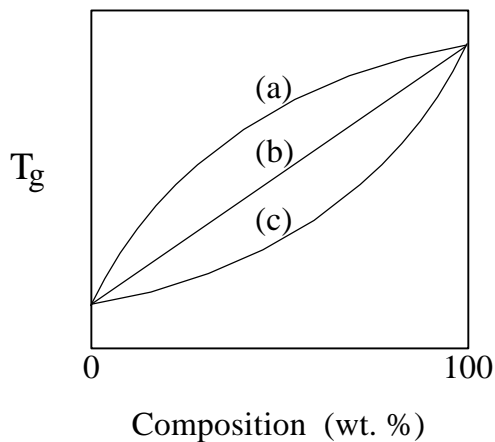


Figure 2-3: Some commonly observed dependencies of  $T_g$  on composition for miscible polymer blends. Additivity for  $T_g$  is illustrated (b) as well as positive (a) and negative (c) deviations thereof.

The attraction of being able to relate the glass transition temperature of a miscible blend to the  $T_g$  values of the pure components has led to the development of several predictive expressions. Basic thermodynamics form the basis from which most of these

expressions are developed, and an examination of the derivation procedures will allow better inspection of the simplifications necessary to achieve the commonly utilized equations. The basic approach used in these derivations was outlined by Couchman<sup>30,31</sup>, and these references will serve as a guide for the following discussion. The entropy of a blend in both the liquid (l) and glassy (g) states can be expressed as an additive function of the pure component entropies plus the corresponding excess change in entropy due to mixing ( $\Delta S_m$ ):

$$S^l = \sum_i w_i S_i^l + \Delta S_m^l \quad \text{and} \quad S^g = \sum_i w_i S_i^g + \Delta S_m^g \quad \text{Eqn. 2-13}$$

where  $w_i$  is the weight fraction of species  $i$ . If the glass transition temperature of the mixture ( $T_g$ ) is treated as a second order thermodynamic transition, the different expressions for the entropy of the mixture in the glassy state and the liquid state must provide continuity of the entropy at  $T_g$  (i.e.  $S^l = S^g$  at  $T = T_g$ ). This allows the following expression to be derived:

$$\sum_i w_i (S_i^l - S_i^g) = \Delta S_m^g - \Delta S_m^l \quad \text{at } T = T_g \quad \text{Eqn. 2-14}$$

Changes in entropy are easily expressed in terms of the heat capacity, and the entropy values for the pure species at the mixture  $T_g$  can be determined from a reference state entropy and the entropy change associated with changing the temperature from the reference temperature to  $T_g$ . Using the species glass transition temperatures as reference states is convenient because the reference state in the glass is identical to that in the liquid for a component, thus allowing the reference state entropies to cancel when the entropy expressions are substituted into Eqn. 2-14, thus resulting in:

$$\sum_i w_i \int_{T_{gi}}^{T_g} \frac{\Delta C_{p_i}}{T} dT = \Delta S_m^g - \Delta S_m^l \quad \text{where } \Delta C_{p_i} = C_{p_i}^l - C_{p_i}^g \quad \text{Eqn. 2-15}$$

The assumption that the values of  $\Delta C_{p_i}$  are largely independent of temperature allows integration to give:

$$\ln T_g = \frac{w_1 \Delta C_{p1} \ln T_{g1} + w_2 \Delta C_{p2} \ln T_{g2} + \Delta S_m^g - \Delta S_m^l}{w_1 \Delta C_{p1} + w_2 \Delta C_{p2}} \quad \text{Eqn. 2-16}$$

Using similar approaches, expressions for the glass transition of a miscible blend can be developed using enthalpy as a basis, again assuming  $\Delta C_{p_i}$  to be temperature independent:

$$T_g = \frac{w_1 \Delta C_{p1} T_{g1} + w_2 \Delta C_{p2} T_{g2} + \Delta H_m^g - \Delta H_m^l}{w_1 \Delta C_{p1} + w_2 \Delta C_{p2}} \quad \text{Eqn. 2-17}$$

and through the use of the thermodynamic variable of volume:

$$T_g = \frac{w_1 (\Delta \alpha_1 / \rho_1) T_{g1} + w_2 (\Delta \alpha_2 / \rho_2) T_{g2} + \Delta V_m^g - \Delta V_m^l}{w_1 (\Delta \alpha_1 / \rho_1) + w_2 (\Delta \alpha_2 / \rho_2)} \quad \text{Eqn. 2-18}$$

In Eqn. 2-18,  $\Delta \alpha_i$  represents the difference between the liquid and glassy thermal expansion coefficients for a pure species,  $\rho_i$  denotes the density of a pure component, and, for derivation purposes, the ratio of these two parameters is considered to be an insignificant function of temperature.

It is clear that the above equations cannot be used without knowledge of the nature of excess mixing properties in both the liquid and glassy states. To eliminate the excess property terms from the predictive expressions requires the use of one of two possible assumptions. One assumption is that the excess properties are negligible for both the liquid and glassy states. This is certainly not valid in a general sense, because, although the changes in entropy with mixing are certainly small for high molecular weight blend components (assuming strong self-associations are absent), values of  $\Delta H_m$  and  $\Delta V_m$  are known to be substantial for many miscible polyblend systems. A second approach to eliminating the necessity of excess property values in the blend  $T_g$  predictions is to assume that the excess properties are equivalent in the liquid and glassy states such that they cancel in the predictive expressions. However, there is no justification for this second assumption either, and no conceptual difficulty exists with regards to a discontinuity in excess properties at the glass transition of a miscible mixture as explained by Goldstein<sup>32</sup>. In fact the whole concept of an excess property in the glassy state is somewhat undefined<sup>33</sup>

as will be explained. As is well known, temperature and pressure can both be varied for a material in either the liquid or glassy state, thus serving as experimental justification for the development of the Ehrenfest relationships. However, blend concentration and temperature are the variables of interest in the formulation of predictive  $T_g$  expressions. Illustrated in Figure 2-4 is a thermodynamic cycle composed of constant temperature and constant composition steps traversing both the liquid and glassy states for an amorphous two-component miscible blend system. Step 4 of this cycle is an experimental impossibility because composition changes in the glassy state, which require extensive diffusion of the components, are not possible due to the low mobility afforded the molecules in the glass. Angell et al<sup>33</sup> state that the “...only sort of mixing conceptually compatible with the glassy state is ‘ideal mixing’, i.e., a process in which labels are changed but positions remain inviolate...” This definition of mixing in the glassy state does not allow volume contraction (negative  $\Delta V_m^g$ ) nor the formation of specific enthalpic interactions between the different blend species in the glass which are not present between molecules of the pure components. In summary, the glass transition of miscible polymer blends cannot be rigorously predicted using the thermodynamic approach formulated above due to the inability to eliminate excess properties from  $T_g$  predictions without the use of unfounded assumptions and, at a more basic level, due to the undefined nature of excess mixing properties in the glassy state.

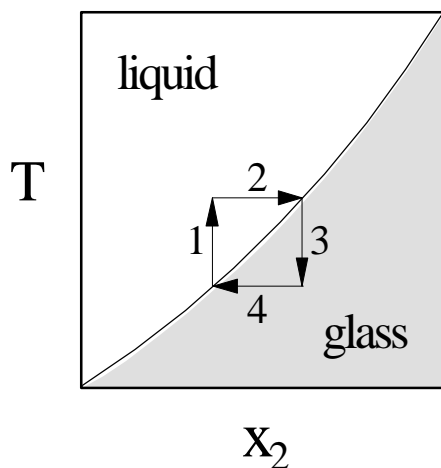


Figure 2-4: Thermodynamic cycle which cannot be performed experimentally (step 4 is

impossible) for an amorphous miscible blend system. Figure adapted from reference 33.

The commonly used expressions in the prediction of blend  $T_g$  values are all simplifications of either Eqn. 2-16, 2-17, or 2-18. If the excess entropy properties are assumed negligible or equivalent for the liquid and glassy states then the Couchman-Karasz expression<sup>34</sup> is obtained from Equation 2-16:

$$\ln T_g = \frac{w_1 \Delta C_{p1} \ln T_{g1} + w_2 \Delta C_{p2} \ln T_{g2}}{w_1 \Delta C_{p1} + w_2 \Delta C_{p2}} = \frac{w_1 \ln T_{g1} + K w_2 \ln T_{g2}}{w_1 + K w_2} \quad \text{Eqn. 2-19}$$

where  $K = \Delta C_{p2} / \Delta C_{p1}$ . The Couchman-Karasz equation is sometimes used in its approximate form (see Addendum for derivation) which is as follows, again with  $K = \Delta C_{p2} / \Delta C_{p1}$ :

$$T_g = \frac{w_1 \Delta C_{p1} T_{g1} + w_2 \Delta C_{p2} T_{g2}}{w_1 \Delta C_{p1} + w_2 \Delta C_{p2}} = \frac{w_1 T_{g1} + K w_2 T_{g2}}{w_1 + K w_2} \quad \text{Eqn. 2-20}$$

Equation 2-20 can also be obtained through the use of Equation 2-17 if the excess enthalpy parameters are deemed insignificant or are assumed equal for the liquid and glassy states. In a similar manner, elimination of the volume changes upon mixing from Equation 2-18 allows simplification to give the Gordon-Taylor<sup>35</sup> equation:

$$T_g = \frac{w_1 (\Delta\alpha_1 / \rho_1) T_{g1} + w_2 (\Delta\alpha_2 / \rho_2) T_{g2}}{w_1 (\Delta\alpha_1 / \rho_1) + w_2 (\Delta\alpha_2 / \rho_2)} = \frac{w_1 T_{g1} + K w_2 T_{g2}}{w_1 + K w_2} \quad \text{Eqn. 2-21}$$

where  $K = (\rho_1 \Delta\alpha_2) / (\rho_2 \Delta\alpha_1)$ . The parameters necessary to predict blend  $T_g$  values can be reduced down to the pure component glass transition temperatures and the component weight fractions by applying additional assumptions to Eqns. 2-19, 2-20, and 2-21. Assuming that the  $K$  parameter is equal to 1.0, the Couchman-Karasz (Equation 2-19) expression becomes a logarithmic additivity expression for  $T_g$ :

$$\ln T_g = w_1 \ln T_{g1} + w_2 \ln T_{g2} \quad \text{Eqn. 2-22}$$

and Eqns. 2-20 and 2-21 simplify to the weight-average rule of mixtures using the same assumption:

$$T_g = w_1 T_{g1} + w_2 T_{g2} \quad \text{Eqn. 2-23}$$

Another set of assumptions can be employed (see Addendum) to simplify the Gordon-Taylor equation to a form equivalent to the Fox equation<sup>36</sup> developed for predicting the glass transition of random copolymers:

$$\frac{1}{T_g} = \frac{w_1}{T_{g1}} + \frac{w_2}{T_{g2}} \quad \text{Eqn. 2-24}$$

Although the expressions above (Eqns. 2-19 to 2-24) were all derived from the basic thermodynamic approach leading to Eqns. 2-16 to 2-18, different assumptions were employed in their development. Therefore, the compositional variation of  $T_g$  predicted for a blend system depends greatly on which simplified equation is used. This is clearly evident in Figure 2-5 which presents experimental  $T_g$  data for the atactic polystyrene (a-PS) / poly(2,6-dimethyl-1,4-phenylene oxide) (PPO) blend system as well as predictions based on the Gordon-Taylor (volume additivity), Couchman-Karasz (entropy additivity), and Fox equations.<sup>31</sup> In addition to the realization that the predictions can be markedly different depending on the equations employed, an important concept to gain from Figure 2-5 is that the Fox equation (Eqn. 2-24) does not represent volume additivity, a common misconception. The Fox equation can be derived from the Gordon-Taylor volume additivity equation but the use of the additional assumptions  $\rho_1=\rho_2$  and  $\Delta\alpha_1 T_{g1} = \Delta\alpha_2 T_{g2}$  is necessary (see Addendum to this section).

There are additional expressions attempting to predict the glass transition temperature of miscible polyblends as a function of blend content. Some of the approaches merely add higher order composition terms ( $w_1^2$ ,  $w_1w_2$ , etc...) with empirical weights and are accordingly not based upon sound principles. Other approaches attempt to introduce the effect of component interactions using a thermodynamic basis similar to the approach explained previously. However, these derivations are also subject to the aforementioned dubious understanding concerning the relative nature of liquid and glassy excess properties. It is really the *difference* between the strength of interactions, and accompanying effect on excess properties, for the glassy state relative to the liquid state which dictates the glass transition behavior of a miscible polyblend. It is therefore not useful in the context of this review to develop an in-depth discussion of other predictive

approaches which do not contribute much additional insight into how to resolve the fundamental difficulty of rigorously predicting the glass transition temperature of miscible blends.

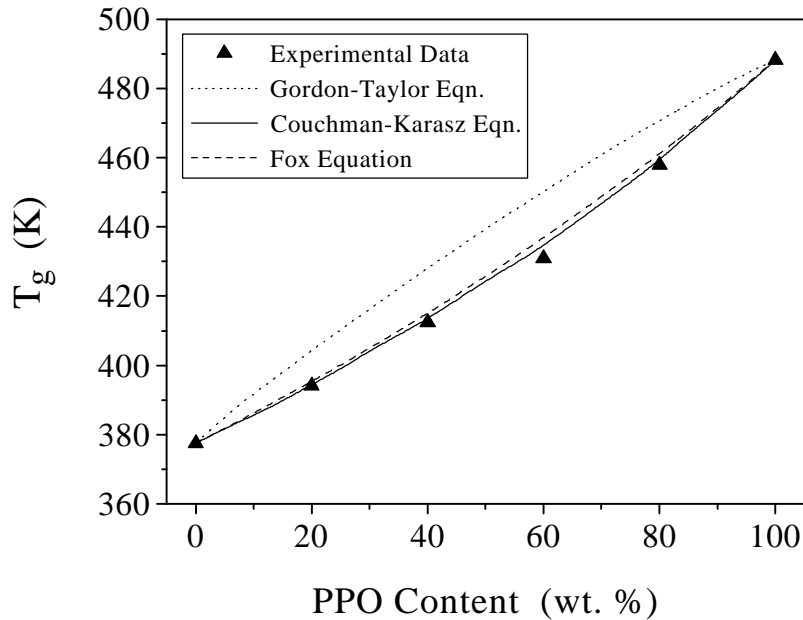


Figure 2-5: Experimental and predicted  $T_g$  values for the a-PS/PPO blend system. Gordon-Taylor and Couchman-Karasz predictions as well as experimental data replotted from reference 31. Prediction using Fox equation calculated based upon the indicated  $T_g$  values of the pure components.

---

### Addendum to Section 2.2.1

#### Convert Couchman-Karasz to approximate form

Start with the Couchman-Karasz expression:

$$\ln T_g = \frac{w_1 \Delta C_{p1} \ln T_{g1} + w_2 \Delta C_{p2} \ln T_{g2}}{w_1 \Delta C_{p1} + w_2 \Delta C_{p2}}$$

Add and subtract the term  $w_2 \Delta C_{p2} \ln T_{g1}$  in the numerator of the above and rearrange to give:

$$\ln T_g = \frac{(w_1 \Delta C_{p1} + w_2 \Delta C_{p2}) \ln T_{g1} + w_2 \Delta C_{p2} (\ln T_{g2} - \ln T_{g1})}{w_1 \Delta C_{p1} + w_2 \Delta C_{p2}}$$

Simplify and combine log terms:

$$\ln \left( \frac{T_g}{T_{g1}} \right) = \frac{w_2 \Delta C_{p2} \ln \left( \frac{T_{g2}}{T_{g1}} \right)}{w_1 \Delta C_{p1} + w_2 \Delta C_{p2}}$$

Add and subtract 1.0 in the natural log terms:

$$\ln \left( \frac{T_g}{T_{g1}} + 1 - 1 \right) = \frac{w_2 \Delta C_{p2} \ln \left( \frac{T_{g2}}{T_{g1}} + 1 - 1 \right)}{w_1 \Delta C_{p1} + w_2 \Delta C_{p2}}$$

$$\ln \left( 1 + \frac{T_g - T_{g1}}{T_{g1}} \right) = \frac{w_2 \Delta C_{p2} \ln \left( 1 + \frac{T_{g2} - T_{g1}}{T_{g1}} \right)}{w_1 \Delta C_{p1} + w_2 \Delta C_{p2}}$$

Employ the approximation  $\ln(1+y) \approx y$  which is valid when  $y$  is a small fractional number.

For example:

$$\ln \left( 1 + \frac{T_{g2} - T_{g1}}{T_{g1}} \right) \approx \frac{T_{g2} - T_{g1}}{T_{g1}}$$

When  $T_{g1} = 300\text{K}$  and  $T_{g2} = 350\text{K}$ , the left and right side of the above approximation agree

to within 8%, and this approximation becomes even more applicable when the  $T_g$  difference is smaller. Use of this approximation results in the following:

$$\frac{T_g - T_{g1}}{T_{g1}} = \frac{w_2 \Delta C_{p2} \left( \frac{T_{g2} - T_{g1}}{T_{g1}} \right)}{w_1 \Delta C_{p1} + w_2 \Delta C_{p2}}$$

Rearrangement gives the approximate Couchman-Karasz equation:

$$T_g = \frac{w_1 \Delta C_{p1} T_{g1} + w_2 \Delta C_{p2} T_{g2}}{w_1 \Delta C_{p1} + w_2 \Delta C_{p2}} = \frac{w_1 T_{g1} + K w_2 T_{g2}}{w_1 + K w_2}$$

where  $K = \Delta C_{p2} / \Delta C_{p1}$ .

### Simplify the Gordon-Taylor equation to the Fox equation

Start with the Gordon-Taylor equation:

$$T_g = \frac{w_1(\Delta\alpha_1 / \rho_1)T_{g1} + w_2(\Delta\alpha_2 / \rho_2)T_{g2}}{w_1(\Delta\alpha_1 / \rho_1) + w_2(\Delta\alpha_2 / \rho_2)} = \frac{w_1 T_{g1} + K w_2 T_{g2}}{w_1 + K w_2}$$

where  $K = (\rho_1 \Delta\alpha_2) / (\rho_2 \Delta\alpha_1)$ . Assume densities are equivalent for the two components and use the Simha-Boyer<sup>37</sup> rule which states that  $\Delta\alpha T_g \approx \text{constant}$ . Use of these two assumptions allows the substitution  $K = T_{g1} / T_{g2}$  which results in:

$$T_g = \frac{w_1 T_{g1} + w_2 T_{g1}}{w_1 + \left(T_{g1}/T_{g2}\right)w_2} = \frac{T_{g1}}{w_1 + \left(T_{g1}/T_{g2}\right)w_2}$$

The fact that the weight fractions of the two components must add to equal unity ( $w_1 + w_2 = 1$ ) was utilized in the above simplification. Inverting this equation and simplifying results in the Fox equation:

$$\frac{1}{T_g} = \frac{w_1}{T_{g1}} + \frac{w_2}{T_{g2}}$$

---

### **2.2.2 Barrier and Mechanical Properties**

In the review of polymer-polymer miscibility, it was mentioned that it is common for a negative  $\Delta V_m$  to occur for polyblends which derive their miscibility from specific interactions. This heightened state of molecular packing for the blends in comparison to the pure polymers influences the mechanical properties in the glassy state. The compositional dependence of specific volume at room temperature is presented in Figure 2-6 as well as the corresponding modulus data for the a-PS/PPO blend system studied by Kleiner and coworkers.<sup>38,39</sup> Because the a-PS/PPO blends are more densely packed than expected based upon the densities of the pure components, mobility is less than expected

for the blends which leads to the observed positive deviation of mechanical stiffness. Based on research on the a-PS/PPO system performed by Kambour et al<sup>40</sup>, compressive yield stress is another mechanical property which exhibits a similar synergy to that observed for tensile modulus as is evident in Figure 2-7. The negative  $\Delta V_m$  observed for this polyblend system in the glassy state also causes some mechanical responses to be less than desirable. This can be observed in Figure 2-7 which indicates that the crack propagation energy is lower for the a-PS/PPO blends than anticipated based upon additivity of the responses for the components in pure form.

The barrier properties of miscible polymer blends are also influenced by the compositional dependence of density. Intuitively, the solubility and diffusivity of small molecules in glassy polymer films are expected to be related to the amount of unoccupied volume surrounding the polymer chain segments. The sorption rate and equilibrium sorption of n-hexane are indeed influenced by the variation of specific volume with blend content for the a-PS/PPO blend system investigated by Hopfenberg, Stannett, and Folk.<sup>41</sup> This data displayed in Figure 2-8 indicates negative compositional deviations from additivity for the sorption properties of the blend, and the magnitudes of these deviations correlate with the negative deviations of specific volume from additivity. A miscible blend system composed of atactic poly(methyl methacrylate) (a-PMMA) and a statistical copolymer of polystyrene and polyacrylonitrile containing 30 wt.% acrylonitrile (SAN30) was investigated by Gsell, Pearce, and Kwei<sup>42</sup>. These researchers observed that the small-molecule transport properties are influenced by the variation of specific volume with composition for this blend system. This variation is quite different from the specific volume function exhibited by the a-PS/PPO system, however. The a-PMMA/SAN30 system, whose miscibility is a result of the copolymer repulsion effect, displays a nearly linear dependence of specific volume on composition and a similar compositional dependence for water vapor diffusivity as illustrated in Figure 2-9.

It is apparent from the previously discussed studies that both mechanical and barrier properties of miscible blend systems are closely related to the variation of the macroscopic volume with blend concentration. In a similar manner, the compositional dependence of mechanical and barrier characteristics of miscible polyblends have also been

experimentally correlated by Hill and coworkers<sup>43,44</sup> with the molecular free volume as probed using positron annihilation lifetime spectroscopy (PALS). Certainly the relative state of packing developed during glass formation in an amorphous miscible blend is also expected to play a role in influencing the physical aging behavior of the blend relative to the aging characteristics of the pure components. This review will now consider research efforts aimed at understanding the physical aging of miscible blends.

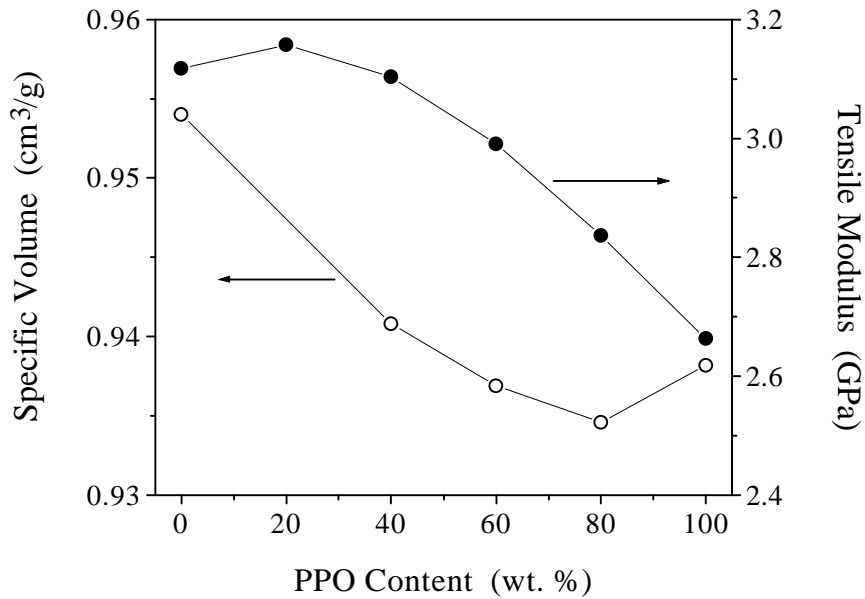


Figure 2-6: Room temperature specific volume and tensile modulus for a-PS/PPO blend system. Data replotted from references 38 and 39.

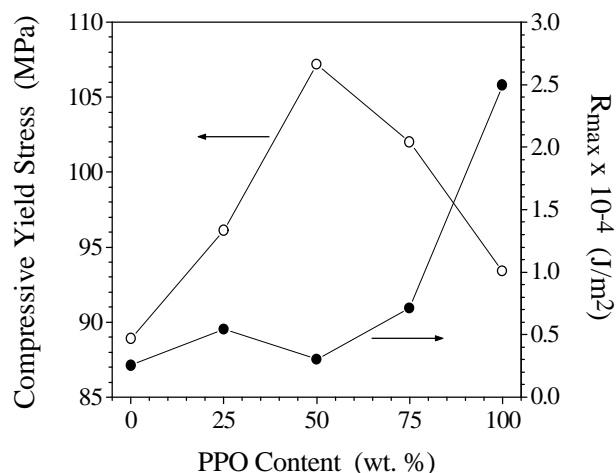


Figure 2-7: Compressive yield stress and maximum crack propagation energy ( $R_{max}$ ) at room temperature for a-PS/PPO blend system. Double-cantilever beam specimens used for crack propagation tests. Data replotted from reference 40.

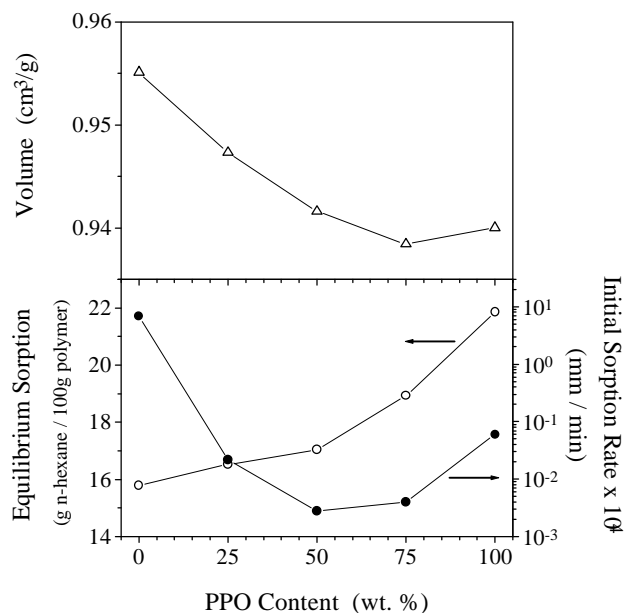


Figure 2-8: Specific volume at 23°C (upper plot) and n-hexane vapor sorption properties at 40°C (lower plot) for a-PS/PPO blends. Prior to testing, samples were annealed for 2 hours at  $T_g + 20^\circ\text{C}$  after solution casting. Sorption data obtained using a ratio of partial pressure to equilibrium vapor pressure (activity) of 0.98. Data replotted from reference 41.

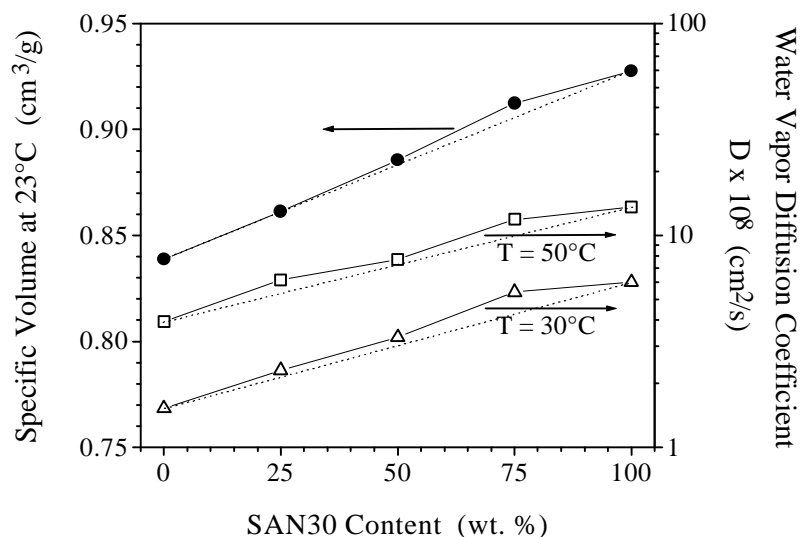


Figure 2-9: Specific volume at 23°C and water vapor diffusion coefficient at 30°C and 50°C for blends of poly(methyl methacrylate) and poly(styrene-co-acrylonitrile)(30 wt.% acrylonitrile). Data replotted from reference 42.

## 2.3 References

- <sup>1</sup> J. W. Barlow and D. R. Paul, *Polym. Eng. Sci.*, **21(15)**, 985 (1981).
- <sup>2</sup> J. M. G. Cowie, *Polymers: Chemistry and Physics of Modern Materials*, second edition, Blackie Academic and Professional, London, 1991.
- <sup>3</sup> D. R. Paul, in *Multicomponent Polymer Materials* (ed. D. R. Paul and L. H. Sperling), Chapter 1, Advances in Chemistry Series, Vol. 211, American Chemical Society, Washington, DC, 1986.
- <sup>4</sup> N. P. Balsara, in *Physical Properties of Polymers Handbook* (ed. J. E. Mark), Chapter 19, A.I.P. Press, Woodbury, NY, 1996.
- <sup>5</sup> O. Olabisi, L. M. Robeson, and M. T. Shaw, *Polymer-Polymer Miscibility*, Academic Press, New York, 1979.
- <sup>6</sup> R. Koningsveld, M. H. Onclin, and L. A. Kleintjens, in *Polymer Compatibility and Incompatibility: Principles and Practices* (ed. K. Solc), MMI Press Symposium Series, Vol. 2, Harwood Academic Publishers, London, 1982.
- <sup>7</sup> H. Marand, personal communication (*Physical Chemistry of High Polymers*, class lectures/notes, Virginia Polytechnic Institute and State University, Fall Semester 1995).
- <sup>8</sup> P. J. Flory, *J. Chem. Phys.*, **10**, 51 (1942).
- <sup>9</sup> M. L. Huggins, *J. Phys. Chem.*, **46**, 151 (1942).

- <sup>10</sup> S. L. Rosen, *Fundamental Principles of Polymeric Materials*, Second Edition, John Wiley and Sons, Inc., New York, 1993.
- <sup>11</sup> N. E. Weeks, W. J. MacKnight, and F. E. Karasz, *J. Appl. Phys.*, **48**, 4068 (1977).
- <sup>12</sup> A. Maconnachie, R. P. Kambour, D. M. White, S. Rostami, D. J. Walsh, *Macromolecules*, **17**, 2645 (1984).
- <sup>13</sup> B. Riedl, R. E. Prud'homme, *J. Polym. Sci.: Part B: Polym. Phys.*, **26**, 1769 (1988).
- <sup>14</sup> R. P. Kambour, J. T. Bendler, and R. C. Bopp, *Macromolecules*, **16(5)**, 753 (1983).
- <sup>15</sup> G. ten Brinke, F. E. Karasz, and W. J. MacKnight, *Macromolecules*, **16(12)**, 1827 (1983).
- <sup>16</sup> D. R. Paul and J. W. Barlow, *Polymer*, **25**, 487 (1984).
- <sup>17</sup> E. M. Woo, J. W. Barlow, and D. R. Paul, *Polymer*, **26**, 763 (1985).
- <sup>18</sup> M. Suess, J. Kressler, and H. W. Kammer, *Polymer*, **28**, 957 (1987).
- <sup>19</sup> J. M. G. Cowie and D. Lath, *Macromol. Chem., Macromol. Symp.*, **16**, 103 (1988).
- <sup>20</sup> N. Nishimoto, H. Keskkula, and D. R. Paul, *Polymer*, **30**, 1279 (1989).
- <sup>21</sup> P. C. Painter, J. F. Graf, and M. M. Coleman, *Macromolecules*, **24(20)**, 5630 (1991).
- <sup>22</sup> I. C. Sanchez, in *Polymer Compatibility and Incompatibility: Principles and Practices* (ed. K. Solc), MMI Press Symposium Series, Vol. 2, Harwood Academic Publishers, London, 1982.
- <sup>23</sup> D. R. Paul and J. W. Barlow, in *Polymer Compatibility and Incompatibility: Principles and Practices* (ed. K. Solc), MMI Press Symposium Series, Vol. 2, Harwood Academic Publishers, London, 1982.
- <sup>24</sup> H. A. Schneider and E. A. DiMarzio, *Polymer*, **33**, 3453 (1992).
- <sup>25</sup> C. D. Han and J. K. Kim, *Polymer*, **34**, 2533 (1993).
- <sup>26</sup> T. K. Kwei, T. Nishi, and R. F. Roberts, *Macromolecules*, **7(5)**, 667 (1974).
- <sup>27</sup> P. T. Inglefield, A. A. Jones, P. Wang, and C. Zhang, *Mat. Res. Soc. Symp. Proc.*, **215**, 133 (1991).
- <sup>28</sup> S. Li, L. C. Dickinson, and J. C. W. Chien, *J. Appl. Polym. Sci.*, **43**, 1111 (1991).
- <sup>29</sup> H. A. Schneider, H.-J. Cantow, C. Wendland, and B. Leikauf, *Makromol. Chem.*, **191**, 2377 (1990).
- <sup>30</sup> P. R. Couchman, *Phys. Letters*, **70A(2)**, 155 (1979).
- <sup>31</sup> P. R. Couchman, *Macromolecules*, **20(7)**, 1712 (1987).
- <sup>32</sup> M. Goldstein, *Macromolecules*, **18(2)**, 277 (1985).
- <sup>33</sup> C. A. Angell, J. M. Sare, and E. J. Sare, *J. Phys. Chem.*, **82(24)**, 2622 (1978).
- <sup>34</sup> P. R. Couchman and F. E. Karasz, *Macromolecules*, **11(1)**, 117 (1978).
- <sup>35</sup> M. Gordon and J. S. Taylor, *J. Appl. Chem.*, **2**, 493 (1952).
- <sup>36</sup> T. G. Fox, *Bull. Am. Phys. Soc.*, **1**, 123 (1956).
- <sup>37</sup> R. Simha and R. F. Boyer, *J. Chem. Phys.*, **37**, 1003 (1962).
- <sup>38</sup> L. W. Kleiner, F. E. Karasz, and W. J. MacKnight. *Polym. Eng. Sci.* **19(7)**, 519 (1979).
- <sup>39</sup> J. R. Fried, *Ph.D. Dissertation*, University of Massachusetts (1976).
- <sup>40</sup> R. P. Kambour and S. A. Smith, *J. Polym. Sci.: Polym. Phys. Ed.*, **20**, 2069 (1982).
- <sup>41</sup> H. B. Hopfenberg, V. T. Stannett, and G. M. Folk, *Polym. Eng. Sci.*, **15(4)**, 261 (1975).

- <sup>42</sup> T. C. Gsell, E. M. Pearce, and T. K. Kwei, *Polymer*, **32(9)**, 1663 (1991).
- <sup>43</sup> M. D. Zipper, G. P. Simon, M. R. Tant, J. D. Small, G. M. Stack, and A. J. Hill, *Polymer International*, **36**, 127 (1995).
- <sup>44</sup> A. J. Hill, M. D. Zipper, M. R. Tant, G. M. Stack, T. C. Jordan, and A. R. Schultz, *J. Phys.: Condens. Matter*, **8**, 3811 (1996).

# Chapter 3

## Review -- Previous Studies Concerned with the Physical Aging of Miscible Polymer Blends

---

The majority of the research to be discussed later is concerned with developing an understanding of the physical aging of miscible polymer blends. Before the details of this research endeavor are established, however, it is important to review the present understanding of the physical aging of miscible polymer blends in order to clearly justify the research which was performed in this study. Literature dealing with the physical aging of miscible polymer blends will be critically reviewed, and all of the literature resulting from an exhaustive search will be discussed, making this review truly comprehensive in nature. The nonequilibrium nature of miscible polyblends has been studied using enthalpy relaxation/recovery measurements and by following changes in mechanical response. Research in these two areas will be discussed in approximate chronological order, and additional insight and analysis, beyond that provided in the literature, will be provided where appropriate.

### 3.1 Enthalpy Relaxation Investigations

Perhaps the earliest investigation of structural relaxation behavior of miscible polymer blends was a study by Kwei and coworkers<sup>1</sup> published in 1978. Atactic poly(methyl methacrylate) (a-PMMA) and poly(styrene-*co*-acrylonitrile) (SAN) with 25.3% AN were melt blended and the enthalpy recovery following isothermal annealing at 85°C was investigated for the miscible blend system as a function of composition. Since the glass transition temperatures of the pure components were very similar ( $T_g = 103.5^\circ\text{C}$  for a-PMMA and  $T_g = 106.5^\circ\text{C}$  for SAN) and the blend  $T_g$  values displayed intermediate behavior relative to the values of the neat polymers, performing aging experiments at a fixed temperature of 85°C provided essentially the same temperature difference ( $\Delta T = T_g -$

$T_a$ ) throughout the entire composition range. This study established that the enthalpy recovery behavior of annealed miscible blend samples heated through the glass transition region exhibited the qualitative features of the characteristic response evident for single component amorphous polymer systems. Although enthalpy relaxation rates were not assessed for the a-PMMA/SAN blend system, it was discovered that the recovered enthalpy after aging for 88 hours at 85°C was approximately the same for the pure components and the blends.

Prest, Luca, and Roberts<sup>2-4</sup> have investigated the enthalpy relaxation response for miscible blends of atactic polystyrene (a-PS) with poly(2,6-dimethyl-1,4-phenylene oxide) (PPO) and for miscible blends of a-PS with poly(vinyl methyl ether) (PVME). The dependence of the enthalpic fictive temperature on aging time was observed to be independent of composition for the a-PS/PPO blends at aging temperatures from 15 to 40°C below  $T_g$ , and hence structural relaxation rates did not vary with PPO content. Although the calorimetric glass transition behavior was broadened for the a-PS/PPO blends compared to the  $T_g$  breadths of the pure components, no compositional dependence was observed for the relaxation time distribution breadth which was inferred from the enthalpy relaxation response for the a-PS/PPO system. This led the authors to the conclusion that concentration fluctuations do not play any significant role in the aging process for the a-PS/PPO polyblends. As was mentioned previously in Chapter 2, blends of a-PS and PVME have extremely broad glass transition responses observed by DSC. The authors did note that the enthalpic aging behavior of a-PS/PVME blends suggested relaxation time distributions which were much broader than those of pure a-PS and PVME. This apparent influence of concentration fluctuations became even more pronounced for a-PS/PVME blends which were heated above the LCST region prior to quenching into the glassy state. This research on the enthalpy relaxation behavior of a-PS/PPO and a-PS/PVME blends is only briefly detailed by the authors in symposium proceedings,<sup>2-4</sup> and, although the authors' discussion relies upon the presence of data, scarcely any of it is given in these references. The authors referred to a more extensive manuscript in preparation, but apparently this paper has yet to be published.

It was recognized that enthalpy relaxation could help elucidate phase behavior of polymer blends by Feijoo et al<sup>5</sup> and Shalaby and Bair<sup>6</sup> in the early 1980's. Later, enthalpy relaxation was clearly shown by ten Brinke, Ellis, and coworkers<sup>7-10</sup> as well as Jorda and Wilkes<sup>11</sup> to be a useful probe in the determination of miscibility of polymer blends when the component  $T_g$  values were in close proximity to one another. As discussed previously, the presence of a single glass transition temperature for a binary polymer mixture is indicative of miscibility, but this criteria cannot be used when there is significant overlap of the glass transition regions of the pure components. Upon sub- $T_g$  annealing, however, if the blend is immiscible then the amorphous components age independently and the appearance of two distinct endothermic recovery peaks is evident upon heating the aged blend through the glass transition region(s).<sup>‡</sup> The general findings of research in this area can be summarized via the schematic presented in Figure 3-1, and research efforts have been thoroughly reviewed in an article by ten Brinke et al.<sup>13</sup> In the course of these studies, the enthalpy relaxation behavior of blends which were found to display miscibility was not clearly compared in a quantitative manner to that of the pure components. In a later publication, however, Oudhuis and ten Brinke<sup>14</sup> referred back to these publications<sup>7-10</sup> and made the general statement that, for miscible blend systems containing polymers with similar  $T_g$  values, the rates of enthalpy relaxation were largely the same for the pure components and the blends.

The enthalpy relaxation of a 50/50wt. solution blend of atactic polystyrene and poly(vinyl methyl ether) has been investigated and contrasted with the relaxation of the two pure blend constituents by Cowie and Ferguson.<sup>15,16</sup> The reference temperature used was the enthalpic fictive temperature for a freshly quenched sample,  $T_{g,f}$ , which was close in value to the DSC midpoint glass transition temperature,  $T_g$ . The enthalpy relaxation was performed isothermally below  $T_{g,f}$ , and the recovered  $\Delta H$  data as a function of aging

---

<sup>‡</sup> Distinct aging characteristics of components in immiscible blends is also manifested in volume relaxation. This concept has been used to allow volume relaxation of one component of an immiscible amorphous polyblend to supercede the relaxation of the other component in order to generate surface relief for microtomed samples, thus allowing phase morphology to be investigated without etching.<sup>12</sup>

time was fit using the Cowie-Ferguson (CF) model which utilizes the KWW stretched exponential relaxation function as indicated below:

$$\Delta H(t_a) = \Delta H_\infty [1 - \phi(t_a)] \quad \text{where } \phi(t_a) = \exp[-(t_a / \tau)^\beta] \quad \text{Eqn. 3-1}$$

The variables  $\tau$  and  $\beta$  are the well-known KWW parameters while  $\Delta H_\infty$  is the total amount of enthalpy relaxation for a sample isothermally aged to enthalpic equilibrium. As is evident from the above expression, the Cowie-Ferguson model incorporates the linear form of the stretched exponential function for the dimensionless decay function which is defined as follows for enthalpy relaxation:

$$\phi(t_a) = \frac{\Delta H_\infty - \Delta H(t_a)}{\Delta H_\infty} \quad \text{Eqn. 3-2}$$

It is this author's opinion that it is not entirely appropriate to use a linear decay function to represent isothermal physical aging which, as was detailed in the previous review of the glassy state, is non-linear. In the CF approach,  $\Delta H_\infty$  is usually treated as an empirical fitting parameter rather than being determined by performing aging until enthalpic equilibrium is reached or by extrapolating the liquid enthalpy curve to the aging temperature ( $\Delta H_\infty \approx \Delta C_p (T_g - T_a)$ ). For an aging temperature equal to  $T_{g,f} - 10^\circ\text{C}$ , the resulting best-fit  $\Delta H_\infty$  parameters for the a-PS/PVME system are indicated in Table 3-I along with independent estimates of  $\Delta H_\infty$  which the authors assessed by extrapolation of the liquid portion of the enthalpy curves for freshly quenched reference samples. Considering the CF values of  $\Delta H_\infty$ , the parameter for the 50/50wt. blend is not intermediate to the values of the pure materials. Because of this and the fact that the ratio of  $\Delta H_\infty$  for the blend to that of PVME is close to the weight fraction of PVME in the blend (ratio = 0.38, weight fraction = 0.50), the authors suggested that the majority of the structural relaxation in the blend could be attributed to the PVME component. However, there is certainly need for caution in accepting this speculative conclusion as will now be discussed.

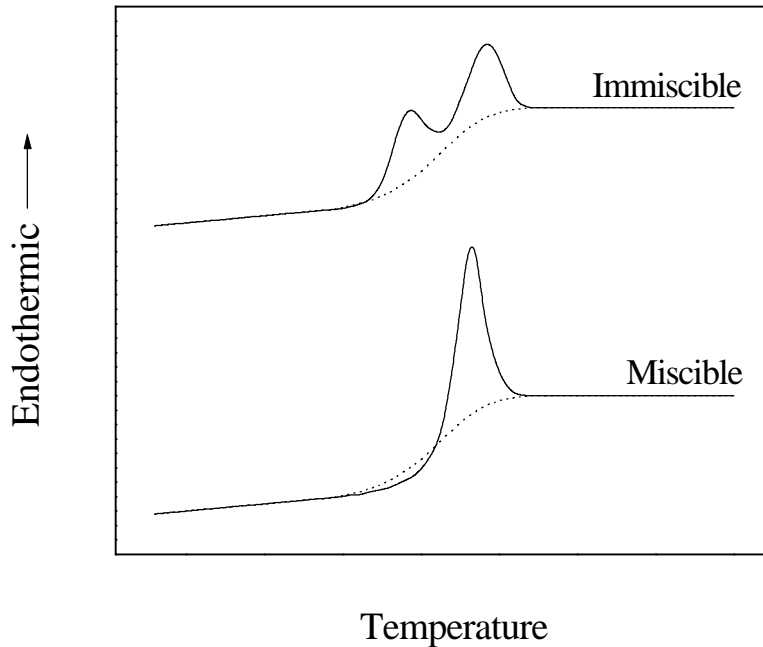


Figure 3-1: Schematic of typical enthalpy recovery behavior (solid lines) following isothermal annealing in the glassy state for binary polymer blends with components possessing similar glass transition temperatures. Dashed lines represent generalized heating scans for freshly quenched blends.

The suggestion by Cowie and Ferguson that the aging in the blend was predominantly due to relaxation of the PVME component is unsettled for several reasons. First, the extrapolated values of  $\Delta H_{\infty}$  indicated that  $\Delta H_{\infty}$  was higher for the 50/50wt. blend than for pure PVME, thus suggesting a different picture than the values determined through the CF fitting procedures. Also, the  $\Delta H$  data which was fit using the CF model had not yet reached equilibrium. The implication of this fact is that a model containing an equilibrium parameter ( $\Delta H_{\infty}$ ) was fit to  $\Delta H$  data which had not clearly reached a plateau with respect to  $\log(t_a)$ . The danger in such a fitting procedure can easily be illustrated via the application of the Cowie-Ferguson model to the example data sets presented in Figure 3-2. As can be seen from the corresponding fitting parameters in Table 3-II, all of the CF equation variables are extremely sensitive to data fluctuations in the absence of  $\Delta H$  data near to, and after attainment of, equilibrium. If indeed the Cowie-Ferguson  $\Delta H_{\infty}$  parameters were truly representative of the behavior of the investigated PVME/a-PS

system, then there is another explanation for the reduced CF  $\Delta H_{\infty}$  value for the 50/50wt. blend relative to the pure component values. Miscible blends of PVME with a-PS are unusual in that the glass transition breadths are considerably greater than the breadths of PVME and a-PS in pure form. The glass transition breadth of the 50/50wt. blend studied by Cowie and Ferguson was 38°C in contrast to the respective values of 3.4°C and 6.7°C for PVME and a-PS. The aging temperatures employed for the blend ranged from -23°C to -3°C which certainly overlapped with the onset glass transition temperature,  $T_{g,o}$ , for the blend which was equal to -14°C. In fact, the aging performed at  $T_{g,f} - 10^{\circ}\text{C}$  for the blend was at a temperature over 10°C higher than the transition onset. The implication of this knowledge is that portions of the blend were likely near or at enthalpic equilibrium before aging was even commenced at  $T_a = T_{g,f} - 10^{\circ}\text{C}$ , logically resulting in a lower  $\Delta H_{\infty}$  value in comparison to the values of the pure components whose aging performed at 10°C below  $T_{g,f}$  was also below  $T_{g,o}$ . This last point which dealt with the breadth of the glass transition has also been mentioned by Oudhius and ten Brinke.<sup>14</sup>

Table 3-I:  $\Delta H_{\infty}$  for PVME, a-PS, and 50/50wt. Blend Aged at  $T_a = T_{g,f} - 10^{\circ}\text{C}$  \*

Material	$\Delta H_{\infty}$ (fit to CF) [J/g]	$\Delta H_{\infty}$ (extrapolated) [J/g]
PVME	2.83 ( $\pm 0.02$ )	3.90
50/50wt. Blend	1.08 ( $\pm 0.02$ )	5.47
a-PS	3.20	not available

\* Data from references 15 and 16

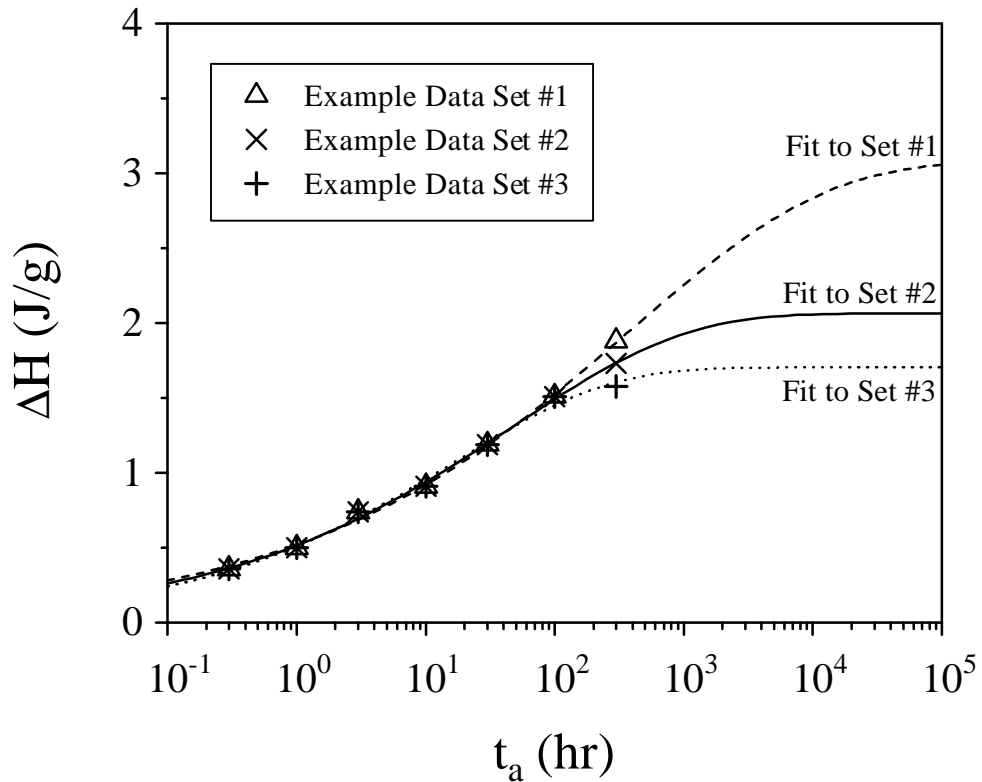


Figure 3-2: Example fits using the Cowie-Ferguson model for illustrative enthalpy recovery “data” which has not yet reached equilibrium. The data sets are identical with the exception of the values at  $t_a = 300$  hours.

Table 3-II: Cowie-Ferguson Parameters Corresponding to Illustrative Fits in Figure 3-2

	$\Delta H_\infty$ [J/g]	$\tau$ [hr]	$\beta$
Fit to Set #1	3.1 ( $\pm 0.7$ )	379 ( $\pm 212$ )	0.28 ( $\pm 0.03$ )
Fit to Set #2	2.1 ( $\pm 0.2$ )	46 ( $\pm 21$ )	0.33 ( $\pm 0.02$ )
Fit to Set #3	1.7 ( $\pm 0.1$ )	17 ( $\pm 6$ )	0.37 ( $\pm 0.03$ )

The effect of blend composition on enthalpy recovery was investigated by Mijovic and coworkers<sup>17,18</sup> for the miscible blend system a-PMMA/SAN following isothermal annealing at temperatures 20, 35, and 50°C below  $T_g$ . Using values of  $\Delta H_\infty$  obtained via extrapolation of the liquid enthalpy curve down to  $T_a$ , the enthalpy relaxation decay functions ( $\phi(t_a) = [\Delta H_\infty - \Delta H(t_a)] / \Delta H_\infty$ ) were compared as a function of composition for the three aging temperature employed. The key finding was that relaxation appeared to proceed at a slightly greater rate for the SAN-rich blends compared to blends with a high PMMA concentration for aging performed at  $T_g - 20^\circ\text{C}$  and  $T_g - 35^\circ\text{C}$ . The decay functions for the a-PMMA/SAN system were essentially identical for aging performed 50°C below  $T_g$  which implies that enthalpy relaxation was independent of composition at this lower aging temperature. Using the Tool-Narayanaswamy-Moynihan (TNM) approach with the typical empirical relaxation time function (see Chapter 1), the DSC heating traces for freshly quenched (unaged) samples were fit by allowing all four model parameters to vary, and the compositional variation of the parameters are evident in Figure 3-3. The authors did not directly comment on the trends exhibited by the model parameters and any associated significance. From Figure 3-3 it can be seen that the parameter  $x$ , which can be thought of as the fractional significance of the actual temperature versus the fictive temperature in determining the relaxation times, appears to display nearly linear intermediate behavior for the blends relative to the pure materials. The parameter associated with the relaxation time breadth,  $\beta$ , also displays an essentially linear compositional dependence. Nothing conclusive can be stated with regard to the other two parameters,  $\Delta h^*$  and  $\ln A$ , since increases in both parameters act in similar ways to shift a predicted curve to higher temperatures, and these effects appeared to offset each other for the a-PMMA/SAN system as can be seen by the opposing compositional trends for these two variables. A more informative approach would be to determine values for the  $\Delta h^*$  parameter independently through techniques involving the heating/cooling rate dependence of the fictive temperature<sup>19</sup>, and then use these fixed  $\Delta h^*$  values during subsequent fitting of heat capacity curves. The compositional dependence of the parameters aside, all of the unaged a-PMMA/SAN heat capacity curves were shown to be

fit quite well in this investigation, and application of the resulting TNM model parameters to the experimental decay functions for the isothermally aged samples also resulted in adequate predictions within experimental error.

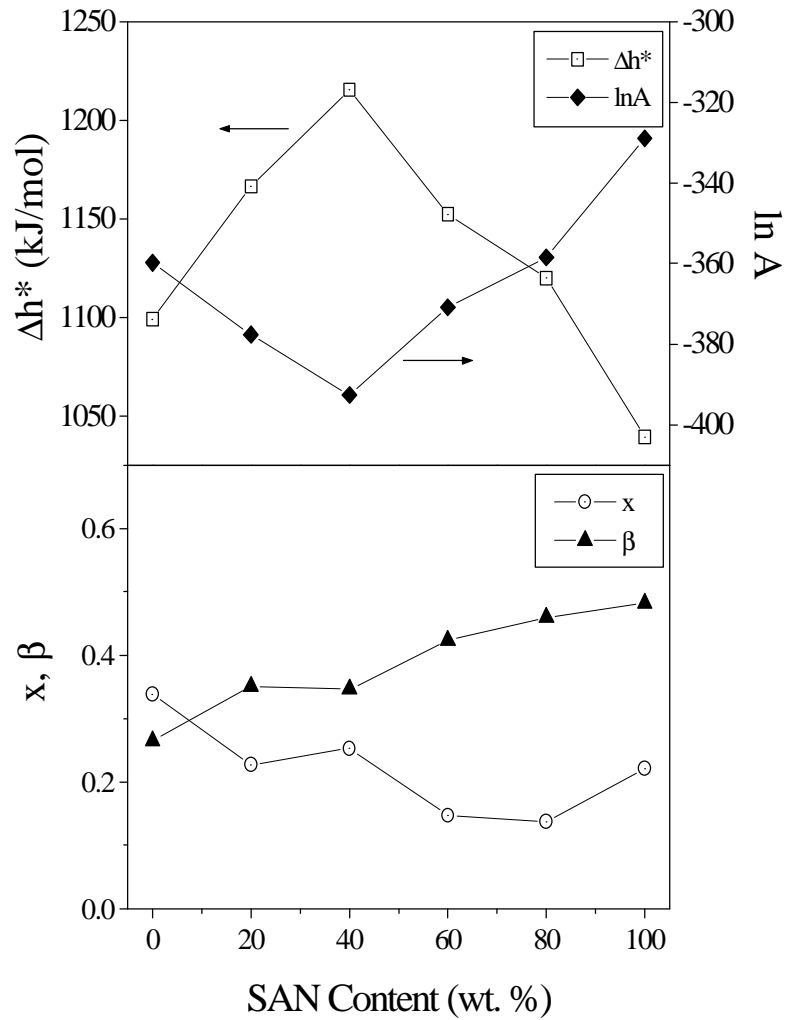


Figure 3-3: Tool-Narayanaswamy-Moynihan parameters fit to normalized DSC heating scans for freshly quenched a-PMMA/SAN samples (100°C/min cooling, 10°C/min heating). Parameters replotted from reference 18.

The enthalpy relaxation of miscible a-PS/PPO blends was studied by Elliot and Cowie, and the influence of blend composition on aging was detailed in Elliot's Ph.D. dissertation.<sup>20</sup> Comparisons were made based upon Cowie-Ferguson model parameters determined from curve fitting to the enthalpy recovery data, and a representative portion of this data is indicated in Figure 3-4. The relaxation time parameter,  $\tau$ , which was assessed by fitting the enthalpy recovery data to the CF model is indicated as a function of composition for the blend system in Figure 3-5a. The trends in the parameter  $\tau$  can also be associated with the average relaxation time  $\langle \tau \rangle$  since there were no substantial compositional variations in  $\beta$ , the parameter associated with the relaxation time breadth. The longer relaxation times evident for the blends relative to those of pure a-PS and PPO were stated by the authors to be consistent with the notion that relaxation hindrances were provided by specific interactions between the components in the blend, although no direct evidence for this connection was presented. It should be pointed out that the  $\Delta H$  data which was fit to the Cowie-Ferguson model had not approached equilibrium, and in fact the  $\Delta H$  data increased in an approximately linear manner with respect to  $\log(t_a)$  (see Figure 3-4). In order to provide another comparison between the aging responses observed for the blends and pure polymers, besides contrasting the CF parameters, the relaxation data of Elliot and Cowie was reanalyzed by this author to determine the values of the enthalpy relaxation rate,  $\beta_H$ . The resulting variation of  $\beta_H$  with blend PPO content is depicted in Figure 3-5b, and interpretation of the enthalpy relaxation data in this manner is inconsistent with the CF relaxation time parameters shown in Figure 3-5a. Although the CF values of  $\tau$  were greater for the blends in comparison to the pure polymers, the enthalpy relaxation rates were faster for the blends which implies lower relative relaxation times. This again highlights the problem with using CF parameters to make quantitative comparisons when fitting is performed on  $\Delta H$  data not obtained close enough to equilibrium. The physical interpretation of the single relaxation time parameter determined from the linear decay function approach is also problematic since structural relaxation is widely viewed as a non-linear process which is characterized by relaxation times which increase as aging progresses.

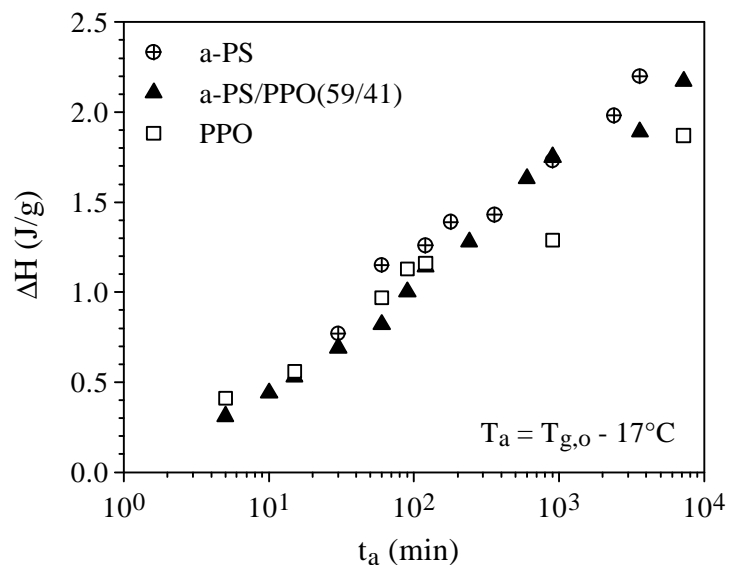


Figure 3-4: Sample of enthalpy relaxation data used to determine  $\tau$  and  $\beta_H$  in Figure 3-5 (data replotted from reference 20).

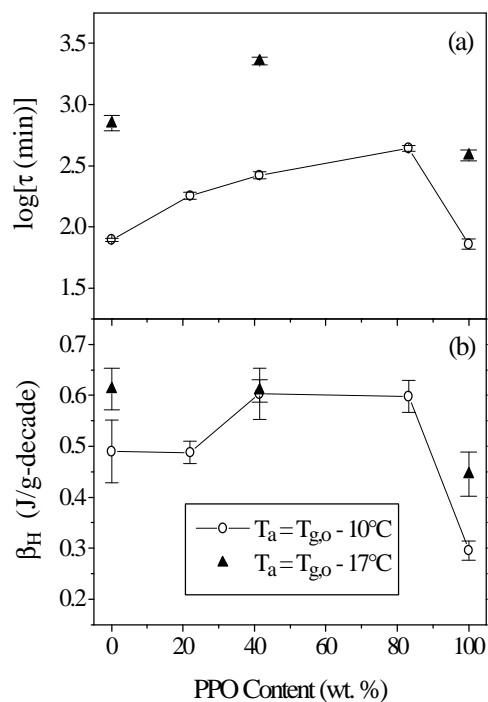


Figure 3-5:(a) Relaxation time,  $\tau$ , from the Cowie-Ferguson model fit to enthalpy relaxation data for a-PS/PPO blends (replotted from reference 20). (b) Enthalpy relaxation rates determined (by this author) from the same  $\Delta H$  data.

An investigation of structural relaxation behavior of miscible a-PS/PPO blends prepared by solution blending was also undertaken by Oudhuis and ten Brinke.<sup>14</sup> This study followed the compositional dependence of enthalpy recovery after isothermal annealing at a temperature 15°C below the onset glass transition temperature,  $T_{g,o}$ . The enthalpy relaxation data were essentially linear with respect to  $\log(t_a)$  for the range of aging times investigated and, hence, rates of enthalpy relaxation ( $\beta_H$  values) can be determined from the data of Oudhuis and ten Brinke for the purposes of this review. These relaxation rates (Figure 3-6) are in agreement with the qualitative observation established by the authors that enthalpy relaxation was significantly slower for the blends relative to the pure components. The  $\beta_H$  values assessed from their data, however, appear to be substantially higher than might be expected which suggests that the  $\Delta H$  data are much larger than expected. For example, the  $\beta_H$  for a-PS was found to be approximately 2.3 J/g-decade which is roughly three times greater than tabulated values for this material aged at a comparable undercooling.<sup>21</sup> It is possible that the  $\Delta H$  values provided by the authors were incorrectly determined from integration of subtracted heat capacity curves which were first made dimensionless via normalization using  $\Delta C_p$  and the heating rate. This would make sense since the DSC traces were also fit using the TNM approach by the authors in this investigation which requires such a normalization endeavor. If the discrepancy is in fact due to the normalization, then the observed trend in  $\beta_H$  is likely still valid because  $\Delta C_p$  typically only varies 0.06 J/g-°C throughout the entire composition range for the a-PS/PPO blend system.<sup>20</sup> The slower aging rates for the blends were attributed to concentration fluctuations in the blend resulting in broader glass transitions for the blends in comparison to the pure component breadths (DSC transition breadths were equal to 5.6, 8.1, and 14.9°C for a-PS, PPO, and 50/50wt. blend, respectively). According to the authors, the significance of this glass transition breadth difference between the blends and the pure polymers was that the blends possessed regions which were further from the aging temperature because aging was performed at a fixed distance of 15°C below the onset glass transition temperature. It was hypothesized that these less-mobile regions possessed longer relaxation times thus resulting in decreased overall

structural relaxation rates for the blends. The inability of the TNM four-parameter model to adequately describe the enthalpy recovery heat capacity curves for the aged blends was also credited to the presence of concentration fluctuations.

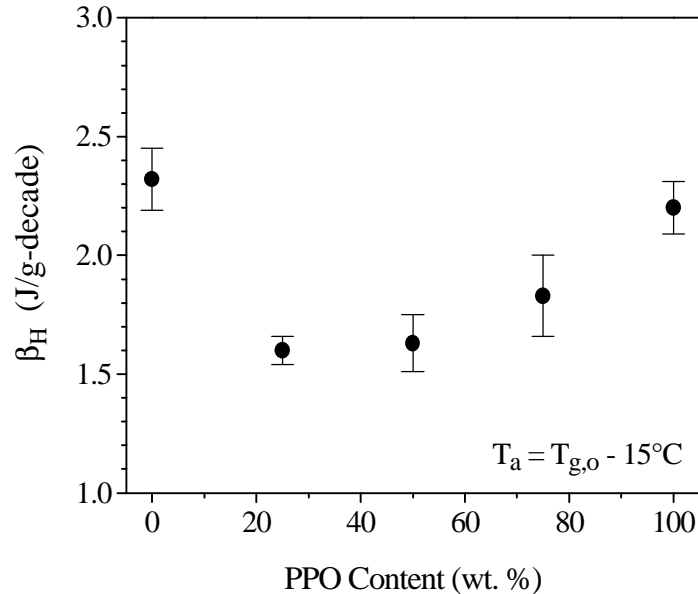


Figure 3-6: Enthalpy relaxation rates for a-PS/PPO blends determined (by this author) from data presented in reference 14 (see text for possible explanation of unusually high  $\beta_H$  values).

A miscible blend of SAN with a random copolymer of styrene and methyl methacrylate (SrMMA) was prepared in 50/50wt. composition via solution blending, and the enthalpy relaxation of this blend and the pure constituents during aging at 20°C below  $T_g$  was investigated by Pauly and Kammer.<sup>22</sup> The enthalpy recovery results were fit using the Cowie-Ferguson model and the results are detailed in Table 3-III. No apparent approaches to equilibrium were evident in the  $\Delta H$  data which exhibited approximately linear increases with  $\log(t_a)$ . Because the data were not obtained close to equilibrium, the parameters obtained using the CF approach should be compared with caution, and the uncharacteristically high value of  $\beta$  assessed for the blend underscores this warning. According to the results of this fitting, the average relaxation time values, determined from  $\tau$  and  $\beta$  parameters, indicate that the blend relaxes faster (shorter  $\langle \tau \rangle$ ) than the pure

species which is in agreement with enthalpy relaxation rates independently determined by this author from the enthalpy recovery data. The authors suggested that the relaxation in the blend was due mainly to relaxation of the SAN component since SAN and the blend possessed similar  $\Delta H_{\infty}$  values, but this conclusion is illogical considering that the blend contained only 50% by weight of SAN. If the relaxation was mainly due to the SAN component, then  $\Delta H_{\infty}$  for the blend should have a value which is half that observed for the aging of pure SAN.

Table 3-III: Enthalpy Relaxation Parameters for SAN/SrMMA System for  $T_a = T_g - 20^{\circ}\text{C}$  \*

Material	$T_g$ [ $^{\circ}\text{C}$ ]	Cowie-Ferguson Model Fit				$\beta_H$ <sup>†</sup> [J/g-decade]
		$\Delta H_{\infty}$ [J/g]	$\tau$ [hr]	$\beta$	$\langle \tau \rangle$ [hr]	
SAN	105	3.08	44	0.28	520	0.67 ( $\pm 0.17$ )
50/50wt. Blend	106	3.60	55	0.84	61	2.02 ( $\pm 0.25$ )
SrMMA	107	2.84	88	0.29	981	0.71 ( $\pm 0.13$ )

\* Table based on data and fitting parameters from reference 22

<sup>†</sup>  $\beta_H$  independently assessed (by this author) from original enthalpy relaxation data

Miscible blends of amorphous polyimides have recently been studied by Campbell, Goodwin, Mercer, and Reddy,<sup>23</sup> and this research included an examination of enthalpy recovery after physical aging. Poly(ether imide) (PEI) and a polyimide based upon phenylindane (Ciba-Geigy XU-218) were blended and the compositional dependence of enthalpy relaxation behavior was studied for aging temperatures ranging from 5 to 17 $^{\circ}\text{C}$  below  $T_g$ . The results were fit using the Cowie-Ferguson model, allowing free variation of all three parameters,  $\tau$ ,  $\beta$ , and  $\Delta H_{\infty}$ . From this fitting effort, the relaxation distribution breadth parameter,  $\beta$ , was found to be independent of concentration, in contrast to the observation that the  $\beta$  values assessed from dynamic mechanical relaxation behavior in the glass transition region were lower for the blends compared to the pure polymers. Values for the characteristic enthalpy relaxation time,  $\tau$ , were larger for the blends relative to pure

component additivity. According to the authors, this finding was consistent with concentration fluctuations and with the apparent densification which occurred upon mixing these two polymers. Again, these results are subject to cautious regard due to the aforementioned problem with the use of a linear decay function for a non-linear enthalpy relaxation process.

### 3.2 Effect of Physical Aging on Mechanical Properties

Changes in mechanical properties upon sub- $T_g$  annealing were investigated by Paul et al<sup>24</sup> for a miscible blend system of bisphenol-A polycarbonate and a copolyester composed of 1,4-cyclohexanedimethanol and a 20/80 mixture of isophthalic and terephthalic acids. Samples with copolyester contents ranging from 0 to 100 wt.% were quenched into the glassy state from above the melting temperature of the copolyester and subsequently aged at  $T_g-15^\circ\text{C}$ . The tensile stress-strain characteristics measured at room temperature indicated that physical aging resulted in increases in modulus and yield strength and decreases in ultimate strength and elongation at break for the blends and pure polymers. Only two aging times other than  $t_a = 0$  were employed in this study and, accordingly, rates of mechanical property changes with respect to  $\log(\text{aging time})$  could not be precisely determined. In general, the mechanical property changes due to aging appeared to exhibit simple linear relationships with respect to blend composition. Although volume relaxation rates were not quantitatively measured, a comparison of the density values before physical aging and after aging for 96 hours at  $T_g-15^\circ\text{C}$  suggested that volume relaxation rates were essentially linear with blend composition, a feature consistent with the mechanical property results. The changes in density due to physical aging appeared not to be influenced by the fact that the blends exhibited freshly quenched density values which were greater than additive compared to the pure constituent densities.

Physical aging effects in a-PS/PPO blends with compositions of 10 and 30 wt.% PPO have been observed using dynamic mechanical analysis by Johari, Monnerie, and

coworkers.<sup>25</sup> Samples were cooled from above  $T_g$  to  $T_g-15^\circ\text{C}$  and dynamic mechanical measurements were made during subsequent isothermal annealing for this down-jump thermal history. The memory effect was also probed by cooling from the equilibrium liquid state to  $T_g-20^\circ\text{C}$ , aging there for 8 hours, heating rapidly to  $T_g-15^\circ\text{C}$ , and then annealing at  $T_g-15^\circ\text{C}$  while probing the dynamic mechanical response. The blends displayed the typical “breathing” response described earlier in this review for the memory experiment, and, for long annealing times at  $T_g-15^\circ\text{C}$ , the memory response curve matched the approach to equilibrium for the down-jump experiment. This aging study did not investigate the non-equilibrium characteristics for the pure components, and thus insight into the compositional nature of dynamic mechanical aging behavior in the glassy state cannot be gained. The non-equilibrium behavior of the a-PS/PPO(70/30) blend was also studied using dielectric analysis,<sup>26</sup> and the results were similar to those obtained from dynamic mechanical analysis. The dielectric study also probed the nature of secondary relaxations in the a-PS/PPO blend system as well in blends of a-PS with PVME. It was noted that the location of the secondary relaxation for both blend systems occurred in the same temperature region (for a fixed frequency) as pure atactic polystyrene. As the content of PPO and PVME was increased in the blends with a-PS, the magnitude of the secondary relaxation increased, suggesting movement of PPO and PVME along with the a-PS segments. This cooperativity observed in the secondary relaxation response for these blend systems may have implications on physical aging of the blends, particularly when aging is performed far below the glass transition temperature.

Mijovic and coworkers<sup>27-29</sup> studied changes in stress relaxation behavior upon annealing in the glassy state for a-PS/PPO and a-PMMA/SAN blend systems as a function of composition for the aging temperatures of 20, 35, and  $50^\circ\text{C}$  below  $T_g$ . The stress relaxation data was obtained in accordance with Struik’s protocol,<sup>30</sup> and the data for aging times of 2, 4, and 8 hours was then fit using the KWW stretched exponential decay function. For these two miscible polyblend systems, a single relaxation time distribution parameter,  $\beta = 0.41$ , was suitable in describing the stress relaxation data irrespective of aging time, aging temperature, and blend composition. A notable result of this work<sup>29</sup> was that the relaxation times determined from the stress relaxation data fitting endeavor for the

a-PMMA/SAN were comparable to the relaxation times determined from the previously mentioned phenomenological modeling of the enthalpy recovery behavior for this blend system. Values of the mechanical aging rate ( $\mu$ ) were not determined from the stress relaxation data obtained for the three aging times which were utilized in this study. However, the  $\log(\text{aging time})$  dependence of the KWW relaxation times can be used to assess aging rates since the  $\beta$  parameter was held constant for the stress relaxation curve fits. The stress relaxation aging rates were determined in this manner (by this author) for the a-PMMA/SAN and a-PS/PPO blend systems, and the results are presented in Figure 3-7 and Figure 3-8. It is difficult to discern any clear trends for  $\mu$  with respect to composition for both blend systems, possibly due to errors in the aging rates resulting from the use of only three aging times in the aging rate determination. The values of  $\mu$  are also subject to any fitting errors associated with the relaxation time parameters. Stress relaxation measurements as a function of aging time were also made on an amorphous 70/30 blend of a-PMMA and poly(vinylidene fluoride) (PVDF) and on a 50/50 a-PMMA/PVDF semicrystalline blend. The amount of PVDF crystallinity in the second blend was such that the miscible amorphous phase had a 70/30 a-PMMA/PVDF composition, identical to the wholly amorphous blend. These two blends provided the means of assessing the role of crystalline regions on stress relaxation aging behavior while keeping the composition of the miscible amorphous phase constant. For the amorphous a-PMMA/PVDF blend, the  $\beta$  parameter was found to be 0.41, the value also found for the a-PS/PPO and a-PMMA/SAN blend systems independent of blend composition. The influence of aging on the  $\tau$  parameter was comparable for the amorphous a-PMMA/PVDF blend relative to the aging behavior observed for the other amorphous polyblends. In stark contrast, the stress relaxation response for the semicrystalline material indicated an extremely broad relaxation time distribution ( $\beta$  values ranging from 0.1 to 0.2). In addition, physical aging did not seem to result in noticeable changes in relaxation times for the semicrystalline blend for the employed aging times of 2, 4, and 8 hours.

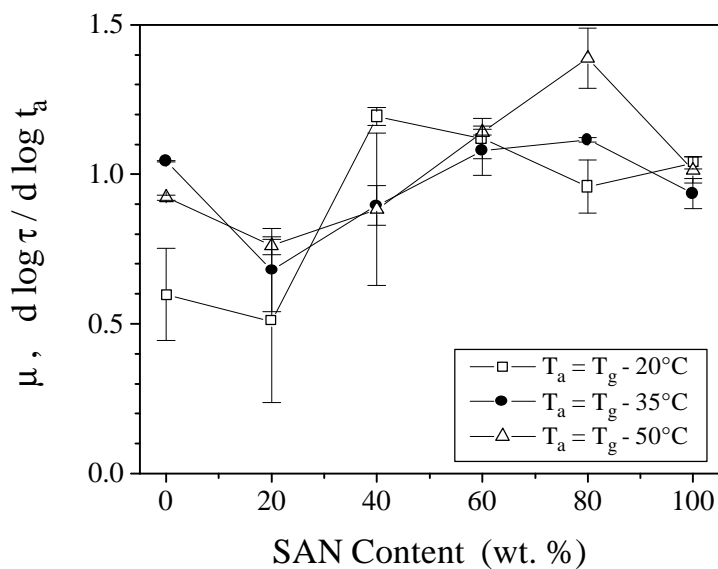


Figure 3-7. Stress relaxation aging rate as a function of composition and aging temperature for a-PMMA/SAN blend system. Aging rates determined (by this author) from KWW relaxation times given in reference 28 for aging times of 2, 4, and 8 hours.

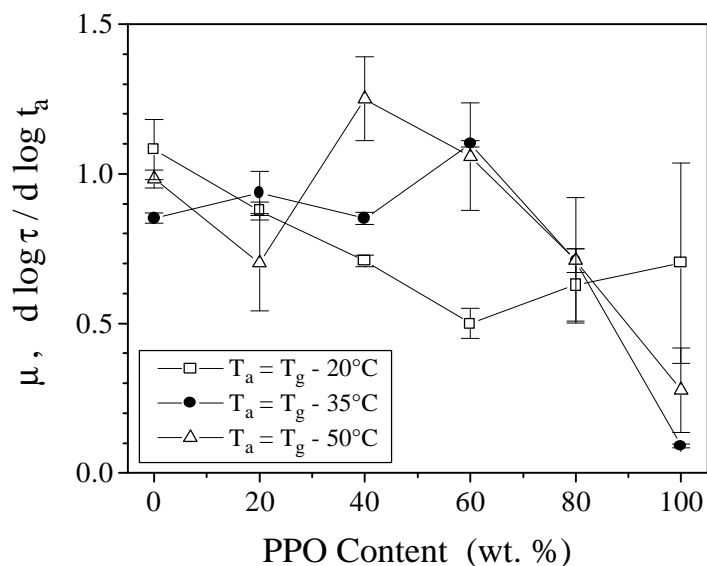


Figure 3-8. Stress relaxation aging rate as a function of composition and aging temperature for a-PS/PPO blend system. Aging rates determined (by this author) from KWW relaxation times given in reference 28 for aging times of 2, 4, and 8 hours.

Chang et al.<sup>31,32</sup> examined the influence of physical aging on stress relaxation behavior of miscible binary blends which were dilute in one component. Physical aging was performed at undercoolings of 15, 20, 25, and 30°C relative to  $T_g$  and stress relaxation was performed as a function of aging time in accordance with procedures recommended by Struik.<sup>30</sup> The three miscible blends studied, prepared via solution casting, were a-PS/PPO(90/10wt.), a-PS/PVME (90/10wt.), and a-PMMA/poly(ethylene oxide) (PEO) (85/15wt.), and it should be noted that the a-PMMA/PEO blend exhibited no indication of PEO crystallinity as determined by DSC. The stress relaxation data for the blends at fixed values of  $T_a$  and  $t_a$  were fit using the KWW expression. The fitting results for the blends were compared to those obtained for the major components for the a-PS/PVME and a-PMMA/PEO systems and compared to the fitting parameters for both neat components in the case of the a-PS/PPO blend system (stress relaxation was not performed on neat PVME or PEO). The KWW  $\beta$  parameter was allowed to vary with different undercoolings and materials but was held fixed with respect to aging time. This restraint assumed maintenance of the shape of the relaxation time distribution during isothermal aging, solely attributing the change in stress relaxation with increasing  $\log(t_a)$  to a shift of the distribution to longer times. Accordingly, time – aging time superposition was performed in order to assess values of the shift factor,  $\mu$ , from the average relaxation time  $\langle \tau \rangle$ :

$$\mu = \left( \frac{\partial \log \langle \tau \rangle}{\partial \log t_a} \right)_{T_a} \quad \text{Eqn. 3-3}$$

Compared to pure a-PS, the a-PS/PPO(90/10) blend and the a-PS/PVME (90/10) blend exhibited higher stress relaxation aging rates ( $\mu$  values), and mechanical aging of the a-PMMA/PEO(85/15) blend was retarded compared to the aging response of pure a-PMMA. These mechanical aging rate responses were explained in terms of differences in packing density, or free volume fraction, for the blends when compared to the major blend components at fixed undercoolings ( $T_g-T$ ). Positron annihilation lifetime spectroscopy (PALS) indicated that the fractional free volumes for the a-PS/PPO(90/10) and a-PS/PVME (90/10) blends were greater than pure a-PS, and the a-PMMA/PEO(85/15)

blend possessed a free volume fraction lower than a-PMMA. While the free volume fractions of the blends were compared to that of the major component comprising each blend, no comparisons were made relative to additivity of the free volume fractions of the pure components. The average relaxation times at an aging time of 240 minutes and the aging shift factors for the a-PS/PPO blend and pure components are presented in Figure 3-9 and Figure 3-10 as respective functions of  $T_g - T_a$  and  $T_{g,o} - T_a$ .<sup>§</sup> The heightened glass transition breadth for the blend relative to the breadths for a-PS and PPO appears to have a noticeable influence on the scaling behavior of  $\mu$  depending on whether the onset or midpoint glass transition temperature is used as a reference, suggesting that concentration fluctuations do play a role in blend aging behavior. Concentration fluctuations were also manifested in the relaxation time distribution for the a-PS/PVME(90/10) blend which was much broader than that for pure a-PMMA, as inferred from the KWW exponent which was 0.38 for the blend and 0.45 for a-PMMA at  $T_a = T_g - 20^\circ\text{C}$ . Another interesting observation is that the aging rates for the a-PS/PPO(90/10) blend appear to be lower than expected based upon additivity because the blend aging rates are closer to those for pure PPO than expected given the amount of PPO in the blend (Figure 3-9b). Of great significance in understanding the physical aging of miscible blends would be an investigation of the compositional dependence of free volume fraction and physical aging behavior for these blends, but this study only involved a single 10 wt.% blend composition in all cases.

---

<sup>§</sup> The definition of the onset of the glass transition used by the authors was based upon the temperature where the first deviation occurred from the linearity of the glassy heat capacity regions. The breadth of the glass transition assessed in this manner is larger than that determined using the standard definitions.

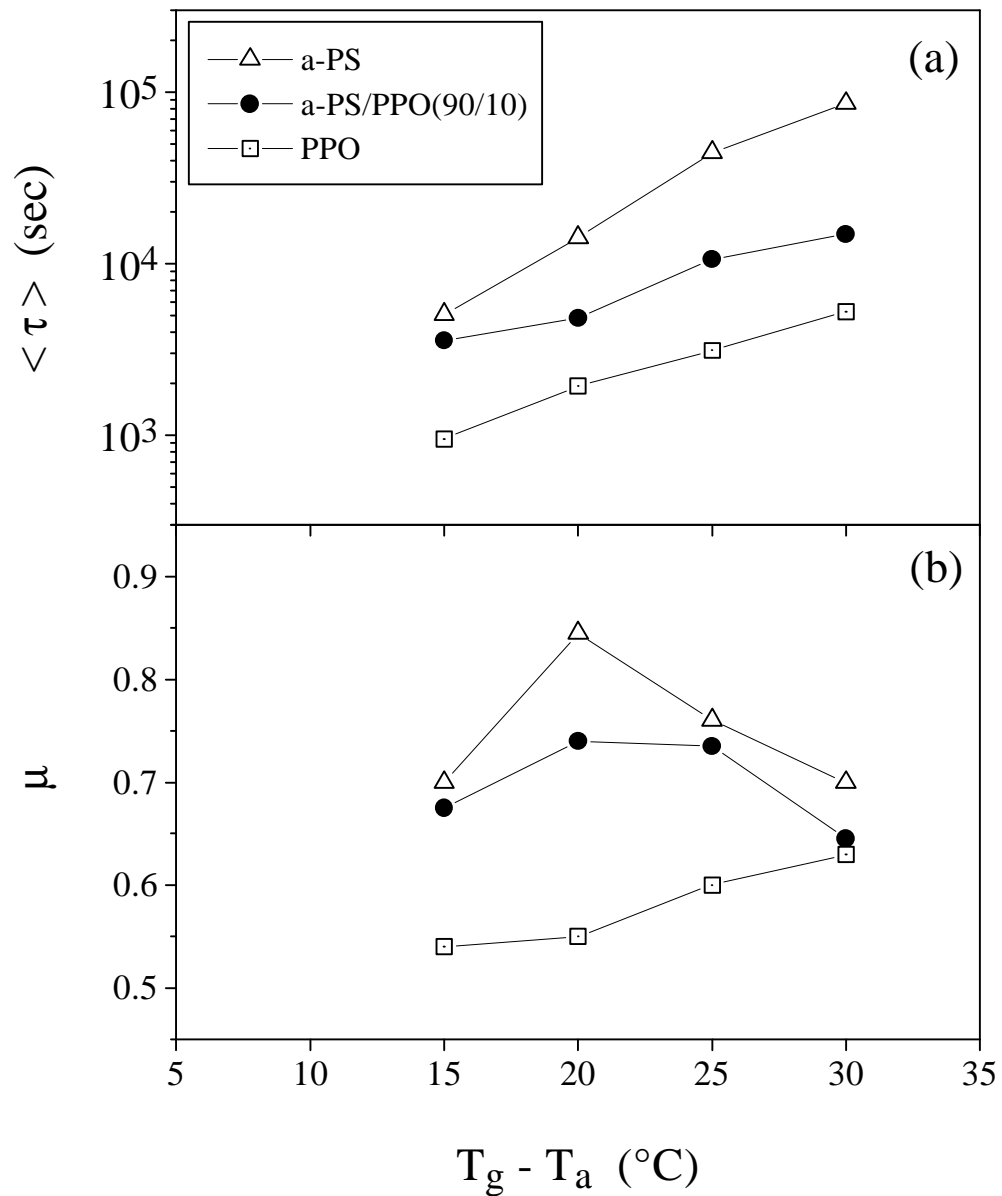


Figure 3-9: (a) Average KWW relaxation time at  $t_a = 240$  min. and (b) aging shift factor,  $\mu$ , determined from stress relaxation data for a-PS/PPO system. The aging temperature is scaled with respect to  $T_g$ . Data are replotted from references 31 and 32.

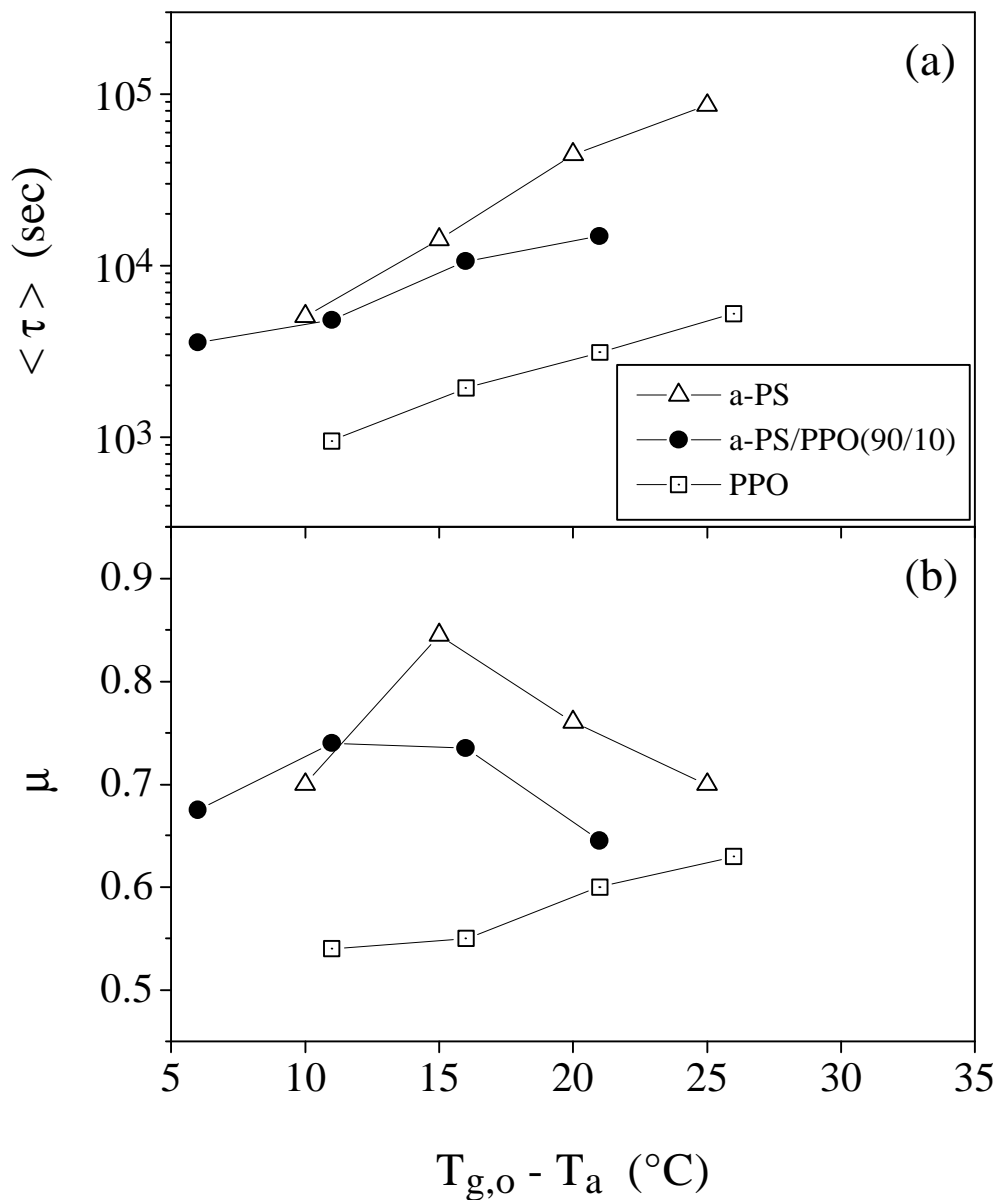


Figure 3-10: (a) Average KWW relaxation time at  $t_a = 240$  min. and (b) aging shift factor,  $\mu$ , determined from stress relaxation data for a-PS/PPO system. The aging temperature is scaled with respect to  $T_{g,o}$ . Data are replotted from references 31 and 32.

### 3.3 References

- <sup>1</sup> K. Naito, G. E. Johnson, D. L. Allara, and T. K. Kwei. *Macromolecules*, **11**, 1260 (1978).
- <sup>2</sup> W. M. Prest, Jr. and F. J. Roberts, Jr., in *Thermal Analysis*, vol. II (ed. B. Miller), John Wiley and Sons, New York, 1982, pp. 973-978.
- <sup>3</sup> W. M. Prest, Jr., D. J. Luca, and F. J. Roberts, Jr., in *Thermal Analysis in Polymer Characterization* (ed. E. A. Turi), Heyden, Philadelphia, 1981, pp. 25-42.
- <sup>4</sup> W. M. Prest, Jr., D. J. Luca, and F. J. Roberts, Jr., *Bull. Am. Phys. Soc.*, **26**, 399 (1981).
- <sup>5</sup> J. L. Feijoo, A. J. Muller, and J. R. Acosta. *J. Mater. Sci. Lett.*, **5**, 1193 (1986).
- <sup>6</sup> S. W. Shalaby and H. E. Bair. in *Thermal Characterization of Polymeric Materials* (ed. E. A. Turi), Academic Press, New York, 1981, p. 365 (Chapter 4).
- <sup>7</sup> M. Bosma, G. ten Brinke, and T. S. Ellis. *Macromolecules*, **21**, 1465 (1988).
- <sup>8</sup> R. Grooten and G. ten Brinke. *Macromolecules*, **22**, 1761 (1989).
- <sup>9</sup> G. ten Brinke and R. Grooten. *Colloid Polym. Sci.*, **267**, 992 (1989).
- <sup>10</sup> T. S. Ellis. *Macromolecules*, **23**, 1494 (1990).
- <sup>11</sup> R. Jorda and G. L. Wilkes. *Polym. Bull.*, **20**, 479 (1988).
- <sup>12</sup> F. Lednický, J. Hromádková, and J. Kolarik. *Polymer Testing*, **11**, 205 (1992).
- <sup>13</sup> G. ten Brinke, L. Oudhuis, and T. S. Ellis. *Thermochimica Acta*, **238**, 75 (1994).
- <sup>14</sup> A. A. C. M. Oudhuis and G. ten Brinke. *Macromolecules*, **25(2)**, 698 (1992).
- <sup>15</sup> J. M. G. Cowie and R. Ferguson. *Macromolecules*, **22(5)**, 2307 (1989).
- <sup>16</sup> J. M. G. Cowie and R. Ferguson. *Macromolecules*, **22(5)**, 2312 (1989).
- <sup>17</sup> J. Mijovic, T. Ho, and T. K. Kwei. *Polym. Eng. Sci.*, **29(22)**, 1604 (1989).
- <sup>18</sup> T. Ho and J. Mijovic. *Macromolecules*, **23(5)**, 1411 (1990).
- <sup>19</sup> I. M. Hodge, *J. Non. Cryst. Solids*, **169**, 211 (1994).
- <sup>20</sup> S. Elliot. Ph.D. Dissertation (advisor: J. M. G. Cowie), Heriot-Watt Univ., UK, 1990.
- <sup>21</sup> J. M. Hutchinson, *Prog. Polym. Sci.*, **20**, 703 (1995).
- <sup>22</sup> S. Pauly and H. W. Kammer. *Polym. Networks Blends*, **4**, 93 (1994).
- <sup>23</sup> J. A. Campbell, A. A. Goodwin, F. W. Mercer, and V. Reddy, *High Perform. Polym.*, **9**, 263 (1997).
- <sup>24</sup> E. A. Joseph, M. D. Lorenz, J. W. Barlow, and D. R. Paul, *Polymer*, **23**, 112 (1982).
- <sup>25</sup> J.Y. Cavaille, S. Etienne, J. Perez, L. Monnerie, G.P. Johari, *Polymer*, **27**, 686 (1986).
- <sup>26</sup> K. Pathmanathan, G. P. Johari, J. P. Faivre, and L. Monnerie, *J. Polym. Sci.: Part B: Polym. Phys.*, **24**, 1587 (1986).
- <sup>27</sup> J. Mijovic, S. T. Devine, and T. Ho, *J. Appl. Polym. Sci.*, **39**, 1133 (1990).
- <sup>28</sup> T. Ho, J. Mijovic, and C. Lee, *Polymer*, **32(4)**, 619 (1991).
- <sup>29</sup> J. Mijovic and T. Ho, *Polymer*, **34(18)**, 3865 (1993).
- <sup>30</sup> L. C. E. Struik, *Physical Aging in Amorphous Polymers and Other Materials*, Elsevier, New York, 1985.
- <sup>31</sup> G.-W. Chang, Ph.D. Dissertation (advisor: A. M. Jamieson), Case Western Reserve Univ., 1993.
- <sup>32</sup> G.-W. Chang, A. M. Jamieson, Z. Yu, and J. D. McGervey. *J. Appl. Polym. Sci.*, **63**, 483 (1997).

## Chapter 4

### Physical Aging Behavior of Miscible Blends Containing Atactic Polystyrene and Poly(2,6-dimethyl-1,4-phenylene oxide)

---

---

#### Chapter Synopsis

The influence of blend composition on physical aging behavior was assessed for miscible blends of atactic polystyrene (a-PS) and poly(2,6-dimethyl-1,4-phenylene oxide) (PPO). At aging temperatures of 15°C and 30°C below the midpoint glass transition temperature ( $T_g$ ), the a-PS/PPO blends exhibited volume relaxation rates which were retarded compared to additivity based upon the aging rates for pure a-PS and PPO. This negative deviation diminished with increased undercooling, and eventually the volume relaxation rates displayed a nearly linear trend with respect to composition at the greatest undercooling of 60°C which was employed. The glass transition breadths were greater for the blends compared to the pure homopolymers, but rescaling the volume relaxation data with respect to the onset to the glass transition temperature region did not significantly alter the observed rate trends. The heightened state of packing in the blends and the compositional nature of secondary relaxations, both influenced by the presence of specific attractive interactions in the blend system, were conjectured to be the causes for the variation of volume relaxation rate with composition and undercooling. For aging at 30°C below  $T_g$ , the dependence of enthalpy relaxation rate on composition was similar to that observed for volume relaxation. A comparison of volume and enthalpy decay rates for aging performed at  $T_g-60^\circ\text{C}$  was obscured by the fact that different enthalpy relaxation trends were noted depending on which indirect method was used to infer the relaxation from the recovery curves measured using differential scanning calorimetry. Mechanical aging rates determined from time-aging time superposition of creep compliance data showed significantly less than additive behavior for the blends aged at  $T_g-30^\circ\text{C}$ , but unlike the volume relaxation results, this trend persisted at the 60°C undercooling. The initial mechanical behavior prior to aging appeared to be predominantly influenced by the compositional nature of glassy density for the blend system at both undercoolings, but the influence of the changing structure on mechanical response changes during aging was different at  $T_g-60^\circ\text{C}$  compared to  $T_g-30^\circ\text{C}$ .

## 4.1 Introduction

The glassy state is inherently nonequilibrium from a thermodynamic standpoint. During cooling a glass-forming liquid, thermal contraction occurs as the free volume surrounding the molecules decreases. The relative mobility of the molecular segments becomes increasingly inhibited, in a manner which could be considered a molecular “log jam”, and a nonequilibrium glassy state is formed. The formation of the nonequilibrium glass occurs when the relaxation times become large relative to the time frame allowed for molecular rearrangements, a time frame dictated by the quench rate. Departure from equilibrium constitutes a driving force for relaxation in the glassy state and, consequently, decreases in the volume, enthalpy, and entropy occur due to localized molecular motion in the glassy state. The temporal changes in the thermodynamic variables of the glass are often termed structural relaxation and, considered together, result in a decrease in the free energy of the system. The changes that occur in the thermodynamic state, in turn, result in changes in numerous characteristics including mechanical, optical, and barrier properties. These property changes associated with the time-dependent nature of the glassy state have been described in great detail by several fine reviews.<sup>1-5</sup> The time-dependent nature of the thermodynamic variables in the glassy state (structural relaxation) as well as interrelated changes in bulk application properties are collectively referred to as physical aging. Because physical aging is a consequence of the non-equilibrium glassy state, it is thermoreversible unlike chemical or thermo-oxidative aging.

In principle, all materials can form an amorphous glassy phase if quenched rapidly enough from the liquid state to avoid complete crystallization. For polymer systems, achieving high crystal contents is not common, and many commercially important polymers are completely amorphous. Therefore, most polymeric materials which are used at temperatures below their glass transition temperature region possess significant glassy contents. Also, relative to inorganic glasses, polymer glasses are often utilized at temperatures which are nearer to the glass transition temperature region where physical aging rates are significant. These factors combine to make physical aging of

polymeric materials an important issue within the industrial community, and this research area has attracted much interest accordingly.<sup>5</sup>

This research investigation is concerned with the nonequilibrium glassy behavior of miscible polymer blends. Because the nature of the glassy state formed from simple liquids is far from being completely defined, it may initially seem premature to probe the temporal nature of more complex multicomponent polymeric glasses. However, the undertaken research is timely for at least two reasons. From a practical standpoint, the use of polymer blends is becoming increasingly widespread for the purpose of developing economically viable materials with novel combinations of application properties. These properties of interest can undergo significant time-dependent changes (physical aging) below the glass transition due to the nonequilibrium nature of the glassy state. Also, the introduction of complexities can provide a means of isolating the effects of certain molecular features on glassy state relaxations. For example, insight into the influence of intermolecular forces on the nonequilibrium behavior of the glassy state may be provided by the study of miscible polymer blend systems with specific interactions present between the blend components. Physical aging of amorphous miscible polymer blends has been investigated to some extent,<sup>6-20</sup> and an in-depth review of these investigations is provided elsewhere.<sup>21</sup> The majority of this past research was focused upon enthalpy relaxation/recovery measurements and none of the studies considered volume relaxation behavior. The goal of the present research study is to extensively investigate physical aging as a function of both blend composition and aging temperature for a widely studied, and commercially important, miscible blend system which is comprised of atactic polystyrene and poly(2,6-dimethyl-1,4-phenylene oxide). Both volume relaxation and enthalpy recovery measurements are included in this study in order to understand the time-dependent structural state for the blends and pure components. The degree to which the physical aging process induces changes in the small-strain mechanical creep response for the a-PS/PPO blend system is also an integral component of this investigation. Where possible, this study attempts to derive suitable interpretation of the aging results in terms of molecular-based concepts.

## 4.2 Experimental Details

### 4.2.1 Blend Preparation and Characterization

Blends of atactic polystyrene (a-PS) and poly(2,6-dimethyl-1,4-phenylene oxide) (PPO) were prepared by mixing at 265°C for 15 minutes in a Brabender (Model 5501) melt mixer using a mixing speed of 70 RPM. Blends with compositions of 25, 50, 75, and 87.5 wt.% PPO were generated. The PPO material was obtained from Polysciences (Cat.# 08974) and has a weight-average molecular weight ( $M_w$ ) of approximately 50,000 g/mol. The a-PS material employed in this study is produced by Dow Chemical (Dow 685D) and the number- and weight-average molecular weights for this polymer are 174,000 and 297,000 g/mol, respectively, as determined by gel permeation chromatography.<sup>22</sup> All polymer materials were dried under vacuum conditions at 70°C before blending. Films were compression molded from the neat materials and blends, and the resulting films had an approximate thickness of 0.2 mm. All materials were stored in a desiccator cabinet prior to testing. The inflection glass transition temperature ( $T_g$ ) was investigated as a function of blend composition in a differential scanning calorimeter (Perkin Elmer DSC 7) for samples weighing 8 to 11 mg at a heating rate of 10°C/minute following a quench from the equilibrium liquid state ( $T_g+50^\circ\text{C}$ ) at 200°C/min (see *Enthalpy Relaxation Measurements* section for further DSC details). The breadth of the glass transition was also assessed for the blend system from the DSC scans. Density measurements were made at 23°C using a pycnometer manufactured by Micromeritics (Model AccuPyc 1330).

### 4.2.2 Enthalpy Relaxation Measurements

Prior to aging, samples weighing approximately 10 mg were loaded in aluminum pans and quenched into the glassy state at 200°C/min in the DSC after annealing at  $T_g+50^\circ\text{C}$  for 10 minutes. Samples were aged isothermally at  $T_g-30^\circ\text{C}$  ( $\pm 0.5^\circ\text{C}$ ) in ovens under nitrogen purge for various amounts of time ranging from 1 to 300 hours. Each sample was then scanned in the Perkin Elmer DSC 7 from  $T_g-70^\circ\text{C}$  to  $T_g+50^\circ\text{C}$  using a heating rate of 10°C/minute (first heat). In order to provide an unaged reference with which to compare an aged DSC trace, each sample was then annealed in the DSC at

$T_g+50^\circ\text{C}$  for 10 minutes, quenched at  $200^\circ\text{C}/\text{min}$ , and scanned from  $T_g-70^\circ\text{C}$  to  $T_g+50^\circ\text{C}$  at  $10^\circ\text{C}/\text{minute}$  (second heat). It was necessary to hold the DSC sample for 2 minutes at  $T_g-70^\circ\text{C}$  to allow control of the heat signal before initiation of the second heat. It is expected that this short amount of time at this low temperature has a negligible effect on the structural state of the sample. The extent of enthalpy recovery was determined from the first and second heating scans using two methods to be described later. A third heat was employed in some cases following annealing at  $T_g+50^\circ\text{C}$  for 10 minutes and quenching at  $200^\circ\text{C}/\text{min}$ . This third scan was performed in order to illustrate, by comparison with the second heat, the thermal stability of the material under the conditions employed during DSC testing. All DSC testing utilized a nitrogen purge. An instrument baseline was generated every two hours of testing at a heating rate of  $10^\circ\text{C}/\text{minute}$  using empty pans with lids in the reference and sample cells. The ice content in the ice/water bath was maintained at approximately 30-50% by volume during all testing. The DSC temperature was calibrated using the melting points of indium and tin, and the heat flow was calibrated using the heat of fusion of indium.

#### ***4.2.3 Volume Relaxation Measurements***

Isothermal volume relaxation was monitored for the a-PS/PPO blend system using a precision mercury dilatometry apparatus described in detail elsewhere.<sup>22</sup> Samples used were compression molded bar samples with weights in the range of 4 to 5 g (approximate dimensions: 1 cm x 1 cm x 4 cm). After a sample was encased in the glass bulb of a capillary dilatometer, the dilatometer was placed under vacuum and was subsequently filled with triple-distilled mercury. A vacuum was pulled on the filled dilatometer for approximately two days to remove any entrapped air bubbles, and the dilatometer was allowed to equilibrate at atmospheric pressure for one day following this de-gassing procedure. Just prior to volume relaxation measurements, the materials were annealed in the dilatometers for 10 minutes at  $T_g+50^\circ\text{C}$  using an oil bath and then quenched using an ice bath. The sample in the dilatometer was then isothermally annealed at the desired aging temperature in a Haake model N4-B oil bath with temperature control fluctuations less than  $0.01^\circ\text{C}$ . The height change of the mercury in the capillary was assessed as a function of aging time using a calibrated linear voltage differential transducer and

converted to volume change based on the cross sectional area of the capillary. The order of the undercoolings (relative to  $T_g$ ) which were used for each blend sample was: 30, 60, 30, 15, 30, 45°C. After volume relaxation measurements were complete at one undercooling, the material was annealed 50°C above  $T_g$  and requenched into the glassy state where densification was followed at the next undercooling. The three experiments performed at  $T_g-30^\circ\text{C}$  allowed a measure of error to be obtained for the volume relaxation rate data.

The thermodynamic state of the quenched dilatometer samples was essentially identical to that of the quenched DSC samples used to assess enthalpy relaxation as was verified in the following manner. Films of a-PS were alternately stacked with Teflon® films (thickness = 0.12 mm) to form a composite bundle with the approximate dimensions of a typical dilatometer sample, and this film bundle was encapsulated in a dilatometer bulb with mercury and de-gassed in the typical manner. The encased material was then annealed in the bulb at  $T_g+50^\circ\text{C}$  for 10 minutes and quenched to room temperature by immersion of the dilatometer bulb in an ice bath. Following this quench, the a-PS films were extracted from the bulb and then the outer and center layers were used to generate ~10 mg DSC samples. These samples were subsequently scanned in the DSC from  $T_g-70^\circ\text{C}$  to  $T_g+50^\circ\text{C}$  at 10°C/minute, annealed at  $T_g+50^\circ\text{C}$  for 10 minutes, quenched at 200°C/min, and scanned a second time from  $T_g-70^\circ\text{C}$  to  $T_g+50^\circ\text{C}$  at 10°C/minute. Fictive temperature ( $T_f$ ) calculations were performed on both heating scans for the two film samples using the Perkin Elmer analysis software provided with the instrument. The first heats of the outer and center film samples provided  $T_f$  values of 103.5°C and 103.0°C, respectively. The second heats for both samples yielded essentially equivalent fictive temperatures equal to 103.4°C, a value also obtained for a-PS samples which were freshly quenched (DSC quench at 200°C/min) and which were not previously subjected to enclosure in the dilatometer bulb. The issue is not whether the center of the dilatometry sample lags behind the surface of the sample during the quench into the glassy state because this is necessarily the case based upon heat transfer limitations. Of importance is the effective rate of cooling experienced by the sample during glass formation, and based upon the above study it is clear that the outside and center of the dilatometry sample experienced very similar rates of cooling. The center

portion may have experienced a slightly lower cooling rate as evidenced by its lower  $T_f$  value compared to that for the center region, but this cooling rate discrepancy is certainly not very different on a logarithmic scale. The structural state generated upon glass formation depends on the logarithm of the cooling rate, and typical apparent activation energies lead to increases of 2 to 7°C in  $T_f$  with a ten-fold increase in cooling rate. Because the initial fictive temperatures generated by the DSC and dilatometry quenching conditions were comparable, the initial structural states of the samples were deemed essentially equivalent for the volume and enthalpy relaxation experiments.

#### ***4.2.4 Creep Compliance Testing***

The influence of physical aging on tensile creep compliance behavior was assessed during isothermal aging. The testing was performed on initially unaged film samples which were freshly quenched between steel plates at room temperature after free-annealing at  $T_g+50^\circ\text{C}$  for 10 minutes. The small-strain creep response was probed after aging times of 1.5, 3, 6, 12, and 24 hours using the procedure established by Struik.<sup>1</sup> A Seiko thermal mechanical analyzer (model TMA 100) was used to test the samples possessing the following approximate dimensions: length of 30 mm, thickness of 0.2 mm, and width of 3 mm. The step stress applied to the samples during the creep measurements was kept small in order to insure that the total strain was kept well below 0.3% (the majority of total strain values were less than 0.15%). This enables a sample to be intermittently tested for its mechanical response during isothermal physical aging without the testing procedure significantly affecting the state of the sample after the stress is removed and the sample is allowed to recover. The total time during which the stress is applied is one-tenth of the total cumulative aging time, such that any aging which occurs during the creep test can be neglected.

#### ***4.2.5 Dynamic Mechanical Testing***

Dynamic mechanical measurements (tensile) were made with a Seiko DMS 210 using samples (0.2 mm thick, 20 mm long, 5 mm wide) which were freshly quenched between steel plates at room temperature after free-annealing at  $T_g+50^\circ\text{C}$  for 10 minutes. The testing procedure involved a heating rate of 2°C/min, a nitrogen purge, and a

frequency of 1 Hz. The dynamic mechanical spectra were determined for the blends and pure polymers from  $-140^{\circ}\text{C}$  to above the  $\alpha$ -relaxation temperature region.

### 4.3 Results and Discussion

Changes in the thermodynamic state of a glassy material during the physical aging process can be followed by directly monitoring volume changes using dilatometry or by inferring enthalpy changes by means of differential scanning calorimetry. Both of these approaches were employed in this investigation of the a-PS/PPO miscible blend system, and the results will be detailed and discussed. Compositional dependence of both dynamic mechanical response and glassy state packing will also be considered because these elements will provide some insight into the observed structural relaxation rate trends. Finally, the discussion will consider the mechanical response changes during physical aging as determined by creep compliance testing.

When considering the time-dependent glassy properties of miscible polymer blends and comparing them to the responses yielded by the pure constituents, the compositional dependence of  $T_g$  is an extremely pertinent issue. A valid comparison of physical aging rates for different glassy materials aged at a fixed temperature is not afforded when the glass transition temperatures are widely different. Atactic polystyrene and poly(2,6-dimethyl-1,4-phenylene oxide) have glass transition temperatures that are different by greater than  $100^{\circ}\text{C}$ , and, for the purpose of this study, aging rate comparisons are made at a fixed undercooling relative to the glass transition temperature which varies with blend composition. Glass transition results for the a-PS/PPO blends and the pure components are given in Table 4-I, and aging temperatures were selected relative to the inflection (midpoint) glass transition temperatures measured by DSC. The DSC glass transition data were obtained using a heating rate of  $10^{\circ}\text{C}/\text{min}$  immediately following a quench into the glassy state at  $200^{\circ}\text{C}$ , and, hence, these results reflect the responses for freshly quenched samples. Another important aspect to consider is the breadth of the glass transition for the blends, and this issue will be dealt with shortly.

### 4.3.1 Volume Relaxation

The time-dependent nature of the thermodynamic state for a glassy material can be assessed by determining volume changes via dilatometry,<sup>23,24</sup> and the densification of the blends and neat polymers was thus measured. Relaxation of volume in the glassy state is often found to display a linear dependence on  $\log(\text{time})$ , a consequence of the nonlinear (self-limiting) nature of the structural relaxation process. With the exception of very short times and when the volume closely approaches the equilibrium volume ( $V_\infty$ ) at long times, isothermal volume relaxation at constant pressure can be described by the following expression, where  $b_V$  is the volume relaxation rate:<sup>1,23</sup>

$$b_V = -\frac{1}{V} \frac{dV}{d \log t_a} \quad \text{Eqn. 4-1}$$

This approach is valid for isothermal volume relaxation following a fast quench or down-jump into the glassy state from the equilibrium liquid state, and this was essentially the experimental procedure employed for this study.

Isothermal volume relaxation was performed at temperatures equal to 15, 30, 45, and 60°C below  $T_g$  for each blend composition. Physical aging studies are often limited to temperatures less than 15°C below  $T_g$  because relevant time scales are experimentally amenable to characterizing relaxation all the way to equilibrium. However, glassy polymers are not typically used as rigid structural materials at temperatures so near to the glass-rubber softening temperature region. This research study undertook a practical approach and employed more realistic undercoolings. Representative volume relaxation results are indicated in Figure 4-1 for a-PS, PPO, and the 50/50 blend. Volume relaxation rates determined from the dilatometry data are provided for all of the compositions and undercoolings in Figure 4-2. Inspection of the  $b_V$  data reveals interesting trends. The blend aging rates at  $T_g-15^\circ\text{C}$  and  $T_g-30^\circ\text{C}$  are clearly less than additive based upon the rates for pure a-PS and PPO. This negative deviation appears to diminish and eventually disappear upon aging at temperatures deeper in the glassy state. Forthcoming discussion will attempt to provide explanation for these features.

An investigation of structural relaxation behavior of miscible a-PS/PPO blends was also undertaken by Oudhuis and ten Brinke,<sup>16</sup> and these researchers assigned responsibility for the observed aging results to the heightened glass transition breadth for

the blends. Their study followed the compositional dependence of enthalpy recovery after isothermal annealing at a temperature 15°C below the onset glass transition temperature (as opposed to the midpoint glass transition temperature used for reference purposes by the present authors). The authors qualitatively noted that the enthalpy relaxation was significantly slower for the blends relative to the pure components. The slower aging rates for the blends were attributed to concentration fluctuations in the blends which caused broader glass transitions in comparison to the pure components. According to the authors, the significance of this glass transition breadth difference between the blends and the pure polymers was that the blends, compared to pure a-PS and PPO, possessed regions which were further from the aging temperature. It was reasoned that these less-mobile regions possessed longer relaxation times thus resulting in decreased overall structural relaxation rates for the blends compared to the pure homopolymers.

It now remains to test whether the retarded volume relaxation rates observed here for the blends at undercoolings of 15°C and 30°C can be rationalized based upon the glass transition breadth issue. Table 4-I provides the experimental glass transition results for the a-PS/PPO blend system. Values of the onset ( $T_{g,onset}$ ) and the end ( $T_{g,end}$ ) temperatures of the DSC glass transition were determined via the standard technique which is employed by the instrument software. In addition, the start of the glass transition ( $T_{g,start}$ ) was determined for each material, and this temperature represents the point where the first significant deviation from the glassy heat response occurs during heating. Because the  $T_{g,start}$  values were of nearly equivalent distances below the respective  $T_{g,onset}$  values for the blends and neat polymers, no advantage is given by using  $T_{g,start}$  versus  $T_{g,onset}$  for comparative scaling arguments. In order to determine the importance of the glass transition breadth, the volume relaxation rate data was scaled with respect to  $T_{g,onset}$  as well as  $T_g$ . The contrasting  $b_V$  results are illustrated in Figure 4-3. Applying interpolation/extrapolation to the data scaled relative to  $T_{g,onset}$  (along the dotted lines), in order to obtain constant undercooling data, results in essentially the same trends exhibited in Figure 4-2. Therefore, the presence of concentration fluctuations and their influence on glass transition breadth cannot be held responsible to any significant extent for the observed trends in volume relaxation rate.

An understanding of the negative deviation noted in the volume relaxation rate versus composition data can be gained by considering the glassy packing features of the blend system. The volumes of freshly quenched samples were measured using pycnometry at room temperature, and thermal expansion coefficients (Chapter 5) were subsequently used to determine the state of packing as a function of composition at the undercoolings of 30°C and 60°C. The resulting specific volume results are plotted in Figure 4-4, and it is apparent that the blends are much more densely packed in the glassy state compared to expectations based upon the densities of the pure components. This is, in fact, a well established feature of this blend system.<sup>25</sup> This enhanced packing for the blends is a result of the interactions present between a-PS and PPO which modify the glass formation process during cooling. The nature of segmental cooperativity for the a-PS/PPO blends and its influence on glass transition kinetics is described in Chapter 5. Based upon the specific volume data, it is not surprising that the blends age slower than additive expectations at  $T_g-15^\circ\text{C}$  and  $T_g-30^\circ\text{C}$ . Prior to aging, the blends have less free volume than the neat polymers and intrinsically have lower mobility than additive behavior would suggest. This causes the initial volume decay for the blends upon annealing to be retarded relative to additivity, and this decay causes relaxation times to sharply increase further because the glassy structures are already more highly packed for the blends. This suggests how the heightened state of packing for the a-PS/PPO blends could influence the self-limiting structural relaxation process. These arguments may help explain the negative deviation observed in the  $b_v$  versus composition data for undercoolings of 15°C and 30°C, but they cannot account for the change in the  $b_v$  trend which occurred upon aging at undercoolings which were deeper within the glassy state.

Inspection of dynamic mechanical responses for the blends and pure species can help illuminate the reason for the stark difference between the volume relaxation results at  $T_g-60^\circ\text{C}$  and those at  $T_g-30^\circ\text{C}$ . The dynamic mechanical spectra are given in Figure 4-5 for all of the blend compositions investigated. Preliminary research indicated that the dynamic mechanical response of PPO is sensitive to moisture,<sup>26</sup> (note Figure 4-6) and particular care was taken, therefore, to insure that all samples were dry prior to testing. The compositional dependence of the glass transition temperature, and breadth thereof, can be observed from the spectra, and relevant parameters are listed Table 4-I. The onset

of the  $\tan\delta$  peak was arbitrarily defined for comparative purposes as the temperature at which the  $\tan\delta$  reached a value of 0.15 during heating. From the loss modulus data, a broad secondary relaxation is noted for pure PPO in the vicinity of  $-80^\circ\text{C}$  ( $\gamma$ -relaxation) and atactic polystyrene displays a relaxation ( $\beta$ -relaxation) with a relatively low intensity at approximately  $20^\circ\text{C}$ . The locations of these sub- $T_g$  relaxations are comparable to the findings of published studies.<sup>27-33</sup> Some researchers<sup>30,31</sup> have additionally noted a weak  $\beta$ -relaxation for PPO between the  $\alpha$  and  $\gamma$  processes. Similar to the results of this current study, Karasz and coworkers<sup>32</sup> did not observe the  $\beta$ -relaxation for PPO.

A comparison of the secondary relaxation responses evident for the blends with the sub- $T_g$  behavior exhibited by pure a-PS and PPO is possible from the DMA data. Although the  $\alpha$ -relaxation (glass-rubber softening transition) temperature region varies systematically with composition as expected, unusual behavior is present in this blend system with regard to secondary relaxations. It is apparent that the blends possess relaxation peaks in essentially the same temperature window where the secondary relaxation process occurs for a-PS, and, interestingly, this relaxation does not diminish with increasing PPO content to the extent that would be expected if only motion of a-PS is held responsible for the relaxation. An excellent dielectric study has been carried out on two a-PS/PPO blends containing 10 and 30 wt.% PPO by Monnerie and coworkers,<sup>9</sup> and the intensity of the peak in the location of the  $\beta$ -relaxation for a-PS was found to increase with PPO content. PPO is substantially more dielectrically active than a-PS due to its greater polarity, and, hence, this dielectric analysis resulted in the important conclusion that PPO motion must accompany the movement of a-PS. Indeed, this cooperative behavior is most certainly responsible for the secondary relaxation behavior observed here by dynamic mechanical analysis. Again, specific attractive interactions between the different molecular species are playing a key role.

It now remains to connect the secondary relaxation features evident in the blends to their structural relaxation behavior. Struik originally noted that the temperature dependence of volume relaxation rates appeared to qualitatively mimic the shape of the dynamic mechanical  $\tan(\delta)$  response with temperature, including local increases in aging rates with respect to temperature in the vicinity of secondary relaxations.<sup>34</sup> Therefore, the

difference in the dynamic mechanical loss intensity (constant frequency) observed for one glassy temperature compared to another may be a semi-quantitative predictor of the relative rates of structural relaxation for the two temperatures. A comparison of the role of blend content on the dynamic loss modulus for undercoolings of 30°C and 60°C is not overly informative as can be seen in Figure 4-7a. The ratio of the loss modulus values at  $T_g-30^\circ\text{C}$  and  $T_g-60^\circ\text{C}$  does, however, appear to be a useful quantity because a remarkable similarity is observed between the compositional dependence of this parameter and that observed for the ratio of volume relaxation rates (Figure 4-7b). As was indicated previously, the dependence of glassy packing on blend content does not change in going from  $T_g-30^\circ\text{C}$  to  $T_g-60^\circ\text{C}$  (Figure 4-4). The reduced mobility associated with the enhanced packing for the blends compared to that of a-PS and PPO may be counteracted at temperatures deep within the glassy state ( $T_g-60^\circ\text{C}$ ) by the extra localized mobility in the blends associated with the unusual cooperative secondary relaxation behavior in the blends. This can help explain the change in the  $b_v$  versus PPO content trend which occurred with increased undercooling. To reiterate the key aspects of the preceding discussion, this investigation has developed a rationale for the observed dependence of volume relaxation rate on both blend composition and aging temperature. This rationale was developed by contrasting both the state of packing acquired upon glass formation and the sub- $T_g$  dynamic relaxation behavior of the blends with the respective characteristics of the pure species.

#### ***4.3.2 Enthalpy Relaxation/Recovery***

Now that an adequate understanding of the volume relaxation data has been developed, it is useful to consider how the enthalpy relaxation process proceeds in comparison to the time-dependent behavior of volume for the blend system. Typical enthalpy recovery experiments were carried out following annealing for varied amounts of time at aging temperatures of  $T_g-30^\circ\text{C}$  and  $T_g-60^\circ\text{C}$ . Representative first and second DSC heating traces are indicated in Figure 4-8 and Figure 4-9 for the different blend compositions. Using the standard subtraction procedure, values of the recovered enthalpy ( $\Delta H$ ) were determined, and it is assumed that these positive enthalpies represent the negative enthalpy changes which occurred during the aging interims. The enthalpy

recovery results are given in Figure 4-10. As will become evident later, transforming the  $\Delta H$  data into fictive temperature ( $T_f$ ) results is informative. It is useful to have a parameter which quantifies the structural state of a glass, and a commonly utilized order parameter is the fictive temperature,  $T_f$ , introduced by Tool.<sup>35,36</sup> The fictive temperature is defined as the temperature at which the system would possess the equilibrium thermodynamic volume or enthalpy if instantaneously heated, a concept which is nicely illustrated in a review by Hutchinson.<sup>4</sup> During isothermal physical aging, the aging temperature ( $T_a$ ) is constant but the structural, or fictive, temperature decreases toward  $T_a$  as structural relaxation progresses. The decrease in enthalpy during the annealing process can be simply related to the corresponding decrease in fictive temperature using the known difference between the liquid and glassy heat capacity for the material of interest. Assuming that the recovered enthalpy reflects the relaxed enthalpy, but with opposite sign, the following relaxation rate can be determined from the values of the slope ( $d\Delta H/d\log(t_a)$ ) provided by the data in Figure 4-10:

$$-\frac{dT_f}{d\log(t_a)} = \frac{1}{\Delta C_p} \frac{d\Delta H}{d\log(t_a)} \quad \text{Eqn. 4-2}$$

Consideration of the temperature dependence of  $\Delta C_p$  is necessary in order to properly evaluate Eqn. 4-2, and Table 4-II provides the relevant data for the a-PS/PPO blend system. Using this approach, the relaxation rates were determined from the data given in Figure 4-10 for aging temperatures of 30 and 60°C below  $T_g$ , and the results are provided in Figure 4-11a. Discussion of this rate data will be undertaken shortly.

Another means of characterizing the enthalpy recovery response is by direct measurement of the fictive temperatures from the enthalpy recovery DSC scans (first heats) using the DSC instrument analysis software. An example of the determination method employed by the software is illustrated in Figure 4-12 for enthalpy recovery heating traces which were exhibited by the 50/50 blend. This technique enables relaxation rates ( $-dT_f/d\log(t_a)$  values) to be determined, and these are given in Figure 4-11b. Both analysis techniques provided similar trends in these rates with respect to blend composition at the aging temperature of  $T_g-30^\circ\text{C}$ , but notable differences are present at the undercooling of 60°C. At  $T_g-60^\circ\text{C}$ , the blends relax much slower than additive for the rates determined from the  $\Delta H$  data while the direct determination of  $T_f$  values yielded

essentially a linear trend with respect to composition. A possible source of this discrepancy is evident upon closer scrutiny of the enthalpy recovery DSC traces in Figure 4-9. For the blends containing 25 and 50 wt.% PPO, the recovery curves undershoot the unaged reference scans (second heats) following the endothermic recovery bumps. Such undershoots were not apparent for samples which were annealed at  $T_g-60^\circ\text{C}$  for short aging times, and the degree of undershoot appeared to become more pronounced with increased aging time. The cause for this very reproducible behavior is not known, but it leads to a reduction in the apparent recovered enthalpy, thus resulting in low recovery rates when the method employing the  $\Delta H$  data is used. It is undeniable that caution must be exerted when interpreting recovery response and attempting to directly correlate it to the prior relaxation event. Following aging at  $T_g-60^\circ\text{C}$ , if the enthalpy recovery events for the a-PS/PPO25 and a-PS/PPO50 blends are atypically broad, particularly at the low temperature side of the pre- $T_g$  endothermic peaks, these breadths may not be able to be discerned decently relative to the underlying glassy heat capacity responses. Some positive area may have been omitted, as a result, when integrating the curves generated by subtracting the reference scans from the recovery scans. Hence, the negative area associated with unusual undershoot behavior may not have been offset to the extent it should have been. The measurement of fictive temperatures may be a more appropriate methodology for materials, such as these blends, where the determination of  $\Delta H$  appears to be problematic.

Determination of relaxation rates based upon changes in fictive temperature can also be assessed for volume. This can be accomplished by dividing the  $b_V$  values by the relevant jumps in thermal expansion coefficient at  $T_g$  ( $\Delta\alpha$ ), values of which are given elsewhere in Chapter 5. Values of the volume relaxation rate ( $-dT_f/d\log(t_a) = b_V/\Delta\alpha$ ) are plotted in Figure 4-13 in order to compare with the rates determined for enthalpy. The rate trends are quite similar for volume and enthalpy at  $T_g-30^\circ\text{C}$ , irrespective of which technique was used to assess the enthalpy relaxation rate. For the undercooling of  $60^\circ\text{C}$ , the direct  $T_f$  calculation procedure appeared to provide enthalpy relaxation rates which exhibited a compositional dependence similar to that obtained for volume. A valid comparison of direct volume relaxation data with indirect enthalpy relaxation measurements can never be made without some question, particularly in this situation

where very different trends result from the two distinct methods used to analyze the same enthalpy recovery data. However, based upon the above suggestion that the fictive temperature approach may be the best technique for indirectly assessing enthalpy relaxation, it appears as though volume and enthalpy display similar relaxation rates for the blend system at both undercoolings of 30 and 60°C.

### ***4.3.3 Aging-Induced Changes in Creep Compliance Behavior***

In order to gain insight into the influence of the changing glassy structure on mechanical response for the a-PS/PPO blend system, small-strain creep compliance measurements were made as a function of aging time. Typical data are displayed in Figure 4-14 for a-PS, PPO, and the 50/50 blend. Horizontal and vertical shifting were used in the typical manner to generate master curves, and time-aging time superposition appeared to be sufficiently valid for the blends and pure species. The degree of horizontal shifting can be used to determine a parameter,  $\mu$ , which may be considered a mechanical aging rate, and this parameter is defined as:

$$\mu = \frac{d \log(a_{t_a})}{d \log(t_a)} \quad \text{where: } a_{t_a} = \frac{\tau(t_a)}{\tau(t_{a,ref})} \quad \text{Eqn. 4-3}$$

The compliance curve at an aging time of 6 hours was selected as the reference, and the shift factor ( $a_{t_a}$ ) was determined from the amount of shifting to the left on the log(time) axis which was required in order to superimpose a data set with the reference curve. The values of  $\mu$  were subsequently determined, and these results along with the vertical shift rates are shown in Figure 4-15. The dependence of  $\mu$  on blend composition indicates that the blends age much slower than additive at both  $T_g$ -30°C and  $T_g$ -60°C. It is difficult to state with extreme confidence that discernible trends are present in the vertical shift rate data because of the large error bars. It does appear as though the compositional trends for the vertical shift rates mimic, to a certain extent, the corresponding relationships observed between  $\mu$  and PPO content.

Further analysis of the creep compliance master curves can provide information concerning relaxation times and their breadth. The master curves were fit using the stretched exponential expression:

$$D(t) = D_0 \exp\left(\frac{t}{\tau}\right)^{\beta} \quad \text{Eqn. 4-4}$$

The  $\tau$  parameter represents the most probable relaxation time for the reference aging time, and  $\beta$  provides a measure of the distribution of relaxation times. A single relaxation time is given by  $\beta=1$ , and the distribution broadens as  $\beta$  decreases from this value towards zero. Because it is more useful to compare the relaxation times before any significant aging has occurred, the relaxation times determined from the fits were scaled back to an aging time of 0.6 hours using the  $\mu$  values. During ensuing discussion, the relaxation times at this short aging time of 0.6 hours will be assumed to be representative of the initial creep compliance behavior prior to aging. The relaxation parameters are indicated in Figure 4-16 as a function of aging time and undercooling. The relaxation time distributions were broader for the blends in comparison to the pure polymers, and this is not surprising based upon the broader glass transition responses yielded by the blends. Also, the relaxation time distribution appears to broaden with increased undercooling for both the blends and neat homopolymers. This leads to the expectation that the distribution also broadens with increased aging time for a given undercooling. Although time-aging time superposition may not be valid in the strictest sense, decent superposition of the data was apparent and the degree of shifting can still be informative. The role of composition on  $\tau$  at  $t_a=0.6$  hr indicates that the blends are inherently less mobile than additive for both undercoolings, and this is consistent with the negative deviation observed for the specific volume versus composition data. The additional mobility which was manifested in the volume relaxation responses at  $T_g-60^\circ\text{C}$  due to the cooperative secondary relaxations for the blends, as was previously hypothesized, apparently did not play a significant role in the unaged mechanical relaxation times for the blends compared to the influence of packing features.

Although the dependence of the initial relaxation time on composition can be rationalized, the increases in the relaxation times during aging, which define the mechanical aging rates, show some unusual behavior. The negative deviation in  $\mu$  with respect to composition at  $T_g-60^\circ\text{C}$  is a peculiar result because the volume relaxation rates were essentially linear with PPO content at this undercooling. One of the characteristics which is often linked in a causal manner to mechanical mobility is free volume. A

pertinent quantity is, therefore, the degree to which a reduction in volume affects the mechanical properties during aging. The sensitivity parameter,  $S$ , indicates the extent to which mechanical property changes are influenced by the changing structure:<sup>1</sup>

$$S = \frac{2.303\mu}{b_V} \quad \text{Eqn. 4-5}$$

Inspection of the variation of sensitivity with composition and undercooling in Figure 4-17 reveals that the increase in sensitivity upon going from  $T_g-30^\circ\text{C}$  to  $T_g-60^\circ\text{C}$  is less than expected for the blends relative to the behavior of a-PS and PPO. As was stated earlier, no significant difference in the role of PPO content on the initial mechanical relaxation behavior was evident for an aging temperature of  $T_g-30^\circ\text{C}$  compared to  $T_g-60^\circ\text{C}$ . The evaluation of the sensitivity parameter, however, revealed that the importance of aging-induced densification in dictating the degree to which the creep response shifts to longer times became noticeably diminished for the blends compared to additivity for aging performed deeper within the glassy state at  $T_g-60^\circ\text{C}$ .

#### 4.4 Conclusions

The physical aging process was investigated as a function of blend composition and aging temperature for the a-PS/PPO blend system by employing volume relaxation, enthalpy relaxation/recovery, and creep compliance measurements. At aging temperatures of  $15^\circ\text{C}$  and  $30^\circ\text{C}$  below the midpoint glass transition temperature ( $T_g$ ), the a-PS/PPO blends exhibited volume relaxation rates which were retarded compared to additivity based upon the aging rates for pure a-PS and PPO. Broader glass transitions for the blends in comparison to a-PS and PPO were not responsible for this volume relaxation trend as was proven by rescaling the data with respect to the onset of the glass transition temperature. A heightened state of glassy packing for the blends was held responsible for the volume relaxation behavior at  $T_g-15^\circ\text{C}$  and  $T_g-30^\circ\text{C}$ . The negative deviation in the volume relaxation data diminished with increased undercooling, and eventually the volume relaxation rates displayed a nearly linear trend with respect to composition at the greatest undercooling of  $60^\circ\text{C}$  which was employed. This change in trend is conjectured to be caused by a unique cooperative secondary relaxation process in

the blends in the vicinity of the  $\beta$ -relaxation for a-PS which played more of an active role for aging performed deep in the glassy state. Enthalpy recovery experiments were performed following aging at undercoolings of 30°C and 60°C, and two methods were used to analyze the data in order to infer the relaxation which occurred during the annealing process. Both techniques gave similar results for aging performed at  $T_g-30^\circ\text{C}$ , and the compositional dependence of enthalpy relaxation was similar to that observed for volume at this aging temperature. Due to unusual enthalpy recovery responses for the blends with 25 and 50 wt.% PPO following aging at  $T_g-60^\circ\text{C}$ , a discrepancy existed between the trends exhibited by the enthalpy relaxation data using the two methods. Therefore, a comparison of volume and enthalpy relaxation rates was inconclusive at the undercooling of 60°C. The variation of mechanical aging rate with composition exhibited a significant negative deviation from additivity, and this trend featuring substantially retarded aging rates was present at both undercoolings of 30 and 60°C which were investigated. The compositional dependence of glassy packing appeared to be the governing influence on the initial mechanical behavior prior to aging at both temperatures of  $T_g-30^\circ\text{C}$  and  $T_g-60^\circ\text{C}$ . Strength for this argument was provided by the relaxation time parameters which were determined by fitting the creep compliance data. However, although the dependence of the initial mechanical response on the unaged state of packing for the blend system was similar for the undercooling of 30°C compared to 60°C, the sensitivity of mechanical property changes to the volume relaxation response was quite different for the blends at the two aging temperatures. The relaxation time distribution breadths inferred from the creep compliance master curves by stretched exponential fits applied to the data indicated that the blends possessed broader distributions than the pure components. This was consistent with glass transition breadths measured by both differential scanning calorimetry and dynamic mechanical analysis.

Table 4-I: Glass Transition Temperature Results

PPO content (wt.%)	DSC: 10°C/min heating scan following 200°C/min quench into glassy state				DMA: 1 Hz, 2°C/min heating	
	T <sub>g</sub> (°C)	T <sub>g,onset</sub> (°C)	T <sub>g,end</sub> (°C)	T <sub>g,start</sub> (°C)	tand peak temp. (°C)	tand peak onset (°C)
0	103	100	106	92	121	103
25	127	122	132	115	146	127
50	149	142	155	134	169	147
75	170	164	177	154	195	172
87.5	195	189	200	179	217	195
100	215	211	218	201	229	212

Table 4-II: Observed Differences Between Liquid and Glassy Heat Capacities

PPO Content (wt. %)	$\Delta C_{p,g}$ (J/g-K)	$\Delta C_p / \Delta C_{p,g}$ at T <sub>g</sub> -30°C	$\Delta C_p / \Delta C_{p,g}$ at T <sub>g</sub> -60°C
0	0.268	1.11	1.20
25	0.263	1.09	1.26
50	0.245	1.14	1.27
75	0.232	1.16	1.23
87.5	0.217	1.13	1.21
100	0.213	1.13	1.24

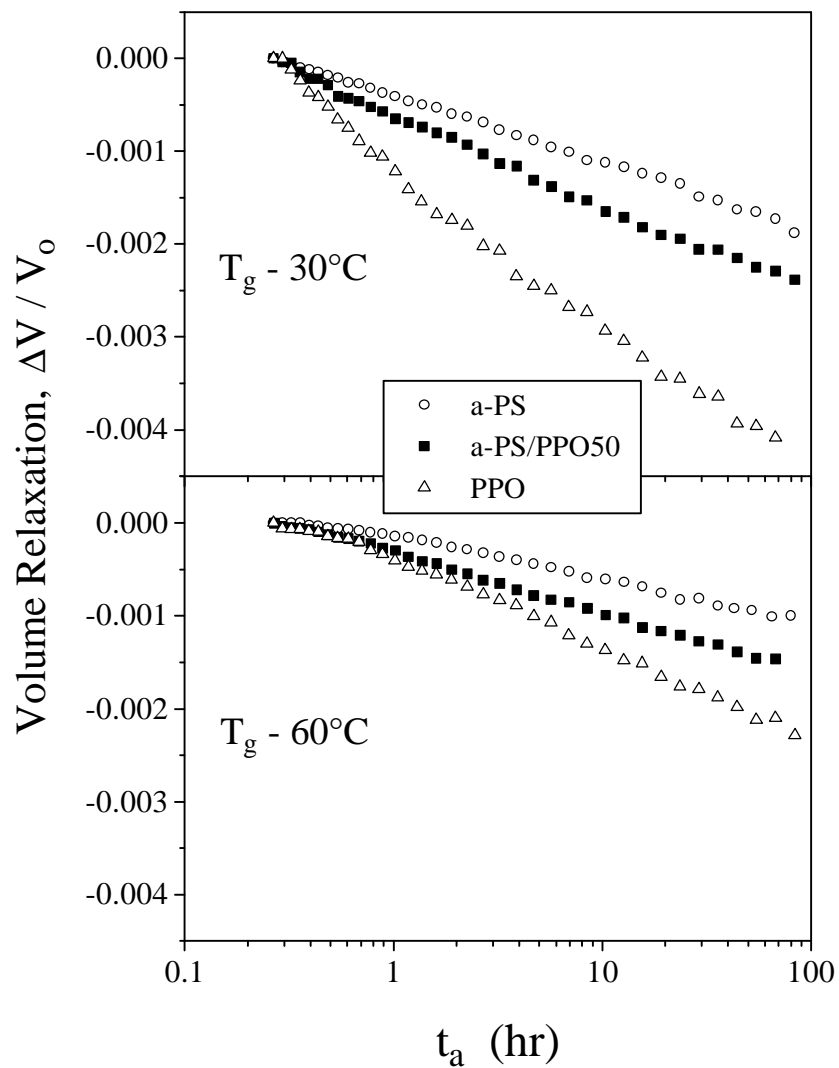


Figure 4-1: Representative volume relaxation data at undercoolings of 30°C and 60°C. An aging time of 0.25 hr was used as the reference for determining volume differences ( $\Delta V$  values). The negative slope of each data set represents the volume relaxation rate,  $b_V$ , and data points between 0.6 hr and 80 hr were used in the rate determination.

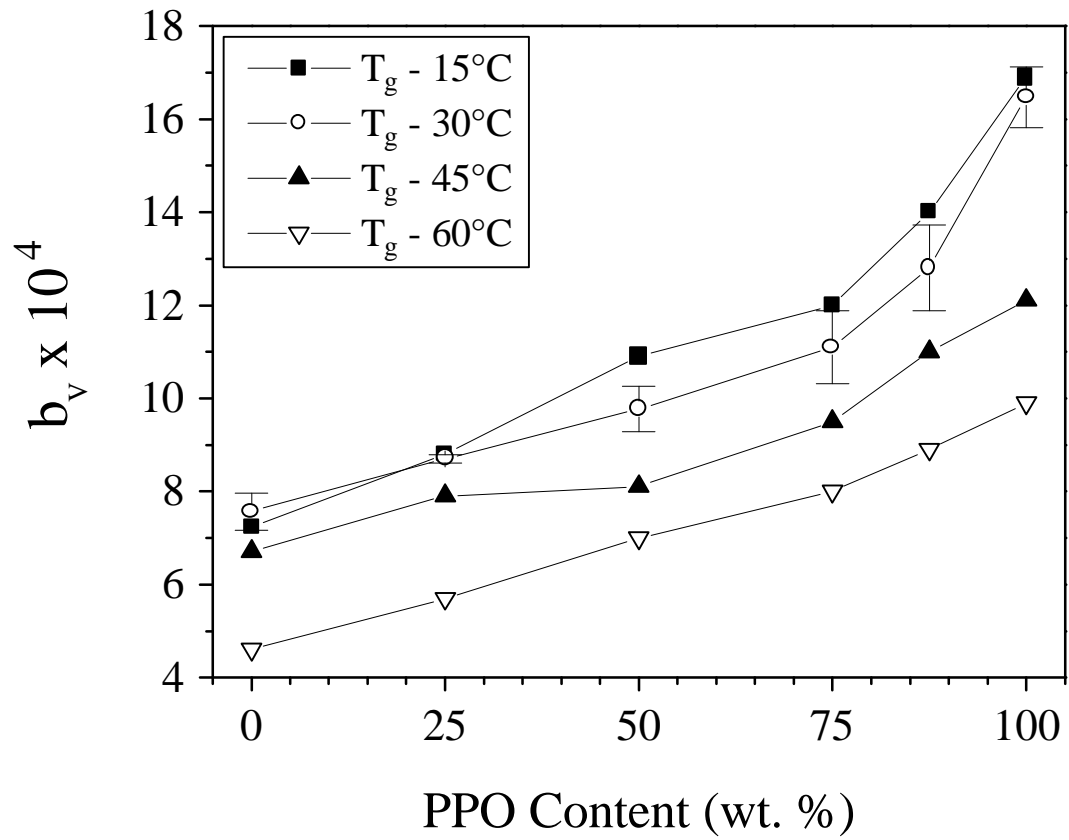


Figure 4-2: Volume relaxation rate as a function of composition for the indicated undercoolings.

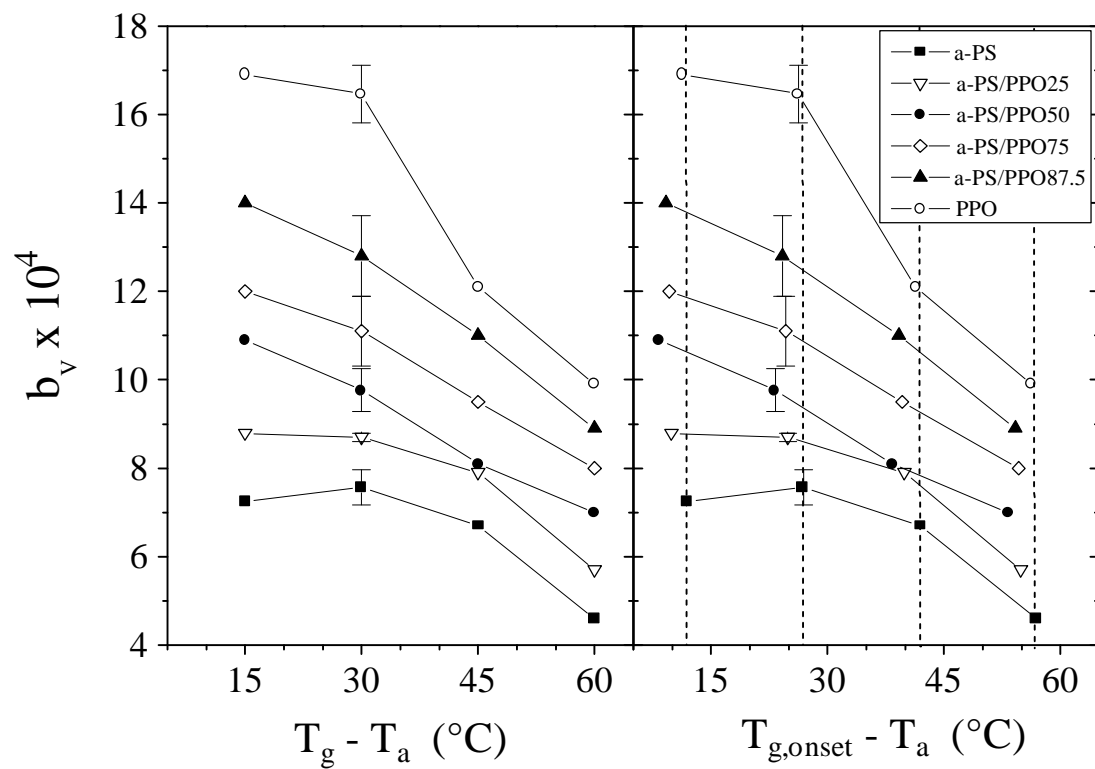


Figure 4-3: Volume relaxation rates replotted as a function of undercooling. Both the midpoint and onset DSC glass transition temperatures are employed as references.

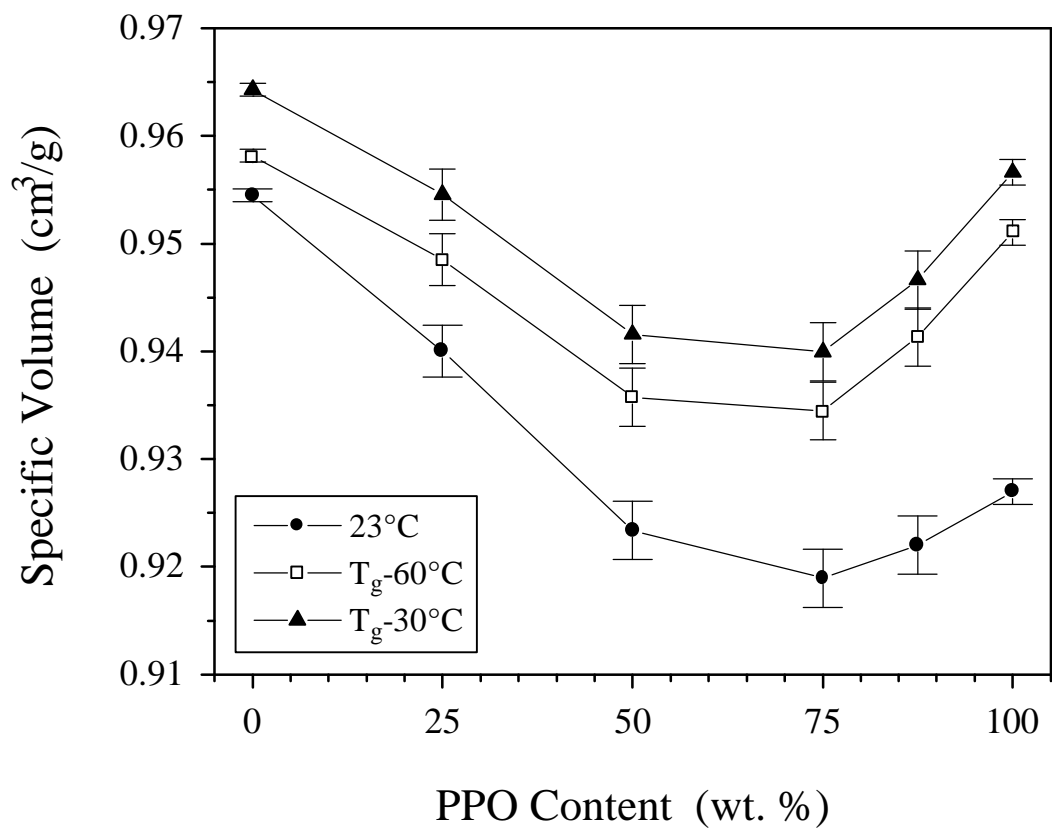


Figure 4-4: Dependence of specific volume on blend composition for freshly quenched glassy samples.

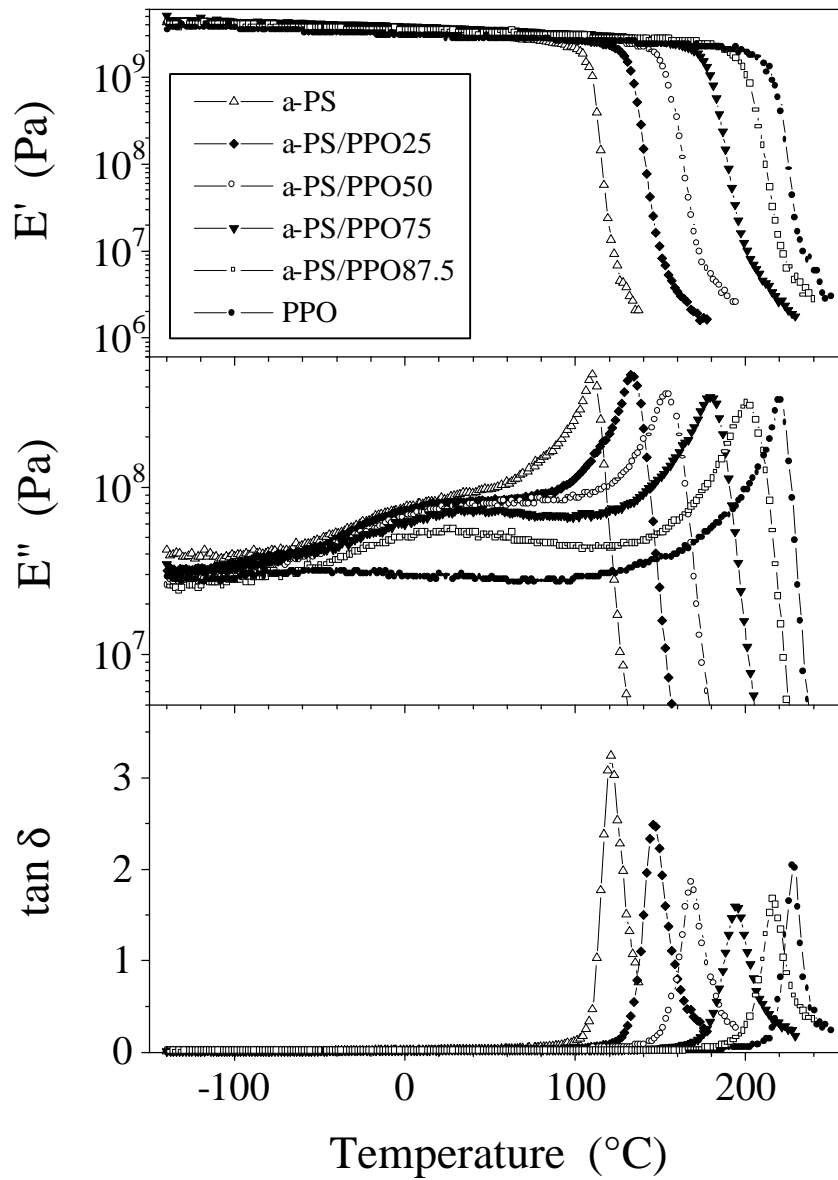


Figure 4-5: Dynamic mechanical response for freshly quenched samples using a heating rate of 2°C/min and a frequency of 1 Hz.

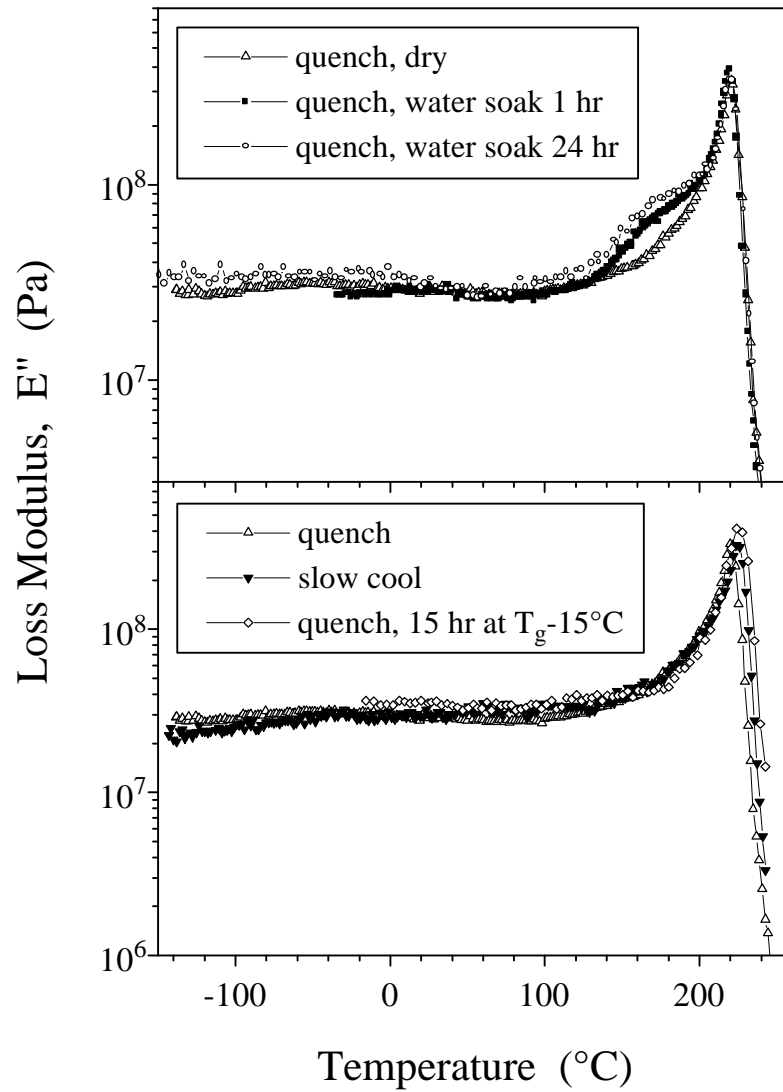


Figure 4-6: Dynamic mechanical response using a heating rate of 2°C/min and a frequency of 1 Hz for PPO samples with the indicated pre-treatments.

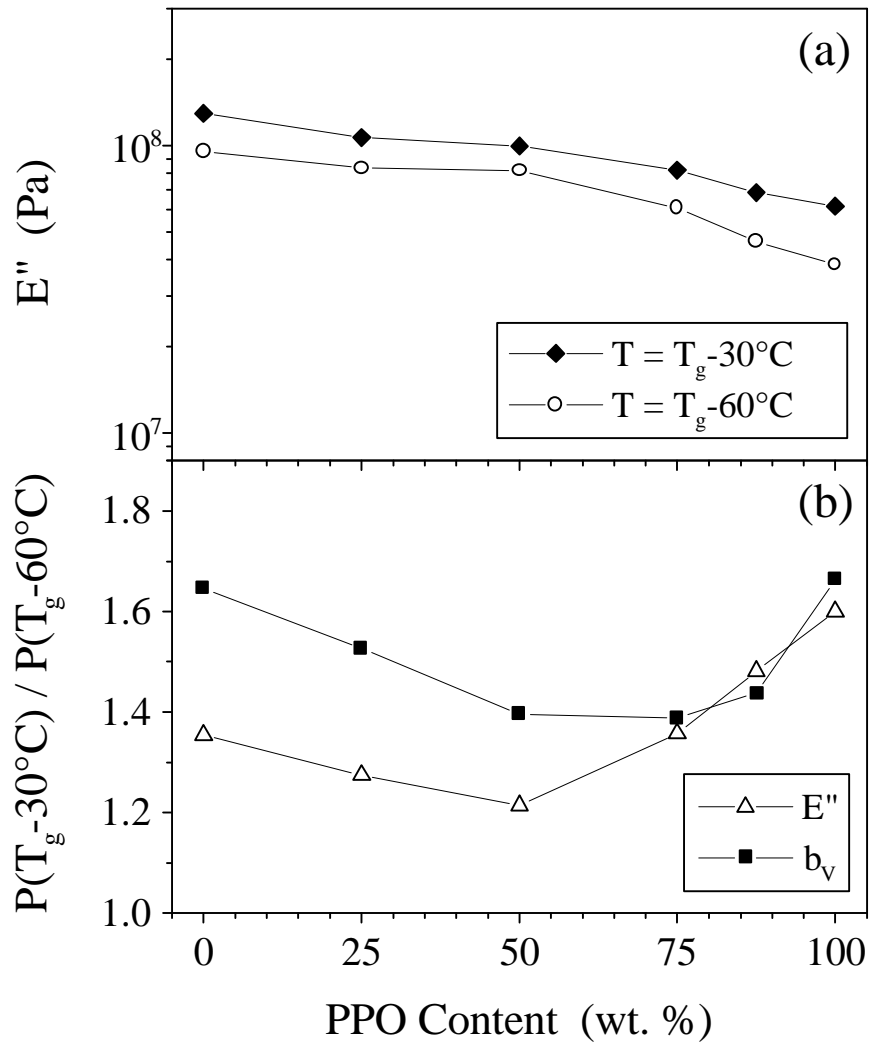


Figure 4-7: Loss modulus at the indicated temperatures (a); and a comparison of property (P) ratios for loss modulus and volume relaxation rate. See text for additional details.

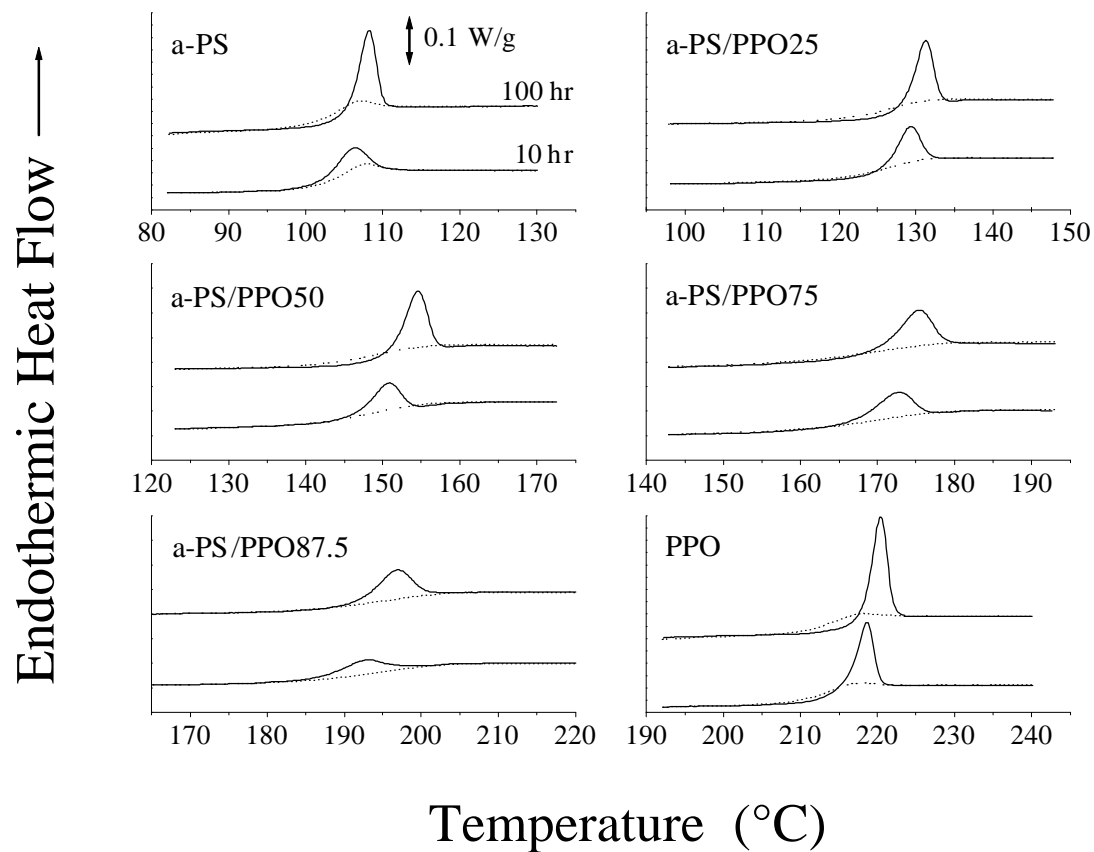


Figure 4-8: Representative DSC enthalpy recovery traces during heating at 10°C/min following annealing at  $T_g - 30^\circ\text{C}$ . The dotted lines represent the second heats after freshly quenching the samples into the glassy state at 200°C/min.

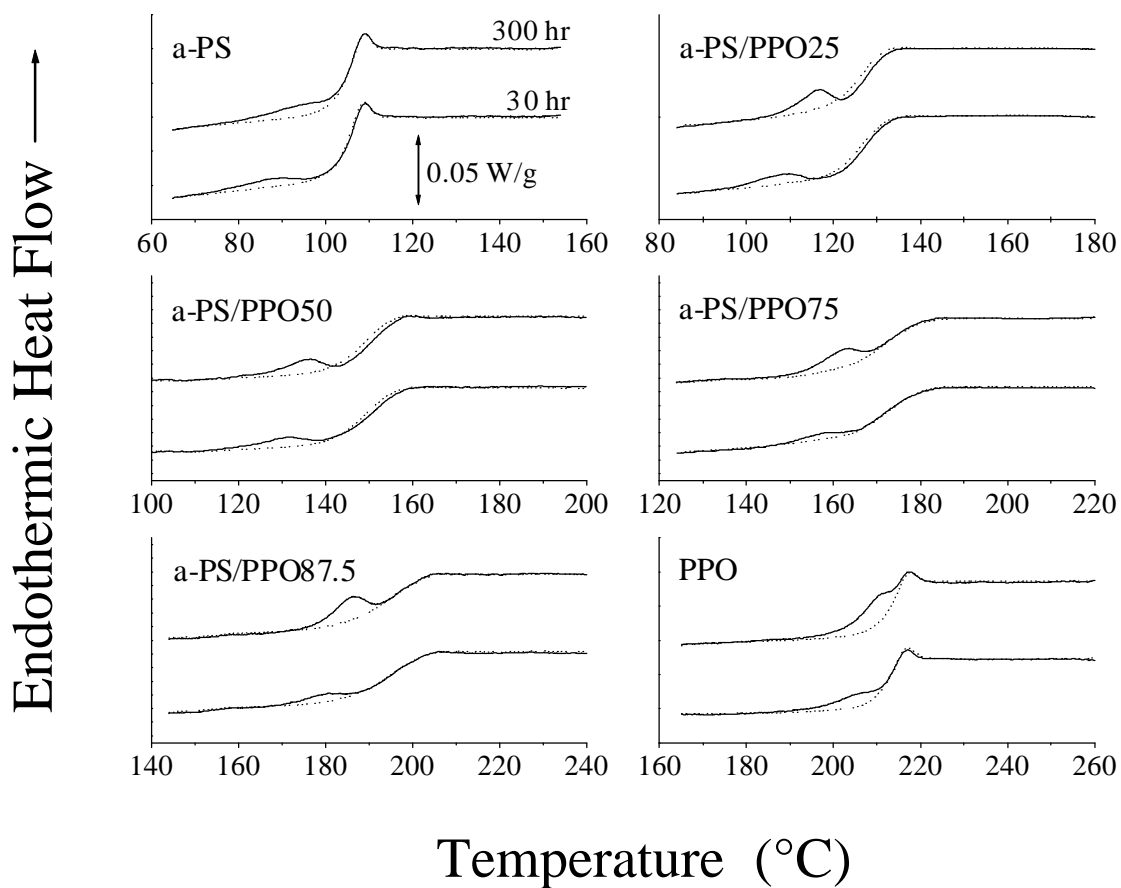


Figure 4-9: Representative DSC enthalpy recovery traces during heating at 10°C/min following annealing at  $T_g - 60^\circ\text{C}$ . The dotted lines represent the second heats after freshly quenching the samples into the glassy state at 200°C/min. Note that the scale is different than that used in Figure 4-8.

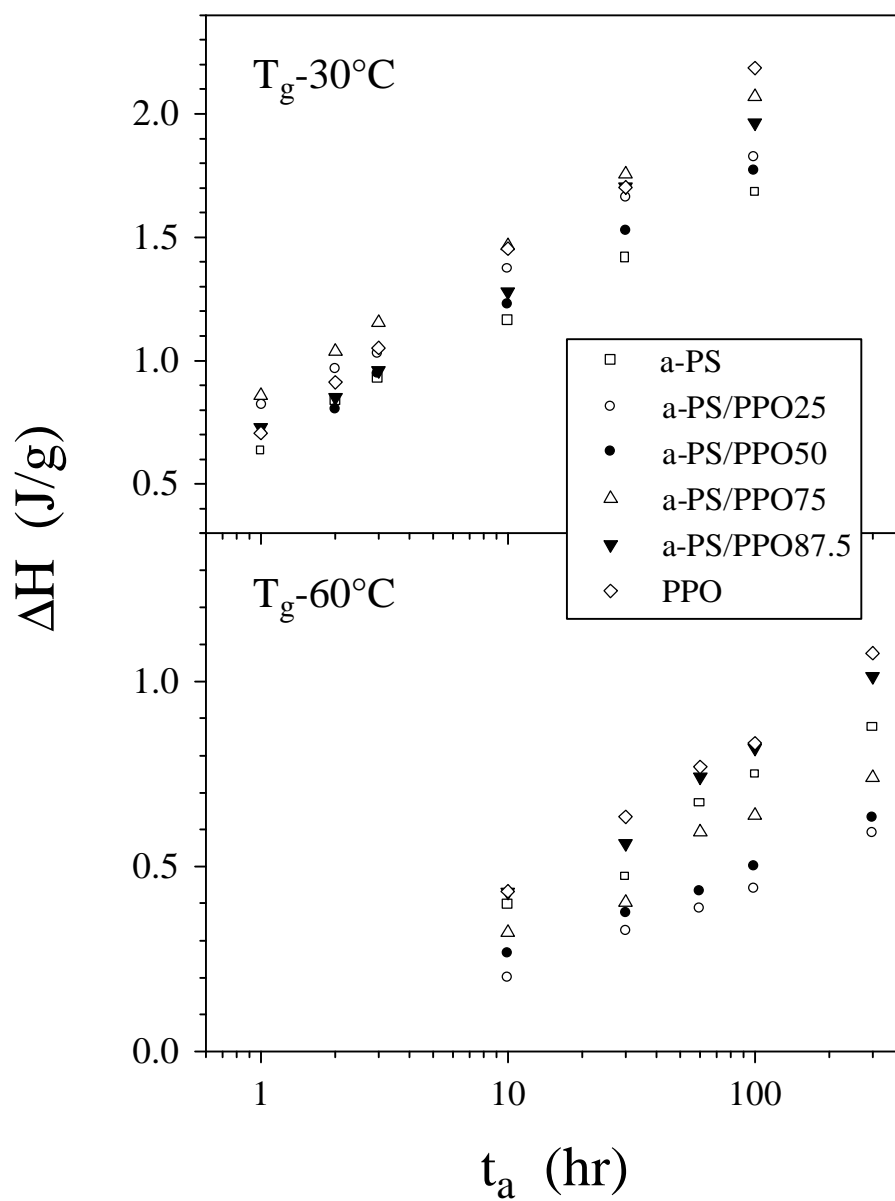


Figure 4-10: Recovered enthalpy ( $\Delta H$ ) as a function of aging time for undercoolings of  $30^\circ\text{C}$  and  $60^\circ\text{C}$ . Each data point represents the average  $\Delta H$  from three DSC enthalpy recovery experiments, and approximately 200 DSC runs were performed in order to generate this plot.

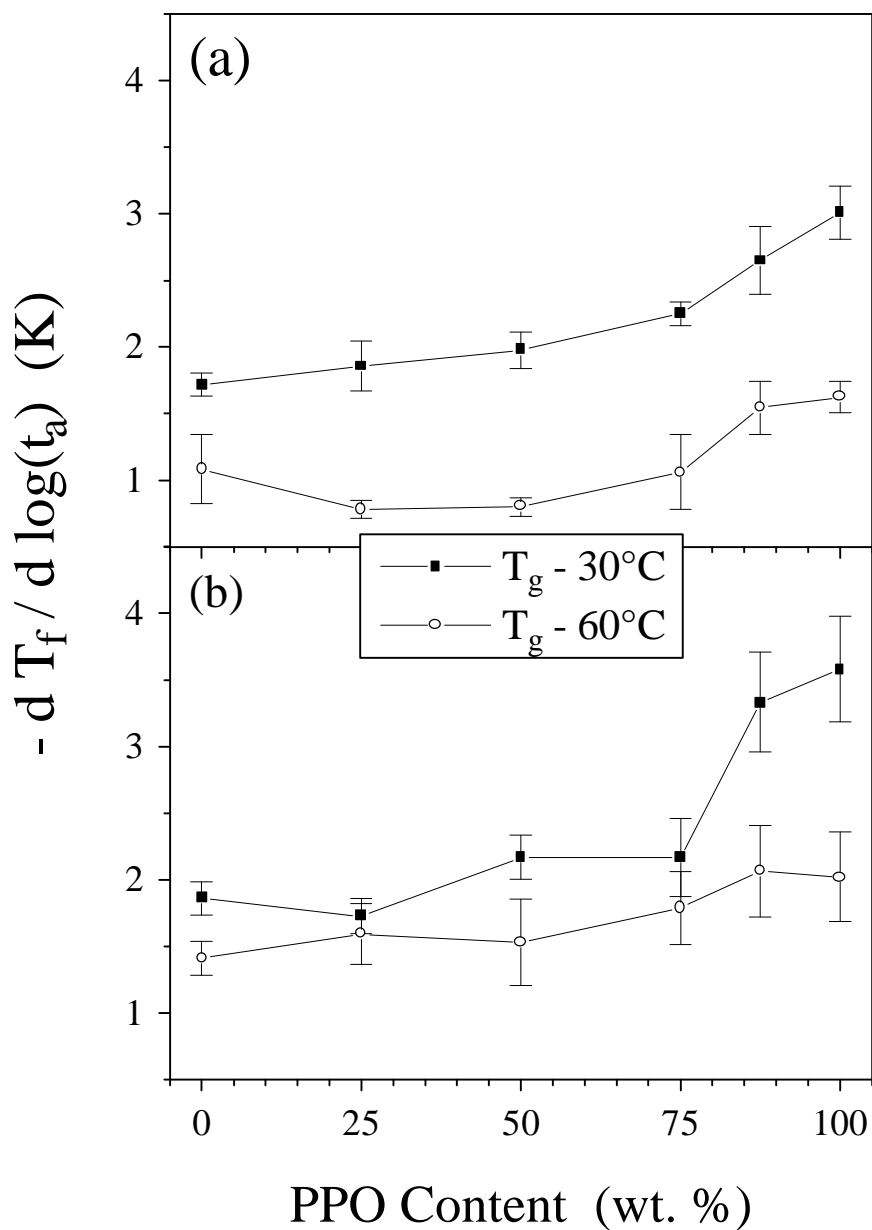


Figure 4-11: Rate of change of enthalpic fictive temperature during aging. Rates were determined: (a) from the  $\Delta H$  data; and (b) from the first heating scans using the software provided with the DSC instrument. See text for additional details.

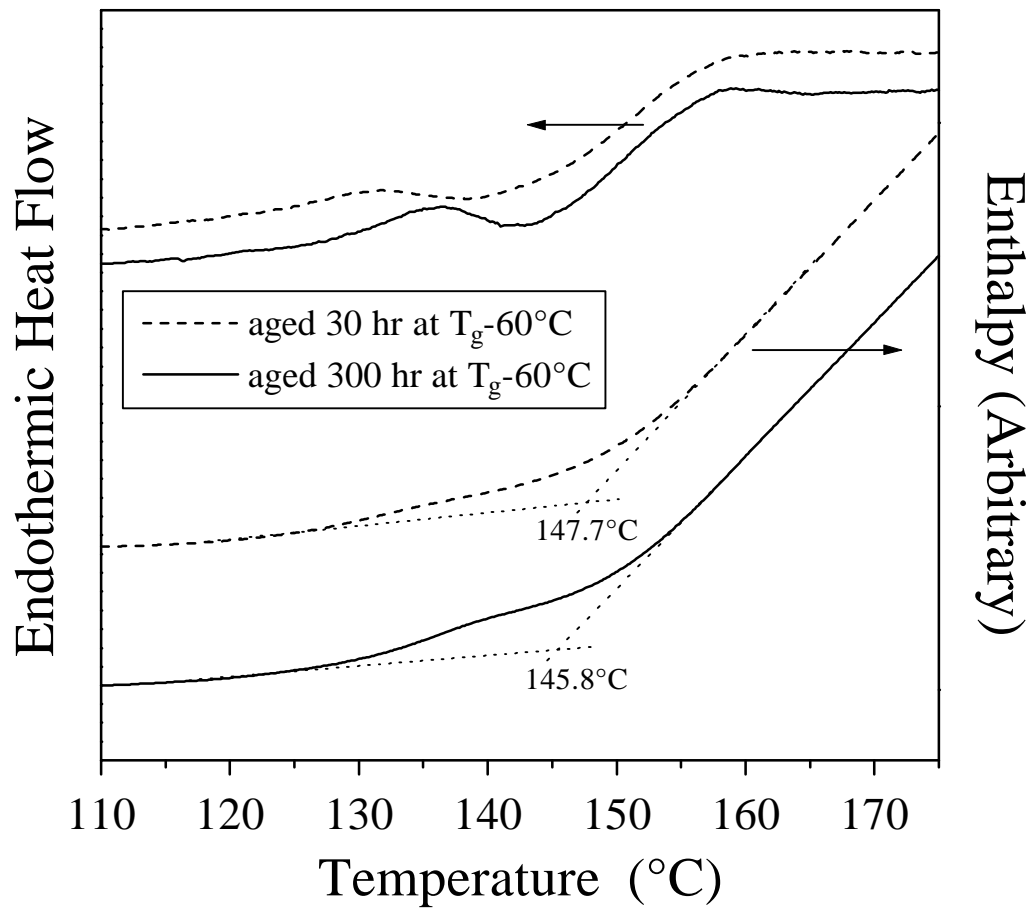


Figure 4-12: Illustration of enthalpic fictive temperature assessment for a-PS/PPO50 blend aged at  $T_g - 60^\circ\text{C}$ .

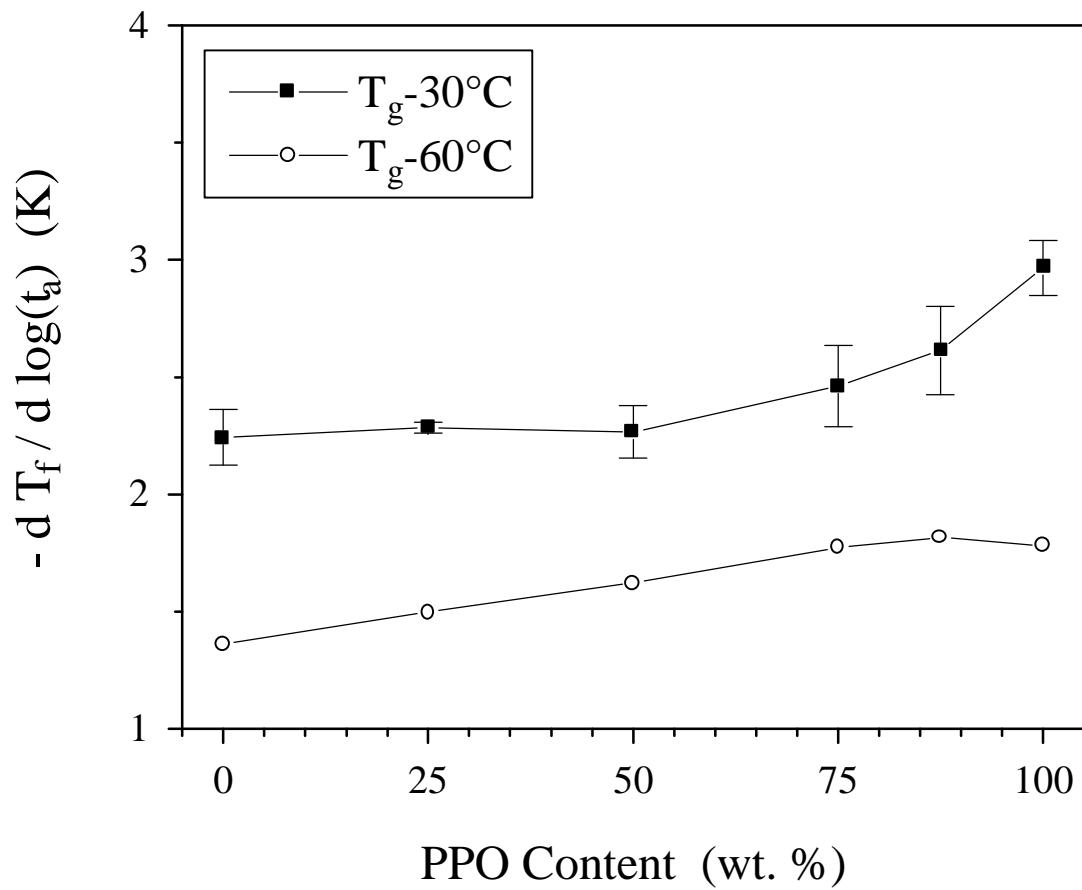


Figure 4-13: Rate of change of volumetric fictive temperature during aging. See text for additional details.

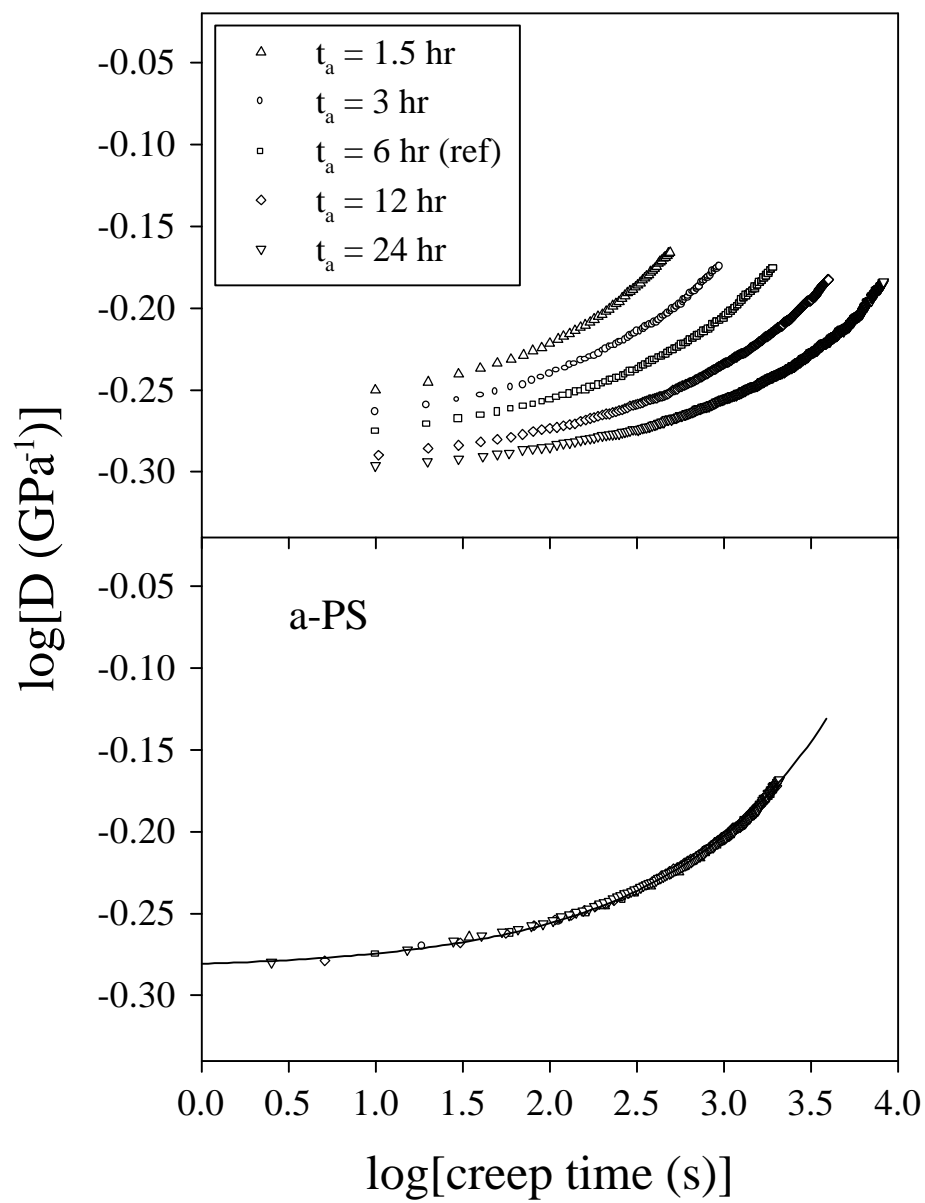


Fig. 4-14(a)

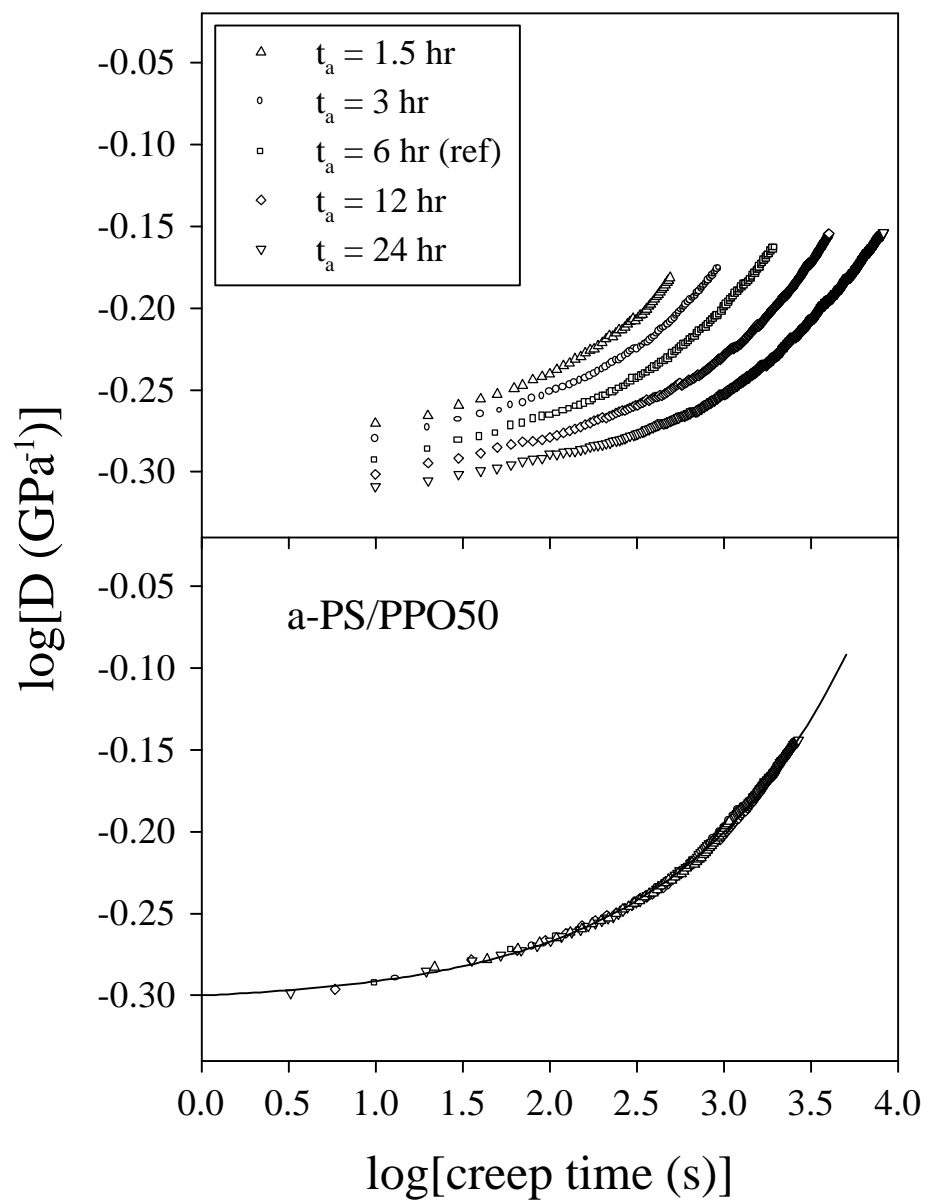


Fig. 4-14(b)

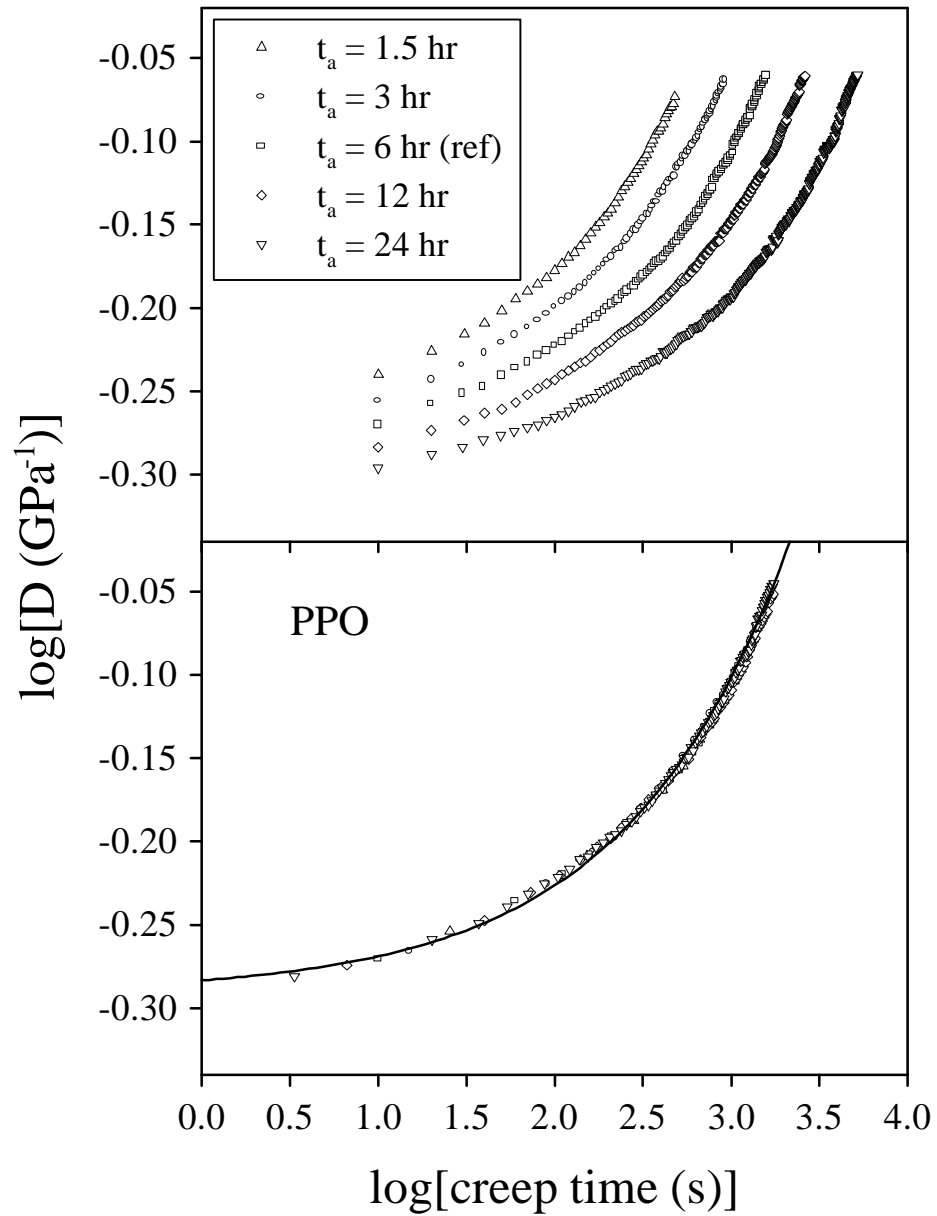


Fig. 4-14(c)

Figure 4-14: Creep compliance responses for a-PS (a), a-PS/PPO50 (b), and PPO (c) aged at  $T_g-30^\circ\text{C}$ . Upper plots depict the data as a function of aging time, and the lower plots are the master curves generated at a reference aging time of 6 hr as well as the stretched exponential fits to the master curve data. For clarity, only every fifth data point is included in the master curves.

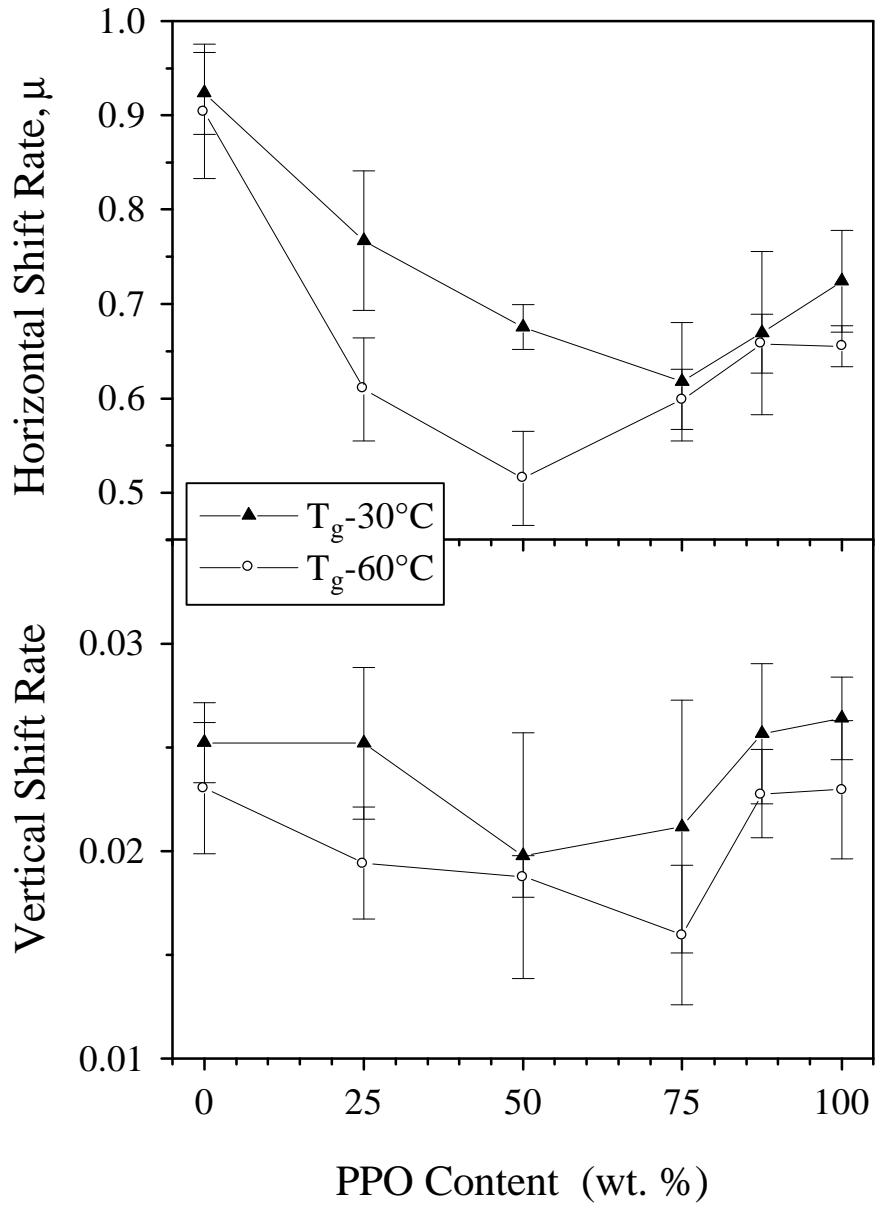


Figure 4-15: Mechanical aging rates determined from horizontal and vertical shift factors used during formation of creep compliance master curves.

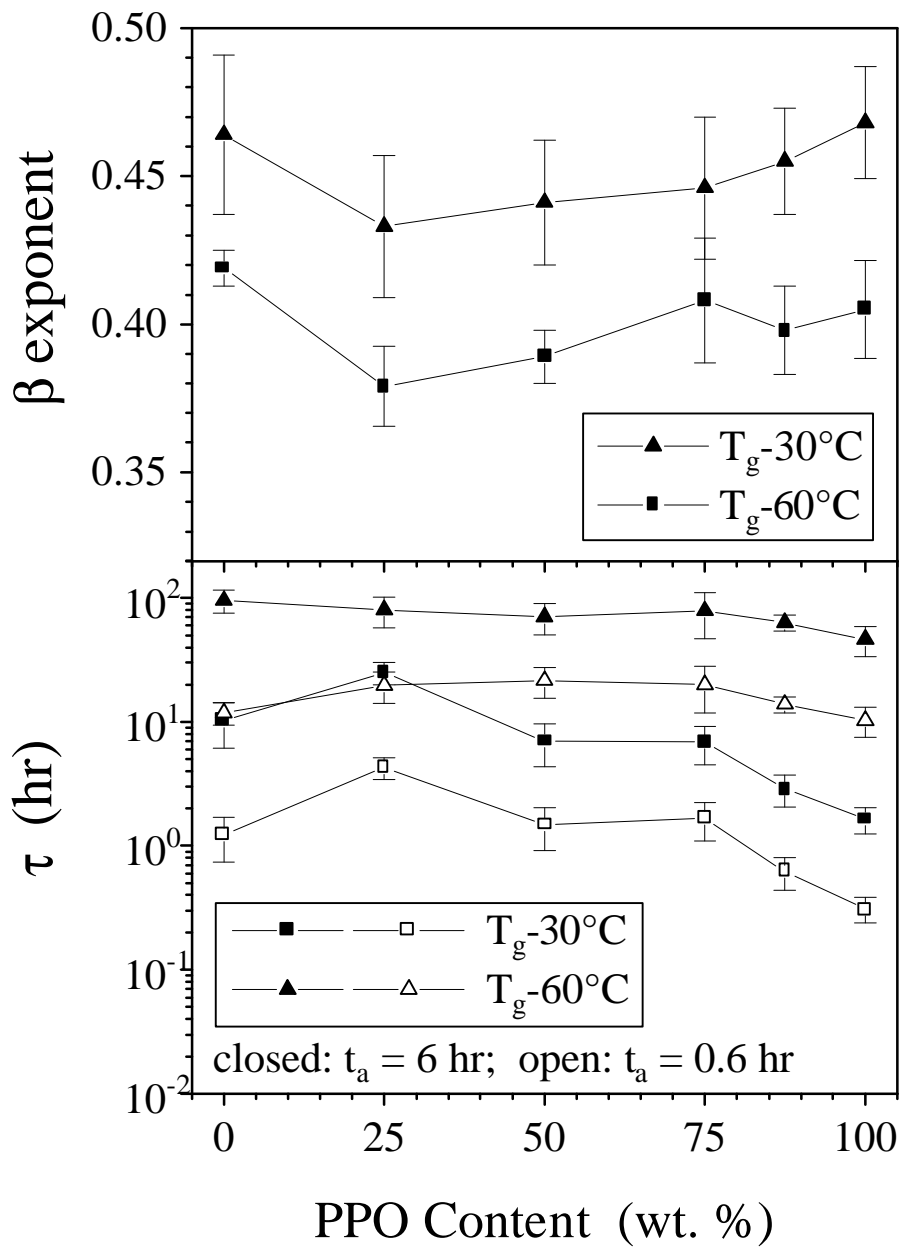


Figure 4-16: Variation of the stretched exponential function parameters  $\tau$  and  $\beta$  with composition for creep compliance response at  $T_{g,-30^{\circ}\text{C}}$  and  $T_{g,-60^{\circ}\text{C}}$ .

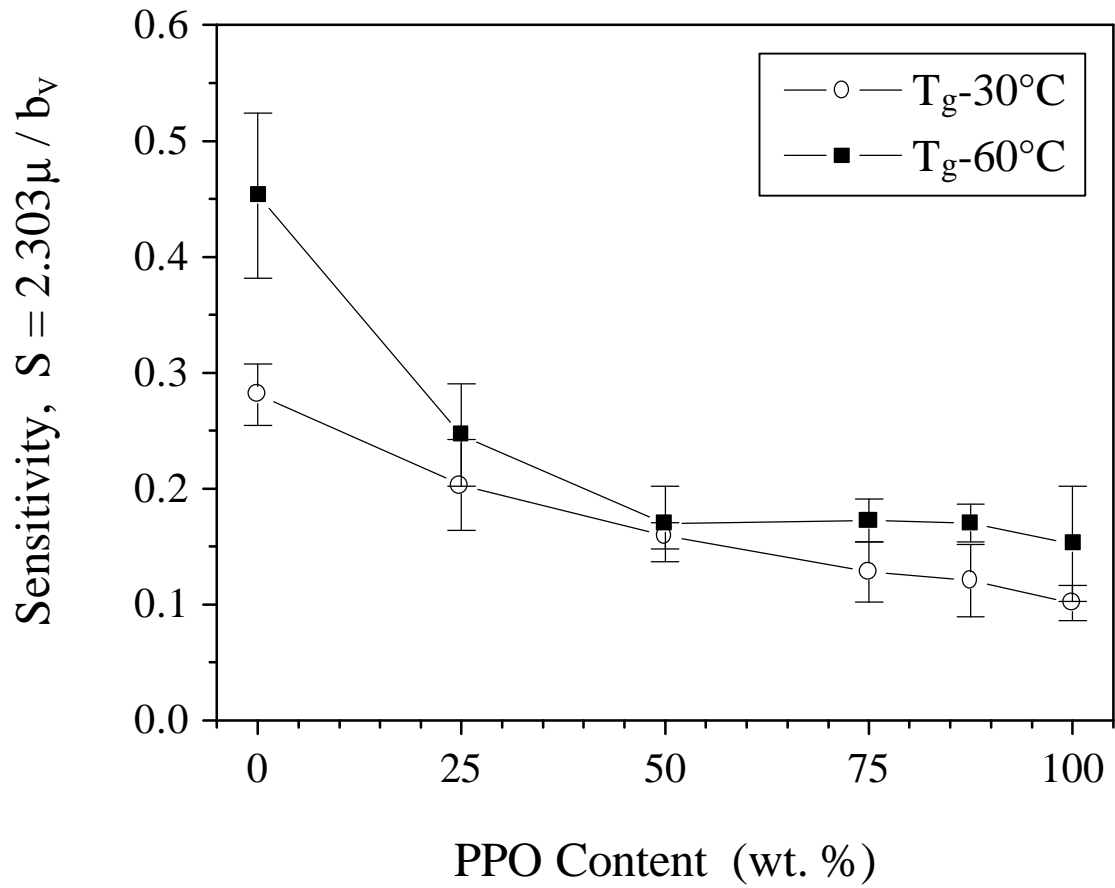


Figure 4-17: Sensitivity of mechanical creep changes to structural volume changes for the blend system at undercoolings of 30°C and 60°C.

## 4.5 References

- 1 Struik, L. C. E. *Physical Aging in Amorphous Polymers and Other Materials*, Elsevier, New York, 1978.
- 2 O'Reilly, J. M. *CRC Critical Rev. in Solid State and Matl. Sci.*, 1987, **13(3)**, 259.
- 3 Tant, M. R. and Wilkes, G. L. *Polym. Eng. Sci.*, 1981, **21(14)**, 874.
- 4 Hutchinson, J. M. *Prog. Polym. Sci.*, 1995, **20**, 703.
- 5 McKenna, G. B. in 'Comprehensive Polymer Science, Vol. 2, Polymer Properties' (eds. C. Booth and C. Price), Pergamon, Oxford, UK, 1989, pp 311-362 (Chapter 10).
- 6 Prest, W. M., Jr., Luca, D. J., and Roberts, F. J., Jr., in 'Thermal Analysis in Polymer Characterization' (ed. E. A. Turi), Heyden, Philadelphia, 1981, pp. 24-42.
- 7 Prest, W. M., Jr. and Roberts, F. J., Jr., in 'Thermal Analysis, Proceedings of the Seventh International Conference on Thermal Analysis' (ed B. Miller), John Wiley and Sons, New York, 1982, Vol 2, pp.973-8.
- 8 Cavaille, J. Y., Etienne, S., Perez, J., Monnerie, L. and Johari, G. P. *Polymer* 1986, **27**, 686.
- 9 Pathmanathan, K., Johari, G. P., Faivre, J. P., and Monnerie, L. *J. Polym. Sci., Part B: Polym. Phys.* 1986, **24**, 1587.
- 10 Bosma, M., ten Brinke, G., and Ellis, T. E. *Macromolecules* 1988, **21**, 1465.
- 11 Cowie, J. M. G. and Ferguson, R. *Macromolecules* 1989, **22**, 2312.
- 12 Mijovic, J., Ho, T., and Kwei, T. K. *Polym. Eng. Sci.* 1989, **29**, 1604.
- 13 Ho, T. and Mijovic, J. *Macromolecules* 1990, **23**, 1411.
- 14 Elliot, S. *Ph.D. Dissertation*, Heriot-Watt University (U.K.), 1990.
- 15 Ho, T., Mijovic, J., and Lee, C. *Polymer* 1991, **32**, 619.
- 16 Oudhuis, A. A. C. M. and ten Brinke, G. *Macromolecules* 1992, **25**, 698.
- 17 Pauly, S. and Kammer, H. W. *Poly. Networks Blends* 1994, **4**, 93.
- 18 Chang, G.-W., Jamieson, A. M., Yu, Z., and McGervey, J. D. *J. Appl. Polym. Sci.* 1997, **63**, 483.
- 19 Campbell, J. A., Goodwin, A. A., Mercer, F. W., and Reddy, V. *High Perform. Polym.*, 1997, **9**, 263.
- 20 Cowie, J. M. G., McEwen, I. J., and Matsuda, S. *J. Chem. Soc., Faraday Trans.*, 1998, **94**, 3481.
- 21 Robertson, C. G. *Ph.D. Dissertation*, Virginia Polytechnic Institute and State University, 1999.
- 22 Shelby, M. D. *Ph.D. Dissertation*, Virginia Polytechnic Institute and State University, 1996.
- 23 Greiner, R. and Schwarzl, F. R. *Rheol. Acta*, 1984, **23(4)**, 378.
- 24 Marvin R. S. and McKinney, J. E. in 'Physical Acoustics', Vol. II B (ed. W. P. Mason), Academic, New York, 1965.
- 25 Kleiner, L. W., Karasz, F. E. and MacKnight, W. J. *Polym. Eng. Sci.*, 1979, **19**, 519.
- 26 Robertson, C. G. and Wilkes, G. L. in *Structure and Properties of Glassy Polymers* (eds. M. R. Tant and A. J. Hill), ACS Books, Washington DC, 1998, p. 133.
- 27 Chung, C. I. and Saur, J. A. *J. Polym. Sci., Part A-2*, 1971, **9**, 1097.
- 28 Illers, K. H. and Jenckel, E. *J. Polym. Sci.*, 1959, **41**, 528.
- 29 Yano, O. and Wada, Y. *J. Polym. Sci., Part A-2*, 1971, **9**, 669.

- 30 Yee, A. F. *Polym. Eng. Sci.*, 1977, **17**, 213.
- 31 De Petris, S., Frosini, V., Butta, E., and Baccaredda, M. *Makromol. Chem.*, 1967, **109**, 54.
- 32 Karasz, F. E., MacKnight, W. J., and Stoelting, J. *J. Appl. Phys.*, 1970, **41**, 4357.
- 33 Ko, J., Park, Y., and Choe, S. *J. Polym. Sci., Part B: Polym. Phys.* 1998, **36**, 1981.
- 34 Struik, L. C. E. *Polymer*, 1987, **28**, 1869.
- 35 Tool, A. Q. *J. Am. Ceram. Soc.*, 1946, **29**, 240.
- 36 Tool, A. Q. *J. Res. Natl. Bur. Stand.*, 1946, **37**, 73.

# Chapter 5

## Glass Formation Kinetics for Miscible Blends of Atactic Polystyrene and Poly(2,6-dimethyl-1,4-phenylene oxide)

---

---

### Chapter Synopsis

Kinetic behavior in the glass formation region was observed by differential scanning calorimetry (DSC) and dynamic mechanical analysis (DMA) for miscible blends composed of atactic polystyrene (a-PS) and poly(2,6-dimethyl-1,4-phenylene oxide) (PPO). The relaxation time build-up with cooling was more severe for the blends in the glass transition region compared to additive behavior based upon the responses of the blend components, and attractive interactions between the blend components were held responsible for this result. This greater degree of segmental cooperativity for the blends compared to pure a-PS and PPO provided insight into physical aging trends, and a connection between sub- $T_g$  aging rates and glass formation kinetics emerged from this investigation. The blends which were rich in PPO exhibited dynamic mechanical loss data which were slightly skewed at the low frequency side of the  $\alpha$ -relaxation dispersion compared to the stretched exponential function fits, and this behavior was likely the consequence of composition fluctuations. Thermal expansion coefficients were obtained above and below the  $T_g$  region, and glassy state densities were determined for freshly quenched samples. This information, in combination with the results of a previous investigation by Zoller and Hoehn [Zoller, P.; Hoehn, H. H. *J. Polym. Sci.: Polym. Phys. Ed.* **1982**, *20*, 1385], indicated that the heightened state of glassy density for these blends compared to the pure polymers was completely kinetic in origin and was not a feature of the thermodynamics of miscibility. This study provided, therefore, a convincing argument against the common interpretation of the compositional dependence of glassy specific volume as a reflection of  $\Delta V_{\text{mix}}$  features associated with the thermodynamics of mixing in the liquid state. However, evidence suggested that the extrapolated glass transition temperatures for the blends in the limit as cooling rate approaches zero, which may represent true thermodynamic transitions, were governed by glassy density features which mirror the liquid state  $\Delta V_{\text{mix}}$  behavior.

## 5.1 Introduction

One of the most widely studied blend systems is that comprised of atactic polystyrene (a-PS) and poly(2,6-dimethyl-1,4-phenylene oxide) (PPO). It is uncommon for a pair of high molecular weight polymers to form completely miscible mixtures, but blends of these two components display miscibility throughout the entire composition range. Mixtures of a-PS and PPO have been investigated with regards to component interactions and miscibility,<sup>1-7</sup> glass transition behavior,<sup>8-10</sup> thermodynamic characteristics,<sup>11-14</sup> barrier properties,<sup>15-17</sup> mechanical properties,<sup>18-22</sup> orientation and relaxation behavior studied by rheo-optical techniques,<sup>23-26</sup> dielectric and dynamic mechanical responses,<sup>8,18,27-29</sup> rheology,<sup>30,31</sup> physical aging,<sup>32-39</sup> and free volume properties determined using positron annihilation lifetime spectroscopy.<sup>38,40</sup> This list is not intended to provide a comprehensive description of research on a-PS/PPO polyblends but rather to give representative examples of previous investigations of this prevalent blend system. Mixtures of a-PS and PPO have received attention in the research arena, in part, because the blend system has significant industrial importance.<sup>41</sup> Therefore, scientific interest in the a-PS/PPO polymer blends proceeds from the atypical extent of miscibility exhibited by this amorphous polymer pair, and this interest is further fueled by the industrial significance of these polyblends.

It is well recognized that the glassy densities of the a-PS/PPO blends are significantly greater than rule-of-mixtures predictions.<sup>12,17-19,39,42</sup> This behavior has been assigned responsibility for heightened modulus<sup>19</sup> and reduced small molecule transport properties<sup>17</sup> in the glassy state for the miscible blends relative to additive contributions from pure a-PS and PPO, to cite a few examples. The increased degree of molecular packing for the a-PS/PPO blends is often interpreted as a thermodynamic effect associated with the component interactions which are responsible for miscibility. It must be remembered, however, that the glassy state is inherently nonequilibrium. If the kinetics of glass formation for the blends are unique compared to the pure polymers due to the attractive interactions between a-PS and PPO in the mixtures, then the compositional dependence of glassy density for freshly quenched samples may simply be a reflection of this behavior. With this issue as an impetus, the goal of this study was to

investigate the glass formation kinetics as a function of composition for the a-PS/PPO system using dynamic mechanical analysis and differential scanning calorimetry. An extensive investigation of physical aging behavior for the a-PS/PPO blend system has been recently performed,<sup>39</sup> and the glass formation kinetics established in this present study will enable a better understanding of the volume and enthalpy relaxation rate trends to be developed. The kinetic information will additionally allow insight to be developed with respect to the difference between the density vs. composition trends observed for the equilibrium liquid state and the nonequilibrium glassy state. Related issues associated with predicting glass transition temperatures as a function of composition using a thermodynamic approach will also be discussed.

## 5.2 Experimental Details

### 5.2.1 Blend Preparation

A model 5501 Brabender melt mixer was used to create blends of atactic polystyrene (a-PS) and poly(2,6-dimethyl-1,4-phenylene oxide) (PPO). Drying of the polymer materials was accomplished under vacuum at 70°C for 2 days prior to blending. The polystyrene pellets were plasticated first in the mixer at 265°C using a speed of 20 RPM, and then the PPO powder was added slowly. Blending was then accomplished at 265°C using a mixing speed of 70 RPM for 15 minutes. Blends were generated with PPO contents of 25, 50, 75, and 87.5 wt.% PPO. The PPO material with  $M_w \approx 50,000$  g/mol was obtained from Polysciences (Cat.# 08974). The a-PS polymer used in this investigation was supplied by Dow Chemical Company (Dow 685D). The number- and weight-average molecular weights for this a-PS material were determined by gel permeation chromatography to be 174,000 and 297,000 g/mol, respectively.<sup>43</sup> Compression molding was performed in order to generate ca. 0.2 mm thick films of the neat materials and blends, and the materials were stored in a dessicator cabinet prior to testing. The blend composition nomenclature to be employed in this paper is a-PS/PPOXX where XX denotes the wt.% of PPO in the blend.

### ***5.2.2 Differential Scanning Calorimetry***

The dependence of fictive temperature on cooling rate was studied using differential scanning calorimetry (DSC) for the blends and pure components with a Perkin-Elmer DSC 7. Each sample with weight ca. 10 mg was loaded in an aluminum pan with lid and annealed in the DSC for 10 minutes at 50°C above  $T_g$  (the glass transition temperature,  $T_g$ , used for all reference purposes in this communication is the inflection DSC glass transition temperature measured during heating at 10°C/min following a quench from above  $T_g$  at 200°C/min). The sample was then cooled at a fixed cooling rate to  $T_g-50^\circ\text{C}$  prior to a heating scan at 10°C/min to a temperature of  $T_g+50^\circ\text{C}$ . The sample was held at  $T_g-50^\circ\text{C}$  for two minutes between the cooling and heating scans in order to provide complete control of the temperature and heat flow before the heating scan was initiated. This necessity was particularly relevant at the highest cooling rates. This minor amount of annealing time at a temperature relatively deep within the glassy state is not expected to significantly alter the structural state of the sample. Six cooling rates of 1, 3, 10, 30, 60, and 100°C/min were employed and a fixed heating rate of 10°C/min was utilized. The Perkin-Elmer software was used in order to analyze the heating scans to determine the calorimetric fictive temperatures. A nitrogen purge was employed during all DSC testing, and the ice content in the ice/water bath was maintained at approximately 30-50% by volume during all testing. Baseline scans were obtained approximately every two hours during testing using a heating rate of 10°C/minute. Any data scans collected for the materials between two baselines were discarded if the baselines exhibited substantial deviation from each other. The temperature was calibrated using the onset melting points of tin and indium, and calibration of the heat signal was achieved using the heat of fusion of indium.

### ***5.2.3 Dynamic Mechanical Analysis***

A Seiko DMS 210 was used to make dynamic mechanical measurements in tension. The samples possessed approximate dimensions of 0.2 mm x 5 mm x 20 mm. The samples were freshly quenched after free-annealing at  $T_g+50^\circ\text{C}$  for 10 minutes prior

to testing. The dynamic mechanical analysis (DMA) was performed at temperatures in the  $\alpha$ -relaxation temperature region (ca. 5°C below to 30°C above the calorimetric  $T_g$ ) using frequencies ranging from 0.01 to 20 Hz.

#### ***5.2.4 Thermal Mechanical Analysis***

Linear thermal contraction was monitored during cooling the isotropic a-PS/PPO materials at 1°C/min using a model TMA 100 Seiko thermal mechanical analyzer (TMA). The temperature range used was from  $T_g+20^\circ\text{C}$  to a final temperature of 50°C. The samples were characterized by the following approximate dimensions: length of 25 mm, thickness of 0.2 mm, and width of 3 mm. A small tensile load was placed on the sample during testing but this did not induce any significant degree of creep. This was verified by holding the sample in tension for 15 minutes at  $T_g+20^\circ\text{C}$  and noting that negligible creep had occurred during this interim. Density measurements were made at 23°C using a pycnometer manufactured by Micromeritics (Model AccuPyc 1330) in order to convert the relative density behavior assessed from the TMA cooling data into actual volume versus temperature curves.

### **5.3 Results and Discussion**

Time-temperature superposition of dynamic mechanical loss data in the segmental dispersion ( $\alpha$ -relaxation) region and evaluation of the cooling rate dependence of DSC glass transition response were performed for the a-PS/PPO blend system. Discussion of the resulting kinetic information afforded by these analyses will be given, and the concepts of fragility and segmental cooperativity will be employed in order to compare the blends with the pure components. An intriguing connection between physical aging rates and the cooperativity associated with the glass formation process will then be revealed. The glassy and equilibrium liquid density characteristics will also be contrasted for the blend system, and the implication of noted differences on the ability to predict the glass transition temperatures for the blends will be considered.

### ***5.3.1 Glass Formation Kinetics from DSC and DMA***

Differential scanning calorimetry can provide useful information about the kinetic nature of the glass transition response. The calorimetric glass transition behavior during heating at 10°C/min was assessed for the a-PS/PPO materials following a quench into the glassy state at various rates ranging from 1°C/min to 100°C/min. A sampling of the scans which resulted from these experiments is provided in Figure 5-1. The blends displayed broader relaxation responses compared to the pure components, and a quantitative breadth comparison will be undertaken later. Beyond a visual comparison of the glass transition behavior for the materials, the DSC data can be further analyzed to give quantitative kinetic information. The relationship between the cooling rate ( $q_c$ ) which is employed during glass formation and the structural, or fictive, temperature which is assessed from the subsequent heating scan can be used to quantify the kinetics of glass formation.<sup>44</sup> The fictive temperature,  $T_f$ , which Tool introduced<sup>45,46</sup> is a parameter which can be used as a measure of the structural state of a glass. The fictive temperature is defined as the temperature at which a glassy material would possess the equilibrium thermodynamic state if heated to that temperature. Illustration of the determination of fictive temperature is provided elsewhere.<sup>39,47</sup> The Perkin-Elmer analysis software allowed straightforward determination of the fictive temperature from each DSC scan. The extent of relaxation time build-up during the glass formation process was quantified through the use of a parameter known as fragility which was developed by Angell.<sup>48-50</sup> The fragility can be simply defined by the slope of the kinetic data plotted in the form indicated in Figure 5-2. Inspection of the compositional dependence of fragility measured using this DSC approach will be undertaken after a description of kinetic data assessed using dynamic mechanical analysis is first given.

The polymer relaxation window which was probed using the DSC protocol mentioned above was limited, and Arrhenius response appeared to be well verified for the materials within this range. However, inspection of a wider range of relaxation data via dynamic mechanical analysis revealed that the glass formation process was characterized by nonArrhenius behavior for the blends and pure polymers. Scaling of dynamic mechanical loss data was performed by generating master curves for loss modulus data obtained at frequencies and temperatures in the glass formation region. Data was

assessed for frequencies ranging from 0.01 to 20 Hz at temperatures from approximately  $T_g-5^\circ\text{C}$  to  $T_g+30^\circ\text{C}$  (the  $T_g$  value which will be used for all reference purposes in this communication is the calorimetric inflection value determined at a heating rate of  $10^\circ\text{C}/\text{min}$  immediately following a quench from well above  $T_g$  at  $200^\circ\text{C}/\text{min}$ ). Relaxation in this regime is often referred to as the segmental dispersion, and the mechanical response is designated as the  $\alpha$ -relaxation for an amorphous polymer. Loss modulus data were reduced into master curves by application of the time-temperature superposition principle, and representative results for PPO and the a-PS/PPO75 blend are given, respectively, in Figure 5-3 and Figure 5-4. Values of the shift factor,  $a_T$ , were assessed from the extent of horizontal shifting which was necessary to superimpose the loss modulus data at selected temperatures with the data obtained at the reference temperature. The shift factor data were then rescaled with respect to a reference temperature equal to the calorimetric glass transition temperature for each material, and these converted data were subsequently plotted in  $T_g$ -normalized Arrhenius form. Each data set was also fit using the well-known Williams-Landel-Ferry (WLF) equation.<sup>51</sup>

$$\log(a_T) = \log\left(\frac{\tau}{\tau_g}\right) = \frac{-C_1(T - T_g)}{C_2 + T - T_g} \quad \text{Eqn. 5-1}$$

The WLF parameters which were developed as a result of this fitting are given in Table 5-I, and selected shift factor data and WLF fits are provided in Figure 5-5. This information developed from the dynamic mechanical results can be further used to discuss the influence of blend composition on fragility and segmental cooperativity which will now be commenced.

The kinetic behavior of the blends and neat polymers can be contrasted using the relaxation data obtained by differential scanning calorimetry and dynamic mechanical analysis. Values of fragility,  $m$ , were determined from the dynamic mechanical relaxation data according to:

$$m = \left. \frac{d \log \tau}{d(T_g/T)} \right|_{T=T_g} = \frac{C_1 T_g}{C_2} \quad \text{Eqn. 5-2}$$

Using this equation, fragility versus PPO content relationships developed from DSC and DMA data can be contrasted, and Figure 5-6 represents such a comparison. Both

techniques indicate that the blends displayed more fragile responses compared to neat a-PS and PPO. Another interesting aspect is that greater fragilities were measured from the DSC data compared to the DMA results. However, the general shape of the fragility versus composition trends are quite similar for both the DMA and DSC data despite the disparity between the magnitudes of the fragility values obtained by the two methods.

Interpretation of the nonArrhenius segmental relaxation behavior of the blends and pure polymers in terms of the Adam-Gibbs<sup>52</sup> cooperativity concept can provide a useful means of contrasting the glass formation responses of the materials. Relaxation of a glass former can be conceptualized as involving intramolecular relaxation of molecular segments, enabled by way of rotation about bonds for example, combined with intermolecular effects associated with crowding of the segments and chemical interactions. The intermolecular features affect the ability of a given segment to undergo an intramolecular relaxation event. Cooperativity, wherein multiple segments must relax simultaneously, is therefore necessary for relaxation to occur. The number of such segments in a relaxing domain is given by the parameter  $z$ , and the general observation of an activation energy which increases during cooling toward the  $T_g$  region can be explained by increases in  $z$ . Of interest is the degree of required cooperativity at the point where departure from the liquid state into the nonequilibrium glass occurs during cooling, and the domain size at this temperature  $T_g$  is denoted by  $z_g$ . Further explanation of the cooperativity approach is offered in Chapter 7 where it is shown that the cooperativity at  $T_g$  can be evaluated from the dynamic mechanical scaling results according to:

$$z_g = (T_g / C_2)^2 \quad \text{Eqn. 5-3}$$

The dependence of  $z_g$  on blend composition was generated using this approach, and the resulting trend is depicted in Figure 5-7. It is evident from this data that significantly larger cooperative domain sizes at  $T_g$  were associated with the segmental relaxation behavior of the blends relative to additivity of the pure component responses.

The intermolecular forces present between a-PS and PPO which are responsible for miscibility may also lead to the greater degree of cooperative behavior for the blends compared to the pure components. Specific attractive interactions are present between a-PS and PPO in their blends, and these interactions are generally considered to be

associated with aromatic donor/acceptor behavior.<sup>6,7</sup> The direct thermodynamic consequences of these specific interactions have been observed. For example, the Flory-Huggins “chi” interaction parameter and enthalpy of mixing were found to be negative for the blend system.<sup>2,11</sup> The presence of these interactions in the blends altered the kinetics of glass formation for the blends compared to neat a-PS and PPO by allowing a greater degree of segmental cooperativity to be developed for the blends prior to departure into the glassy state. A discussion of the implications of this glass formation cooperativity behavior on the physical aging characteristics of the blend system will be entertained later. Also, a probable connection between the variations in  $z_g$  and glassy density with blend composition will be mentioned.

Satisfactory loss modulus master curves were generated for all of the a-PS/PPO materials, and this fact was implied previously during consideration of shift factor data for the materials. No significant difference was noted for the blends compared to pure a-PS and PPO with respect to the applicability of time-temperature scaling for the range of temperatures and frequencies used. In support of this apparent reducibility of the mechanical data for the blends, Lin and Aklonis<sup>21</sup> were able to successfully generate stress relaxation master curves in the glass-rubber softening dispersions of a-PS/PPO blends. According to Cavaille et al.,<sup>28</sup> decent master curves could be obtained from dynamic loss and storage moduli for a-PS and blends containing 10, 20, and 30 wt.% PPO in the  $\alpha$ -relaxation region, but closer inspection revealed that time-temperature superposition was not well confirmed for either the blends or pure atactic polystyrene. Roland, Ngai, and coworkers<sup>53-57</sup> have studied segmental relaxation of various miscible polymer blends in detail using dielectric and dynamic mechanical testing. Failure of superposition was suggested to be a general expectation for miscible polymer blends according to these researchers due to heterogeneity of dynamic relaxation behavior, although this failure was not always borne out by the experimental data. Both failure and success of the time-temperature correspondence principle when applied to segmental and terminal relaxation regimes for miscible blends was revealed via research performed by Colby et al.<sup>58-61</sup> It may be that time-temperature superposition was not completely valid for the a-PS/PPO blends investigated herein, and the formation of master curves was merely the consequence of the limited range of frequencies provided by dynamic

mechanical analysis compared to, for instance, dielectric spectroscopy. Even if this was the case for the a-PS/PPO system, the scaling of the dynamic mechanical data still provided critical information about differences in the average segmental relaxation time responses for the blends compared to the glass formation behavior of the pure polymers.

An indication of the relaxation time distribution can be acquired from the dynamic mechanical data for each material. A mathematical representation of a distribution of relaxation times about the most probable relaxation time,  $\tau$ , is given by the Kohlrausch-Williams-Watts<sup>62-64</sup> (KWW) function:

$$\phi(t) = \exp\left[-\left(\frac{t}{\tau}\right)^\beta\right] \quad \text{Eqn. 5-4}$$

When the value of the  $\beta$  exponent is equal to 1.0 then relaxation is exponential with only a single relaxation time, and as  $\beta$  decreases the relaxation time distribution broadens. The KWW function can be applied numerically in order to predict the shape of the loss modulus  $\alpha$ -relaxation dispersion in the frequency domain, and this process is detailed in Chapter 7. Comparison of the predictions generated using different values of  $\beta$  with the loss modulus master curves allowed values of this parameter to be determined for the a-PS/PPO blend system. Examples of the predictions which best matched the loss modulus data are provided by the solid lines in Figure 5-3 and Figure 5-4. The results of this fitting process enabled the effect of blend composition on  $\beta$  to be determined, and discussion of this information will be given later after mention is made of the determination of  $\beta$  from the DSC data. In general, the KWW function captured the shape of the loss modulus behavior for the pure polymers and the blends with 25 wt% and 50 wt.% PPO. The higher blend compositions of 75 wt.% and 87.5 wt.% PPO, however, exhibited slight, but noticeable, skewing of the loss modulus data at the low frequency end of the dispersions compared to the KWW fits. This can be observed from the data for the a-PS/PPO75 blend shown in Figure 5-4. This particular asymmetry is consistent with the influence of concentration fluctuations as described by Roland and Ngai.<sup>57</sup> However, the asymmetric broadening effect noted here for the a-PS/PPO blends is quite small in comparison to the behavior observed for other miscible blends, for example blends of atactic polystyrene and poly(vinyl methyl ether) (PVME).<sup>55</sup> Blends of a-PS

and PVME are quite different than miscible a-PS/PPO blends in that the a-PS/PVME mixtures have much broader glass transitions despite the fact the disparities between the glass transition temperatures of the pure components are nearly the same for the two blend systems. For example, the 50/50 (wt./wt.) blend of a-PS and PVME has a DSC glass transition breadth of approximately 50°C,<sup>65</sup> which is far greater than the breadth of the glass transition for a-PS/PPO50 which is on the order of 20°C (see Figure 5-1).

Modeling was performed in order to gain insight into the relaxation time distributions from the differential scanning calorimetry results so that a contrast between distributions from DMA and DSC could be made. The modeling utilized the Tool-Narayanaswamy-Moynihan scheme in combination with the nonlinear Adam-Gibbs relaxation time function. The parameter specification process and the details of the numerical modeling approach are well documented in Chapter 8. Parameters which were specified from the dynamic mechanical data were applied to the DSC data, but the value of  $\beta$  was allowed to vary. Values for the Adam-Gibbs parameters  $\Delta\mu$  and  $T_0$  were determined from the WLF constants. The Vogel temperature,  $T_0$ , represents the temperature where the relaxation time appears to diverge toward an infinite value, and this temperature asymptote is expressed as:  $T_0 = T_g - C_2$ . The Adam-Gibbs  $\Delta\mu$  parameter represents the activation energy associated with the intramolecular relaxation of a molecular segment in the absence of cooperative interferences due to other segments. A value of  $\Delta\mu$  can be inferred from the high temperature limiting behavior of the WLF equation which is fit to the experimental shift factor data, and the value is accordingly given by:  $\Delta\mu = 2.303RC_1C_2$ . As can be observed from Table 5-I, the results for  $\Delta\mu$  were 13.8 kJ/mol (3.3 kcal/mol) for a-PS and 32.7 kJ/mol (7.8kcal/mol) for PPO with intermediate values for the blends. Confirmation for the interpretation of  $\Delta\mu$  as the activation energy governing rotation about backbone bonds is provided by molecular mechanics calculations<sup>35</sup> for PPO which indicate that the energy barrier to rotation is approximately 34 kJ/mol which is very similar to the value calculated from the WLF constants. Also, the value of  $\Delta\mu$  assessed from the dynamic mechanical scaling data for a-PS is consistent with typical C-C backbone bond rotation activation energies.<sup>66</sup> The Adam-Gibbs pre-exponential constant, A, can be varied in order to match each prediction with the location of the experimental DSC glass transition heat flow change (the A

parameter serves merely to shift the predictions along the temperature scale without otherwise altering the shape of the predicted responses). In this manner, all of the necessary model parameters were fixed except for the KWW exponent,  $\beta$ , which was varied in order to describe the DSC data. Adequate fits of the DSC data were obtained for the pure polymers and the blends using this methodology as is clearly indicated in Figure 5-8.

The influence of blend composition on the relaxation time distribution can now be inspected based upon the dynamic mechanical and differential scanning calorimetry data. The dependence of  $\beta$  on composition is plotted in Figure 5-9, and the blends displayed broader distributions (lower  $\beta$  values) compared to pure a-PS and PPO based upon both the DSC and DMA results. This is certainly not a surprising result based upon qualitative breadth comparisons which can be made, for example, by visual inspection of the DSC scans given in Figure 5-1. A comparison of the  $\beta$  values for neat a-PS and PPO obtained by the different techniques shows that the equilibrium mechanical relaxation time distributions are broader for the pure components relative to the calorimetric distributions. This is similar to the findings of Bero and Plazek which indicated a substantially narrower relaxation time distribution for the thermodynamic property of volume compared to the distribution assessed from creep mechanical response for an epoxy material.<sup>67</sup> What is quite interesting from the results provided in Figure 5-9 is that the difference between the DMA and DSC  $\beta$  values became diminished with increasing PPO content, and the  $\beta$  parameters from the two technique were essentially equivalent for the blends with 75 wt.% and 87.5 wt.% PPO. One insinuation which can be made based upon this unique observation is that concentration fluctuations contribute more to the broadening of the calorimetric glass transition than to the broadening of the dynamic mechanical  $\alpha$ -relaxation dispersion compared to the relevant breadths for the pure polymers. However, the interactions between the blend species can also be expected to broaden the relaxation time distribution compared to the pure polymer distributions as will be mentioned shortly. It is, therefore, difficult to attribute any broadening effects solely to concentration fluctuations. Further strength for the fact that the relative calorimetric and mechanical relaxation time distributions are quite different for the blends compared to neat a-PS and PPO is provided by Figure 5-10 which displays the

compositional dependence of a less refined comparison of the  $T_g$  breadths assessed by DSC and DMA.

The blends were found to be more fragile (cooperative) compared to additive expectations based upon the behavior of a-PS and PPO, and comparatively broader relaxation time distributions were noted for the blends. The combination of these two results is in accord with the general correlation which has been observed between the nonexponential and nonArrhenius characteristics of glass formers by Böhmer, Ngai, Angell, and Plazek<sup>68</sup>. This correlation is reproduced in Figure 5-11 along with the DMA results for the a-PS/PPO blend system. The expectation that intermolecular interactions influence the characteristic of fragility (Chapter 7) and the general interrelationship between fragility and  $\beta$  suggests that the broadening of the relaxation time distributions for the miscible blends may be due, to some extent, to the specific interactions between a-PS and PPO. It is often assumed that broader glass transition responses for miscible polymer blends composed of polymers with widely different  $T_g$  values are associated with compositional microheterogeneities, but it should be emphasized that attractive interactions can also broaden the relaxation time distribution in addition to the effect of these composition fluctuations. It appears that a combination of these effects are present for the a-PS/PPO blends because the slope of the fragility vs.  $\beta$  data is not quite as steep as the general linear trend between these two parameters observed for the other polymer materials.

### ***5.3.2 Correlation between Aging Rates and Glass Transition Cooperativity***

The segmental cooperativity results for the a-PS/PPO blends provided insight into their physical aging response during sub- $T_g$  annealing. Aging rates determined at 30°C below  $T_g$  are plotted in Figure 5-12 versus blend composition for the properties of volume and enthalpy, and these results are part of an extensive aging study on this blend system which is disclosed in another communication.<sup>39</sup> The rates are presented in terms of the variation of fictive temperature with respect to  $\log(\text{aging time})$ . Inspection of the data indicates that the aging rates trends are characterized by less than additive behavior. The influence of composition on these volume and enthalpy relaxation rates was previously attributed to the enhanced state of packing in the glassy state for the blends

compared to additive expectations based upon the specific volumes of the pure components (Chapter 4). Comparison of the  $z_g$  versus composition data, which is also given in Figure 5-12, with the variations of the aging rates with composition suggests that the aging rates may be connected to the glass transition cooperativity. Indeed, an indirect relationship appears to exist between the aging rates at  $T_g-30^\circ\text{C}$  and the degree of required cooperativity which is developed during cooling as can be attested to via Figure 5-13. This correlation was first noted for this blend system, and it was subsequently expanded to include the data from other amorphous polymer materials (see Chapter 7). It initially appeared that this cooperativity-based explanation for the aging rate data represented an alternative to the interpretation which involved glassy density features. As will soon be clear, the unique cooperativity behavior for the blends, which was influenced by the presence of attractive interactions, caused the negative deviation in the specific volume versus composition data compared to a rule-of-mixtures relationship. Therefore, the different explanations for the aging results at  $T_g-30^\circ\text{C}$  which were based upon specific volume results for freshly quenched samples and based upon the cooperativity data were actually synonymous.

### ***5.3.3 Origin of Negative Excess Volumes in the Glassy State: Kinetic vs. Thermodynamic Considerations***

When the enhanced degree of segmental cooperativity was discovered for the blends of a-PS and PPO, a question which arose was whether packing features in the glassy state were related to these kinetics or whether the compositional variation of glassy density was a result of mixing thermodynamics. Upon inspection of the literature, an answer to this question became immediately evident. An excellent pressure-volume-temperature (PVT) study was performed on the a-PS/PPO blend system by Zoller and Hoehn.<sup>12</sup> Relevant specific volume data from this previous study are plotted in Figure 5-14. The specific volume values at  $20^\circ\text{C}$  and  $300^\circ\text{C}$  were directly replotted from the data provided by Zoller and Hoehn, and the volumes at  $250^\circ\text{C}$  were calculated from the values at  $300^\circ\text{C}$  using the reported thermal expansion coefficients. The temperatures of  $250^\circ\text{C}$  and  $300^\circ\text{C}$  are both above the glass transition temperature of PPO, and thus equilibrium thermodynamic characteristics can be observed at these conditions. Surprisingly, no

volume contraction with mixing was evident in the liquid state while a pronounced densification effect was observed from the glassy data at 20°C which is well below the glass transition temperature region of a-PS. The specific volume characteristics in the nonequilibrium glassy state did not reflect the equilibrium liquid thermodynamics. Confirmation of the results generated by Zoller and Hoehn was achieved based upon research performed for the purpose of this present study. Thermal contraction data were obtained for the a-PS/PPO materials using linear dilatometry and glassy density results were assessed using pycnometry. This data is presented in Figure 5-15. The jump in thermal expansion coefficient at  $T_g$ ,  $\Delta\alpha$ , is plotted as a function of composition in Figure 5-16, and these results were comparable to those obtained by Zoller and Hoehn. In general, this data supports the previous findings which provided evidence that the enhanced glassy packing for the a-PS/PPO blends is a purely kinetic phenomenon.

The negative deviation of specific volume in the glassy state relative to additivity for the a-PS/PPO blends is consistent with the general statement made by Angell<sup>69</sup> that glass formers with a greater degree of fragility tend to be more closely packed in the glassy state. Because the blends can develop a greater degree of segmental cooperativity during cooling prior to formation of the nonequilibrium glassy state, they are able to develop densities which are closer to their ground states of amorphous packing. A more cooperative, or fragile, glass former has a kinetic glass transition temperature which is closer to the Vogel temperature,  $T_0$ , which represents the limit for the glass transition as cooling rate approached zero. If an infinitely slow cooling rate could be employed then a glass former would, in principle, settle into an equilibrium glassy state which is in the ground state of amorphous packing according to Gibbs and DiMarzio.<sup>70</sup> Thus, the positive deviation of the  $z_g$  vs. composition data can logically account for the commonly observed negative deviation in specific volume versus composition results compared to additive contributions from a-PS and PPO. Interactions between a-PS and PPO in the blends influence the kinetics of glass formation for the blends and enable the blends to develop denser glassy structures compared to the pure polymers. To summarize these critical findings, *the glassy density characteristics of a-PS/PPO blends are kinetic in origin and are not a consequence of the thermodynamics of miscibility.*

The nature of apparent excess property behavior for polymer blends can play an important role when an attempt is made to generate an understanding of kinetic glass transition temperature versus composition data based upon an approach which is based upon thermodynamics. This issue will be specifically addressed for the glass transitions of the a-PS/PPO blends using a predictive thermodynamic approach derived from a volume standpoint. The difference between the volume versus composition trends for the liquid and glassy states will be integral to this forthcoming discussion.

Predictive expressions for the glass transition temperature of a miscible blend can be developed using thermodynamic arguments. The general thermodynamic approach was nicely outlined by Couchman,<sup>71,72</sup> and this treatment resulted in the following expression for the glass transition temperature for a miscible blend when volume was employed as the thermodynamic variable of interest:

$$T_g = \frac{w_1(\Delta\alpha_1/\rho_1)T_{g,1} + w_2(\Delta\alpha_2/\rho_2)T_{g,2} + \Delta V_{\text{mix}}^g - \Delta V_{\text{mix}}^l}{w_1(\Delta\alpha_1/\rho_1) + w_2(\Delta\alpha_2/\rho_2)} \quad \text{Eqn. 5-5}$$

The subscripts 1 and 2 signify, respectively, component 1 and component 2 which comprise the mixture, and the superscripts indicate the glassy (g) and liquid (l) states. In the above expression,  $\Delta\alpha_i$  represents the difference between the liquid and glassy thermal expansion coefficients for a pure species,  $\rho_i$  denotes the density of a pure component, and, for derivation purposes, the ratio of these two parameters is considered to be an insignificant function of temperature. The weight fraction of component  $i$  in the blend is given by  $w_i$ . It is clear that the above equation cannot be used without knowledge of the excess volume properties associated with mixing in both the liquid and glassy states. To eliminate the excess property terms from the predictive expressions requires the use of one of two possible assumptions. One assumption is that the excess volumes are negligible for both the liquid and glassy states, but this is certainly not valid in a general sense for miscible polyblends. A second approach to eliminating the  $\Delta V_{\text{mix}}$  parameters is to assume that the excess properties are equivalent in the liquid and glassy states such that they cancel in the predictive expression. However, there is no justification for this second assumption either, and no conceptual difficulty exists with regards to a

discontinuity in excess properties at the glass transition of a miscible mixture as explained by Goldstein.<sup>73</sup> Of course, the whole concept of excess properties due to mixing which are defined in the glassy state is problematic because it is a practical impossibility to mix two polymers in the glassy state, and this issue was raised by Angell et al.<sup>74</sup> Elimination of the excess volume parameters using one of these two unfounded assumptions allows simplification of Eqn. 5-5 to give the familiar Gordon-Taylor<sup>75</sup> equation:

$$T_g = \frac{w_1(\Delta\alpha_1/\rho_1)T_{g,1} + w_2(\Delta\alpha_2/\rho_2)T_{g,2}}{w_1(\Delta\alpha_1/\rho_1) + w_2(\Delta\alpha_2/\rho_2)} = \frac{w_1T_{g,1} + Kw_2T_{g,2}}{w_1 + Kw_2} \quad \text{Eqn. 5-6}$$

where  $K = (\rho_1\Delta\alpha_2)/(\rho_2\Delta\alpha_1)$ . Using the Gordon-Taylor equation, the glass transition temperatures of miscible polymer blends can be predicted from the properties of the pure components. A comparison of the glass transition temperature results (DSC, 10°C/min heating) for the a-PS/PPO blend system with the Gordon-Taylor predictions obtained using Eqn. 5-6 is made in Figure 5-17. The Gordon-Taylor expression significantly overpredicted the blend glass transition data. It must be recalled that the excess volume properties were eliminated in the development of this equation. It was, however, previously illustrated that the excess volumes in the liquid state were negligible in the liquid state while the apparent excess volumes associated with the glassy state were sizable negative values. Using the results of Zoller and Hoehn, predictions were generated using Eqn. 5-5. These predictions agreed with the experimental data quite well as is illustrated in Figure 5-17. An interesting observation was that the Gordon-Taylor equation could decently capture the dependence of  $T_0$  on composition which suggests that values of  $\Delta V_{\text{mix}}$  were nearly equivalent for the liquid and glassy states. If the Vogel temperatures represent true glass transitions then the equilibrium glassy states of the a-PS/PPO blends appear to have specific volumes which display a linear dependence on composition which is similar to the dependence experimentally observed in the equilibrium liquid state. In other words, evidence suggests that the discrepancy between excess volume properties for the liquid and glassy states of the a-PS/PPO system is eliminated upon consideration of the equilibrium glasses as opposed to the nonequilibrium glasses.

## 5.4 Conclusions

Both dynamic mechanical analysis and differential scanning calorimetry techniques revealed that the a-PS/PPO blends were characterized by more severe relaxation time increases during cooling in the glass formation temperature region. This pronounced increase in fragility, or cooperativity, for the blends compared to pure a-PS and PPO was likely the consequence of the specific interactions present between the species in the blends. The enhanced cooperativity for the blends resulted in retarded aging rates of the a-PS/PPO mixtures compared to additivity, and an inverse correlation between aging rates and glass transition cooperativity was accordingly discovered. Relaxation time distributions were broader for the blends and it was suggested that both the specific interactions and composition fluctuations contribute to this broadening effect. The distribution breadths were broader by DMA compared to DSC for the neat polymers, but this discrepancy was diminished for the miscible blends. It was shown that appreciable contraction with mixing did not occur in the equilibrium liquid state. The negative  $\Delta V_{\text{mix}}$  values which were inferred from the glassy state packing behavior were, therefore, not attributed to the thermodynamics of mixing but rather to the unique cooperativity characteristics noted for the blends.

Table 5-I. Relaxation Parameters

PPO Content [wt. %]	$T_g$ [K]*	$C_{1,g}$	$C_{2,g}$ [K]	$\Delta\mu$ [kJ/mol]	$T_0=T_g-C_{2,g}$	$\ln(A)$
0	376	15.1	47.8	13.8	328	-30.2
25	401	15.5	50.2	14.9	351	-33.7
50	422	17.5	54.8	18.4	367	-36.9
75	443	17.4	62.2	20.7	381	-36.3
87.5	468	18.0	68.9	23.7	399	-38.5
100	488	20.4	83.8	32.7	404	-40.0

\*  $T_g$  data are the inflection values measured by DSC during heating at 10°C/min for freshly quenched samples

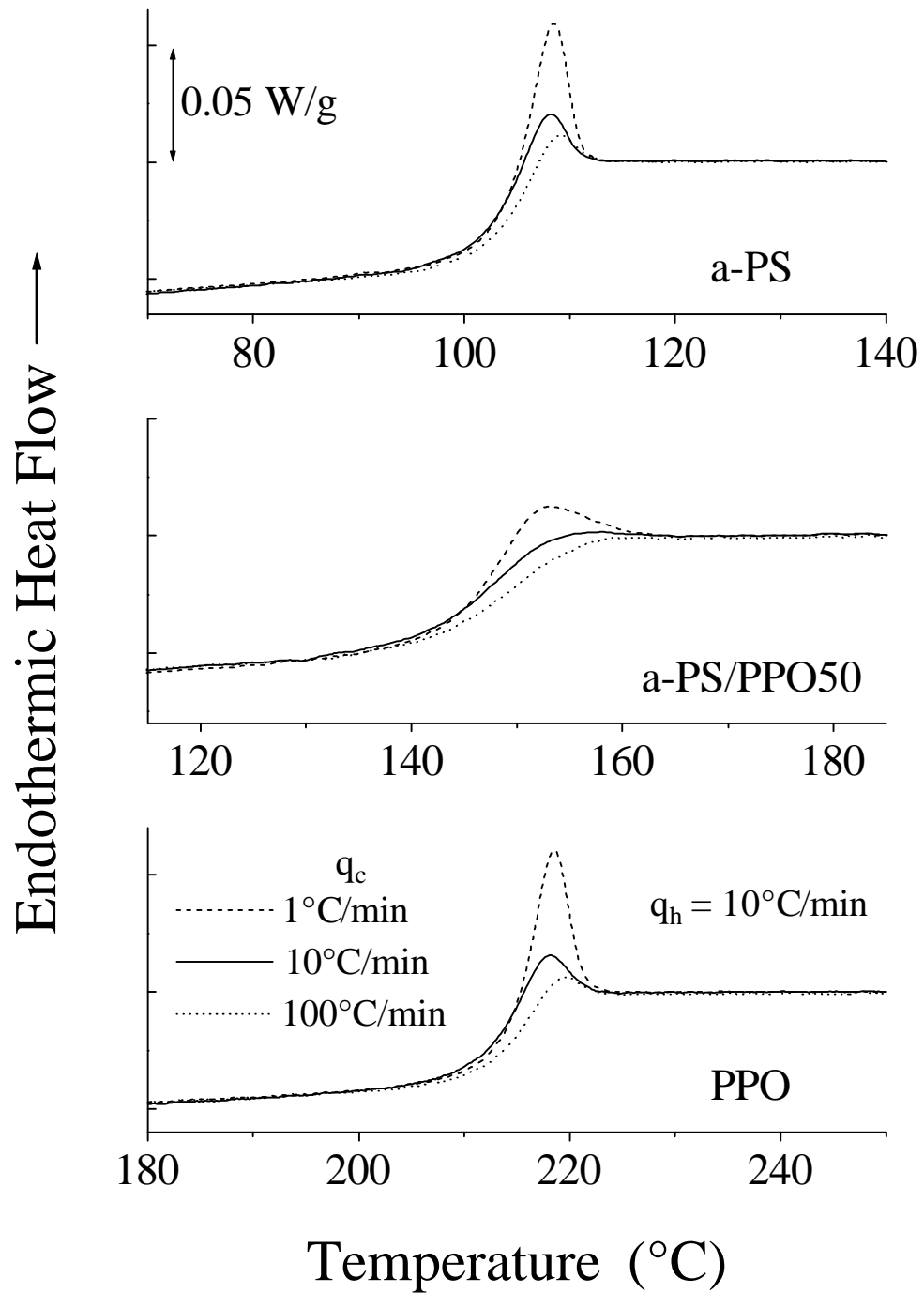


Figure 5-1. DSC glass transition responses during heating at  $10^\circ\text{C}/\text{min}$  following a quench from above  $T_g$  at the indicated cooling rates.

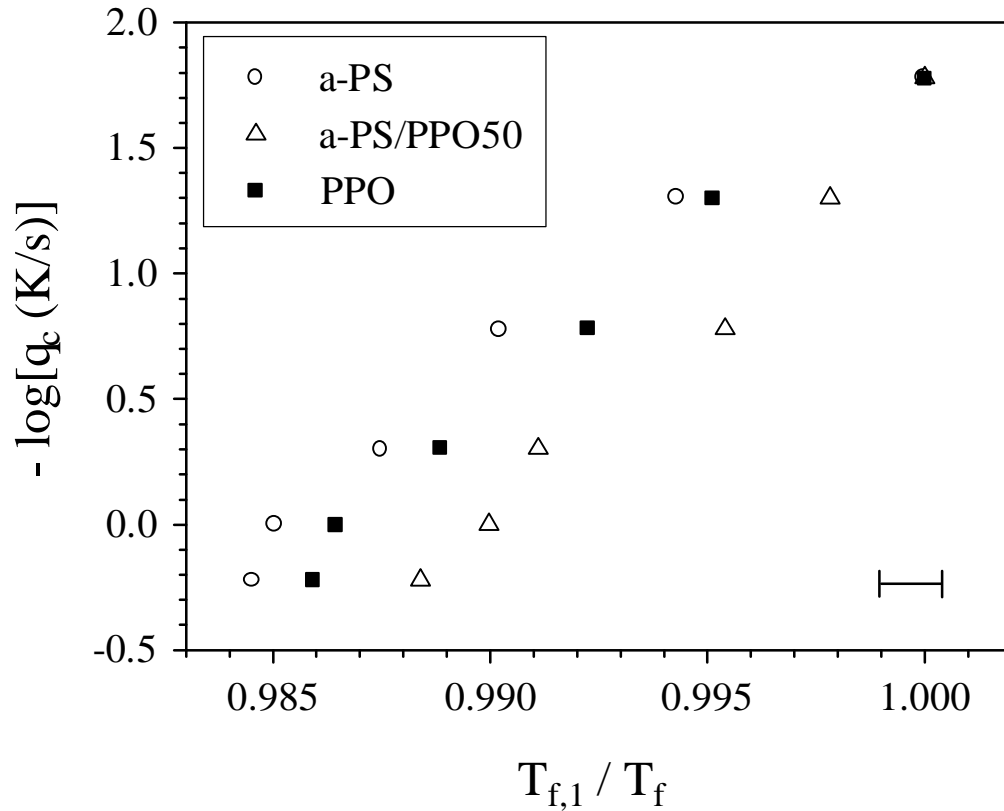


Figure 5-2. Relationship between the cooling rate and the fictive temperature assessed from the DSC heating scans at 10°C/min. The fictive temperature associated with the cooling rate of 1°C/min,  $T_{f,1}$ , is used as a normalization constant for each material. The magnitude of a typical error bar associated with the normalized fictive temperature data is given in the plot.

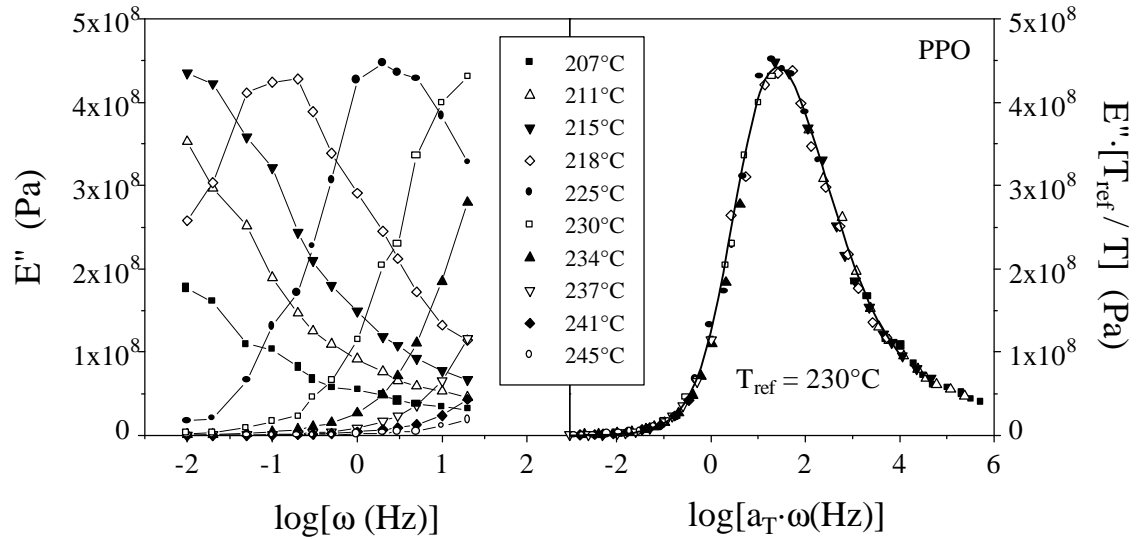


Figure 5-3. Dependence of loss modulus on frequency and temperature for PPO in the glass formation ( $\alpha$ -relaxation) region. The plot on the right is the master curve which was generated by time-temperature superposition, and the solid line represents the KWW function which was fit to the master curve data. Vertical shifting of the loss modulus data was accomplished using the temperature ratio  $T_{\text{ref}} / T$  (where temperatures are in units of K).

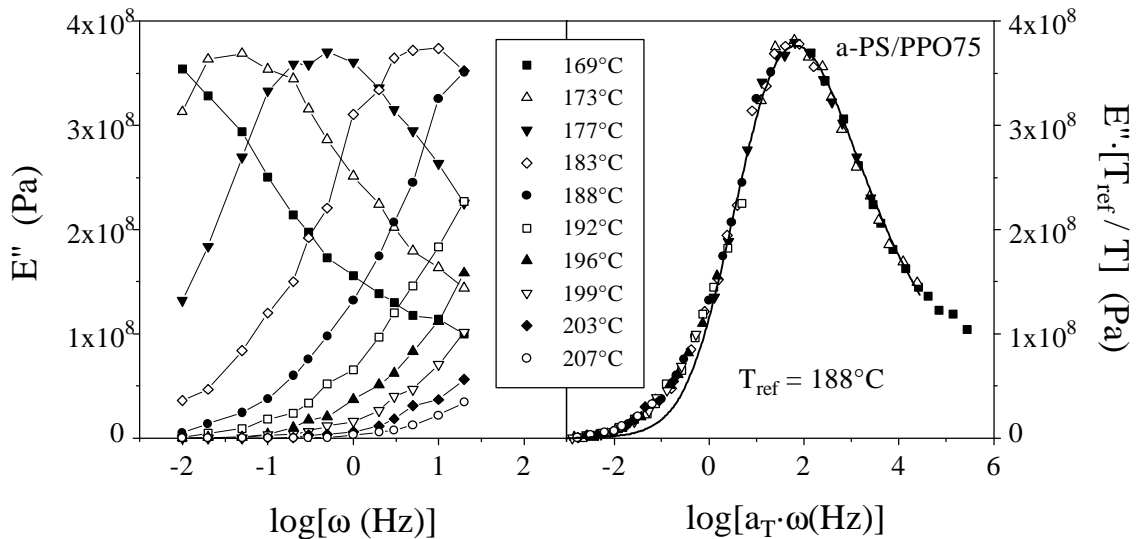


Figure 5-4. Dependence of loss modulus on frequency and temperature for the a-PS/PPO75 blend in the glass formation ( $\alpha$ -relaxation) region. The plot on the right is the master curve which was generated by time-temperature superposition, and the solid line represents the KWW function which was fit to the master curve data. Vertical shifting of the loss modulus data was accomplished using the temperature ratio  $T_{\text{ref}} / T$  (where temperatures are in units of K).

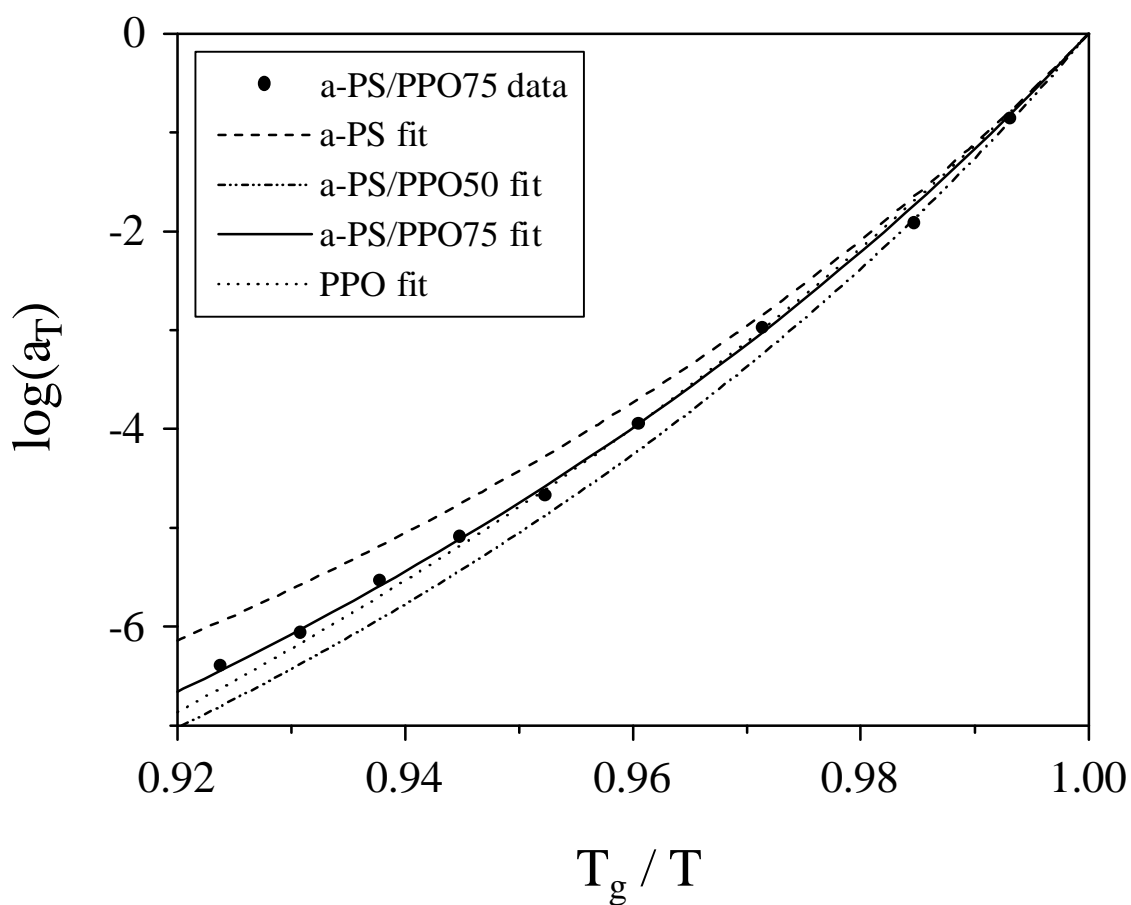


Figure 5-5. NonArrhenius behavior of segmental relaxation times in the glass formation temperature range. The shift factor data and associated WLF fits (lines) were converted from the reference temperatures used during time-temperature superposition of loss modulus data to the DSC glass transition temperatures. Only selected data and fits are shown in order to maintain clarity.

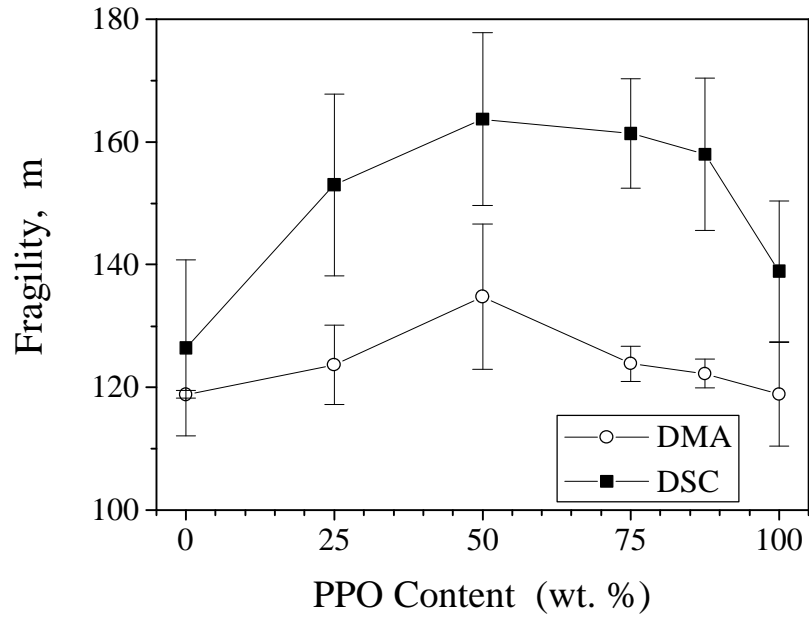


Figure 5-6. Influence of blend composition on fragility determined from DSC and DMA data.

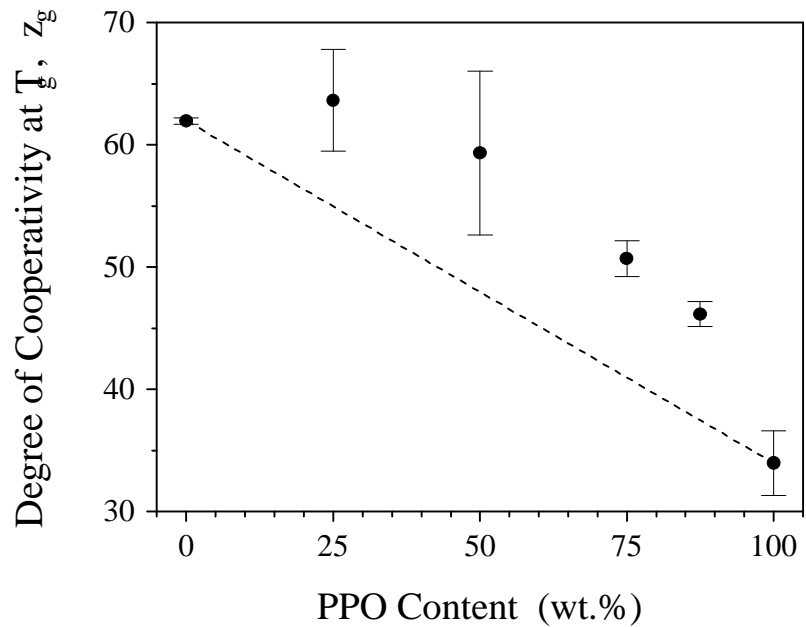


Figure 5-7. Cooperative domain size at  $T_g$  for the a-PS/PPO polyblends determined from DMA relaxation time scaling behavior. The dashed line represents pure component additivity.

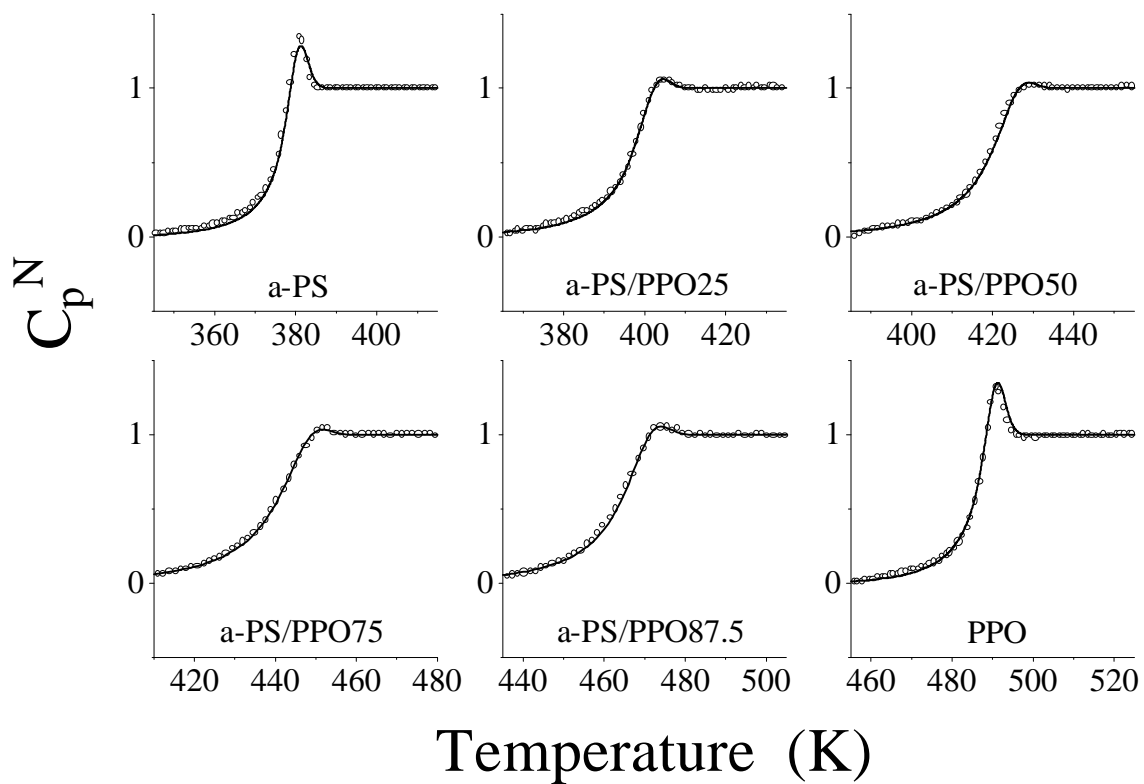


Figure 5-8. Normalized DSC heat flow data (symbols) for a-PS/PPO blends obtained during heating at 10K/min following a quench from above  $T_g$  at 10K/min. The solid lines are the AG/TNM fits to the data. See text for additional details.

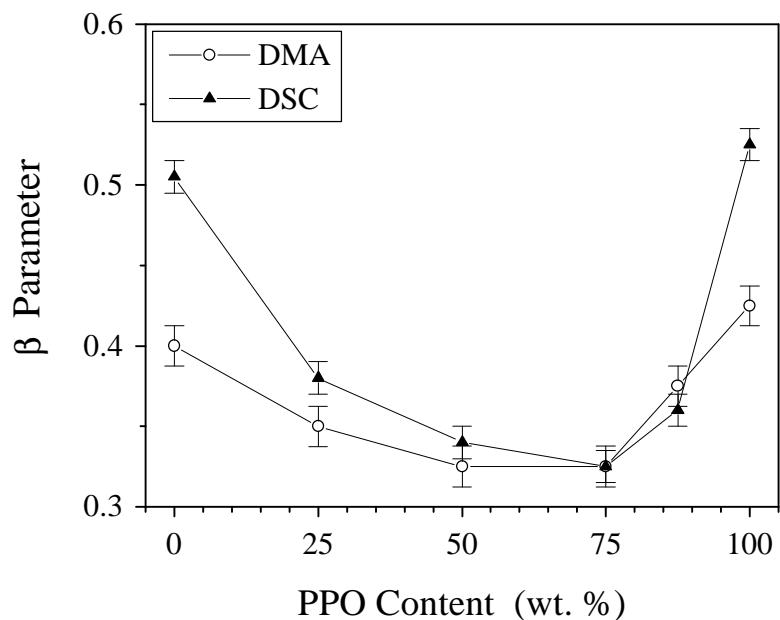


Figure 5-9. Role of PPO content on the  $\beta$  parameter assessed from DSC and DMA data.

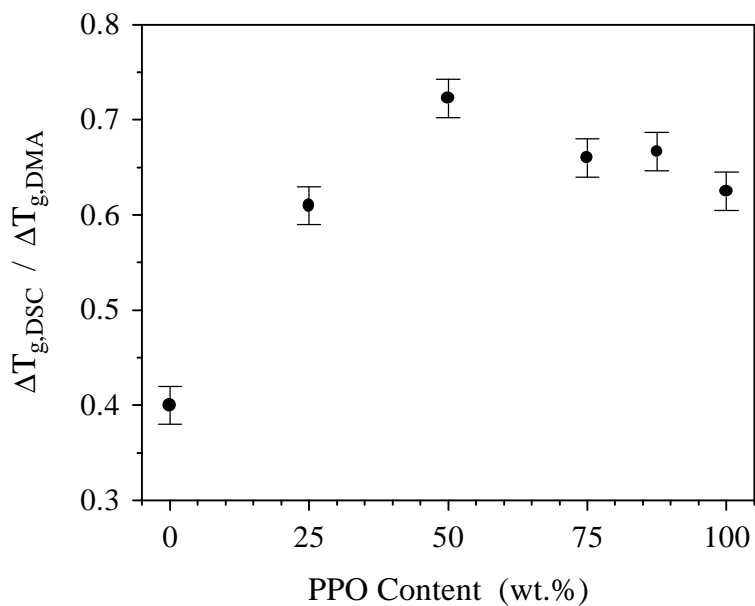


Figure 5-10. Compositional dependence of the ratio of DSC glass transition breadth to the breadth assessed from DMA data. The DSC breadth was determined from heating scans at 10°C/min and the DMA transition breadth assessed from the peak width at half height of the  $\tan\delta$  peaks obtained at 1 Hz and during heating at 2°C/min.<sup>39</sup>

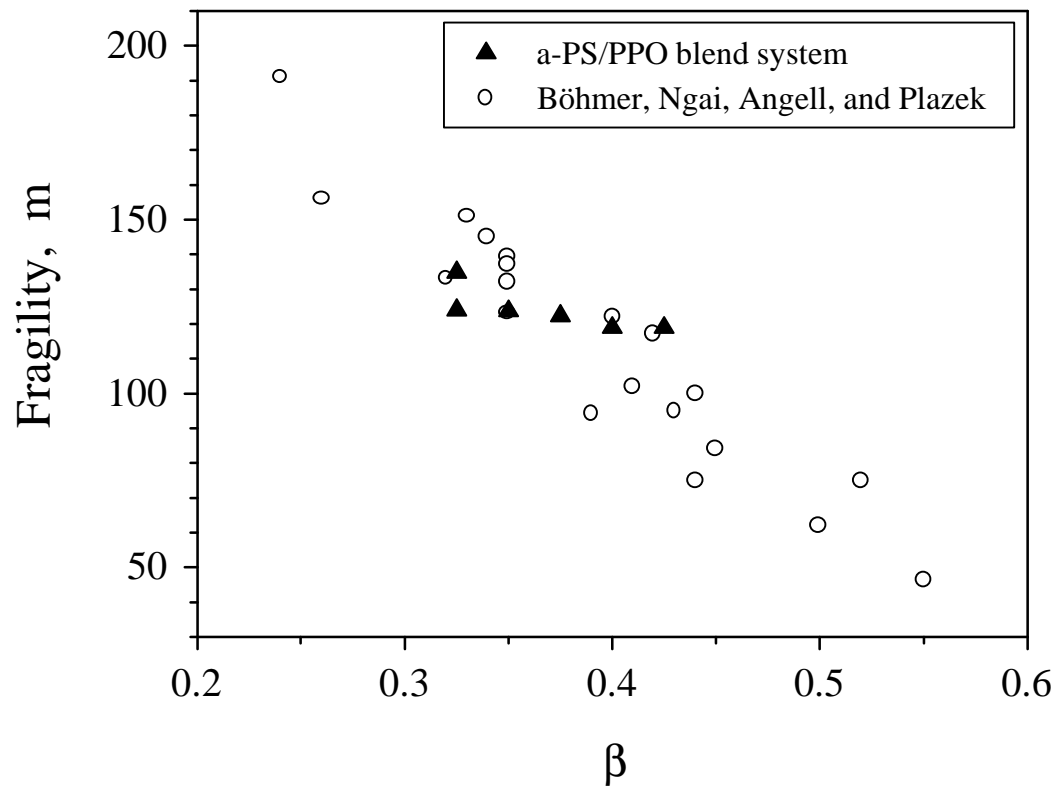


Figure 5-11. Comparison of the trend between fragility and  $\beta$  observed for the a-PS/PPO system via DMA with the literature trend for polymers reported by Böhmer et al.

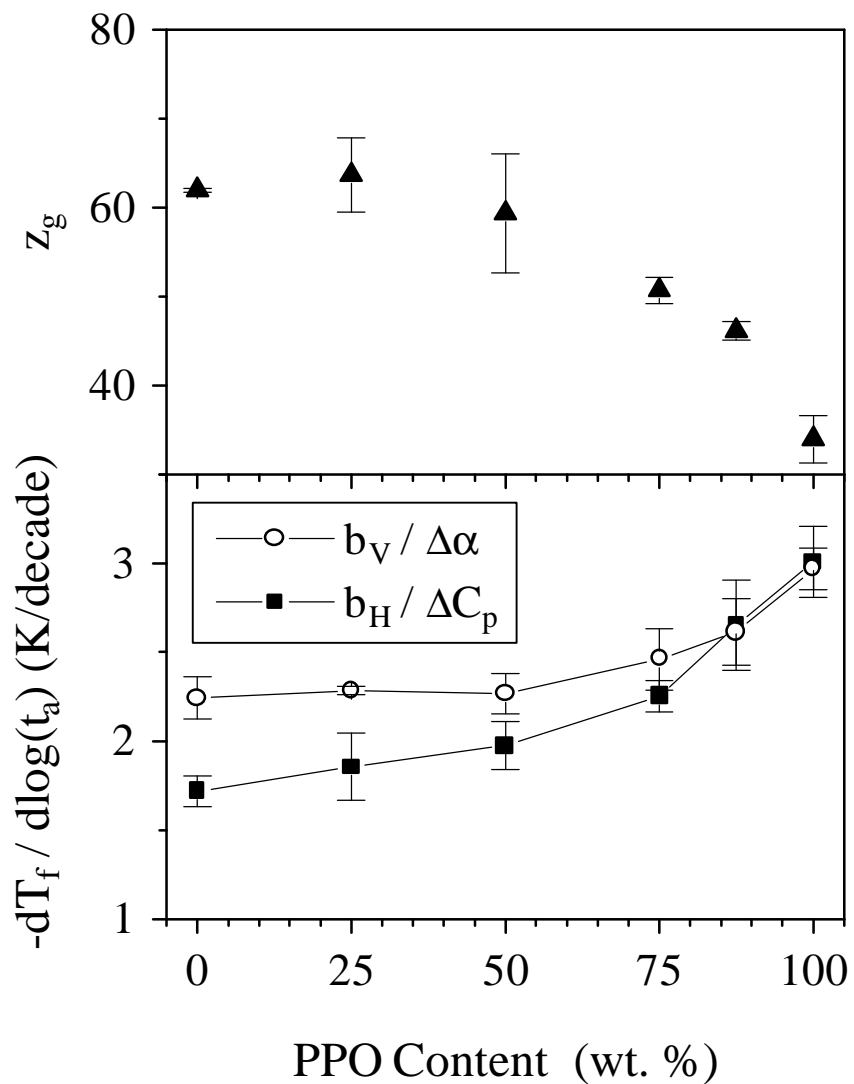


Figure 5-12. Variation of glass transition cooperativity,  $z_g$ , (upper plot) and aging rates at  $T_a=T_g-30^\circ\text{C}$  (lower plot) with blend composition.

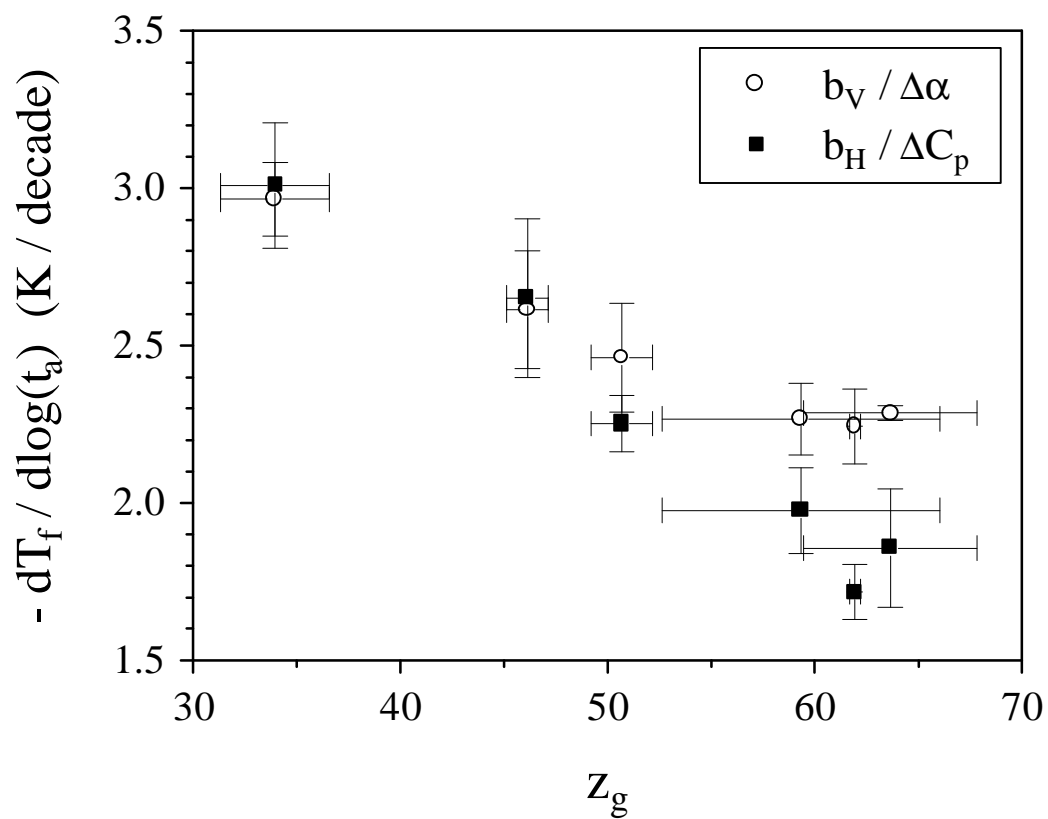


Figure 5-13. Apparent correlation between structural relaxation rates at  $T_a = T_g - 30^\circ\text{C}$  and glass transition cooperativity for the a-PS/PPO blend system.

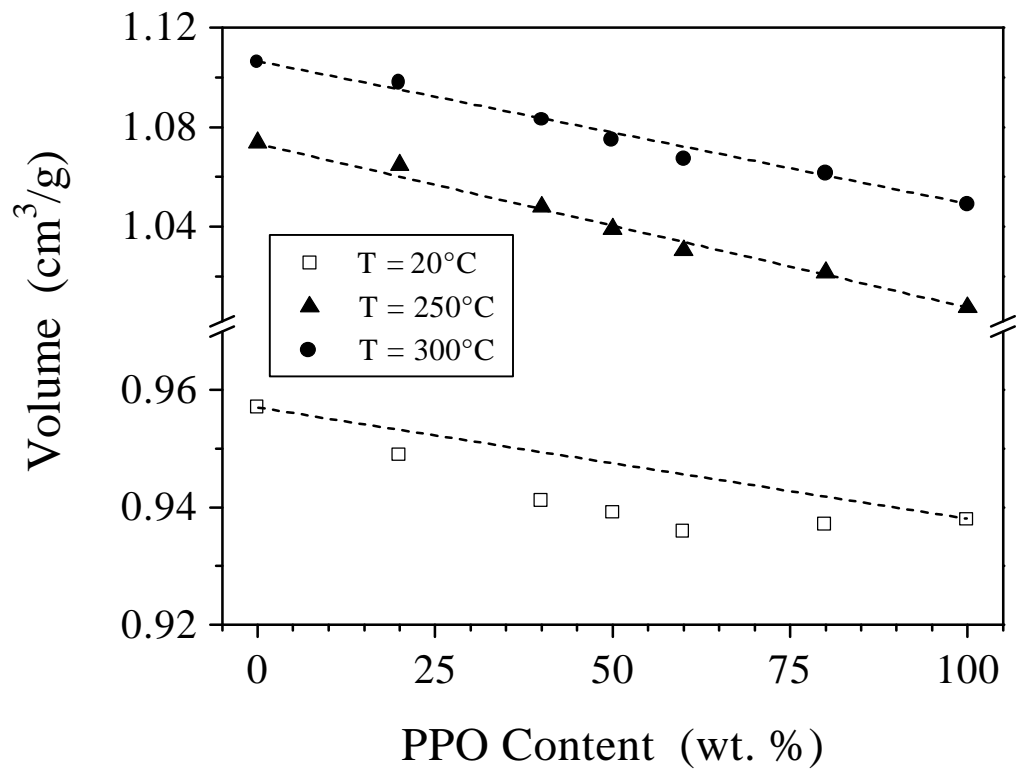


Figure 5-14. Compositional dependence of specific volume for the a-PS/PPO blend system plotted based upon results of Zoller and Hoehn.<sup>12</sup> The dashed lines connect the data points for the pure polymers and thus represent additive behavior.

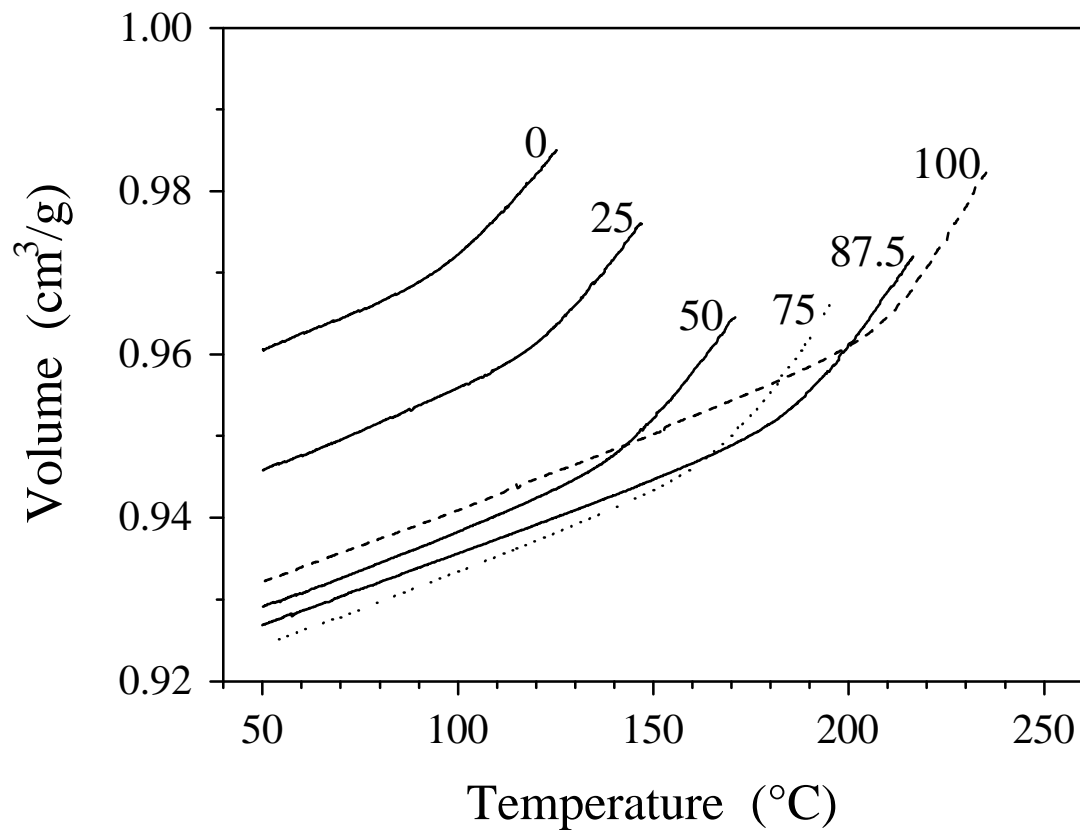


Figure 5-15. Thermal contraction responses for the a-PS/PPO blends during cooling at 1°C/min. The numbers represent the PPO content in wt.%.

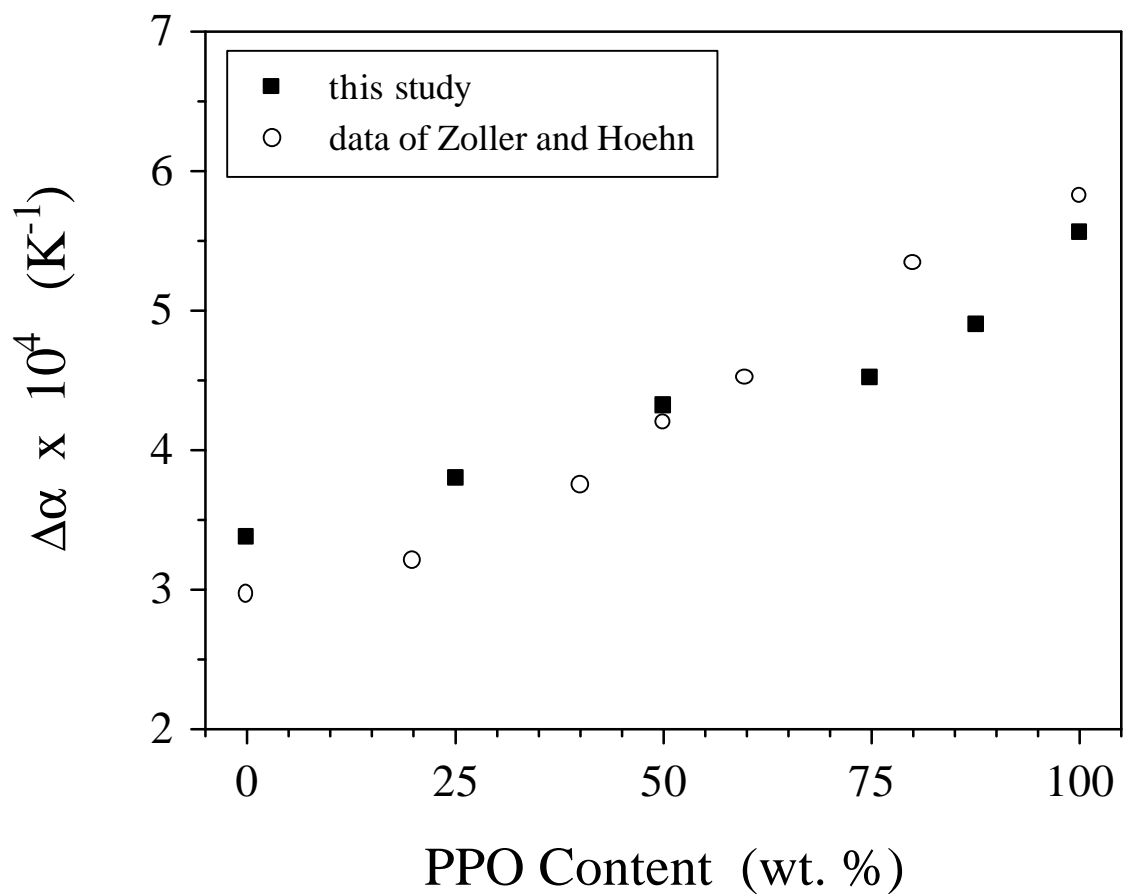


Figure 5-16. Jump in thermal expansion coefficient at  $T_g$  as a function of blend composition. Data are from this study and from the investigation performed by Zoller and Hoehn.<sup>12</sup>

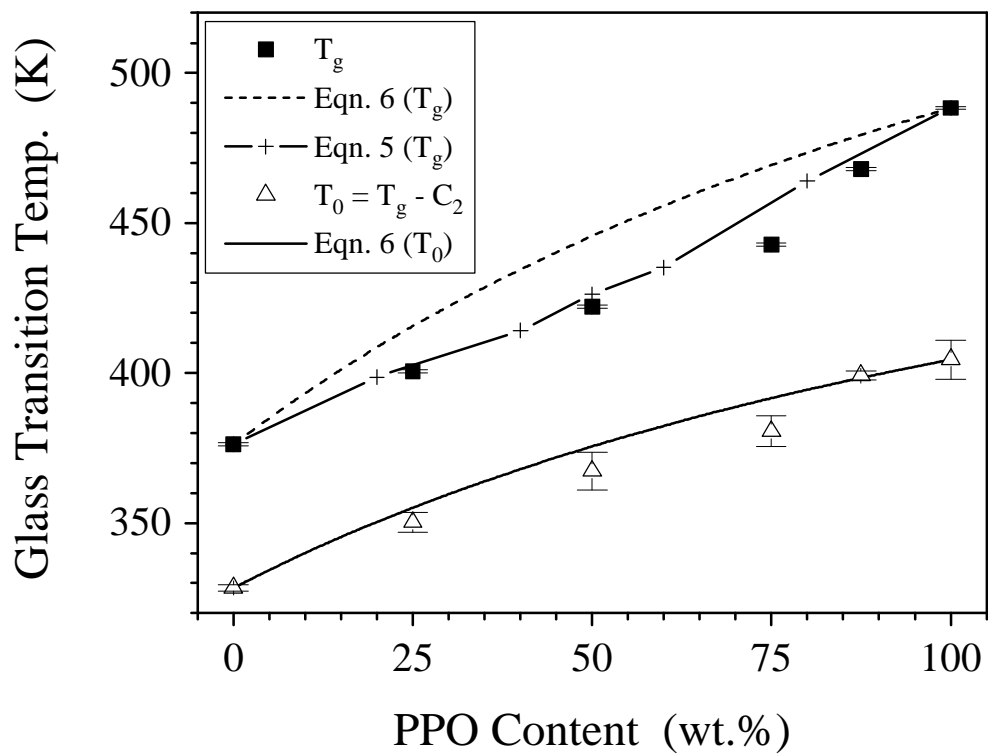


Figure 5-17. Compositional variation of DSC glass transition temperature,  $T_g$ , and Vogel temperature,  $T_0$ . Also plotted are predictions for both  $T_g$  and  $T_0$ .

## 5.5 References

- <sup>1</sup> E. O. Stejskal, J. Schaefer, M. D. Sefcik, and R. A. McKay, *Macromolecules* **14**, 275 (1981).
- <sup>2</sup> A. Maconnachie, R. P. Kambour, D. M. White, S. Rostami, and D. J. Walsh, *Macromolecules* **17**, 2645 (1984).
- <sup>3</sup> G. R. Mitchell and A. H. Windle, *J. Polym. Sci.: Polym. Phys. Ed.* **23**, 1967 (1985).
- <sup>4</sup> P. T. Inglefield, A. A. Jones, P. Wang, and C. Zhang, *Mat. Res. Soc. Symp. Proc.* **215**, 133 (1991).
- <sup>5</sup> S. Li, L. C. Dickinson, and J. C. W. Chien, *J. Appl. Polym. Sci.* **43**, 1111 (1991).
- <sup>6</sup> H. Feng, Z. Feng, H. Ruan, and L. Shen, *Macromolecules* **25**, 5981 (1992).
- <sup>7</sup> S. H. Goh, S. Y. Lee, X. Zhou, and K. L. Tan, *Macromolecules* **32**, 942 (1999).
- <sup>8</sup> A. R. Shultz and B. M. Beach, *Macromolecules* **7**, 902 (1974).
- <sup>9</sup> M. A. de Araujo, R. Stadler, and H.-J. Cantow, *Polymer* **29**, 2235 (1988).
- <sup>10</sup> H. A. Schneider, H.-J. Cantow, C. Wendland, and B. Leikauf, *Makromol. Chem.* **191**, 2377 (1990).
- <sup>11</sup> N. E. Weeks, F. E. Karasz, and W. J. MacKnight, *J. Appl. Phys.* **48**, 4068 (1977).
- <sup>12</sup> P. Zoller and H. H. Hoehn, *J. Polym. Sci.: Polym. Phys. Ed.* **20**, 1385 (1982).
- <sup>13</sup> R. K. Jain, R. Simha, and P. Zoller, *J. Polym. Sci.: Polym. Phys. Ed.* **20**, 1399 (1982).
- <sup>14</sup> T. S. Chow, *Macromolecules* **23**, 4648 (1990).
- <sup>15</sup> C. H. M. Jacques, H. B. Hopfenberg, and V. Stannett, *Polym. Eng. Sci.*, **13**, 81 (1973).
- <sup>16</sup> C. H. M. Jacques and H. B. Hopfenberg, *Polym. Eng. Sci.*, **14**, 441 (1974).
- <sup>17</sup> H. B. Hopfenberg, V. T. Stannett, and G. M. Folk, *Polym. Eng. Sci.*, **15**, 261 (1975).
- <sup>18</sup> A. F. Yee, *Polym. Eng. Sci.* **17**, 213 (1977).
- <sup>19</sup> L. W. Kleiner, F. E. Karasz, and W. J. MacKnight, *Polym. Eng. Sci.* **19**, 519 (1979).
- <sup>20</sup> R. P. Kambour and S. A. Smith, *J. Polym. Sci.: Polym. Phys. Ed.* **20**, 2069 (1982).
- <sup>21</sup> K. S. C. Lin and J. J. Aklonis, *Macromolecules* **16**, 376 (1983).
- <sup>22</sup> C. Creton, J.-L. Halary, and L. Monnerie, *Polymer* **40**, 199 (1998).
- <sup>23</sup> L. H. Wang and R. S. Porter, *J. Polym. Sci.: Polym. Phys. Ed.* **21**, 1815 (1983).
- <sup>24</sup> C. Bouton, V. Arrondel, V. Rey, P. Sergot, J. L. Manguin, B. Jasse, and L. Monnerie, *Polymer* **30**, 1414 (1989).
- <sup>25</sup> Y. Zhao, R. E. Prud'homme, and C. G. Bazuin, *Macromolecules* **24**, 1261 (1991).
- <sup>26</sup> K. Kawabata, T. Fukuda, Y. Tsujii, and T. Miyamoto, *Macromolecules* **26**, 3980 (1993).
- <sup>27</sup> Pathmanathan, K., Johari, G. P., Faivre, J. P., and Monnerie, L. *J. Polym. Sci., Part B: Polym. Phys.* 1986, **24**, 1587.
- <sup>28</sup> J. Y. Cavaille, S. Etienne, J. Perez, L. Monnerie, and G. P. Johari, *Polymer* **27**, 549 (1986).
- <sup>29</sup> J. Ko, Y. Park, and S. Choe, *J. Polym. Sci., Part B: Polym. Phys.* **36**, 1981 (1998).
- <sup>30</sup> W. M. Prest, Jr. and R. S. Porter, *J. Polym. Sci., Part A-2* **10**, 1639 (1972).
- <sup>31</sup> S. Wu, *J. Polym. Sci., Part B: Polym. Phys.* **25**, 2511 (1987).
- <sup>32</sup> Prest, W. M., Jr., Luca, D. J., and Roberts, F. J., Jr., in 'Thermal Analysis in Polymer Characterization' (ed. E. A. Turi), Heyden, Philadelphia, 1981, pp. 24-42.

- 33 Prest, W. M., Jr. and Roberts, F. J., Jr., in 'Thermal Analysis, Proceedings of the  
Seventh International Conference on Thermal Analysis' (ed B. Miller), John Wiley  
and Sons, New York, 1982, Vol 2, pp.973-8.
- 34 Cavaille, J. Y., Etienne, S., Perez, J., Monnerie, L. and Johari, G. P. *Polymer* 1986,  
**27**, 686.
- 35 Elliot, S. *Ph.D. Dissertation*, Heriot-Watt University (U.K.), 1990.
- 36 Ho, T., Mijovic, J., and Lee, C. *Polymer* 1991, **32**, 619.
- 37 Oudhuis, A. A. C. M. and ten Brinke, G. *Macromolecules* 1992, **25**, 698.
- 38 Chang, G.-W., Jamieson, A. M., Yu, Z., and McGervey, J. D. *J. Appl. Polym. Sci.*  
1997, **63**, 483.
- 39 C. G. Robertson and G. L. Wilkes, "Physical Aging Behavior of Miscible Blends  
Containing Atactic Polystyrene and Poly(2,6-dimethyl-1,4-phenylene oxide)"  
(Chapter 4).
- 40 H.-L. Li, Y. Ujihira, A. Nanasawa, and Y. C. Jean, *Polymer* **40**, 349 (1999).
- 41 The NORYL<sup>®</sup> and PREVEX<sup>®</sup> polymer product lines of General Electric Plastics are  
based upon these blends.
- 42 Y. Agari, M. Shimada, and A. Ueda, *Polymer* **38**, 2649 (1997).
- 43 Shelby, M. D. *Ph.D. Dissertation*, Virginia Polytechnic Institute and State  
University, 1996.
- 44 I. M. Hodge, *J. Non. Cryst. Solids*, **169**, 211 (1994).
- 45 Tool, A. Q. *J. Am. Ceram. Soc.*, 1946, **29**, 240.
- 46 Tool, A. Q. *J. Res. Natl. Bur. Stand.*, 1946, **37**, 73.
- 47 Hutchinson, J. M. *Prog. Polym. Sci.*, 1995, **20**, 703.
- 48 Angell, C. A. *Science* **1995**, 267, 1924.
- 49 Angell, C. A.; Monnerie, L.; Torell, L. M., in *Structure, Relaxation, and Physical  
Aging of Glassy Polymers* (eds. R. J. Roe and J. M. O'Reilly), *Mat. Res. Symp. Proc.*  
**1991**, 215, 3.
- 50 Angell, C. A. *J. Non-Cryst. Solids* **1991**, 131-133, 13.
- 51 Williams, M. L.; Landel, R. F.; Ferry, J. D. *J. Am. Ceram. Soc.*, **1955**, 77, 3701.
- 52 Adam, G.; Gibbs, J. H. *J. Chem. Phys.* **1965**, 43, 139.
- 53 Ngai, K. L.; Plazek, D. J. *Macromolecules* **1990**, 23, 4282.
- 54 Roland, C. M.; Ngai, K. L.; *Macromolecules* **1991**, 24, 2261.
- 55 Roland, C. M.; Ngai, K. L.; *Macromolecules* **1992**, 25, 363.
- 56 Ngai, K. L.; Roland, C. M.; O'Reilly, J. M.; Sedita, J. S. *Macromolecules* **1992**, 25,  
3906.
- 57 Roland, C. M.; Ngai, K. L.; *J. Rheology* **1992**, 36, 1691.
- 58 Colby, R. H. *Polymer* **1989**, 30, 1275.
- 59 Kumar, S. K.; Colby, R. H., Anastasiadis, S. H.; Fytas, G. *J. Chem. Phys.* **1996**, 105,  
3777.
- 60 Pathak, J. A.; Colby, R. H.; Kamath, S. Y.; Kumar, S. K.; Stadler, R.  
*Macromolecules* **1998**, 31, 8988.
- 61 Pathak, J. A.; Colby, R. H.; Floudas, G.; Jerome, R. *Macromolecules* **1999**, 32, 2553.
- 62 R. Kohlrausch, *Pogg. Ann. Phys.*, **91**, 198 (1854).

- <sup>63</sup> R. Kohlrausch, *Pogg. Ann. Phys.*, **119**, 352 (1863).
- <sup>64</sup> G. Williams and D. C. Watts, *Trans. Faraday Soc.*, **66**, 80 (1970).
- <sup>65</sup> H. A. Schneider, H.-J. Cantow, C. Wendland, and B. Leikauf, *Makromol. Chem.* **191**, 2377 (1990)
- <sup>66</sup> Matsuoka, S. *Relaxation Phenomena in Polymers*, Munich: Hanser Publishers, 1992.
- <sup>67</sup> C. A. Bero and D. J. Plazek, *J. Polym. Sci.: Part B: Polym. Phys.* **29**, 39 (1991).
- <sup>68</sup> Böhmer, R.; Ngai, K. L.; Angell, C. A.; Plazek, D. J. *J. Chem. Phys.*, **1993**, 99, 4201.
- <sup>69</sup> C. A. Angell, *Proc. Natl. Acad. Sci.*, **92**, 6675 (1995).
- <sup>70</sup> J. H. Gibbs and E. A. DiMarzio, *J. Chem. Phys.*, **28(3)**, 373 (1958).
- <sup>71</sup> P. R. Couchman, *Phys. Letters*, **70A(2)**, 155 (1979).
- <sup>72</sup> P. R. Couchman, *Macromolecules*, **20(7)**, 1712 (1987).
- <sup>73</sup> M. Goldstein, *Macromolecules*, **18(2)**, 277 (1985).
- <sup>74</sup> C. A. Angell, J. M. Sare, and E. J. Sare, *J. Phys. Chem.*, **82(24)**, 2622 (1978).
- <sup>75</sup> M. Gordon and J. S. Taylor, *J. Appl. Chem.*, **2**, 493 (1952).

# Chapter 6

## Physical Aging Behavior for Miscible Blends of Poly(methyl methacrylate) and Poly(styrene-co-acrylonitrile)

---

---

### Chapter Synopsis

Volume relaxation behavior was measured in the glassy state as a function of blend composition for miscible blends of poly(methyl methacrylate) (PMMA) and poly(styrene-co-acrylonitrile) (SAN) possessing 25 wt.% acrylonitrile. The volume relaxation rates displayed an approximately linear dependence on blend composition for all of the aging temperature employed which were 15, 30, and 45°C below  $T_g$ . This blend system is thought to derive its miscibility via the copolymer repulsion effect, and significant attractive interactions are absent between the blend components. Consistent with the lack of specific interactions, no unique behavior was observed for the blends compared to the pure polymers in terms of glass transition fragility observed by differential scanning calorimetry or based upon the variation of density with composition. The secondary dynamic mechanical relaxation process for PMMA was observed in the PMMA/SAN blends, and the intensity of the relaxation diminished with increasing SAN content in the blend. The volume aging results were consistent with the fragility, density, and secondary relaxation features of the blend system. An apparent failure of time-aging time superposition was observed for creep compliance data obtained for neat PMMA for aging performed at  $T_g-30^\circ\text{C}$ . This failure was likely the consequence of aging-induced changes in the  $\alpha$ -relaxation relaxation response which were distinct from the changes in the overlapping secondary relaxation process in PMMA.

### 6.1 Introduction

The nonequilibrium nature of the glassy state results in time-dependent changes in properties of amorphous materials during their use at temperatures below the glass transition temperature region, and this relaxation process is known as physical aging. Research on physical aging has recently received much attention; a survey of the

literature from the years 1987 to 1998 reveals that over 800 publications appeared in that interim which were concerned with, to some extent, nonequilibrium glassy behavior.<sup>1</sup> What is remarkable given this high degree of activity in this research area is that a comprehensive understanding of the physical aging process has yet to be generated from a basic molecular standpoint. The study of the time-dependent glassy state of miscible polymer blends can provide a way of assessing the role of chemical interactions on the physical aging process, thus aiding in revealing how physical aging is influenced by intermolecular characteristics. Previous investigations by considered the physical aging (Chapter 4) and glass formation kinetics (Chapter 5) of the miscible blend system composed of atactic polystyrene (a-PS) and poly(2,6-dimethyl-1,4-phenylene oxide) (PPO). The presence of specific attractive interactions is a well established attribute of the a-PS/PPO blends.<sup>2,3</sup> In contrast, blends of atactic poly(methyl methacrylate) (PMMA) with statistical copolymers of styrene and acrylonitrile (SAN) derive their miscibility by means of a repulsive effect which will be presently described. Investigating the aging behavior as a function of blend composition for PMMA/SAN blends can, therefore, enable an informative comparison to be made with the previously disclosed aging results for miscible blends of a-PS and PPO.

Mixtures of high molecular weight polymers typically require a negative change in enthalpy with mixing,  $\Delta H_{\text{mix}}$ , in order to insure that miscibility is energetically favorable.<sup>4</sup> Specific attractive interactions between the different blend species which are not present in the pure polymers can accomplish this. In blends where at least one component is a random copolymer, miscibility does not need to be a result of specific interactions but rather the necessary negative value of the Flory-Huggins interaction parameter,  $\chi$ , can be derived from a repulsive effect.<sup>5-11</sup> As an example, the interaction parameter can be expressed as follows<sup>5,6</sup> for a blend of a homopolymer (A) made up of type 1 segments and a random copolymer (B) composed of molecular units 2 and 3:

$$\chi_{A,B} = b \chi_{1,2} + (1-b) \chi_{1,3} - b(1-b) \chi_{2,3} \quad \text{Eqn. 6-1}$$

The variable  $b$  denotes the mole fraction of the type 2 repeat unit in the copolymer, and the  $\chi$  subscripts indicate which two molecular units are associated with each binary interaction parameter. A negative interaction parameter between the homopolymer and

the copolymer ( $\chi_{A,B}$ ) can be obtained for a range of copolymer compositions even if the interaction parameters between all of the different segments are all greater than zero. This can occur if more repulsion exists between the chemically linked copolymer units 2 and 3 than is present between either of these units and the homopolymer unit 1:

$$0 < \chi_{1,2} < \chi_{2,3} \quad \text{and} \quad 0 < \chi_{1,3} < \chi_{2,3} \quad \text{Eqn. 6-2}$$

with the magnitudes of the inequalities dictated by the copolymer composition, b. Poly(methyl methacrylate) is not miscible with either polystyrene or polyacrylonitrile but yet it can form miscible blends with poly(styrene-*co*-acrylonitrile) for statistical copolymers with approximately 9 to 35 wt.% acrylonitrile due to the copolymer repulsion effect.<sup>9,11</sup>

Study of the PMMA/SAN blend system by <sup>13</sup>C NMR was performed by Feng et al.<sup>12</sup> These authors suggested that miscibility was not a consequence of the copolymer repulsion effect but rather due to attractive interactions between the carbonyl of PMMA and the phenyl side group on the polystyrene repeat unit of the SAN copolymer. The attractive interactions between PMMA and SAN are quite weak, however, and cannot alone explain the miscibility between PMMA and SAN which is observed despite the fact that miscible blends of PMMA cannot be formed with either polystyrene or polyacrylonitrile. Kwei et al.<sup>13</sup> noted evidence for interaction involving the carbonyl group of PMMA in mixtures of PMMA and SAN by means of infrared absorption measurements, but they concluded that only ca. 3% of the PMMA repeat units contributed to the shifted carbonyl band. The result of Feng and coworkers that some attractions exist between the phenyl group of the SAN copolymer and the carbonyl of PMMA is not being refuted. What is being stated is that the predominant opinion concerning the PMMA/SAN blends is that miscibility is a result of the copolymer repulsion effect,<sup>9-11,14</sup> and the present authors are also proponents of this view.

The goal of this investigation was to characterize the sub- $T_g$  volume relaxation as a function of composition for blends of PMMA and SAN. This research was initiated in order to contrast the aging behavior for the a-PS/PPO and PMMA/SAN blend systems in view of their differences in the nature of interactions and associated miscibility. A few physical aging studies of the PMMA/SAN blends have been reported in the literature.

Kwei and coworkers<sup>13</sup> performed a limited examination of enthalpy relaxation/recovery as part of a comprehensive study of the physical properties of PMMA/SAN blends. Aging was probed by Mijovic et. al<sup>15-19</sup> for blends of PMMA and SAN by assessing changes in both enthalpy and stress relaxation response. Changes in stress relaxation due to the physical aging process were also recently investigated for the PMMA/SAN blend system by Cowie, McEwen, and Matsuda.<sup>20</sup> Further details of these studies will be included later where appropriate. None of these prior studies, however, characterized volume relaxation behavior of PMMA/SAN polymer blends which represents the focus of this present communication.

## **6.2 Experimental Details**

### ***6.2.1 Preparation and Characterization of Blends***

Atactic poly(methyl methacrylate) (PMMA) and a statistical copolymer of styrene and acrylonitrile containing 25 mol.% acrylonitrile (SAN) were melt blended for 15 minutes at 170°C and 70 RPM in a Brabender (Model 5501) melt mixer. The atactic PMMA was obtained from Aldrich Chemical Company (Cat. # 44,574-6) and has a  $M_w$  of approximately 350,000 g/mol. The SAN material is reported to have an approximate  $M_w$  of 165,000 g/mol and this polymer was also obtained from Aldrich (Cat. # 18,285-0). The polymer materials were dried under vacuum conditions at 70°C before blending. Blends with compositions of 25, 50, and 75 wt. % SAN were made. The nomenclature PMMA/SANXX will be used to describe each blend where XX represents the SAN content in units of wt. %. Films of approximate thickness 0.2 mm were compression molded from PMMA, SAN, and the blends at 175°C. Glass transition responses were measured by differential scanning calorimetry (DSC) for samples which were freshly quenched into the glassy state at a rate of 200°C/min (see Differential Scanning Calorimetry section). The midpoint, or inflection, glass transition temperature,  $T_g$ , was measured and an indication of the transition breadth was also obtained for each material. Specific volume data were assessed at 23°C using a pycnometer manufactured by Micromeritics (Model AccuPyc 1330) for samples which were freshly quenched from  $T_g+30^\circ\text{C}$ .

### ***6.2.2 Volume Relaxation Measurements***

Volume relaxation experiments were performed on the neat materials and the blends using a mercury dilatometry apparatus constructed by Shelby.<sup>21</sup> Compression molded samples of approximate weight 6 g (dimensions ca. 1.0 cm x 1.5 cm x 4 cm) were sealed in the glass bulbs of the dilatometers. The dilatometers were then filled with mercury and de-gassed under vacuum. Prior to each run, the encased sample was equilibrated at 30°C above  $T_g$  using a Fisher Scientific 1006D oil bath and subsequently quenched to 0°C using an ice bath. The dilatometer and enclosed sample was then placed back into the oil bath after the bath was cooled to the desired aging temperature of 15, 30, or 45°C below  $T_g$ . Isothermal annealing was then performed for approximately four days while volume changes were assessed from the height of the mercury in the capillary of the glass dilatometer using a linear voltage differential transducer. Three runs were conducted at the undercooling of 30°C in order to provide an indication of the measurement error. Experimental details beyond those given here can be found in Chapter 4 and elsewhere.<sup>21</sup>

### ***6.2.3 Creep Compliance Measurements***

The influence of physical aging on small-strain tensile creep compliance behavior was assessed for neat PMMA during isothermal aging at  $T_a = T_g - 30^\circ\text{C}$ . Each sample was cut and tested after a piece of PMMA film was rapidly quenched from  $T_g + 30^\circ\text{C}$  to well below  $T_g$  by placing it between two steel plates at room temperature. Using the procedure established by Struik,<sup>22</sup> the small-strain creep response was probed after aging times of 1.5, 3, 6, 12, and 24 hours. A Seiko thermal mechanical analyzer (model TMA 100) was used to test the samples which possessed a length of 25 mm length, thickness of 0.2 mm, and a width of 3 mm (approximate dimensions). Creep measurements on the blends were not performed because an apparent failure of time-aging time superposition was noted for pure PMMA (see Results and Discussion).

#### ***6.2.4 Differential Scanning Calorimetry***

The kinetic nature of the glass transition was probed using differential scanning calorimetry (DSC). A properly calibrated Perkin Elmer DSC7 was used, and the sample and reference cells of this instrument were constantly kept under a nitrogen purge during measurements and while the instrument was idle. The temperature was calibrated using tin and indium, and the heat flow was calibrated using indium. Particular care was taken with respect to maintaining the ice/water bath and insuring that changes in the instrument baseline were not occurring during the measurements. Each sample weighing approximately 10 mg was cooled in the calorimeter from  $T_g+50^\circ\text{C}$  to  $T_g-50^\circ\text{C}$  at a fixed rate of 1, 3, 10, 30, 60, or  $100^\circ\text{C}/\text{min}$  and then measurements were made as the sample was then heated back to  $T_g+50^\circ\text{C}$  at  $10^\circ\text{C}/\text{min}$ . Three samples were tested for each cooling rate, and this testing was performed for all of the blend compositions. Fictive temperature calculations were conducted on the heating scans using the Perkin Elmer analysis software.

#### ***6.2.5 Dynamic Mechanical Analysis***

Dynamic mechanical measurements were made in tension using a Seiko DMS 210. The samples had the approximate dimensions of 0.2 mm x 5 mm x 10 mm long. The testing was performed on freshly quenched samples which were generated by annealing films at a temperature of  $T_g+30^\circ\text{C}$  for 10 minutes and then quenching them to well below  $T_g$  by placing them between steel plates at room temperature. The testing procedure involved a heating rate of  $2^\circ\text{C}/\text{min}$ , a nitrogen purge, and a frequency of 1 Hz. The dynamic mechanical response was assessed accordingly for each material from approximately  $-140^\circ\text{C}$  to above the  $\alpha$ -relaxation temperature region.

#### ***6.2.6 Thermal Contraction Measurements***

A model TMA 100 Seiko thermal mechanical analyzer was used to measure linear thermal contraction during cooling the PMMA, SAN, and PMMA/SAN50 materials at  $1^\circ\text{C}/\text{min}$  from  $T_g+20^\circ\text{C}$  to  $50^\circ\text{C}$ . The samples possessed the following approximate dimensions: length of 25 mm, thickness of 0.2 mm, and width of 3 mm. A very small tensile load was maintained during testing but this did not induce any significant amount

of creep as was verified by holding the sample in tension for 15 minutes at  $T_g+20^\circ\text{C}$ . Four samples were tested for each material and density measurements were made on the samples after the cooling runs were all performed. The four samples were cut up and combined for testing at  $23^\circ\text{C}$  using the Micromeritics AccuPyc 1330 pycnometer in order to transform the relative density behavior assessed for the isotropic samples during cooling into actual volume versus temperature curves.

### 6.3 Research and Discussion

The isothermal decay of volume in the glassy state was assessed as a function of both aging temperature and blend composition, and the information gained from this experimentation will be presented and discussed. Specifically, an attempt to gain an understanding of the volume relaxation results will be undertaken based upon supporting data concerning the influence of blend composition on: (1) initial density prior to aging; (2) kinetics of the glass formation process; and (3) intensity of secondary relaxation processes. This will permit a thorough comparison of the volume aging behavior of the PMMA/SAN and a-PS/PPO blend systems.

#### 6.3.1 Physical Aging Results

Dilatometry was used to follow decreases in volume during sub- $T_g$  annealing for PMMA, SAN, and their blends. The aging temperature,  $T_a$ , values which were employed were 15, 30, and  $45^\circ\text{C}$  below the inflection DSC glass transition temperatures measured during heating freshly quenched samples at  $10^\circ\text{C}/\text{min}$ . The glass transition temperature used as the reference temperature for the aging experiments did not vary substantially with blend composition as is attested to by the data plotted in Figure 6-1a. Some representative volume relaxation results obtained at  $T_g-30^\circ\text{C}$  are provided by Figure 6-2. To quantify the volume aging behavior and enable comparisons to be made, each volume relaxation rate,  $b_V$ , was determined according to the following:<sup>22,23</sup>

$$b_V = -\frac{1}{V} \frac{dV}{d \log t_a} \quad \text{Eqn. 6-3}$$

The influences of composition and undercooling ( $T_g - T_a$ ) on volume relaxation rate can be observed from Figure 6-3. Volume relaxation rates increased in an essentially linear manner with regards to SAN content for both the undercoolings of 15°C and 30°C. For the aging temperature of  $T_g - 45^\circ\text{C}$ ,  $b_v$  was noted to be independent of blend composition. Explanation of the observed volume relaxation rate trends is reserved for later in the discussion.

The volume relaxation trends presented herein are, in general, comparable with the results of the previous studies which investigated enthalpy relaxation/recovery for the PMMA/SAN blends. Kwei and coworkers<sup>13</sup> annealed PMMA/SAN samples for 88 hours at 85°C, which was an aging temperature of approximately  $T_g - 20^\circ\text{C}$  for the neat polymers and blends, and noted that the degree of enthalpy recovery was essentially constant with respect to composition. These enthalpy recovery data were unlike the volume relaxation results at a similar undercooling of  $T_g - 15^\circ\text{C}$  presented in this communication in that the volume relaxation rates were found to increase with SAN content. Physical aging was only a minor component of this previous study by Kwei et al., and measurements of the degree of enthalpy recovery as a function of  $\log(\text{aging time})$  were not made to assess enthalpy aging rates. The limited enthalpy recovery data acquired for annealing at 85°C for 88 hours did provide an indication that the blends displayed relaxation/recovery characteristics which were intermediate to the responses for pure PMMA and SAN. The present volume relaxation study supports this general result. A more comprehensive examination of enthalpy relaxation/recovery was later undertaken for the PMMA/SAN blend system by Mijovic et al.<sup>16</sup> The conclusions reached by these researchers are quite consistent with the volume relaxation results presented here; the decay of enthalpy with  $\log(\text{aging time})$  was essentially intermediate for the blends compared to the pure components and increased with SAN content at  $T_g - 20^\circ\text{C}$  and  $T_g - 35^\circ\text{C}$  while the rate of enthalpy relaxation was independent of composition at  $T_g - 50^\circ\text{C}$ . Therefore, these new dilatometric findings are consistent with trends present in published enthalpy relaxation data. The remaining challenge is to develop an understanding of the trends, a venture which will be commenced shortly.

At the outset of this study, the intention was to also characterize the mechanical aging of the PMMA/SAN materials. Such an endeavor, however, turned out to be

problematic due to concern for whether Struik's<sup>24</sup> time-aging time superposition was valid for PMMA and, as an extension, for blends of PMMA with SAN. Small-strain creep compliance response was measured for PMMA following aging at 82°C ( $T_g-30^\circ\text{C}$ ) for aging times of 1.5, 3, 6, 12, and 24 hours. Typical results which were obtained following this testing procedure are presented in Figure 6-4a. An attempt to superimpose all of the creep data via horizontal and vertical shifting was performed with the outcome represented by the apparent master curve shown in Figure 6-4b. Although a fair master curve could be formed, some question concerning the applicability of time-aging time superposition remained. The creep data points in the middle of this apparent master curve (Figure 6-4b) exhibit noticeable discord relative to each other which brings into scrutiny the reducibility of the data according to the typical time-aging time principle. When only superposition of the long time portions of the creep data was performed, excellent reduction of the long time data was possible as is illustrated in Figure 6-4c. However, the short time response appeared to display a dependence on aging time not accounted for by the horizontal and vertical shifting necessary to superimpose the long time data. This behavior was observed for all three PMMA samples testing under these conditions.

The apparent failure of the superposition for the PMMA creep data is consistent with expectations based upon creep studies performed by Read and coworkers<sup>25,26</sup> on polymers with overlapping primary and secondary mechanical relaxations. When two distinct relaxations both exert some influence on the data in the experimental window accessible by the mechanical measurements, it is anticipated that thermorheological complexity will be the result. An intense secondary relaxation is a characteristic feature of PMMA and this relaxation significantly overlaps with the  $\alpha$ -relaxation (glass transition). This is a well established feature of the dynamic mechanical behavior of PMMA.<sup>27</sup> This relaxation, albeit reduced in magnitude, is also present in the PMMA/SAN blends as is illustrated in Figure 6-5. Further discussion of the secondary relaxations for the blends will be entertained later. The typical effect of aging on the  $\alpha$ -relaxation of an amorphous polymer is a shift of the associated relaxation time distribution to longer times while the temperature/frequency location of secondary relaxations remains unaffected by the aging process.<sup>26,28,29</sup> While there is some debate

concerning whether the intensity of a secondary relaxation diminishes with physical aging,<sup>28-32</sup> the aging process clearly influences the  $\alpha$ - and  $\beta$ -relaxations differently. Therefore, when the primary and secondary relaxation processes overlap in the temperature and time regions where mechanical aging studies are performed, failure of the time-aging time superposition can result.

Both failure and success of the time-aging time superposition principle as applied to PMMA has been observed. Failure of time-aging time superposition has been clearly established for the small-strain creep behavior of PMMA at 40°C and 60°C by McKenna and Kovacs,<sup>33</sup> but these researchers found that decent superposition of creep data could be performed at 80°C, unlike the present study which indicated questionable superposition at a similar aging temperature of 82°C ( $T_g-30^\circ\text{C}$ ). An examination of mechanical aging of the PMMA/SAN blend system has been performed by Mijovic and coworkers as well as Cowie et al. and these stress relaxation studies indicated no evidence of failure of time-aging time superposition for any of the neat materials or blends. This successful mechanical data reduction observed in the study by Cowie et al. is not surprising given the relatively close proximity of the aging temperatures to the glass transition temperature. The investigated undercoolings were all less than 30°C, and the influence of the secondary relaxation on the experimentally accessible creep response becomes diminished relative to the  $\alpha$ -relaxation contribution as temperature is increased. The complete success of superposition noted in the study by Mijovic et al. is unexpected, however, because these researchers utilized aging temperatures down to  $T_g-50^\circ\text{C}$  which, for neat PMMA, is an aging temperature in close proximity to 60°C where McKenna and Kovacs found clear failure of time-aging time superposition for this material. An in-depth study of the applicability of the time-aging time reduction scheme to mechanical data for glassy blends of PMMA and SAN, although certainly warranted, is outside the scope of this present investigation. If Struik's reduction principle is invalid in a general sense for pure PMMA and for PMMA/SAN blends, then mechanical aging rates cannot be precisely compared with the goal of determining the influences of composition and temperature on mechanical aging behavior.

### ***6.3.2 Interpretation of Aging Results and Comparison with a-PS/PPO System***

Study of the miscible blend system comprised of atactic polystyrene and poly(2,6-dimethyl-1,4-phenylene oxide) revealed that the compositional variation of glassy density, fragility, and secondary relaxation intensity could provide insight into physical aging results for the blends (Chapters 4 and 5). These characteristics were also investigated for the PMMA/SAN blend system of current interest. This information will be employed in order to understand the noted variation of volume relaxation rate with composition and aging temperature for the PMMA/SAN system, and this will further enable the aging behavior of the a-PS/PPO and PMMA/SAN blend systems to be contrasted.

Quenching an amorphous polymer into the glassy state captures a certain amount of free volume which can further decrease during physical aging. The free volume which is present prior to aging controls, in addition to other chemical and structural features, the initial degree of mobility at a given temperature in the glassy state. This initial mobility can influence the subsequent rate of volume relaxation during annealing due to the self-limiting character of the physical aging process. Self-limitation describes the circular process wherein mobility enables the structural rearrangements necessary for a reduction in the volume toward the equilibrium state, and this densification serves to further retard the mobility. Accordingly, the initial amount of free volume which is captured by the quenching process can influence the rate of volume relaxation during aging. It was observed that unaged density characteristics could help explain the compositional dependence of volume relaxation rates for the a-PS/PPO blend system aged at undercoolings of 15°C and 30°C. Negative deviation in freshly quenched specific volumes were observed for the a-PS/PPO blends compared to additivity and a comparable deviation was also noted from the  $b_v$  versus composition data at  $T_g-15^\circ\text{C}$  and  $T_g-30^\circ\text{C}$ . The volume relaxation rates obtained for aging the a-PS/PPO system at  $T_g-60^\circ\text{C}$  were linear with composition, however, and this will be addressed later during consideration of the effects of secondary relaxations on aging rates. In contrast to the excess volume characteristics in the glassy state for blends of a-PS and PPO, the variation of specific volume with composition for freshly quenched samples of the PMMA/SAN materials displayed an essential linear trend as can be seen in Figure 6-1b. A linear

dependence of volume relaxation rate on SAN content was also obtained for all of the undercoolings employed in this PMMA/SAN aging study (Figure 6-3) which was consistent with the specific volume data prior to aging. A linear dependence of  $b_v$  on composition was noted for the PMMA/SAN blends at the undercoolings of 15, 30, and 45°C, but the slope of the dependence varied with undercooling. Inspection of secondary relaxation characteristics for the PMMA/SAN system will generate insight into the reason for the changes in the slope with variations in the aging temperature.

Previous research on the a-PS/PPO blend system indicated a close tie between the glass formation kinetics and excess volumes in the glassy state for the blends. The variation of the initial glassy density (induced by a quench from above  $T_g$ ) with blend composition is influenced by the relative kinetics of glass formation for the miscible blends compared to the behavior observed for the pure components. The negative excess volumes observed for the a-PS/PPO blends in the glassy state are not present at temperatures in the liquid state.<sup>34</sup> The negative excess volumes for the blends in the glassy state are due to the fact that the specific interactions between the a-PS and PPO components heighten the fragility (cooperativity) of the blends compared to pure a-PS and PPO (Chapter 5). Volume contraction with mixing is typically inferred from glassy state density versus composition data even though mixing of the amorphous polymers occurs in the liquid state above the highest component  $T_g$ . This proved to be an inappropriate approach for the case of the a-PS/PPO blends where it was clear that the negative  $\Delta V_{\text{mix}}$  values noted in the glassy state were caused by kinetic, rather than thermodynamic, effects. This proved that the presence of specific interactions caused the increased density for the blends compared to additivity in the glassy state which in turn affected the subsequent volume relaxation rate behavior at  $T_g-15^\circ\text{C}$  and  $T_g-30^\circ\text{C}$ .

It was mentioned previously that the PMMA/SAN blends do not possess attractive interactions between the components comparable to those present between a-PS and PPO in their miscible mixtures. The positive deviation of fragility from additivity due to the interactions between a-PS and PPO in the blends caused the negative deviation in the specific volume versus PPO content data in the glassy state. It is informative to consider the fragility characteristics of the PMMA/SAN blends and compare them to the glass formation kinetics of the neat polymers. It is not the intention of the authors to

reiterate the details of the fragility concept in this present communication; a detailed explanation with appropriate reference citations is provided in Chapters 5 and 7. Glass transition kinetic characteristics were not assessed from dynamic mechanical  $\alpha$ -relaxation data of the PMMA/SAN materials because of concern for the convoluting influence of the intense secondary relaxation which overlaps the  $\alpha$ -relaxations of pure PMMA and the blends (Figure 6-5). However, consideration of DSC heating scans through the glass transition region can provide quantitative information about glass transition kinetics if the cooling rate employed just prior to the heating scans (fixed heating rate) is systematically varied.<sup>35</sup> Such an approach was used in this investigation, and some typical DSC results for the PMMA/SAN materials are indicated in Figure 6-6 as a function of blend composition. A value of fictive temperature,<sup>36-38</sup>  $T_f$ , was determined from each heating trace using the Perkin-Elmer software. The relationship between cooling rate,  $q_c$ , and fictive temperature is shown in Figure 6-7 for PMMA, SAN, and the PMMA/SAN50 blend. The slope of each data set plotted in the manner indicated in Figure 6-7 provides a measure of fragility. Information concerning the dependence of fragility on SAN content was generated accordingly with the resulting trend indicated in Figure 6-8. Because the fragility characteristics of the PMMA/SAN blends are linearly intermediate to the fragility characteristics of neat PMMA and SAN, the variation of specific volume with composition should be similar for the liquid and glassy states unlike the a-PS/PPO results. Thermal contraction experiments carried out during cooling at 1°C using linear dilatometry bear out this anticipation as can be seen from the data presented in Figure 6-9. Quantitative thermal expansion parameters resulting from the thermal contraction tests are given in Table 6-I. The cooling curve for the 50/50 blend is essentially intermediate to the data of PMMA and SAN in both the liquid and glassy states. Because strong attractive interactions are not present between PMMA and SAN in the blends, no increased fragility behavior was noted for the blends compared to the pure component responses which resulted in the maintenance of the liquid state excess volume for the 50/50 blend upon cooling into the nonequilibrium glassy state. This observation is in stark contrast to the behavior of the a-PS/PPO blend system.

Characterization of secondary relaxation intensity as a function of blend composition can enable an understanding to be developed concerning changes in  $b_V$  versus blend composition trends which occur as aging temperature is varied. It was observed that the a-PS/PPO blends possessed secondary relaxations in the vicinity of the  $\beta$ -relaxation for neat atactic polystyrene (Chapter 4). The intensity of the relaxation, however, did not diminish in a simple manner with increasing PPO content due to additional motion of the PPO which occurred in cooperation with the a-PS secondary dispersion. The fact that the variation of  $b_V$  with composition changed from a trend characterized by negative deviation from additivity at  $T_g-30^\circ\text{C}$  to a linear trend at  $T_g-60^\circ\text{C}$  was attributed to these secondary relaxation characteristics. It was discovered that an indication of the change in mobility in going from one glassy temperature to another could be obtained by a ratio of the loss modulus values at these two temperatures for a fixed set of testing conditions. The variation of this loss modulus ratio with blend composition was remarkably comparable to the compositional dependence of a similar ratio determined for volume relaxation rate for the a-PS/PPO blend system. This suggested that a dynamic mechanical spectrum can provide some prediction of relative volume relaxation rates of an amorphous polymer for two substantially different glassy temperatures (temperature difference of  $30^\circ\text{C}$ ), an observation which supported earlier work by Struik.<sup>39</sup> The secondary relaxation process for PMMA was observed to be present in the PMMA/SAN blends (Figure 6-5). Unlike the a-PS/PPO dynamic mechanical results, the secondary relaxation intensities of the PMMA/SAN blends decreased with decreasing PMMA content in a fashion consistent with the fact that only motion of PMMA was responsible for the dynamic dispersion. The curiosity arose in this study as to whether the dynamic mechanical responses could help explain the variation of the volume relaxation rate results with aging temperature for the PMMA/SAN blends based upon the prior success of this approach in the investigation of the a-PS/PPO blend system. The ratio of properties at  $T_g-15^\circ\text{C}$  to those at  $T_g-45^\circ\text{C}$  were determined for the properties of loss modulus and volume relaxation rate which were measured for the PMMA/SAN system. The results are plotted in Figure 6-10. It can be concluded from the similarity of the loss modulus and  $b_V$  ratio parameters that the reduction in the slope of the volume relaxation rate versus SAN content which occurred with increasing

undercooling (Figure 6-3) was due to the compositional dependence of secondary relaxation intensity.

Comparison of the two blend systems has enabled the development of an informative picture of the physical aging process for miscible blends. Contrasting the PMMA/SAN and a-PS/PPO blend systems allowed some understanding of the role of attractive interactions on the volume relaxation process to be gained. It must be pointed out that these two blend systems have an important difference which is beyond their distinction concerning the nature of interactions. The glass transition temperatures of PMMA and SAN are quite similar while the glass transition temperature of PPO is approximately 100°C higher than that of a-PS. Concentration fluctuations in the a-PS/PPO blends, therefore, introduce more heterogeneity with regards to mobility than is caused by local variations in composition for the PMMA/SAN blends. It was shown, however, that the presence of concentration fluctuations was not responsible for the observed trends in volume relaxation rate for the a-PS/PPO blend system (Chapter 4). Although the comparison of the PMMA/SAN and a-PS/PPO systems was not perfect, considerable progress was made nonetheless towards attaining a comprehensive understanding of the influence of intermolecular features on the glass formation and volume relaxation processes.

## 6.4 Conclusions

The effects of aging temperature and composition on volume relaxation rate,  $b_v$ , were investigated for blends of PMMA and SAN. Volume relaxation rates were found to be essentially linear with composition for the aging temperatures of 15, 30, and 45°C below  $T_g$ . Fragility determined from differential scanning calorimetry and unaged density in the glassy state were both linear with SAN content in the blends which helped to explain the noted dependence of volume relaxation rate on composition. The slope of the linear  $b_v$  versus SAN content decreased as aging was performed deeper in the glassy state. The secondary relaxation process for PMMA was observed in the blends and decreased systematically in intensity as the amount of PMMA was decreased in the

blends. The noted effect of aging temperature on the volume relaxation rates was attributed to the secondary relaxation characteristics. All of the above observations were consistent with the lack of attractive interactions between the components in these blends. The results of this study were contrasted with previously obtained data for the a-PS/PPO blend system, and a better understanding of the role of interactions on volume relaxation emerged as a result.

Table 6-I: Results from thermal contraction experiments

Material	midpoint $T_g$ (°C)	$\alpha_g \times 10^4$ (K <sup>-1</sup> )	$\alpha_l \times 10^4$ (K <sup>-1</sup> )	$\Delta\alpha \times 10^4$ (K <sup>-1</sup> )
PMMA	98.9 (±0.4)	2.5 (±0.2)	5.0 (±0.2)	2.5
PMMA/SAN50	98.0 (±0.3)	2.3 (±0.3)	5.4 (±0.2)	3.1
SAN	97.4 (±0.3)	2.3 (±0.2)	5.9 (±0.1)	3.6

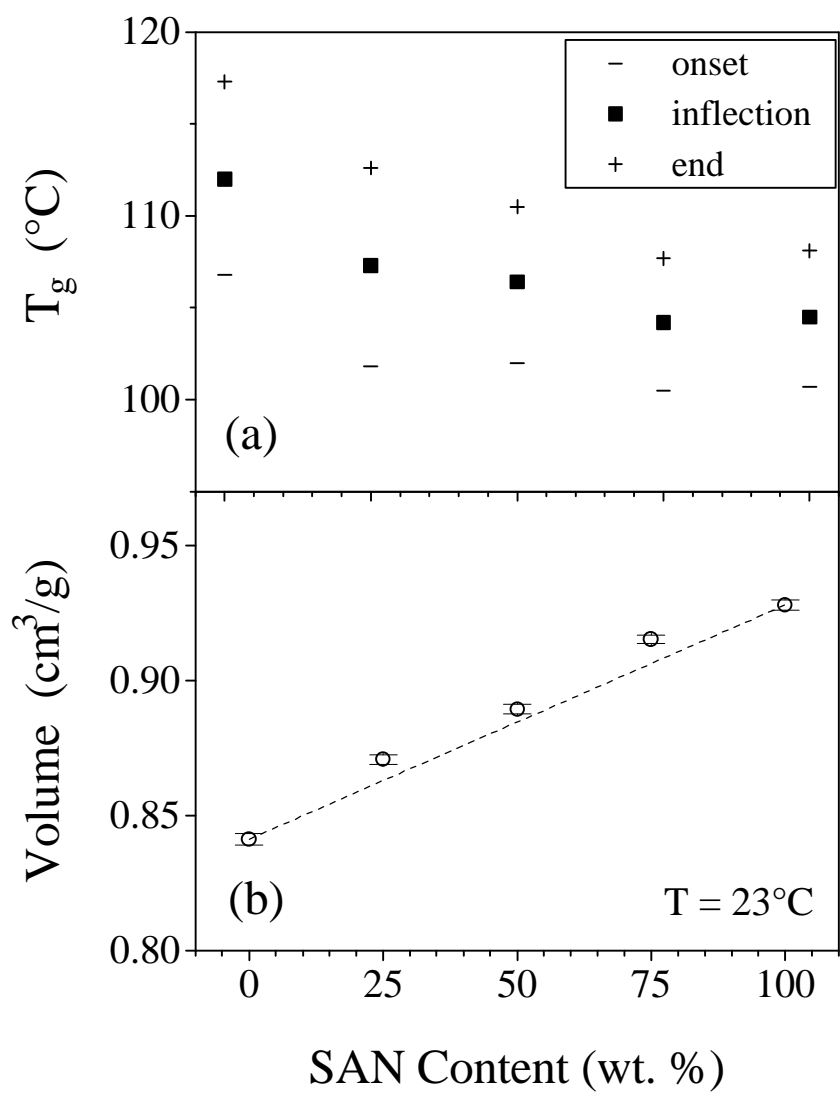


Figure 6-1. (a) DSC glass transition temperature results and (b) room temperature specific volume data.

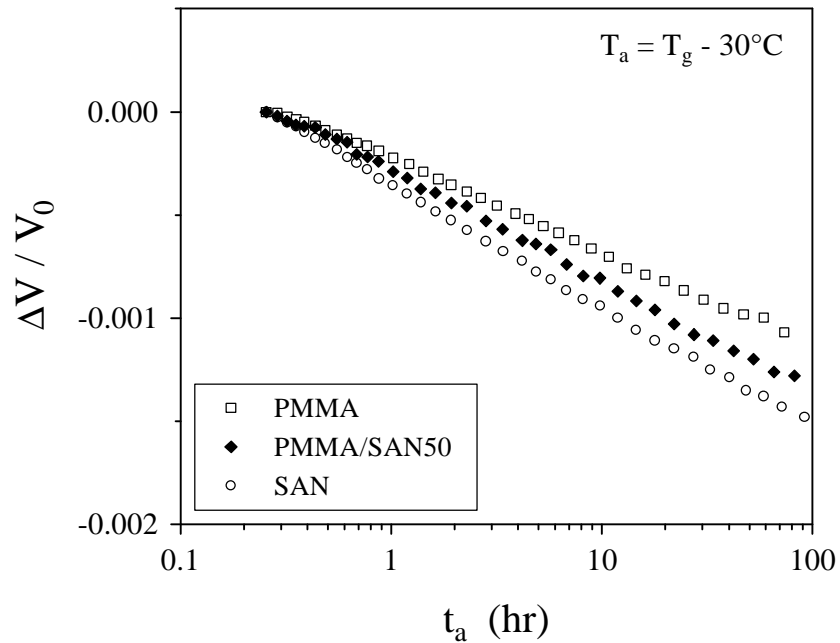


Figure 6-2. Typical volume relaxation results for aging performed at  $T_g - 30^\circ\text{C}$ . An aging time of 0.25 hr was used as the reference for determining volume differences ( $\Delta V$  values). The negative slope of each data set represents the volume relaxation rate,  $b_V$ , and data points between 0.6 hr and 80 hr (approx.) were used in the rate determination.

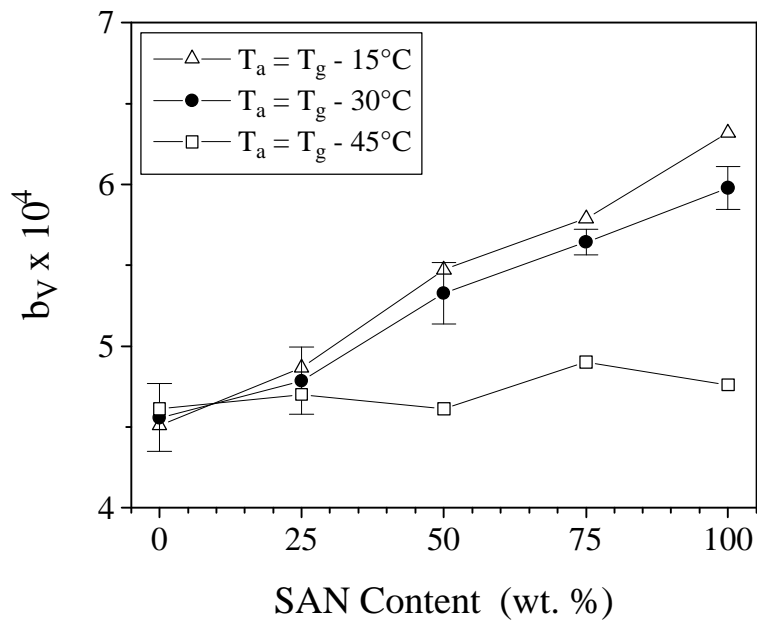


Figure 6-3. Variation of volume relaxation rate with composition and aging temperature.

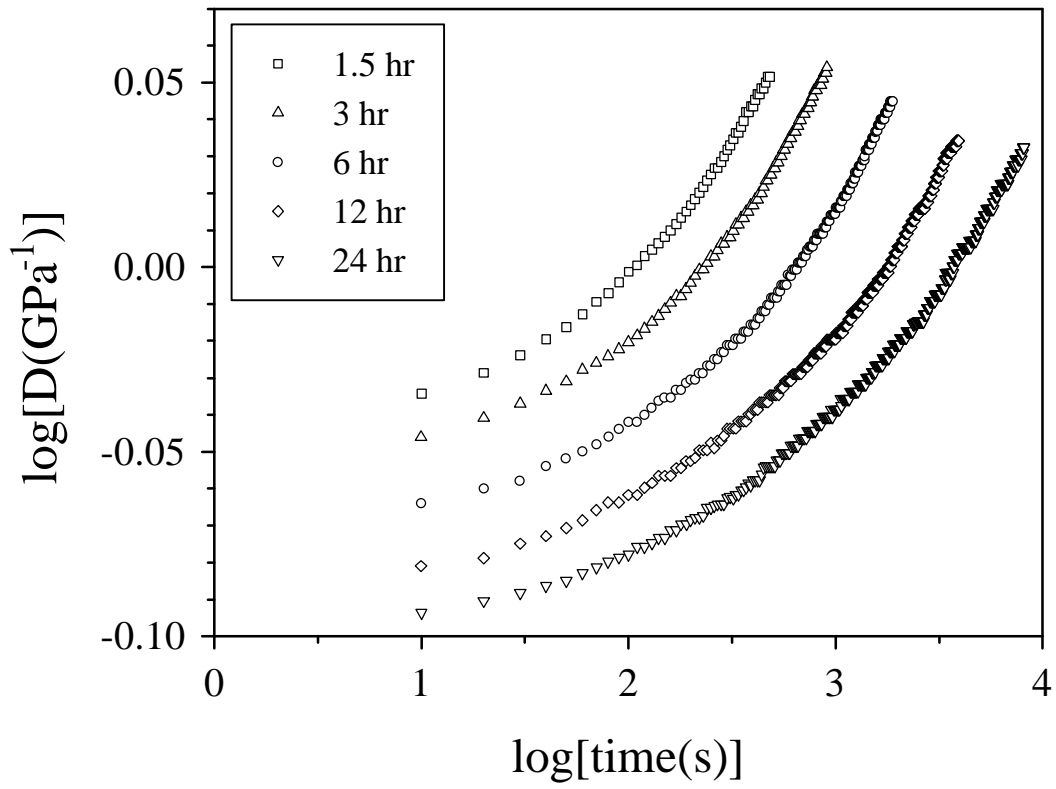


Fig. 6-4a

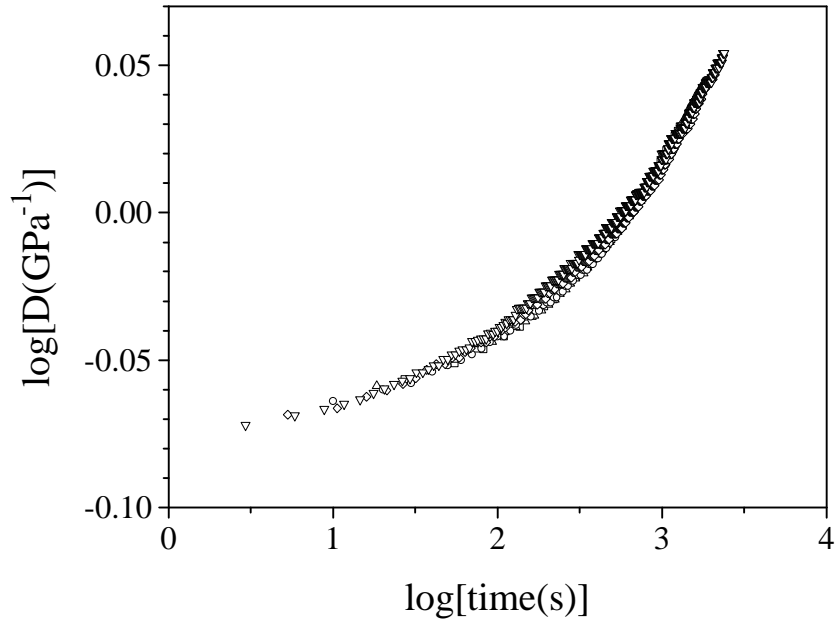


Fig. 6-4b

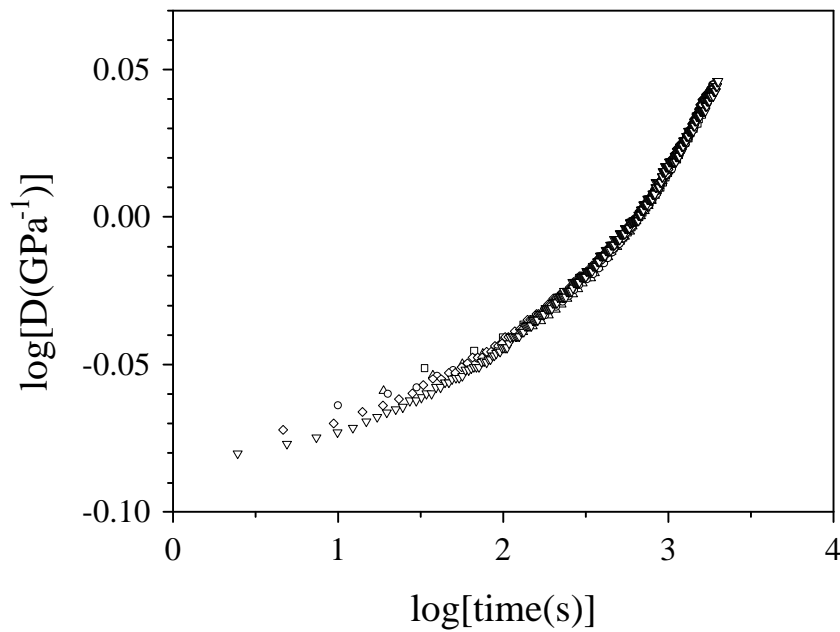


Fig 6-4c

Figure 6-4. (a) Creep compliance behavior for PMMA following aging at  $T_g-30^\circ\text{C}$  for the indicated aging times; (b) Attempt to generate a master curve via horizontal and vertical shifting in order to superimpose the entire data set for each aging time; (c) Attempt to superimpose the long time portion of the creep data. The reference response used during the superposition attempts was that obtained at an aging time of 6 hours.

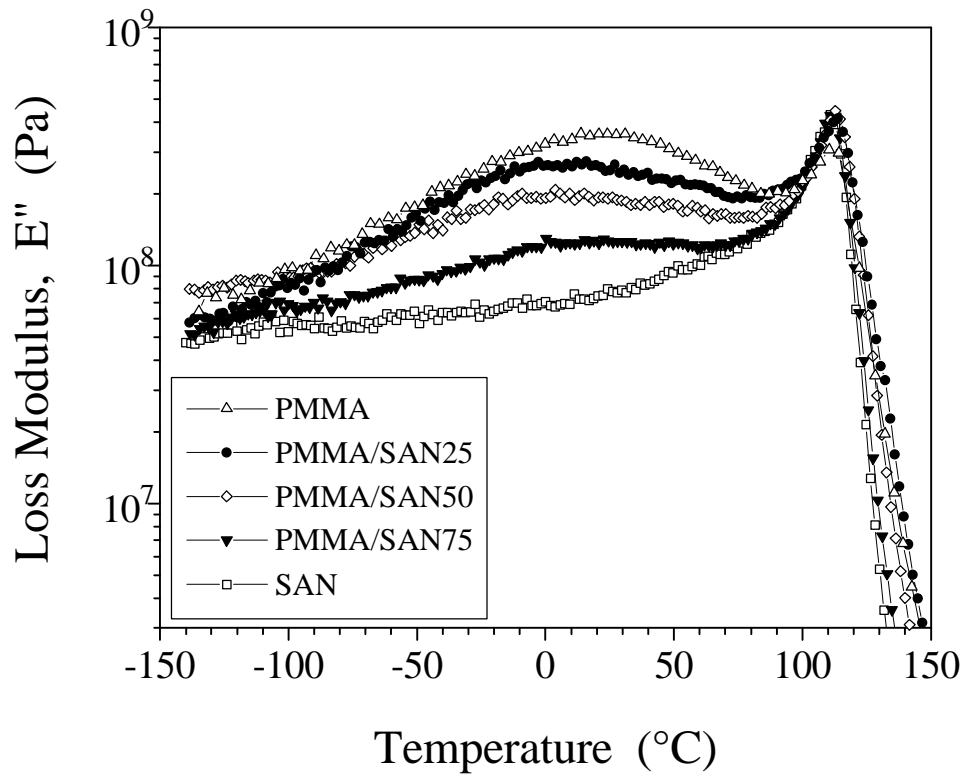


Figure 6-5. Loss modulus data obtained at a heating rate of 2°C/min using a testing frequency of 1 Hz.

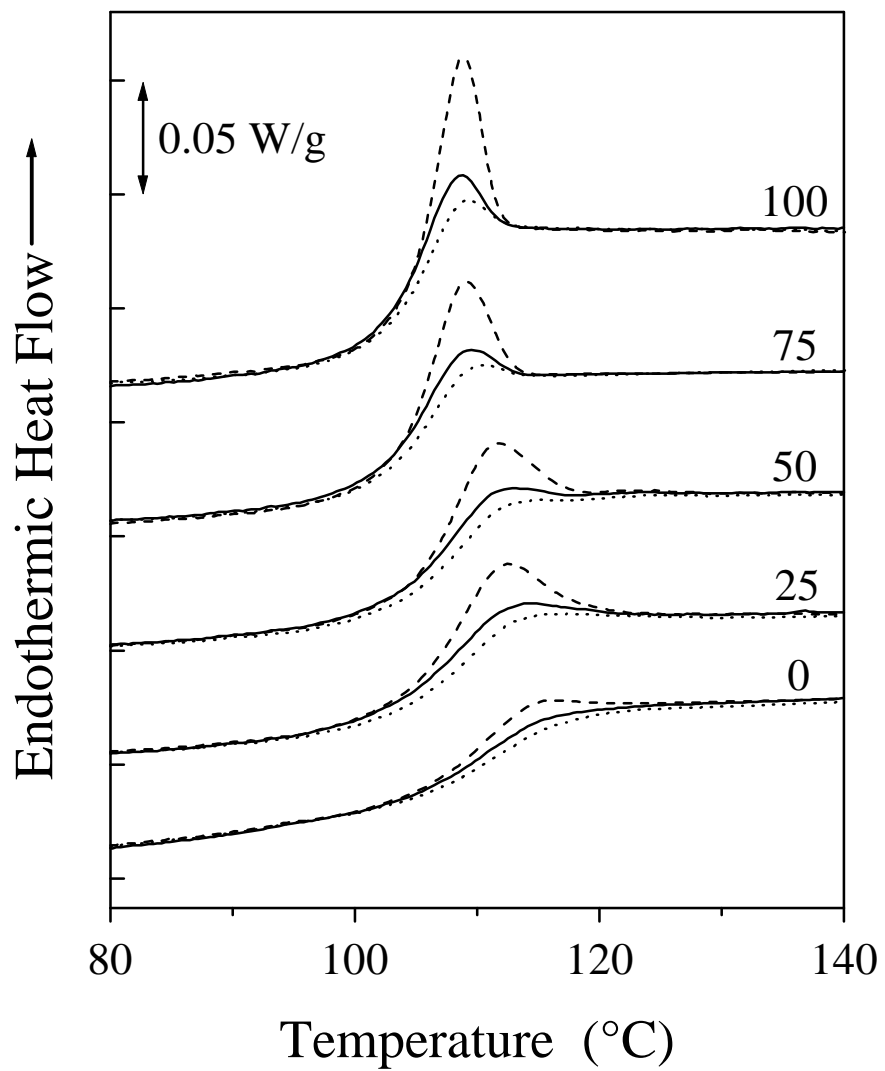


Figure 6-6. DSC heating traces obtained during heating at 10°C/min following cooling at 1°C/min (dashed lines), 10°C/min (solid lines), and 100°C/min (dotted lines). The numbers represent the SAN content in wt.%.

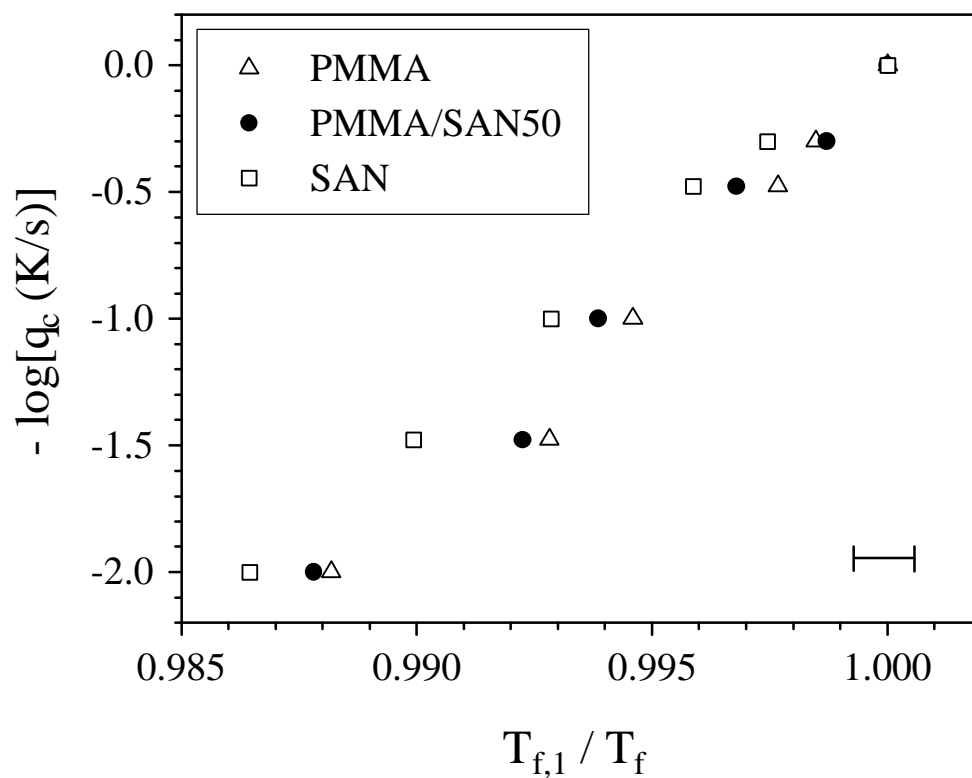


Figure 6-7. Relationship between the cooling rate ( $q_c$ ) and the fictive temperature assessed from the DSC heating scans at  $10^\circ\text{C}/\text{min}$ . The fictive temperature associated with the cooling rate of  $1^\circ\text{C}/\text{min}$ ,  $T_{f,1}$ , is used as a normalization constant for each material. The magnitude of a typical error bar associated with the normalized fictive temperature data is given in the plot.

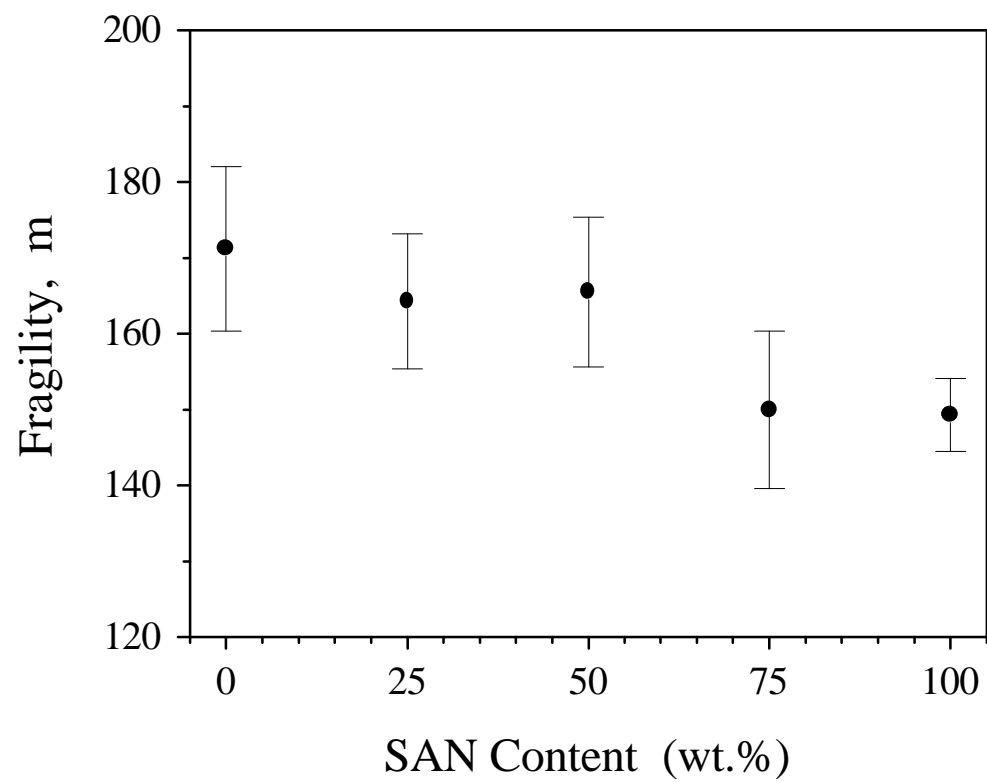


Figure 6-8. Influence of blend composition on the fragility determined from the DSC data.

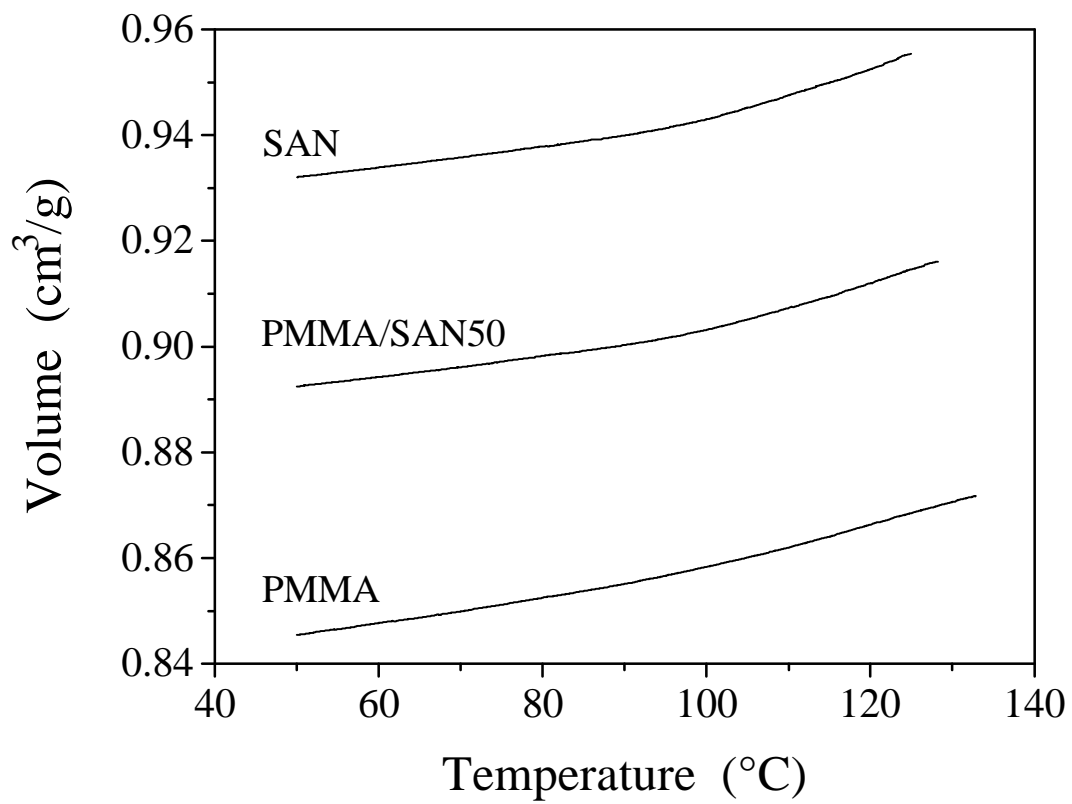


Figure 6-9. Thermal contraction responses assessed during cooling at 1°C/min.

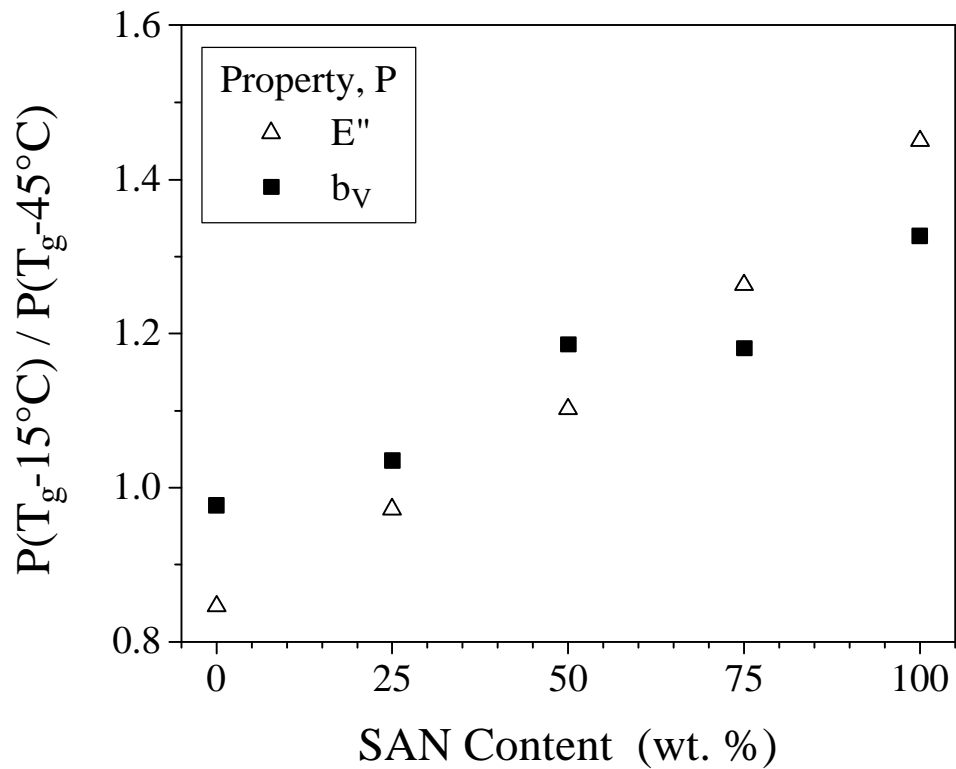


Figure 6-10. Ratio of property value at  $T_g-15^\circ\text{C}$  to value at  $T_g-45^\circ\text{C}$  for the properties of volume relaxation rate and loss modulus (1 Hz, heating at  $2^\circ\text{C}/\text{min}$ , freshly quenched sample).

## 6.5 References

- 1 ISI Science Citation Index, search: "physical aging", "physical ageing", "volume relaxation", or "enthalpy relaxation"
- 2 H. Feng, Z. Feng, H. Ruan, and L. Shen, *Macromolecules* **25**, 5981 (1992).
- 3 S. H. Goh, S. Y. Lee, X. Zhou, and K. L. Tan, *Macromolecules* **32**, 942 (1999).
- 4 J. W. Barlow and D. R. Paul, *Polym. Eng. Sci.*, **21**, 985 (1981).
- 5 R. P. Kambour, J. T. Bendler, and R. C. Bopp, *Macromolecules*, **16**, 753 (1983).
- 6 G. ten Brinke, F. E. Karasz, and W. J. MacKnight, *Macromolecules*, **16**, 1827 (1983).
- 7 D. R. Paul and J. W. Barlow, *Polymer*, **25**, 487 (1984).
- 8 E. M. Woo, J. W. Barlow, and D. R. Paul, *Polymer*, **26**, 763 (1985).
- 9 M. Suess, J. Kressler, and H. W. Kammer, *Polymer*, **28**, 957 (1987).
- 10 J. M. G. Cowie and D. Lath, *Makromol. Chem., Macromol. Symp.*, **16**, 103 (1988).
- 11 N. Nishimoto, H. Keskkula, and D. R. Paul, *Polymer*, **30**, 1279 (1989).
- 12 H. Feng, C. Ye, and Z. Feng, *Polymer Journal*, **28**, 661 (1996).
- 13 K. Naito, G. E. Johnson, D. L. Allara, and T. K. Kwei, *Macromolecules* **11**, 1260 (1978).
- 14 N. Higashida, J. Kressler, and T. Inoue, *Polymer*, **36**, 2761 (1995).
- 15 J. Mijovic, S. T. Devine, and T. Ho, *J. Appl. Polym. Sci.*, **39**, 1133 (1990).
- 16 J. Mijovic, T. Ho, and T. K. Kwei, *Polym. Eng. Sci.*, **29**, 1604 (1989).
- 17 T. Ho and J. Mijovic, *Macromolecules* **23**, 1411 (1990).
- 18 T. Ho, J. Mijovic, and C. Lee, *Polymer* **32**, 619 (1991).
- 19 J. Mijovic and T. Ho, *Polymer* **34**, 3865 (1993).
- 20 J. M. G. Cowie, I. J. McEwen, and S. Matsuda, *J. Chem. Soc., Faraday Trans.*, **94**, 3481 (1998).
- 21 Shelby, M. D. *Ph.D. Dissertation*, Virginia Polytechnic Institute and State University, 1996.
- 22 L. C. E. Struik, *Physical Aging in Amorphous Polymers and Other Materials*, Elsevier, New York, 1978.
- 23 Greiner, R. and Schwarzl, F. R. *Rheol. Acta*, 1984, **23**, 378.
- 24 Struik, L. C. E. *Physical Aging in Amorphous Polymers and Other Materials*, Elsevier, New York, 1978.
- 25 B. E. Read, P. E. Tomlins, and G. D. Dean *Polymer* **31**, 1204 (1990).
- 26 B. E. Read *J. Non-Cryst. Solids* **131-133**, 408 (1991).
- 27 N. G. McCrum, B. E. Read, and G. Williams, *Anelastic and Dielectric Effects in Polymeric Solids*, Dover Publications, New York, 1967, pp. 238-255.
- 28 L. C. E. Struik *Polymer* **28**, 57 (1987). (**CHECK THIS**)
- 29 R. Diaz-Calleja, A. Ribes-Greus, and J. L. Gomez-Ribelles *Polymer* **30**, 1433 (1989).
- 30 E. Muzeau, G. Vigier, and R. Vassoille *J. Non-Cryst. Solids* **172-174**, 575 (1994).
- 31 G. P. Johari *J. Chem. Phys.* **77**, 4619 (1982).
- 32 L. Guerdoux and E. Marchal *Polymer* **22**, 1199 (1981).
- 33 G. B. McKenna and A. J. Kovacs *Polym. Eng. Sci.* **24**, 1138 (1984).
- 34 P. Zoller and H. H. Hoehn, *J. Polym. Sci.: Polym. Phys. Ed.* **20**, 1385 (1982).
- 35 I. M. Hodge, *J. Non. Cryst. Solids*, **169**, 211 (1994).

- <sup>36</sup> Tool, A. Q. *J. Am. Ceram. Soc.*, 1946, **29**, 240.
- <sup>37</sup> Tool, A. Q. *J. Res. Natl. Bur. Stand.*, 1946, **37**, 73.
- <sup>38</sup> Hutchinson, J. M. *Prog. Polym. Sci.*, 1995, **20**, 703.
- <sup>39</sup> L. C. E. Struik *Polymer* **28**, 1869 (1987).

# Chapter 7

## Correlation Between Physical Aging Rates and Glass Transition Cooperativity (Fragility): Part 1. Experimental Results

---

---

### Chapter Synopsis

The results of this study indicate that normalized physical aging rates for volume and enthalpy correlate well with glass transition cooperativity for numerous amorphous polymer materials aged at 30°C below the glass transition temperature. The nonArrhenius relaxation time behavior in the glass formation region observed using dynamic mechanical analysis can be used to determine a measure of the glass transition cooperativity ( $z_g$ ) based upon the general Adam-Gibbs approach. The  $z_g$  parameter represents the most probable number of segments in a hypothetical cooperative domain at the glass transition temperature. It is demonstrated that the glass transition cooperativity can be simply determined from the Williams-Landel-Ferry scaling of segmental relaxation times in the glass formation temperature region. During cooling from above  $T_g$ , the ability to develop a larger number of cooperatively relaxing segments in a domain prior to the onset of the nonequilibrium glassy state appears to result in a slower structural relaxation rate upon subsequent annealing in the glassy state. This connection is consistent with the interrelationships among the nonArrhenius, nonexponential, and nonlinear relaxation characteristics of glass formers observed by Hodge [*Macromolecules* **1983**, *16*, 898] and by Böhmer, Ngai, Angell, and Plazek [*J. Chem. Phys.* **1993**, *99*, 4201].

### 7.1 Introduction

Physical aging is the term used to describe time-dependent changes in properties arising from the nonequilibrium thermodynamic nature of the glassy state. Relaxation of volume and enthalpy (structural relaxation) and the accompanying changes in mechanical, barrier, and optical properties must be understood in order to help insure that the performance of a polymer in the glassy state does not diminish to an unacceptable level during its

application lifetime. The physical aging process poses a serious practical problem and also presents a challenge to scientists attempting to attain a fundamental understanding of the glassy state. Accordingly, the study of nonequilibrium relaxations in the glassy state continues to be a very active area of research.

Although a completely acceptable definition of the glass transition and glassy state has yet to emerge in terms of basic physical principles, the general phenomenological features of glass-forming materials are established to a large extent. During cooling toward the glass transition region, the relaxation times and viscosity of an amorphous material increase rapidly in a nonArrhenius manner. The kinetic behavior of materials in the glass formation temperature region is additionally characterized by a distribution of relaxation times, and this nonexponentiality is also observed for relaxations in the glassy state. Departure into a nonequilibrium glassy state during cooling is a consequence of the increasing relaxation times, and glassy state relaxations are often described as nonlinear due to a dependence on both the temperature and the time-dependent structural state.

Correlations between the nonArrhenius, nonexponential, and nonlinear characteristics of glassy materials have been noted. A connection between the nonArrhenius and nonexponential features of glassy materials was initially proposed in 1983 by Hodge<sup>1</sup> based upon a trend observed between parameters employed in the phenomenological modeling of enthalpy relaxation/recovery data, and this correlation was later strengthened by the incorporation of results for additional glass formers.<sup>2</sup> The link between the nonArrhenius and nonexponential relaxation response has also been conclusively established for numerous glass formers by Böhmer, Ngai, Angell, and Plazek<sup>3,4</sup> using the results from predominantly viscoelastic and dielectric measurements. In addition, Hodge<sup>1,2</sup> indicated that nonexponentiality and nonlinearity appear to be interrelated features as revealed via phenomenological modeling efforts. The dependence of the nonArrhenius segmental relaxation characteristics on chemical structural details has been investigated for numerous glass-forming polymers by Roland, Ngai, and other researchers,<sup>5-8</sup> thus aiding in developing an understanding of the influence of molecular structure on the severity of the relaxation time build-up with cooling. The molecular-level interpretation of glass transition kinetics and the apparent unifying ties between the

characteristic relaxation phenomena of glass formers are critical elements to consider in the formulation of a fundamental understanding of the glass transition and nonequilibrium glassy state.

This investigation examines the possible connection between structural relaxation rates and glass transition cooperativity for glassy polymer materials. Dynamic mechanical analysis allows the nonArrhenius segmental dynamics to be probed, and an index of cooperativity at  $T_g$  can be developed based upon the molecular-based rationale of cooperative relaxation provided by the Adam-Gibbs approach. The relaxation of volume and enthalpy at an aging temperature ( $T_a$ ) of 30°C below  $T_g$  can be assessed following a quench into the glassy state, allowing the determination of any connections between these physical aging rates and the cooperativity observed during glass formation. The attempt to interrelate aging rates and cooperativity for glassy polymer materials will employ data from research efforts of the present authors and will also incorporate literature data in order to illustrate the generality of any observed trends. If the structural relaxation rates vary in a regular fashion with respect to the glass transition cooperativity, and if cooperativity response can be understood in terms of molecular features, then the prediction of aging rates from chemical structural characteristics may eventually become a reality.

## **7.2 Experimental Details**

This scientific contribution makes use of data for numerous glass-forming polymer systems in order to develop a general correlation between aging behavior and the kinetics of glass formation. The majority of this data is detailed in other papers by the present authors or in published work by other scientists. Because the experimental details are of great importance, the reader is encouraged to consult these sources of additional information which will be referred to later. To illustrate the methodology for determining glass transition cooperativity, this study will utilize previously unpublished data for an amorphous thermoplastic polyimide. Physical aging data for this polyimide material are reported in Chapter 9.

### **7.2.1 Material**

The material to be used as an illustrative example is a commercial amorphous polyimide in the Regulus<sup>®</sup> series of polyimides produced by Mitsui Toatsu Chemicals, Inc. This polyimide is described in Chapter 9. The polyimide material was obtained in 0.1 mm thick films and these films were freshly quenched into the glassy state after free annealing above  $T_g$  prior to all testing to insure isotropic and unaged samples. Calorimetric information for this polyimide was obtained at a heating rate of 10°C/min using a Perkin Elmer (model DSC 7) differential scanning calorimeter (DSC). The inflection, or midpoint, glass transition temperature ( $T_g$ ) at this rate was measured to be 239°C and the difference in liquid and glass heat capacities,  $\Delta C_p$ , was determined to be 0.236 J/g-K at  $T_g$ . This data reflects the average thermal behavior for over 10 samples which were freshly quenched into the glassy state in the DSC at 200°C/min after annealing at 50°C above  $T_g$  for 10 minutes. Because the kinetic glass transition temperature mentioned above was obtained in heating as opposed to cooling, it may be more appropriate to discuss this transition temperature as a fictive temperature ( $T_f$ ), or structural temperature.<sup>9</sup> The value of the fictive temperature for freshly quenched samples of the polyimide was 238°C, as determined from the DSC scans using the Perkin Elmer analysis software.

### **7.2.2 Differential Scanning Calorimetry**

The cooling rate dependence of fictive temperature was investigated for the polyimide using a Perkin Elmer (model DSC 7) differential scanning calorimeter (DSC). A sample weighing approximately 10 mg was loaded in an aluminum pan with lid and annealed in the DSC for 10 minutes at 50°C above  $T_g$ . The sample was then cooled at a fixed cooling rate to  $T_g-50^\circ\text{C}$  prior to a heating scan at 10°C/min to a final temperature of  $T_g+50^\circ\text{C}$ . It was necessary to hold the sample for 2 minutes at  $T_g-50^\circ\text{C}$  to allow precise control of the heat signal before initiation of the heating scan, and it is expected that this short amount of time at this low temperature has a negligible effect on the structural state of the sample. The testing incorporated six cooling rates of 0.3, 1, 3, 10, 30, and 100°C/min and employed a fixed heating rate of 10°C/min. The heating scans were

analyzed using the Perkin Elmer software in order to determine the calorimetric fictive temperatures. The same sample was utilized for all six cooling rate experiments to eliminate sample error in the assessment of activation energy from the cooling rate dependence of fictive temperature. The sample did not suffer any significant chemical degradation during these thermal cycles as was verified at the end of the six cooling rate experiments by repeating the first experiment and comparing the two comparable DSC heating traces which were found to be essentially identical. The DSC testing utilized a nitrogen purge, and the ice content in the ice/water bath was maintained at approximately 30-50% by volume during all testing. Instrument baselines were generated at a heating rate of 10°C/minute using empty pans with lids in the reference and sample cells. If a substantial difference was noted between subsequent baseline runs, then any scans collected between these baseline scans were discarded. The DSC temperature was calibrated using the onset melting points of indium and tin, and the heat flow was calibrated using the heat of fusion of indium.

### ***7.2.3 Dynamic Mechanical Analysis***

Dynamic mechanical measurements (tensile) were made with a Seiko DMS 210 using polyimide samples which were freshly quenched after free-annealing at  $T_g+50^\circ\text{C}$  for 10 minutes. The sample dimensions were characterized by a thickness of 0.1 mm, width of 5 mm, and a length suitable to enable a grip-to-grip distance of 10 mm to be employed. A nitrogen gas purge was used during the testing. The dynamic mechanical analysis (DMA) of the polyimide was performed in the  $\alpha$ -relaxation region at temperatures from approximately 5°C below to 30°C above the calorimetric  $T_g$  using frequencies ranging from 0.01 to 20 Hz.

## **7.3 Results and Discussion**

The ultimate purpose of this study is to experimentally investigate the existence of a link between the structural relaxation process and the kinetics of glass formation. It is

therefore necessary to detail the methodology employed for the purpose of assessing the nonArrhenius and nonexponential glass-forming characteristics. Dynamic mechanical analysis is one useful tool for providing quantitative details about both of these relaxation responses, as will be described, and differential scanning calorimetry can yield supplemental information. The presentation of experimental methods for assessing glass formation features will also include discussion which describes the cooperativity concept and its relationship to the observed relaxation time features in the glass formation region. This discussion will specifically highlight a simple method for characterizing the conceptual number of cooperatively relaxing molecular segments at the glass transition temperature, following the general approach of Adam and Gibbs. The most probable number of segments which must relax together at  $T_g$ ,  $z_g$ , will then be used as an index of glass transition cooperativity. Any trends in the volume and enthalpy relaxation rates for amorphous polymer materials annealed at  $T_g-30^\circ\text{C}$  can then be observed with respect to  $z_g$ .

### ***7.3.1 Determination of glass formation characteristics***

As a glass-forming material is cooled from the liquid state, the increase of relaxation times does not follow Arrhenius behavior, but instead the activation energy increases as temperature is decreased in the glass formation region. Time-temperature superposition allows shift factors ( $a_T$  values) to be generated which indicate how the most probable relaxation time,  $\tau$ , at a selected temperature compares to that at a reference state temperature, typically the midpoint glass transition temperature measured by calorimetry ( $T_g$ ). The empirically developed Williams-Landel-Ferry (WLF) equation is useful in representing the experimentally determined relaxation time scaling behavior in the glass formation region:<sup>10</sup>

$$\log(a_T) = \log\left(\frac{\tau}{\tau_g}\right) = \frac{-C_1(T - T_g)}{C_2 + T - T_g} \quad \text{Eqn. 7-1}$$

The values for the parameters  $C_1$  and  $C_2$  depend on the choice of the reference temperature in the general WLF expression, but for the purposes of this study the

inflection glass transition temperature measured calorimetrically at a rate of 10°C/min will always be the reference temperature at which WLF parameters are reported. The parameters  $C_1$  and  $C_2$  will therefore be used interchangeably with  $C_{1,g}$  and  $C_{2,g}$ , where the subscript g designates that the reference temperature for the WLF parameters is  $T_g$ . The nonArrhenius nature of glass formation is shown in Figure 7-1 where the WLF function is plotted using the parameters given in the caption. The responses represented by curves A and B in Figure 7-1 are contrasted for the purpose of illustrating that amorphous materials, relative to each other, can display distinctly different behavior in the glass-forming region. Discussion of methods for quantitatively distinguishing the nonArrhenius responses for different amorphous polymers will be undertaken later, employing the concepts of fragility and cooperativity.

The assessment of dynamic mechanical response as a function of frequency ( $\omega$ ) in the glass formation temperature region can enable the determination of the nonArrhenius relaxation behavior for an amorphous material. The glass former of immediate interest is a commercial amorphous polyimide material (see *Experimental Details*), and the dynamic loss ( $E''$ ) data corresponding to the  $\alpha$ -relaxation for this polymer is indicated in Figure 7-2. Information concerning the dependence of relaxation time on temperature can be obtained from the amount of horizontal shifting necessary to superimpose the response at one temperature with that at the reference temperature. The horizontal shift factor,  $a_T$ , represents the degree of shifting along the  $\log(\text{frequency})$  axis. In the typical manner, a very small amount of vertical shifting was applied a priori to the loss modulus data prior to horizontal shifting in order to account for the temperature dependence of modulus:  $E''(\omega a_T, T)/T = E''(\omega, T_{\text{ref}})/T_{\text{ref}}$ . The application of the time-temperature superposition principle to the loss modulus data for the polyimide material resulted in the formation of a master curve which is presented in Figure 7-3.

The scaling behavior of segmental relaxation times can be evaluated from the temperature-dependent horizontal shift factors employed during superposition. The horizontal shift factor ( $a_T$ ) represents how the most probable relaxation time,  $\tau$ , at a specific temperature compares with that at the reference temperature:  $a_T = \log(\omega_{\text{ref}}/\omega) = \log(\tau/\tau_{\text{ref}})$ . A reference temperature ( $T_{\text{ref}}$ ) of 250°C was used in the formation of the

master curve given in Figure 7-3, but of greater interest is the relaxation time scaling behavior with respect to the glass transition temperature. The midpoint glass transition temperature for freshly quenched polyimide samples was found to be 239°C via DSC using a 10°C/min heating rate, and the horizontal shift factors obtained for a reference temperature of 250°C were converted relative to this  $T_g$  value. The temperature-dependent  $a_T$  data were fitted using the Williams-Landel-Ferry equation, and the resulting WLF parameters were then converted using the following:  $C_{1,g}C_{2,g} = C_{1,ref} C_{2,ref}$  and  $T_g - C_{2,g} = T_{ref} - C_{2,ref}$ . Transformation of the shift factors and the associated WLF fit was accomplished by this conversion, and the results are indicated in the  $T_g$ -normalized Arrhenius plot given by Figure 7-4. Deviation from a simple thermally-activated Arrhenius process can be clearly observed from this shift factor data which displays curvature. This dynamic mechanical analysis approach was applied to other glass-forming polymer materials for the purpose of contrasting the deviations from Arrhenius relaxation time behavior, and such comparisons will be undertaken later.

Insight into the kinetics of glass formation can also be gained by an examination of the influence of cooling rate on glass transition response determined by differential scanning calorimetry. The basic approach is to cool the amorphous liquid into the glassy state at various cooling rates and then compare the subsequent DSC heating scans, all performed at a fixed heating rate.<sup>2</sup> The heating scans for the polyimide which reflect different cooling rates used during glass formation are indicated in Figure 7-5. The structural temperature, or fictive temperature ( $T_f$ ), was determined as a function of the cooling rate ( $\dot{q}_c$ ) by analyzing each scan using the Perkin Elmer software. Fictive temperature is often employed as a parameter to describe the kinetic nature of the glass transition and nonequilibrium glassy state, and a brief illustration of the definition of  $T_f$  will be undertaken during mention of isothermal structural relaxation rates. The range of cooling rates which can be realistically employed in this DSC approach is limited and, accordingly, the relaxation response behavior is only probed in the immediate vicinity of the glass transition region. Therefore, this approach can only yield a measure of the apparent activation energy at  $T_g$  and cannot be used to determine WLF parameters. The

apparent activation energy at the glass transition temperature ( $\Delta E_{a,g}$ ) can then be determined:

$$\Delta E_{a,g} = -R \frac{d \ln(\dot{q}_c)}{d(1/T_f)} \quad \text{Eqn. 7-2}$$

The calorimetric activation energy for the polyimide was determined in this manner from the slope of the data plotted in Figure 7-6. The apparent activation energy determined using this methodology can then be compared with that assessed from DMA. The DSC value of  $\Delta E_{a,g}$  was found to be 1480 kJ/mol, and the DMA value was determined to be 1450 kJ/mol from the WLF parameters:  $\Delta E_{a,g} = 2.303RC_1(T_g)^2 / C_2$ . These two independent  $\Delta E_{a,g}$  values are nearly equal for the polyimide material, but, in general, equivalence of these activation energy values is certainly not a physical necessity for the distinct viscoelastic and calorimetric responses.

Insight into the segmental relaxation time response during glass formation can be acquired using dynamic mechanical and dielectric techniques, and the question now arises as to how to quantify the nonArrhenius response in order to compare different materials. It is useful to re-examine the general nonArrhenius behavior depicted in Figure 7-1 and discuss the origin of the difference between the two hypothetical WLF curves depicted in this plot. Although the normal applicability range of the WLF equation is from the calorimetric  $T_g$  to approximately 100K above  $T_g$ ,<sup>11</sup> the functionality is extended in Figure 7-1 for illustrative purposes because the limiting behavior can provide interesting insight. The relaxation times appear to display Arrhenius behavior in the limit of high temperatures as is evident from the constant slope behavior in Figure 7-1 as  $T_g/T$  approaches zero. As the glass transition temperature range is approached upon cooling, the activation energy of relaxation time response increases, and the relaxation times appear to diverge due to a kinetic temperature asymptote. From the WLF expression, this kinetic temperature limit is given by  $T_0 = T_g - C_2$ . The origin of the difference between the two WLF curves in Figure 7-1 is due to variation of the  $C_2$  parameter, which has values of 50K for curve A and 100K for curve B. Inspection of the WLF data given for numerous polymers in a recent review by Ngai and Plazek<sup>12</sup> reveals that 50K and 100K represent reasonable values for polymer materials.

Angell has developed the concept of “fragility” to compare the nonArrhenius glass formation characteristics of liquids.<sup>13-15</sup> One way to contrast the difference between curves A and B in Figure 7-1 is the slope in the glass transition region, and a definition of fragility, represented by the symbol  $m$ , is given by:

$$m = \left. \frac{d \log \tau}{d(T_g/T)} \right|_{T=T_g} = \frac{C_1 T_g}{C_2} \quad \text{Eqn. 7-3}$$

The  $m$  parameter is essentially a normalization of the apparent activation energy ( $\Delta E_{a,g}$ ) in the glass transition region ( $m = \Delta E_{a,g}/(2.303RT_g)$ ). Recently, Angell has utilized a different quantitative representation of fragility,  $F$ :<sup>16</sup>

$$F = \frac{T_0}{T_g} = 1 - \frac{C_2}{T_g} \quad \text{Eqn. 7-4}$$

where it is assumed that the Williams-Landel-Ferry  $C_1$  parameter is a constant. Although the WLF equation is sometimes considered to have universal constants, it is clear that unique fragility characteristics require differences in the  $C_2$  parameter. The kinetic temperature asymptote,  $T_0$ , represents where the equilibrium relaxation times appear to diverge toward infinity (recall that  $T_0 = T_g - C_2$ ). How close this asymptote is to the glass transition temperature dictates the severity of the nonArrhenius behavior during glass formation. If the kinetic limit represents a true thermodynamic glass transition, then fragility given by the second definition may be considered a measure of how close the kinetic glass transition approaches the true thermodynamic glass transition temperature. Glasses with a low and high degree of fragility are classified, respectively, as strong and fragile glasses.

Recognition of the influence that segmental cooperativity can have on relaxation times leads to a different, albeit related, measure of glass forming behavior compared to the fragility approach. Adam and Gibbs were the first to establish in a detailed manner the conceptual treatment of cooperatively rearranging domains. It was asserted by Adam and Gibbs that equilibrium relaxation times should be inversely related to configurational

entropy ( $S_c$ ).<sup>17</sup> This assumption that  $\log(\tau)$  is proportional to  $1/S_c$  has its basis derived from: (1) the prediction of a true glass transition temperature ( $T_2$ ) according to the theoretical treatment of Gibbs and DiMarzio where the configurational entropy of an amorphous polymer system becomes zero; and (2) the *apparent* divergence of equilibrium relaxation times at  $T_0$  when extrapolated into the glassy state. Because this assumption is used as a basis, the Adam-Gibbs approach should not be considered a rigorous theoretical treatment but rather should be treated as a conceptual aid which can be used to rationalize the observed relaxation response in terms of cooperativity between molecular segments. To this end, the notion of cooperative relaxation is a useful concept which includes some molecular-based features, as will become evident.

The approach taken in this study is to employ the cooperativity concept in a general sense in order to develop a new index of nonArrhenius behavior which is simple to determine and which may have some molecular significance. The observation of an activation energy that increases during cooling a glass-forming liquid can be explained in terms of enhanced cooperativity between relaxing segments. A conceptual picture of cooperativity can be developed by breaking a glass-forming material down into primitive relaxing segments, or “beads”. These segments can relax in an intramolecular manner which, in the case of a segment of a linear polymer, would involve rotation about backbone bonds. Because of packing (free volume) considerations and intermolecular attractions between neighboring segments, such an intramolecular relaxation of one segment may require cooperative movement of the segments surrounding it. Therefore, while the primitive relaxation of a single segment may have an associated activation energy ( $\Delta\mu$ ), the observed activation energy ( $\Delta E$ ) is greater by a factor of  $z$ , where  $z$  is the number of segments which must relax together in concert ( $\Delta E = z \Delta\mu$ ). A pictorial representation of hypothetical domains with  $z = 7$  is given in Figure 7-7, and this picture is based upon the depiction given by Matsuoka and Quan.<sup>18,19</sup> The influence of this segmental cooperativity on the activation energy is illustrated in Figure 7-8. As an amorphous material is cooled from the liquid state, the free volume and configurational entropy decrease and the influence of polarity and specific interactions becomes enhanced as segments become more crowded. These features lead to an increase in  $z$  and can

explain the nonArrhenius relaxation time response. An apparent activation energy can be determined from any relaxation time expression by evaluating the derivative  $Rd\ln(\tau)/d(1/T)$  at the temperature of interest. If the WLF behavior in the extrapolated high temperature limit can be thought to represent the independent relaxation of segments without the additional influence of cooperativity ( $z=1$ ), then the activation energy in the limit of  $1/T \rightarrow 0$  ( $T \rightarrow \infty$ ) is the primitive activation energy given by:

$$\Delta\mu = 2.303RC_1C_2 \quad \text{Eqn. 7-5}$$

The temperature dependence of the apparent activation energy according to the WLF equation can similarly be represented by:

$$\Delta E(T) = 2.303RC_1C_2 [T/(T-T_g+C_2)]^2 \quad \text{Eqn. 7-6}$$

The cooperativity approach suggests that:

$$\Delta E = z \Delta\mu \quad \text{Eqn. 7-7}$$

This use of this expression enables the following expression for  $z$  to be developed based upon the WLF description of nonArrhenius behavior:

$$z(T) = \frac{\Delta E(T)}{\Delta\mu} = \left( \frac{T}{T - T_g + C_2} \right)^2 \quad \text{Eqn. 7-8}$$

This expression describes the most probable cooperative domain size in the equilibrium liquid state. The temperature dependence of  $z$  according to this expression is illustrated in Figure 7-9 for the WLF behavior corresponding to curve A in Figure 7-1. This dependence of domain size on temperature represents the equilibrium liquid state, but of interest is the value of  $z$  at  $T_g$  ( $z_g$ ) where departure from equilibrium into the glassy state occurs during cooling. When  $T = T_g$ , the value of  $z_g$  can be simply determined from the above equation:

$$z_g = (T_g/C_2)^2 \quad \text{Eqn. 7-9}$$

Relaxation times depart from the WLF response as the nonequilibrium glassy state is formed during cooling as the generalized behavior in Figure 7-10 illustrates. The question which naturally arises is whether the rate of relaxation during sub- $T_g$  annealing at an aging

temperature ( $T_a$ ) is influenced by the particular domain size which a material is able to develop during cooling prior to vitrification. *Do different amorphous polymers possess distinct values of glass transition cooperativity, and, if so, do structural relaxation rates correlate with  $z_g$ ?*

In addition to the nonArrhenius relaxation time behavior, it is desirable to quantify the distribution of relaxation times which leads to nonexponential (nonDebye) relaxation response. In the context of the cooperativity approach, the presence of a relaxation time distribution implies the existence of either a distribution of  $z$  values or a coupling between the cooperatively relaxing domains with the most probable  $z$  value. Determination of the nonexponential characteristics associated with the glass formation temperature region is afforded by a temperature and frequency investigation of the dynamic mechanical response. The time-dependent stretched exponential, or Kolrausch-Williams-Watts (KWW), decay function,  $\phi(t)=\exp[-(t/\tau)^\beta]$ , is often used to mathematically define a relaxation time distribution. The parameter  $\tau$  represents the most probable relaxation time and the stretching exponent  $\beta$  is related to the distribution of relaxation times. For exponential response where only a single characteristic relaxation time governs relaxation behavior,  $\beta$  assumes a value of 1.0. However, as the distribution of relaxation times broadens according to the KWW decay function,  $\beta$  decreases from 1.0 toward zero. The KWW function can be transformed to the frequency ( $\omega$ ) domain in order to allow prediction of dynamic mechanical loss modulus data:<sup>20</sup>

$$\frac{E''(\omega)}{E_\infty - E_0} = \omega \int_0^\infty \phi(t) \cos(\omega t) dt \quad \text{Eqn. 7-10}$$

In the above equation, the quantity  $E_\infty - E_0$  represents the relaxation strength for the dynamic mechanical glass transition ( $\alpha$ -relaxation). A value of  $\tau$  and  $\beta$  can be selected and then the above equation can be numerically integrated to allow prediction of the shape of the loss modulus master curve as a function of frequency. A series of predictions have been generated in this manner using numerous values of  $\beta$ , incremented by 0.025, and these predictions can be compared with experimental loss modulus data in order to determine the appropriate value of  $\beta$  which is necessary to describe the distribution of

relaxation times for a given material. A careful numerical approach was necessary because the integrand is a product of decay and cosine terms and, therefore, the nature of the integrand exhibits substantial changes due to variations in frequency. The results of these predictions are tabulated in the *Appendix* section of this chapter, and select curves are illustrated in Figure 7-11. This information is supplied in order to enable other researchers interested in characterizing the nonexponential nature of amorphous materials to do so with relative ease. The relaxation time parameter was set at  $\tau = 10$  seconds in the generation of these predictions, and the predictions need to be shifted along the  $\log(\text{frequency})$  axis when attempting to characterize the breadth of the loss modulus master curve. Also, a value of the relaxation strength,  $E_\infty - E_0$ , must be selected in order to vertically scale the predicted maximum to the peak value of the loss modulus. The solid line in Figure 7-3 represents the KWW prediction ( $\beta=0.45$ ) which provided the best representation of the loss modulus master curve for the polyimide material. Using this method, the nonexponential nature of glass-forming polymers can be compared, in particular using the  $\beta$  parameter as a measure of nonexponentiality.

### ***7.3.2 Correlation between structural relaxation rates and cooperativity***

The  $z_g$  and  $\beta$  parameters can be used to describe the nonArrhenius and nonexponential relaxation time responses, respectively, and it now remains to develop a means of characterizing the nonlinear relaxation in the nonequilibrium glassy state. Following a quench from above  $T_g$ , isothermal annealing in the glassy state generally leads to an approximate dependence of property changes on the logarithm of aging time ( $t_a$ ), and, hence, physical aging is often described as a self-limiting process. The structural relaxation process can be characterized by aging rates which reflect the changes of the thermodynamic variables with respect to  $\log(\text{aging time})$ . Volume relaxation can be directly measured via dilatometry, and the relaxation of enthalpy can be inferred using recovery responses determined using differential scanning calorimetry. Isothermal aging rates for volume and enthalpy, respectively represented by  $b_v$  and  $b_H$ , can then be determined using the definitions:  $b_v = -(1/V)dV/d\log(t_a)$  and  $b_H = d(\Delta H)/d\log(t_a)$ .<sup>21</sup> These aging rates are not applicable at very short aging times where an aging rate lag is often

observed nor at very long aging times when the system starts to approach equilibrium. This latter applicability concern is not an issue for this study which employs an aging temperature of 30K below  $T_g$  where close approach to equilibrium is not typical for the experimental aging time frames utilized (maximum aging times ranged from 100 to 300 hours).

For the comparison of aging rates for different glass formers, it is informative to normalize the volume and enthalpy relaxation rates in a manner which indicates the relaxation of the fictive temperature ( $T_f$ ). The reductions in volume and enthalpy can be thought to depend on both the actual temperature and the changing structural (fictive) temperature, and this nonlinearity leads to the observed self-limiting behavior. Tool<sup>22,23</sup> pioneered the use of fictive temperature to describe the kinetic nature of the glass transition and glassy state, and this parameter is often employed to characterize the changing structural state during relaxation in the glassy state. It is a worthwhile endeavor to illustrate the definition of fictive temperature for those less familiar with this descriptive parameter, and Figure 7-12 is provided for this purpose. The solid line in Figure 7-12 represents a quench from the equilibrium liquid state into the nonequilibrium glassy state, and for the freshly quenched state (state 0) at the aging temperature ( $T_a$ ), the fictive temperature is equal to the kinetic  $T_g$  observed during the quench. As aging progresses during annealing at  $T_a$  (0→1→2), the fictive temperature decreases as is clear from the relative  $T_f$  values defined by the extrapolations (dotted lines) in the diagram. The concept of fictive temperature can also be employed in order to assess the kinetic nature of glass formation as was introduced during discussion of the DSC data for the polyimide material. If different cooling rates are employed during cooling, then a slower cooling rate will enable the material to settle into a lower structural state before the formation of the glassy state relative to a fast quench. Therefore, a reduction in cooling rate results in a decrease in the initial fictive temperature associated with the freshly quenched glass. Because fictive temperature is considered a useful structural parameter, it is desirable to connect the measured volume and enthalpy relaxation rates to the associated changes in  $T_f$ . Using Figure 7-12, this connection is a simple geometric exercise where changes in the thermodynamic variables can be transformed to changes in  $T_f$  using the difference between the slopes in the liquid and

glassy regions. It can be simply shown that the aging rate of interest,  $-dT_f/d\log(t_a)$ , is given by the quantity  $b_H / \Delta C_p$  for enthalpy relaxation and for volume relaxation is represented by  $b_V / \Delta\alpha$ . Although relaxation rates for both enthalpy and volume are herein converted to temporal changes in  $T_f$  in order to allow a more fundamental comparison of glassy relaxation responses for various amorphous polymers, the authors are certainly not asserting that the fictive temperatures for volume and enthalpy are necessarily equivalent. Methods for characterizing the glass transition cooperativity and structural relaxation rates have been detailed. The results can now be studied for the purpose of developing a general connection between the relaxation response in the nonequilibrium glassy state and the glass formation behavior of an amorphous material. Several amorphous polymer materials have been investigated and the relevant results, including aging rates at  $T_g-30K$ , are detailed in Table 7-I and Table 7-II. Also tabulated are some data for additional glassy polymers which have been studied by other researchers.<sup>24-32</sup> A plot of the normalized aging rates for volume and enthalpy versus the glass transition cooperativity is presented in Figure 7-13, and a clear trend emerges from this data. It appears that, during cooling from above  $T_g$ , the ability to develop a larger number of cooperatively relaxing segments in a domain prior to the onset of the nonequilibrium glassy state results in a slower structural relaxation rate upon subsequent annealing in the glassy state. The only data point noticeably outside the general trend exhibited in this plot is that corresponding to poly(methyl methacrylate), and this aberration may be due to the influence of the uncharacteristically intense secondary relaxation which is typical for this polymer.<sup>33</sup> The experimental trend observed between  $-dT_f/d\log(t_a)$  and  $z_g$  can be represented well by a single-parameter empirical expression which can be developed based upon reasonable physical limits associated with the cooperativity approach. The smallest possible value allowed for  $z_g$  is 1.0, and it is reasonable to expect that the structural relaxation rate should diverge to infinity as this non-cooperative extreme is approached. At the other end of the range of possibilities for  $z_g$  is the case where the glass transition cooperativity becomes so large that, in principle, the material sample in its entirety may be considered a single cooperative domain. No structural relaxation in the glassy state should be possible

for this situation where  $z_g$  approaches infinity. A simple empirical expression which captures these two logical limits is:

$$-\frac{dT_f}{d \log(t_a)} = \frac{J}{z_g - 1} \quad \text{Eqn. 7-11}$$

This expression can represent the data in Figure 7-13 with a value of the fitting constant,  $J$ , equal to 130 K, and this empirical description indicated by the solid line in the plot fits the data well with the exception of the PMMA outlier. Conversion of Eqn. 7-11 to volume relaxation rate and incorporation of the definition for  $z_g$  results in:

$$b_V = \frac{\Delta\alpha J}{(T_g/C_2)^2 - 1} \quad \text{Eqn. 7-12}$$

where  $J=130\text{K}$  for  $T_a=T_g-30\text{K}$ . This empirical representation of the data does not have any physical basis, but it is intriguing nonetheless because of the wealth of data which it can simply capture.

The trend between the normalized structural relaxation rates and the glass transition cooperativity is consistent with the inverse relationship between fragility ( $m$ ) and  $\beta$  and the direct relationship between the nonlinearity ( $x$ ) and  $\beta$  parameters which have been previously observed by Hodge<sup>1,2</sup> and Böhmer et al.<sup>3,4</sup> In considering the empirical nonlinear relaxation time function commonly employed to model enthalpy relaxation/recovery,<sup>1,2</sup> it is evident that the greater the value of the fractional nonlinearity parameter,  $x$ , the more the relaxation depends on the actual temperature compared to the time-dependent structural temperature. Therefore, relaxation is less self-retarded for greater  $x$  values, and, accordingly, structural relaxation should proceed at a greater rate with respect to  $\log(t_a)$ . This intuitive direct relationship between  $x$  and  $-dT_f/d\log(t_a)$  suggests that the observed correlation between the normalized aging rates and  $z_g$  developed in this study is entirely consistent with the established relationship between the nonArrhenius and nonexponential phenomenological characteristics in combination with the connection between nonlinearity and nonexponentiality features. To further clarify this

point, the trend observed between  $-dT_f/d\log(t_a)$  and  $z_g$  can be rationalized from the combination of: (1) the close tie between fragility ( $m$ ) and  $z_g$  wherein increases in fragility correspond to increases in  $z_g$ ; (2) the inverse relationship between  $m$  and  $\beta$ ; (3) the observation that  $x$  appears to be an increasing function of  $\beta$ ; and (4) the expected direct relationship between  $x$  and  $-dT_f/d\log(t_a)$  which was established using the above argument.

It is expected that  $z_g$  and  $\beta$  are also correlated because of the well-established connection between fragility ( $m$ ) and the  $\beta$  parameter. In order to expand the data set for inspecting any relationship between nonexponentiality and glass transition cooperativity, the values of fragility given for amorphous polymers by Böhmer and coworkers<sup>4</sup> were converted to  $z_g$  data. This conversion involves the assumption that the Williams-Landel-Ferry  $C_1$  parameter can be considered to be approximately constant. Angell has suggested a physical basis for fixing the value of  $C_1$  because this parameter should represent the logarithmic difference between the segmental relaxation time at  $T_g$  ( $\tau_g$ ) and the relaxation time in the limit of high temperatures ( $\tau_0$ ). Values for  $\tau_g$  and  $\tau_0$  are typically of the magnitude  $10^2$  and  $10^{-14}$ , respectively, and a  $C_1$  parameter equal to 16 is consistent with these relaxation times.<sup>34</sup> Using the assumption that  $C_1$  has a constant value of 16, fragilities from the literature can be converted to  $z_g$  values via the following:

$$z_g = \left( \frac{m}{C_1} \right)^2 \approx \left( \frac{m}{16} \right)^2 \quad \text{Eqn. 7-13}$$

The parameters in Table 7-II and the converted literature data provide the means for an extensive inspection of any association between  $\beta$  and  $z_g$ , and Figure 7-14 exhibits the results of this examination. A clear, notwithstanding broad, correlation is observed between  $\beta$  and  $z_g$ . Plausible extrapolated limits for this relationship are: relaxation is exponential ( $\beta=1$ ) for independent segmental relaxation ( $z_g=1$ ) where coupling between relaxing segments is absent; and the approach of  $\beta$  toward zero is associated with the divergence of  $z_g$  ( $z_g \rightarrow \infty$ ).<sup>35</sup>

Extension of the observed connection between  $\beta$  and  $z_g$  for the collection of amorphous polymer materials to a single material leads to the expectation that  $z$  and  $\beta$  are intimately related for a glass-forming material which suggests general failure of the time-

temperature superposition principle. If the relationship between  $\beta$  and  $z$  holds for a material, then, as the most probable domain size grows in size during cooling and the most probable relaxation time increases, the relaxation time distribution broadens. This association between degree of intermolecular cooperativity and relaxation time distribution is a natural prediction of the coupling model of Ngai and coworkers,<sup>36-39</sup> although the coupling parameter,  $n = 1 - \beta$ , is considered to be the independent parameter, in opposition to the causality suggested by the discussion given here. This raises a key issue concerning the apparent correlation observed between the normalized structural relaxation rates with  $z_g$ . One cannot undeniably consider  $z_g$  as the direct influence on the structural relaxation rates because of the association between  $\beta$  and  $z_g$ .

An attempt to deduce the manner by which glass transition cooperativity ( $z_g$ ) is influenced by intra- and intermolecular features, however limited, is a worthwhile endeavor. Before this is undertaken, however, some cautionary statements are necessary. The following arguments presuppose that the  $\Delta\mu$  parameter inferred from the extrapolated segmental relaxation response is an indication of the average activation energy governing intramolecular bond rotation. Not only does the ensuing discussion rely on the assignment of physical meaning to extrapolated behavior, but it also assumes validity of the cooperativity approach. It should be re-emphasized that the Adam-Gibbs cooperativity approach is a conceptual aid and not a rigorous treatment. With these caveats in mind, the following discussion will attempt to sort out the expected influences of intra- and intermolecular effects on  $z_g$ .

The nature of intermolecular forces between molecular segments is certainly of relevance when employing an approach based upon the concept of cooperative relaxation. It is easier to note the potential role of intermolecular attractions if the intramolecular features remain constant. When comparing two glass-forming polymers with the same intramolecular bond rotation activation energy, the  $C_2$  parameter should be approximately the same for both materials. This statement comes from the recognition that the activation energy is represented by  $\Delta\mu = 2.303RC_1C_2$  in addition to the assumption that  $C_1$  is largely invariable for different materials. All else being equal, if one of these two polymers has the potential for stronger intermolecular attractions relative to the other polymer, then the

glass transition temperature region will be higher, in general, due to the influence of these specific interactions. The introduction of attractive intermolecular forces increases  $T_g$ , and, relative to a fixed intramolecular activation energy (fixed  $C_2$ ), this results in an increase in the glass transition cooperativity according to  $z_g=(T_g/C_2)^2$ .

It is a more difficult task to intuitively discuss changes in cooperativity due to variations in intramolecular activation energy for materials which are otherwise similar from an intermolecular standpoint. In general, restraints on intramolecular chain mobility negatively affect the ability of a glass former to densely pack into the glassy state, and, accordingly, an increase in  $\Delta\mu$  might be expected to result in a stronger (less fragile) glass-former with a lower  $z_g$ . This expectation should initially be considered with caution because an increase in average bond rotation activation energy typically induces an increase in  $T_g$  as well which should increase cooperativity based upon the expression for  $z_g$ . Consideration of the necessary conditions to keep  $z_g$  unaffected despite an increase in  $\Delta\mu$  will assist in sorting out which effect, packing restraint or  $T_g$  increase, should be dominant. Consider two fictional amorphous polymers designated as “polymer A” and “polymer B”. Let polymer A have a glass transition temperature of 400K and possess a primitive activation energy ( $\Delta\mu$ ) of 15kJ/mol. Otherwise similar to polymer A from an intermolecular standpoint, polymer B has a  $\Delta\mu$  equal to 30kJ/mol. A two-fold increase in  $\Delta\mu$  from approximately 15 to 30 kJ/mol (3.6 to 7.2 kcal/mol) is associated with  $C_2$  increasing from 50 to 100 when  $C_1$  is constant at a value of 16. To maintain identical  $z_g$  values for the two polymers would require:  $(T_{g,A} / 50)^2 = (T_{g,B} / 100)^2$ . Despite the fact that the activation energies are both reasonable values for polymeric materials, the  $T_{g,B}$  necessary to keep  $z_g$  constant would be 800K, a value well out of the range of typical glass transition temperatures. In short, an increase in  $\Delta\mu$  should predominantly result in a decrease in glass transition cooperativity because  $C_2$  should increase more than  $T_g$  does.

Intra- and intermolecular characteristics influence the location of the glass transition temperature for an amorphous polymer. Molecular features also affect the cooperativity increases during cooling and the ensuing glass formation process, and a natural question is what association, if any, exists between  $T_g$  and  $z_g$ . An investigation of the relationship between these two parameters is afforded by Figure 7-15. This figure also

displays a plot of fragility ( $m$ ) versus the glass transition temperature. The data for both fragility and glass transition cooperativity exhibit complex relationships with  $T_g$ . The extent of nonArrhenius relaxation time build-up during cooling, quantified by either  $m$  or  $z_g$ , appears to exhibit a maximum with respect to  $T_g$  for the numerous polymer materials represented in Figure 7-15. This dependence is not without question, however, due to the extent of scatter present within the data. An in-depth explanation of the apparent maximum is not currently offered, but a possible explanation may center around the different relative contributions of intra- and intermolecular characteristics to  $T_g$  and the nonArrhenius glass formation behavior. Although increases in rotational energy barriers and in the capacity for intermolecular attractions should both lead to an increase in  $T_g$ , it is expected that changes in these molecular characteristics act in opposite ways in determining the glass transition cooperativity as described earlier.

What is quite clear from this study is that rates of structural relaxation at  $T_g-30K$  exhibit a convincing dependence on the degree of segmental cooperativity developed prior to glass formation during cooling. Differences in cooperativity/fragility characteristics can, therefore, explain why the volume relaxation rates vary substantially in magnitude when comparing the aging behavior of various polymer glasses at a fixed undercooling of 30K. The variation in  $b_v$  at  $T_g-30K$  for different polymers is evident from the data of Greiner and Schwarzl<sup>27</sup> which is shown in Figure 7-16. Certainly the approach taken here cannot assist in understanding the differences between the shapes of the  $b_v$  versus temperature curves for the different glassy polymers. Secondary relaxations can influence the volume relaxation rates in the glassy state as Struik noted.<sup>40</sup> At aging temperatures near  $T_g$ , such as the undercooling of 30K employed in this study, the influence of secondary relaxations is diminished on a relative basis. It is in this aging temperature range where the prediction of aging-induced densification from glass formation characteristics, and ultimately from chemical features, may be a realistic possibility.

## 7.4 Conclusions

The relaxation characteristics of numerous glassy polymers were investigated and a clear correlation between structural relaxation rates and glass transition cooperativity (fragility) was exposed. The general Adam-Gibbs approach was used to assess the nonArrhenius segmental relaxation time behavior, and the temperature dependence of the most probable number of molecular segments which were sufficiently constrained to require simultaneous cooperative relaxation was determined from the Williams-Landel-Ferry description of equilibrium relaxation time scaling. During cooling, the capacity for developing a large number of cooperative segments at  $T_g$  ( $z_g$ ) prior to glass formation apparently dictates slower volume and enthalpy relaxation rates during subsequent annealing at  $T_g-30K$ . The observed connection between the aging rates and glass transition cooperativity is consistent with the relationships between nonArrhenius, nonexponential, and nonlinear established in the literature. Because some insight into the role of intra- and intermolecular features in nonArrhenius relaxation time response is currently available, the established connection between aging rates and  $z_g$  is encouraging in terms of the future prediction of physical aging behavior from molecular characteristics.

Table 7-I: Parameters describing glass transition and aging responses

Material	$T_g$ DSC (K)	$C_1$	$C_2$ (K)	$\Delta\alpha \times 10^4$ ( $K^{-1}$ )	$\Delta C_p$ (J/g-K)	$b_v \times 10^4$	$b_H$ (J/g per decade)
SAN	378	13.7	38.8	3.55	0.364	5.98	---
PS	376	15.1	47.8	3.38	0.268	7.57	0.511
PS/PPO25	401	15.5	50.2	3.81	0.263	8.70	0.532
PS/PPO50	422	17.5	54.8	4.31	0.245	9.77	0.552
PS/PPO75	443	17.4	62.2	4.51	0.232	11.1	0.606
PS/PPO87.5	468	18.0	68.9	4.90	0.217	12.8	0.650
PPO	488	20.4	83.8	5.55	0.213	16.5	0.724
polyimide	512	19.8	68.7	---	0.236	---	0.589
PVC	358 <sup>24</sup>	13.4 <sup>24</sup>	28.7 <sup>24</sup>	3.18 <sup>25</sup>	0.310 <sup>26</sup>	3.0 <sup>27</sup>	---
PMMA	390 <sup>28</sup>	10.5 <sup>28</sup>	29.0 <sup>28</sup>	2.30 <sup>25</sup>	0.335 <sup>26</sup>	4.2 <sup>27</sup>	---
PC	423 <sup>29</sup>	13.4 <sup>29</sup>	47.3 <sup>29</sup>	3.72 <sup>25</sup>	0.191 <sup>26</sup>	7.3 <sup>27</sup>	---
PSf	458 <sup>30</sup>	18.3 <sup>30</sup>	77.3 <sup>30</sup>	3.40 <sup>31</sup>	0.232 <sup>26</sup>	11.2 <sup>30</sup>	---
PEI	490 <sup>30</sup>	16.7 <sup>30</sup>	89.4 <sup>30</sup>	3.05 <sup>25</sup>	---	13.0 <sup>30</sup>	---

Upper portion of table represents data from this work and lower portion provides literature data.

The literature values of  $C_1$  and  $C_2$  reported at some temperature other than  $T_g$  were converted to  $T_{ref}=T_g$ .

Table nomenclature: styrene-co-acrylonitrile statistical copolymer with 25 % acrylonitrile (SAN); atactic polystyrene (PS), poly(2,6-dimethyl-1,4-phenylene ether) (PPO); miscible PS/PPO blends with XX wt.%

PPO (PS/PPOXX); polyimide described in this paper (polyimide); poly(vinyl chloride) (PVC); atactic poly(methyl methacrylate) (PMMA); bisphenol-A polycarbonate (PC); common engineering polymer polysulfone (PSf); common engineering polymer poly(ether imide) (PEI).

Table 7-II: Relaxation parameters

Material	T <sub>g</sub> DSC (K)	$\beta$	$\Delta\mu$		z <sub>g</sub>	fragility, m	b <sub>v</sub> / $\Delta\alpha$
			(kJ/mol)	(kcal/mol)			
SAN	378	0.375	10.2	2.4	95	133	1.68
PS	376	0.400	13.8	3.3	62	119	2.24
PS/PPO25	401	0.350	14.9	3.6	64	124	2.28
PS/PPO50	422	0.325	18.4	4.4	59	135	2.27
PS/PPO75	443	0.325	20.7	4.9	51	124	2.46
PS/PPO87.5	468	0.375	23.7	5.7	46	122	2.61
PPO	488	0.425	32.7	7.8	34	119	2.97
polyimide	512	0.450	26.0	6.2	56	147	---
PVC	358	0.24 <sup>32</sup>	7.4	1.8	156	167	0.94
PMMA	390	0.34 <sup>32</sup>	5.8	1.4	181	141	1.83
PC	423	0.35 <sup>32</sup>	12.1	2.9	80	120	1.96
PSf	458	0.40 <sup>30</sup>	27.1	6.5	35	108	3.29
PEI	490	0.35 <sup>30</sup>	28.6	6.8	30	92	4.26

Upper portion of table represents data from this work and lower portion provides literature data. See Table 7-I for material nomenclature.

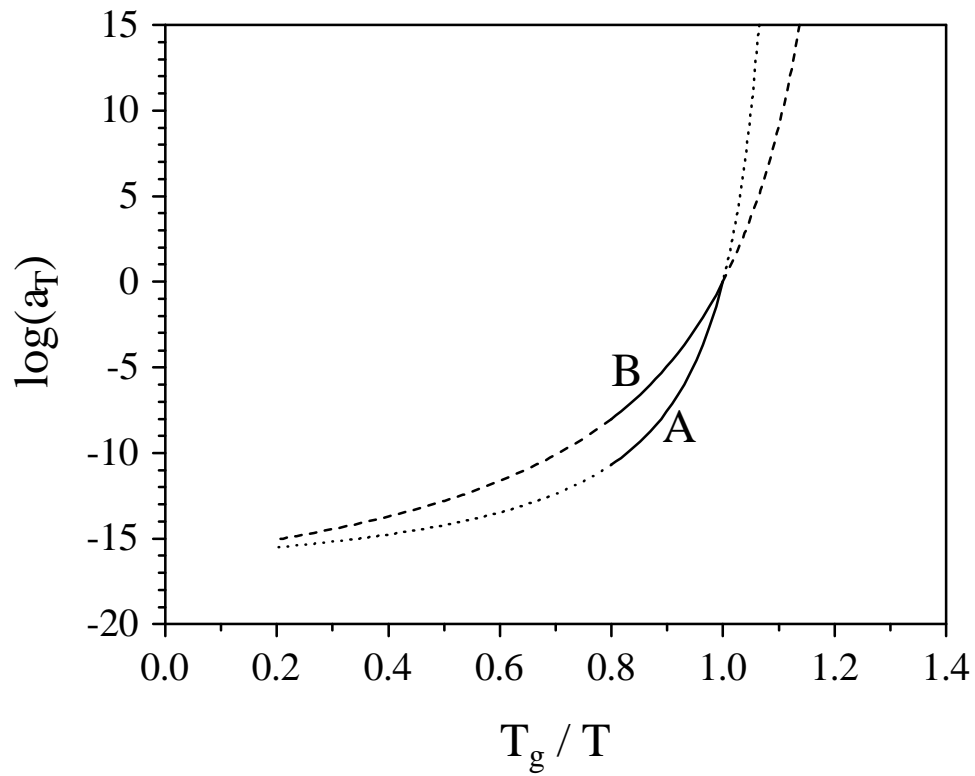


Figure 7-1: Generalized segmental relaxation time behavior in glass-forming temperature region. The curves are generated using the Williams-Landel-Ferry expression with  $T_g=400\text{K}$ ,  $C_1=16$ , and  $C_2=50\text{K}$  for curve A and  $C_2=100\text{K}$  for curve B.

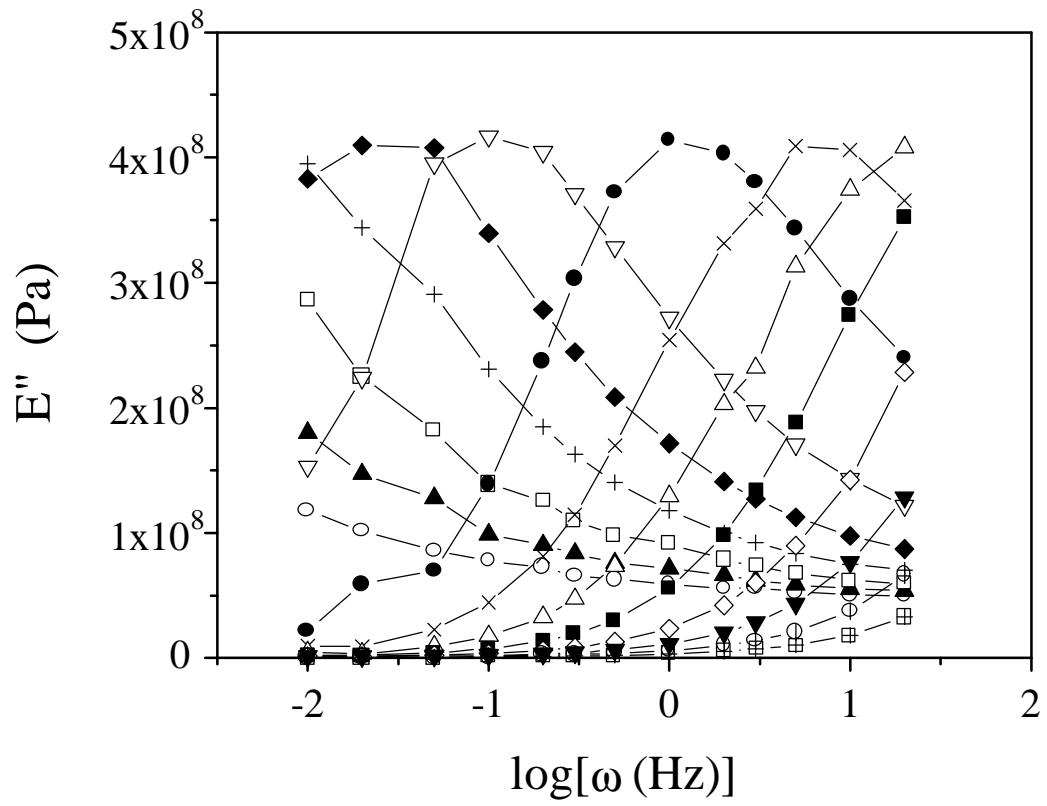


Figure 7-2: Dynamic mechanical loss data as a function of frequency and temperature for the amorphous polyimide. See Figure 7-3 for the symbol legend.

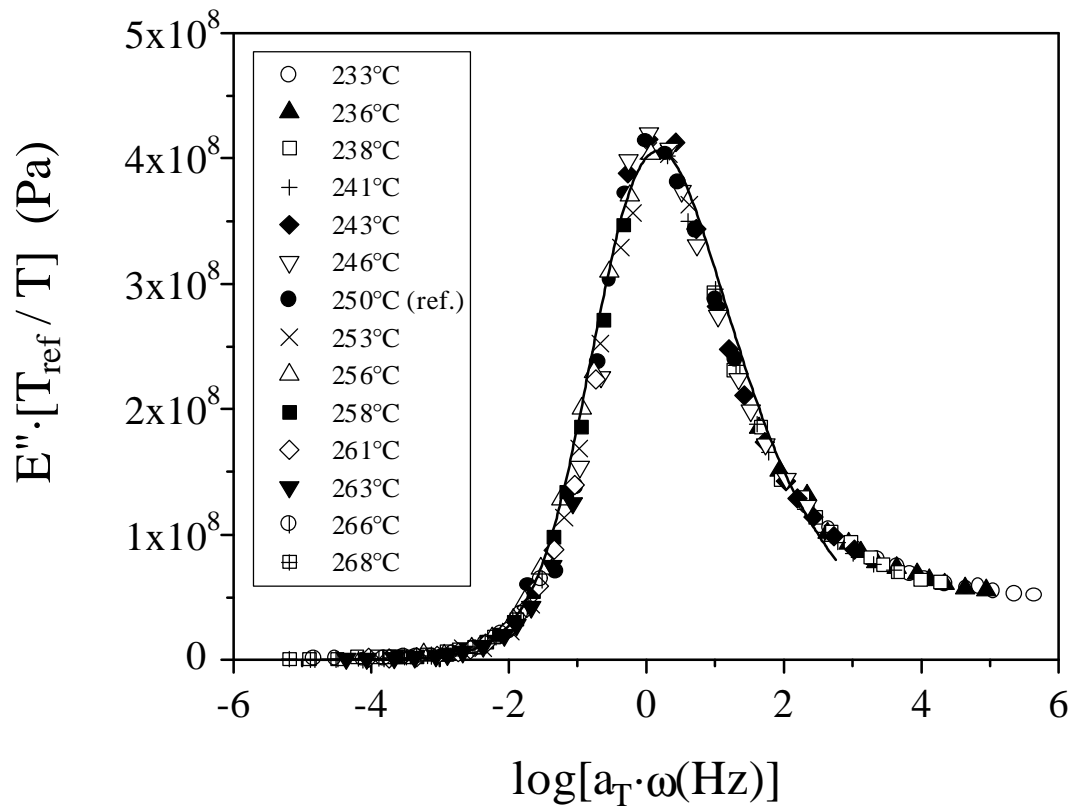


Figure 7-3: Loss modulus master curve obtained by superposition of the data in Figure 7-2. The solid line is the stretched exponential function fit to the data ( $\beta=0.45$ )

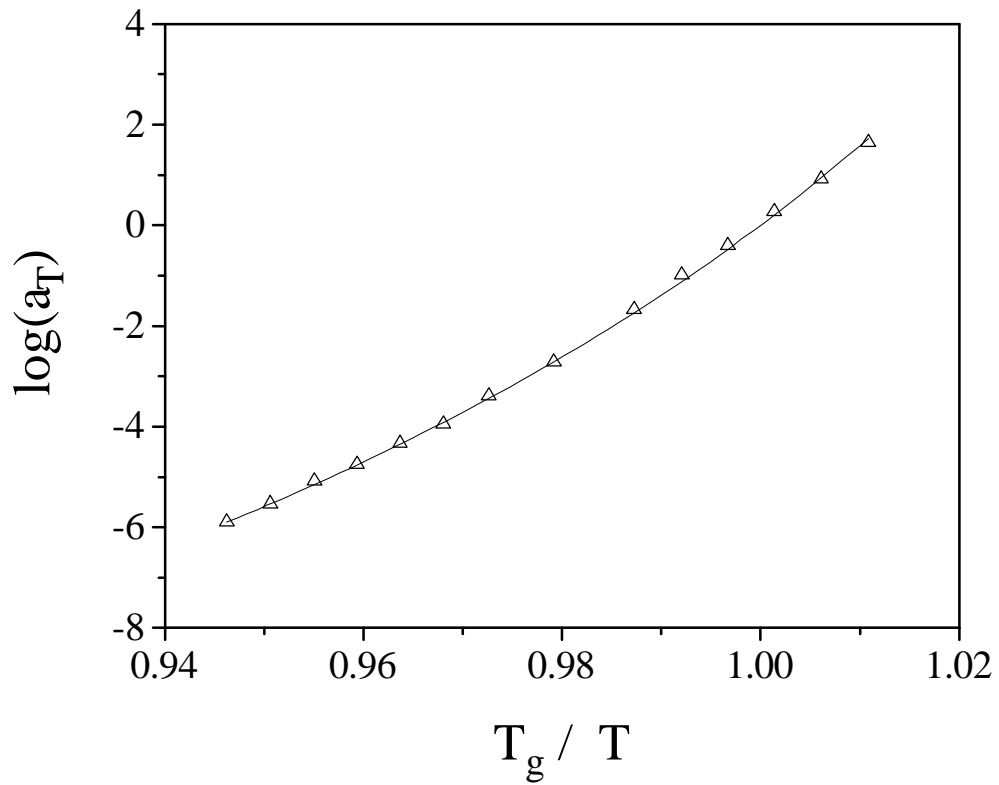


Figure 7-4: Shift factor plot illustrating glass transition cooperativity for the amorphous polyimide investigated. The shift factors were converted from the reference temperature of 250°C used during superposition of the loss modulus data to a reference temperature of 239°C which is the calorimetric  $T_g$ . The solid line represents the WLF fit.

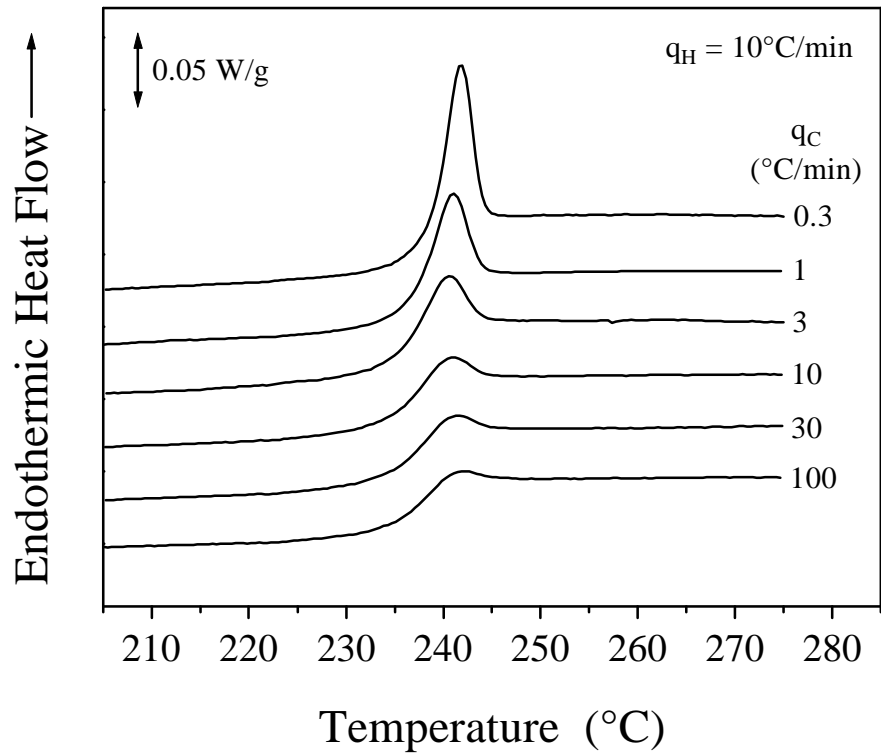


Figure 7-5: DSC glass transition response during heating at  $10^\circ\text{C}/\text{min}$  for the amorphous polyimide material following cooling from  $T_g+50^\circ\text{C}$  at the indicated cooling rates.

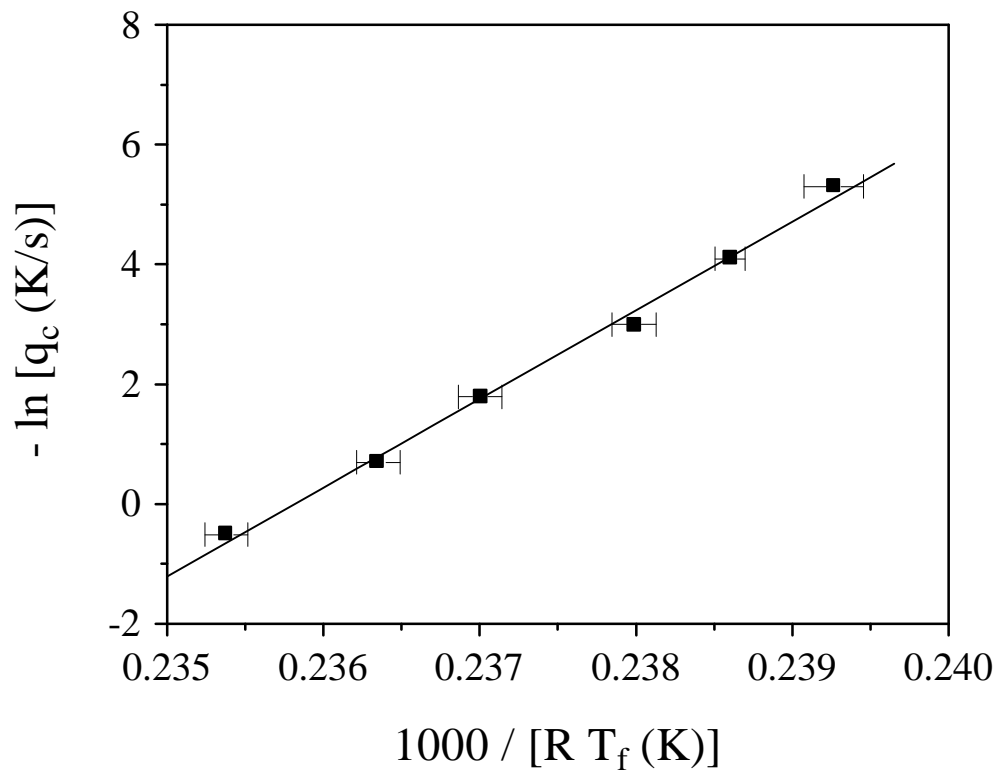


Figure 7-6: Arrhenius plot of the cooling rate dependence of calorimetric fictive temperature for the polyimide material.

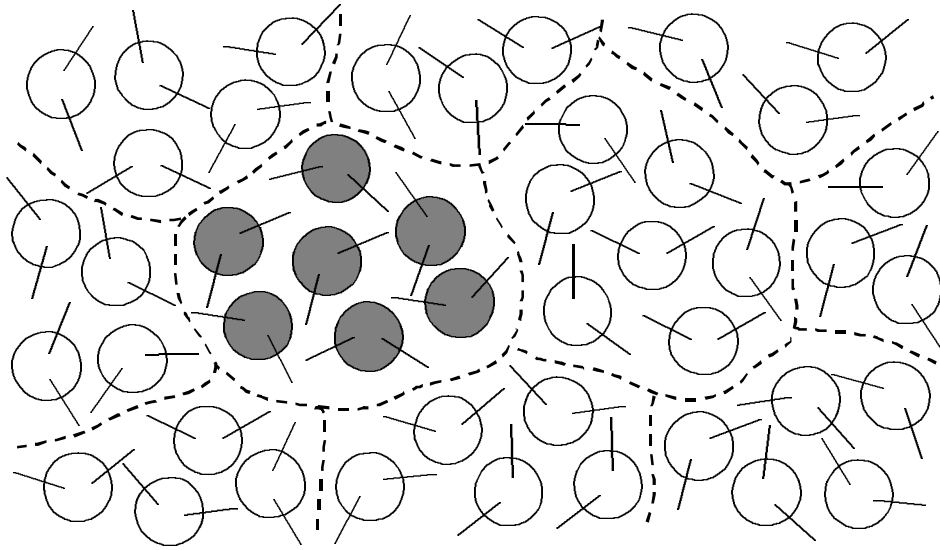


Figure 7-7. Two-dimensional depiction of cooperative relaxation domains with  $z = 7$ . Schematic adapted from representation given by Matsuoka and Quan.<sup>18,19</sup>

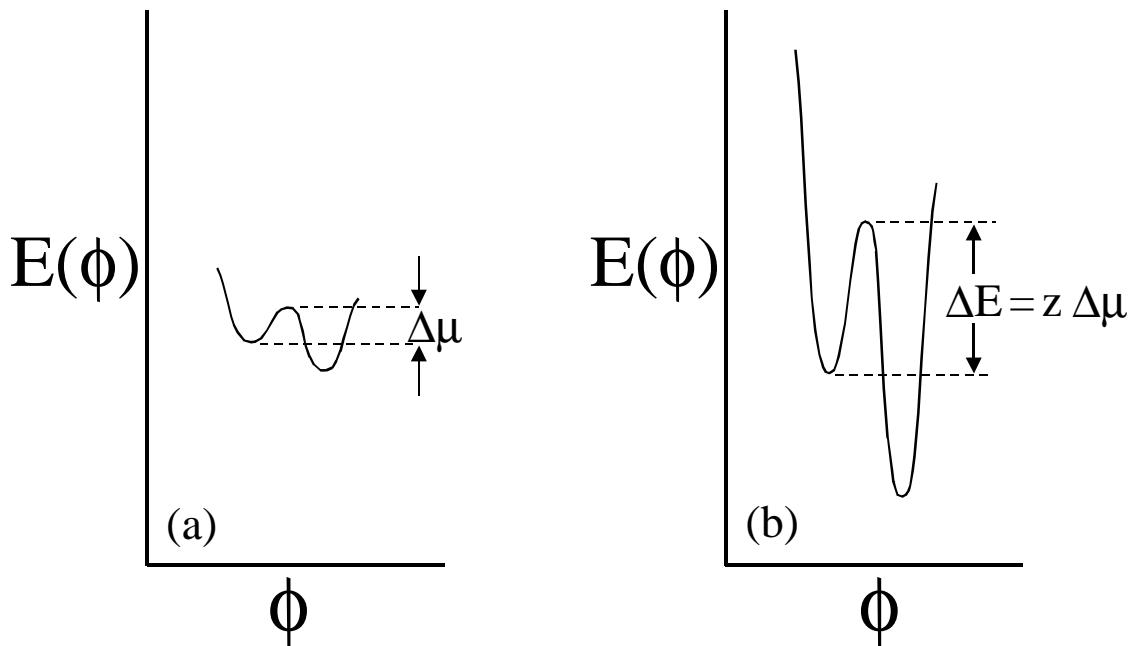


Figure 7-8: Schematic which illustrates activation energy associated with intramolecular relaxation of molecular segments: (a) independent relaxation of one segment; (b) cooperative relaxation of  $z$  segments. The intramolecular relaxation depicted involves rotation of backbone bonds from second-lowest to lowest energy state ( $\phi$  is the angle of rotation).

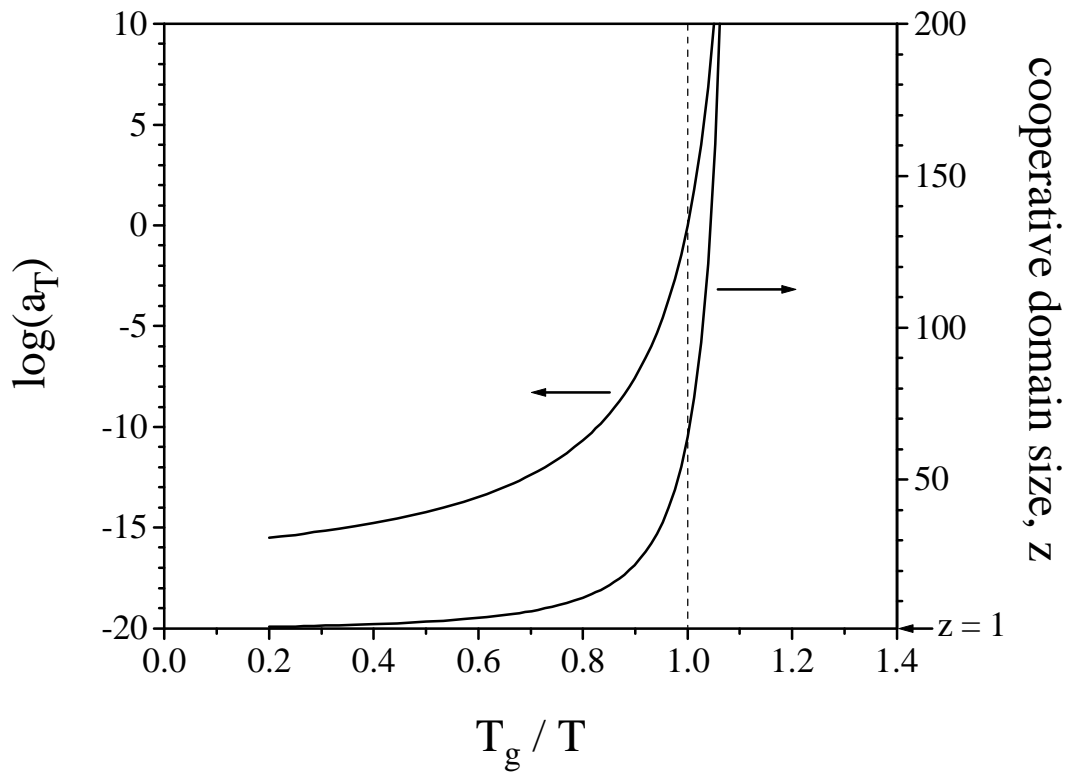


Figure 7-9. WLF behavior (curve A from Figure 7-1) and the associated temperature dependence of the most probable cooperative domain size.

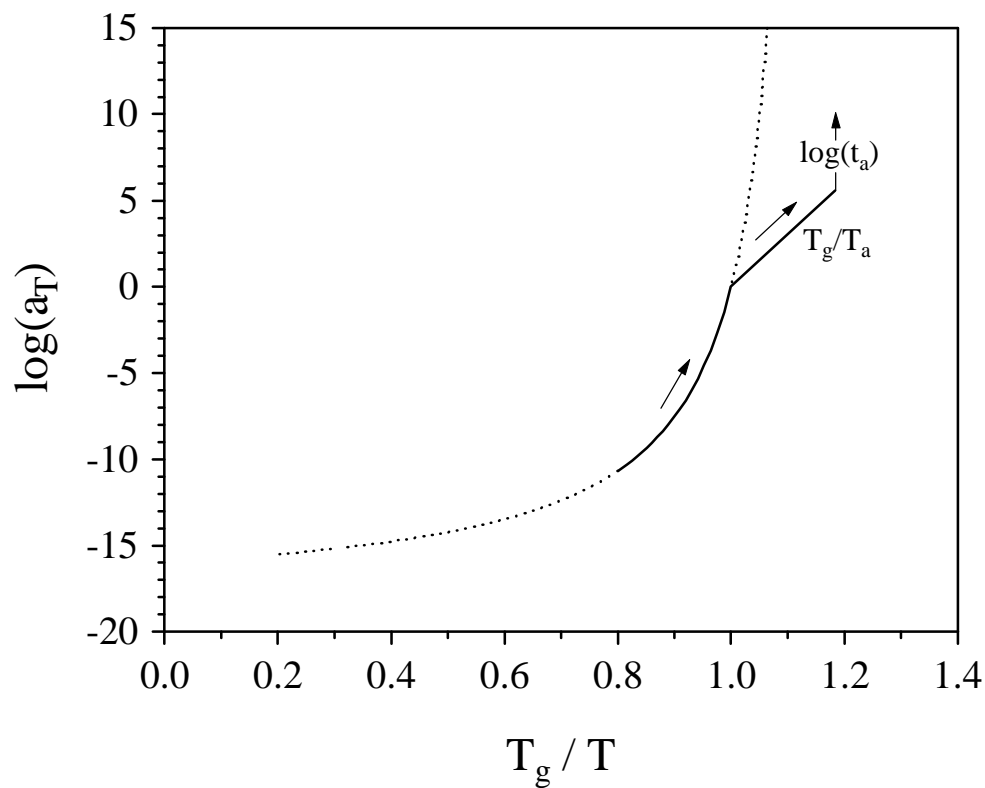


Figure 7-10: Departure into the non-equilibrium glassy state from the equilibrium nonArrhenius segmental relaxation response in the glass formation region. The segmental relaxation response indicated is from curve A in Figure 7-1.

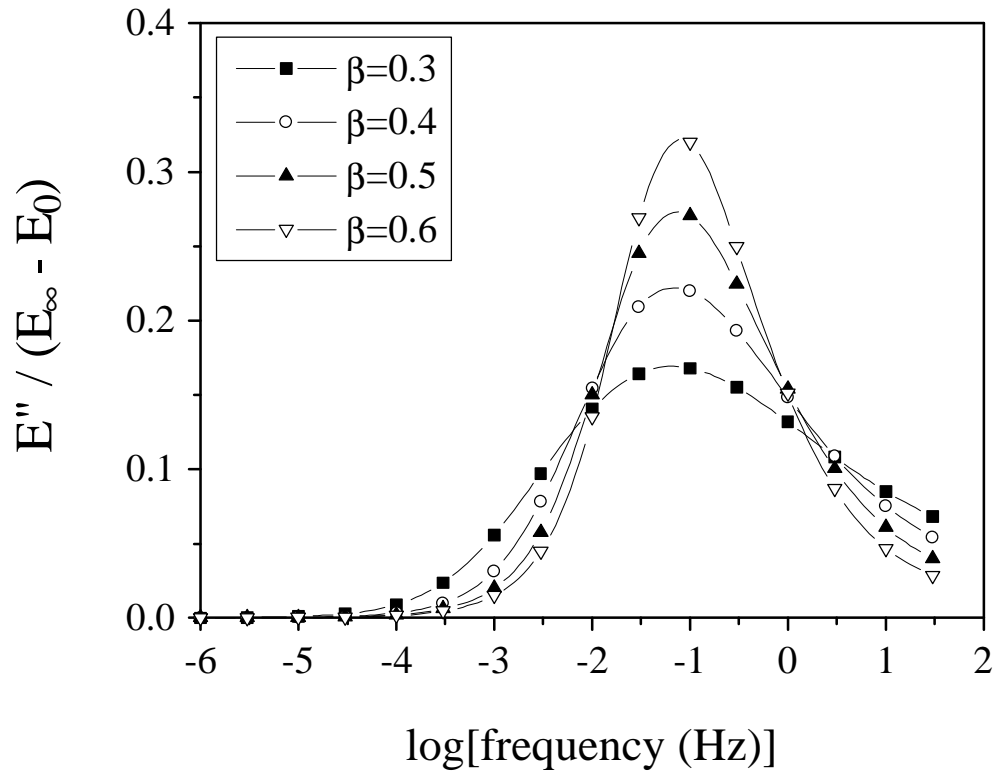


Figure 7-11: Predicted loss modulus using KWW function numerically transformed to frequency domain. A fixed relaxation time ( $\tau = 10$  sec) was used in the predictions and the stretching exponent was varied as indicated.

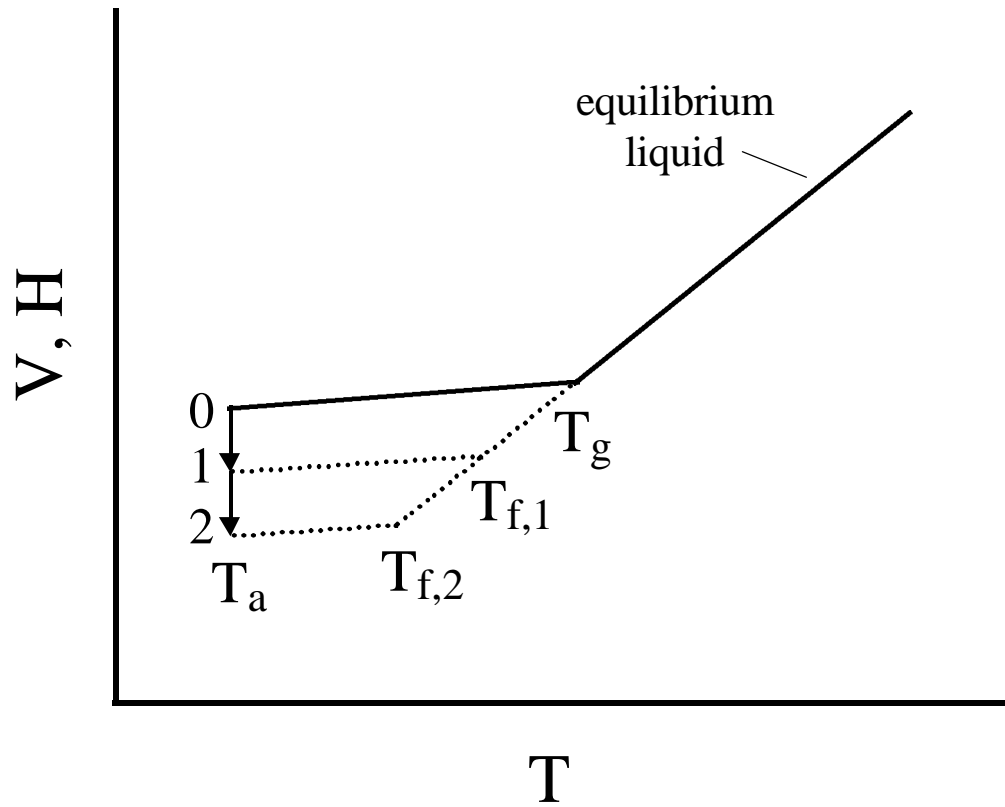


Figure 7-12: Illustration of fictive temperature changes during isothermal annealing in the glassy state.

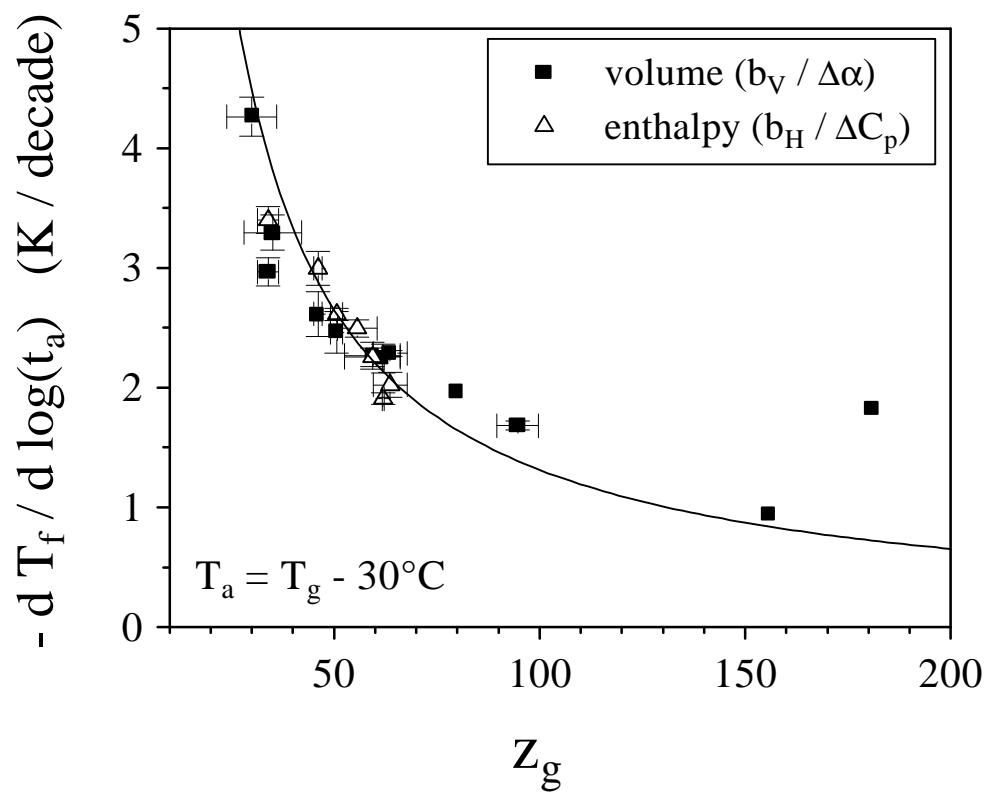


Figure 7-13: Apparent correlation between structural relaxation rates at  $T_g-30^\circ\text{C}$  and glass transition cooperative domain size.

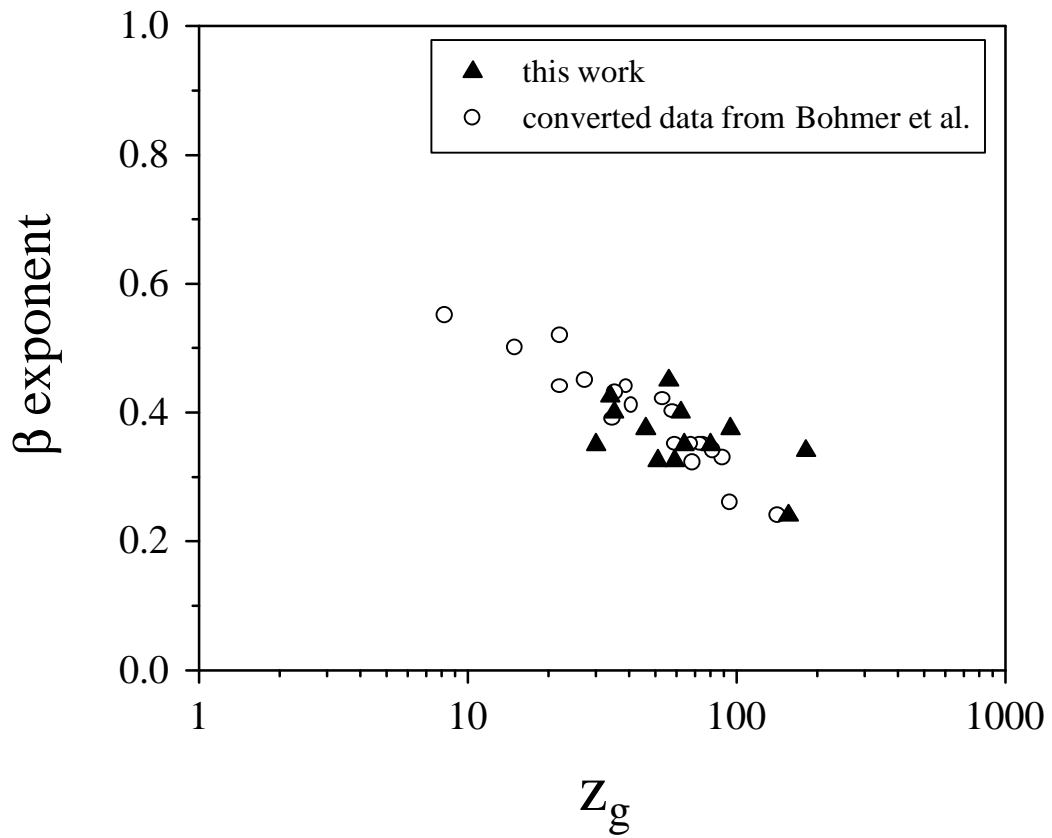


Figure 7-14. Apparent correlation between  $\beta$  and most probable cooperative domain size at the glass transition temperature for amorphous polymers. The solid triangles are from this paper (Table 7-II) and the open circles are converted data from Böhmer et al.<sup>3</sup> Literature fragility data were converted to  $z_g$  data using assumption  $C_1 = 16$ .

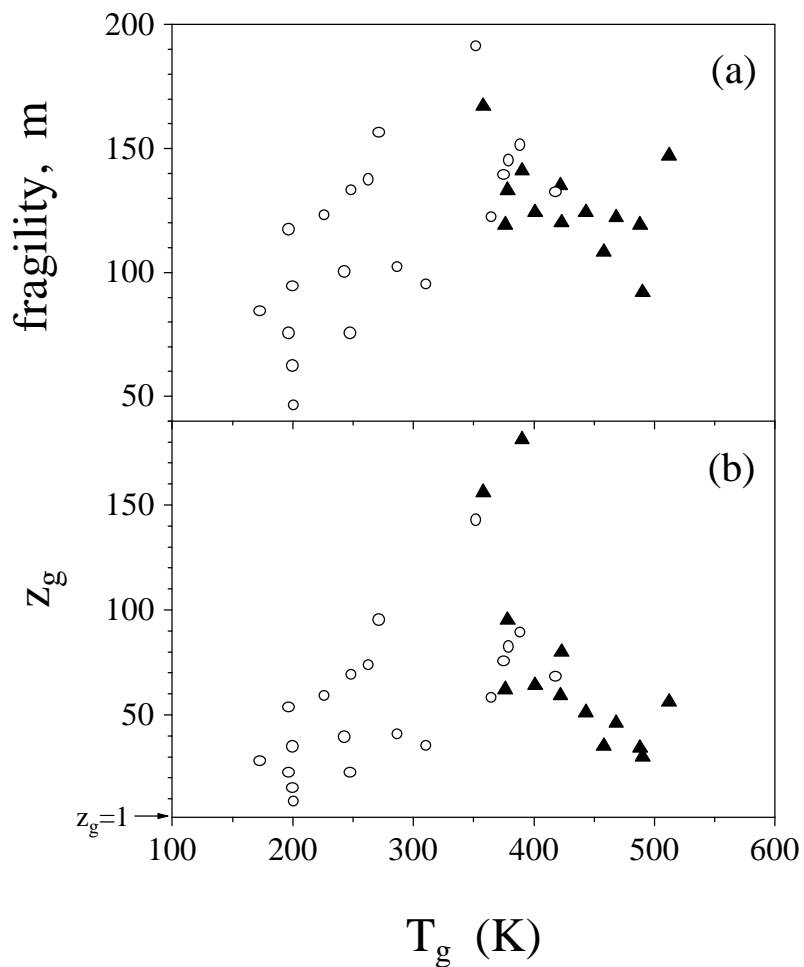


Figure 7-15. Fragility and  $z_g$  plotted versus glass transition temperature for amorphous polymers. The solid triangles are from this paper (Table 7-II) and open circles are from Böhmer et al.<sup>4</sup> Literature fragility data were converted to  $z_g$  data using assumption  $C_1 = 16$ .

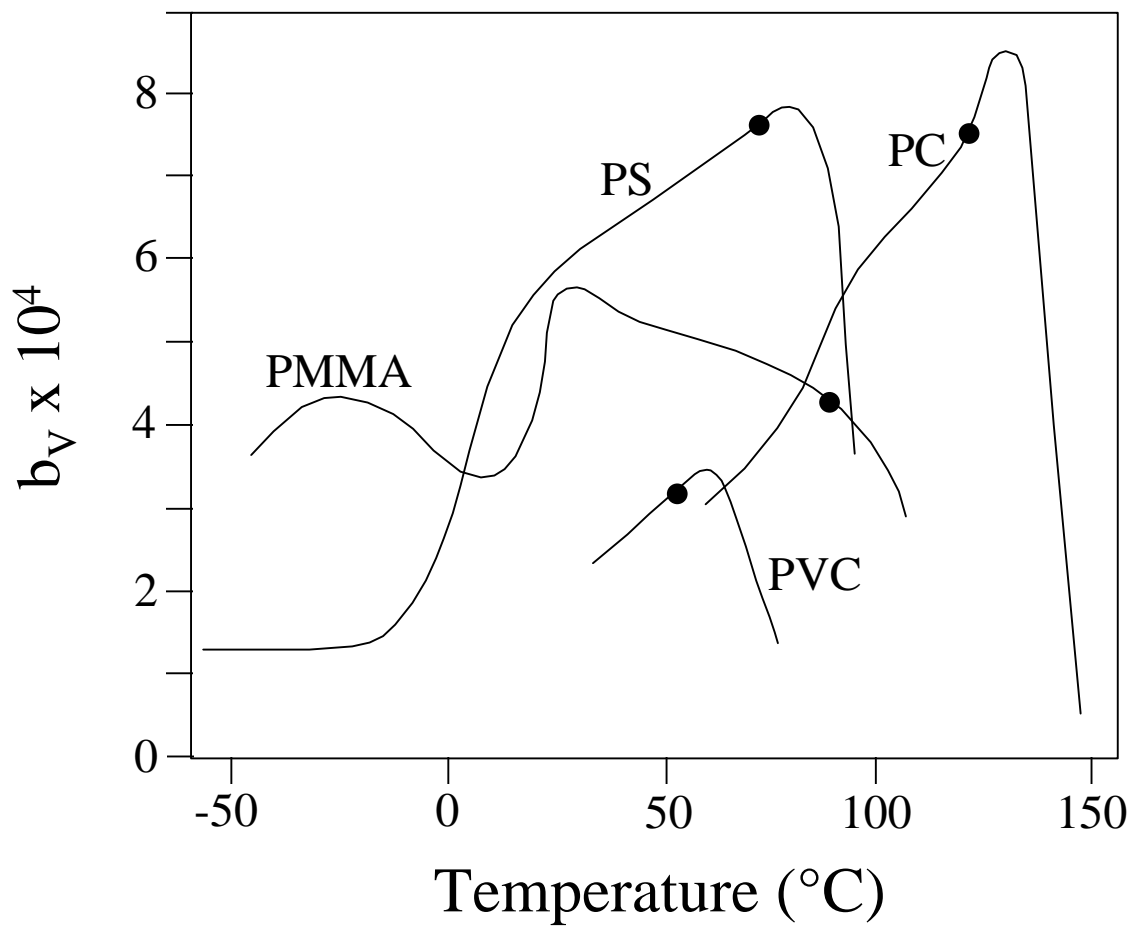


Figure 7-16. Volume relaxation rates for various glassy polymers. Figure adapted from reference 27. Each solid circle marks the volume relaxation aging rate at  $T_g-30\text{K}$ .

## 7.5 Appendix

The following tabulated results represent the numerical transformation of the KWW stretched exponential function to predict the loss modulus in the frequency domain. These predictions can be easily compared with dielectric and dynamic mechanical loss data in order to characterize the relaxation time distribution using the KWW expression.

Table 7-III: Predicted values of  $E''/(E_\infty - E_0)$  for low values of  $\beta$  (using  $\tau = 10$  sec)

log[f(Hz)]	$\beta = 0.3$	$\beta = 0.325$	$\beta = 0.35$	$\beta = 0.375$	$\beta = 0.4$	$\beta = 0.425$
-6.0	9.323E-5	6.676E-5	5.090E-5	4.072E-5	3.382E-5	2.894E-5
-5.5	2.789E-4	1.995E-4	1.519E-4	1.214E-4	1.007E-4	8.608E-5
-5.0	9.275E-4	6.633E-4	5.049E-4	4.032E-4	3.343E-4	2.855E-4
-4.5	2.767E-3	1.990E-3	1.510E-3	1.210E-3	1.000E-3	8.541E-4
-4.0	8.907E-3	6.540E-3	5.010E-3	4.010E-3	3.330E-3	2.840E-3
-3.5	2.356E-2	1.844E-2	1.463E-2	1.189E-2	9.920E-3	8.490E-3
-3.0	5.581E-2	4.890E-2	4.232E-2	3.648E-2	3.156E-2	2.758E-2
-2.5	9.724E-2	9.404E-2	8.955E-2	8.419E-2	7.839E-2	7.254E-2
-2.0	1.406E-1	1.461E-1	1.503E-1	1.532E-1	1.548E-1	1.551E-1
-1.5	1.643E-1	1.763E-1	1.878E-1	1.988E-1	2.092E-1	2.191E-1
-1.0	1.680E-1	1.812E-1	1.943E-1	2.073E-1	2.202E-1	2.330E-1
-0.5	1.552E-1	1.654E-1	1.752E-1	1.845E-1	1.934E-1	2.019E-1
0.0	1.317E-1	1.371E-1	1.417E-1	1.454E-1	1.485E-1	1.508E-1
0.5	1.082E-1	1.096E-1	1.101E-1	1.099E-1	1.090E-1	1.075E-1
1.0	8.495E-2	8.334E-2	8.110E-2	7.834E-2	7.520E-2	7.179E-2
1.5	6.808E-2	6.497E-2	6.151E-2	5.785E-2	5.411E-2	5.037E-2

Table 7-IV: Predicted values of  $E''/(E_\infty - E_0)$  for high values of  $\beta$  (using  $\tau = 10$  sec)

$\log[f(\text{Hz})]$	$\beta = 0.45$	$\beta = 0.475$	$\beta = 0.5$	$\beta = 0.525$	$\beta = 0.55$	$\beta = 0.575$	$\beta = 0.6$
-6.0	2.536E-5	2.266E-5	2.056E-5	1.891E-5	1.758E-5	1.649E-5	1.559E-5
-5.5	7.535E-5	6.724E-5	6.097E-5	5.601E-5	5.202E-5	4.877E-5	4.607E-5
-5.0	2.498E-4	2.228E-4	2.019E-4	1.854E-4	1.721E-4	1.612E-4	1.523E-4
-4.5	7.469E-4	6.659E-4	6.032E-4	5.537E-4	5.139E-4	4.814E-4	4.545E-4
-4.0	2.480E-3	2.210E-3	2.010E-3	1.840E-3	1.710E-3	1.600E-3	1.510E-3
-3.5	7.440E-3	6.630E-3	6.010E-3	5.510E-3	5.120E-3	4.790E-3	4.520E-3
-3.0	2.441E-2	2.190E-2	1.990E-2	1.830E-2	1.700E-2	1.593E-2	1.505E-2
-2.5	6.696E-2	6.185E-2	5.731E-2	5.338E-2	4.999E-2	4.711E-2	4.465E-2
-2.0	1.542E-1	1.524E-1	1.498E-1	1.465E-1	1.429E-1	1.390E-1	1.351E-1
-1.5	2.284E-1	2.370E-1	2.449E-1	2.521E-1	2.585E-1	2.641E-1	2.688E-1
-1.0	2.457E-1	2.583E-1	2.708E-1	2.832E-1	2.955E-1	3.078E-1	3.199E-1
-0.5	2.099E-1	2.175E-1	2.247E-1	2.316E-1	2.380E-1	2.440E-1	2.497E-1
0.0	1.524E-1	1.535E-1	1.539E-1	1.539E-1	1.533E-1	1.524E-1	1.510E-1
0.5	1.054E-1	1.030E-1	1.002E-1	9.714E-2	9.385E-2	9.039E-2	8.681E-2
1.0	6.821E-2	6.452E-2	6.080E-2	5.710E-2	5.347E-2	4.993E-2	4.652E-2
1.5	4.671E-2	4.317E-2	3.980E-2	3.661E-2	3.362E-2	3.085E-2	2.828E-2

## 7.6 References

- <sup>1</sup> Hodge, I. M. *Macromolecules* **1983**, *16*, 898.
- <sup>2</sup> Hodge, I. M. *J. Non-Cryst. Solids*, **1994**, *169*, 211.
- <sup>3</sup> Böhmer, R.; Angell, C. A. *Materials Science Forum* **1993**, *119-121*, 485.
- <sup>4</sup> Böhmer, R.; Ngai, K. L.; Angell, C. A.; Plazek, D. J. *J. Chem. Phys.*, **1993**, *99*, 4201.
- <sup>5</sup> Roland, C. M.; Ngai, K. L. *J. Non-Cryst. Solids*, **1994**, *172-174*, 868.
- <sup>6</sup> Santangelo, P. G.; Ngai, K. L.; Roland, C. M. *Macromolecules* **1993**, *26*, 2682.
- <sup>7</sup> Roland, C. M.; Ngai, K. L. *Macromolecules* **1991**, *24*, 5315.
- <sup>8</sup> Connolly, M.; Karasz, F.; Trimmer, M. *Macromolecules* **1995**, *28*, 1872.
- <sup>9</sup> Plazek D. J.; Ngai, K. L., in *Physical Properties of Polymers Handbook*, (ed. J. E. Mark), American Institute of Physics Press, Woodbury, NY, 1996, Chapter 12, pp. 139-159.
- <sup>10</sup> Williams, M. L.; Landel, R. F.; Ferry, J. D. *J. Am. Ceram. Soc.*, **1955**, *77*, 3701.
- <sup>11</sup> McKenna, G. B., in *Comprehensive Polymer Science, Vol. 2, Polymer Properties* (ed. C. Booth and C. Price), Pergamon, Oxford, UK, 1989, pp 311-362 (Chapter 10).
- <sup>12</sup> K. L. Ngai and D. J. Plazek, in *Physical Properties of Polymers Handbook* (ed. J. E. Mark), AIP Press, Woodbury, NY, 1996, pp. 341-362 (Chapter 25).
- <sup>13</sup> Angell, C. A. *Science* **1995**, *267*, 1924.
- <sup>14</sup> Angell, C. A.; Monnerie, L.; Torell, L. M., in *Structure, Relaxation, and Physical Aging of Glassy Polymers* (eds. R. J. Roe and J. M. O'Reilly), *Mat. Res. Symp. Proc.* **1991**, *215*, 3.
- <sup>15</sup> Angell, C. A. *J. Non-Cryst. Solids* **1991**, *131-133*, 13.
- <sup>16</sup> Angell, C. A. *J. Res. Natl. Inst. Stand. Technol.*, **1997**, *102*, 171.
- <sup>17</sup> Adam, G.; Gibbs, J. H. *J. Chem. Phys.* **1965**, *43*, 139.
- <sup>18</sup> Matsuoka, S. *Relaxation Phenomena in Polymers*, Munich: Hanser Publishers, 1992.
- <sup>19</sup> Matsuoka, S.; Quan, X. *Macromolecules* **1991**, *24*, 2770.
- <sup>20</sup> Williams, G., in *Comprehensive Polymer Science, Vol. 2, Polymer Properties* (ed. C. Booth and C. Price), Pergamon, Oxford, UK, 1989, pp. 601-632 (Chapter 18).
- <sup>21</sup> Hutchinson, J. M. *Prog. Polym. Sci.* **1995**, *20*, 703.
- <sup>22</sup> Tool, A. Q. *J. Am. Ceram. Soc.* **1946**, *29*, 240.
- <sup>23</sup> Tool, A. Q. *J. Res. Natl. Bur. Stand* **1946**, *37*, 73.
- <sup>24</sup> Colmenero, J.; Arbe, A.; Alegria, A. *J. Non-Cryst. Solids*, **1994**, *172-174*, 126.
- <sup>25</sup> Colucci, D. M.; McKenna, G. B. in *Structure and Dynamics of Glasses and Glass Formers* (eds. C. A. Angell, K. L. Ngai, J. Kieffer, T. Egami, and G. U. Nienhaus), *Mat. Res. Symp. Proc.* **1997**, *455*, 171.
- <sup>26</sup> Wen, J. in *Physical Properties of Polymers Handbook* (ed J. E. Mark), American Institute of Physics Press, Woodbury, NY, 1996, Chapter 9, pp. 101-109.
- <sup>27</sup> Greiner, R.; Schwarzl, F. R. *Rheol. Acta* **1984**, *23*, 378.
- <sup>28</sup> Plazek, D. J.; Tan, V.; O'Rourke, V. M. *Rheol. Acta* **1974**, *13*, 367.
- <sup>29</sup> Mercier, J. P.; Groeninckx, G. *Rheol. Acta* **1969**, *8*, 516.
- <sup>30</sup> Muggi, M. W.; Ward, T. C. (Chemistry Dept., Virginia Tech), unpublished data.
- <sup>31</sup> Zoller, P. *J. Polym. Sci., Polym. Phys. Ed.* **1978**, *16*, 1261.
- <sup>32</sup> Plazek, D. J.; Ngai, K. L. *Macromolecules* **1991**, *24*, 1222.

- <sup>33</sup> McCrum, N. G.; Read, B. E.; Williams, G. *Anelastic and Dielectric Effects in Polymeric Solids*, John Wiley and Sons Ltd., London, 1967.
- <sup>34</sup> Angell, C. A. *Polymer* **1997**, *38*, 6261.
- <sup>35</sup> Hodge, I. M. *J. Res. Natl. Inst. Stand. Technol.* **1997**, *102*, 195.
- <sup>36</sup> Ngai, K. L. *Comments Solid State Phys.* **1979**, *9*, 127.
- <sup>37</sup> Ngai, K. L. *Comments Solid State Phys.* **1980**, *9*, 141.
- <sup>38</sup> Rajagopal, A. K.; Ngai, K. L.; Teitler, S. *J. Non-Cryst. Solids*, **1991**, *131-133*, 282.
- <sup>39</sup> Ngai, K. L.; Rendell, R. W. *J. Non-Cryst. Solids*, **1991**, *131-133*, 942.
- <sup>40</sup> Struik, L. C. E. *Polymer* **1987**, *28*, 1869.

# Chapter 8

## Correlation Between Physical Aging Rates and Glass Transition Cooperativity (Fragility): Part 2. Adam-Gibbs Predictions

---

---

### Chapter Synopsis

The Adam-Gibbs (AG) cooperativity approach is employed in combination with the Tool-Narayanaswamy-Moynihan (TNM) formalism in order to predict glassy state structural relaxation. Using parameters developed from the equilibrium segmental relaxation time response above  $T_g$ , the nonlinear Adam-Gibbs relaxation time function is applied to the nonequilibrium glassy state in order to test whether the Adam-Gibbs model is consistent with the experimentally noted correlation between structural relaxation rates at  $T_g-30^\circ\text{C}$  and glass transition cooperativity (fragility). The Adam-Gibbs theory is not a rigorous treatment and recent theoretical work by DiMarzio and Yang [DiMarzio, E. A.; Yang, A. J. M. *J. Res. Natl. Inst. Stand. Technol.* **1997**, *102*, 135] has established grounds for questioning the Adam-Gibbs premise that the logarithm of the equilibrium relaxation time in the glassy state is inversely related to configurational entropy. The nonlinear Adam-Gibbs function can, however, semi-quantitatively predict the observed correlation between structural relaxation rates and glass transition cooperativity. The Adam-Gibbs model can capture the shape of the experimental correlation observed for numerous glassy polymers but slightly underpredicts the relaxation rates. This latter feature is likely due to narrower relaxation time distributions for both volume and enthalpy relaxation relative to the distribution breadth inferred from the dynamic mechanical response in the  $\alpha$ -relaxation region. Inadequacies associated with the prediction of glassy state relaxations using the Adam-Gibbs model are noted and discussed, and conditions leading to the apparent breakdown of the AG/TNM numerical modeling procedure are described.

## 8.1 Introduction

The phenomenological modeling of relaxations in the nonequilibrium glassy state attracts interest due to the desire to characterize and ultimately predict physical aging behavior relevant to the application of glassy materials. Research which involves descriptive and predictive modeling efforts is also driven by the necessity to inspect the degree to which proposed models can realistically capture the physics associated with glass-forming materials. One particular relaxation function worth critical examination is the description given by the Adam-Gibbs (AG) configurational entropy model,<sup>1</sup> and this present investigation is aimed at testing the predictive capability of this model. Chapter 7 presented a strong experimental connection between structural relaxation rates in the glassy state and the nonArrhenius kinetics of glass formation, and this correlation provides a unique means of probing the performance of the Adam-Gibbs relaxation model.

The experimental observation of a general link between segmental dynamics in the glass-forming temperature range and glassy state relaxation of volume and enthalpy suggests that the chemical/structural features of amorphous materials influence both responses in related ways. Therefore, the Adam-Gibbs approach is worth consideration because it incorporates the notion of segmental cooperativity which may be thought to reflect both intra- and intermolecular characteristics. The equilibrium Adam-Gibbs model is consistent with the nonArrhenius build-up of relaxation times during cooling toward the glass transition temperature region in the glass formation temperature region. In addition, application of nonlinear extensions of the Adam-Gibbs model to relaxations in the nonequilibrium glassy state has encountered some success. For example, research by Scherer,<sup>2,3</sup> Moynihan et al.,<sup>4</sup> and Hodge<sup>5,6</sup> has indicated the ability of the AG function, in combination with the Tool-Narayanaswamy-Moynihan (TNM) methodology, to allow a reasonable representation of nonequilibrium relaxation data for glassy materials.

The Adam-Gibbs model has been successfully employed to describe relaxation characteristics, but one cannot discount the recent theoretical and experimental contradictions which suggest incorrect physics involved with the model when applied to the glassy state. It is generally accepted that the Adam-Gibbs model does not have a

rigorous theoretical foundation and should be appropriately classified as a conceptual aid.<sup>7,8</sup> In addition, one of the basic assertions of the Adam-Gibbs model has recently come under scrutiny from both theoretical and experimental standpoints. The feature in question concerns the inverse relationship between the logarithm of equilibrium relaxation time and configurational entropy which presupposes that the equilibrium relaxation times are infinite in value for all temperatures below the thermodynamic transition temperature,  $T_2$ , predicted by Gibbs and DiMarzio.<sup>9</sup> The implication of this assertion is that equilibrium relaxation times in the glassy state follow the extrapolation of the nonArrhenius relaxation time response above  $T_g$  which can be described by expressions such as the Williams-Landel-Ferry (WLF) equation.<sup>10</sup> Recent theoretical work by DiMarzio and Yang<sup>11</sup> has predicted that the viscosity displays an Arrhenius dependence on temperature in the glassy state under conditions of thermodynamic equilibrium. Also, physical aging investigations by O'Connell and McKenna<sup>12,13</sup> have indicated that equilibrium mechanical relaxation times in the glassy state display Arrhenius behavior which deviates from the WLF response determined above  $T_g$ . Therefore, both theoretical and experimental grounds for questioning the applicability of the Adam-Gibbs model to glassy state relaxations have been recently established.

Further examination of the AG relaxation function is certainly warranted. From one perspective, the AG approach appears to contain some truth and thus has merit. The model captures the WLF scaling behavior above  $T_g$  from an entropy standpoint as opposed to a free volume basis, and nonlinear extensions of the model can allow reasonable fits of nonequilibrium glassy responses. Conversely, the caveats related to the lack of theoretical fortitude and the questionable predictions of the model for the equilibrium glassy state cannot be ignored. The use of the AG relaxation function to predict glassy relaxations in this research effort is designed as a test and should not be misinterpreted as the present authors' advocacy of the fundamental legitimacy of the Adam-Gibbs approach. Questions to be addressed in this investigation include: (1) whether a single set of parameters can adequately describe both the glass formation behavior and sub- $T_g$  relaxation associated with the physical aging process; and (2) whether

the Adam-Gibbs approach can capture the experimental correlation between aging rates and cooperativity.

## 8.2 Results and Discussion

Before comparing experimental results and Adam-Gibbs predictions, it is necessary to outline the modeling approach and provide details of the parameter specification process. The numerical application of the Adam-Gibbs relaxation time expression via the Tool-Narayanaswamy-Moynihan scheme will be described, and mention will be made of some noted limitations. Finally, a critical examination will be undertaken with regard to the predictive capabilities of the nonlinear AG relaxation time function, particularly its ability to capture the observed link between structural relaxation rates at  $T_g-30^\circ\text{C}$  and the degree of cooperativity observed in the glass transition region.

### 8.2.1 Model Description

One of the most commonly employed approaches for modeling relaxation in the nonequilibrium glass is the Tool-Narayanaswamy-Moynihan (TNM) method.<sup>14-18</sup> An alternate, but very comparable, approach to describing the phenomenological features of glassy state relaxations is offered by the Kovacs-Aklonis-Hutchinson-Ramos (KAHR) model.<sup>19</sup> A brief outline of the TNM formalism is detailed here because it is used in this study. An informative synopsis of the KAHR method is presented elsewhere in a review by McKenna.<sup>20</sup> When nonexponentiality is introduced via the stretched exponential function (Kolrausch-Williams-Watts (KWW) function<sup>21,22</sup>), the general TNM expression which can be applied to thermal programs involving continuous cooling, heating, and annealing steps takes on the following form:

$$T_f(T) = T_{\text{init}} + \int_{T_{\text{init}}}^T \left\{ 1 - \exp \left[ - \left( \int_{t(T'')}^{t(T)} \frac{dt'}{\tau(T, T_f)} \right)^\beta \right] \right\} dT'' \quad \text{Eqn. 8-1}$$

This approach allows changes in fictive temperature ( $T_f$ ) to be determined during a numerically imposed thermal history through the use of a nonlinear relaxation time function which depends on the actual and fictive temperatures,  $\tau(T, T_f)$ . The TNM expression employs the reduced time concept and superposition of responses. In addition, thermorheological simplicity is assumed to be valid which dictates that  $\beta$  does not vary throughout the simulated thermal cycle. The numerical application of the TNM equation involves discretization of the integrals, a process which is nicely outlined by Mijovic and coworkers.<sup>23</sup>

Use of the TNM formalism necessitates an expression for the most probable relaxation time ( $\tau$ ) which is a function of both temperature and the changing structure, the latter of which is characterized by means of the fictive temperature. Often, the function introduced by Narayanaswamy<sup>16</sup> is used, and the widely recognized form of this equation is given by:<sup>17</sup>

$$\tau = A \exp\left(\frac{x \Delta h}{R T} + \frac{(1-x) \Delta h}{R T_f}\right) \quad \text{Eqn. 8-2}$$

Using a nonlinearity parameter,  $x$ , this Arrhenius expression partitions the activation energy,  $\Delta h$ , in order to separate the effects of temperature and  $T_f$  on relaxation time. The  $A$  parameter is a preexponential constant. Criticisms of this function include the fact that its origin is purely empirical and that the function remains an Arrhenius expression above  $T_g$  (where  $T_f = T$ ) despite the experimental observation of nonArrhenius behavior in the equilibrium liquid state. The model has, nonetheless, enjoyed substantial success in fitting enthalpy recovery DSC traces for glass-forming materials.<sup>6</sup>

As an alternative to the Narayanaswamy equation, a nonlinear form of the Adam-Gibbs relaxation time expression can be developed and incorporated into the TNM modeling approach represented by Eqn. 8-1. In the process of introducing the AG function for  $\tau(T, T_f)$ , it is worthwhile to compare the equilibrium and nonlinear AG functions as well as contrast the expressions for the most probable number of segments in a cooperative domain,  $z$ , which can be developed from them. To reiterate from Chapter 7, the  $z$  parameter represents the most probable number of molecular segments or "beads"

which must move cooperatively for relaxation to occur. The use of a function for the difference between the liquid and glassy heat capacities which is given by  $\Delta C_p(T) = C \cdot T_2/T$  allows the following form of the equilibrium (linear) Adam-Gibbs equation to be developed:<sup>1,6</sup>

$$\tau = A \exp\left(\frac{D}{RT[1-(T_2/T)]}\right) \quad \text{where: } D = \frac{s_c^* \Delta\mu'}{C} \quad \text{Eqn. 8-3}$$

In the above equation, C is the configurational heat capacity at  $T_2$ , the Gibbs-DiMarzio transition temperature. The configurational entropy associated with the independently (non-cooperatively) relaxing molecular segments is represented by the symbol  $s_c^*$ , and  $\Delta\mu'$  is the primitive activation energy associated with rearrangement of one of the segments in a cooperative domain. The prime nomenclature (') applied to the primitive activation energy is used to distinguish it from the comparable activation energy which results from the extrapolation treatment which will be detailed shortly.

The basic cooperativity concept employs the notion that the apparent activation energy is greater than the primitive activation energy due to required segmental cooperativity, and the number of cooperative segments in a domain is equal to z. Assigning an expression for z based upon Eqn. 8-3 is difficult because the number of molecular entities (atoms, bonds, etc.) comprising the molecular segment, or "bead", must be estimated in addition to the associated number of distinct ways that this basic relaxing unit can be arranged. This information is necessary in order to assign a value to  $s_c^*$ . Treating the Adam-Gibbs model in a general manner can provide an alternate means of developing a function  $z(T)$  for the equilibrium case and an expression  $z(T, T_f)$  for the nonlinear case. The extrapolated high temperature limit of the AG model should provide an activation energy which represents non-cooperative relaxation (i.e. relaxation of a single molecular segment without any influence of other segments). Hence, the evaluation of the derivative of  $\ln(\tau)$  with respect to  $1/T$  in the limit as  $T \rightarrow \infty$  should provide a means of evaluating the primitive activation energy,  $\Delta\mu$ , which turns out to be equal to the D parameter ( $\Delta\mu = D$ ). The following relation proceeds from this argument, and this expression will be referred to as the linear (or equilibrium) AG expression:

$$\tau = A \exp\left(\frac{\Delta\mu}{RT[1-(T_2/T)]}\right) \quad \text{Eqn. 8-4}$$

One benefit of this assignment of the primitive activation energy is that explicit expressions for the most probable cooperative domain size,  $z$ , can be easily developed. Upon comparing Eqn. 8-4 with a generalized Arrhenius expression,  $\tau \propto \exp(\Delta E/RT)$  and the cooperativity notion that  $\Delta E = z \cdot \Delta\mu$ , it may be tempting to assign an expression for  $z$  which is equal to  $[1-(T_2/T)]^{-1}$ . However, when one defines the activation energy ( $\Delta E$ ) in the proper manner by the derivative of  $\ln(\tau)$  with respect to  $1/T$  then it is apparent that  $z$  should be expressed as a function of temperature according to:

$$z(T) = \frac{\Delta E(T)}{\Delta\mu} = \frac{R}{\Delta\mu} \frac{d \ln(\tau)}{d(1/T)} = \frac{1}{(1-T_2/T)^2} \quad \text{Eqn. 8-5}$$

The cooperative domain size in the equilibrium state is accordingly predicted to be a function of  $T_2$ , which is a material-dependent parameter, and the temperature. It should be mentioned that the expression for  $z(T)$  provided by Matsuoka and Quan<sup>24-26</sup> is inconsistent with the interpretation presented here.

The same approach which Adam and Gibbs established for the equilibrium liquid state can be generalized and extended into the glassy state, and Hodge details the relevant history associated with the development of this extension in a recent publication.<sup>7</sup> The use of  $T_f$  as the integration limit for evaluating configurational entropy, as opposed to the limit of  $T$  which is used in the equilibrium case, leads to a nonlinear relaxation time function.<sup>5</sup> Using the same function for  $\Delta C_p$  which was employed in deriving Eqn. 8-4, and treating the primitive activation energy as described previously, the following nonlinear AG expression can be formulated:

$$\tau = A \exp\left(\frac{\Delta\mu}{RT[1-(T_2/T_f)]}\right) \quad \text{Eqn. 8-6}$$

The cooperative domain size in the glassy state,  $z(T, T_f)$ , can be evaluated from Eqn. 8-6 according to:

$$z(T, T_f) = \frac{R}{\Delta\mu} \left[ \left( \frac{d \ln(\tau)}{d(1/T)} \right)_{T_f} + \left( \frac{d \ln(\tau)}{d(1/T_f)} \right)_T \right] \quad \text{Eqn. 8-7}$$

which yields:

$$z(T, T_f) = \underbrace{\frac{1}{1 - T_2/T_f}}_{\text{isostructural temperature contribution}} + \underbrace{\left( \frac{T_2}{T} \right) \frac{1}{(1 - T_2/T_f)^2}}_{\text{isothermal structure contribution}} \quad \text{Eqn. 8-8}$$

Clearly, the partitioning of  $z$ , and hence the activation energy, into temperature and structure components is a natural outcome of the nonlinear Adam-Gibbs model. The result is comparable in character to the duty of the  $x$  parameter in Narayanaswamy's function (Eqn. 8-2). What is a unique feature of the nonlinear AG model is that it predicts that the *degree of nonlinearity varies during the imposed thermal history for a constant set of parameters*. This can be observed from the diagram presented in Figure 8-1 which was generated using Eqn. 8-5 and Eqn. 8-8 with  $T_g = 400\text{K}$  and  $T_2 = 350\text{K}$  (see figure caption). In this diagram, the fictive temperature decreases towards the actual temperature during annealing at  $370\text{K}$ , and the influence of this relaxation on the relative contributions of temperature and structure to the cooperativity is detailed in the table which is included in Figure 8-1. Because the nonlinearity parameter,  $x$ , does not depend on the actual and fictive temperatures, the Narayanaswamy expression predicts that the degree of nonlinearity remains constant for the relaxation of a glassy material. The Adam-Gibbs and Narayanaswamy expressions obviously depart from each other in the specific treatment of nonlinearity.

Now that the linear and nonlinear versions of the Adam-Gibbs model have been described, it is appropriate to describe the method of specifying the parameters necessary to predict glassy relaxations. The equilibrium AG function can be applied to dynamic mechanical or dielectric data which characterize the segmental dynamics in the glass-forming temperature region. The parameters thus determined can then be applied to the nonequilibrium glassy state via the nonlinear version of the AG model in an attempt to

predict relaxation behavior. The WLF expression, which is essentially equivalent in form to the linear AG equation (Eqn. 8-4), is given by:

$$\log(a_T) = \log\left(\frac{\tau}{\tau_g}\right) = \frac{-C_1(T - T_g)}{C_2 + T - T_g} \quad \text{Eqn. 8-9}$$

The WLF parameters which are fit to shift factor scaling data can be converted to AG parameters according to:

$$T_2 \approx T_0 = T_g - C_{2,g} \quad \text{Eqn. 8-10}$$

$$\Delta\mu = 2.303 R C_{1,g} C_{2,g} \quad \text{Eqn. 8-11}$$

$$\ln(A) = \ln(\tau_g) - 2.303 C_{1,g} \quad \text{Eqn. 8-12}$$

The  $T_g$  value measured by DSC, obtained during heating at 10°C for a sample freshly quenched from above  $T_g$  at 200°C/min, is used as a reference temperature during scaling of superposition of dynamic mechanical loss data, and the relaxation time,  $\tau_g$ , at this temperature is on the order of 100 seconds for glass-forming materials. This value of 100 seconds can be used to develop an initial guess for  $\ln(A)$  which can subsequently be modified slightly in order to match the predicted glass transition temperature region with the experimental data. Dynamic mechanical loss data in the glass-forming (segmental) temperature region can be used to obtain a measure of the  $\beta$  parameter as described in Part 1 of this investigation (Chapter 7). All of the necessary modeling parameters can, therefore, be specified from the equilibrium dynamic mechanical response and applied in an attempt to predict glassy state relaxations. The goal is to ascertain whether a single set of parameters for a glass former can adequately describe both liquid and glassy relaxations.

Some specific details are necessary to consider concerning the numerical application of Eqn. 8-1 to the modeling of glassy relaxation behavior. In the execution of this research study, an apparent break-down of the AG/TNM numerical modeling procedure was noted, and it is important to describe this observation which has not been

previously mentioned in the literature. The ensuing discussion of the modeling procedure assumes some familiarity with the numerical application of the TNM method which is described elsewhere.<sup>6,23,27</sup>

Specific discussion of the procedural details associated with the numerical modeling aspect of this study is essential based upon potential problems associated with the typical approach used in the literature. In considering Eqn. 8-1, it is evident that this expression is implicit in  $T_f$ . In the calculations, therefore, the fictive temperature from the previous numerical step (i-1) was used as a guess for  $T_f$  at step i, and an iterative procedure was then performed until the calculated  $T_f$  displays changes less than 1E-6 K between consecutive iterations. The importance of iteration can be realized by inspecting Figure 8-2 which depicts thermal cycles which were predicted with and without the iterative procedure using parameters determined from dynamic mechanical data for an amorphous polyimide material that was mentioned in Chapter 7. The polyimide parameters used for the predictions were:  $T_2 = 443\text{K}$ ,  $\Delta\mu=26.0\text{ kJ/mol}$ ,  $\ln(A) = -43.0$ , and  $\beta = 0.45$ . Based upon observations which are summarized via Figure 8-2, all of the model calculations to be discussed incorporated the  $T_f$  iteration loop in the FORTRAN code. For those simulated thermal histories involving an isothermal sub- $T_g$  annealing component, the total aging time was divided into 100 logarithmically spaced time steps for the numerical calculations. In order to use the TNM expression, the cooling and heating portions of the thermal cycles must be divided into small temperature steps, each followed by a short annealing period consistent with the cooling/heating rate applied experimentally. It is commonly held<sup>6</sup> that a temperature step ( $\Delta T$ ) of 1.0 K is suitable for most cooling/heating cycles even without an iterative component to the fictive temperature calculation procedure, although an iterative approach is recommended for situations where rapid changes in  $T_f$  occur (e.g. during the heating cycle for a well-annealed glassy material where a high degree of recovery occurs in the  $T_g$  region). The temperature step was varied in this study in order to explore the effect on the calculated relaxation response, and values of  $\Delta T$  equal to 0.25, 0.5 and 1.0 K were employed. No significant effect of the temperature step was evident for the predicted relaxation associated with the thermal histories represented by Figure 8-3 and Figure 8-4 (see figure captions). The temperature

program used to generate Figure 8-3 was essentially a 10 K/min quench followed by a 10K/min heating step (thermal history A). A short anneal of two minutes was included between the cooling and heating components of thermal history A in order to match the relevant experimental cycle. The cycle associated with Figure 8-4, designated as thermal history B, involved a 200 K/min quench, a one hour annealing period at  $T_g-30K$ , and finally a heating phase at 10 K/min back into the equilibrium liquid state. In contrast to these two temperature programs, thermal cycles which resulted in a large degree of glassy relaxation/recovery did exhibit an influence of the temperature step in the glass transition region of the heating portion of the predictions. Figure 8-5 displays the predicted relaxation for a cycle similar to thermal history A with the exception that the cooling rate employed was 1 K/min (thermal history C), and it is clear that the predicted heating response was significantly affected by the value of  $\Delta T$ . Such a problem can be rectified by reducing the temperature step even further. It was discovered that reducing  $\Delta T$  to a value of 0.1 K for thermal history C did not substantially change the predicted variation of  $T_f$  with temperature compared to that obtained using a temperature step equal to 0.25, thus confirming that  $\Delta T \leq 0.25$  was suitable to insure valid predicted results. *What this exercise reveals is that the often utilized temperature step of 1 K may be quite inadequate for some thermal cycles of interest.* A temperature program which results in even greater glassy relaxation/recovery than thermal history C is a quench into the glassy state at 200 K/min followed by 100 hr of annealing at  $T_g-30K$  before a heating program at 10 K/min back into the liquid state (thermal history D). A complete break-down in the numerical predictions was noted in the heating portion of thermal history D as is clearly evident in Figure 8-6. Not only was there a dependence of the glassy recovery response on  $\Delta T$ , but also large discontinuities were noted in all of the predictions in the transition region. Reduction of the temperature step to values of 0.1 K and 0.05 K did not eliminate the apparent failure of the numerical procedure.

Thermal cycles which incite a large degree of enthalpy recovery upon heating through the  $T_g$  region should be treated cautiously with respect to fitting DSC enthalpy recovery traces via the AG/TNM methodology. According to O'Reilly,<sup>28</sup> the temperature step size can also influence TNM calculations which incorporate the Narayanaswamy

function as opposed to the AG function, although slower heating rates greatly diminish the effect by reducing the magnitude of the overshoot in the recovery region. Indeed, this latter feature was evident from the predicted thermal cycles illustrated here; the thermal cycles which resulted in a relatively low degree of recovery during heating through the glass transition temperature region did not display a significant dependence of the predicted heating response on the temperature step size nor was any evidence of a gross discontinuity evident in the predictions. It should be emphasized that the cooling and annealing portions of all the predicted relaxation responses presented herein do not exhibit any features which result in questioning the soundness of the numerical approach which uses cooling/heating temperature steps (absolute values) in the range of 0.25 to 1 K and partitions the aging time as mentioned previously. Modeling experimental data such as isothermal volume relaxation or DSC cooling traces does not appear to be problematic according to these predictions. Unfortunately, the predominant use of the TNM modeling approach involves fitting experimental DSC heating traces using numerical optimization routines. Such an endeavor may provide adequate representation of the data while disguising underlying problems with the numerical procedure. Critical inspection of the physics involved with the models and the comparison of model parameters fit to relaxation data cannot be accomplished in a meaningful fashion if the numerical procedure is suspect.

Another caution to be aware of when fitting DSC heating traces is the presence of temperature gradients in the sample which are not accounted for within the framework of the modeling effort. The temperature gradient across a 0.2 mm thick polymer film sample was determined using a Perkin Elmer DSC 7 for a heating rate of 10 °C/min according to common procedure by placing indium below and on top of the sample. The resulting response can be observed from Figure 8-7 which indicates that the gradient across the sample in the glassy state was approximately 1°C. Such a gradient is expected to have a relatively small influence on the enthalpy recovery behavior, but the artificial broadening and shifting of the glass transition response due to heat transfer considerations is expected to be significant at higher heating rates. The importance of accounting for experimental temperature gradients has been emphasized by Hutchinson and coworkers<sup>29</sup> as well as

O'Reilly and Hodge.<sup>30</sup> In addition, Simon<sup>31</sup> recently developed a modified approach to performing TNM model calculations which incorporates temperature gradients.

### ***8.2.2 Comparison of Predictions with Experimental Data***

A test of the predictive capabilities of the Adam-Gibbs model can now be considered. The nonlinear Adam-Gibbs relaxation time function was incorporated into the TNM phenomenological approach in order to predict nonequilibrium glassy relaxation behavior using parameters specified from the dynamic mechanical response in the equilibrium thermodynamic state above  $T_g$ . Previous discussion has furnished sufficient details about the model and its numerical application to allow an efficient comparison of predictions and data which is unencumbered by background information. Isothermal structural relaxation rates can be predicted from, for example, the annealing portion of the plot given by Figure 8-6. The time dependence of the predicted  $T_f$  during isothermal annealing following a quench from above  $T_g$  at 200°C/min is indicated for the polyimide material in Figure 8-8 for various aging temperatures. The rate of change of fictive temperature with respect to  $\log(\text{aging time})$  was determined from the predictions for annealing times between 1 and 100 hours, a range which corresponds to the experimental time frame employed.<sup>32</sup> This rate can then be converted to an enthalpy relaxation rate ( $b_H$ ) by dividing by the difference between the liquid and glassy heat capacities,  $\Delta C_p$ , and a volume relaxation rate ( $b_V$ ) can be similarly determined by dividing by the difference between the liquid and glassy thermal expansion coefficients,  $\Delta\alpha$  (consult Chapter 7). A comparison of the predicted enthalpy relaxation rates for the polyimide material with the associated experimental data<sup>32</sup> is enabled by inspection of Figure 8-8. Although the magnitudes of the predicted rates are within reason compared to the data, the predictions clearly do not allow adequate representation of the entire data set. A similar conclusion can be drawn from contrasting predicted and experimental volume relaxation rates for atactic polystyrene (Figure 8-10). The parameters which were used to predict the volume relaxation behavior of atactic polystyrene were:  $T_2 = 328\text{K}$ ,  $\Delta\mu = 13.8\text{ kJ/mol}$ ,  $\ln(A) = -30.2$ , and  $\beta = 0.4$ . These relaxation parameters were assigned based upon equilibrium

dynamic mechanical data. Based upon these results, a single set of parameters, based upon knowledge of relaxation behavior above  $T_g$ , appears inadequate to predict structural relaxation rates as a function of aging temperature.

One possible difference between the dynamic mechanical relaxation parameters and those necessary to describe the thermodynamic variables in the glassy state has nothing to do with the additional contribution of nonlinearity but rather the difference between mechanical and volumetric, or enthalpic, relaxation in general. Bero and Plazek<sup>33</sup> noted that the mechanical relaxation time distribution for an epoxy material was significantly broader than the distribution determined from volume measurements. A similar conclusion can be drawn from this present investigation. The AG/TNM method was used to predict DSC heating traces for the polyimide material, and increasing the  $\beta$  parameter without otherwise changing the parameters determined from the DMA data allowed excellent fitting of the data. This is depicted in Figure 8-11. The use of the DMA  $\beta$  parameter predicted a broader glass transition response than was observed experimentally via DSC. In addition, the  $\beta$  parameter necessary to describe the glassy relaxation/recovery behavior varied with thermal history as can be observed from this plot. This data suggests the presence of thermorheological complexity, but the TNM formalism does not allow the incorporation of this feature.

The critical test in this study, as was mentioned earlier, is whether the AG/TNM modeling approach can generate the trend observed between aging rates and glass transition cooperativity. The index of glass transition cooperativity which was used to characterize and distinguish the various glassy polymers investigated was the cooperative domain size at  $T_g$ ,  $z_g$ , and it is important that Chapter 7 be consulted regarding this parameter and its determination. The experimental results are reproduced from Chapter 7 in Figure 8-12, and it is evident from this data that more cooperative (fragile) glass formers display slower aging rates during annealing in the glassy state at a temperature of  $T_g-30^\circ\text{C}$ . Calculations using the AG/TNM model were also performed using  $\beta$  values of 0.3, 0.45, and 0.6 (see Figure 8-12 caption for modeling details), and these predictions are plotted in Figure 8-12 along with the experimental data. The AG/TNM predictions are consistent with the data trend; the shape of the predicted curves match that exhibited by

the data including the sharp upturn at the lower end of the  $z_g$  spectrum. It should be mentioned that the glass-forming polymers which are represented by Figure 8-12 possessed equilibrium DMA values of  $\beta$  which were largely in the range of 0.3 to 0.45. Therefore, the AG/TNM calculations underpredict the experimental data slightly, a feature which may be associated with the difference between the mechanical relaxation time distribution and the distributions associated with the thermodynamic variables in the glassy state. A broad correlation between  $\beta$  and  $z_g$  was also noted in this study (Chapter 7) which again suggests the need for including thermorheological complexity in the prediction of relaxation for glass formers. If the  $\beta$  parameter was allowed to decrease with increasing  $z_g$ , the shape of the experimental trend could be captured to an even greater extent with the exception of the outlier at the highest  $z_g$  value which was mentioned in Part 1. In general, the Adam-Gibbs model does pass the critical examination posed by the aging rate vs.  $z_g$  data trend, and the model certainly earns some degree of merit as a predictive tool in the process.

### 8.3 Conclusions

This investigation scrutinized the ability of the nonlinear Adam-Gibbs relaxation time function to predict structural relaxation behavior in the nonequilibrium glassy state using the vehicle of the Tool-Narayanaswamy-Moynihan methodology. It was observed that the use of a single set of parameters determined from the linear dynamic mechanical response above  $T_g$  cannot provide a detailed prediction of the structural relaxation behavior. For example, the magnitude of each predicted aging rate was in the general vicinity of the experimental data, but the detailed variation of isothermal structural relaxation rates with aging temperature could not be decently captured. The relaxation time distribution which was inferred by fitting DSC data of an amorphous polyimide material was narrower (lower  $\beta$  value) than that determined from the dynamic mechanical loss data in the  $\alpha$ -relaxation, and the  $\beta$  parameter exhibited a dependence on the DSC thermal history. Despite the shortcomings of the Adam-Gibbs model, the AG/TNM

approach could predict the experimentally observed link between aging rates and glass transition cooperativity, a link which represents a rigorous test of relaxation models. The correlation generated via the AG/TNM modeling effort slightly underpredicted the experimental data, however, which may be a manifestation of mechanical relaxation time distributions which are broader than the comparable distributions assessed from volume and enthalpy characteristics.

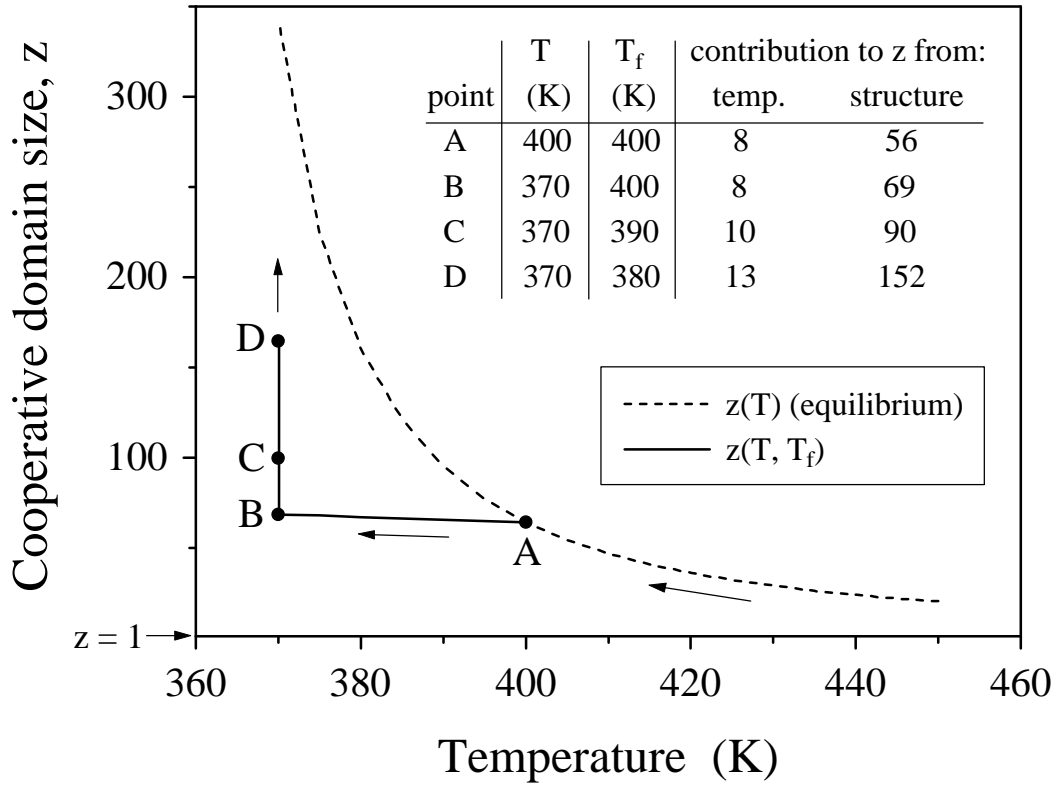


Figure 8-1. Illustration of the temperature and structure contributions to the most probable cooperative domain size. The calculations use a  $T_g$  (during cooling as shown) equal to 400 K and a value of 350 K for  $T_2$ . For illustrative purposes, it is assumed that limited structural relaxation occurs during cooling from A to B such that the fictive temperature remains constant in the glassy state until annealing is commenced at 370 K.

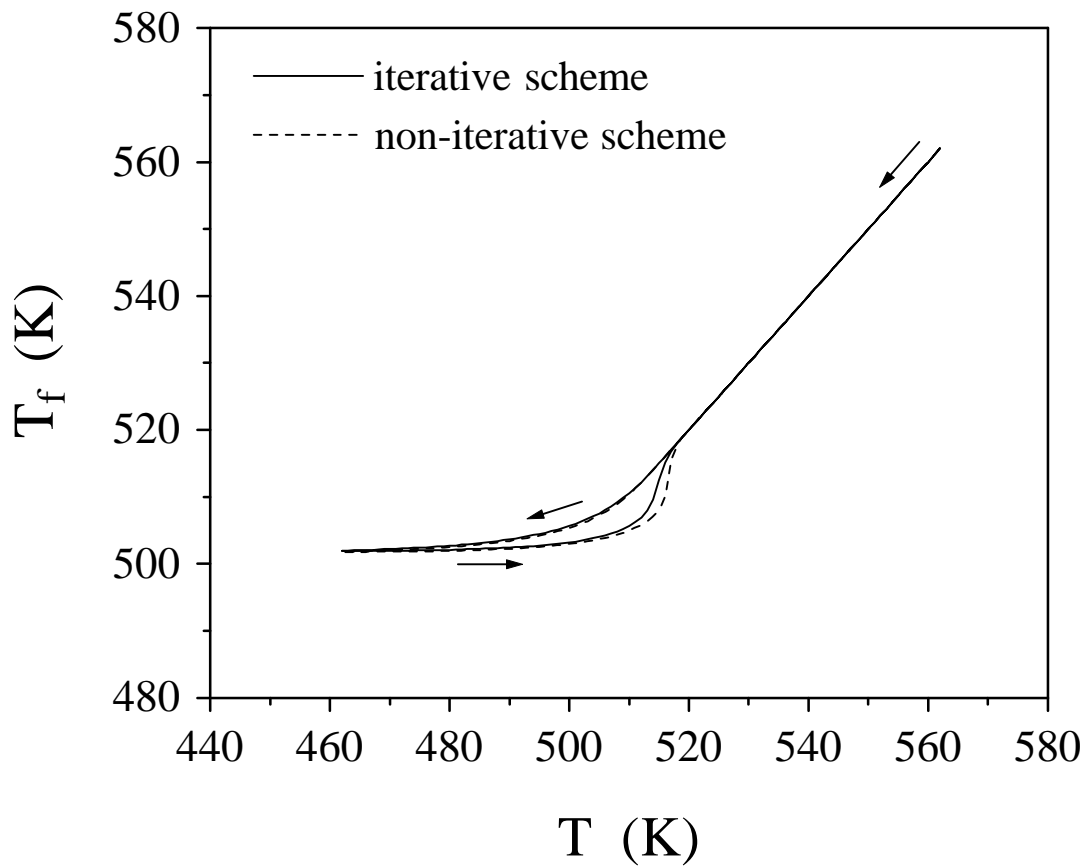


Figure 8-2: AG/TNM predictions for thermal history involving cooling from  $T_g+50\text{K}$  at  $1\text{K}/\text{min}$ , annealing for 2 minutes at  $T_g-50\text{K}$ , and heating to  $T_g+50\text{K}$  at  $10\text{K}/\text{min}$ . The model parameters employed were assessed from DMA data for the polyimide material. The curves indicate the influence of including an iterative procedure for  $T_f$  evaluation during the numerical prediction using a temperature step size of  $1.0\text{ K}$ .

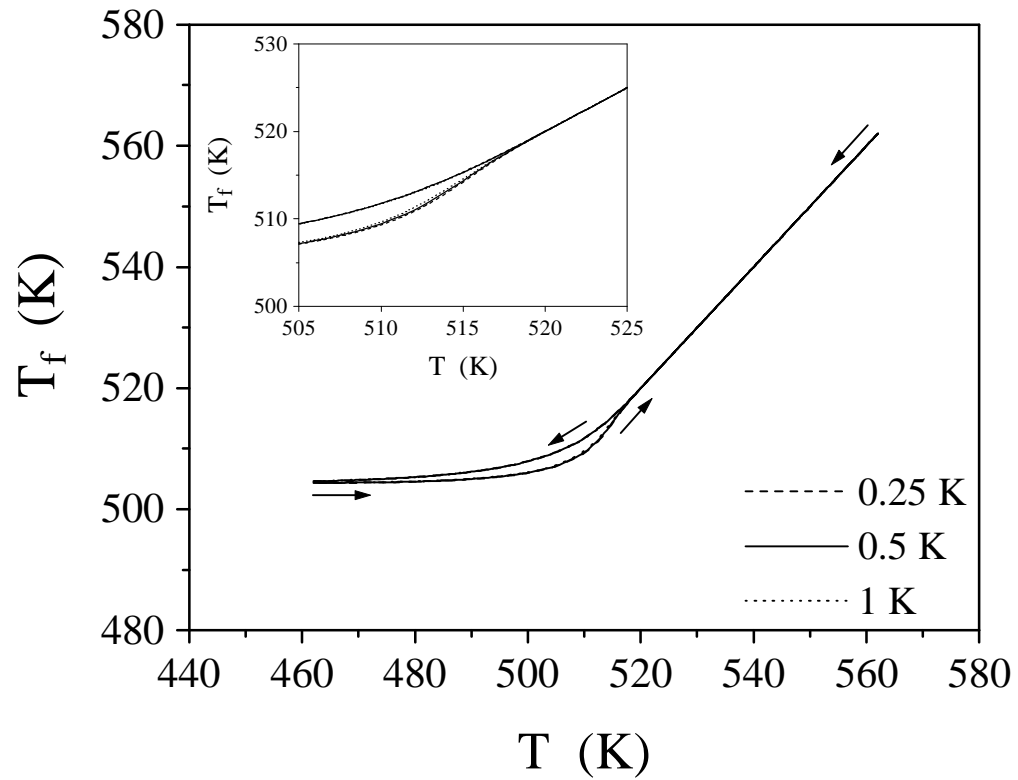


Figure 8-3: AG/TNM predictions for thermal history involving cooling from  $T_g+50K$  at  $10K/min$ , annealing for 2 minutes at  $T_g-50K$ , and heating to  $T_g+50K$  at  $10K/min$ . The model parameters employed were assessed from DMA data for the polyimide material. The curves represent the different temperature steps employed in the numerical technique.

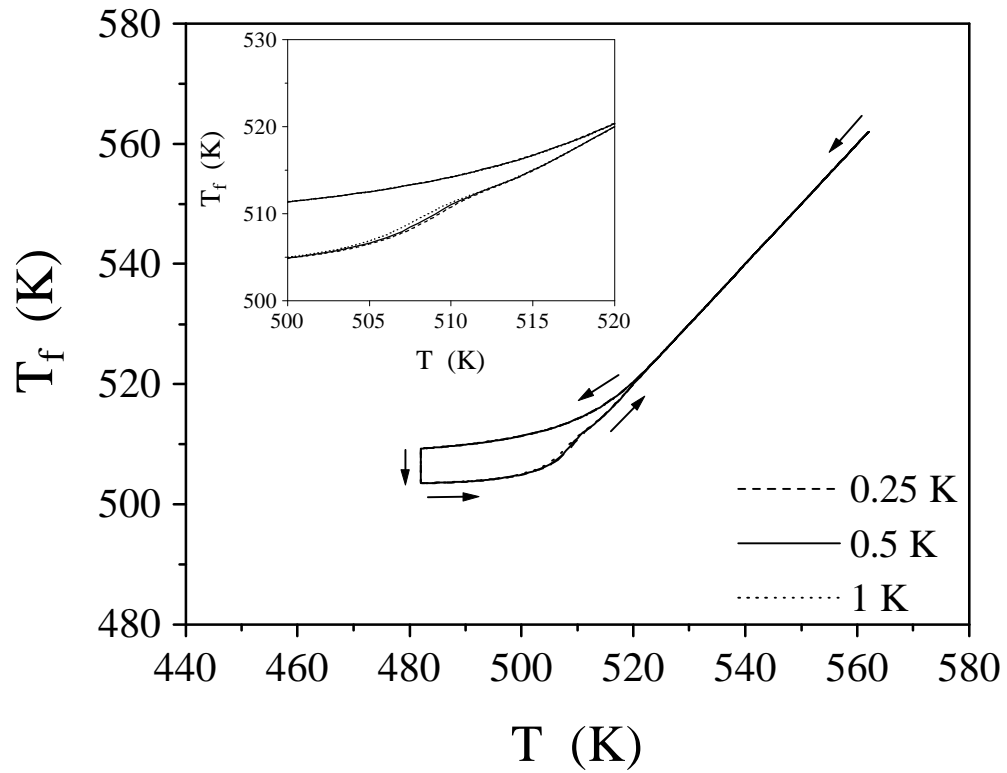


Figure 8-4: AG/TNM predictions for thermal history involving cooling from  $T_g+50K$  at  $200K/min$ , annealing for 1 hour at  $T_g-30K$ , and heating to  $T_g+50K$  at  $10K/min$ . The model parameters employed were assessed from DMA data for the polyimide material. The curves represent the different temperature steps employed in the numerical technique.

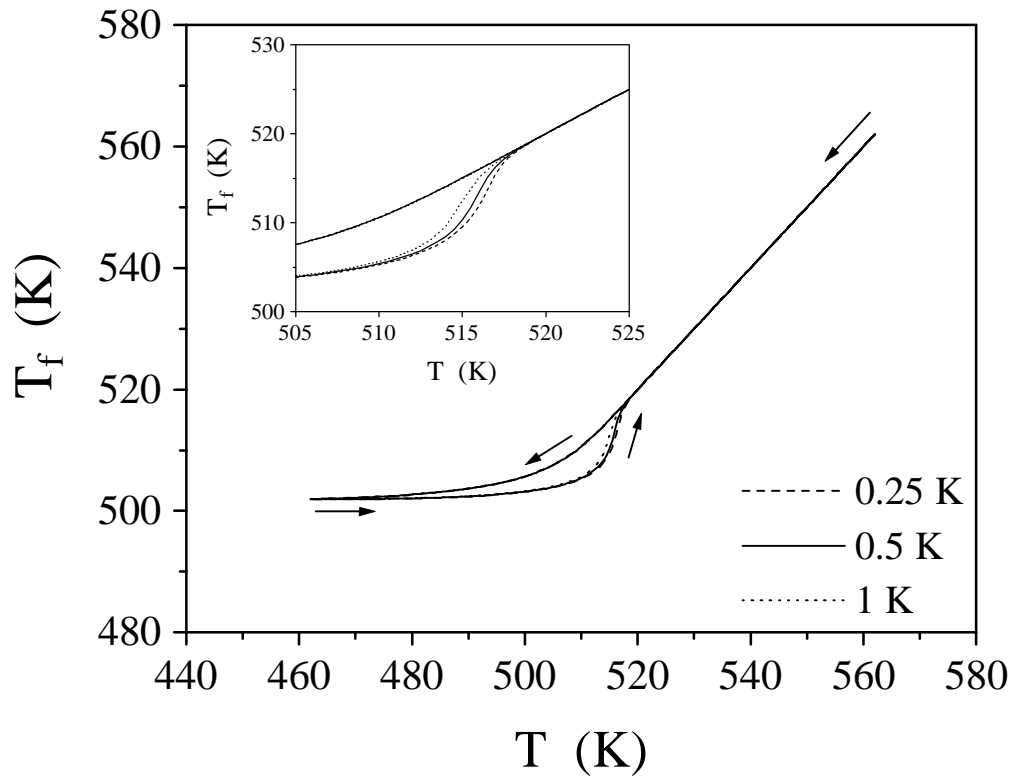


Figure 8-5: AG/TNM predictions for thermal history involving cooling from  $T_g+50K$  at  $1K/min$ , annealing for 2 minutes at  $T_g-50K$ , and heating to  $T_g+50K$  at  $10K/min$ . The model parameters employed were assessed from DMA data for the polyimide material. The curves represent the different temperature steps employed in the numerical technique.

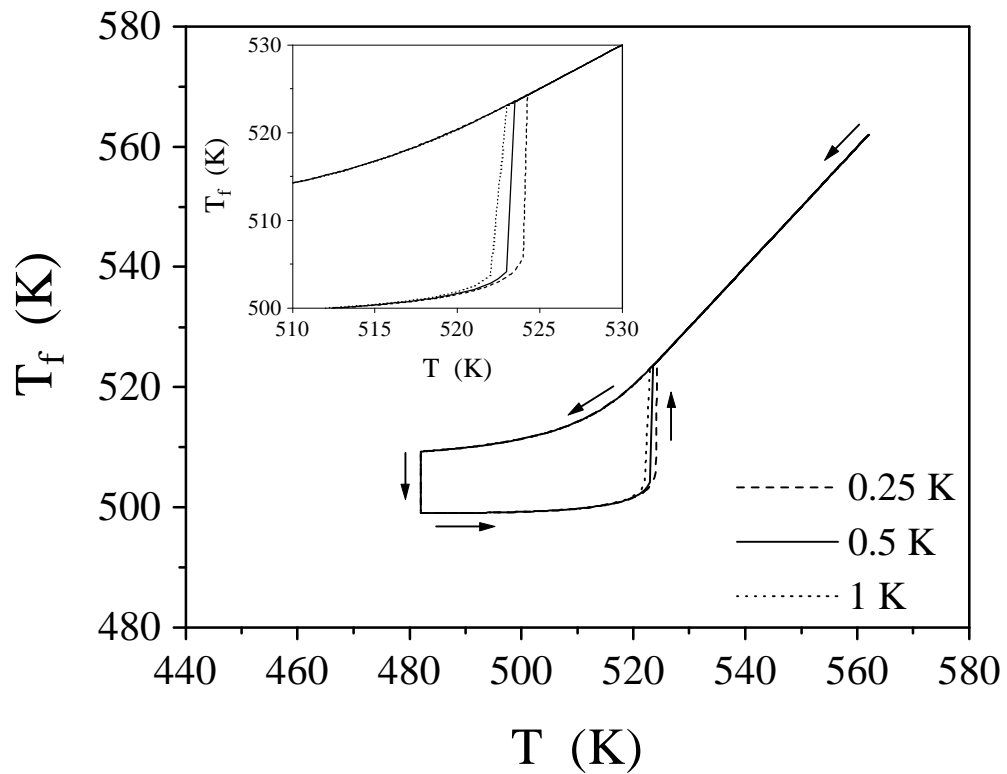


Figure 8-6: AG/TNM predictions for thermal history involving cooling from  $T_g+50K$  at  $200K/min$ , annealing for 100 hours at  $T_g-30K$ , and heating to  $T_g+50K$  at  $10K/min$ . The model parameters employed were assessed from DMA data for the polyimide material. The curves represent the different temperature steps employed in the numerical technique.

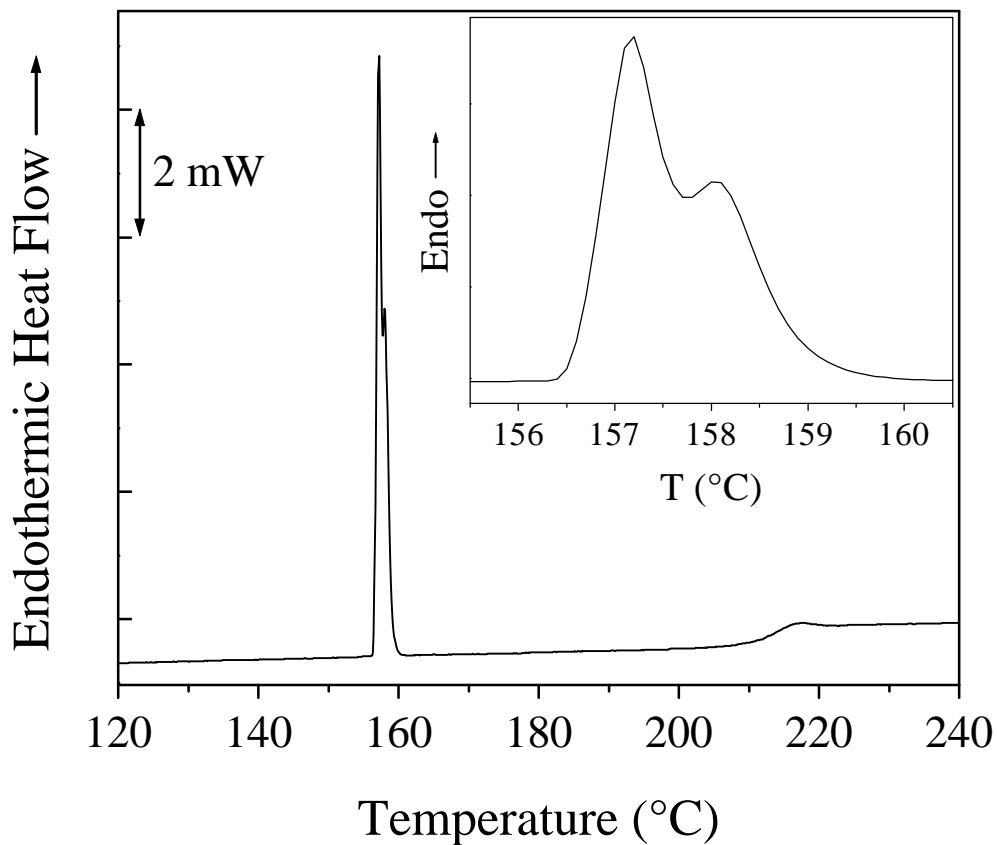


Figure 8-7: DSC heating scan at 10°C/min for a poly(2,6-dimethyl-1,4-phenylene oxide) (PPO) film sample (thickness approx. 0.2 mm) sandwiched between two indium samples. Indium (1.6 mg) was melted in the DSC pan, the PPO sample (8.3 mg) was then placed in the pan, and additional indium (1.0 mg) was melted on top. A lid was finally placed on top and the pan was crimped. A quench from above the  $T_g$  of PPO into the glassy state at 200°C/min was then performed prior to the heating scan at 10°C/min shown in the figure.

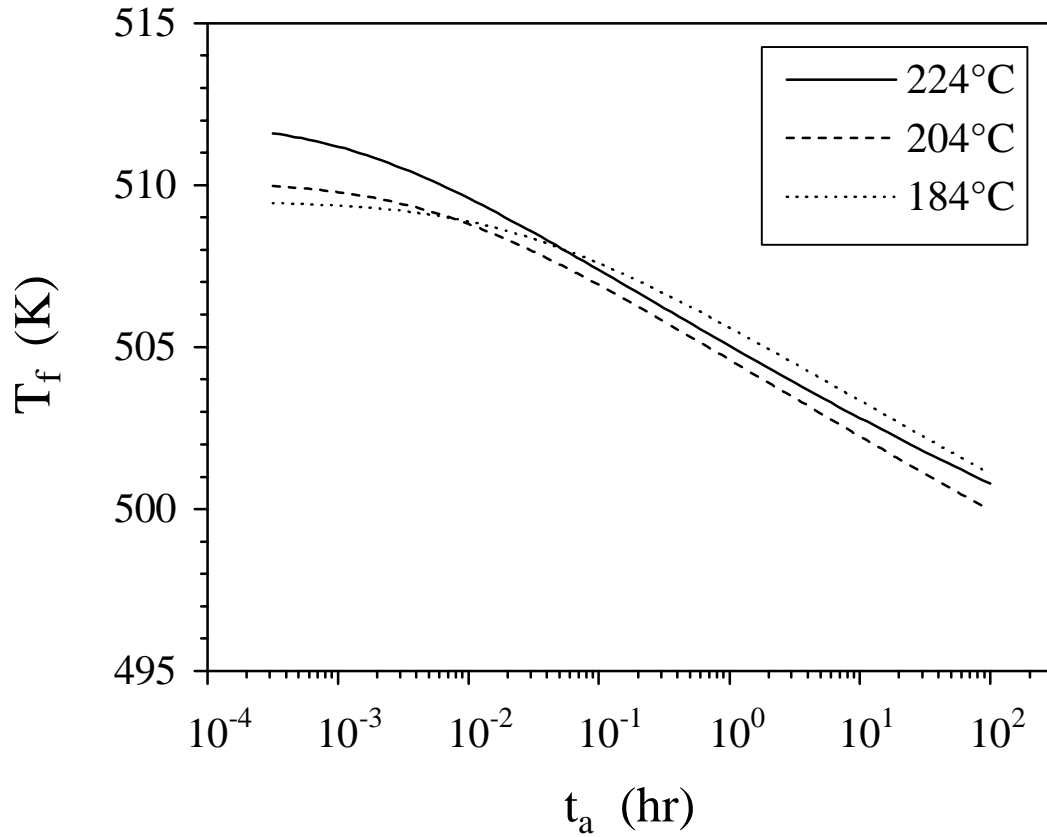


Figure 8-8: AG/TNM predictions during annealing at the indicated aging temperatures following a quench from  $T_g+50K$  ( $289^\circ C$ ) at  $200K/min$ . The model parameters employed were assessed from DMA data for the polyimide material. The negative rate of change of the predicted  $T_f$  with respect to  $\log(t_a)$  was evaluated for aging times between 1 and 100 hours for each annealing temperature and converted to a  $b_H$  value by division by  $\Delta C_p$ .

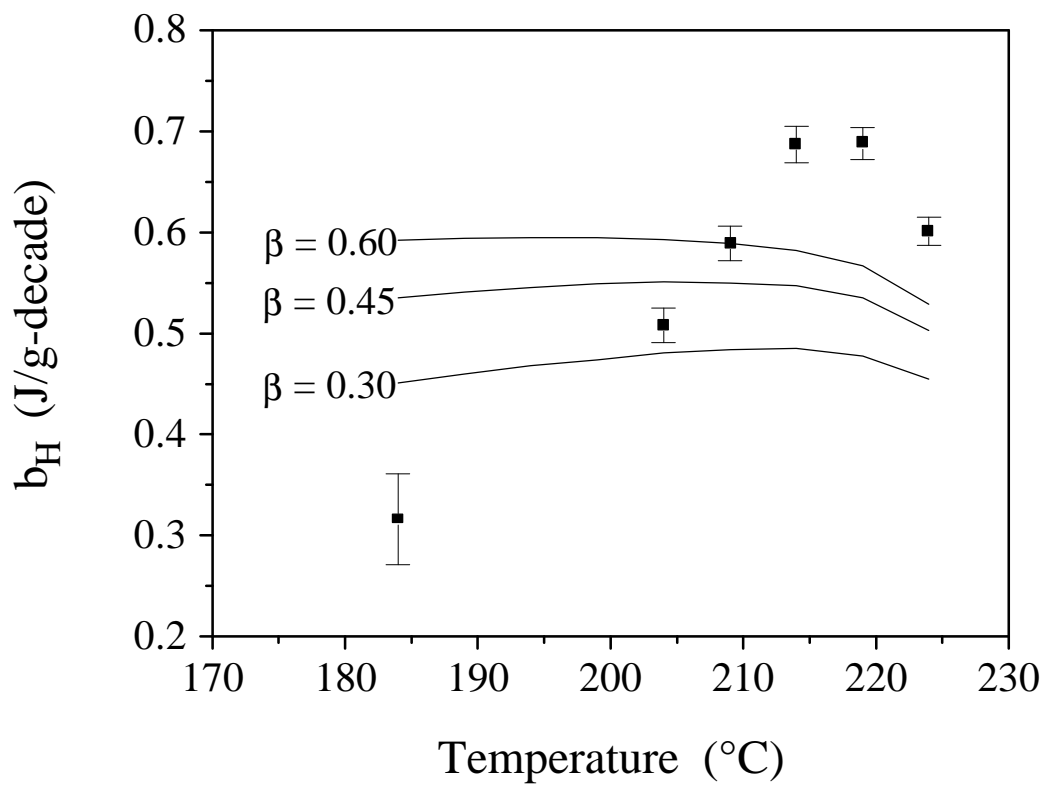


Figure 8-9: Comparison of AG/TNM predictions and experimental enthalpy relaxation rate data for the polyimide material ( $T_g = 239^\circ\text{C}$ ). The  $\beta$  parameter was varied as indicated in the plot ( $\beta = 0.45$  for DMA data).

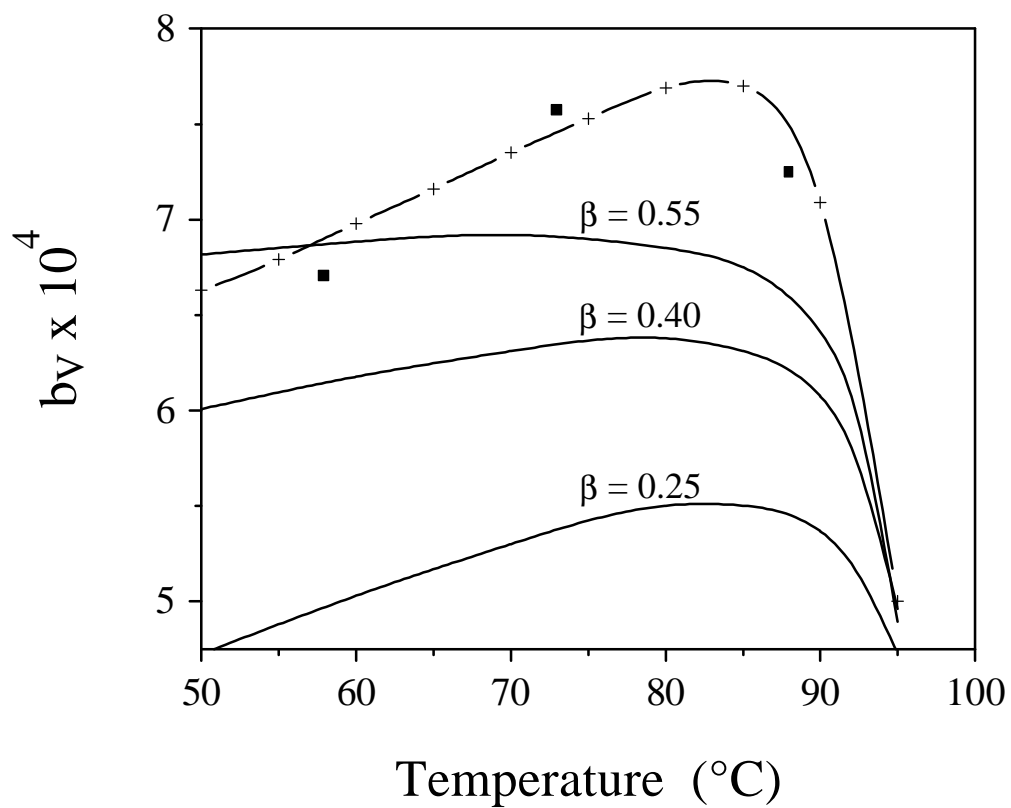


Figure 8-10: Volume relaxation rates for atactic polystyrene. Plotted are the experimental data trend from Greiner and Schwarzl (— + —) and this work (■). Also indicated are AG/TNM predictions using the given values of the  $\beta$  parameter ( $\beta = 0.4$  for DMA data).

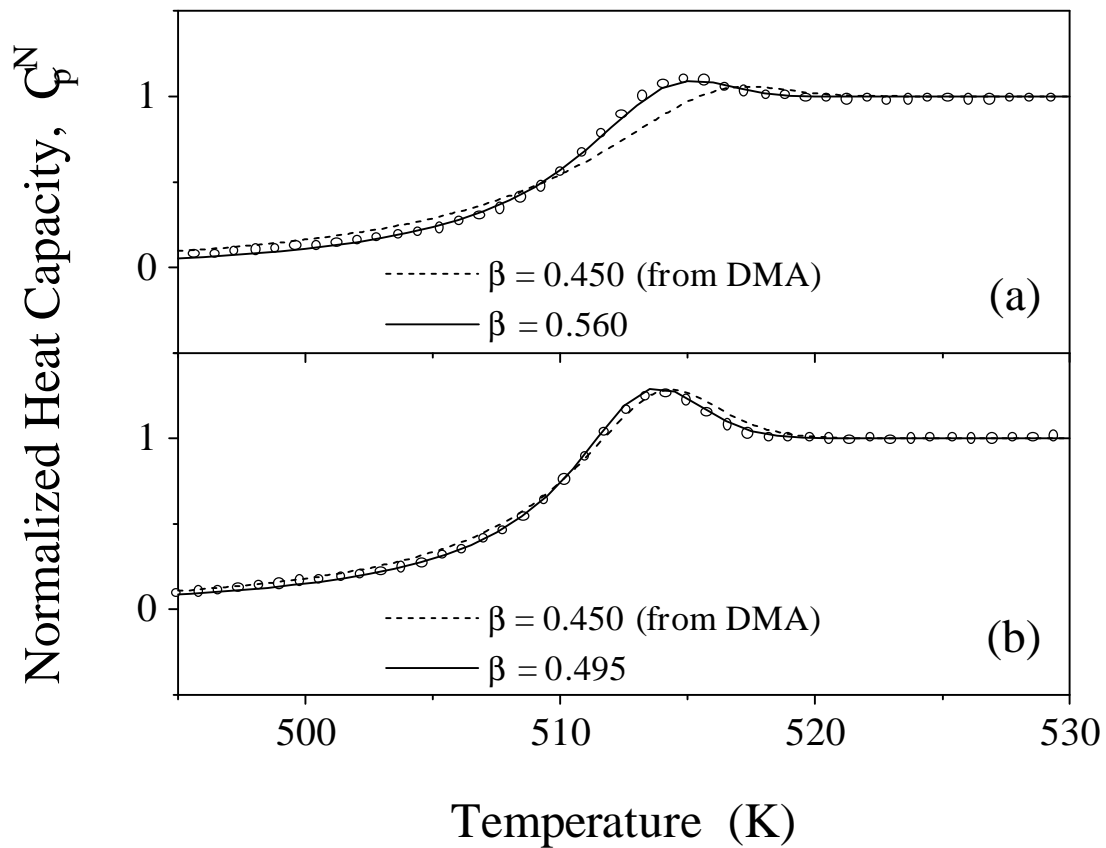


Figure 8-11: Comparison of AG/TNM predictions (lines) and normalized experimental DSC heating traces (symbols) at 10°C/min for the polyimide material following cooling from  $T_g+50^\circ\text{C}$  at: (a) 100°C/min; and (b) 10°C/min. A short hold of 2 minutes at  $T_g-50^\circ\text{C}$  was performed after the quench and prior to the heating scan. Refer to Chapter 7 for experimental details.

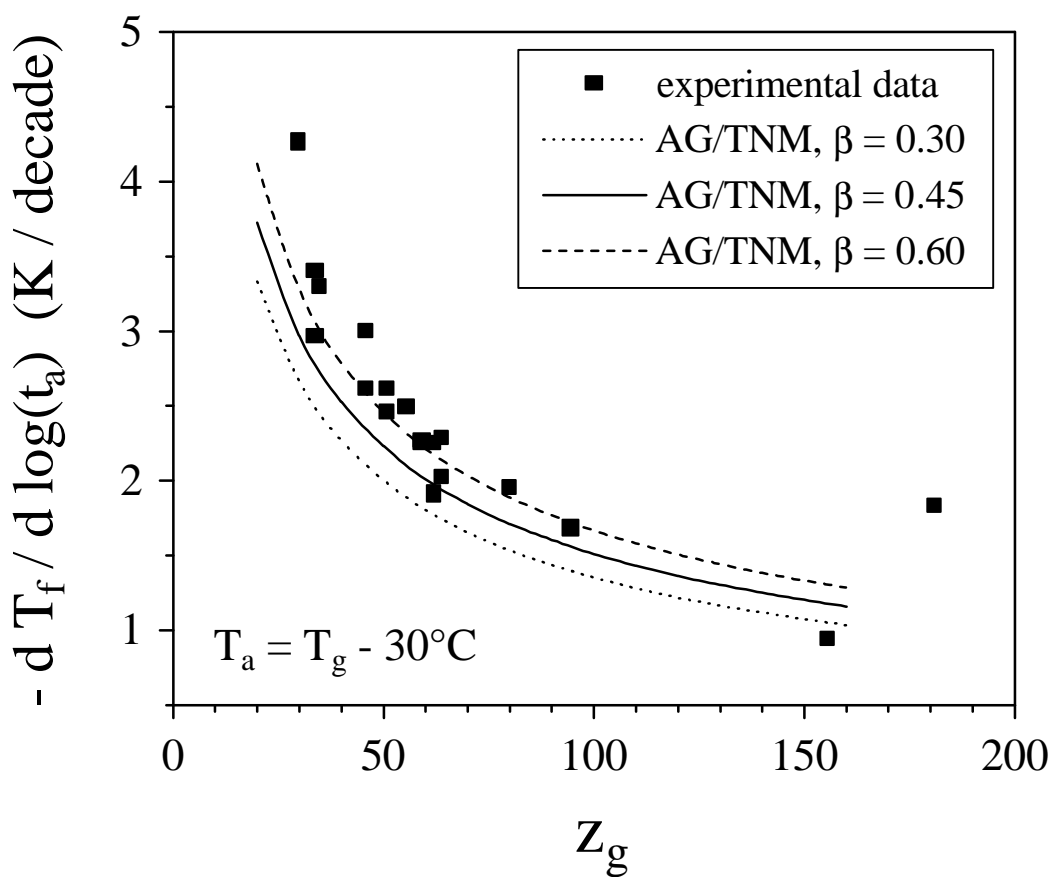


Figure 8-12: Apparent correlation between structural relaxation rates at  $T_g-30^\circ\text{C}$  and glass transition cooperativity (data from part 1). For the predictions,  $\tau_g = 100$  sec,  $T_g = 400$  K,  $C_{1,g} = 16$ , and  $C_{2,g}$  was varied between 31.6 and 89.4 K to give  $z_g$  which varied from 160 to 20.

#### 8.4 References

- <sup>1</sup> Adam, G.; Gibbs, J. H. *J. Chem. Phys.* 1965, 43, 139.
- <sup>2</sup> Scherer, G. W. *J. Am. Ceram. Soc.* 1984, 67, 506.

- 3 Scherer, G. W. *J. Am. Ceram. Soc.* 1986, 69, 374.
- 4 Crichton, S. N.; Moynihan, C. T. *J. Non-Cryst. Solids*, 1988, 102, 222.
- 5 Hodge, I. M. *Macromolecules* 1987, 20, 2897.
- 6 Hodge, I. M. *J. Non-Cryst. Solids*, 1994, 169, 211.
- 7 Hodge, I. M. *J. Res. Natl. Inst. Stand. Technol.* 1997, 102, 195.
- 8 Angell, C. A. *J. Res. Natl. Inst. Stand. Technol.* 1997, 102, 171.
- 9 Gibbs, J. H.; DiMarzio, E. A. *J. Chem. Phys.* 1958, 28, 373.
- 10 Williams, M. L.; Landel, R. F.; Ferry, J. D. *J. Am. Ceram. Soc.* 1955, 77, 3701.
- 11 DiMarzio, E. A.; Yang, A. J. M. *J. Res. Natl. Inst. Stand. Technol.* 1997, 102, 135.
- 12 O'Connell, P. A.; McKenna, G. B. *Proc. NATAS 25<sup>th</sup> Annual Conference* 1997, 420.
- 13 O'Connell, P. A.; McKenna, G. B. *Proc. SPE ANTEC '98* 1998, II, 2152.
- 14 Tool, A. Q. *J. Am. Ceram. Soc.* 1946, 29, 240.
- 15 Tool, A. Q. *J. Res. Natl. Bur. Stand.* 1946, 37, 73.
- 16 Narayanaswamy, O. S. *J. Am. Ceram. Soc.* 1971, 54, 491.
- 17 Moynihan, C. T.; Easteal, A. J.; DeBolt, M. A.; Tucker, J. *J. Am. Ceram. Soc.* 1976, 59, 12.
- 18 Moynihan, C. T.; et al. *Ann. NY Acad. Sci.* 1976, 279, 15.
- 19 Kovacs, A. J.; Aklonis, J. J.; Hutchinson, J. M.; Ramos, A. R. *J. Polym. Sci., Polym. Phys. Ed.* 1979, 17, 1097.
- 20 McKenna, G. B. in *Comprehensive Polymer Science, Vol. 2, Polymer Properties* (eds. C. Booth and C. Price), Pergamon, Oxford, 1989.
- 21 Kohlrausch, R. *Pogg. Ann. Phys.* 1854, 91, 198.
- 22 Williams G.; Watts, D. C. *Trans. Faraday Soc.* 1970, 66, 80.
- 23 Mijovic, J.; Nicolais, L.; D'Amore, A.; Kenny, J. M. *Polym. Eng. Sci.* 1994, 34, 381.
- 24 Matsuoka, S.; Quan, X. *Macromolecules* 1991, 24, 2770.
- 25 Matsuoka, S.; Quan, X. *J. Non-Cryst. Solids* 1991, 131-133, 293.
- 26 Matsuoka, S. *J. Res. Natl. Inst. Stand. Technol.* 1997, 102, 213.
- 27 Hodge, I. M.; Berens, A. R. *Macromolecules* 1982, 15, 762.
- 28 J. M. O'Reilly, personal communication.
- 29 Hutchinson, J. M.; Ruddy, M.; Wilson, M. R. *Polymer* 1988, 29, 152.
- 30 O'Reilly, J. M.; Hodge, I. M. *J. Non-Cryst. Solids* 1991, 131-133, 451.
- 31 Simon, S. L. *Macromolecules* 1997, 30, 4056.
- 32 Robertson, C. G.; Monat, J. E.; Wilkes, G. L. "Physical Aging of an Amorphous Polyimide: Enthalpy Relaxation and Mechanical Property Changes", *J. Polym. Sci.: Part B: Polym. Phys.*, accepted for publication.
- 33 Bero, C. A.; Plazek, D. J. *J. Polym. Sci.: Part B: Polym. Phys.* 1991, 29, 39.

# Chapter 9

## Physical Aging of an Amorphous Polyimide: Enthalpy Relaxation and Mechanical Property Changes

---

---

### Chapter Synopsis

The physical aging behavior of an isotropic amorphous polyimide possessing a glass transition temperature of approximately 239°C was investigated for aging temperatures ranging from 174 to 224°C. Enthalpy recovery was evaluated as a function of aging time following sub- $T_g$  annealing in order to assess enthalpy relaxation rates, and time-aging time superposition was employed in order to quantify mechanical aging rates from creep compliance measurements. With the exception of aging rates obtained for aging temperatures close to  $T_g$ , the enthalpy relaxation rates exhibited a significant decline with decreasing aging temperature while the creep compliance aging rates remained relatively unchanged with respect to aging temperature. Evidence suggests distinctly different relaxation time responses for enthalpy relaxation and mechanical creep changes during aging. The frequency dependence of dynamic mechanical response was probed as a function of time during isothermal aging, and failure of time-aging time superposition was evident from the resulting data. Compared to the creep compliance testing, the dynamic mechanical analysis probed the shorter time portion of the relaxation response which involved the additional contribution of a secondary relaxation, thus leading to failure of superposition. Room temperature stress-strain behavior was also monitored after aging at 204°C, with the result that no discernible embrittlement due to physical aging was detected despite aging-induced increases in yield stress and modulus.

## 9.1 Introduction

The inherent nonequilibrium nature of the glassy state causes amorphous materials to be characterized by time-dependent changes in properties when utilized at temperatures below the glass transition temperature region, a feature known as physical aging. The rapidly decreasing mobility as the glass transition temperature region is approached during cooling from the equilibrium liquid state prevents the maintenance of thermodynamic equilibrium as vitrification occurs. This kinetic process results in a thermodynamic driving force in the glassy state which causes the volume, enthalpy, and entropy to exhibit decreases during annealing, and these decreases are enabled by localized segmental motion. This time-dependent behavior which is observed for the thermodynamic properties of the glassy state is often referred to as structural relaxation, although the term physical aging also applies in a more general sense. In turn, the changing thermodynamic state affects such important characteristics as mechanical, barrier, and optical properties.<sup>1-3</sup>

Studies concerned with the physical aging of amorphous polymer materials with glass transition temperatures in excess of 200°C have been quite limited in comparison to research on their lower- $T_g$  counterparts. The research investigation to be disclosed in this communication involves the physical aging of a commercial polyimide material with a high glass transition temperature of 239°C. Previous research efforts which studied the physical aging of poly(ether imide) (PEI) and other amorphous polyimide materials are of particular relevance to this work and will first be briefly reviewed.

Physical aging investigations have been performed on the engineering polymer poly(ether imide) ( $T_g \approx 210^\circ\text{C}$ ), and the first reported study of the time-dependent nature of this polymer in the nonequilibrium glassy state was performed by Hay et al.<sup>4,5</sup> This research effort investigated the enthalpy recovery behavior of PEI, and the time to reach enthalpic equilibrium was assessed as a function of aging temperature. The times to reach equilibrium for the variable of enthalpy were found to be comparable to equilibrium relaxation times for the glass transition ( $\alpha$ -relaxation) region determined from dielectric and dynamic mechanical analyses. These researchers<sup>4</sup> also suggested that structural relaxation does not occur at all below the temperature asymptote where the  $\alpha$ -

relaxation times appear to diverge to infinity (i.e. a kinetic temperature limit or a possible true thermodynamic glass transition temperature), a conjecture which is questionable given experimental evidence otherwise.<sup>6-9</sup>

The physical aging response of PEI has also been studied by Brennan and Feller<sup>10</sup> for aging temperatures within a very extensive range of  $T_g-140^\circ\text{C}$  to  $T_g-20^\circ\text{C}$ . These researchers studied enthalpy recovery as well as changes in dynamic mechanical properties and room temperature stress-strain behavior for PEI. The physical aging process induced an increase in yield stress and a decrease in strain at break, and the severity of both of these changes appeared to diminish as the aging temperature was decreased. Changes in the frequency response of storage modulus due to physical aging were used to assess aging rates using time-aging time superposition with the result of obtaining uncharacteristically high aging rates for the aging temperatures close to the glass transition temperature. These authors also noted a reduction in the strength of a secondary dynamic mechanical relaxation ( $\beta$ -relaxation) due to the physical aging process. Enthalpy relaxation/recovery was also examined for the PEI material, although a quantitative determination of relaxation rates was not made.

The time-dependence of enthalpy and dynamic storage modulus in the glassy state of PEI was considered by Yoshida<sup>11</sup> for aging temperatures from 10 to  $25^\circ\text{C}$  below the glass transition temperature. Nonexponential decay functions with a time-independent relaxation time parameter (i.e. linear decay functions) were applied to the data and characteristic relaxation times were found to be essentially equivalent for enthalpy relaxation and the time-dependent behavior of storage modulus. This implies a strong connection between the changing structural state and the dynamic mechanical response during physical aging. However, the application of a linear decay function to glassy state relaxations may be inappropriate as will be discussed later.

An excellent examination of the nonequilibrium glassy nature of PEI was performed by Simon, Plazek, and coworkers.<sup>12-14</sup> This study evaluated volume relaxation, enthalpy relaxation/recovery, and creep compliance response changes for PEI. The relaxation of these properties was contrasted for aging performed at an aging temperature which was  $9.5^\circ\text{C}$  below the fictive temperature for a freshly quenched sample,  $T_{f,0}$ . Of great significance was the observation that the time to reach equilibrium

was the same for volume, enthalpy, and mechanical response at this aging temperature. However, the approach toward equilibrium displayed different behavior for the three properties. This investigation also included a modeling endeavor by Simon<sup>14</sup> which was employed in an attempt to provide an adequate phenomenological description of the enthalpy recovery behavior.

The nonequilibrium glassy behavior of a polyimide material was studied by Venditti and Gillham<sup>15</sup> by following changes in free-oscillation torsional response due to physical aging. A polyamic acid was synthesized from benzophenone tetracarboxylic acid dianhydride and from two aromatic diamines which were oxy-dianiline and meta-phenylene-dianiline. This polyamic acid was fully imidized on a glass fiber braid to form a polyimide material with a glass transition temperature of approximately 304°C, and the viscoelastic behavior was subsequently characterized using torsional braid analysis. The viscoelastic response was monitored during isothermal aging for an impressive aging temperature range of 10 to 282°C, and, in addition, the temperature dependence of dynamic response was evaluated after aging and compared to the scan for a freshly quenched (unaged) sample. Isothermal physical aging rates for the dynamic mechanical properties declined as the aging temperature was decreased, but the rates were still nonzero even at the lowest temperatures investigated and appeared to be influenced by the presence of a secondary relaxation. According to the authors, the physical aging could be thermally reversed by heating to temperatures above the aging temperature but still below  $T_g$  for aging performed deep within the glassy state, because the temperature region of aging recovery was localized about the aging temperature at these large undercoolings.

Research studies on the physical aging response of high- $T_g$  amorphous polymers are limited in number, but this fact does not reflect a lack of importance concerning research in this area. Changes in properties at ambient temperature are anticipated to be slow for glassy polymers with high glass transition temperatures because this end-use temperature is far below  $T_g$ . However, these materials are often utilized at much higher temperatures. The ability to employ these polymers as rigid structural materials at high temperatures is a desirable feature, but these application temperatures are much closer to the glass transition temperature where physical aging becomes a significant concern.

This provides justification for the present research investigation which is concerned with the time-dependent glassy behavior of a commercial polyimide material with a high glass transition temperature ( $T_g \approx 239^\circ\text{C}$ ). Thermodynamic changes in the glassy state of this polyimide are followed using enthalpy relaxation/recovery measurements, and changes in the mechanical response are monitored by means of creep compliance, dynamic mechanical, and stress-strain testing techniques. An attempt to interrelate the physical aging of mechanical performance with the rate of structural relaxation is also made. A focused physical aging study, such as the investigation to be disclosed, inevitably contributes in a more general sense due to the current lack of fundamental and comprehensive understanding of the glass transition and the nonequilibrium glassy state. The study of high- $T_g$  polymers with relatively stiff backbone structures may assist in developing an understanding of how the kinetics of glass formation and physical aging correlate with chemical features, both intramolecular and intermolecular.

## 9.2 Experimental Details

### 9.2.1 Material

The material used in this investigation is a commercial polyimide material produced by Mitsui Toatsu Chemicals, Inc. Specifically, this material is an amorphous polyimide in the Regulus<sup>®</sup> series of polyimides. This polymer is reportedly comprised of the molecular repeat unit given in Figure 9-1 in addition to a proprietary comonomer, the incorporation of which is intended to eliminate the possibility of crystallization through disruption of chain symmetry.<sup>16</sup> Inspection of the wide angle x-ray scattering pattern revealed only a diffuse amorphous halo with absolutely no evidence of crystalline diffraction for a polyimide sample which had been annealed for 30 minutes at a temperature of  $50^\circ\text{C}$  above the glass transition temperature region, thus confirming the wholly amorphous character of this polyimide. In addition, no evidence of crystallinity was detected via DSC for a polyimide sample with the same thermal history. The polyimide material was obtained in film form with a thickness of approximately 0.1 mm, and a minor amount of biaxial orientation in the as-received film was inferred via

approximately 2% shrinkage of the film after heating to above the glass transition temperature region. This did not affect this investigation, however, because samples were freshly quenched after free annealing above the glass transition temperature prior to all testing. Calorimetric information for this polyimide was obtained at a heating rate of 10°C/min using a Perkin Elmer (model DSC 7) differential scanning calorimeter (DSC). The inflection, or midpoint, glass transition temperature ( $T_g$ ) at this rate was measured to be 238.9°C ( $\pm 0.2^\circ\text{C}$ ) and the difference in liquid and glass heat capacities at the glass transition temperature,  $\Delta C_{p,g}$ , was determined to be 0.236 J/g-K ( $\pm 0.002$  J/g-K). This data reflects the average thermal behavior for over 10 samples which were freshly quenched in the DSC from the equilibrium liquid state into the glassy state at 200°C/min just prior to testing. The equilibrium liquid state referred to here is the state of a sample after annealing at 50°C above  $T_g$  for 10 minutes. Because the kinetic glass transition temperature mentioned above was obtained in heating as opposed to cooling, it may be more appropriate to discuss this transition temperature as a fictive temperature ( $T_f$ ), or structural temperature.<sup>17</sup> The value of the fictive temperature for freshly quenched samples of the polyimide,  $T_{f,0}$ , was 238.4°C ( $\pm 0.2^\circ\text{C}$ ), as determined from the DSC scans using the Perkin Elmer analysis software.

### ***9.2.2 Enthalpy Relaxation Study***

Prior to aging, samples weighing approximately 10 mg were loaded in aluminum pans and quenched into the glassy state at 200°C/min in a Perkin Elmer (model DSC 7) differential scanning calorimeter after annealing at  $T_g+50^\circ\text{C}$  for 10 minutes. Samples were then aged isothermally at 184, 204, 209, 214, 219, and 224°C ( $\pm 0.5^\circ\text{C}$ ) in ovens under a nitrogen purge for aging times ranging from 1 to 300 hours. Each sample was then scanned in the DSC from  $T_g-50^\circ\text{C}$  to  $T_g+50^\circ\text{C}$  using a heating rate of 10°C/minute (first heat). In order to provide an unaged reference with which to compare an aged DSC trace, each sample was then annealed in the DSC at  $T_g+50^\circ\text{C}$  for 10 minutes, quenched at 200°C/min, and scanned from  $T_g-50^\circ\text{C}$  to  $T_g+50^\circ\text{C}$  at 10°C/minute (second heat). It was necessary to hold the sample for 2 minutes at  $T_g-50^\circ\text{C}$  to allow precise control of the heat signal before initiation of the second heat, and it is expected that this short amount of time at this low temperature has a negligible effect on the structural state of the sample.

Extent of enthalpy relaxation was determined from the first and second heating scans using a method to be described later. Three samples were tested for each aging condition. A third heat was employed in some cases following annealing at  $T_g+50^\circ\text{C}$  for 10 minutes and quenching at  $200^\circ\text{C}/\text{min}$  in order to illustrate, by comparison with the second heat, the thermal stability of the material under the conditions employed during DSC testing. All DSC testing utilized a nitrogen purge. An instrument baseline was generated for every two hours of testing at a heating rate of  $10^\circ\text{C}/\text{minute}$  using empty pans with lids in the reference and sample cells. If a substantial difference was noted between subsequent baseline runs, then any data collected between these baseline scans were discarded. The ice content in the ice/water bath was maintained at approximately 30-50% by volume during all testing. The DSC temperature was calibrated using the melting points of indium and tin, and the heat flow was calibrated using the heat of fusion of indium.

The preparation of the initial glassy sample prior to the aging process is crucial to obtaining aged and reference DSC scans which can be simply shifted along the heat flow axis to provide excellent agreement both below and above the temperature region where enthalpy recovery occurs, alignment which is essential for accurately determining the recovered enthalpy ( $\Delta H$ ). The best preparation involves quenching the encased sample into the glassy state in the DSC using the same cooling rate to be utilized later between the first and second heats. This technique helps to insure that the initial sample is seated well within the DSC pan, does not contain stresses, and has the same structural state as is induced in the sample just prior to the second heating scan. Otherwise, the first heating scan after aging can be influenced thus preventing proper alignment of the aged and reference scans. This can then lead to an erroneous assessment of the recovered enthalpy as has been observed in preliminary work by the present authors. The stability of the instrument baseline is also of great importance as implied earlier.

### ***9.2.3 Tensile Stress-Strain Testing***

Tensile measurements were made at room temperature using an Instron model 4400R mechanical testing apparatus. Dogbone-shaped specimens were cut from the polyimide films and these samples had a thickness of 0.1 mm, a width of 2.75 mm, and a

gauge length of 7 mm. A grip distance of 10 mm was employed during testing, but the gauge length was used in the calculation of strain (a strain extensometer was not utilized). Two crosshead speeds of 2.54 and 25.4 mm/min were used in this mechanical property study. The polyimide film material was free-annealed at  $T_g+50^\circ\text{C}$  for 10 minutes, quenched into the glassy state between two steel plates at room temperature and cut into tensile test specimens. Unaged specimens were tested as well as samples which were first aged at  $204^\circ\text{C}$  in an oven with a nitrogen purge for times of 10, 30, 100, and 300 hours. For each thermal history, ten samples were tested to gain statistical confidence in the measured stress-strain characteristics.

#### ***9.2.4 Creep Compliance Measurements***

The influence of physical aging on tensile creep compliance behavior was assessed during isothermal aging. The small-strain creep response was probed after aging times of 1.5, 3, 6, 12, and 24 hours using the procedure established by Struik. The amount of time that stress was applied to the sample was one-tenth of the cumulative aging time in order to allow any aging which occurred during creep to be neglected. A Seiko thermal mechanical analyzer (model TMA 100) was used with tensile fixtures to test samples possessing a length of 30 mm and a cross sectional area of approximately  $0.3\text{ mm}^2$ . The step stress applied to the samples during the creep measurements was kept small in order to insure that the total strain was small. The majority of total strain values were less than 0.1% and none were greater than 0.3%. The testing was performed on initially unaged samples which were freshly quenched after free-annealing at  $T_g+50^\circ\text{C}$  for 10 minutes. Three samples were tested at each aging temperature. The temperature during isothermal aging varied less than  $1^\circ\text{C}$  along the length of the sample as was verified by altering the position of the thermocouple within the environmental chamber.

#### ***9.2.5 Dynamic Mechanical Analysis***

Dynamic mechanical analysis (DMA) was performed in tensile mode using a Seiko DMS 210. The polyimide film material was free-annealed at  $T_g+50^\circ\text{C}$  for 10 minutes and quenched into the glassy state between two steel plates at room temperature

prior to testing in order to provide isotropic and unaged specimens. The sample dimensions were characterized by a thickness of 0.1 mm, width of 5 mm, and a length suitable to enable a grip-to-grip distance of 20 mm to be employed in the instrument. The dynamic mechanical spectrum of the material was characterized by heating at 2°C/min from -140°C to above the glass transition ( $\alpha$ -relaxation) temperature region using a frequency of 1 Hz. Samples were aged in the dynamic mechanical analyzer at aging temperatures of 174, 184, 204, and 224°C, allowing the dynamic mechanical response to be probed every 15 minutes during aging up to a total aging time of 24 hours. This DMA testing during isothermal physical aging incorporated 13 frequencies ranging from 0.01 to 20 Hz.

### **9.3 Results and Discussion**

This investigation considers the time-dependent nature of the thermodynamic state and associated changes in the mechanical response for an amorphous thermoplastic polyimide material in the nonequilibrium glassy state. Enthalpy relaxation can be assessed indirectly using differential scanning calorimetry, serving as a measure of the changing thermodynamic structural state during the physical aging process. This will be detailed as well as an examination of the influence of aging assessed by changes in tensile stress-strain properties, creep compliance behavior, and dynamic mechanical response. Finally, an introspective discussion will consider some complexities involved in attempting to relate mechanical and structural aging rates.

#### ***9.3.1 Enthalpy Relaxation Rates***

Following a quench from above the glass transition region, the changing thermodynamic state during isothermal annealing in the glassy state is characterized by decreases in volume and enthalpy. Enthalpy relaxation/recovery measurements were utilized in this study as an assessment of the structural relaxation process for the polyimide material. It must be remembered, however, that this is just one means of characterizing the changing thermodynamic state, and volume relaxation may display different behavior than that observed for enthalpy relaxation. Research by Oleinik<sup>18</sup>

suggests that volume relaxation and enthalpy relaxation can be related for a material by differences in the thermal expansion coefficient and heat capacity for the liquid and glassy states. In contrast, the decay of enthalpy and volume toward equilibrium cannot be simply interrelated according to work by Simon et al.<sup>13</sup> and Cowie and coworkers.<sup>19</sup> Changes in enthalpy for a glassy polymer cannot be directly followed during isothermal physical aging, but, upon heating in a DSC through the glass transition region into the equilibrium liquid state, the reduction in enthalpy which occurred during the aging interim is recovered. Subtracting the DSC scan for the freshly quenched sample (second heat after annealing at  $T_g+50^\circ\text{C}$  for 10 minutes) from the scan for the aged sample (first heat) and then integrating the result provides an enthalpy difference value essentially equivalent to the reduction in enthalpy which took place during the actual aging period. Aging samples for different amounts of time prior to this enthalpy recovery measurement technique allows an isothermal enthalpy relaxation rate ( $b_H$ ) to be determined as follows:<sup>20</sup>  $b_H = d(\Delta H)/d\log(t_a)$ , where  $t_a$  is the isothermal aging time at the aging temperature ( $T_a$ ), and  $\Delta H$  is the endothermic area determined from the subtraction procedure. This equation does not represent the data well for very short aging times or when the system is close to reaching the equilibrium state. A positive value of the recovered enthalpy ( $\Delta H$ ) in the above expression reflects a negative change in enthalpy which occurred during the physical aging process.

The representative enthalpy recovery behavior for the polyimide is shown as a function of aging temperature and aging time in Figure 9-2. The amount of recovered enthalpy increases with the extent of annealing at each aging temperature, and evidence for significant enthalpy relaxation is observed even at the lowest aging temperature of  $184^\circ\text{C}$  ( $T_a = T_g - 55^\circ\text{C}$ ). At this undercooling of  $55^\circ\text{C}$ , the enthalpy recovery response is broad and begins at temperatures noticeably below the  $T_g$  region. The enthalpy relaxation data exhibit essentially linear behavior with respect to  $\log(t_a)$  for the aging temperatures and aging times investigated (Figure 9-3), allowing enthalpy relaxation rates to be simply assessed. In Figure 9-4 is illustrated the dependence of enthalpy relaxation rate ( $b_H$ ) on aging temperature, a trend characterized by a maximum rate observed near  $215^\circ\text{C}$  and a decline in relaxation rate as temperature is decreased from

this point. Similar temperature dependencies have been observed for the volume relaxation of various glassy polymers.<sup>1,21</sup>

### ***9.3.2 Changes in Stress-Strain Response***

In order to assess the influence of physical aging on the practical mechanical performance of the polyimide material, tensile stress-strain behavior was evaluated at room temperature for samples which were aged at 204°C. Typical response curves are presented in Figure 9-5 for testing performed at an extension rate of 2.54 mm/min for samples with a gauge length equal to 7 mm. An enhancement in modulus and yield stress were brought about as a result of the physical aging process, as can be observed from Figure 9-6. In this plot, the data for the unaged material is arbitrarily placed at an aging time of 0.01 hr for comparative purposes. The lack of trend for the strain at yield ( $\epsilon_y$ ) with increased aging is likely a consequence of the competing effects of yield stress and modulus increases; an increase in the initial slope of the stress-strain response leads to a reduction in  $\epsilon_y$  while the development of a higher stress associated with yielding increases  $\epsilon_y$ . In contrast to the small-strain properties, surveying the ultimate properties as a function of aging time (Figure 9-7) reveals no significant effect of physical aging. After the yielding process, the influence of physical aging is not evident with respect to stress at break, strain at break, and toughness (energy to fail).

While increases in modulus and yield stress are in accord with expectations, the absence of aging-induced changes in failure properties is unusual.<sup>22-30</sup> Although the data are not shown here, testing was also performed using a ten-fold greater crosshead speed of 25.4 mm/min with similar results. Large stresses as well as dilatation of polymers in tensile deformation due to the Poisson effect have been thought to rejuvenate, or de-age, polymer glasses.<sup>1,31,32</sup> Also, research performed by Delin et al.<sup>33</sup> indicates the possibility that rejuvenation may occur even at small strains during dynamic testing of glassy materials. If rejuvenation did occur for the polyimide material investigated here, then it was not realized until after the yield point. Physical aging was manifested in both modulus and yield stress changes but the influence of aging appeared to diminish after the yielding process. Excellent experimental work by McKenna and coworkers<sup>34-37</sup> using a torsional dilatometer has provided strong evidence for a decoupling between

stress/strain fields and the structure (volume) of the glass, although Struik attempted to argue against this decoupling in a recent communication.<sup>38</sup> Despite the lack of observed aging-induced embrittlement via tensile testing for the polyimide material, physical aging may still have a marked effect on impact properties because it is unlikely that the high speed impact testing would enable structural rejuvenation prior to failure. It is also possible that physical aging did exert some small influence on break stress, toughness, and strain at failure which was merely not discernible due to the substantial error bars associated with the failure properties. Petrie and coworkers<sup>22</sup> subjected a freshly quenched amorphous poly(ethylene terephthalate) material to annealing at 51°C ( $T_g \approx 75^\circ\text{C}$ ) for 1.5 hr. This aging resulted in a reduction in tensile strain at break of approximately 0.10 compared to the performance of the unaged material, and a transition from ductile to brittle behavior was observed due to the aging-induced disappearance of the yielding process. With the degree of embrittlement found by these researchers in mind, it is possible that a total change in strain at break equal to 0.1 is hidden within the errors associated with the tensile failure measurements for the polyimide material.

### ***9.3.3 Mechanical Aging Effects Observed by Creep and DMA***

Creep compliance measurements were employed in order to quantify mechanical aging rates for comparison with the enthalpy relaxation rates and to enable the assessment of relaxation time characteristics. Using the general testing procedure established by Struik<sup>1</sup>, creep compliance ( $D(t)$ ) curves were obtained after aging times of 1.5, 3, 6, 12, and 24 hr for the polyimide material aged at temperatures ranging from 174 to 224°C. The data obtained during aging at 204°C are displayed in Figure 9-8 as well as the master curve generated by horizontal and vertical shifting of the compliance curves on the double logarithm plot to superimpose with the reference aging time data at  $t_a = 6$  hr. Horizontal shifting of the data to form a master curve assumes that aging shifts the relaxation time distribution to longer times but does not alter its shape. This assumption was justified by the similarity in curvature of the creep compliance response curves obtained as a function of aging time for a given aging temperature. The amount of horizontal shifting can be related to a mechanical aging rate,  $\mu$ , which is defined as:<sup>1</sup>

$$\mu = \frac{d \log(a_{t_a})}{d \log(t_a)} \quad \text{where: } a_{t_a} = \frac{\tau(t_a)}{\tau(t_{a,\text{ref}})} \quad \text{Eqn. 9-1}$$

The shift factor,  $a_{t_a}$ , relates the relaxation time  $\tau$  at a particular aging time ( $\tau(t_a)$ ) to the relaxation time at the reference aging time ( $\tau(t_{a,\text{ref}})$ ), and  $\log(a_{t_a})$  is the amount of horizontal shift to the left on the  $\log(\text{time})$  axis. A small amount of vertical shifting is also necessary to obtain reasonable superposition. The rate of shifting,  $\nu$ , along the  $\log(D)$  axis due to physical aging can be determined from the aging time dependence of the vertical shift factor ( $a_\nu$ ):

$$\nu = \frac{d \log(a_\nu)}{d \log(t_a)} \quad \text{where: } a_\nu = \frac{D_0(t_{a,\text{ref}})}{D_0(t_a)} \quad \text{Eqn. 9-2}$$

The parameter  $D_0$  is the limit of the compliance as time goes to zero, and hence may be related to an instantaneous elastic response of the material. Once a master curve is formed, a stretched exponential function can be applied to the curve to develop values for the most probable relaxation time ( $\tau$ ) at the reference aging time and the stretching exponent ( $b$ ) which is inversely related to the relaxation time distribution breadth:

$$D(t) = D_0 \exp\left(\frac{t}{\tau}\right)^b \quad \text{Eqn. 9-3}$$

The result of fitting this function to the master curve at  $T_a = 204^\circ\text{C}$  is evident in Figure 9-8b. A comparison of the stretched exponential functions assessed at  $t_a = 6$  hr for the different aging temperatures is given in Figure 9-9, and the relevant fitting parameters are listed in Table 9-I.

The mechanical aging rates determined from the creep compliance data can be contrasted with the rates of structural relaxation represented by the values of  $b_H$ , and these different rates are compared in Figure 9-10. The goal is not to contrast the absolute values of the rates but rather to inspect the effect of aging temperature on the different rates. Close to the glass transition temperature region, the mechanical and enthalpic aging rates appeared to be reduced in value as the aging temperature was increased as is commonly observed. At larger undercoolings, it is evident that the rate of enthalpy relaxation declined with decreasing aging temperature while the creep compliance aging rates remained fairly constant. The observation that the creep compliance aging rates

appear to maintain high values as aging temperature is decreased while the structural relaxation rates decrease is consistent with other research findings; a comparison of the aging temperature effects on the rate of mechanical aging<sup>1</sup> with those determined for volume relaxation rates<sup>21</sup> reveals similar differences for other glassy polymers.

It was stated earlier that vertical shifting was necessary for adequate superposition of the creep compliance aging data. Values of the vertical shift rate,  $\upsilon$ , are indicated as a function of aging temperature in Figure 9-11. Also indicated in this plot is the logarithmic rate of increase for stress-strain Young's modulus ( $E$ ) for aging performed at 204°C. The magnitude of this rate is comparable to the value of  $\upsilon$  determined from vertical shifting of the creep compliance data obtained at the same aging temperature. This similarity is consistent with the notion that the necessity of vertical shifting may be related, in part, to changes in the limiting elastic character of the material ( $D_0 = 1 / E_0$ ) due to the densification that occurs with the physical aging process.

Physical aging is also evident in dynamic mechanical property changes.<sup>11,15,39,40</sup> A mechanical aging rate ( $\mu$ ) can be determined from isothermal changes in the frequency response of dynamic storage modulus in a manner comparable to that used for the creep compliance data. Before describing the attempt to apply time-aging time superposition to isothermal dynamic mechanical data for the polyimide, it is useful to refer to the dynamic thermal-mechanical spectrum at a fixed frequency ( $f$ ) of 1 Hz (Figure 9-12), so that it is clear where the isothermal aging measurements were obtained relative to the characteristic relaxations for this material. The isothermal dynamic mechanical testing was performed at temperatures from 174 to 224°C, temperatures which are in the region between the glass transition relaxation ( $\alpha$ -relaxation) and the broad secondary  $\beta$ -relaxation. The variations of the dynamic storage ( $E'$ ) and loss ( $E''$ ) moduli with increasing  $\log(t_a)$  during annealing at 204°C are given in Figure 9-13, and it is evident that the storage modulus exhibits increases with aging, comparable to the behavior of the Young's modulus determined from the initial slope of the stress-strain curves. It is more useful to consider  $E'$  data as a function of inverse frequency for constant values of aging time, and the data plotted in this manner are depicted in Figure 9-14a. In a manner similar to that employed for the creep data, horizontal and vertical shifting were used to develop a master curve at a reference aging time of 6 hr (Figure 9-14b). Decent

superposition is apparent from this  $E'$  master curve, although it is difficult to evaluate the validity of superposition because the storage modulus at a given aging time does not exhibit much change in value for the frequency range used. Comparison of this  $E'$  master curve with the creep compliance master curve at the same aging temperature of 204°C (Figure 9-8b) reveals that, on a relative basis, the creep master curve displays much larger changes in mechanical response than the storage modulus curve despite the fact that the number of time decades covered by both measurement techniques are comparable. However, the range of frequency ( $f$ ) values used during DMA testing was from 20 to 0.01 Hz which corresponds, respectively, to a time ( $t$ ) range from 0.008 to 16 seconds ( $t = 1/(2\pi f)$ ). Because the shortest creep time was approximately 15 seconds, it is not surprising that the storage modulus changes are quite small given the limited degree of creep which was evident at the short time end of the compliance curves.

The relatively small changes in storage modulus with respect to both frequency and aging time do not permit adequate scrutiny of the applicability of time-aging time superposition. Before aging rates can be developed from the degree of shifting applied to the storage modulus data, it is necessary to inspect the variation in dynamic loss modulus ( $E''$ ) due to aging. The dependence of loss modulus on inverse frequency is indicated in Figure 9-15a for the various aging times. Clearly the influence of both the  $\alpha$ -relaxation and the  $\beta$ -relaxation are present in the experimental time window probed during the dynamic testing (the  $\beta$ -relaxation causes the upturn in the loss modulus data at the short end of the time scale). An attempt to superimpose the  $E''$  data via vertical and horizontal shifting is depicted in Figure 9-15b, and decent superposition of the data was not possible. Similar difficulties with superposition of dynamic loss data were apparent for the other aging temperatures. Therefore, aging rates were not determined from the dynamic mechanical data due to the thermorheological complexity evident. The relative influence of aging on primary and secondary relaxations is not clear in the literature.<sup>10,15,41-45</sup> One of the controversial aspects is whether the aging-induced intensity reduction observed for the secondary relaxation is real or actually reflects an influence of physical aging on the high frequency (short time) tail of the primary relaxation which is partly underlying the secondary relaxation response. Although questions remain concerning the influence of aging on secondary relaxations, the overlap of the secondary

relaxation with the primary relaxation certainly resulted in failure of time-aging time superposition for this dynamic mechanical investigation of the polyimide material. The very short time character of creep mechanical response can also be influenced by secondary relaxations,<sup>46</sup> but the creep measurements were made for the polyimide material within a time-frame outside the region where the secondary relaxation can play a role. Accordingly, the creep compliance curves exhibited good superimposability.

#### ***9.3.4 Discussion of Mechanical-Structural Aging Rate Interrelationships***

One of the well established features of relaxation in the glassy state is nonlinearity, where the relaxation time is not only a function of temperature but also depends on the changing structure (volume, etc.) of the glassy state. As relaxation proceeds during physical aging, the material densifies and configurational entropy decreases. This decreases the mobility, in turn making it more difficult for further structural relaxation to occur. This is the essence of nonlinear, or self-limiting, behavior which leads to the typical dependence of volume and enthalpy decreases on the logarithm of aging time as opposed to linear time during isothermal aging following a quench from above  $T_g$ . The general nonlinear stretched exponential decay function for isothermal relaxation includes a relaxation time which depends on structure, and hence time, and assumes that the relaxation time distribution remains invariant (constant **b** exponent):<sup>8,47</sup>

$$\phi(t_a) = \frac{\Delta H_\infty - \Delta H(t_a)}{\Delta H_\infty} = \exp \left[ - \left( \int_0^{t_a} \frac{dt}{\tau(t)} \right)^b \right] \quad \text{Eqn. 9-4}$$

A value of **b** equal to 1.0 represents the presence of only a single relaxation time and the relaxation time distribution represented by the above expression broadens as **b** decreases from this value towards zero. The parameter  $\Delta H_\infty$  represents the difference between the enthalpy of the freshly quenched sample from one which has been aged to equilibrium. This can be determined from where the recovered enthalpy ( $\Delta H$ ) reaches a plateau with respect to  $\log(t_a)$  or can be estimated by:  $\Delta H_\infty = \Delta C_p(T_{f,0} - T_a)$ . The  $\Delta C_p$  is the difference between the liquid and glassy heat capacities and is temperature dependent. In order to easily obtain relaxation times and values of the stretching exponent (**b**), some researchers

inappropriately apply the linear form of the decay function to the nonlinear glassy state. The linear form assumes that the most probable relaxation time is a constant, thus:

$$\phi(t_a) = \frac{\Delta H_\infty - \Delta H(t_a)}{\Delta H_\infty} = \exp\left[-\left(\frac{t}{\tau}\right)^b\right] \quad \text{Eqn. 9-5}$$

However, the structural relaxation time is anticipated to continually increase during aging, and hence the physical meaning of the relaxation time parameters determined in such a manner is not evident. To further compound the fundamental problems associated with this linear approach, the  $\Delta H_\infty$  parameter is sometimes treated as a variable and is fit to the enthalpy recovery data along with the two other variables, despite the fact that the recovered enthalpy data has not reached equilibrium or even begun to approach a plateau with respect to  $\log(\text{aging time})$ .

To see if the relaxation times and associated dependencies on aging time are comparable for mechanical and structural aging behavior, an attempt was made to predict the nonlinear behavior of enthalpy relaxation using relaxation times developed from the analysis of the creep compliance data. It must be emphasized that this is an exercise to test the relative relaxation behavior for creep and enthalpy aging responses, and there is certainly no a priori justification for using mechanical relaxation data to predict changes in the thermodynamic state due to aging. The previous application of the linear stretched exponential function (Eqn. 9-3) to the creep compliance master curves was indeed appropriate because the aging time dependence of relaxation times was accounted for by the horizontal curve shifting used to generate the master curve at the reference aging time of 6 hr. The aging time dependence of the relaxation time for creep can be simply written from Eqn. 9-1 as:

$$\tau(t_a) = \tau(t_{a,\text{ref}}) \left( \frac{t_a}{t_{a,\text{ref}}} \right)^\mu \quad \text{Eqn. 9-6}$$

This function can be put into Eqn. 9-4 and used in conjunction with the  $\tau(t_{a,\text{ref}})$  and  $\mu$  data to attempt to predict enthalpy relaxation decay functions. Values of  $b$  equal to 0.3, 0.45, and 0.6 were selected and used for the predictions in order to assess the influence of relaxation time distribution at each aging temperature. Because the relaxation times at

short aging times (below  $t_a=1.5$  hr) were not known for the creep compliance behavior, Eqn. 9-6 cannot be applied to short times where a lag is commonly observed prior to the development of a constant aging rate. Accordingly, the numerical integration of Eqn. 9-4 assumed that the relaxation time was constant for aging times equal to and below 1 hr. The numerical integration of Eqn. 9-4 employed an initial time step of 1 hr from  $t_a=0$  to  $t_a=1$  and then used logarithmically spaced time steps for the remainder of the integration. In determining the experimental decay functions, values of  $\Delta H_\infty$  were estimated using the method given above. The difference between the liquid and glassy heat capacities,  $\Delta C_p$ , varied with temperature for the polyimide and was heightened with increased undercooling in comparison to the difference at  $T_g$  ( $\Delta C_{p,g} = 0.236$  J/g-K). Values of the ratio  $\Delta C_p/\Delta C_{p,g}$  were determined to be 1.30, 1.21, 1.16, and 1.09 at the temperatures of 184, 204, 214, and 224°C, respectively, and these were used to determine  $\phi(t_a)$  from the enthalpy recovery data. A comparison of the experimental decay functions with those predicted from the creep compliance relaxation time functions are indicated in Figure 9-16. The use of creep relaxation time functions predicted much faster enthalpy relaxation than was indicated by the experimental data, and variation of the  $b$  parameter within the reasonably large range from 0.3 to 0.6 did not remedy this situation.

The experimental enthalpy decay functions were subsequently fit using the (inappropriate) linear decay function (Eqn. 9-5) to obtain estimates of the “characteristic” relaxation time and to illustrate the inadequacy of this approach. Fits allowing free variation of both  $\tau$  and  $b$  were performed (Figure 9-17), and the results are listed in Table 9-II. Because this linear fitting approach does not allow for nonlinear, or self-limiting, relaxation time behavior characterized by relaxation times which increase during aging, the observed experimental enthalpy recovery data can only be decently represented by the linear decay function by improper modification of the nonexponentiality character of the equation. In other words, the inability of this approach to include the dependence of the most probable relaxation time on  $\log(t_a)$  necessitates inappropriate broadening of the relaxation time distribution by reduction of the value of  $b$  in order to fit the experimental structural relaxation response. This results in the assessment of  $b$  parameters which are atypically low in value and have no physical meaning. Cowie and coworkers<sup>19,48</sup> claim that the introduction of a relaxation time which depends on the changing structural state

is not necessary to adequately represent experimental decay data for isothermal aging, and the linear stretched exponential function can satisfactorily describe the data. It may be true that the data can be fit well via this approach, but the worth of such a venture becomes diminished if some of the physics are lost in the process. The use of the linear nonexponential function to describe the structural relaxation process ignores the distinction between the separate phenomenological features of nonlinearity and nonexponentiality which was established by the influential work of Kovacs.<sup>49</sup>

The fitting endeavor using the linear decay function did provide an indication that the values of  $\tau$  for enthalpy relaxation of the polyimide are orders of magnitude greater than those found for creep aging behavior. This comparative relaxation time behavior is clearly seen by contrasting the relaxation times given in Table 9-I with those provided in Table 9-II. Also, the same conclusion can be drawn from the failed attempt to represent the enthalpy decay data with the creep compliance relaxation data. It must be reasserted that some caution must be exerted concerning interpreting the relaxation time parameters for enthalpy relaxation due to the discussion given above. Similar to the findings given here, McKenna and coworkers<sup>34</sup> noted that mechanical relaxation times were shorter than those exhibited by volume for an epoxy glass. A different epoxy material was studied by Bero and Plazek,<sup>50</sup> and aging responses were assessed for creep and volume. Although the shortest relaxation times for volume and creep compliance were found to be of similar magnitude, the spectra was broader and the average relaxation time was greater for the mechanical response, a result which is different from the observation of McKenna's research group. Another study by Mijovic and Ho<sup>51</sup> found that relaxation times were comparable for enthalpy and stress relaxation aging responses of poly(methyl methacrylate), poly(styrene-co-acrylonitrile), and their blends. In recent papers by Simon et al.<sup>13</sup> and Cowie and coworkers<sup>52</sup>, excellent reviews are included which describe the efforts of numerous researchers concerned with comparing volume, enthalpy, and mechanical responses in the nonequilibrium glassy state. What is clear from these surveys is that there exists no general consensus with regards to relative aging behavior for different properties. Additional research is necessary to resolve these issues. It may eventually be concluded that relative changes in properties due to physical aging depend

on the chemical and structural details of the glassy material being studied, and, consequently, the development of generalities may not be possible.

Given all of the evidence, it is quite clear that the enthalpy relaxation and creep compliance changes have very distinct relaxation time characteristics. It is intuitive that the underlying glassy structure influences the mechanical relaxation characteristics but the connection is certainly not trivial. A comparison of enthalpy relaxation rates with mechanical aging rates from a direct relaxation time perspective is not appropriate because  $b_H$  and  $\mu$  are related to changes in relaxation times during physical aging in opposite ways. For the nonlinear structural relaxation process, the enthalpy relaxation rate is *inversely* proportional to the rate of relaxation time increase with respect to  $\log(\text{aging time})$ . As the relaxation times increase during structural relaxation, the molecular motion which enables changes in the thermodynamic state of the material becomes more retarded. Therefore, lower enthalpy relaxation rates are associated with greater changes in relaxation times which occur during aging. In contrast, the mechanical aging rate ( $\mu$ ) is defined as the rate of shift of the mechanical response to longer times during physical aging, and therefore  $\mu$  is *directly* proportional to the rate of relaxation time increase with respect to  $\log(\text{aging time})$ . While the changing mechanical response during aging may reflect the time-dependent nature of the thermodynamic state, there appears to be no reason to expect the relaxation times, or the rates of change thereof, to be the same for enthalpy and mechanical properties.

## 9.4 Conclusions

The physical aging behavior of an amorphous polyimide was studied using DSC and mechanical property testing for aging performed at temperatures from 15 to 65°C below  $T_g$ . Enthalpy relaxation rates and mechanical aging rates from creep compliance data were determined as a function of aging temperature. The rate of enthalpy relaxation decreased with decreasing aging temperature, but the creep compliance aging rates remained largely unchanged. Thermorheological complexity prevented the application of

the time-aging time superposition principle to dynamic mechanical data, and this complexity was caused by an overlap of the primary and secondary relaxation processes within the frequency domain used during isothermal aging. Room temperature stress-strain behavior as a function of aging time at 204°C indicated no discernible embrittlement due to physical aging despite commonly observed increases in yield stress and modulus, a phenomenon possibly related to rejuvenation enabled via the yielding process. The change in stress-strain modulus with aging was comparable in magnitude to the vertical shift rate used to improve the superimposability of creep data obtained at the same aging temperature of 204°C. An attempt to predict enthalpy relaxation rates using relaxation time aging characteristics assessed from creep compliance data indicated that relaxation times were much greater for enthalpy relaxation relative to creep mechanical behavior.

Table 9-I. Stretched exponential fitting parameters for creep compliance master curves (reference:  $t_a = 6$  hr)

$T_a$ (°C)	$D_0$ (GPa <sup>-1</sup> )	$\tau$ (hr)	$b$
174	0.398 (±0.001)	69.0 (±4.2)	0.460 (±0.007)
184	0.404 (±0.001)	34.5 (±1.0)	0.420 (±0.002)
204	0.401 (±0.002)	10.7 (±0.4)	0.487 (±0.007)
214	0.410 (±0.001)	5.41 (±0.10)	0.483 (±0.005)
224	0.419 (±0.005)	0.551 (±0.018)	0.455 (±0.009)

Table 9-II. Fitting parameters for linear stretched exponential decay function applied to enthalpy relaxation data

$T_a$ (°C)	$\tau$ (hr)	$b$
184	5,260,000 (±3,600,000)	0.299 (±0.035)
204	226,000 (±117,000)	0.225 (±0.012)
214	12,800 (±5,200)	0.209 (±0.015)
224	123 (±8)	0.197 (±0.006)

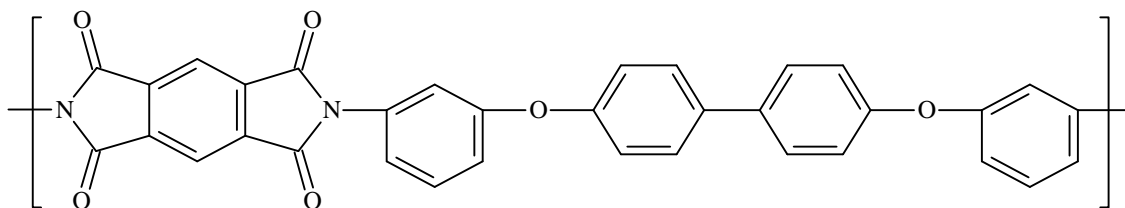


Figure 9-1. Predominant chemical repeat unit for the polyimide used in this investigation. The incorporation of a proprietary comonomer serves to disrupt chain symmetry and prevent crystallizability of the polymer.

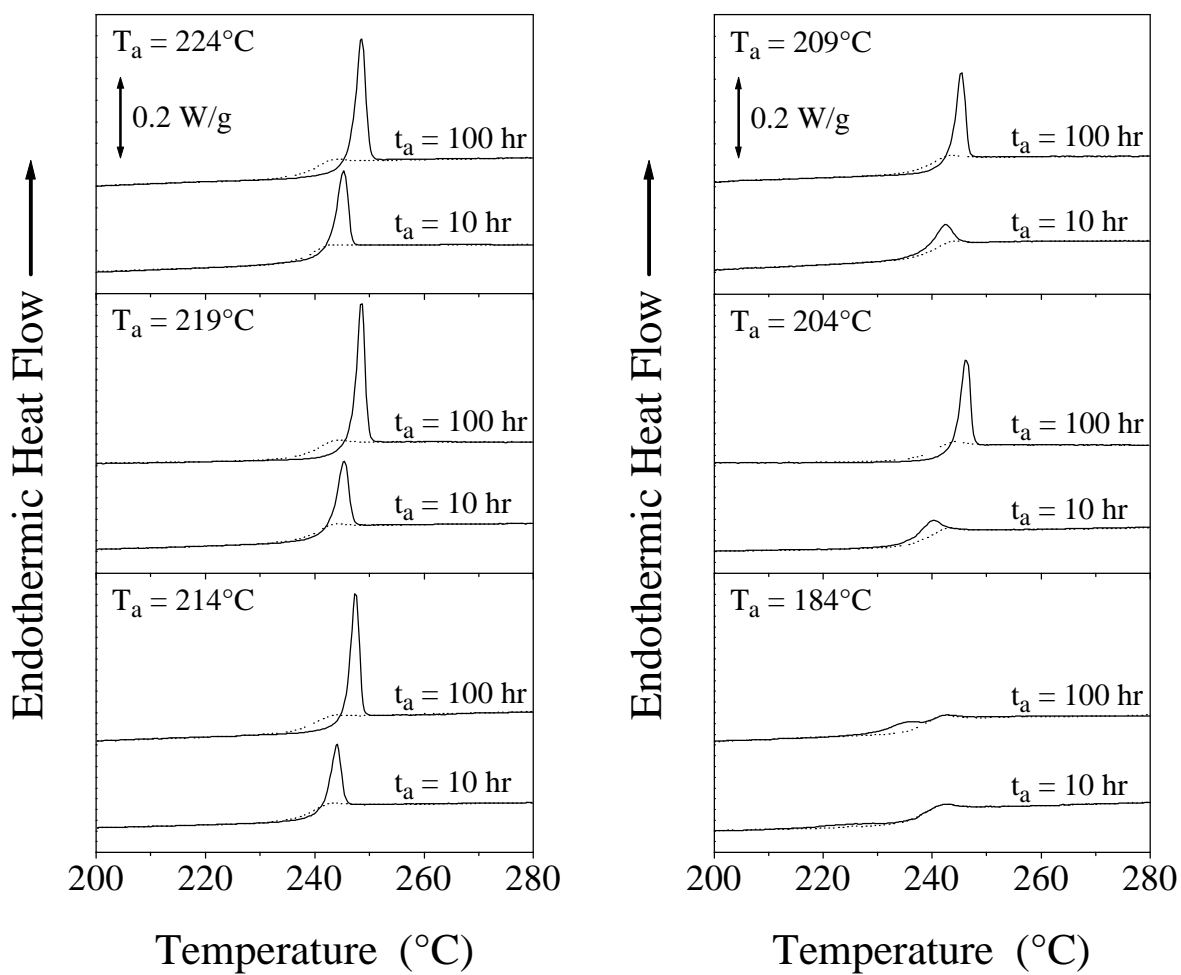


Figure 9-2. DSC scans ( $10^\circ\text{C}/\text{min}$  heating) illustrating enthalpy recovery behavior following aging at the indicated temperatures. Each dotted line represents the second scan immediately following a quench into the glassy state.

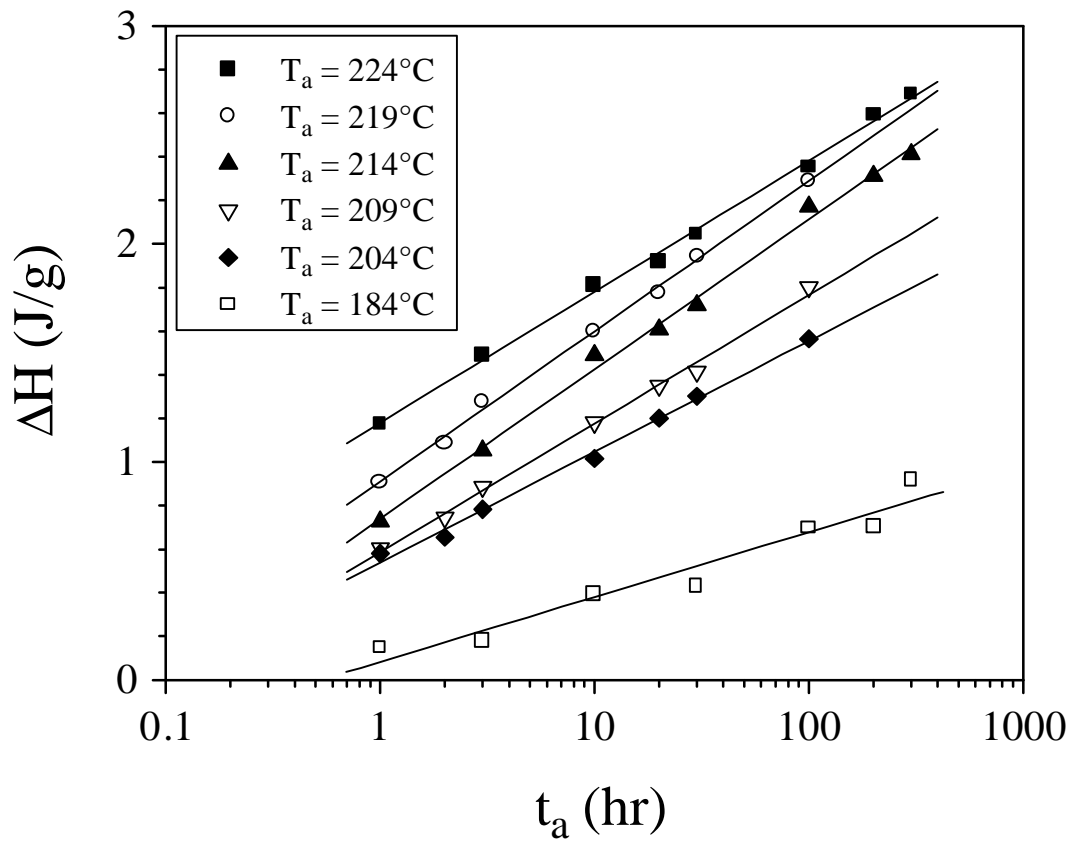


Figure 9-3. Dependence of recovered enthalpy ( $\Delta H$ ) on aging time for aging performed at the indicated temperatures. The lines are linear fits to the data for the given axes (linear y, logarithmic x) and the slope of each line is  $b_H$ . Each data point represents the average  $\Delta H$  value from three samples.

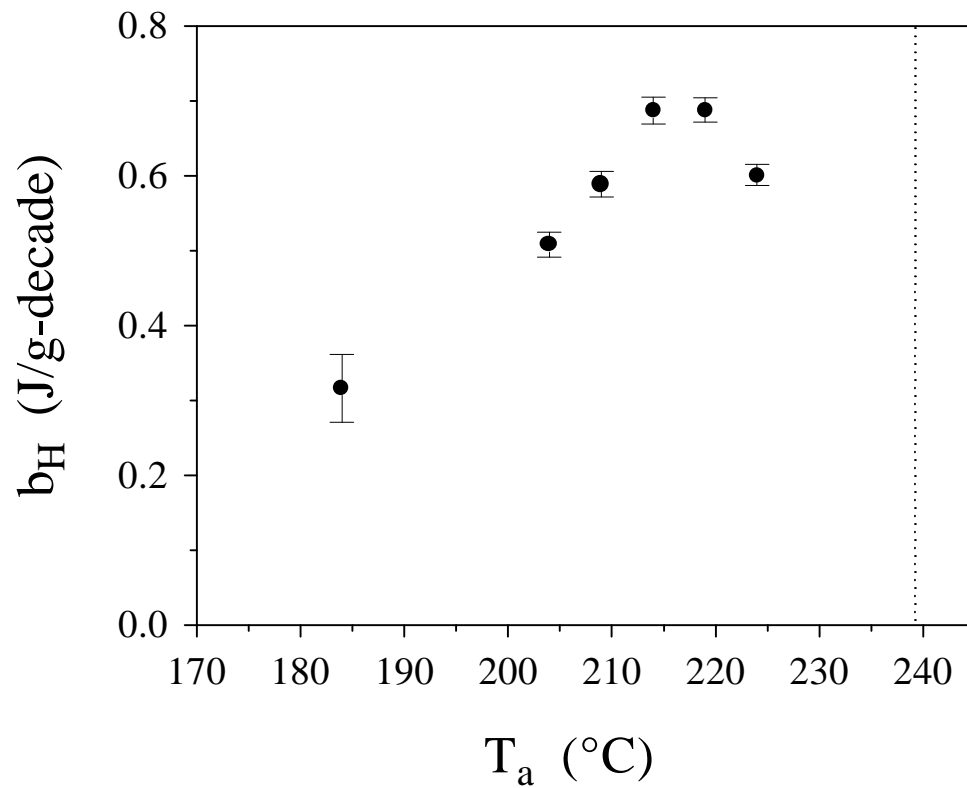


Figure 9-4. Enthalpy relaxation rate ( $b_H$ ) as a function of aging temperature. The dotted line indicates the location of the kinetic  $T_g$  determined via DSC for a freshly quenched sample using a 10°C/min heating rate.

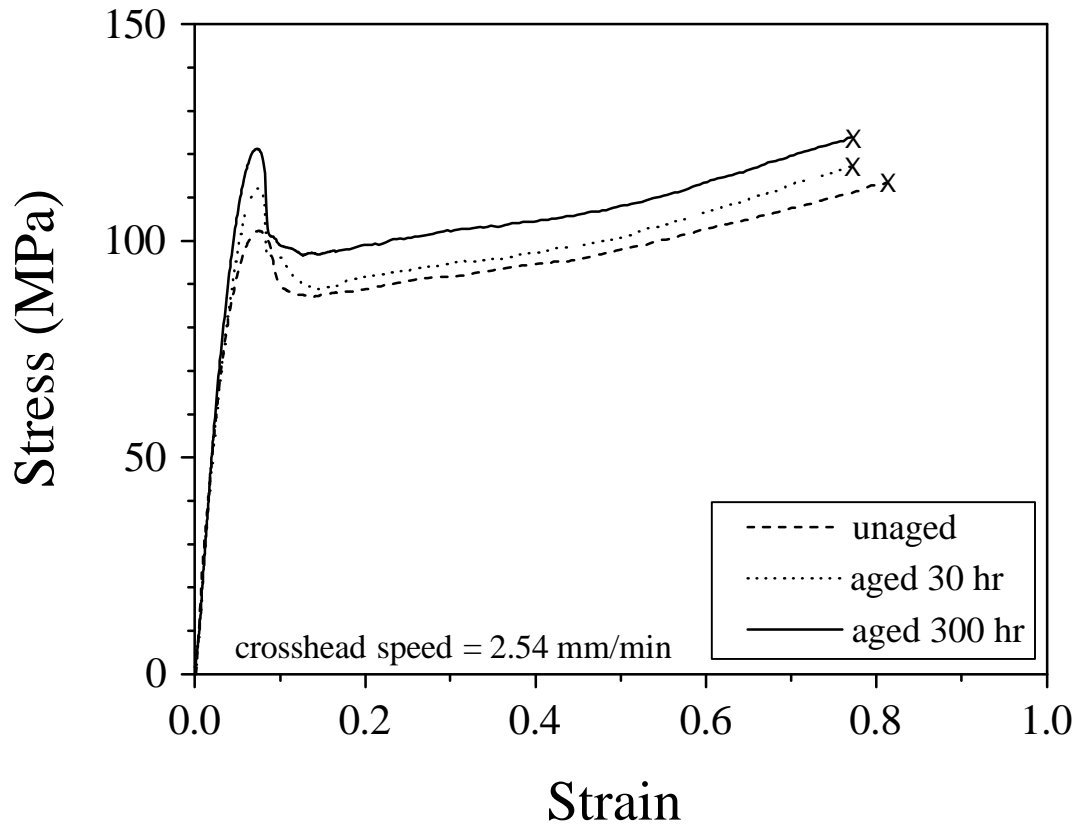


Figure 9-5. Effect of physical aging at  $T_a = 204^\circ\text{C}$  on the engineering stress-strain (tensile) behavior measured at room temperature using a rate of 2.54 mm/min (sample gauge length = 7 mm). Each indicated curve is representative of the average response for the 10 samples tested at each condition.

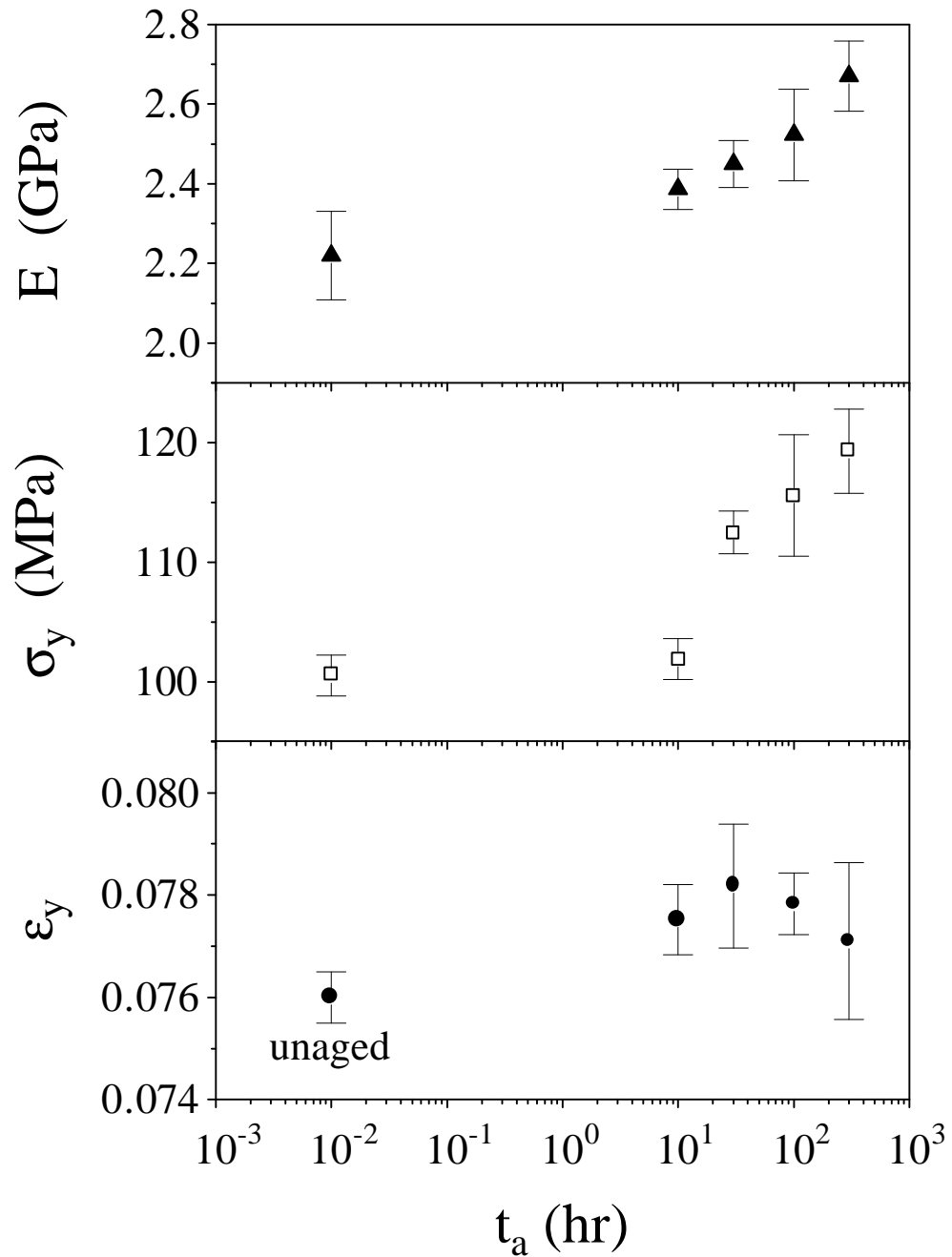


Figure 9-6. Effect of physical aging at 204°C on modulus ( $E$ ), yield stress ( $\sigma_y$ ), and strain at yield ( $\epsilon_y$ ) determined from tensile testing at room temperature using a testing rate of 2.54 mm/min. Data plotted at  $t_a = 10^{-2}$  hr are for unaged material.

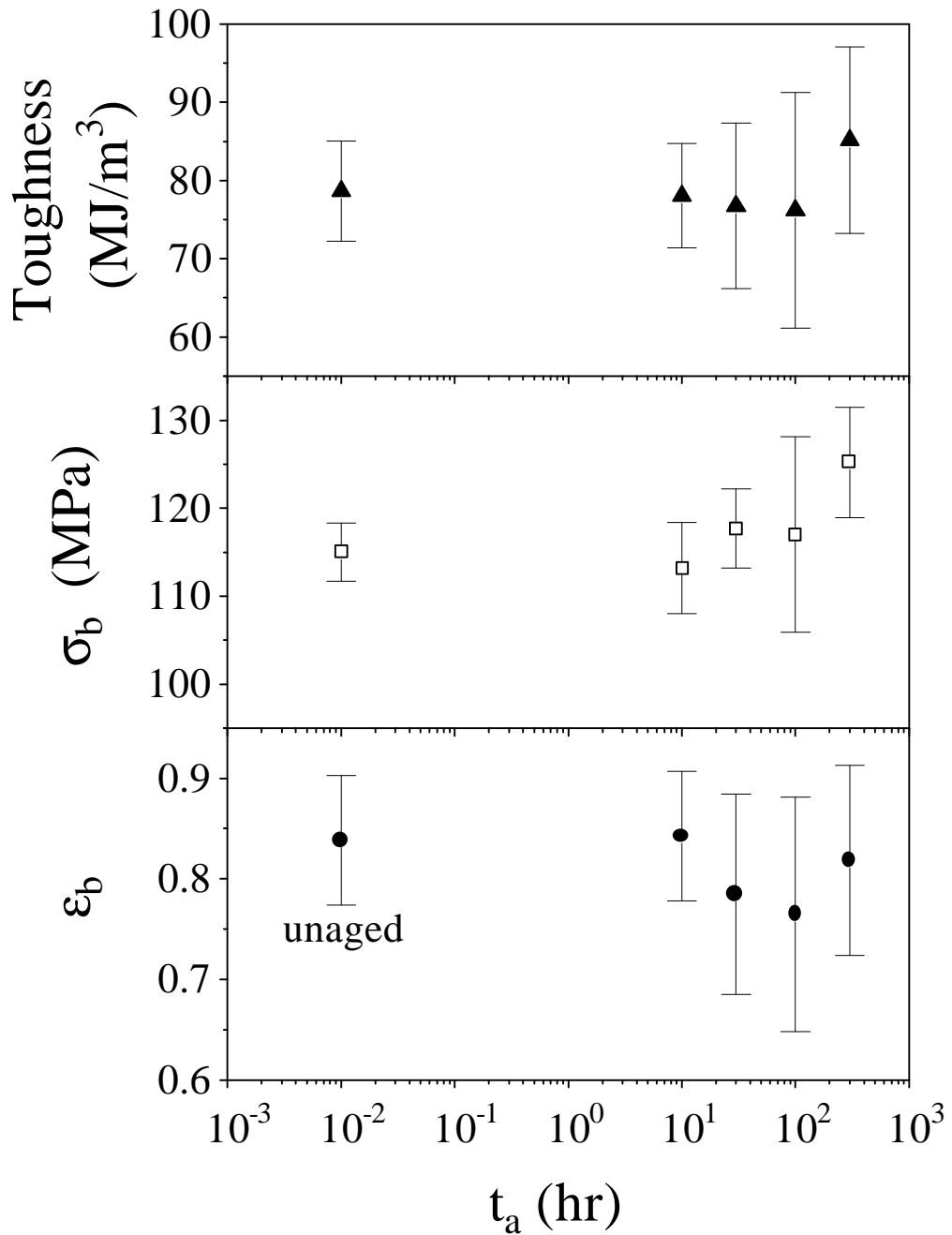


Figure 9-7. Effect of physical aging at 204°C on toughness, stress at break ( $\sigma_b$ ), and strain at break ( $\epsilon_b$ ) determined from tensile testing at room temperature using a testing rate of 2.54 mm/min. Data plotted at  $t_a = 10^{-2}$  hr are for unaged material.

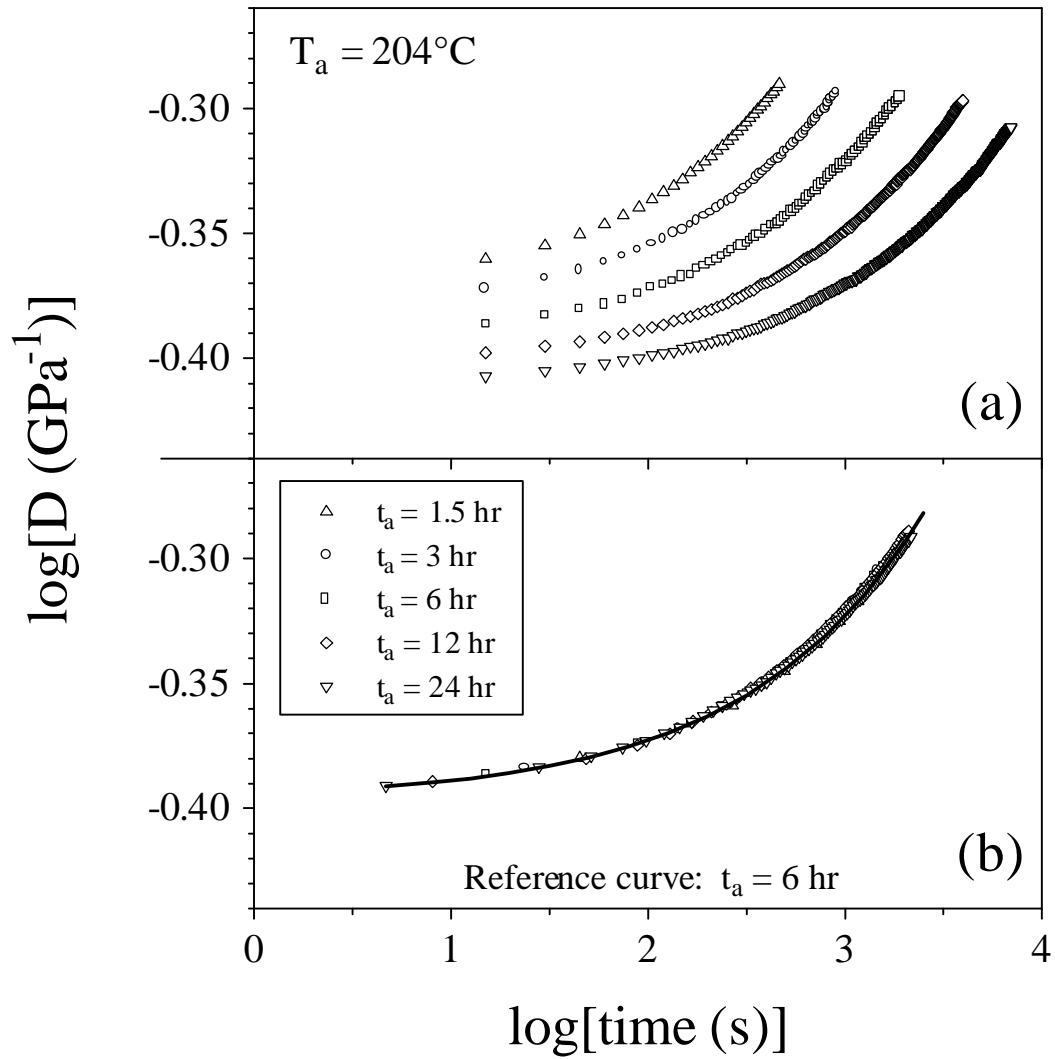


Figure 9-8. (a) Tensile creep compliance response after aging at  $204^\circ\text{C}$  for the indicated aging times. (b) Master curve at a reference aging time of 6 hr generated by horizontal and vertical shifting. For clarity, only every fifth data point indicated for each aging time data set in the master curve. The solid line is the best fit of the stretched exponential function to the master curve.

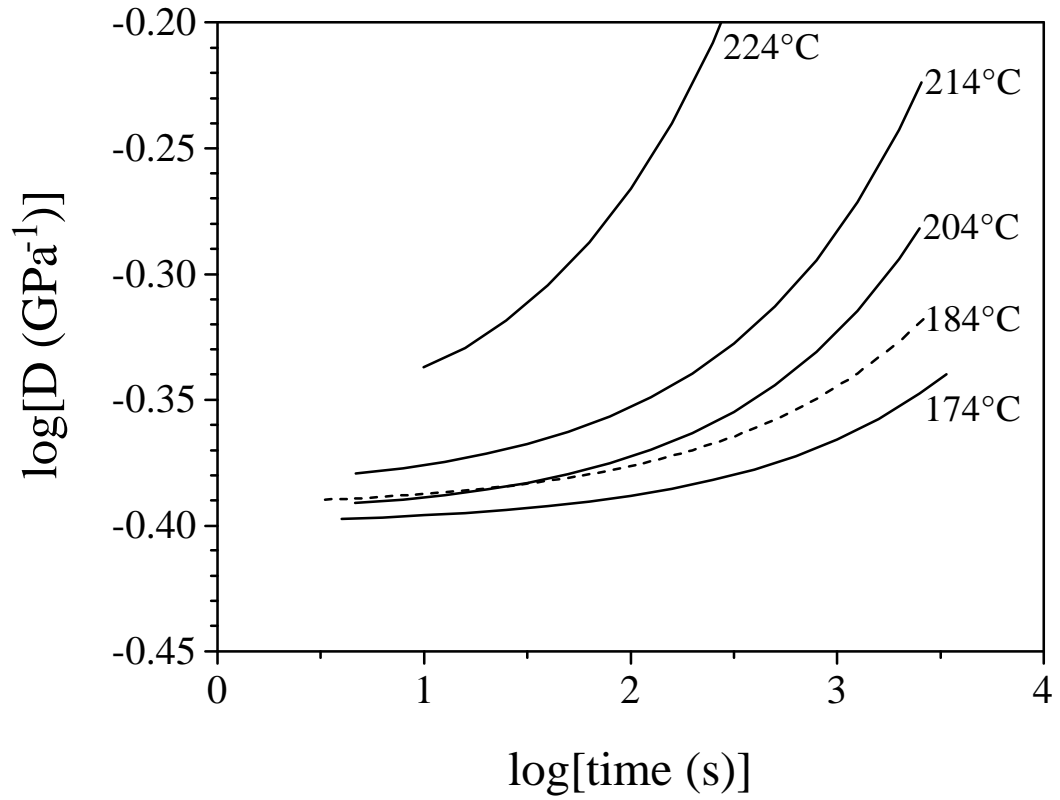


Figure 9-9. Comparison of creep compliance master curves (reference:  $t_a = 6$  hr) for the aging temperatures indicated. The curves represent the stretched exponential functions which were fit to the master curves.

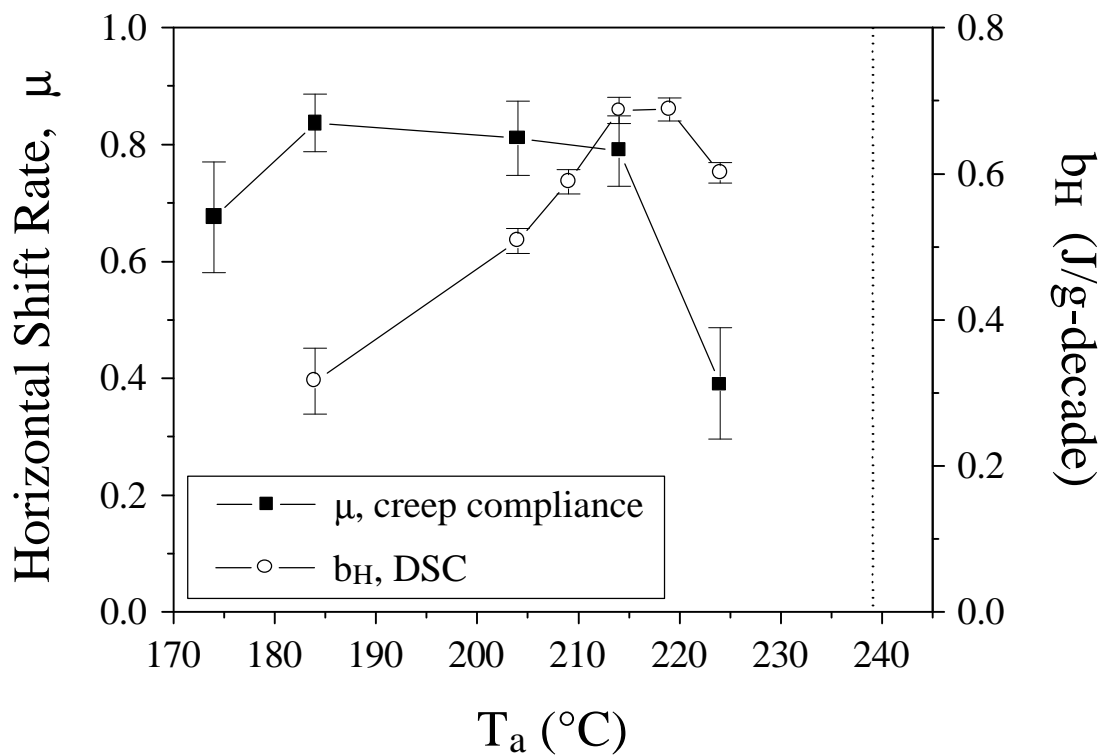


Figure 9-10. Mechanical aging rate ( $\mu$ ) as a function of aging temperature determined from the rate of horizontal shifting used in the generation of master curves for creep compliance data. Also shown are enthalpy relaxation rate ( $b_H$ ) data. The dotted line indicates the location of the kinetic  $T_g$  determined via DSC for a freshly quenched sample using a 10°C/min heating rate.

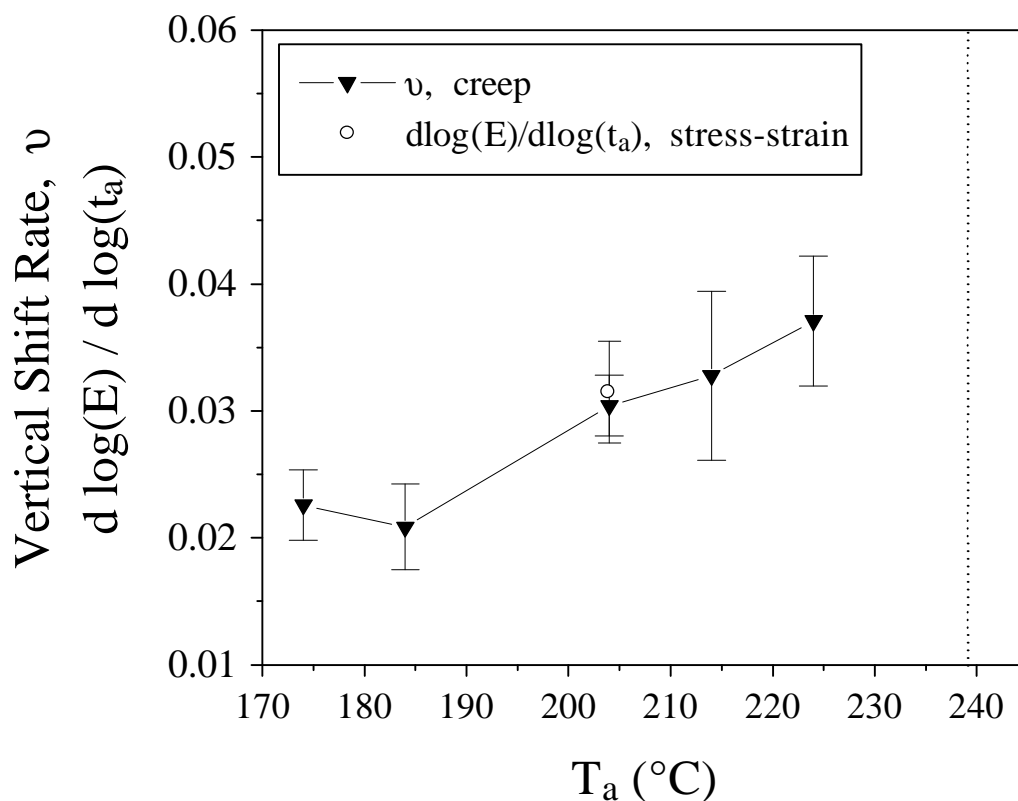


Figure 9-11. Rate of vertical shifting necessary for adequate superposition of creep compliance data to form master curves. Also indicated is the derivative of  $\log(\text{modulus})$  with respect to  $\log(t_a)$  for the stress-strain tensile modulus. The dotted line indicates the location of the kinetic  $T_g$  determined via DSC for a freshly quenched sample using a  $10^\circ\text{C}/\text{min}$  heating rate.

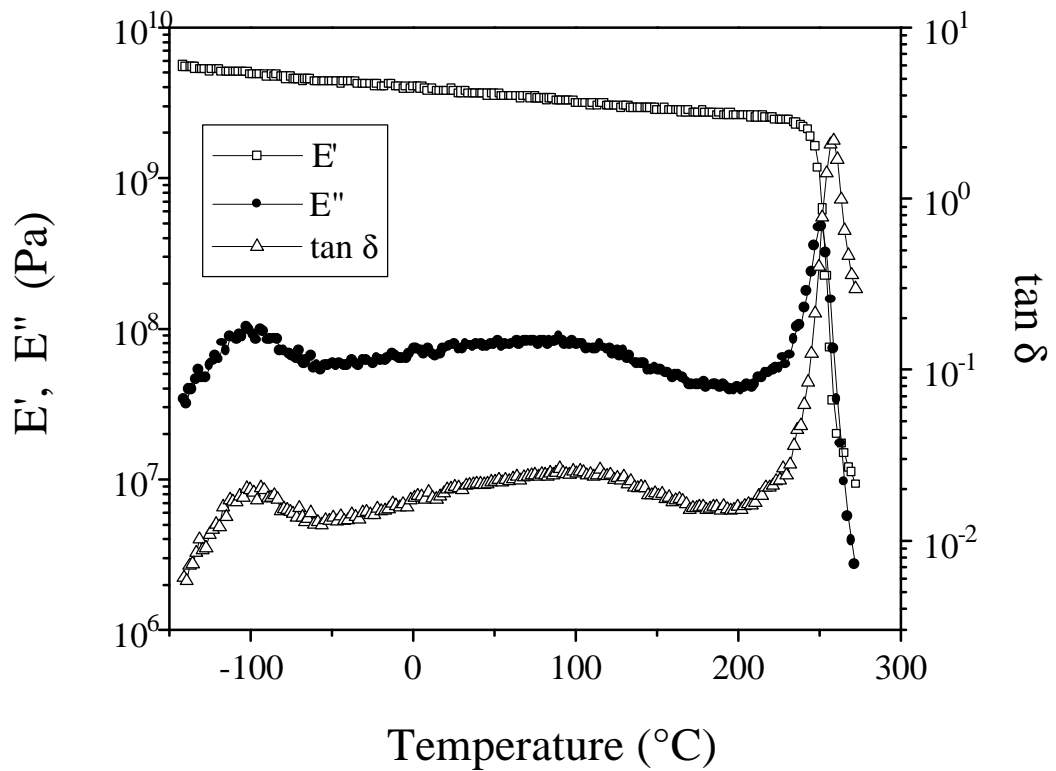


Figure 9-12. Dynamic mechanical spectrum for a freshly quenched sample measured in tension at a frequency of 1 Hz and using a heating rate of 2°C/min.

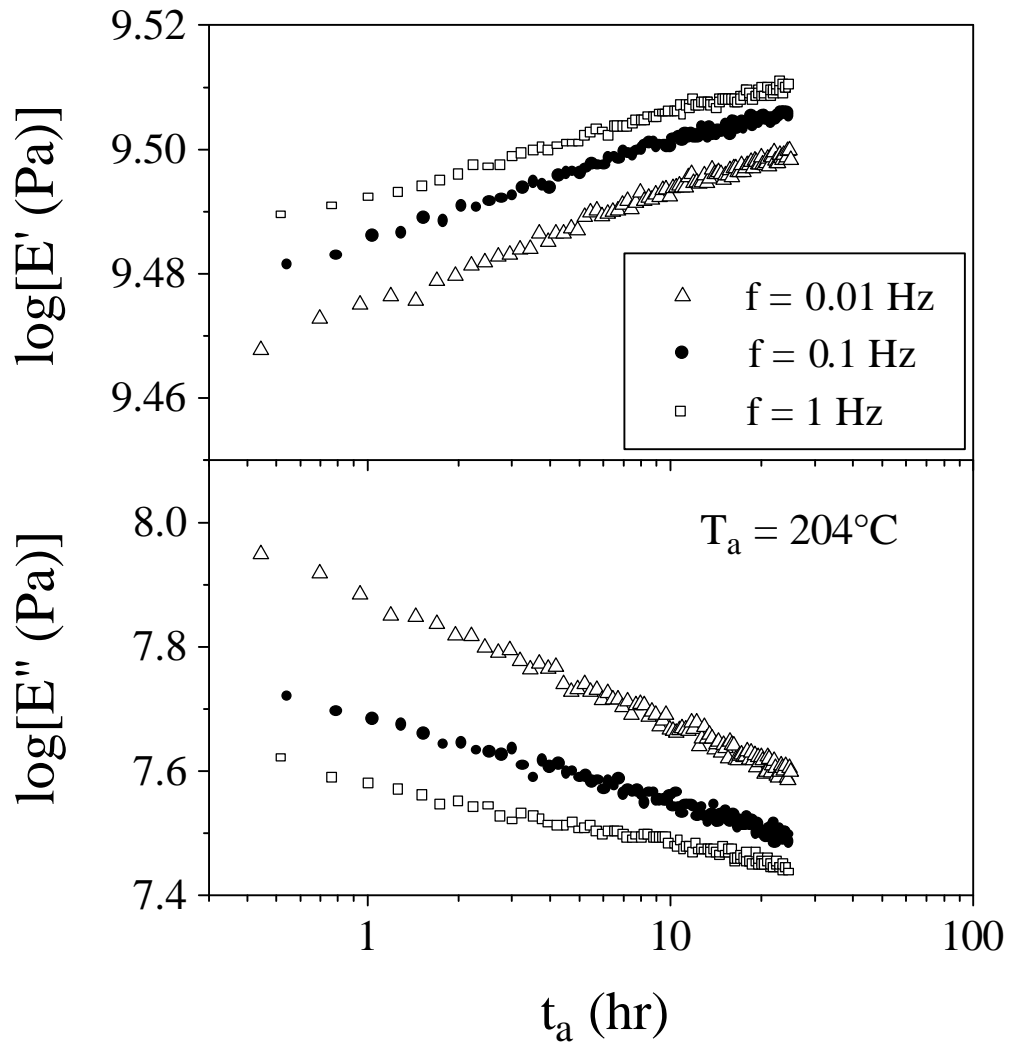


Figure 9-13. Changes in dynamic storage ( $E'$ ) and loss ( $E''$ ) moduli during physical aging at  $204^\circ\text{C}$ . Testing was performed using 13 frequencies ranging from 0.01 Hz to 20 Hz although only the data for 0.01, 0.1, and 1 Hz are shown.

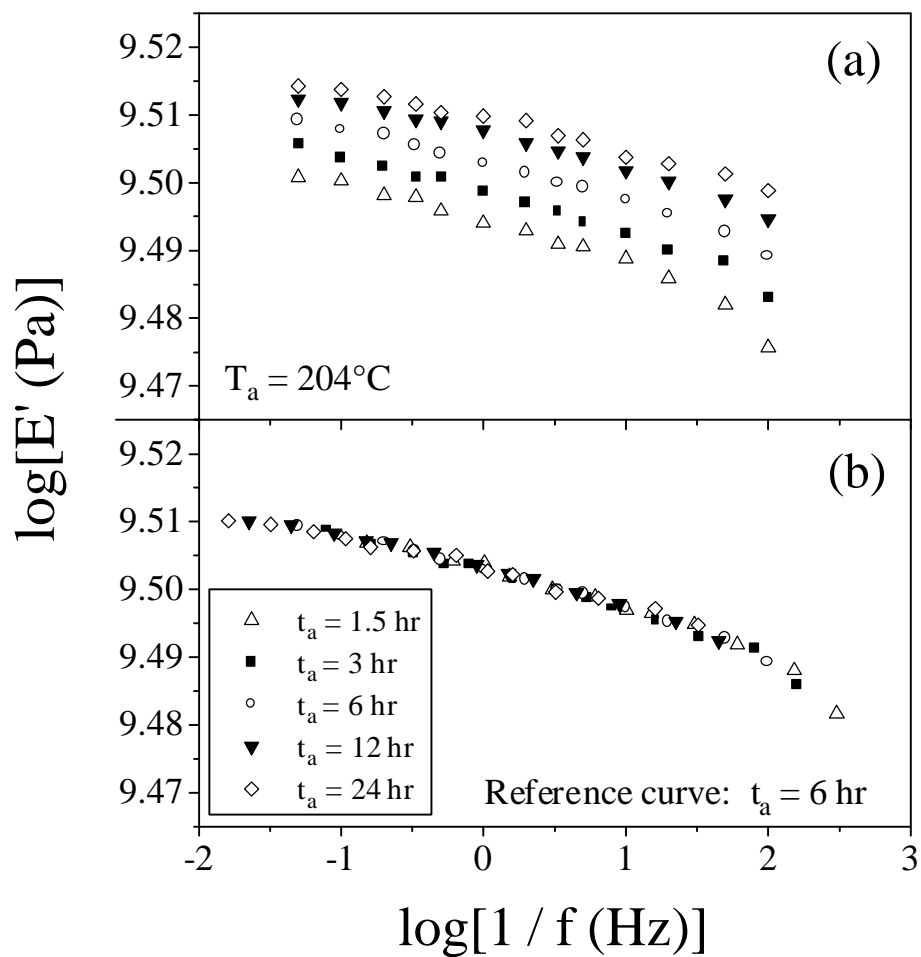


Figure 9-14. (a) Storage modulus response after aging at  $204^\circ\text{C}$  for the indicated aging times. (b) Master curve at a reference aging time of 6 hr generated by horizontal and vertical shifting.

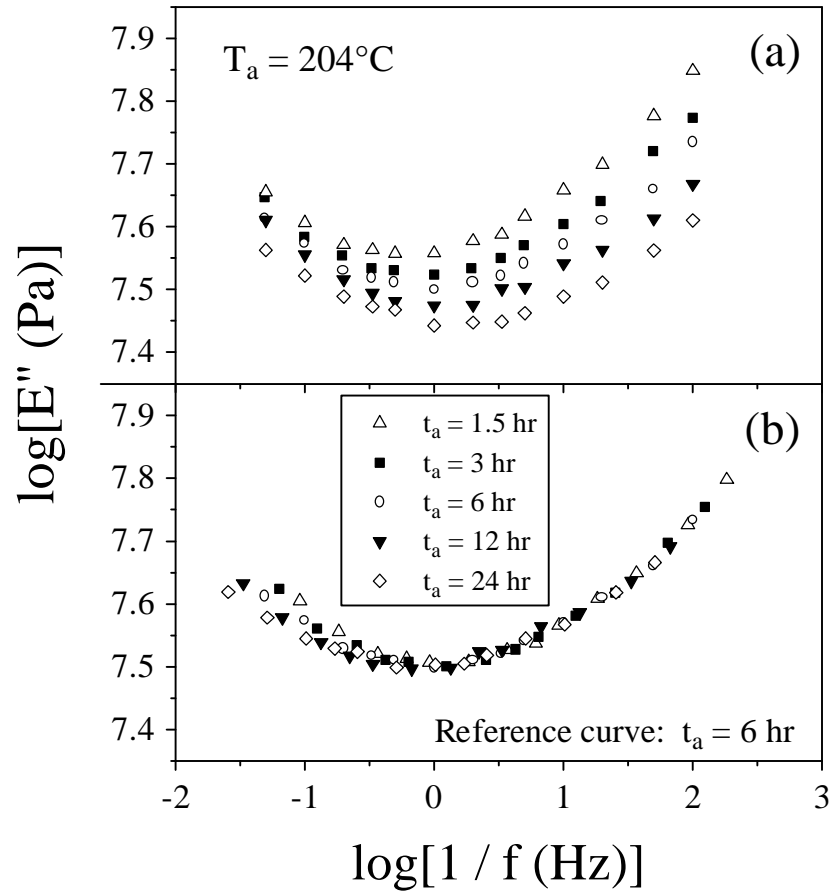


Figure 9-15. (a) Loss modulus response after aging at  $204^\circ\text{C}$  for the indicated aging times. (b) Attempt to generate master curve at a reference aging time of 6 hr by horizontal and vertical shifting.

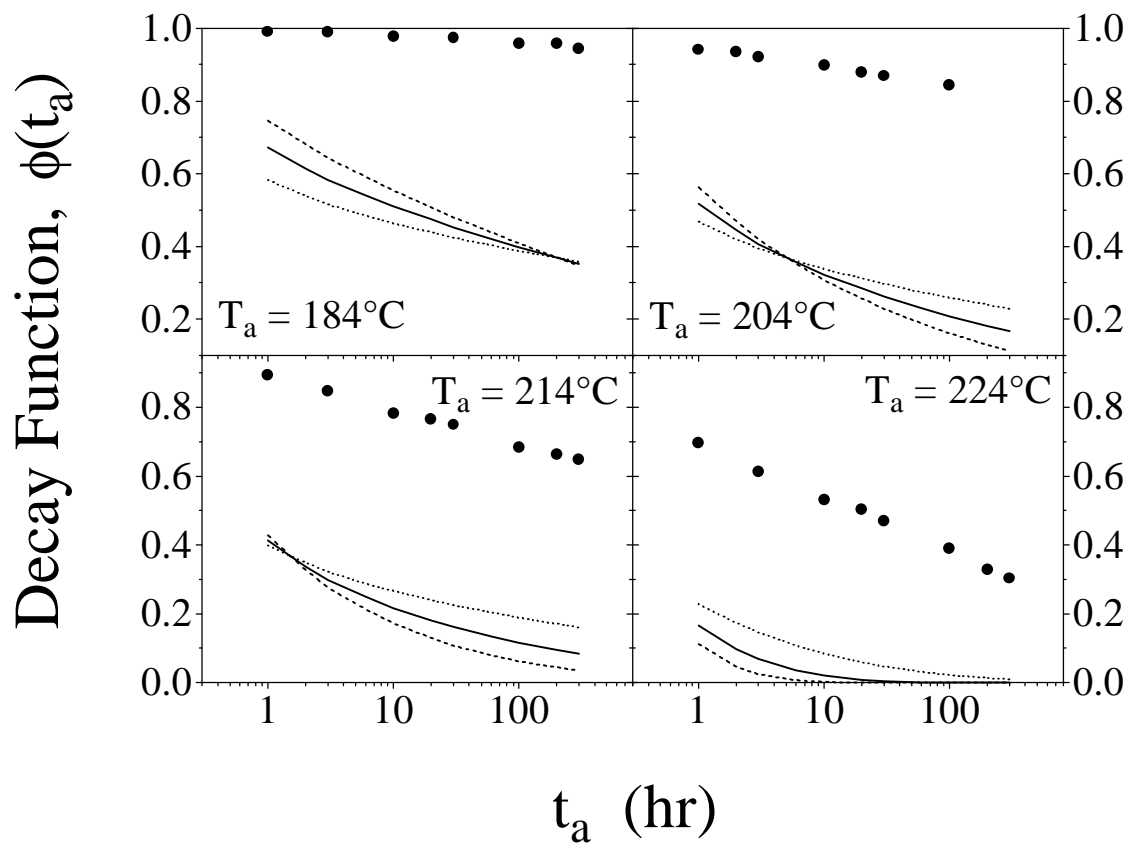


Figure 9-16. Decay function for enthalpy relaxation at indicated aging temperatures. Experimental data presented as well as nonlinear predictions using relaxation time function determined from creep compliance data. The predictions employ the  $b$  values fit to the creep data (solid lines) as well as  $b = 0.3$  (dotted lines) and  $b = 0.6$  (dashed lines).

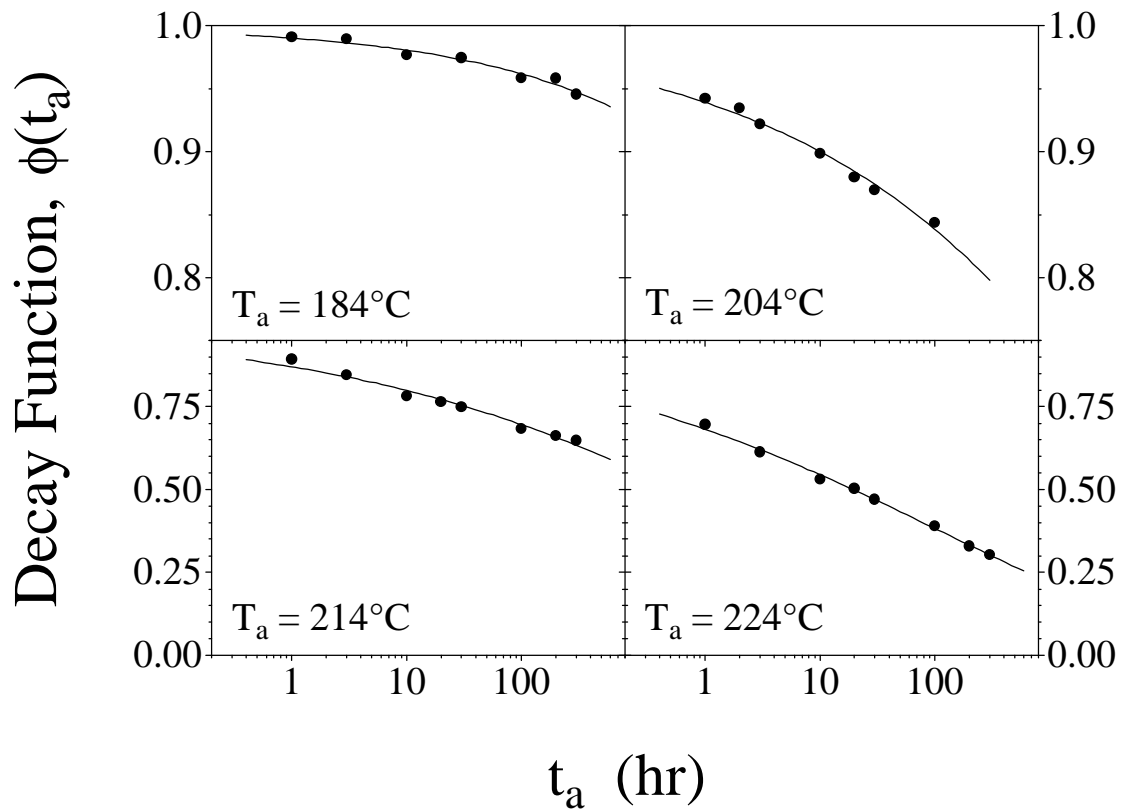


Figure 9-17. Enthalpy relaxation decay functions for aging at 184, 204, 214, and 224°C. Each solid line represents the linear stretched exponential fit. See text for additional details.

## 9.5 References

- <sup>1</sup> L. C. E. Struik, *Physical Aging In Amorphous Polymers and Other Materials*, Elsevier, New York, 1978.
- <sup>2</sup> G. B. McKenna, in *Comprehensive Polymer Science, Vol. 2: Polymer Properties*, C Booth and C. Price, eds., Pergamon, Oxford, 1989, Chapter 10, pp. 311-361.
- <sup>3</sup> M. R. Tant and G. L. Wilkes, *Polym. Eng. Sci.*, **21**, 874 (1981).
- <sup>4</sup> A. A. Goodwin and J. N. Hay, *Polymer Commun.*, **31**, 338 (1990).
- <sup>5</sup> F. Biddlestone, A. A. Goodwin, J. N. Hay, and G. A. C. Mouledous, *Polymer*, **32**, 3119 (1991).
- <sup>6</sup> L. C. E. Struik, *Polymer*, **28**, 1869 (1987).
- <sup>7</sup> R. Wimberger-Friedl and J. G. deBruin, *Macromolecules*, **29**, 4992 (1996).
- <sup>8</sup> I. M. Hodge, *J. Non-Cryst. Solids*, **169**, 211 (1994).
- <sup>9</sup> E. Muzeau, G. Vigier, and R. Vassoille, *J. Non-Cryst. Solids*, **172-174**, 575 (1994).
- <sup>10</sup> A. B. Brennan and F. Feller III, *J. Rheology*, **39**, 453 (1995).
- <sup>11</sup> H. Yoshida, *Thermochimica Acta*, **266**, 119 (1995).
- <sup>12</sup> I. Echeverria, P.-C. Su, S. L. Simon, and D. J. Plazek, *J. Polym. Sci.: Part B: Polym. Phys.* **33**, 2457 (1995).
- <sup>13</sup> S. L. Simon, D. J. Plazek, J. W. Sobieski, and E. T. McGregor, *J. Polym. Sci.: Part B: Polym Phys.*, **35**, 929 (1997).
- <sup>14</sup> S. L. Simon, *Macromolecules*, **30**, 4056 (1997).
- <sup>15</sup> R. A. Venditti and J. K. Gillham, *J. Appl. Polym. Sci.*, **45**, 1501 (1992).
- <sup>16</sup> P. M. Hergenrother, *SPE Conference on High Temperature Polymers and Their Uses*, Case Western Reserve University, Oct. 2-4, 1989.
- <sup>17</sup> D. J. Plazek and K. L. Ngai, in *Physical Properties of Polymers Handbook*, J. E. Mark., ed., American Institute of Physics Press, Woodbury, NY, 1996, Chapter 12, pp. 139-159.
- <sup>18</sup> E. F. Oleinik, *Polymer J.*, **19**, 105 (1987).
- <sup>19</sup> J. M. G. Cowie, S. Harris, and I. J. McEwen, *Macromolecules*, **31**, 2611 (1998).
- <sup>20</sup> J. M Hutchinson, *Prog. Polym. Sci.* **20**, 703 (1995).
- <sup>21</sup> R. Greiner and F. R. Schwarzl, *Rheol. Acta*, **23**, 378 (1984).
- <sup>22</sup> R. M. Mininni, R. S. Moore, J. R. Flick, and S. E. B. Petrie, *J. Macromol. Sci.*, **B8**, 343 (1973).
- <sup>23</sup> D. G. LeGrand, *J. Appl. Polym. Sci.*, **13**, 2129 (1969).
- <sup>24</sup> J. H. Golden, B. L. Hammant, and E. A. Hazell, *J. Appl. Polym. Sci.*, **11**, 1571 (1967).
- <sup>25</sup> J. M. Crissman and G. B. McKenna, *J. Polym. Sci.: Part B: Polym. Phys.* **25**, 1667 (1987).
- <sup>26</sup> J. M. Crissman and G. B. McKenna, *J. Polym. Sci.: Part B: Polym. Phys.* **28**, 1463 (1990).
- <sup>27</sup> J. C. Arnold, *J. Polym. Sci.: Part B: Polym. Phys.* **31**, 1451 (1993).
- <sup>28</sup> J. C. Arnold, *Polym. Eng. Sci.*, **35**, 165 (1995).
- <sup>29</sup> A. C.-M. Yang, R. C. Wang, and J. H. Lin, *Polymer*, **37**, 5751 (1996).

- 30 G. M. Gusler and G. B. McKenna, *Polym. Eng. Sci.*, **37**, 1442 (1997).
- 31 S. Matsuoka, H. E. Bair, S. S. Bearder, H. E. Kern, and J. T. Ryan, *Polym. Eng. Sci.*,  
**18**, 1073 (1978).
- 32 S. Matsuoka and H. E. Bair, *J. Appl. Phys.*, **48**, 4058 (1977).
- 33 M. Delin, R. W. Rychwalski, J. Kubat, C. Klason, and J. M. Hutchinson, *Polym. Eng.*  
*Sci.*, **36**, 2955 (1996).
- 34 M. M. Santore, R. S. Duran, and G. B. McKenna, *Polymer*, **32**, 2377 (1991).
- 35 C. G'Sell and G. B. McKenna, *Polymer*, **33**, 2103 (1992).
- 36 W. K. Waldron, Jr., G. B. McKenna, and M. M. Santore, *J. Rheology*, **39**, 471 (1995).
- 37 G. B. McKenna, *J. Res. Natl. Inst. Stand. Technol.*, **99**, 169 (1994).
- 38 L. C. E. Struik, *Polymer*, **38**, 4053 (1997).
- 39 A. J. Kovacs, R. A. Stratton, and J. D. Ferry, *J. Phys. Chem.*, **67**, 152 (1963).
- 40 J. Perez, J. Y. Cavaille, R. Diaz Calleja, J. L. Gomez Ribelles, M. Montleon Pradas,  
and A. Ribes Greus, *Makromol. Chem.*, **192**, 2141 (1991).
- 41 G. P. Johari and M. Goldstein, *J. Chem. Phys.* **53**, 2372 (1970).
- 42 J. Haddad and M. Goldstein, *J. Non-Cryst. Solids*, **30**, 1 (1978).
- 43 G. P. Johari, *J. Chem. Phys.*, **77**, 4619 (1982).
- 44 R. Diaz-Calleja, A. Ribes-Greus, and J. L. Gomez-Ribelles, *Polymer*, **30**, 1433  
(1989).
- 45 E. Muzeau, G. Vigier, R. Vassoille, and J. Perez, *Polymer*, **36**, 611 (1995).
- 46 B. E. Read and G. D. Dean, *Polymer*, **25**, 1679 (1984).
- 47 G. W. Scherer, *Relaxation in Glass and Composites*, Wiley, New York, 1986.
- 48 J. M. G. Cowie, S. Harris, and I. J. McEwen, *J. Polym. Sci.: Part B: Polym. Phys.* **35**,  
1107 (1997).
- 49 A. J. Kovacs, *Fortschr. Hochpolym.-Forsch.*, **3**, 394 (1964).
- 50 C. A. Bero and D. J. Plazek, *J. Polym. Sci.: Part B: Polym. Phys.* **29**, 39 (1991).
- 51 J. Mijovic and T. Ho, *Polymer*, **34**, 3865 (1993).
- 52 J. M. G. Cowie, R. Ferguson, S. Harris, and I. J. McEwen, *Polymer*, **39**, 4393 (1998).

# Chapter 10

## Long-Term Volume Relaxation of Bisphenol-A Polycarbonate and Atactic Polystyrene

---

---

### Chapter Synopsis

Volume relaxation was assessed using dilatometry for two years at ambient temperature conditions (between 19 and 24°C) for bisphenol-A polycarbonate (PC) and atactic polystyrene (a-PS) after quenching the materials from above the respective glass transition temperatures. A peculiar increase in the negative slope of volume versus  $\log(\text{aging time})$  data was first noted for PC at room temperature by Wimberger-Friedl and de Bruin [*Macromolecules* **1996**, 29, 4992], and this change in volume relaxation rate occurred after an aging time of approximately  $10^7$  seconds (ca. 115 days). The present study also observed such an unusual densification process for PC which confirmed the previous findings. In contrast, the decay of volume for a-PS displayed the typical self-limiting behavior with no noticeable change in volume relaxation rate, and this provided an argument against the interpretation of the odd densification for PC as a general characteristic of glassy polymers.

## 10.1 Introduction

A few years ago, a study by Wimberger-Friedl and de Bruin<sup>1</sup> appeared in the literature and provided convincing evidence against the picture of physical aging as a self-limiting process. Upon quenching an amorphous polymer from above the glass transition temperature into the glassy state, densification occurs in the nonequilibrium glassy state as the material attempts to achieve the preferred thermodynamic state. The decrease in free volume during this physical aging process is thought to enact a corresponding decrease in mobility which, in turn, further limits the ability of the material to relax and densify. This circular process, which is known as self-limitation or self-retardation, is generally considered to be responsible for the dependence of isothermal volume relaxation on  $\log(\text{aging time})$ , as opposed to linear time, during the aging process induced by a quench into the glassy state. The data obtained by Wimberger-Friedl and de Bruin for bisphenol-A polycarbonate (PC) aged at 23°C indicated that the rate of decrease of volume with respect to  $\log(\text{aging time})$  was constant up to an aging time of approximately  $10^7$  seconds where a transition to a much greater volume relaxation rate was noted. These results were clearly in opposition to the self-limitation concept.<sup>2-4</sup> In view of the significance of these findings, the goal of this presently disclosed study was to independently verify the long-term volume relaxation behavior of PC near room temperature (ca. 21°C). Also, investigation of the densification behavior of another common glassy polymer, atactic polystyrene (a-PS), was also performed in order to inspect whether the unusual volume relaxation behavior of PC was specific to that material or general to many polymers.

## 10.2 Experimental Details

The polymers utilized in this investigation were Makrolon 2608, a bisphenol-A polycarbonate produced by Bayer, and an atactic polystyrene material manufactured by Dow which has the resin designation 685D. The approximate number average molecular weight for the PC material was 16,500 g/mol, and the number and weight average molecular weights for the atactic polystyrene were 174,000 and 297,000 g/mol,

respectively.<sup>5</sup> The  $T_g$  values were 147°C and 103°C, respectively, for PC and a-PS. These glass transition temperatures were obtained using a Perkin Elmer DSC7 during heating at 10°C/min following a quench into the glassy state at 200°C/min. Glass dilatometers were constructed using precision glass tubing with an inner diameter of 1.829 mm ( $\pm 0.0004$  mm) for the capillary portion. The tubing was obtained from Ace Glass. A large amount of film for each sample (approximately 60 g) was placed inside a dilatometer and sealed. Triple-distilled mercury was then used to fill the dilatometers under vacuum conditions. The filled dilatometers were then de-gassed under vacuum for ca. two days, and the dilatometers were allowed to stand for one day upon removal of the vacuum. The encased polymer samples were annealed for 15 minutes at  $T_g + 20^\circ\text{C}$  in a Haake model N4-B oil bath, and then rapidly quenched into the glassy state by immersion of the dilatometers in an ice water bath. The dilatometers were then placed into an insulated oil bath kept at room temperature. The reference time which was used as the zero aging time was 15 minutes after the dilatometers were placed into the room temperature oil bath after removal from the ice water bath. The aging temperature was predominantly between 20°C and 22°C, but extremes of 19°C and 24°C were noted throughout the aging interim which was two years. However, during measurement of the mercury height in the capillaries using a cathetometer manufactured by Gaertner Scientific Corp., the oil bath temperature was controlled to temperatures between 21.35°C and 21.42°C. A Haake D1 circulating heater was used to heat the oil bath when necessary for measurements, and liquid nitrogen was employed when some measure of cooling was required. The temperature of the bath and the dilatometers contained therein was assessed using a precision thermocouple made by Ertco-Hart (model 850). Due to the small temperature discrepancies, the height measurements were corrected based upon the thermal expansion behavior for the polymer samples and the mercury.

### 10.3 Results and Discussion

The densification results for PC which were assessed in this study confirm the volume relaxation behavior noted by Wimberger-Friedl and de Bruin. The long-term volume relaxation data for PC which were obtained during aging at ca. 21°C are

presented in Figure 10-1. A change in volume relaxation rate was clearly observed from the measured densification, and this occurred in the aging time vicinity of  $10^7$  seconds, comparable to the previous study. Wimberger-Friedl and de Bruin speculated that this apparent transition may represent the realization of the glass transition. This hypothesis opposes the principle of a Vogel temperature which represents the apparent temperature limit where the equilibrium relaxation times corresponding to the  $\alpha$ -relaxation (glass transition) appear to diverge to infinity. The Vogel temperature for PC is approximately  $100^\circ\text{C}$ ,<sup>6</sup> and this suggests that the observation of the glass transition near room temperature should not occur based upon the current understanding of the kinetics of glass formation. An alternate explanation of the change in volume relaxation rate at ca.  $10^7$  seconds for PC can be developed without the necessity of invoking the presence of a transition. If a slow densification process which varied with respect to linear time occurred in conjunction with the typical  $\log(\text{time})$ -dependent physical aging, then this could also explain the volume relaxation rate data for bisphenol-A polycarbonate. If an extremely slow linear volume relaxation process characterized by, for example,  $d(\Delta V/V_0)/dt = -1.6\text{E-}11 \text{ sec}^{-1}$  is subtracted from the total densification, then the apparent transition disappears as is indicated in Figure 10-2. The hypothetical linear process does not impact the initial portion of the volume data plotted versus  $\log(\text{aging time})$ , but its influence becomes increasingly evident at long times because of the disparity between linear and logarithmic time. This thought argument is not intended to suggest that a linear densification does in fact occur in addition to the self-limiting physical aging process for PC. Rather, the objective of this illustration is to suggest that the peculiar acceleration of volume relaxation rate which happened near  $10^7$  seconds does not have to be the consequence of a transition.

Volume relaxation was also monitored for atactic polystyrene at  $21^\circ\text{C}$  in parallel with the aging study of bisphenol-A polycarbonate. The observed decay of volume with  $\log(\text{aging time})$  for a-PS is given in Figure 10-3, and the data are characteristic of a self-limiting aging process. The question which remains to be answered is why PC displays the peculiar densification while a-PS exhibits the typical self-limiting aging behavior. It is clear that a more systematic investigation of the long-term aging behavior of numerous

glass-forming polymers at various temperatures must be accomplished before any understanding can be acquired concerning the unusual densification behavior of PC.

#### **10.4 Conclusions**

Confirmation of the peculiar room temperature aging behavior for PC first noted by Wimberger-Friedl and de Bruin was provided by this investigation. It was argued herein, however, that the change in volume relaxation rate did not need to be the result of a thermo-kinetic transition. Atactic polystyrene did not show the unusual densification process exhibited by PC. This indicated that the increase of volume relaxation rate noted at long times for PC is not a general characteristic of glassy polymers.

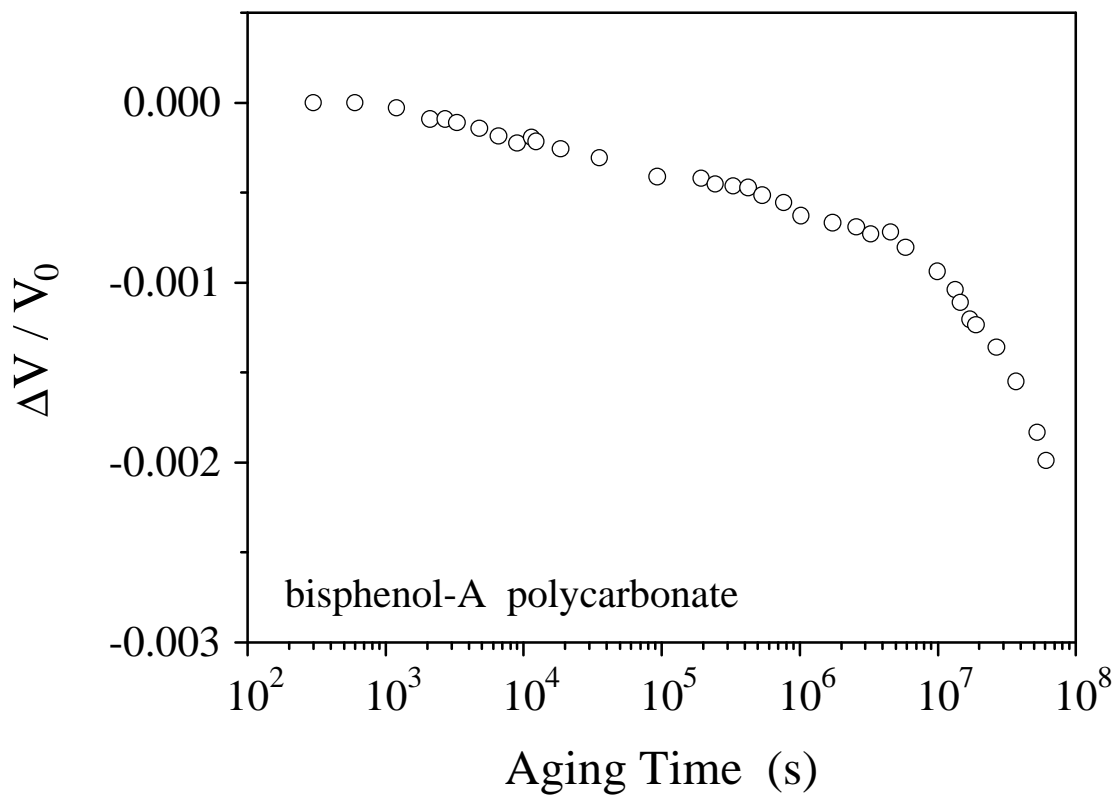


Figure 10-1. Volume relaxation data for bisphenol-A polycarbonate during aging at 21°C.

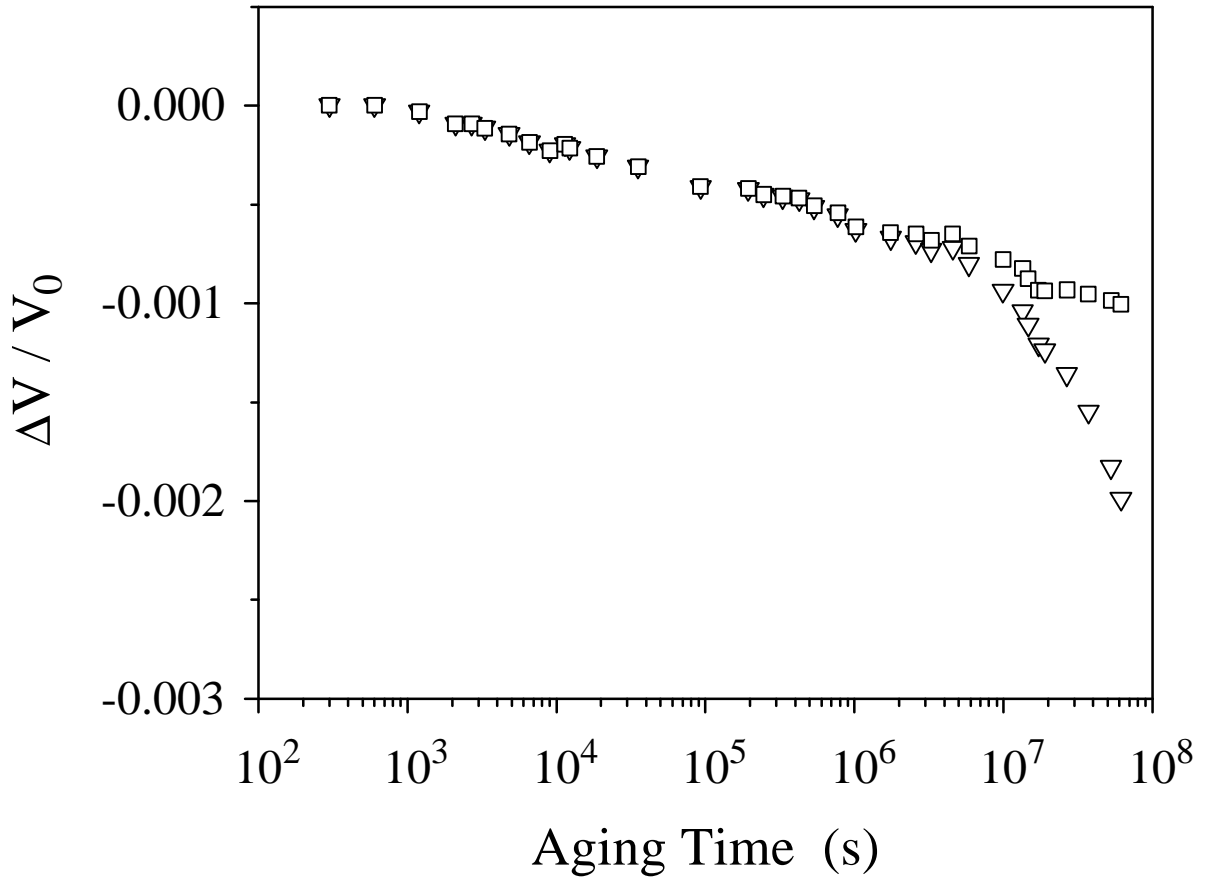


Figure 10-2: Volume relaxation data for bisphenol-A polycarbonate during aging at 21°C (triangles) and the converted data after subtraction of a slow linear volume relaxation process (squares). See text for an explanation of the subtraction.

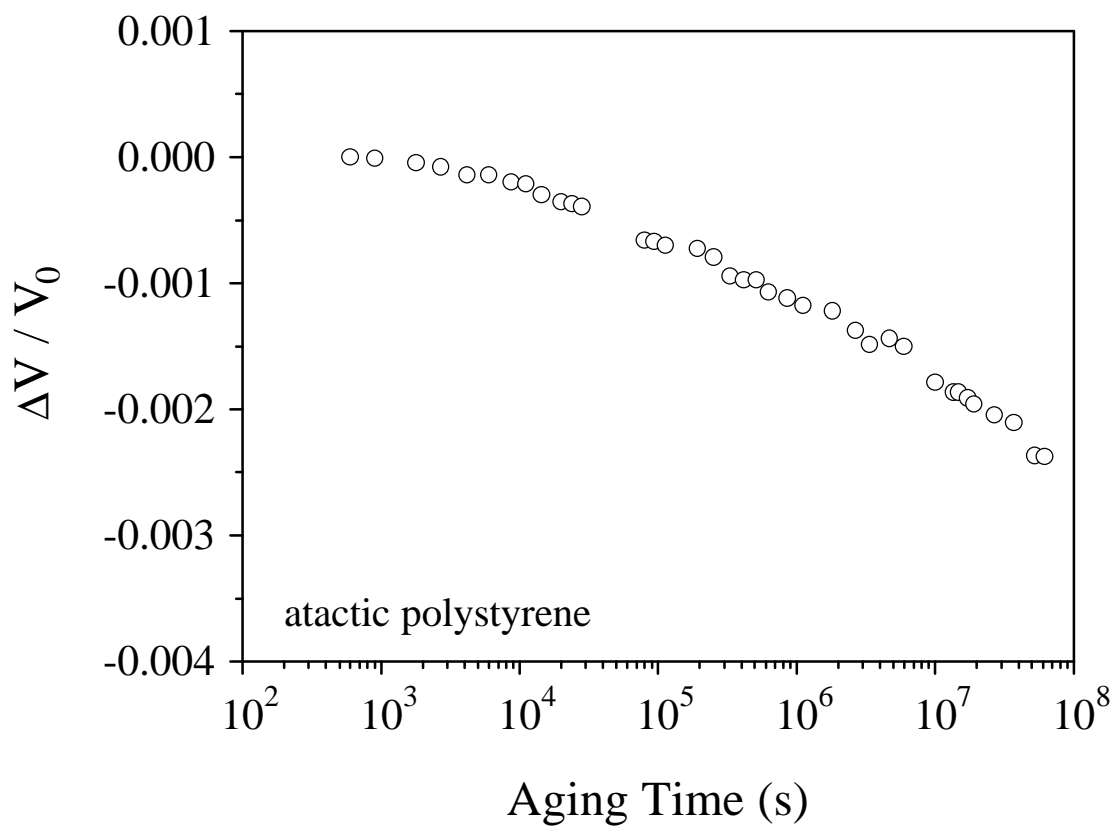


Figure 10-3. Volume relaxation data for atactic polystyrene during aging at 21°C.

## 10.5 References

- <sup>1</sup> Wimberger-Friedl, R.; de Bruin, J. G. *Macromolecules* **1996**, *29*, 4992.
- <sup>2</sup> A. J. Kovacs, *Fortschr. Hochpolym.-Forsch.*, **1964**, *3*, 394.
- <sup>3</sup> G. W. Scherer, *Relaxation in Glass and Composites*, Wiley, New York, 1986.
- <sup>4</sup> L. C. E. Struik, *Physical Aging In Amorphous Polymers and Other Materials*, Elsevier, New York, 1978.
- <sup>5</sup> Shelby, M. D. *Ph.D. Dissertation*, Virginia Polytechnic Institute and State University, 1996.
- <sup>6</sup> Mercier, J. P.; Groenincks, G. *Rheol. Acta* **1969**, *8*, 516.

# Chapter 11

## Refractive Index: A Probe for Monitoring Volume Relaxation of Glassy Polymers During Physical Aging

---

---

### Chapter Synopsis

A positive correlation between refractive index and density has been experimentally illustrated in the literature for numerous materials, including polymers. This relationship was exploited in an attempt to follow the densification of a glassy polymer during the physical aging process. Atactic polystyrene films were aged at 74°C and the refractive index ( $n$ ) was evaluated as a function of aging time ( $t_a$ ) using an Abbe refractometer. The refractive index increased linearly with respect to  $\log(t_a)$ , and this dependence was used in conjunction with experimentally determined values of the thermal expansion coefficient in the glassy state and  $(\partial n / \partial T)_{P, t_a}$  for unaged polystyrene to determine the volume relaxation rate at 74°C. This rate was similar to that obtained for the same polystyrene material using a precision dilatometer, indicating the possibility for using refractive index measurements to quantitatively assess volume relaxation during physical aging.

## 11.1 Introduction

Optical properties are intimately related to the chemical composition and structural features of a polymeric material. Representative examples of such relationships are evident in the Lorentz-Lorenz expression for average refractive index ( $\bar{n}$ ), an important optical property for polymer applications. One form of the Lorentz-Lorenz equation is as follows:<sup>1</sup>

$$\frac{\bar{n}^2 - 1}{\bar{n}^2 + 2} = \frac{\rho N_{av} \sum n_i \bar{\alpha}_i}{3 M_0 \epsilon_0} \quad \text{Eqn. 11-1}$$

where  $N_{av}$  is Avogadro's number, the molecular weight of the polymer repeat unit is denoted by  $M_0$ ,  $\epsilon_0$  is the permittivity of free space constant, the density of the polymer is represented by  $\rho$ , the average polarizability of the  $i^{\text{th}}$  type chemical bond is given the symbol  $\bar{\alpha}_i$ , and  $n_i$  is the number of such bonds per repeat unit. It is clear from the above equation that increasing the average polarizability of the chemical bonds is expected to result in greater refractive index values, if all other factors remain constant. For a given chemical composition, the number of polarizable species per unit volume also influences the velocity of light through a material, hence a positive correlation between refractive index and density. Therefore, knowledge of refractive index changes for a polymer material can provide information concerning density changes.

There are numerous variables which indirectly influence refractive index by altering the density of a polymer. As temperature is increased, a material expands volumetrically which results in a decrease in density and refractive index. The thermal expansion coefficient for a polymer in the glassy state is significantly lower than the coefficient for the polymer at temperatures above the glass transition region. The inflection in a plot of refractive index versus temperature can be used to determine the glass transition temperature associated with the heating/cooling conditions utilized, as has been detailed in the literature.<sup>2-4</sup> The crystalline phase of a semicrystalline polymer is more dense than its amorphous counterpart, and refractometry has additionally been used in assessing the degree of crystallinity for polymer films.<sup>5</sup>

Physical aging of glassy polymers is another area where refractive index measurements can potentially be utilized to probe densification features. When an amorphous polymer is quenched from the liquid state to a temperature below the glass transition temperature region, attainment of thermodynamic equilibrium via structural rearrangement is initially denied due to kinetic considerations.<sup>6</sup> Relaxation can occur with time, and this process, known as physical aging, results in a decrease of the specific volume of the polymer towards the equilibrium state. Although the density changes during physical aging are typically quite small (the density of atactic polystyrene aged 15°C below  $T_g$  increases at an approximate rate of 0.0008 g/cc per decade of aging time<sup>7</sup>), volume relaxation during physical aging may be able to be followed using refractometry provided refractive index measurements can be made with adequate accuracy. Research employing refractometry to provide insight into the non-equilibrium nature of the glassy state has been very limited. The memory effect, first disclosed by the dilatometry experiments of Kovacs<sup>8</sup>, has been investigated for inorganic glasses using refractometry<sup>9-11</sup> as opposed to dilatometry. Jenkel followed the physical aging of polystyrene using refractive index<sup>12</sup>, but a direct quantitative link between refractive index changes and volume relaxation rates has not clearly been made for the physical aging of glassy polymers. This research investigates whether changes in refractive index for atactic polystyrene (a-PS) during isothermal physical aging can be quantitatively related to the corresponding volume changes..

## 11.2 Experimental Details

The material used in this study was Styron 685D, an atactic polystyrene (a-PS) produced by Dow Chemical. This amorphous polymer has a number average molecular weight of 174,000 g/mol and a weight average molecular weight equal to 297,000 g/mol as assessed via gel permeation chromatography. The inflection glass transition temperature ( $T_g$ ) for this material was determined to be 104°C at a heating rate of 10°C/min using a differential scanning calorimeter (Perkin Elmer DSC-7). Films were generated by compression molding a-PS pellets in a picture frame mold at a temperature

of 165°C using a laboratory press with heated platens produced by Pasadena Hydraulics Incorporated. The resulting films, possessing an average thickness of 0.1 mm, were cut into rectangles of suitable size (20 mm x 50 mm) for refractive index testing. In order to insure that the initial films were unaged and unoriented, the film samples were free-annealed at a temperature 50°C above  $T_g$  for 10 minutes and subsequently quenched between two plates at room temperature. The films were then placed into a vacuum oven held at 74°C, and samples were removed from the oven at various aging times for refractive index evaluation. Because the films were unoriented, the refractive index in any direction for the films should be equal to the average refractive index, and the symbols  $n$  and  $\bar{n}$  will, therefore, be used interchangeably in this paper.

Refractive index measurements were made using an Abbe refractometer manufactured by Bellingham and Stanley Ltd. (model 60/ED). The product literature provided for this instrument indicated that it provides refractive indices that are accurate to within 0.0001 refractive index units. A circulating water bath produced by Neslab Instruments Inc. (model Endocal RTE-100) was employed to maintain the temperature of the refractometer prisms and the enclosed sample at a constant value  $\pm 0.1^\circ\text{C}$ . Based on the sensitivity of refractive index to temperature in the glassy state for a-PS, this temperature fluctuation is expected to result in a refractive index error of  $\pm 1.2 \times 10^{-5}$ , a value negligible in comparison to the combined sample and instrument error to be detailed later. Prior to testing the polystyrene film samples, the refractometer was calibrated at 20°C using a contact liquid with a known refractive index of 1.5982 at this temperature. For all of the tests performed, the critical angles were determined with respect to the average Sodium D line (589.3 nm wavelength), and the corresponding refractive index ( $n_D$ ) values were determined to the fifth decimal place using conversion tables for the instrument. In order to minimize diffuse reflection from the surfaces of the a-PS films, a contact fluid based upon hydrogenated terphenyl 1-bromonaphthalene was utilized. The  $n_D$  of the particular fluid used was 1.6423 at 20°C which is a value between the refractive index of a-PS (~1.59) and that of the refractometer prisms (~1.89), in accordance with standard refractometry procedure.<sup>13</sup> To eliminate sample error, it would be desirable to determine the refractive index of a single a-PS film sample after various incremental aging

times. However, the a-PS samples could only be tested once because it was necessary to expose the film samples to the contact fluid in order to make refractive index measurements. Since testing multiple films was unavoidable, five a-PS samples were tested for each aging condition to provide some measure of the statistical significance of the refractive index data.

Volume relaxation of the atactic polystyrene material during physical aging at 74°C was evaluated using a precision dilatometry apparatus constructed by Dr. M. D. Shelby and described in detail elsewhere.<sup>14</sup> A solid bar of the a-PS material with the dimensions 13 mm x 13 mm x 38 mm was prepared in an analogous manner to the previously mentioned films. The bar sample was subsequently enclosed in a glass dilatometer containing a capillary with an inside diameter of 4.16 mm. The dilatometer, encasing the polymer sample, was filled with mercury and then degassed under vacuum for 48 hours to remove any air bubbles. The degassed dilatometer was allowed to equilibrate for 24 hours at room temperature after removal of the vacuum, annealed 10 minutes at a temperature 50°C above  $T_g$  in an oil bath, and then quenched using an ice bath. The a-PS sample in the dilatometer was then isothermally annealed at 74°C in a Haake model N4-B oil bath with temperature control fluctuations less than 0.01°C, and the height change of the mercury in the capillary was assessed with aging time using a calibrated linear voltage differential transducer and converted to volume change based on the cross sectional area of the capillary. This procedure was performed three times in order to determine a volume relaxation rate and its corresponding standard deviation for a-PS undergoing physical aging at 74°C. The thermal expansion coefficient for a-PS in the glassy state was also determined using dilatometry by cooling a sample from above the glass transition region to a temperature of 65°C in the dilatometer at an approximate rate of 1°C/min., recording the capillary height change during cooling, and subtracting the mercury volume change in order to assess the volume change attributed solely to the a-PS sample as a function of temperature.

### 11.3 Results and Discussion

The discussion to follow will explore the potential for using refractive index measurements to monitor the densification of atactic polystyrene during physical aging. First, the experimental data concerning the influence of aging time on the refractive index of atactic polystyrene isothermally aged at 74°C will be presented. This will be followed by details pertaining to the development of two straightforward methods to utilize this data in the determination of the corresponding volume relaxation rate ( $\beta$ ). The volume relaxation rates assessed using the two refractometry approaches will finally be compared to the analogous rate determined for the same a-PS material at the same aging conditions using dilatometry in order to provide an indication of the validity of the refractometry approach developed.

#### *11.3.1 Effect of Physical Aging on Refractive Index*

Film samples of atactic polystyrene were physically aged at 74°C following a quench from the equilibrium rubbery state ( $T = T_g + 50^\circ\text{C}$ ), and refractive index measurements were made as a function of aging time ( $t_a$ ). After removal from the aging chamber, the film samples were cooled to room temperature and the refractive indices were determined at 20°C within 20 minutes from the time of oven removal. It was assumed that negligible additional physical aging occurred during the short 20 minute duration after the samples were removed from the oven because the aging rate is expected to be extremely slow at 20°C relative to the rate at 74°C, a temperature which is much closer to the glass transition temperature region.<sup>7</sup> The effect of aging at 74°C on the refractive index of atactic polystyrene is indicated in Figure 11-1a. The refractive index increased in a linear fashion when plotted as a function of  $\log(t_a)$  and the slope of the linear fit to the data  $(\partial n / \partial \log t_a)_{P,T}$  was found to be  $(3.22 \pm 0.60) \times 10^{-4}$ . The error bars indicated in this plot represent the standard deviations associated with the five samples tested at each aging time. The refractive index error, which represents a combination of

instrument error ( $\pm 0.0001$ ) and sample error, possessed average and maximum values of 0.00015 and 0.00028, respectively. Despite the considerable magnitudes of the error bars, the linear dependence of refractive index on  $\log(t_a)$  is statistically significant as is evident from the correlation coefficient ( $R^2$ ) for the linear fit which is equal to 0.934.

It is often observed that density increases are linearly related to  $\log(t_a)$  during isothermal aging, following a quench from above the glass transition temperature, due to the self-limiting nature of physical aging.<sup>15</sup> The Lorentz-Lorenz relationship (Eqn. 11-1) does not predict refractive index to be a linear function of density, and the experimental observation that refractive index has a linear dependence on aging time does not have a fundamental basis. The refractive index data was replotted in the form of the left hand side of Eqn. 11-1 as illustrated in Figure 11-1b. This plot implies that a linear increase in density with  $\log(t_a)$  occurred during isothermal aging of a-PS at 74°C, as anticipated. However, the degree of linearity for the plot in Figure 11-1b ( $R^2 = 0.934$ ) is identical to the linearity between refractive index and  $\log(t_a)$  which suggests that either plot is suitable to describe the experimentally observed effect of aging on refractive index for the polymer material and conditions utilized in this study. In agreement with this observation, research evaluating the effect of density on refractive index for various polyolefins resulted in the conclusion that plotting refractive index or refractive index expressed in the form of Lorentz-Lorenz equation versus density provides similar degrees of linearity.<sup>13</sup>

### ***11.3.2 Determination of Volume Relaxation Rate from Refractive Index Data***

The volume relaxation rate ( $\beta$ ) is a parameter which can be used to represent the kinetics of volume relaxation during the isothermal physical aging of glassy materials. The volume relaxation rate can be expressed as follows<sup>7</sup>:

$$\beta = -\frac{1}{V} \left( \frac{\partial V}{\partial \log t_a} \right)_{P,T} \quad \text{Eqn. 11-2}$$

The previously discussed increase in refractive index with aging time for atactic polystyrene is a consequence of the densification of the system. Therefore, the value of

$(\partial n / \partial \log t_a)_{P,T}$  observed for a-PS physically aged at 74°C is influenced by the rate of volume relaxation and can potentially be used to determine  $\beta$ . The relationship between  $\beta$  and  $(\partial n / \partial \log t_a)_{P,T}$  can be expressed mathematically using the chain rule of partial differentiation:

$$\beta = -\frac{1}{V} \left( \frac{\partial V}{\partial \log t_a} \right)_{P,T} = - \left( \frac{\partial n}{\partial \log t_a} \right)_{P,T} \left( \frac{\partial T}{\partial n} \right)_{P,t_a} \frac{1}{V} \left( \frac{\partial V}{\partial T} \right)_{P,t_a} \quad \text{Eqn. 11-3}$$

Using the definition of the thermal expansion coefficient in the glassy state ( $\alpha_g$ ), Eqn. 11-3 can be rewritten as:

$$\beta = -\frac{1}{V} \left( \frac{\partial V}{\partial \log t_a} \right)_{P,T} = - \left( \frac{\partial n}{\partial \log t_a} \right)_{P,T} \left( \frac{\partial n}{\partial T} \right)_{P,t_a}^{-1} \alpha_g \quad \text{Eqn. 11-4}$$

This relationship allows determination of the volume relaxation rate from  $(\partial n / \partial \log t_a)_{P,T}$  in conjunction with the change of refractive index with temperature for the unaged material in the glassy state  $(\partial n / \partial T)_{P,t_a}$  and the glassy thermal expansion coefficient. Refractive index data for unaged a-PS is presented as a function of temperature in Figure 11-2. This data was used to determine a value for  $(\partial n / \partial T)_{P,t_a}$  which was equal to  $-(1.17 \pm 0.07) \times 10^{-4} \text{ K}^{-1}$ , a value comparable to the value of  $-1.2 \times 10^{-4} \text{ K}^{-1}$  reported in the literature.<sup>1</sup> Dilatometry was used to determine that  $\alpha_g = (2.21 \pm 0.06) \times 10^{-4} \text{ K}^{-1}$  for the atactic polystyrene material investigated which is consistent with the range of values tabulated for this polymer.<sup>16</sup> Using the experimentally determined values for the parameters  $(\partial n / \partial \log t_a)_{P,T}$ ,  $(\partial n / \partial T)_{P,t_a}$ , and  $\alpha_g$ , and propagating their associated errors using a differential technique, the volume relaxation rate calculated via Eqn. 11-4 was found to be equal to  $(6.08 \pm 1.61) \times 10^{-4}$ . A summary of the parameter values used in this calculation of volume relaxation rate can be found in the upper portion (Method #1) of Table 11-I.

Irrespective of the changing thermodynamic state of the glassy polymer undergoing physical aging, the Lorentz-Lorenz expression should remain valid at any instant in time. Because the chemistry of the system is not changing during physical aging, all of the parameters on the right hand side of Eqn. 11-1 are constant except for density. Therefore, the following expression can be developed based upon this proportionality between density and the left hand side of the Lorentz-Lorenz equation:

$$\frac{1}{L} \left( \frac{\partial L}{\partial \log t_a} \right)_{P,T} = \frac{1}{\rho} \left( \frac{\partial \rho}{\partial \log t_a} \right)_{P,T} = \beta \quad \text{where: } L = \frac{n^2 - 1}{n^2 + 2} \quad \text{Eqn. 11-5}$$

Using this approach (Method #2), the volume relaxation rate determined was equal to  $(4.25 \pm 0.38)E-4$  as is indicated in the lower half of Table 11-I. Direct use of the Lorentz-Lorenz expression (Method #2) slightly underpredicted the volume relaxation rate in comparison to Method #1. As will be detailed in the next section, the  $b_v$  value determined from the refractive index data via Method #1 more closely agrees with the value obtained by dilatometry. The development of Method #2 assumes that density does not influence the polarizability of the chemical bonds, and a possible interrelationship between density and polarizability may have resulted in the noted under-prediction of volume relaxation rate using this method. This possible interrelationship does not pose any problems when using Method #1 due to a canceling effect between density changes (and possible polarizability changes) induced by temperature changes and by physical aging.

### ***11.3.3 Comparison of Aging Rates Determined by Refractometry and Dilatometry***

Volume relaxation rates for glassy materials are commonly assessed through the use of dilatometry. The densification of a-PS during physical aging at 74°C was investigated using a precision mercury dilatometer, and a typical volume relaxation plot providing a slope of  $-\beta$  is presented in Figure 11-3. The average volume relaxation rate for three dilatometry experiments was found to be  $(7.57 \pm 0.41) \times 10^{-4}$  in contrast to the rate calculated based upon the refractive index data via Method #1 which was equal to  $(6.08 \pm 1.61) \times 10^{-4}$ . If the substantial error associated with the  $\beta$  determined by

refractometry is taken into account, the volume relaxation rate determined from refractive index measurements (Method #1) is within experimental error of the  $\beta$  value assessed using dilatometry. This suggests that the technique (Method #1) developed in this investigation for converting refractive index changes during physical aging of glassy polymers to the associated volume relaxation rates can be used quantitatively.

It is anticipated that improvements can be made in order to determine volume relaxation rates using the refractometry approach which more closely match the corresponding rates assessed using dilatometry. The use of a device which allows refractive index determinations with improved accuracy relative to the Abbe refractometer used in this study is expected to improve the agreement between the volume relaxation rates. Additionally, if refractive index measurements could be made on a single polymer film sample as it is incrementally aged, the sample error would be eliminated thus improving the experimental results and the volume relaxation rates calculated from them. A weak secondary relaxation, which occurs in the vicinity of 60°C for atactic polystyrene, has been shown to slightly increase the glassy thermal expansion coefficient above this temperature of 60°C relative to the glassy expansion coefficient observed near room temperature.<sup>17</sup> Although this difference is quite small, it implies that  $(\partial n / \partial T)_{P, t_a}$  near the aging temperature of 74°C may have been slightly different than that determined for the lower temperature range used to determine this parameter, possibly influencing the  $\beta$  calculation. Overall, the best method would be to accurately follow the refractive index for a single polymer film sample *in situ* during the physical aging process and use values of the parameters  $(\partial n / \partial T)_{P, t_a}$  and  $\alpha_g$  determined near the aging temperature in the calculation of the volume relaxation rate using Eqn. 11-4.

## 11.4 Conclusions

For atactic polystyrene isothermally aged at 74°C following a quench from above the glass transition temperature, the refractive index increased linearly with respect to  $\log(t_a)$  due to the densification of the system during physical aging. This linear

relationship was used with experimentally determined values of the thermal expansion coefficient in the glassy state and  $\left(\frac{\partial n}{\partial T}\right)_{P,t_a}$  for the unaged polymer to determine the volume relaxation rate. This rate was equal to  $(6.08 \pm 1.61) \times 10^{-4}$ , a value within experimental error of the volume relaxation rate of  $(7.57 \pm 0.41) \times 10^{-4}$  determined by dilatometry. This technique developed for converting refractive index changes to the rate of volume relaxation appears to be a quantitative alternative to dilatometry for following the densification kinetics associated with physical aging. Due to the difficulty in constructing a dilatometry apparatus providing accurate volume change measurements and the lengthy procedures necessary to remove entrapped air from the dilatometer prior to testing, the refractometry approach explored in this study may in fact be an easier method of following volume relaxation as well.

Table 11-I: Summary of parameters used to calculate  $\beta$  from refractive index data

Method #1	$\left(\frac{\partial n}{\partial \log t_a}\right)_{P,T}$	$\left(\frac{\partial n}{\partial T}\right)_{P,t_a}$ [K <sup>-1</sup> ]	$\alpha_g$ [K <sup>-1</sup> ]	$\beta$
Eqn. 11-4	$(3.22 \pm 0.6) \text{E-4}$	$(-1.17 \pm 0.07) \text{E-4}$	$(2.21 \pm 0.06) \text{E-4}$	$(6.08 \pm 1.61) \text{E-4}$
Method #2	$\frac{n^2 - 1}{n^2 + 2}$ (Average Value)	$\left(\frac{\partial L}{\partial \log t_a}\right)_{P,T}$ where: $L = \frac{n^2 - 1}{n^2 + 2}$		$\beta$
Eqn. 11-5	$0.3373 \pm 0.0002$	$(1.43 \pm 0.06) \text{E-4}$		$(4.25 \pm 0.38) \text{E-4}$

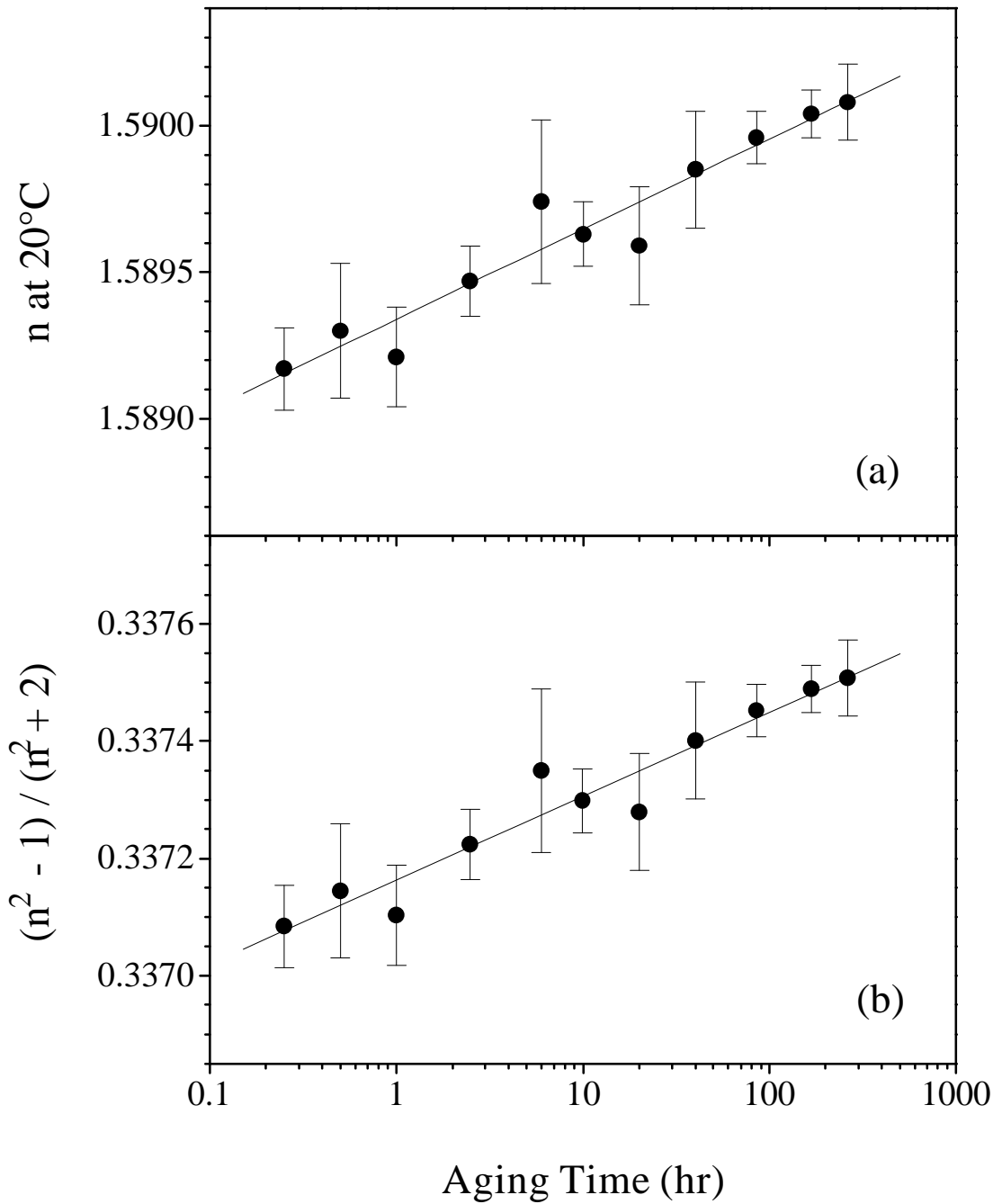


Figure 11-1: Refractive index at  $20^\circ\text{C}$  as a function of aging time for a-PS films aged at  $74^\circ\text{C}$  (a) and data replotted in the form of the Lorentz-Lorenz relationship (b). Straight lines represent linear fits to the data.

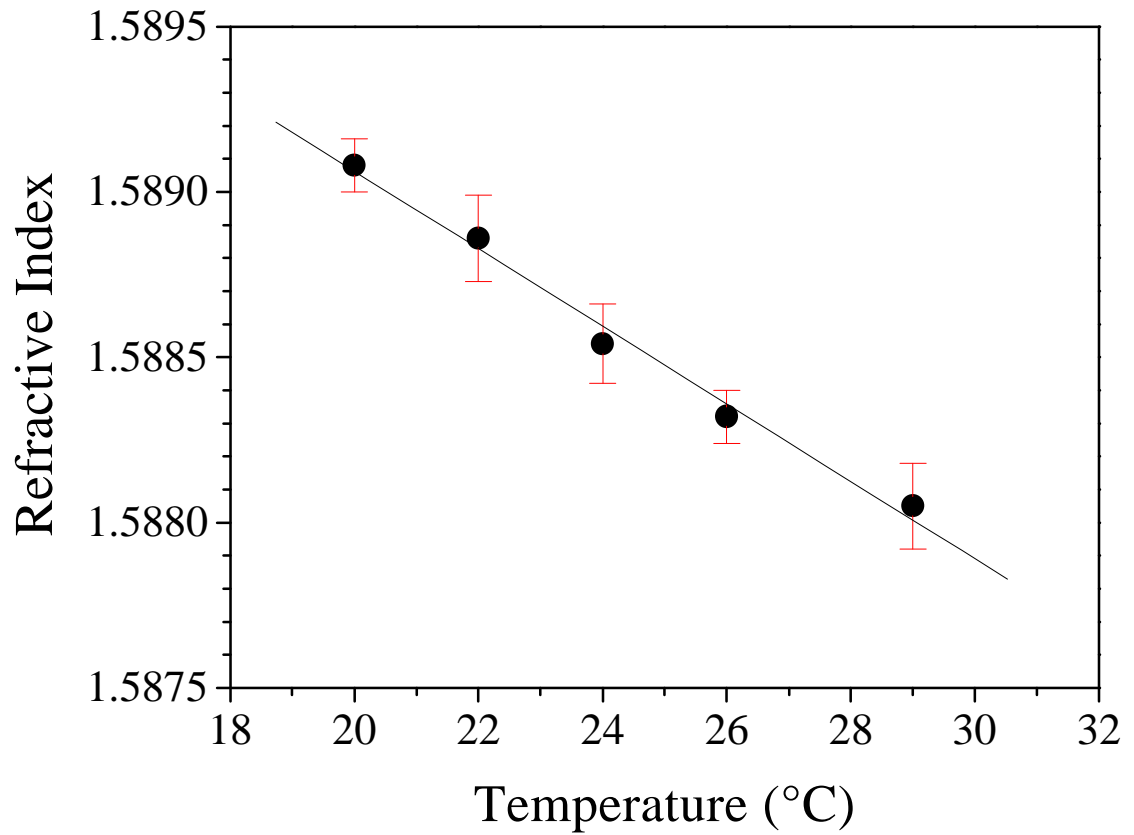


Figure 11-2: Refractive index as a function of temperature for unaged a-PS films. The solid line represents the linear fit used to determine  $(\partial n / \partial T)_{P, t_a}$

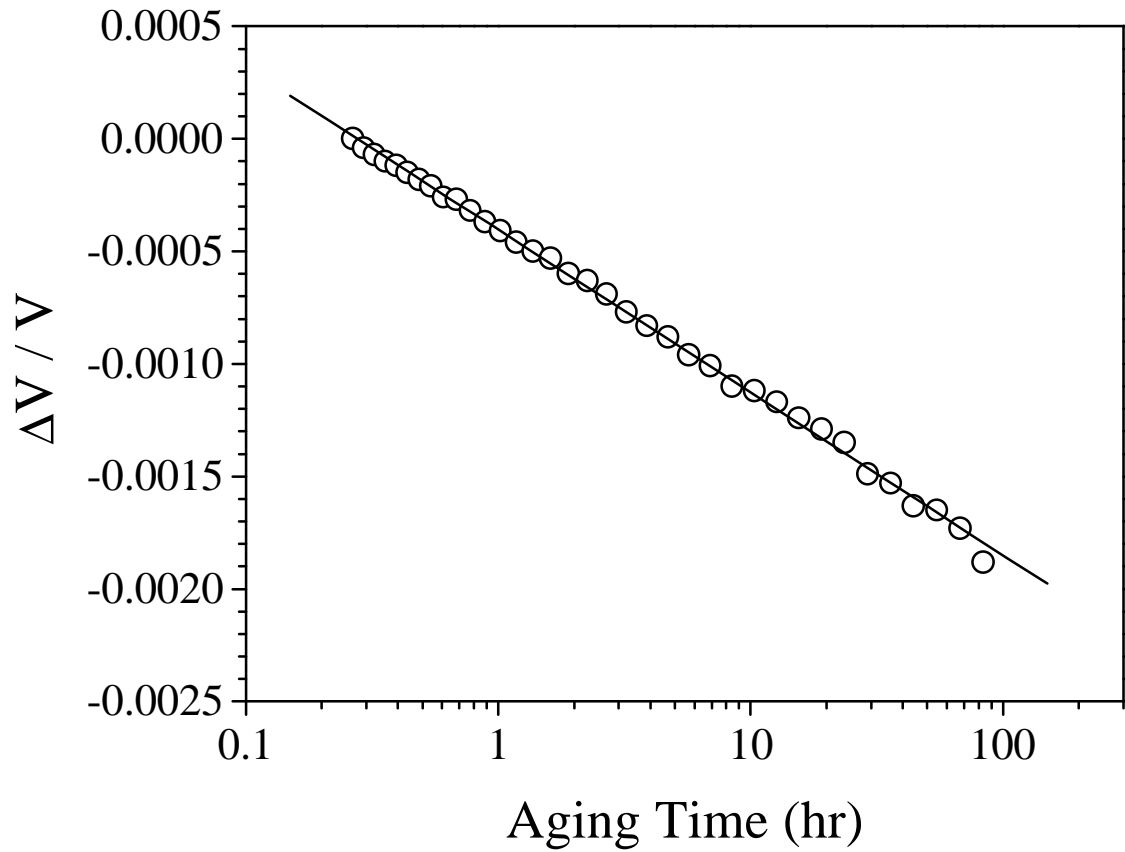


Figure 11-3: Volume relaxation plot for a-PS during aging at 74°C obtained using dilatometry. Volume changes referenced to  $t_a = 0.25$  hr. The slope of the linear fit is equal to  $-\beta$ .

### 11.5 References

- <sup>1</sup> Mills, N. J. in 'Encyclopedia of Polymer Science and Engineering' 2nd Edn. (Eds. H. F. Mark, N. M. Bikales, C. G. Overberger, G. Menges, and J. I. Kroschwitz), John Wiley and Sons, New York, 1987, Vol. 10, pp. 493-540.
- <sup>2</sup> Stützel, P., Tegtmeier, H. D., and Tacke, M. *Infrared Phys.* 1988, **28**, 67.
- <sup>3</sup> Krause, S. and Lu, Z.-H. *J. Polym. Sci., Part A-2* 1981, **19**, 1925.
- <sup>4</sup> Beaucage, G., Composto, R., and Stein, R. S. *J. Polym. Sci., Part B: Polym. Phys.* 1993, **31**, 319.
- <sup>5</sup> Samuels, R. J. *J. Polym. Sci., Polym. Phys. Ed.* 1974, **12**, 1417.
- <sup>6</sup> McKenna, G. B. in 'Comprehensive Polymer Science, Vol.2: Polymer Properties' (Eds. C. Booth and C. Price), Pergamon, Oxford, 1990, pp.311-362.
- <sup>7</sup> Hutchinson, J. M. *Prog. Polym. Sci.* 1995, **20**, 703.
- <sup>8</sup> Kovacs, A. J. *Fortschr. Hochpolym. Forsch.* 1963, **3**, 394.
- <sup>9</sup> Spinner, S. and Napolitano, A. *J. Res. Nat. Bur. Stand.* 1966, **70A**, 147.
- <sup>10</sup> Boesch, L., Napolitano, A. and Macedo, P. B. *J. Amer. Ceram. Soc.* 1970, **53**, 148.
- <sup>11</sup> Moynihan, C. T., Macedo, P. B., Montrose, C. J., Gupta, P. K., DeBolt, M. A., Dill, J. F., Dom, B. E., Drake, P. W., Easteal, A. J., Elterman, P. B., Moeller, R. P., Sasabe, H., and Wilder, J. A. *Ann. NY Acad. Sci.* 1976, **279**, 15.
- <sup>12</sup> Jenkel, E. in 'Struktur und Physikalisches Verhalten der Kunststoffe' ed. K. A. Wolf, Springer, Berlin, 1962, pp. 160-189.
- <sup>13</sup> Pepper, R. E. and Samuels, R. J. in 'Encyclopedia of Polymer Science and Engineering' 2nd Edn. (Eds. H. F. Mark, N. M. Bikales, C. G. Overberger, G. Menges, and J. I. Kroschwitz), John Wiley and Sons, New York, 1987, Vol. 14, pp. 261-298.
- <sup>14</sup> Shelby, M. D. *Ph.D Thesis*, Virginia Tech, Blacksburg, VA, 1996.
- <sup>15</sup> Tant, M. R. and Wilkes, G. L. *Polym. Eng. Sci.* 1981, **21**, 874.
- <sup>16</sup> Brandrup, J. and Immergut, E. H., eds. 'Polymer Handbook' 2nd ed., John Wiley and Sons, New York, 1975, p. V-51.
- <sup>17</sup> Greiner, R. and Schwarzl, F. R. *Rheol. Acta* 1984, **23**, 378.

## Summary and Recommendations for Future Work

---

This research study revealed that the compositional variation of unaged glassy density, fragility, and secondary relaxation intensity, all of which are influenced by molecular interactions, could provide insight into physical aging results for the a-PS/PPO and PMMA/SAN blends. One of the inadequacies which presented itself with regard to contrasting the influence of interactions on the aging behavior of the a-PS/PPO and PMMA/SAN blend systems concerned the many notable differences between the blends. In addition to attaining thermodynamic miscibility by distinct mechanisms (specific attractive interactions for a-PS/PPO and the copolymer repulsion effect for PMMA/SAN), the variation of both secondary relaxation intensity and glass transition temperature with composition displayed unique behavior for the two blends. Nevertheless, a systematic method for understanding and interpreting the aging results was developed in this investigation. It would be preferable to directly compare the structural relaxation characteristics for polymer materials which differ from each other in the nature and strength of chemical interactions but which otherwise display similarities with regard to backbone chemistry, location/intensity of secondary relaxations, etc. Future research contributions which attempt to entertain such revealing comparisons would greatly enhance the current understanding of how intermolecular interactions affect relaxation in the nonequilibrium glassy state.

Investigating the glass formation kinetic behavior for miscible blends of a-PS and PPO revealed that the common thermodynamically-based interpretation of negative mixing volumes inferred from glassy density measurements may not always be correct. The kinetics of glass formation influence the initially frozen-in density which results upon formation of the glassy state during cooling. Because attractive interactions can heighten the fragility (cooperativity) observed for polymer blends compared to the behavior of the pure components, there is no reason to expect that the excess thermodynamic properties associated with the equilibrium liquid state should be maintained upon quenching into the glassy state. Determination of pressure-volume-

temperature characteristics for many amorphous polyblends as a function of composition in the glassy and liquid states would, in combination with fragility measurements, allow a general examination of this observation noted herein for the a-PS/PPO system.

Perhaps the most noteworthy component of this physical aging research endeavor was the general relationship which was uncovered between equilibrium glass transition cooperativity in the liquid state and the structural relaxation behavior in the glassy state of amorphous polymer materials. The significance of this finding was that it generated a better molecular-level understanding of volume and enthalpy relaxation in the nonequilibrium glass because of the current comprehension of glass transition cooperativity, or fragility, in terms of intra- and intermolecular characteristics. While this correlation appeared to be quite valid for an aging temperature of  $T_g-30^\circ\text{C}$ , extension of the relationship to aging temperatures deeper within the glassy state was problematic due to the differences between the various amorphous polymer materials with respect to the location and extent of secondary relaxation behavior. Future research needs to address the molecular mechanism(s) by which localized secondary relaxations affect the dependence of both thermodynamic and mechanical properties on aging time and temperature. This information is necessary to extend and revise the correlation between segmental cooperativity and structural relaxation rates to deal with aging temperatures far below the glass transition temperature where secondary dispersions can play more prominent roles.

The study of the amorphous polyimide material revealed the presence of distinctly different relaxation time characteristics for the decay of enthalpy versus mechanical creep compliance changes during the physical aging process. One of the most uncertain aspects of the scientific literature dealing with research on physical aging is centered around the dubious relationship between thermodynamic and mechanical aging rates and whether or not the properties all reach equilibrium at the same time. A systematic and careful aging study of numerous amorphous polymers which, for example, follows changes in enthalpy, volume, and mechanical creep compliance is needed to clarify this crucial issue.

## Vita

Christopher Robertson was born in Sanford, Maine on October 31, 1970. He was raised in southern Maine and then southeastern Pennsylvania by his parents, Howard and Anne Robertson. After graduating Owen J. Roberts High School in Pottstown, Pennsylvania, he attended Virginia Tech and in 1993 received a Bachelor of Science degree in Chemical Engineering. An internship was then performed in Hickory, North Carolina at the Research, Development, and Engineering division of Siecor, a joint subsidiary of Siemens and Corning which specializes in the fabrication of fiber-optic cables. He then returned to Virginia Tech to pursue a graduate education in Chemical Engineering with a specialization in polymer science and engineering. A Master of Science degree was awarded in 1995 after working with Professor Donald Baird in the area of polymer processing. Upon completion of his Ph.D degree obtained under the guidance of Professor Garth Wilkes, he will commence a postdoctoral research appointment at the Naval Research Laboratory.